ISSN 0021-9673

VOL. 688 NOS. 1 + 2 30 DECEMBER 1994

COMPLETE IN ONE ISSUE

JOURNAL OF CHROMATOGRAPHY A

INCLUDING ELECTROPHORESIS AND OTHER SEPARATION METHODS

ELSEVIER

JOURNAL OF CHROMATOGRAPHY A

INCLUDING ELECTROPHORESIS AND OTHER SEPARATION METHODS

Scope. The *Journal of Chromatography A* publishes papers on all aspects of **chromatography, electrophoresis** and related methods. Contributions consist mainly of research papers dealing with chromatographic theory, instrumental developments and their applications. In the *Symposium volumes*, which are under separate editorship, proceedings of symposia on chromatography, electrophoresis and related methods are published. *Journal of Chromatography B: Biomedical Applications* —This journal, which is under separate editorship, deals with the following aspects: developments in and applications of chromatographic and electrophoretic techniques related to clinical diagnosis or alterations during medical treatment; screening and profiling of body fluids or tissues related to the analysis of active substances and to metabolic disorders; drug level monitoring and pharmacokinetic studies; clinical toxicology; forensic medicine; veterinary medicine; occupational medicine; results from basic medical research with direct consequences in clinical practice.

Submission of Papers. The preferred medium of submission is on disk with accompanying manuscript (see *Electronic manuscripts* in the Instructions to Authors, which can be obtained from the publisher, Elsevier Science B.V., P.O. Box 330, 1000 AH Amsterdam, Netherlands). Manuscripts (in English; *four* copies are required) should be submitted to: Editorial Office of *Journal of Chromatography A*, P.O. Box 681, 1000 AR Amsterdam, Netherlands, Telefax (+31-20) 485 2304, or to: The Editor of *Journal of Chromatography B: Biomedical Applications*, P.O. Box 681, 1000 AR Amsterdam, Netherlands. Review articles are invited or proposed in writing to the Editors who welcome suggestions for subjects. An outline of the proposed review should first be forwarded to the Editors for preliminary discussion prior to preparation. Submission of an article is understood to imply that the article is original and unpublished and is not being considered for publication elsewhere. For copyright regulations, see below.

Publication information. *Journal of Chromatography A* (ISSN 0021-9673): for 1995 Vols. 683–714 are scheduled for publication. *Journal of Chromatography B: Biomedical Applications* (ISSN 0378-4347): for 1995 Vols. 663–674 are scheduled for publication. Subscription prices for *Journal of Chromatography A*, *Journal of Chromatography B: Biomedical Applications* or a combined subscription are available upon request from the publisher. Subscriptions are accepted on a prepaid basis only and are entered on a calendar year basis. Issues are sent by surface mail except to the following countries where air delivery via SAL is ensured: Argentina, Australia, Brazil, Canada, China, Hong Kong, India, Israel, Japan, Malaysia, Mexico, New Zealand, Pakistan, Singapore, South Africa, South Korea, Taiwan, Thailand, USA. For all other countries airmail rates are available upon request. Claims for missing issues must be made within six months of our publication (mailing) date. Please address all your requests regarding orders and subscription queries to: Elsevier Science B.V., Journal Department, P.O. Box 211, 1000 AE Amsterdam, Netherlands. Tel.: (+31-20) 485 3642; Fax: (+31-20) 485 3598. Customers in the USA and Canada wishing information on this and other Elsevier journals, please contact Journal Information Center, Elsevier Science Inc., 655 Avenue of the Americas, New York, NY 10010, USA, Tel. (+1-212) 633 3750, Telefax (+1-212) 633 3764.

Abstracts/Contents Lists published in Analytical Abstracts, Biochemical Abstracts, Biological Abstracts, Chemical Abstracts, Chemical Titles, Chromatography Abstracts, Current Awareness in Biological Sciences (CABS), Current Contents/Life Sciences, Current Contents/Physical, Chemical & Earth Sciences, Deep-Sea Research/Part B: Oceanographic Literature Review, Excerpta Medica, Index Medicus, Mass Spectrometry Bulletin, PASCAL-CNRS, Referativnyi Zhurnal, Research Alert and Science Citation Index.

US Mailing Notice. *Journal of Chromatography A* (ISSN 0021-9673) is published weekly (total 52 issues) by Elsevier Science B.V., (Sara Burgerhartstraat 25, P.O. Box 211, 1000 AE Amsterdam, Netherlands). Annual subscription price in the USA US$ 5389.00 (US$ price valid in North, Central and South America only) including air speed delivery. Second class postage paid at Jamaica, NY 11431. **USA POSTMASTERS**: Send address changes to *Journal of Chromatography A*, Publications Expediting, Inc., 200 Meacham Avenue, Elmont, NY 11003. Airfreight and mailing in the USA by Publications Expediting.

See inside back cover for Publication Schedule, Information for Authors and information on Advertisements.

0021-9673/94/$07.00

Printed in the Netherlands

VOL. 688, NOS. 1 + 2 JOURNAL OF CHROMATOGRAPHY A 30 DECEMBER 1994

CONTENTS

(Abstracts/Contents Lists published in Analytical Abstracts, Biochemical Abstracts, Biological Abstracts, Chemical Abstracts, Chemical Titles, Chromatography Abstracts, Current Awareness in Biological Sciences (CABS), Current Contents/Life Sciences, Current Contents/Physical, Chemical & Earth Sciences, Deep-Sea Research/Part B: Oceanographic Literature Review, Excerpta Medica, Index Medicus, Mass Spectrometry Bulletin, PASCAL-CNRS, Referativnyi Zhurnal, Research Alert and Science Citation Index)

REGULAR PAPERS

Column Liquid Chromatography

Gas Chromatography

(Continued overleaf)

Contents (continued)

SHORT COMMUNICATIONS

Column Liquid Chromatography

Planar Chromatography

BOOK REVIEW

JOURNAL OF CHROMATOGRAPHY A

VOL. 688 (1994)

JOURNAL OF CHROMATOGRAPHY A

INCLUDING ELECTROPHORESIS AND OTHER SEPARATION METHODS

ELSEVIER

Amsterdam – Lausanne – New York – Oxford – Shannon – Tokyo

J. Chromatogr. A, Vol. 688 (1994)

0021-9673/94/$07.00

Printed in the Netherlands

ELSEVIER

Journal of Chromatography A, 688 (1994) 1–23

JOURNAL OF CHROMATOGRAPHY A

Theoretical analysis of band profiles in non-linear ideal countercurrent chromatography

GuoMing Zhong[a,b], Georges Guiochon[a,b,*]

[a]*Department of Chemistry, University of Tennessee, Knoxville, TN 37996-1600, USA*

[b]*Division of Analytical Chemistry, Oak Ridge National Laboratory, Oak Ridge, TN 37831-6120, USA*

First received 17 May 1994; revised manuscript received 10 August 1994

Abstract

The analytical solution of the ideal model of chromatography for the band profile of a single component in overloaded elution is extended to the case of the elution of a rectangular pulse in countercurrent moving-bed chromatography. The formation of concentration shocks and diffuse boundaries resulting from the rectangular injection profile of the feed is discussed for compounds moving in the direction of either the liquid phase or the solid phase. Differences between the solutions obtained for the moving-bed and the fixed-bed problems are examined and explained.

1. Introduction

Conventional implementations of chromatography, whether for analytical or preparative applications are batch processes. A feed solution is injected into a continuous stream of mobile phase which percolates through an immobile bed of a suitable stationary phase packed inside a fixed chromatographic column. The feed components are eventually separated and collected or detected at the end of the column. Then, another cycle starts with the injection of a new batch of feed. This same type of cyclic operation takes place in all classic modes of chromatography, elution, displacement or frontal analysis. These processes have been developed to their current state of sophistication by analytical chemists.

In its present form, the elution process satisfies excellently the requirements for chemical analyses and for the production of small amounts of purified products in the research laboratory. It is relatively easy to prepare columns for liquid chromatography that have a high separation power and a throughput commensurate with the range of production rates needed by the pharmaceutical industry. Therefore, the possibility of scaling up a chromatographic process for large-scale industrial production has attracted considerable attention. There are no reasons, however, for the same implementation which suits so well the needs of analytical chemists to be the most convenient for industrial production. Continuous processes have well known advantages over batch processes and much interest has been devoted to the development of a continuous

* Corresponding author. Address for correspondence: Department of Chemistry, University of Tennessee, Knoxville, TN 37996-1600, USA.

0021-9673/94/$07.00
SSDI 0021-9673(94)00765-9

implementation of the chromatographic process [1]. This objective can be achieved if a relative motion is created between the bed of stationary phase and the point at which the feed is introduced into the column. The main solutions proposed so far are countercurrent chromatography (using a sliding column or a "stationary phase" bed moving along the column) and cross-current chromatography, using a rotary annular column [1]. The former approach is generating increasing interest among separation engineers [1–7]. Note that in these implementations it becomes impossible to distinguish the two phases of a chromatographic system as the mobile and the stationary phase, since both phases move along the column. We shall call the former the liquid phase and the latter the solid phase.

The countercurrent effect can be achieved by sliding the column past the feed injection nozzle (sliding column), by moving continuously the solid adsorbent (moving bed, MB) or by using a series of short columns, instead of a long column, and moving sequentially in the direction of the liquid phase the inlet and outlet ports associated with each connection between successive columns (simulated moving bed, SMB) [1–6]. From the perspectives of modeling and initial process design, both true and simulated countercurrent processes can be considered in the same general way [2], and only a general model of countercurrent moving bed needs to be considered at this stage. Numerous theoretical and experimental investigations of MB and SMB have been published, particularly in the recent past [1–6]. However, owing to the complexity of the problem, our understanding of the phenomenon and our ability of optimize the experimental conditions under which the process is run are still limited.

As has happened in fixed-bed chromatography [7], the understanding of the development, migration and progressive separation of the individual bands of the components of a mixture in moving-bed chromatography would be greatly simplified if we knew the evolution of the profiles of single-component bands during their migration in a countercurrent chromatographic system. The use of the ideal model further simplifies considerably the solution of this latter problem by focusing attention on the influence of the thermodynamics of phase equilibrium [7]. As all implementations of chromatography for preparative purposes are bound to operate at high concentrations, only a moderate amount of dispersion distinguishes the band profiles obtained with actual columns from those predicted by the ideal model [7]. The ideal model has been studied in great detail and its analytical solutions for single- and multi-component problems are now well known for elution, frontal analysis and displacement [7–11]. They have been used as a basis not only for a theoretical understanding of the behavior of chromatographic bands, but also for the development of practical procedures of optimization of the experimental conditions for maximum production rate in preparative chromatography [7,12–16]. As we shall show, the ideal model offers similar interest in moving-bed and simulated moving-bed chromatography.

The purpose of this paper is the study of the simplest problem of countercurrent chromatography, the determination of the concentration profile and the migration of overloaded bands of a single component moving in an ideal column (i.e., having an infinite efficiency) under the conditions of moving bed and a pulse feed (with zero feed flow as in the fixed-bed case). This should provide a link between fixed-bed and moving-bed chromatography, a first step toward a detailed understanding of the properties of countercurrent chromatography and the mechanism of multi-component separations under steady-state conditions. In further publications, a binary mixture and a finite feed flow which differentiates continuous from discontinuous operations will be considered.

2. Theory

As explained in the Introduction, countercurrent moving-bed chromatography is very similar to fixed-bed elution, except for the movement of the solid phase and a finite feed flow. However, in this first stage, the effect of the latter is not considered here. Accordingly, the basic assump-

tions of the ideal model for countercurrent chromatography are [7–11] that (i) the solid and the liquid phases are in constant and instantaneous equilibrium; (ii) there is no axial dispersion in the column; (iii) the process is isothermal; (iv) the column is radially homogeneous, and can be considered as one-dimensional; (v) the liquid phase is not compressible; and (vi) the partial molar volume of the component is the same in the liquid and the solid phases and, accordingly, there is no sorption effect [7]. Hence the column is assumed to have an infinite efficiency. Although actual columns always have a finite efficiency, this efficiency is high in most practical cases, and the influence of the non-linear behavior of the isotherm becomes the controlling factor of band profiles, at least at high concentrations [7]. As shown later, a concentration band may migrate in two opposite directions and exit at two opposite side outlets of the column; we define the raffinate outlet at which the component exits with the liquid phase (after moving in the direction of the liquid phase) and the extract outlet at which the component exits with the solid phase.

2.1. System of equations of countercurrent chromatography

Based on the above assumptions, the mass balance of a retained component is given by

$$\frac{\partial C}{\partial t} + F \cdot \frac{\partial q}{\partial t} + u \cdot \frac{\partial C}{\partial z} - vF \cdot \frac{\partial q}{\partial z} = 0 \tag{1}$$

where C and q are the liquid- and solid-phase concentrations of the component, respectively, t and z are the time and the position in the column, respectively, F is the phase ratio [$F = (1-\varepsilon)/\varepsilon$, ε = total column porosity], u is the flow velocity of the liquid phase and v is the velocity of the moving solid phase. Eq. 1 differs from the conventional mass balance of chromatography only by the second convective term.

This equation is also the mass balance in simulated moving-bed chromatography, provided that the velocity u and v are chosen so that the following two relationships are valid:

$$v = v^{SMB} \tag{2a}$$

$$u + Fv = u^{SMB} \tag{2b}$$

where u^{SMB} and v^{SMB} are the velocities of the fluid (liquid or gas) and the solid phases, respectively, in SMB. Since, in practice, the movement of the solid phase in SMB is achieved by switching sequentially the inlet and outlet ports of each of the series of interconnected sub-columns, the velocity v^{SMB} is such that

$$v^{SMB} = \frac{L_s(1-\varepsilon)}{t_s} \tag{2c}$$

where L_s is the length of each sub-column or column sub-section used in SMB and t_s is the switching interval time, i.e., the time between two successive shifts of the feed injection and product withdrawal points, shifts which are assumed to take place instantaneously.

C and q are related by the adsorption isotherm:

$$q = f(C) \tag{3a}$$

In this work, q is assumed to be differentiable as needed. For the sake of simplicity we consider only a convex-upward isotherm without an inflection point. The extension to a convex-downward isotherm is straightforward and is not discussed here. The simplest and most often used model, the Langmuir isotherm:

$$q = \frac{aC}{1+bC} \tag{3b}$$

where a and b are numerical coefficients, will be used for illustrative examples of our general results.

The initial and boundary conditions correspond to an empty column and to the injection of a rectangular pulse of feed in the middle of the column, respectively. This amendment to the classical definition of the boundary condition is required to account for all the possible movements of the band. As shown later, depending on the experimental conditions, the band (or part of it) can move in the forward or backward direction. Feed injection in the middle of the column differs from conventional practice in

analytical chromatography or in fixed-bed preparative chromatography, in which cases the injection is done at one end of the column. Actually, this condition corresponds to the practice of countercurrent moving-bed chromatography where the feed is introduced at the column center and the separated fractions are collected at its two ends. The initial and boundary conditions are written as

$$C(z, t=0) = 0 \qquad -L < z < L \tag{4a}$$

$$C(z=0, t) = C_0 \qquad 0 < t < t_p \tag{4b}$$

$$C(z=0, t) = 0 \qquad t_p < t \tag{4c}$$

where the initial component concentration in the column is zero, C_0 is the component concentration in the feed and t_p is the injection duration.

2.2. Summary of the results obtained in fixed-bed chromatography

The properties of the band profiles predicted by the ideal model have been abundantly discussed in the case of fixed-bed chromatography [7–16]. In this case, $v = 0$ and the mass balance equation contains only the first three terms in Eq. 1. It results from this equation that a velocity $u_z(C)$ is associated with each concentration C on a diffuse (i.e., continuous) profile. This velocity is given by

$$u_z = \frac{u}{1 + F \cdot \dfrac{dq}{dC}} \tag{5}$$

Thus, in the case of a rectangular pulse injection of width t_p and height C_0, the continuous part of the elution profile (its rear in the case of a convex-downward isotherm such as the Langmuir isotherm) is given by

$$t(C) = t_p + \frac{L}{u_z} = t_p + t_0\left(1 + F \cdot \frac{dq}{dC}\right) \tag{6}$$

Because the isotherm is not linear, u_z depends on the concentration. As a consequence, a concentration discontinuity or shock will form on one side of the profile, whatever the injection profile. In Eq. 5, dq/dC is the slope of the isotherm at concentration C. It increases with decreasing liquid-phase concentration for a convex-upward isotherm, with increasing concentration for a convex-downward isotherm. Thus, the velocity associated with a concentration increases with increasing concentration in the case of a convex-upward isotherm. Fig. 1 illustrates this effect for the Langmuir isotherm (solid line). In this case, high concentrations move faster than low concentrations but, as they cannot pass them [7,10,11], they pile up at the front of the band and a discontinuity or shock is formed. The opposite is true for a convex-downward isotherm, in which case a concentration shock forms at the rear of the band profile.

The velocity of the concentration shock is not given by Eq. 5. Writing a mass balance for the discontinuity, Aris and Amundson [10] have shown that the shock velocity is given by

$$U_s = \frac{u}{1 + F \cdot \dfrac{\Delta q}{\Delta C}} \tag{7}$$

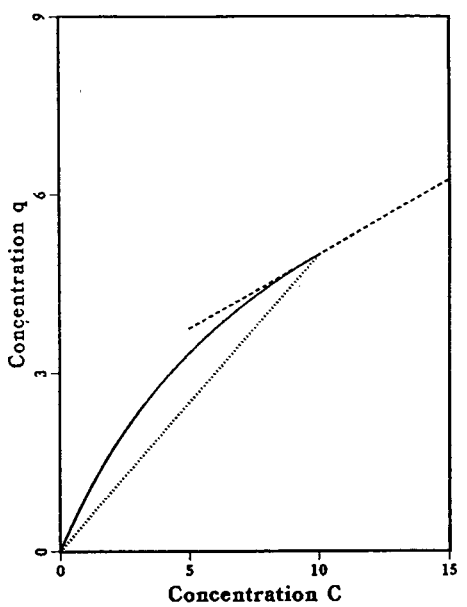

Fig. 1. Langmuir isotherm. Solid line, isotherm; dotted line, tangent to the isotherm at C; dashed line, chord of the isotherm at C. The parameters used in all the figures are phase ratio, $F = 0.25$; injection time, $t_p = 0.5$ s; Langmuir isotherm, $a = 1$ and $b = 0.1$ mM^{-1}. Axes in mM.

where Δq and ΔC are the concentration amplitudes of the shock in the solid and the liquid phase, respectively. The ratio $\Delta q/\Delta C$ is the slope of the chord connecting the two points on the isotherm which correspond to the liquid-phase composition after and before the shock (see Fig. 1). Unless the isotherm has an inflection point, this line goes through the origin.

The retention time of the front shock can be obtained by writing that the band area is constant and equal to the area injected [7,16]. This procedure provides the maximum concentration of the band, given as the root of the algebraic equation

$$\left| q - C \cdot \frac{\mathrm{d}q}{\mathrm{d}C} \right| = \frac{n}{F_v t_0 F} \tag{8}$$

where $n = C_0 t_p F_v$ is the amount injected, $F_v = \varepsilon S u$ is the liquid-phase flow-rate and S is the column cross-sectional area. This equation can be solved in the case of the Langmuir isotherm, giving

$$C_M = \frac{\sqrt{L_f}}{b(1 - \sqrt{L_f})} \tag{9}$$

where L_f is the loading factor or ratio of the sample size to the column saturation capacity:

$$L_f = \frac{n}{F_v t_0 F} = \frac{t_p C_0 b}{t_0 k'_0} \tag{10}$$

where $k'_0 = Fa$ is the limit retention factor at infinite dilution. In the case of the Langmuir isotherm, the retention time, $t_R(C_M)$, of the shock is given by

$$t_R(C_M) = t_p + t_0 + k'_0 t_0 (1 - \sqrt{L_f})^2 \tag{11}$$

A band profile corresponding to this case is shown in Figs. 2 and 3 (solid lines), as a reference for comparison with the profiles obtained in the case of a moving-bed column.

Finally, comparison between Eqs. 5 and 7 shows that the point on a continuous concentration profile, or diffuse boundary, at concentration C moves faster than a shock from concentration 0 to C. Hence, when a rectangular pulse (width t_p, height C_0) is injected into the column, its front shock is stable and moves as a shock at a constant velocity [Eq. 7, $U_s(C_0)$]. Its rear shock is not stable and becomes a diffuse boundary (Eq. 6). The highest point of that

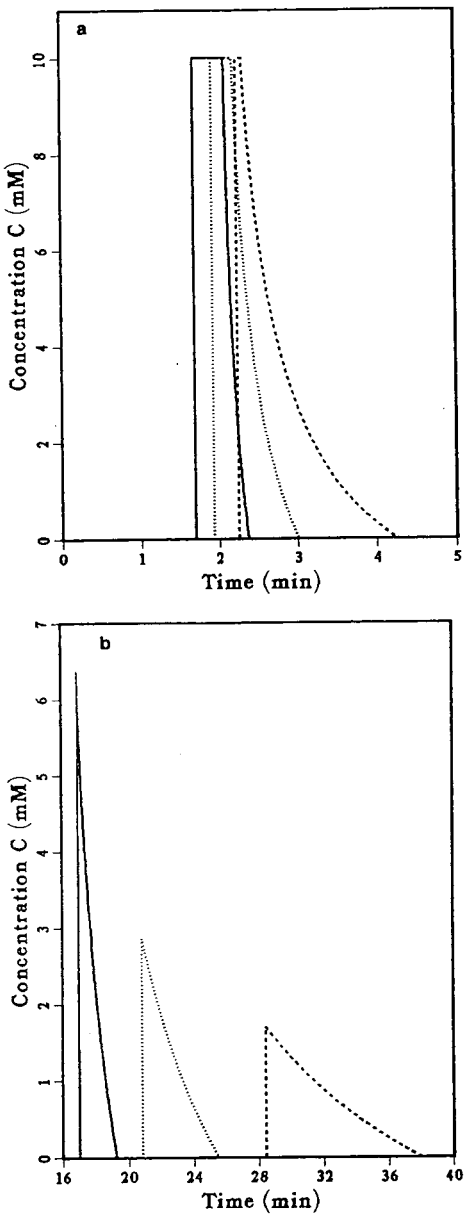

Fig. 2. Positive velocity case. Band profiles at the raffinate outlet. $k'_0 = 0.25$ Solid line, fixed-bed chromatography, $\beta = 0$; dotted line, moving-bed chromatography, $\beta = 1$; dashed line, moving-bed chromatography, $\beta = 2$. Liquid-phase flow velocity, $u = 6.67$ cm/s. Column length: (a) 10 cm; (b) 100 cm.

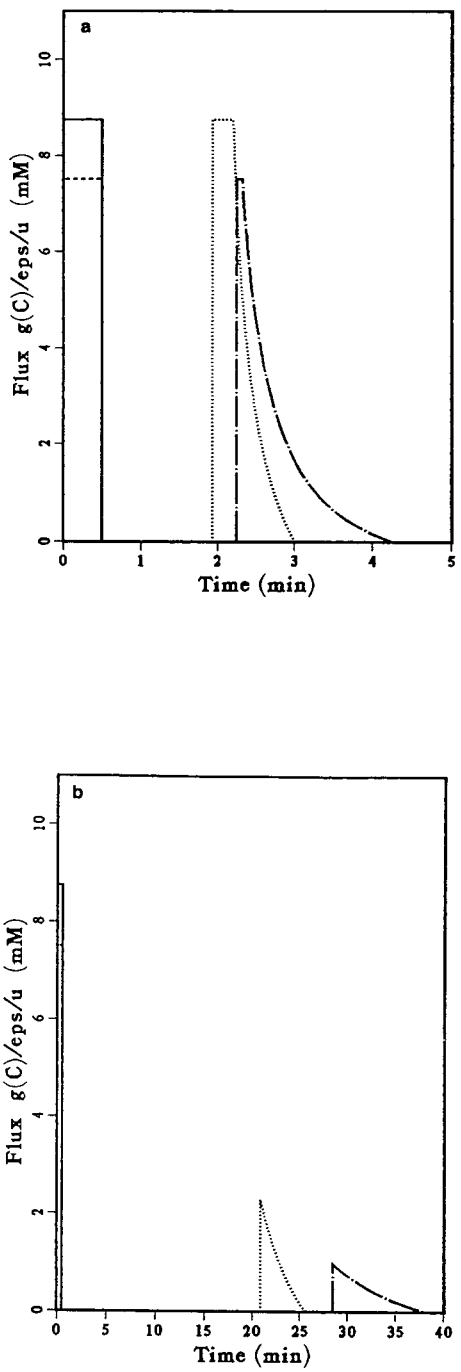

Fig. 3. Positive velocity case. Mass fluxes at the raffinate outlet. Solid line, flux profile at injection or in-flux for $\beta = 1$; dotted line, out-flux profile for $\beta = 1$; dashed line, in-flux profile for $\beta = 2$; chain-dotted line, out-flux profile for $\beta = 2$; liquid-phase flow velocity, $u = 6.67$ cm/s. Column length: (a) 10 cm; (b) 100 cm. eps = ε.

boundary moves faster than the shock, so the injection plateau at C_0 shrinks and eventually disappears. When it disappears, the shock amplitude decreases and so does its velocity (Eq. 7). The shock height is given by Eq. 8 and its position by Eq. 6 as $t_R(C_M)$.

Similar profiles are obtained in countercurrent chromatography, with some significant changes caused by the solid-phase migration.

2.3. General properties of band profiles in countercurrent chromatography

In this section we follow the same approach as in fixed-bed chromatography to derive the equations giving the features of the band profiles during their migration along the column [$C = f(z)$ at $t =$ constant] and those of the elution profiles [$C = f(t)$ at $z = L$ or $z = -L$ according to the band exiting at the raffinate outlet or the extract outlet].

Mass conservation and mass flux

During a classical chromatographic experiment, the concentration of a component is a function of both t and z. There are significant differences in fixed-bed chromatography between elution profiles [i.e., curves $C(t)$ at $z = L$] and concentration profiles along the column or spatial profiles [i.e., curves $C(z)$ at a certain time]. In the latter case, the component in the column is distributed between the two phases and it is the sum of the areas of the liquid- and solid-phase concentration profiles which is conserved. Because of the non-linear behavior of the isotherm and the progressive dilution of the band during its migration, the proportion of the component in each phase at equilibrium varies during elution. The proportion in the solid phase increases during the migration of the band if the isotherm is convex-upward because the average concentration decreases. In the elution profile, however, the entire amount of component is in the liquid phase, so the area of the elution profile is equal to the area of the injection profile. In moving-bed chromatography, by contrast, the history of liquid-phase concentrations at a given point of the column (e.g., at $z = L$) does not have a constant area. Part of the

component moves past the point z with the liquid phase at velocity u, and part with the solid phase at velocity v. The invariant quantity in this case is the integral of the mass flux passing across the column at point z. It must be equal to the total amount injected.

In fixed-bed chromatography, the net mass flux, $g^0(C)$, in any point of the column for a component with a local concentration C is

$$g^0(C) = \varepsilon C u \tag{12}$$

As εu is constant, the mass flux is proportional to the concentration and the area of the liquid-phase concentration profile is proportional to the mass and can represent it.

In a countercurrent moving bed, the solid phase moves in the countercurrent direction and the net flux, $g^\beta(C)$, is

$$g^\beta(C) = \varepsilon C u - (1-\varepsilon) q v = \varepsilon u (C - \beta F q) \tag{13}$$

where $\beta = v/u$ is the ratio of the velocities of the solid and liquid phases in the moving bed column. It is the area of the profile of $g^\beta(C)$ which is constant at any point of the column and, for practical purposes, at $z = 0$ (inlet of the liquid phase and feed in the present case) and at $z = L$ or $z = -L$ (outlets of the liquid phase and component).

Velocity associated with a concentration

In the cases of MB or SMB, Eq. 1 can be rewritten as

$$\frac{\partial C}{\partial t} + u\left(\frac{1-\beta F \cdot \frac{dq}{dC}}{1+F\cdot\frac{dq}{dC}}\right)\frac{\partial C}{\partial z} = 0 \tag{14}$$

This result is very similar to that obtained in elution on a fixed-bed column (Eq. 5), a case in which $\beta = v = 0$. Eq. 14 shows that each concentration propagates in the column at the velocity u_z given by

$$u_z = u\left(\frac{1-\beta F \cdot \frac{dq}{dC}}{1+F\cdot\frac{dq}{dC}}\right) \overset{\text{Langmuir}}{=} u\left[1 - \frac{k_0'(1+\beta)}{(1+bC)^2 + k_0'}\right] \tag{15}$$

Properties similar to those of the elution profiles on a fixed-bed column have been found for the velocity associated with a concentration on a diffuse boundary and for the velocity of the concentration shock in moving-bed chromatography [3,11]. Of special importance, u_z increases with increasing concentration for a convex-upward isotherm. In this case, accordingly, the bands will have a rear diffuse boundary and a front shock, as in the fixed-bed case.

However, in the moving-bed case the velocity associated with a concentration on a diffuse boundary (Eq. 15) may be positive or negative, depending on the sign of $(1 - \beta F\, dq/dC)$. We need to consider separately these two possible cases. In fact, in the most common applications of MB and SMB implementations, the feed will be separated into two fractions on the basis of the sign of the velocities associated with low concentrations of the two pure components. The simplest practical case is the separation of a binary mixture, with one component moving in one direction and the other in the opposite direction.

Shock velocity and mass propagation

When a concentration shock is formed, its velocity is not given by Eq. 15, but by an equation similar to Eq. 7 and derived in the same manner:

$$U_s = u\left(\frac{1-\beta F\cdot\frac{\Delta q}{\Delta C}}{1+F\cdot\frac{\Delta q}{\Delta C}}\right) \overset{\text{Langmuir}}{=} u\left[1 - \frac{k_0'(1+\beta)}{(1+bC)+k_0'}\right] \tag{16}$$

where $\Delta q/\Delta C$ is the slope of the isotherm chord (Fig. 1). Comparison between Eqs. 15 and 16 shows that for a given concentration C, u_z will be larger than U_s in the case of a convex-upward isotherm, as it is in fixed-bed chromatography. Hence the concentration plateau obtained in the case of a rectangular pulse injection (boundary conditions 4b and 4c) shrinks and disappears, leaving a concentration shock of decreasing amplitude which moves at a decreasing velocity.

In fixed-bed chromatography, the migration

velocity of a slice of thickness dz of the profile of a retained component is given by

$$V^0 = \frac{\text{net flux}}{\text{total mass}} = \frac{\varepsilon C u}{\varepsilon C + (1-\varepsilon)q} = \frac{u}{1+\frac{Fq}{C}} \overset{\text{Langmuir}}{=} \frac{u}{1+\frac{k'_0}{1+bC}} \quad (17)$$

Thus, as explained and illustrated elsewhere (Ref. [5], pp. 227–228), the mass of component contained in a slice of column of thickness dz where the concentration is C migrates at the velocity of the shock, U_s (Eq. 16), while the concentration C moves at the velocity u_z. Similarly, in moving-bed chromatography, the migration velocity of a slice of thickness dz of the profile of a retained component is

$$V^\beta = \frac{\text{net flux}}{\text{total mass}} = \frac{\varepsilon C u - (1-\varepsilon)qv}{\varepsilon C + (1-\varepsilon)q} \overset{\text{Langmuir}}{=} u\left(\frac{1-\frac{\beta k'_0}{1+bC}}{1+\frac{k'_0}{1+bC}}\right) \quad (18)$$

In moving-bed chromatography also the mass contained in a column slice of thickness dz propagates at the shock velocity, while concentrations propagate at the faster velocity u_z. However, whereas in fixed-bed chromatography V^0 is always positive and a retained component always moves forward, in moving-bed chromatography, by contrast, the mass velocity, V^β, is proportional to $(1-\beta Fq/C)$ which depends on the velocity ratio, β, and on the local solid- and liquid-phase concentrations, q and C. V^β may be positive, negative or zero.

2.4. Equations for the band profile in the different possible cases

The injection profile is described by Eqs. 4b and 4c. It includes two concentration shocks. The first, at the injection front, enters the column at time $t = 0$; the second, at the injection rear, enters the column at time $t = t_p$. Between these two shocks, there is a concentration plateau at $C = C_0$ with a width t_p. Because the band may change direction of propagation when the shock amplitude decreases (see later), we need to clarify the concepts of the front and rear of the band. We define the band front as the part of the profile which arises from the front shock of the injection pulse, that which enters the column first; the band rear is the part of the profile arising from the rear shock of the rectangular injection front. Owing to the complexity of countercurrent chromatography, the front so defined may be eluted last, which should not be surprising as it may leave the column through the extract exit.

The solution requires now that we distinguish several possibilities, depending on the sign of the velocities associated with the concentration shocks and with the concentration $C = 0$. If the shock velocity is positive, it begins its migration in the direction of the liquid phase. If it is negative, it migrates in the direction of the solid phase. However, if the shock velocity is positive, the velocity of the concentration $C = 0$ can be positive or negative. In the former case, the entire band will eventually elute with the liquid phase. In the latter case, the shock, which migrates in the direction of the liquid phase but erodes progressively and slows, may or may not reach the liquid phase exit. We discuss all these cases in detail.

First case: all concentration velocities are positive, $\beta k'_0 < 1$

In this case, all the concentrations migrate in the direction of the liquid phase. Since for a convex-upward isotherm, dq/dC decreases with increasing concentration, C, the associated velocity (Eq. 15) increases with increasing concentration. Because high concentrations move faster than lower concentrations but cannot pass them, the front shock is stable and will propagate along the column. In contrast, the rear shock is unstable, collapses in a flight of characteristics and spreads continuously [7,10,11].

Since the rear shock becomes a diffuse boundary, each concentration C moves at the velocity given by Eq. 15. The retention time of concentration C at the column outlet is

$$t_R^\beta(C) = t_p + \frac{L}{u_z} = t_p + t_0\left(\frac{1 + F\cdot\frac{dq}{dC}}{1 - \beta F\cdot\frac{dq}{dC}}\right)$$

$$\overset{\text{Langmuir}}{=} t_p + t_0\left[1 + \frac{(1+\beta)k_0'}{(1+bC)^2 - \beta k_0'}\right] \qquad (19a)$$

where t_p results from the injection duration and the fact that the rear diffuse boundary results from the collapse of the rear shock of the injection profile. Since dq/dC decreases with increasing concentration, $t_R^\beta(C)$ also decreases with increasing C. Eq. 19 shows that $t_R^\beta(C)$ increases with increasing β, corresponding to an increase in the effective column length seen by the band which moves against the direction of the solid phase.

The profile ends at the elution time of the concentration $C = 0$:

$$t_R^\beta(0) = t_p + t_0\cdot\frac{1 + k_0'}{1 - \beta k_0'} \qquad (19b)$$

with $k_0' = F[dq/dC]_0$, where $[dq/dC]_0$ is the initial slope of the isotherm.

The front shock of the injection pulse moves at the constant velocity $U_s(C_0)$ as long as the injection plateau is not eroded away (see below). If the injection plateau still exits, the retention time of the shock at the raffinate exit $z = L$ is

$$t_s^\beta(C_0) = \frac{L}{U_s(C_0)} = t_0\left(\frac{1 + F\cdot\frac{\Delta q}{\Delta C}}{1 - \beta F\cdot\frac{\Delta q}{\Delta C}}\right)$$

$$\overset{\text{Langmuir}}{=} t_0\left[1 + \frac{(1+\beta)k_0'}{(1+bC_0) - \beta k_0'}\right] \qquad (20)$$

where $t_0 = L/u$ is the holdup time and $\Delta q/\Delta C = [q(C_0) - q(0)]/C_0$ is the slope of the isotherm chord, as illustrated by the dotted line in Fig. 1 (in the case of the Langmuir isotherm).

Since the rear of the band profile is a diffuse boundary whereas its front is a shock, the two ends of the injection plateau propagate at different velocities. The velocity of the front shock is given by Eq. 16 and its retention time is given by Eq. 20. All concentrations on the rear diffuse boundary move at velocities given by Eq. 15, and their retention times are given by Eq. 19. The point at the rear of the plateau is the highest point of the rear diffuse boundary, with a retention time $t_R^\beta(C_0)$ derived from Eq. 19 with $C = C_0$. For the convex-upward isotherm considered here (see Fig. 1), $dq/dC(C_0) < \Delta q(C_0)/\Delta C = [q(C_0) - q(0)]/C_0$ and $u_z(C_0) > U_s(C_0)$. Hence the velocity of the point of the diffuse profile at $C = C_0$ is larger than the shock velocity. The plateau becomes narrower, shrinks and eventually disappears if the column is long enough. Then, the rear diffuse boundary captures the front, the shock erodes, its height decreases and it slows (see Eq. 16). The tip of the band profile belongs both to the front shock and to the rear diffuse boundary. u_z is larger than U_s for any given value of C. As a consequence, the point at the tip of the shock disappears constantly and the shock keeps becoming shorter and moving more slowly. Therefore, after the concentration plateau at $C = C_0$ has disappeared, Eq. 16 can no longer be used to calculate the retention time of the shock.

This time is easily derived by observing that the total mass in the column must be conserved and that, accordingly, the area of the mass flux at the raffinate end (in the present case) of the column, $z = L$, must be equal to the area of the injection profile [16]. We can calculate the net mass of component leaving the column by integrating the net mass flux profile of the component (Eq. 13) from $C = 0$ to $C = C_M$, where C_M is the maximum concentration of the profile. This gives

$$M^{out} = \int_0^{C_M} [t_R^\beta(C) - t_R^\beta(C_M)]\, dg^\beta(C)$$

$$= t_0\varepsilon u\left\{[C + Fq(C)]\Big|_0^{C_M} - \left(\frac{1 + F\cdot\frac{\Delta q}{\Delta C}}{1 - \beta F\cdot\frac{\Delta q}{\Delta C}}\right) g^\beta(C)\Big|_0^{C_M}\right\} \qquad (21a)$$

The mass flux entering the column is given by the equation

$$M^{in} = \int_0^{C_0} t_p \, dg^\beta(C) = t_p g^\beta(C)|_0^{C_0} \quad (21b)$$

Writing that these two masses are equal gives

$$t_p[C - \beta F q(C)]|_0^{C_0} = t_0 \left\{ [C + Fq(C)]|_0^{C_M} - \frac{1 + F \cdot \frac{dq(C_M)}{dC}}{1 - \beta F \cdot \frac{dq(C_M)}{dC}} [C - \beta F q(C)]|_0^{C_M} \right\} \quad (21c)$$

C_M is obtained as the root of this algebraic equation. Once it is known, its retention time is derived from Eq. 19 as $t_R^\beta(C_M)$.

The above derivations apply to any isotherm, with the only condition that it has no inflection point. In the case of the Langmuir isotherm (Eq. 21c), C_M can be solved in closed form and the maximum concentration of the band is

$$C_M = \frac{L_f^\beta + \sqrt{L_f^\beta (1 + (L_f^\beta - 1)\beta k_0')}}{b(1 - L_f^\beta)} \quad (22)$$

The retention time of the maximum concentration of the band when the injection plateau has been eroded away is given by

$$t_R^\beta(C_M) = t_p + t_0 + t_0(1+\beta)k_0' \times \frac{(1 - L_f^\beta)^2}{L_f^\beta(1 + \beta k_0') + 1 - \beta k_0' + 2\sqrt{L_f^\beta(1 + L_f^\beta \beta k_0' - \beta k_0')}} \quad (23)$$

where L_f^β is the loading factor, or ratio of the sample size and the column saturation capacity:

$$L_f^\beta = \frac{\left(1 - \frac{\beta k_0'}{1 + bC_0}\right) t_p C_0 b}{t_0 k_0'(1 + \beta)} \quad (24)$$

The loading factor is lower in moving-bed chromatography than with a fixed bed of the same length because moving the solid phase backwards effectively increases the length of the column bed along which a component must migrate before eluting out of the column.

Obviously, the solution of the moving-bed problem in the case in which the concentration velocities are all positive is very similar to the solution of fixed-bed chromatography. A comparison of the relevant equations shows that the equations giving the band profile in moving-bed chromatography tend toward those derived for fixed-bed chromatography when the velocity of the solid phase tends toward 0 (see Table 1). A discussion of this comparison follows. It is convenient for the purpose of this discussion to report the retention time of the shock and the elution times of concentrations with respect to those observed under fixed-bed conditions. These expressions can be written explicitly in the case of Langmuir isotherm.

Retention times in fixed-bed and moving-bed chromatography. Assuming that all the experimental conditions are the same for the moving and the fixed beds, except for the movement of the solid phase in the former case, the retention times of a shock of amplitude C and of a concentration C become

$$\tau_s^\beta(C) = \frac{t_s^\beta(C) - t_s^0(C)}{t_s^0(C)} = \frac{1}{\frac{1}{\beta F \cdot \frac{\Delta q}{\Delta C}} - 1} \overset{\text{Langmuir}}{=} \frac{1}{\frac{1 + bC}{\beta k_0'} - 1} \quad (25a)$$

$$\tau_R^\beta(C) = \frac{t_R^\beta(C) - t_R^0(C)}{t_R^0(C)} = \frac{1}{\frac{1}{\beta F \cdot \frac{dq}{dC}} - 1} \overset{\text{Langmuir}}{=} \frac{1}{\frac{(1 + bC)^2}{\beta k_0'} - 1} \quad (25b)$$

where $\tau_s^\beta(C)$ and $\tau_R^\beta(C)$ are the relative differences of the retention times of the front shock of amplitude C and of a concentration C, respectively, between moving-bed and fixed-bed columns. Since in the present case $\beta k_0' < 1$ and $d^2q/dC^2 < 0$ (convex-upward isotherm), we have always $\beta F \, dq/dC < 1$ and, as a consequence, τ_s^β and τ_R^β are positive. They increase with increas-

Table 1

Moving-bed chromatography	Fixed-bed chromatography
General isotherm model, $q = f(C)$	
$t_R^\beta(C) = t_p + t_0\left(\frac{1 + F\cdot\frac{dq}{dC}}{1 - \beta F\cdot\frac{dq}{dC}}\right)$	$t_R^0(C) = t_p + t_0\left(1 + F\cdot\frac{dq}{dC}\right)$
$t_s^\beta(C_0) = t_0\left(\frac{C_0 + Fq_0}{C_0 - \beta Fq_0}\right)$	$t_s^0(C_0) = t_0\left(1 + F\cdot\frac{q_0}{C_0}\right)$
$t_p[C - \beta Fq(C)]]_0^{C_0} = t_0\left\{[C + Fq(C)]]_0^{C_M} - \frac{1 + F\cdot\frac{dq(C_M)}{dC}}{1 - \beta F\cdot\frac{dq}{dC}(C_M)}[C - \beta Fq(C)]]_0^{C_M}\right\}$	$\left\lvert q - C\cdot\frac{dq}{dC}\right\rvert = \frac{n}{F_v t_0 F}$
Case of the Langmuir isotherm, $q = aC/(1 + bC)$	
$t_R^\beta(C) = t_p + t_0\left[1 + \frac{(1+\beta)k_0'}{(1+bC)^2 - \beta k_0'}\right]$	$t_R^0(C) = t_p + t_0\left[1 + \frac{k_0'}{(1+bC)^2}\right]$
$t_s^\beta(C_0) = t_0\left[1 + \frac{(1+\beta)k_0'}{(1+bC_0) - \beta k_0'}\right]$	$t_s^0(C_0) = t_0\left(1 + \frac{k_0'}{1+bC_0}\right)$
$t_R^\beta(C_M) = t_p + t_0 + t_0(1+\beta)k_0'\cdot\frac{(1 - L_f^\beta)^2}{L_f^\beta(1+\beta k_0') + 1 - \beta k_0' + 2\sqrt{L_f^\beta(1 + L_f^\beta\beta k_0' - \beta k_0')}}$	$t_R^0(C_M) = t_p + t_0 + k_0' t_0(1 - \sqrt{L_f})^2$
$L_f^\beta = \frac{\left(1 - \frac{\beta k_0'}{1+bC_0}\right)t_p C_0 b}{t_0 k_0'(1+\beta)}$	$L_f^0 = \frac{nb}{\varepsilon S L k_0'} = \frac{t_p C_0 b}{t_0 k_0'}$

ing β and with decreasing concentration of the component in the liquid phase.

This result is expected. The migration of the solid phase in the direction opposite to the liquid-phase stream and to the direction in which the lesser retained bands migrate increases the apparent column length and the actual migration distance of a band in the column. The larger is β, the longer are the retention times. This effect is illustrated in Fig. 2a and b, which show the band profiles obtained at the end of a short (Fig. 2a, $L = 10$ cm) and a long column (Fig. 2b, $L = 100$ cm), for the same rectangular injection ($C_0 = 10$ mM) and the same velocity of the solid phase. The injection pulse width has been chosen so that the band elutes from the short column before the injection plateau has been eroded away.

Erosion of the injection plateau between the shock and the diffuse boundary. The width of the injection plateau decreases continuously because the highest point on the diffuse boundary moves faster than the shock. The width of this plateau is given by

$$t_R^0(C_0) - t_s^0(C_0) = t_p + t_0\left[\frac{dq}{dC}(C_0) - \frac{\Delta q}{\Delta C}\right] \quad (26a)$$

in the fixed-bed case. In the moving-bed case, it is

$$t_R^\beta(C_0) - t_s^\beta(C_0) = t_p + t_0 \times \left\{\frac{(1+\beta)F\left[\frac{dq}{dC}(C_0) - \frac{\Delta q}{\Delta C}\right]}{\left[1 - \beta F\cdot\frac{dq}{dC}(C_0)\right]\left(1 - \beta F\cdot\frac{\Delta q}{\Delta C}\right)}\right\} \quad (26b)$$

As $\beta\, dq/dC < 1$ and $dq/dC(C_0) < \Delta q/\Delta C(C_0)$, we have

$$t_R^\beta(C_0) - t_s^\beta(C_0) < t_R^0(C_0) - t_s^0(C_0) \quad (26c)$$

The width of the residual injection plateau at the top of the band profile is smaller in the moving-

bed case than in the corresponding fixed-bed case. This is clearly illustrated by the chromatograms calculated in Fig. 2a.

Profile of the diffuse boundary. Both τ_R^β and t_R^0 decrease with increasing liquid phase concentration; so also does $t_R^\beta(C) - t_R^0(C)$, and

$$t_R^\beta(C_0) - t_R^0(C_0) \leq t_R^\beta(C) - t_R^0(C) \leq t_R^\beta(0) - t_R^0(0) \quad (27)$$

This means that the retention time of a given concentration, which increases with decreasing concentration, increases faster in moving-bed than in fixed-bed chromatography. The band width or distance between the band front or shock and its point at any concentration C is larger under moving-bed than under fixed-bed conditions. In other words, the rear diffuse boundary is more diffuse for the moving-bed than for the fixed-bed column and its width increases with increasing β or solid-phase velocity. This effect is illustrated in Fig. 2a and b.

As a consequence, the elution bands are more dilute in moving-bed than in fixed-bed chromatography. This conclusion has no direct consequence, however, on the concentration of the fractions collected in the conventional applications of the method.

Band profile area. In fixed-bed chromatography, the area of the elution band profile represents the mass leaving the column, as explained previously. Because the component mass in the column must be conserved, this area must remain constant and equal to the area of the injection profile. This property is used to determine the maximum concentration of the band, once the injection plateau has been eroded away (see Theory). Inside the column, however neither the area of the liquid-phase nor that of the solid-phase concentration profile remains constant. It is the total concentration ($C + Fq$) profile area that remains constant, whether in fixed-bed or in moving-bed chromatography. This is due to the non-linear behavior of the isotherm which causes a variable proportion of the component to be in each phase at equilibrium.

It is interesting to calculate the area of the liquid-phase concentration profile at the column exit and compare it with the injection area. The area of a rectangular injection pulse is

$$S^{in} = t_p C_0 \quad (28a)$$

The band area at the outlet of column in fixed-bed chromatography is

$$S^{out} = \int_0^{C_0} [t_R^0(C) - t_s^0(C_0)]\,dC = t_p C_0 + t_0 F \int_0^{C_0} \left(\frac{dq}{dC} - \frac{\Delta q}{\Delta C}\right) dC = S^{in} \quad (28b)$$

This result is obtained because $dq|_0^{C_0} = (\Delta q/\Delta C)\Delta C$. This demonstration is general, independent of the isotherm properties, whether convex upward or downward. It results from the fact that the profile is a solution of the mass balance equation and that only the liquid phase leaves the column.

In moving-bed chromatography, the area of the elution profile of the liquid-phase concentration band is

$$S^{out} = \int_0^{C_0} [t_R^0(C) - t_s^0(C_0)]\,dC = t_p C_0 + t_0 F \int_0^{C_0} \left\{ \frac{(1+\beta)\left[\frac{dq(C)}{dC} - \frac{\Delta q}{\Delta C}\right]}{\left[1 - \beta F \cdot \frac{dq(C)}{dC}\right]\left(1 - \beta F \cdot \frac{\Delta q}{\Delta C}\right)} \right\} dC \quad (29a)$$

We have no solution for Eq. 29. However, in the case of the Langmuir isotherm, it simplifies to

$$S^{out} - S^{in} = t_0(1+\beta)k_0' \left\{ \frac{1}{2b\gamma} \ln\left[\frac{(1 + bC_M - \gamma)(1+\gamma)}{(1 + bC_M + \gamma)(1-\gamma)} - \frac{C_M}{(1 + bC_M) - \gamma^2} \right] \right\} > 0 \quad (29b)$$

with $\gamma = \sqrt{\beta k_0'}$. The right-hand side of Eq. 29b is always positive for the case studied here, since it

is equal to 0 when $C_M = 0$ and its first differential with respect to C_M is positive. Thus, the area of the band profile of the liquid-phase concentration is not conserved but is larger at the column outlet than at injection. It increases with increasing β. This reflects the fact that the concentration of the component in the solid phase that enters the column (and is in equilibrium with the exiting liquid phase) is finite and that this phase and the liquid phase move in opposite directions. Hence part of the amount eluted in the liquid phase returns into the column with the solid phase.

As an example, while the areas of the injection profiles of the short and long columns in Fig. 2a and b are identical (dotted line, $\beta = 1$), the areas of the profiles of the liquid-phase concentration obtained at the outlet of each of these two columns are 1.032 (Fig. 2a) and 1.16 (Fig. 2b), respectively, larger for moving-bed than for fixed-bed operation. The problem of the mass conservation is easily solved by considering the local mass flux.

Mass flux and mass conservation. Based on the net mass flux of component given in Eq. 13, we can calculate the masses injected into the column and leaving the column in the case in which a residual injection plateau is included in the elution profile

$$M^{in} = \int_0^{C_0} t_p \, dg^{\alpha}(C) = t_p g^{\alpha}(C)|_0^{C_0} \tag{30a}$$

$$M^{out} = \int_0^{C_0} [t_R^{\alpha}(C) - t_s^{\alpha}(C_0)] \, dg^{\alpha}(C) \tag{30b}$$

$$= \int_0^{C_0} \left[t_p + t_0 \left(\frac{1 + F \cdot \frac{dq}{dC}}{1 - \alpha F \cdot \frac{dq}{dC}} \right) - t_0 \left(\frac{1 + F \cdot \frac{\Delta q}{\Delta C}}{1 - \alpha F \cdot \frac{\Delta q}{\Delta C}} \right) \right] dg^{\alpha}(C)$$

$$= t_p g^{\alpha}(C)|_0^{C_0} + t_0 \varepsilon u \left\{ [C + Fq(C)]|_0^{C_0} - \left(\frac{1 + F \cdot \frac{\Delta q}{\Delta C}}{1 - \alpha F \cdot \frac{\Delta q}{\Delta C}} \right) g^{\alpha}(C)|_0^{C_0} \right\}$$

$$= t_p g^{\alpha}(C)|_0^{C_0} = M^{in} \tag{30c}$$

Mass is indeed conserved, which is expected in the case of the exact solution of a mass balance equation. A similar calculation was used to determine the maximum concentration of the band, and hence its retention time when the shock has been captured by the diffuse boundary, assuming conservation of the net mass flux (Eq. 21). However, it was important to illustrate the difference between fixed-bed and moving-bed problems and to emphasize that, since the solid phase moves in and out the column as well as along it and carries a fraction of the retained component, its contribution to the solute mass flux must be taken into account in the latter case.

Fig. 3 illustrates the time profiles of the in-flux and out-flux for (a) the short and (b) the long column, with the rectangular profiles showing the injection or in-flux profiles and the curved lines showing the out-flux in the case for which $\beta = 1$ (dashed line) and $\beta = 2$ (chain-dotted line). The areas of the in-flux and out-flux profiles are now the same, but note that, although the concentration profiles at injection are the same for the two values of β, the in-flux profiles are different (see Eq. 13).

Second case: the limit velocity is zero, $\beta k_0' = 1$

As in the previous case, any finite concentration migrates at a positive velocity, i.e., in the direction of the liquid phase, but the limit velocity, or velocity associated with the concentration $C = 0$, is zero. This case differs from the first case, in which even the limit velocity is strictly positive (i.e., different from zero). Now the end of the band ($C = 0$) does not move at all, as illustrated in Fig. 4a, which shows concentration profiles along the column. All these

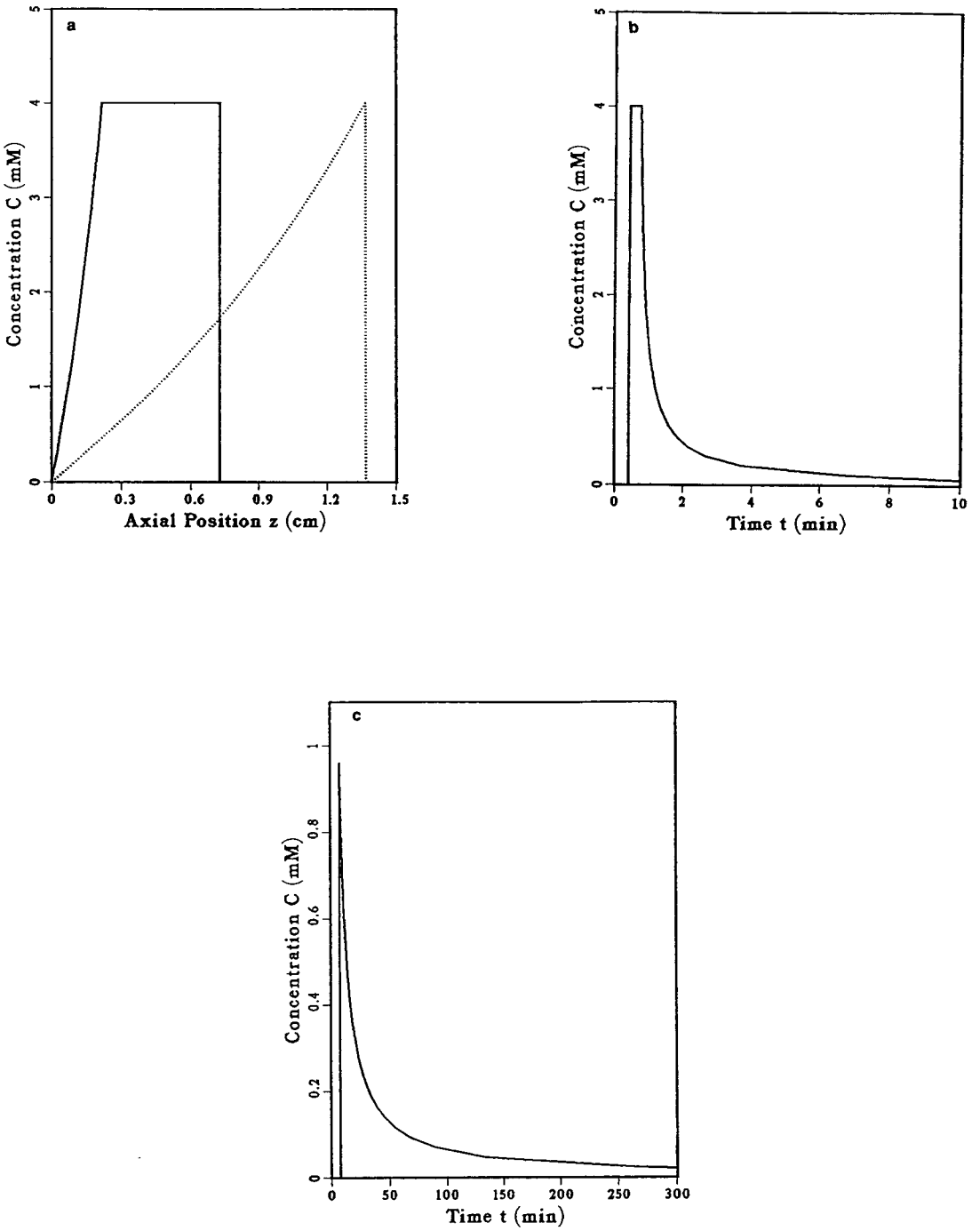

Fig. 4. Non-negative velocity case: $\beta = 4$, $C_0 = 4$ mM. Liquid-phase flow velocity, $u = 5$ cm/s; short column, $L = 0.5$ cm; long column, $L = 5$ cm; middle column, $L = 1.5$ cm, which is just shorter than the characteristic length L^*; two characteristic concentrations $C_1 = 5$ mM and $C_2 = 12.5$ mM. (a) Axial band profiles along the column at two different times: solid line, $t = 0.6$ s; dotted line, $t = 1.13$ s. (b) Temporal band profiles at the raffinate outlet ($z = L$), short column. (c) Same as (b) but long column.

profiles go through the origin. Accordingly, the end of the band, the concentration $C = 0$ will never exit from the column. The profile will tail indefinitely, an exceptional situation with the ideal model and its hyperbolic mass balance equation. The elution profile in the liquid phase is illustrated in Fig. 4b. All the other features of the band profiles are given by the same equations as in the previous case.

Third case: the limit velocity is negative, $\beta k'_0 > 1$

In this case, the retention of the component injected and/or the solid-phase velocity are high. Accordingly, the velocities associated with low concentrations are negative. However, because virtually all solid phases have a saturation capacity, equilibrium isotherms have a horizontal asymptote and dq/dC tends toward zero when C increases indefinitely. Hence there is always, at least in principle, a value of the injection concentration, C_0, which is high enough for the velocity associated with the high concentrations of the diffuse boundary and/or for the front shock of the rectangular injection pulse to have a positive velocity. Accordingly, we must distinguish several cases, depending on the signs of these velocities (see Fig. 5). Let C_1 be the concentration for which $u_z(C_1) = 0$ and C_2 the concentration for which $U_s(C_2) = 0$. C_1 is smaller than C_2 since the isotherm is convex upward and $U_s(C) < u_z(C)$ for all values of C, as illustrated in Fig. 5.

From Eqs. 15 and 16, we derive the equations giving C_1 and C_2:

$$\frac{dq}{dC}(C_1) = \frac{1}{\beta F} \tag{31a}$$

$$\frac{\Delta q}{\Delta C}(C_2) = \frac{1}{\beta F} \tag{31b}$$

For the Langmuir isotherm, these equations can be solved in closed form:

$$C_1 = \frac{1}{b}(\sqrt{\beta k'_0} - 1) \tag{31c}$$

$$C_2 = \frac{1}{b}(\beta k'_0 - 1) \tag{31d}$$

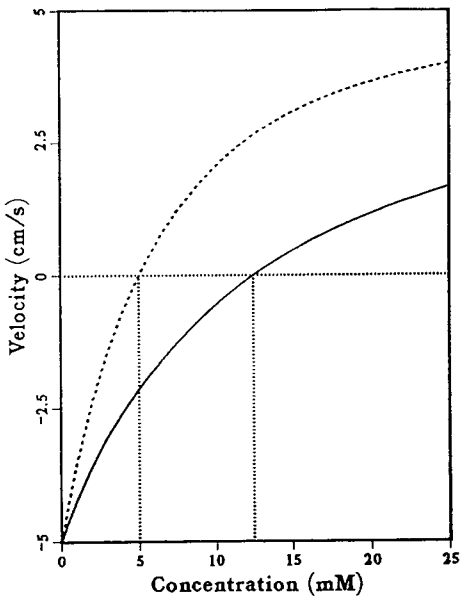

Fig. 5. Definition of the concentrations C_1 and C_2. Solid line, shock velocity, $U_s(C)$; dashed line, velocity associated with a concentration, $u_z(C)$. Experimental conditions as in Fig. 4.

and $C_1 < C_2$. In the figures, $\beta = 9$, $k'_0 = 0.25$, $b = 0.1$ mM^{-1}, so $C_1 = 5$ mM and $C_2 = 12.5$ mM. Note that $\beta = 9$ would probably be an unrealistically high value in many applications but this choice permits informative illustrations of the profiles obtained.

As illustrated in Fig. 5, there are three different cases:

(i) $C_0 < C_1$. The velocities associated with any possible concentrations of the band profiles are negative, $u_z(C) < 0$, $U_s(C) < 0$, $\forall C$. The band migrates in the direction of the solid phase and the component is entirely eluted as an extract [17].

(ii) $C_1 < C_0 < C_2$. The front shock of the rectangular injection pulse has a negative velocity, i.e., moves in the direction of the solid phase. However, the velocities associated with the high concentrations of the band profile ($C_1 < C < C_0$) during injection and immediately after are positive and these concentrations tend to move in the direction of the liquid phase. Concentrations lower than C_1 have a negative associ-

ated velocity and move in the direction of the solid phase.

(iii) $C_2 < C_0$. The concentration of the rectangular pulse injection is high, the front shock of the injection band moves in the direction of the liquid phase and the shock keeps moving in this direction after the front shock has been captured by the rear, diffuse boundary, as long as $C_2 < C_M$. On a diffuse boundary, the high concentrations $C > C_1$ move in the direction of the liquid phase and the low concentrations in the direction of the solid phase.

The first case is simple, the whole band moves in the direction of the solid phase and exits with it through the column entrance, as an extract. The other two cases are more complex. The band will begin moving in the direction of the liquid phase and part of it may reach the exit and elute as a raffinate if the column is short enough. However, because chromatography involves dilution, the band will eventually turn around if the column is long, start moving in the direction of the solid phase, and elute through the column entrance, as an extract.

$C_0 < C_1$, *all velocities are negative.* As all velocities are negative, all concentrations move backwards, in the direction of the solid phase, towards the extract exit. However, as the velocity associated with a concentration increases with increasing concentration, the lower concentrations have the larger backward velocity in absolute value. As a consequence, the low concentrations move backward faster than the high concentrations and the front shock of the rectangular injection pulse is unstable. It collapses into a front diffuse boundary. In contrast and for the same reason, the rear shock of the injection pulse is stable and it propagates as a rear shock.

Accordingly, the retention time of a concentration on the front diffuse boundary is given by the following equation:

$$t_R^\beta(C) = \frac{-L}{u_z} = t_0\left(\frac{F\cdot\frac{dq}{dC}+1}{\beta F\cdot\frac{dq}{dC}-1}\right) \overset{\text{Langmuir}}{=} -t_0\left[1+\frac{(1+\beta)k_0'}{(1+bC)^2-\beta k_0'}\right] \quad (32)$$

The equation differs slightly from Eq. 19, by the lack of the term t_p. This comes from the origin of the diffuse boundary, the collapse of the front shock of the injection. The concentration $C = 0$ exits first, with a retention time

$$t_R^\beta(0) = t_0\cdot\frac{1+k_0'}{\beta k_0'-1} \quad (32b)$$

If part of the injection plateau remains at the time of elution, the end of the band is eluted at time

$$t_s^\beta(C_0) = t_p + \frac{-L}{U_s} = t_p + t_0\left(\frac{F\cdot\frac{\Delta q}{\Delta C}+1}{\beta F\cdot\frac{\Delta q}{\Delta C}-1}\right) \overset{\text{Langmuir}}{=} t_p - t_0\left[1+\frac{(1+\beta)k_0'}{(1+bC_0)-\beta k_0'}\right] \quad (33a)$$

If the rear shock has been captured by the front diffuse boundary, the maximum concentration of the band, C_M, is given by the same mass balance equation (Eq. 21). In the case of a Langmuir isotherm (Eq. 22), the retention time of the shock can be solved in closed form and becomes

$$t_R^\beta(C_M) = -t_0 - t_0(1+\beta)k_0' \times \frac{(1-L_f^\beta)^2}{L_f^\beta(1+\beta k_0')+1-\beta k_0'+2\sqrt{L_f^\beta(1+L_f^\beta\beta k_0'-\beta k_0')}} \quad (33b)$$

Note that in this case, the loading factor, L_f^β, has a negative value since the column length is negative in this direction.

In fact, the solution of the problem in this case is the exact opposite of the solution obtained in the case of a positive velocity, studied in the previous section, the roles of the front and rear shocks of the rectangular injection pulse being exchanged. Accordingly, the parameter t_p, the width of the rectangular injection pulse, appears in those equations of the present solution (negative velocities) whereas it does not in the equations of the other solution (positive velocities), and conversely.

Fig. 6a illustrates the concentration profiles of the band along the column at two different times after the injection. Fig. 6b shows the elution

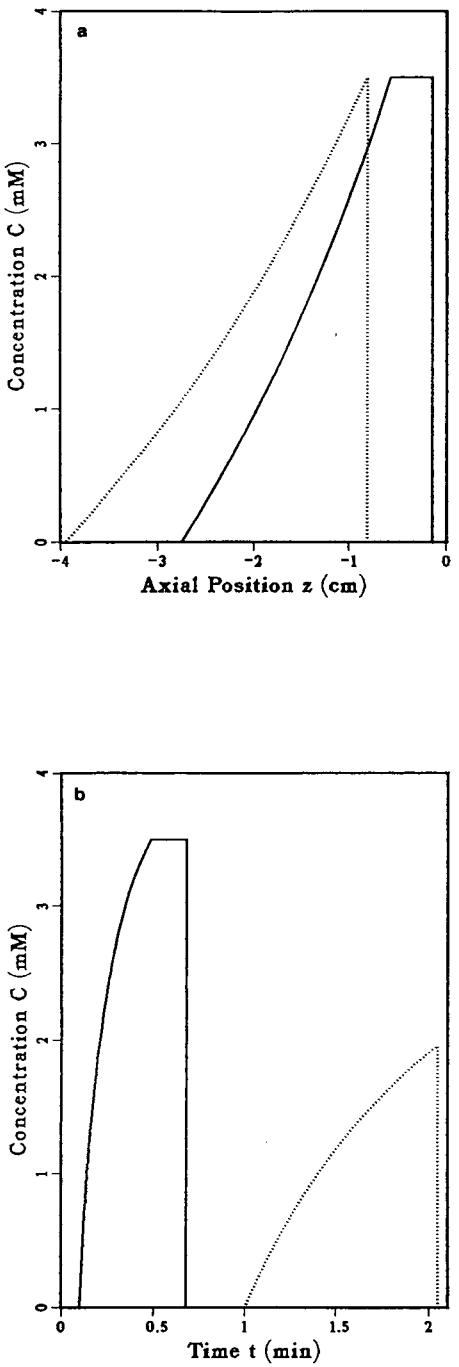

Fig. 6. Negative velocity case: $C_0 < C_1$, $\beta = 9$, $C_0 = 3.5$ mM. Experimental conditions as in Fig. 4. (a) Axial band profiles the column at two different times: solid line, $t = 0.55$ s; dotted line, $t = 0.67$ s. (b) Temporal band profiles at the extract outlet ($z = -L$): solid line, short column; dotted line, long column.

band profiles at the extract exit of a short (solid line) and a long column (dotted line). The former band profile exhibits a residual plateau at the injection concentration and the retention time of the rear shock is given by Eq. 33a. The latter profile is shorter and its maximum concentration is given by Eq. 21 or 33b.

$C_0 = C_1$, *the velocity associated with the concentration* C_0 *is zero*. This is a transition case. When the injection concentration C_0 is equal to C_1, $u_z(C_0) = u_z(C_1) = 0$. Hence the maximum concentration of a diffuse boundary does not move. The front shock of the injection pulse is unstable and a front diffuse boundary is formed as in the previous case. The retention time of a concentration C on this boundary is given by Eq. 32. The top point of this boundary, however, has a velocity equal to zero and it stays at the origin. Fig. 7a shows the concentration profile along the column at three successive times, corresponding to the injection still in progress, the end of the injection and some time afterward. The rear shock cannot move forward as its velocity is negative $[U_s(C) < u_z(C)]$. It cannot move backwards, however, because it is kept at the origin by the injection as long as it is in progress. In this case, there is no injection plateau. However long the injection or short the column, this plateau is reduced to a single point.

When the injection is finished, the rear of the band is a stable shock which has a negative velocity. The front diffuse boundary of the band and its rear shock have the same maximum concentration, C_0. At this concentration, $U_s(C_0) < u_z(C_0)$ and the velocity of the rear shock is lower than the velocity associated with the band maximum. As these velocities are negative, the shock starts moving backwards as soon as the feed injection ends. It moves backwards faster than the top of the diffuse boundary. Hence the tip of the shock (and the top of the band) is eroded progressively and the height of the concentration point at $z = 0$ begins to decrease. Since C_M becomes lower than $C_0 = C_1$, the velocity associated with C_M becomes negative and the band rear shock begins to move backward (Fig. 7a, third profile). The elution profiles are illustrated in Fig. 7b for two different

column lengths. These profiles are characterized by the lack of a plateau at the injection concentration, whatever the width or duration of the injection. Since the injection plateau has been eroded away, the maximum concentration of the band, C_M, is given by Eq. 21 in the general case or Eq. 22 for a Langmuir isotherm.

$C_1 \leq C_0 \leq C_2$, the velocity of the shock is negative, the velocity associated with C_0 is positive. When the injection concentration, C_0, is between C_1 and C_2, the velocity associated with the high concentrations on the diffuse boundary, $u_z(C)$, is positive whereas the velocity associated with the low concentrations is negative. For the intermediate concentration C_1, $u_z(C_1) = 0$. However, the shock velocity, $U_s(C)$ is always negative. This results in a more complex situation than previously encountered.

The rectangular pulse injected into the column begins with a front shock rising from 0 to C_0. This shock cannot move. If it moves backwards, it is unstable and collapses into a diffuse boundary whose highest concentration, C_0, has a positive velocity, and hence should move forward. However, if the concentration C_0 moves forwards it becomes the head of a stable front shock, a shock whose velocity is negative, so this shock should move backwards. Thus, it is physically impossible for the shock to move either forwards or backwards. As in the previous case, the band front does not move but it stays at the injection point.

The situation is the same for all concentrations between C_0 and C_1. These concentrations cannot move in the column. Concentrations lower than C_1 move backwards, as part of a front diffuse boundary, as they do in the first case since their velocities are negative. Concentrations larger than C_1 should move forwards since their associated velocities are positive. However, if they move forwards, they must be part of a stable front shock whose velocity must be negative [since $U_s(C_0) < 0$]. The paradoxical situation is that although a feed at concentration C_0 is pumped into the column, only concentrations lower than C_1 (or larger than C_2, see next

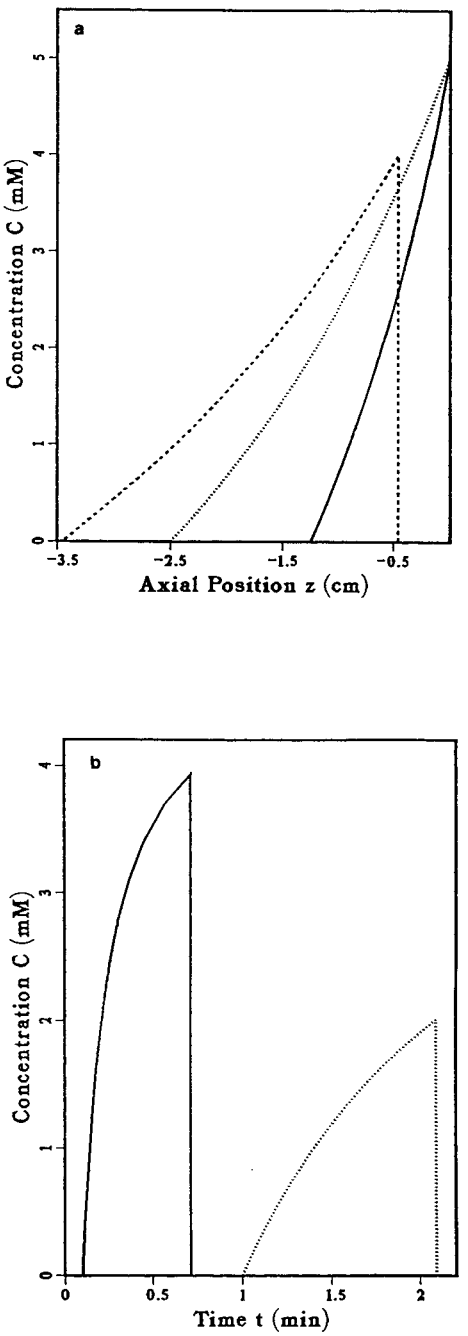

Fig. 7. Negative velocity case: $C_0 = C_1$, $\beta = 9$, $C_0 = 5.0$ mM. Experimental conditions as in Fig. 4. (a) Axial band profiles along the column at three different times: solid line, $t = 0.25$ s; dotted line, $t = 0.5$ s; dashed line, $t = 0.9$ s. (b) Temporal band profiles at the extract outlet ($z = -L$): solid line, short column; dotted line, long column.

section) can move along the column. The column offers an infinite resistance to its penetration by a feed at a concentration intermediate between C_1 and C_2. In other words, there is an instantaneous dilution of the feed from C_0 to C_1, certainly a phenomenon to be avoided.

When the injection is finished, the maximum concentration of the band begins to decrease, the amplitude of the rear shock becomes smaller than C_1 and it begins to move backwards at a velocity which increases progressively as the shock amplitude decreases with progressive dilution. The band profile is given by the same equations as in the previous case.

$C_0 > C_2$, the velocity of the injection shock is positive. When the injection concentration C_0 is higher than C_2, we can distinguish three concentration ranges in the boundaries of the band profile:

(i) when $C \leq C_1$, both the velocity associated with the concentration C, $u_z(C)$, and the shock velocity, $U_s(C)$, are negative;

(ii) when $C_1 \leq C \leq C_2$, the velocity associated with the concentration C is positive and the shock velocity is negative;

(iii) when $C_2 \leq C$, both the velocity associated with the concentration C and the shock velocity are positive.

Thus, the front shock of a rectangular injection pulse has a positive velocity, $U_s(C_0)$; it moves forwards and it is a stable shock. When the rectangular injection pulse ends, the concentration profile along the column is the same as in the case of a component for which the velocities associated with any values of the concentration are positive and whose band moves forward (*First case*). As in this case also, the rear shock is unstable and collapses, because the velocity associated with a concentration increases with increasing concentration. There is a major difference, however: the velocities associated with the low concentrations are negative and these concentrations move backwards while the front shock continues to move forwards. During the whole time when the injection is in process, the concentration C_1 remains stable at the origin. It cannot move as its velocity is zero (Fig. 8a).

As its front moves forwards and its rear moves backwards, the band spreads rapidly and the diffuse boundary captures the shock. The amplitude of the shock begins to decrease and it slows. In contrast to the case when $\beta k'_0 < 1$ (*First case*), the shock velocity can become zero in the present case. This takes place when the shock amplitude becomes equal to C_2. Then the shock stops and starts moving backwards. $u_z(C)$ is still positive, however, and the amplitude of the shock decreases rapidly. As long as the shock amplitude is larger than C_1, the diffuse boundary has the concentration C_1 at the injection point ($z = 0$). The rear shock goes by the injection point when its amplitude becomes equal to C_1. Spatial band profiles observed shortly after the end of the injection and at the time when the diffuse boundary captures the shock are illustrated in Fig. 8a and b.

Depending on the duration of the injection and the column length, part of the feed may exit with the liquid phase, as a raffinate, if the shock can reach $z = L$ during its forward migration, i.e., if the amplitude of the shock when it reaches the exit of the column is such that $C > C_2$. The rest of the injection leaves the column with the solid phase, as an extract. Thus, three types of band profiles can be obtained:

(a) If the column is short and/or the injection duration long enough, the front shock at C_0 reaches the column raffinate exit ($z = L$), followed by the rest of the injection plateau and a diffuse boundary. As the injection plateau is not yet eroded, the retention time of the shock is given by

$$t_s^{\beta}(C_0) = t_0 \left[\frac{1 + F \cdot \frac{\Delta q}{\Delta C}(C_0)}{1 - \beta F \cdot \frac{\Delta q}{\Delta C}(C_0)} \right] \overset{\text{Langmuir}}{=} t_0 \left[1 + \frac{(1+\beta)k'_0}{(1+bC_0) - \beta k'_0} \right] \quad (34)$$

The diffuse boundary of the elution profile is derived from the retention time of a concentration

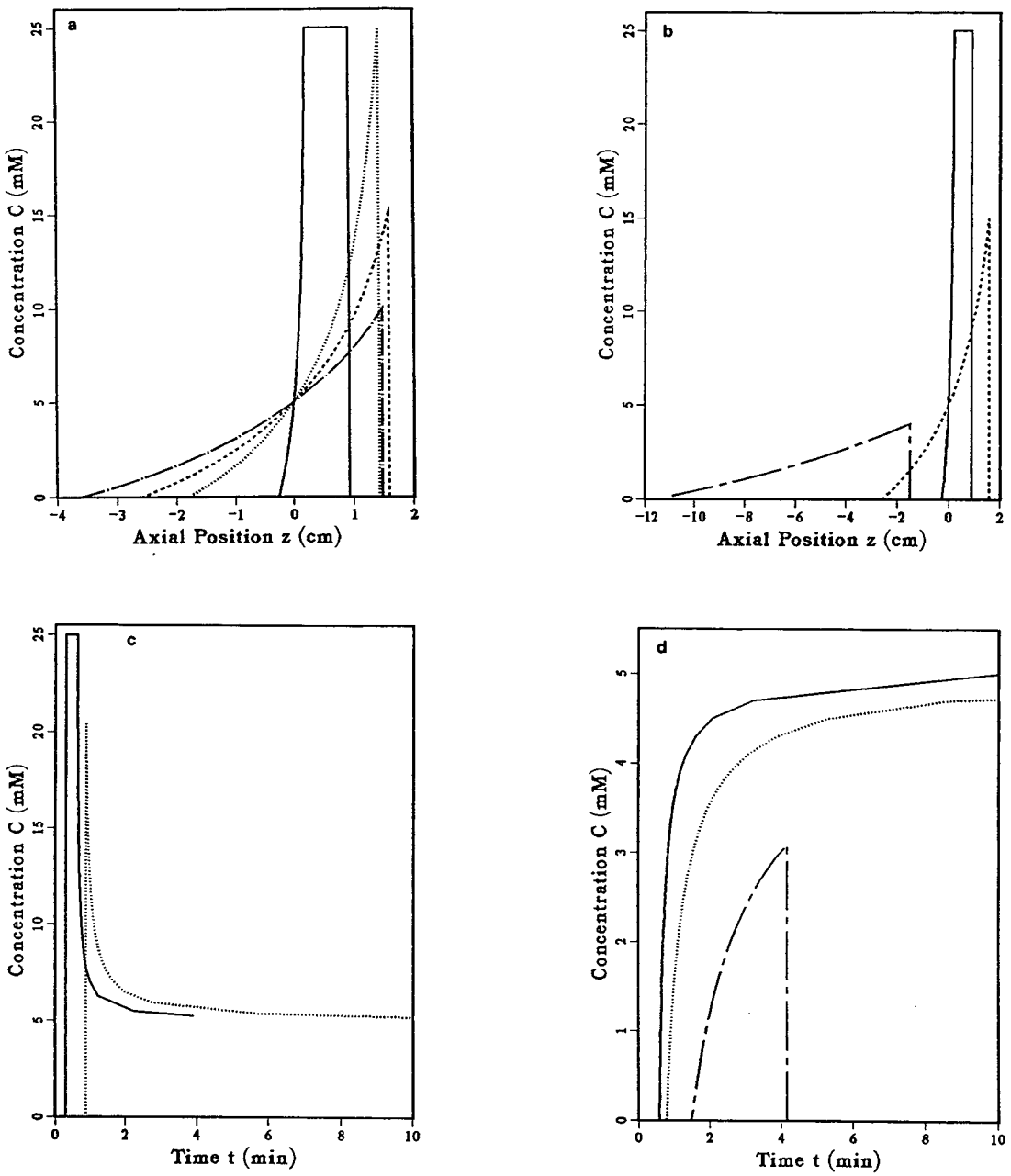

Fig. 8. Negative velocity case: $C_0 > C_2$, $\beta = 9$, $C_0 = 25.0$ mM. Experimental conditions as in Fig. 4. (a) Axial band profiles along the column at four different times: solid line, $t = 0.55$ s; dotted line, $t = 0.86$ s; dashed line, $t = 1.02$ s; chain-dotted line $t = 1.22$ s. $L^* = 1.61$ cm. (b) Axial band profiles along the column at three different times: solid line, $t = 0.55$ s; dashed line, $t = 1.02$ s; chain-dashed line, $t = 1.61$ s. (c) Temporal band profiles consisting of the front shock and the higher part of the rear diffuse boundary at the raffinate outlet ($z = L$): solid line, short column; dotted line, middle column. (d) Temporal band profiles at the extract outlet ($z = -L$): solid line, short column; dotted line, middle column. For both columns, the profiles consist of only the lower part of the rear diffuse boundary. Chain-dashed line, long column; the profile consists of the whole band (the front shock and the whole rear diffuse boundary).

$$t_R^{\beta}(C) = t_p + t_0\left(\frac{F\cdot\frac{dq}{dC}+1}{1-\beta F\cdot\frac{dq}{dC}}\right)$$

$$\overset{\text{Langmuir}}{=} t_p + t_0\left[1+\frac{(1+\beta)k_0'}{(1+bC)^2-\beta k_0'}\right]$$

$$(C \geqslant C_1) \qquad (35)$$

This equation is the same as Eq. 19. The rear of the injection plateau is eluted at time $t_R^{\beta}(C_0)$. If this time is shorter than the retention time of the shock, the latter has been captured by the diffuse boundary and the amplitude of the shock is less than C_0 (see case b).

Only concentrations larger than C_1 can leave the column through the liquid-phase exit (raffinate). Lower concentrations are associated with negative velocities and must leave the column through the other end (extract). Fig. 8c and d show the elution profiles at the raffinate (Fig. 8c) and extract (Fig. 8d) exits. In Fig. 8c, two possibilities are shown, when the profile includes a plateau at the injection concentration and when this plateau has disappeared. These elution profiles never end but have a horizontal asymptote at $C = C_1$ since the retention time of concentration C_1 is infinite. Although the liquid-phase concentration profile has an infinite area, there is no physical impossibility because the outgoing mass flux of the component falls rapidly towards zero when C tends towards C_1 and is zero at $C = C_1$. The area of the component–concentration profile in the liquid phase has no direct physical meaning and is not conservative because there is a finite concentration, $q_1 = f(C_1)$, in the solid phase entering the column at $z = L$ [1]. Only the net mass flux of component leaving the column is conserved. Note the striking difference between the profiles in Fig. 8d, depending on whether the column is or is not long enough for the front shock to change its direction of migration. When the whole sample exits as an extract (chain-dashed line) the elution profile appears normal. When the column is short and the front shock elutes at the raffinate exit, the elution profile has an infinite area. This is a good illustration of the fact that only the mass flux is conservative, while the area of the concentration profile is meaningless in moving-bed chromatography.

The concentrations which are lower than C_1 leave the column with the solid phase at the extract exit ($z = -L$). Typical profiles are shown in Fig. 8d. The equation of the continuous profile is not Eq. 35, but

$$t_R^{\beta}(C) = t_p + \frac{-L}{u_z} = t_p - t_0\left(\frac{1+F\cdot\frac{dq}{dC}}{1-\beta F\cdot\frac{dq}{dC}}\right)$$

$$\overset{\text{Langmuir}}{=} t_p - t_0\left[1+\frac{(1+\beta)k_0'}{(1+bC)^2-\beta k_0'}\right]$$

$$(C \leqslant C_1) \qquad (36)$$

Although similar to Eqs. 32 and 35, this equation differs from Eq. 32 by the presence of t_p and from Eq. 35 by the sign of L. The concentration C_1 remains stagnant anywhere it appears on a diffuse boundary, first at the injection point, then all along the column. It can be eluted only if it is swept out by the passage a shock. If, as in the present case, no shock comes to purge the column, it becomes filled with the component at concentration C_1, a concentration which does not move in either direction.

(b) As we have shown earlier, the amplitude of the shock decreases once it has been captured by the diffuse boundary and the shock slows. Eventually, its velocity becomes zero when the band height has decreased to C_2. Then, the shock turns around to migrate in the opposite direction, pushing the entire band profile backward. Thus, there is a critical column length, L^*, such that if $L < L^*$, the front shock exits with the liquid phase, and some raffinate is collected, whereas if $L > L^*$, the same shock exits, as the rear band shock, through the column entrance, with the solid phase and all the sample is collected as an extract. This critical column length is derived from the integral mass balance equation (Eq. 21), by writing that the maximum concentration of the band, or shock amplitude, C_M, has become equal to C_2. This length is

$$L^* = \frac{t_p u[C_0 - \beta F q(C_0)]}{C_2 + F q(C_2)}$$

$$\overset{\text{Langmuir}}{=} \frac{t_p u C_0 \beta}{C_2(1+\beta)}\left(1 - \frac{\beta k'_0}{1 + bC_0}\right) \quad (37)$$

If the column length is less than L^*, the maximum band concentration C_M is larger than C_2 and the situation is similar (see Fig. 7b, dotted line) to that just described in (a). The maximum band C_M can be obtained from the mass balance, i.e., the injected mass at the feed point must be equal to the sum of the masses leaving the column at both the positive and negative outlets and the mass staying inside the column. Hence C_M is determined by Eq. 21 or 22, and the retention times are given by Eq. 35.

(c) If the column is longer than L^*, the band maximum C_M decreases and becomes lower than C_2 before it can leave the column at its raffinate outlet. In this case, $U_s(C)$ changes sign at concentration C_2 and the front shock stops and changes the direction of its migration from forwards to backwards. This shock remains stable after shifting the direction of its migration. It now moves backwards, in the direction of the solid phase, opposite to the direction of migration of the high concentrations ($C_1 < C < C_2$) on the diffuse boundary. This interaction between the shock and the high concentrations on the diffuse boundary causes a rapid decay of the shock. During all the time when the band shock is in the positive part of the column (i.e., $z > 0$), the diffuse boundary of the band has a concentration equal to C_1 at the origin ($z = 0$). Hence the shock concentration is equal to C_1 when it passes the feed point. Further, concentrations on the diffuse boundary can move backwards only if $C < C_1$. Eventually, the front shock leaves the column at the extract outlet. In this last case, the whole band exits from the column at the extract end and is not split into two fractions as it is in the cases (a) and (b) above.

As the whole band leaves the column at the negative (extract) outlet, $z = -L$, the retention times of the front diffuse boundary is given by Eq. 36, and the band maximum C_M is given by

$$-t_p[C - \beta F q(C)]\Big|_0^{C_0} = t_0\left\{[C + F q(C)]\Big|_0^{C_M} \frac{1 + F \cdot \frac{dq}{dC}(C_M)}{1 - \beta F \cdot \frac{dq}{dC}(C_M)}[C - \beta F q(C)]\Big|_0^{C_M}\right\} \quad (38)$$

For the Langmuir isotherm, C_M can be expressed analytically:

$$C_M = \frac{\sqrt{L_f^\beta[-1 + (L_f^\beta + 1)\beta k'_0]} - L_f^\beta}{b(1 + L_f^\beta)} \quad (39)$$

and the retention time of the band is

$$t_R^\beta(C_M) = t_p - t_0 - t_0(1+\beta)k'_0 \times \frac{(1 + L_f^\beta)^2}{-L_f^{0\beta}(1 + \beta k'_0) + 1 - \beta k'_0 + 2\sqrt{L_f^\beta(-1 + L_f^\beta \beta k'_0 + \beta k'_0)}} \quad (40)$$

Note that, in this case, the rear of the injection profile reaches the column end first, before the front shock of the injection. This is due to the change in the propagation direction of the front shock which results in a negative sign in Eq. 38 replacing a positive sign in Eq. 21. Whereas in all the other cases the column operates as a first in, first out storage device, in this case it operates on the first in, last out principle.

Symbols

a	numerical coefficient in the Langmuir isotherm
b	numerical coefficient in the Langmuir isotherm
C	liquid concentration of the component
C_M	maximum concentration of the profile
C_0	component concentration in the feed
C_1	characteristic concentration [$u_z(C_1) = 0$]
C_2	characteristic concentration [$U_s(C_2) = 0$]
F	phase ratio [$F = (1 - \varepsilon)/\varepsilon$]
F_v	liquid-phase flow-rate ($F_v = \varepsilon S u$)

g^0	net mass flux
$k'_0 = \mathrm{Fa}$	limit retention factor at infinite dilution
L	half the column length
L_f	loading factor or ratio of the sample size to the column saturation capacity
L_s	length of each sub-column or column sub-section in SMB
L^*	critical column length (Eq. 37)
M^{in}	mass flux entering the column
M^{out}	mass flux leaving the column
n	amount injected ($n = C_0 t_p F_v$)
q	solid-phase concentration of the component
S	column cross-sectional area or area of the band profile
t	time
t_p	injection duration
$t_R(C_M)$	retention time of the shock
t_s	switching interval time
U_s	shock velocity
u	flow velocity of the liquid phase
u^{SMB}	velocity of the fluid phase in SMB
$u_z(C)$	velocity associated with a concentration C on a diffuse boundary
V^β	migration velocity of an infinitely thin slice of the profile of a retained component
v	velocity of the moving solid phase
v^{SMB}	velocity of the solid phase in SMB
z	position in the column

Greek letters

β	ratio of the velocities of the solid and the liquid phase in the moving bed column ($\beta = v/u$)
γ	intermediate parameter, $\gamma = \sqrt{\beta k'_0}$
ΔC	concentration amplitude of the shock in the liquid phase
Δq	concentration amplitude of the shock in the solid phase
ε	total column porosity

Superscript

β	characterizes parameters used in countercurrent chromatography

Acknowledgements

This work was supported in part by Grant CHE-92-01663 of the National Science Foundation and by the cooperative agreement between the University of Tennessee and the Oak Ridge National Laboratory. We acknowledge the continuous support of our computational effort by the University of Tennessee Computing Center.

References

[1] G. Ganetsos and P.E. Baker, *Preparative and Production Scale Chromatography*, Marcel Dekker, New York, 1993.
[2] D.M. Ruthven, *Chem. Eng. Sci.* 44 (1989) 1011.
[3] B.B. Fish, R.W. Carr and R. Aris, *AIChE J.* 35 (1989) 80.
[4] B. Balannec and G. Hotier, *Rev. Inst. Fr. Pet.*, 46 (1991) 803.
[5] P.C. Wankat, *Large-Scale Adsorption and Chromatography*, CRC Press, Boca Raton, FL, 1986.
[6] G. Storti, M. Masi, S. Carra and M. Morbidelli, *J. Prep. Chromatogr.*, 1 (1988) 1.
[7] G. Guiochon, S. Golshan-Shirazi and A.M. Katti, *Fundamentals of Preparative and Nonlinear Chromatography*, Academic Press, Boston, MA, 1994.
[8] E. Glueckauf, *Proc. R. Soc. London, Ser. A.*, 186 (1946) 35.
[9] F. Helfferich and G. Klein, *Multicomponent Chromatography—A Theory of Interference*, Marcel Dekker, New York, 1970.
[10] R. Aris and N.R. Amundson, *Mathematical Methods in Chemical Engineering*, Prentice-Hall, Englewood Cliffs, NJ, 1973, Vol. 2.
[11] H.-K. Rhee, R. Aris and N.R. Amundson, *First-Order Partial Differential Equations. II. Theory and Applications of Hyperbolic Systems of Quasilinear Hyperbolic Equations*, Prentice-Hall, Englewood Cliffs, NJ, 1986.
[12] S. Golshan-Shirazi and G. Guiochon, *Anal. Chem.*, 60 (1988) 2364.
[13] B. Lin, S. Golshan-Shirazi, Z. Ma and G. Guiochon, *Anal. Chem.*, 60 (1988) 2647.
[14] G. Guiochon, S. Ghodbane, S. Golshan-Shirazi, J.-X. Huang, A.M. Kati, B. Lin and Z. Ma, *Talanta*, 36 (1989) 19.
[15] B. Lin, Z. Ma, S. Golshan-Shirazi and G. Guiochon, *J. Chromatogr.*, 500 (1990) 185.
[16] S. Golshan-Shirazi and G. Guiochon, *J. Phys. Chem.*, 94 (1990) 495.
[17] D.B. Broughton, *Sep. Sci.*, 19 (1984) 723.

ELSEVIER

Journal of Chromatography A, 688 (1994) 25–29

JOURNAL OF CHROMATOGRAPHY A

29-Silicon NMR evidence for the improved chromatographic siloxane bond stability of bulky alkylsilane ligands on a silica surface

Alex B. Scholten*, Jan W. de Haan, Henk A. Claessens, Leo J.M. van de Ven, Carel A. Cramers

Eindhoven University of Technology, Laboratory of Instrumental Analysis, P.O. Box 513, 5600 MB Eindhoven, Netherlands

First received 5 August 1994; revised manuscript received 28 September 1994

Abstract

A stable bond stationary phase for reversed-phase high-performance liquid chromatography, with a diisobutyl-*n*-octadecylsilane derivatized surface, was studied using ^{29}Si cross-polarization magic angle spinning (CP MAS) NMR. Fumed silica surfaces (Aerosil), trimethylsilylated to different extents, were used to illustrate the effect of ligand surface loading on the hydrogen bonding contribution to the ligand silane CP MAS NMR signal. Spectral comparison of the diisobutyl-*n*-octadecylsilane derivatized silica with the conventional dimethyl-*n*-octadecylsilane derivatized silica revealed significantly decreased hydrogen bonding of residual silanols to the ligand siloxane bond in the diisobutyl-*n*-octadecyl phase. This illustrates the increased steric protection of the ligand siloxane bond by the bulky alkyl substituents, which is assumed to be the reason for the improved hydrolytic stability at low pH of this phase.

1. Introduction

In many applications of reversed-phase high-performance liquid chromatography (RP-HPLC), stationary phase degradation is a major drawback when using alkylsilane-modified silica surfaces because of the hydrolytic instability of siloxane bonds. The lifetime of one column packing may not even be sufficient to perform adequate experimental designs for optimizing separation efficiencies [1]. Consequently, much research was done to identify the most important factors involved in phase deterioration and to design new stationary phases with improved stability. Kirkland et al. proposed that bulky substituents in the silanizing reagent (for example, diisobutyl-*n*-octadecylsilane instead of dimethyl-*n*-octadecylsilane) would result in a more efficient steric protection of the silica surface and, in particular, the ligand siloxane bond [2]. These so-called stable bond phases indeed exhibit superior hydrolytic stability at low pH [3,4]. However, the improved steric protection was not observed as such; it was postulated using the increased chromatographic stability as a criterion.

Of the physicochemical methods used to investigate chromatographic silica surfaces, solid-state NMR has proven to be a powerful tool that enables identification of different chemical sur-

* Corresponding author.

0021-9673/94/$07.00
SSDI 0021-9673(94)00928-7

face structures. The goal of much research has been to relate NMR characteristics of the detected chemical surface species to the observed chromatographic behaviour of silica surfaces [5–11]. In this paper we present ^{29}Si cross-polarization magic angle spinning (CP MAS) NMR evidence for a decreased contribution of hydrogen bonding groups to the ligand silane signal in diisobutyl-*n*-octadecylsilane-modified silica gel compared to the dimethyl-*n*-octadecylsilane analogue. This inhibition of hydrogen bonding is brought about by steric protection of the ligand siloxane bond by the bulky isobutyl substituents.

2. Experimental

The two Zorbax octadecyl phases used in this study were obtained from Rockland Technologies (Newport, DE, USA). One is a dimethyl-*n*-octadecylsilane derivatized silica, Rx-C_{18}, with a carbon content of 12.25% (ligand density = 3.37 μmol/m^2), the other is a diisobutyl-*n*-octadecylsilane derivatized silica, SB-C_{18}, with a carbon content of 9.85% (ligand density = 2.00 μmol/m^2). Both phases were prepared from the same silica substrate: Rx-Sil, with a surface area of 180 m^2/g, a particle size of 5.4 μm, an average pore diameter of 80 Å and a pore volume of 0.45 ml/g (as reported by the manufacturer). In addition, four batches of a fumed silica (Aerosil A-200, Degussa, Frankfurt, Germany), trimethylsilylated to different degrees as described earlier [12], were also studied by ^{29}Si CP MAS NMR. All silicas were dried in vacuum for 8 h at 110°C.

^{29}Si CP MAS NMR spectra were obtained on a Bruker MSL-400 NMR spectrometer (Bruker, Rheinstetten, Germany) at a Larmor frequency of 79.6 MHz. Approximately 250 mg siliceous material was filled into zirconia rotors (7 mm) of the Bruker double bearing type. The magic angle spinning frequency was 2 kHz, using air as the driving gas. Contact time variation revealed that 6 ms was an appropriate setting for comparing the spectra of the Aerosil samples. The contact time for the Zorbax phases was set to 3 ms. The acquisition time was 10 ms and the pulse delay time was 4 s. A total of 3000 free induction decays were added in 1K data points and zero filled to 8K. A line broadening of 20 Hz was applied prior to Fourier transformation. NMR chemical shifts are referenced to liquid tetramethylsilane, using Q_8M_8 (the trimethylsilylester of cubic octameric silicate) as an external reference.

3. Results and discussion

Fig. 1 displays the ^{29}Si CP MAS NMR spectra of the Aerosil samples in the silane ligand region for four different degrees of trimethylsilylation. Clearly, the chemical shift of the maximum of the ligand signal decreases with increasing surface coverage. Also, the asymmetry of the signals due to a shoulder at the left of the peak maximum is evident. Very recently, Haukka and Root [13] reported that a similar shoulder is also evident in the earlier pioneering work on silylated silicas [14,15], but that it never was commented on. They proposed to assign this signal to trimethylsilyl groups produced by the reaction of hexamethyldisilazane (HMDS) with a terminal silanol group of which the oxygen atom is involved in hydrogen bonding and the proton is uncoordinated. Many other authors postulate this type of silanol functionality to be more acidic and thus more reactive towards silanizing reagents such as HMDS [13]. After silylation, the oxygen atom in the ligand siloxane bond can still be involved in hydrogen bonding to the neighbouring silanol functionality, leading to a magnetic deshielding of the silane silicon nucleus (downfield shift of the NMR signal). A rather convincing argument for Haukka and Root's assignment is the observation that the shoulder is less pronounced, or even not present at all, after silylation of high temperature (up to 820°C) pretreated silica substrates. This high temperature curing causes the surface silanols to form siloxane bonds with neighbouring silanols. The resulting lower silanol surface concentration decreases the possibilities of hydrogen bonding of residual silanols to the ligand siloxane bonds

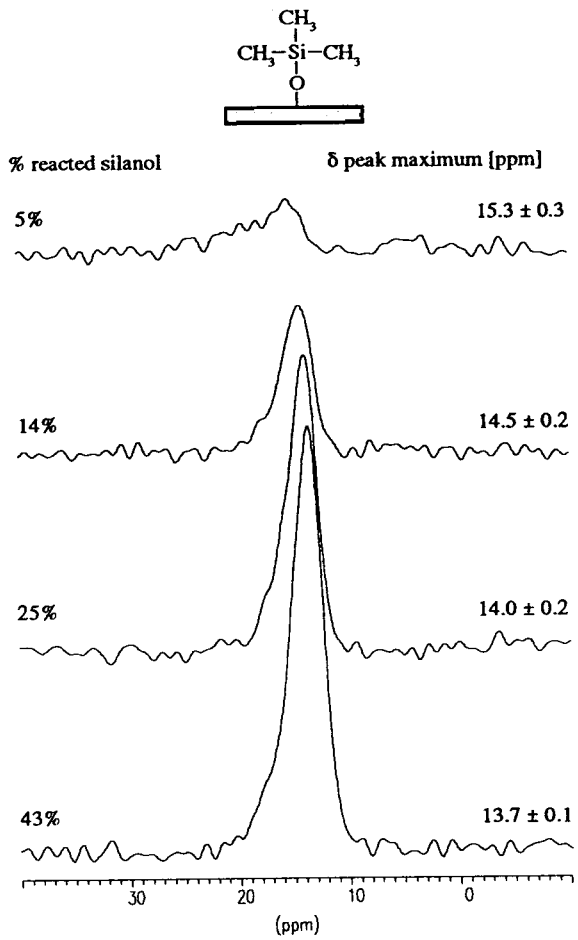

Fig. 1. ^{29}Si CP MAS NMR spectra of Aerosil A-200 with trimethylsiloxane surface coverages and chemical shifts of the peak maxima (± maximum error) as indicated. All spectra are on the same intensity scale.

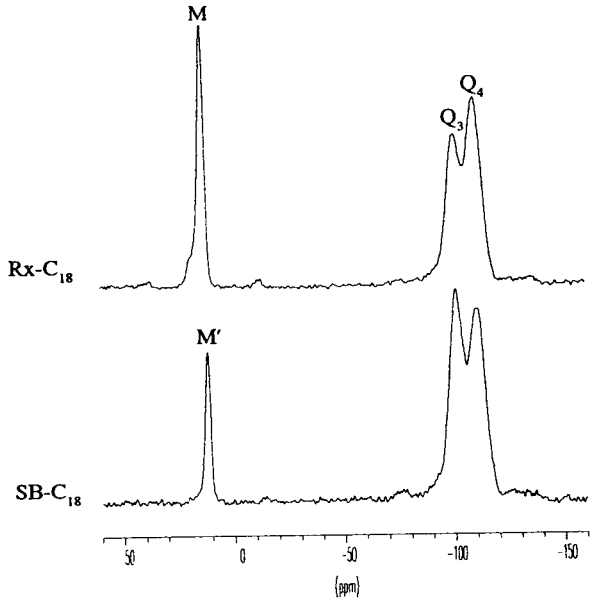

Fig. 2. ^{29}Si CP MAS NMR spectra of the Zorbax octadecyl RP-HPLC phases. Both spectra are on the same intensity scale. M = dimethyl-*n*-octadecylsiloxane, M′ = diisobutyl-*n*-octadecylsiloxane, Q_3 = single silanol, Q_4 = siloxane.

after silylation. Now, Fig. 1 illustrates that in our case, where the silanol surface concentration is decreased by means of trimethylsilylation, the relative contribution of the hydrogen bonding residual silanols to the ligand siloxane signal is decreased because the signal maximum is shifted to lower ppm values.

Fig. 2 displays the ^{29}Si CP MAS NMR spectra of the two Zorbax C_{18} phases. Before considering the asymmetry of the silane ligand NMR signals, it should be noted that the peak maximum of the SB-C_{18} ligand signal is shifted 2 ppm upfield from the maximum of the Rx-C_{18} ligand signal. This is due to the β effect on ^{29}Si upon substitution of two hydrogen atoms for two isopropyl groups. This chemical shift difference is, however, irrelevant in the following discussion. The attention is focused on the degree of asymmetry of both signals. It appears that the shoulder in the SB-C_{18} spectrum is much less pronounced, indicating that the ligand siloxane bond is involved in hydrogen bonding only to a small extent. In the Rx-C_{18} spectrum on the other hand, the shoulder is clearly discernible. It should be noted that the surface coverage by the diisobutyl-*n*-octadecylsilane ligands is much lower than that of the dimethyl-*n*-octadecylsilane ligands (26% vs. 44% of reacted silanols, assuming a generally accepted initial silanol surface concentration of 7.6 μmol/m^2 on a fully hydroxylated silica surface: Kiselev–Zhuravlev constant = 4.6 nm^{-2} [16]). Bearing in mind the result of the trimethylsilylated Aerosil surfaces, where increasing surface coverage is accompanied by a decreasing hydrogen bonding contribution to the NMR signal, the slight asymmetry

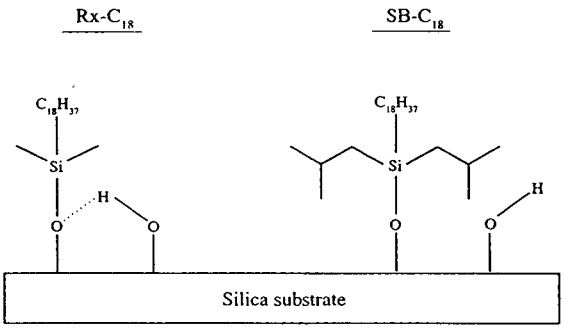

Fig. 3. Schematic drawing of the dimethyl-*n*-octadecylsilyl and the diisobutyl-*n*-octadecylsiloxane surface structures, illustrating the increased steric protection of the ligand siloxane bond by the bulky side groups in the latter.

of the SB-C_{18} ligand NMR signal strongly suggests the superior steric shielding properties of the isobutyl groups. This is schematically illustrated in Fig. 3.

In an attempt to roughly quantify this hydrogen bonding contribution, the spectra of the two *n*-octadecyl phases were deconvoluted using the Bruker Linesim software. As is known from theory, solid-state NMR signals generally have Gaussian line shapes, thus Gaussian functions were used in the spectral deconvolution. A total of three Gaussian line shapes appeared necessary to accurately fit the experimental traces. Fig. 4 shows the results of these simulations and Table 1 summarizes the relevant numerical data. The main peak (nr. 1) in the simulated traces represents silane silicon atoms attached to former single silanol (Q_3) groups, of which the siloxane bond to the silica surface is not involved in hydrogen bonding. The second peak (nr. 2), 2 ppm downfield from the main signal, has an intensity about 4 to 5 times smaller than the main peak. We assign this signal to the silane species after reaction with silanediol (Q_2) groups as the ratio 1:5 reflects the Q_2:Q_3 ratio of the native silica gel. The third Gaussian (nr. 3) is mainly responsible for the asymmetry of the total ligand signal. In line with Haukka and Root's results, this peak is assigned to the ligand siloxane bonds involved in hydrogen bonding.

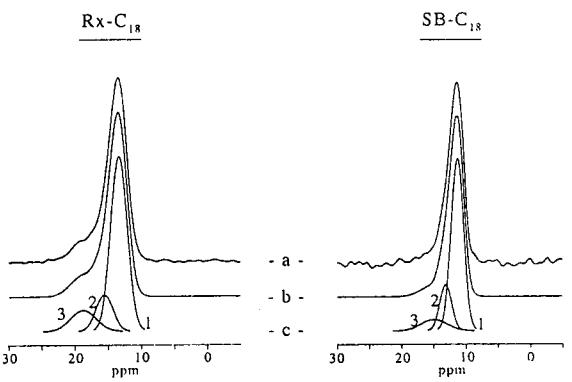

Fig. 4. Experimental (a), simulated (b) and deconvoluted (c) traces of the ligand siloxane signals of the ^{29}Si CP MAS NMR spectra of the Rx-C_{18} phase (left) and the SB-C_{18} phase (right). The numbers next to the individual Gaussians correspond to the peak numbers in Table 1.

From Table 1 several arguments can be deduced to sustain the supposed increased shielding of the ligand siloxane bond in the SB-C_{18} phase. First, peak number 3 has a greater downfield shift compared to the main peak (number 1) 1) in the Rx-C_{18} phase, indicating a stronger hydrogen bond. Second, this peak has a higher intensity and a larger relative area. Furthermore, the main peak (nr. 1) at 11.5 ppm in the

Table 1
Relevant data of the three Gaussian peak shapes used to simulate the experimental ligand silane ^{29}Si CP MAS NMR signal of the Rx-C_{18} and the SB-C_{18} phase

Phase, peak nr.[a]	δ (ppm)	Intensity [b]	Width (Hz)	Relative area (%)
Rx-C_{18}				
1	13.4	95.0 (0.7)	236 (4)	71.6 (0.4)
2	15.7	19.6 (1.0)	242 (7)	15.2 (0.6)
3	18.8	11.3 (0.5)	364 (21)	13.2 (0.7)
SB-C_{18}				
1	11.5	95.6 (0.6)	182 (3)	72.2 (0.4)
2	13.2	25.2 (1.1)	173 (7)	18.1 (0.7)
3	15.1	6.2 (0.3)	378 (22)	9.7 (0.5)

Values in parentheses are ± estimated maximum errors, determined by manual distortion of the separate parameters to the point where visual inspection clearly indicated a lack of fit.

[a] For assignments, see text.

[b] Maximum in the experimental trace = 100.

simulated traces of the SB-C_{18} spectrum has a considerably smaller width than the corresponding peak at 13.4 ppm in the Rx-C_{18} simulated trace. The same is true for peak number 2. This points to a decreased site dispersion for the silane silicon atom caused by the large cloud of isobutyl groups surrounding the silane silicon atom, which is thus effectively shielded from interactions that would contribute to its site dispersion.

Together, these observations strongly suggest the increased steric protection of the ligand siloxane bond in the diisobutyl-*n*-octadecylsilane derivatized surface, especially if the surface loading effect is taken into account too.

4. Conclusions

It is proved, using ^{29}Si CP MAS NMR, that isobutyl side groups of ligand silane chains of a silica based RP-HPLC phase provide a significantly increased steric protection of the ligand siloxane bond compared to their methyl analogues. Hydrogen bonding of residual silanols to the ligand siloxane oxygen atoms is shown to occur much less in the diisobutyl-*n*-octadecylsilane derivatized silica. It is likely that this also explains the increased chromatographic stability at low pH of these stable bond phases, as the siloxane bond is protected from contact with aggressive, hydrolyzing eluents. It has very recently been demonstrated, however, that at high pH stable bond phases degrade more rapidly [17]. At high pH, dissolution of the silica substrate is the major cause of *n*-octadecylsilane stationary phase degradation [18]. The lower surface coverage of diisobutyl-*n*-octadecylsilane phase compared to the dimethyl-*n*-octadecylsilane phase apparently provides a less effective shielding of the underlying silica substrate. Therefore, the term "stable bond" phase refers to the increased stability of the ligand-to-silica siloxane bond.

Acknowledgment

Dr. J.J. Kirkland from Rockland Technologies Inc. is gratefully acknowledged for the donation of the Zorbax phases.

References

[1] B. Bourguignon and D.L. Massart, *Anal. Chim. Acta*, 282 (1993) 33.
[2] J.J. Kirkland, J.L. Glajch and R.D. Farlee, *Anal. Chem.*, 61 (1989) 2.
[3] J.J. Kirkland, C.H. Dilks, Jr. and J.E. Henderson, *LC-GC Int.*, 6 (1993) 436.
[4] A. Houbenová, H.A. Claessens, J.W. de Haan, C.A. Cramers and K. Stulík, *J. Liquid Chromatogr.*, 17 (1994) 46.
[5] K. Albert, R. Brindle, J. Schmid, B. Buszewski and E. Bayer, *Chromatographia*, 38 (1994) 283
[6] K. Albert and E. Bayer, *J. Chromatogr.*, 544 (1991) 370.
[7] R.K. Gilpin and M.E. Gangoda, *J. Magn. Reson.*, 64 (1985) 408.
[8] D.W. Sindorf and G.E. Maciel, *J. Am. Chem. Soc.*, 105 (1983) 1848.
[9] D.M. Bliesner and K.B. Sentell, *Anal. Chem.*, 65 (1993) 1819.
[10] M.J.J. Hetem, J.W. de Haan, H.A. Claessens, L.J.M. van de Ven, C.A. Cramers and J.N. Kinkel, *Anal. Chem.*, 62 (1990) 2288.
[11] M. Hanson, K.K. Unger, J.S. Schmid, K. Albert and E. Bayer, *Anal. Chem.*, 65 (1993) 2249.
[12] A.B. Scholten, H.-G. Janssen, J.W. de Haan and C.A. Cramers, *J. High Resolut. Chromatogr.*, 17 (1994) 77.
[13] S. Haukka and A. Root, *J. Phys. Chem.*, 98 (1994) 1695, and references therein.
[14] D.W. Sindorf and G.E. Maciel, *J. Am. Chem. Soc.*, 103 (1981) 4263.
[15] D.W. Sindorf and G.E. Maciel, *J. Phys. Chem.*, 86 (1982) 5208.
[16] L.T. Zhuravlev, *Colloids Surf. A*, 74 (1993) 71.
[17] J.J. Kirkland, M.A. van Straten and H.A. Claessens, *J. Chromatogr.*, in press.
[18] A.B. Scholten, J.W. de Haan, L.J.M. van de Ven, H.A. Claessens and C.A. Cramers, *Anal. Chem.*, in press.

ELSEVIER

Journal of Chromatography A, 688 (1994) 31–45

JOURNAL OF CHROMATOGRAPHY A

Chromatographic evaluation of alkyl-bonded phases prepared through olefin hydrosilylation on a hydride–silica intermediate

María C. Montes, Cliff van Amen[1], Joseph J. Pesek, Junior E. Sandoval*

Department of Chemistry, San José State University, San José, CA 95192, USA

First received 15 June 1994; revised manuscript received 6 October 1994

Abstract

The chromatographic characterization of alkyl-bonded silica-based stationary phases for HPLC is described. A previously established method involving catalytic hydrosilylation of terminal olefins on a hydride-modified intermediate was used to obtain octyl and octadecyl packings. Generally speaking, the resulting phases were found to be chromatographically equivalent (comparable retention and selectivity) to sorbents produced in a conventional manner using organosilanization. The new bonded phases are, however, significantly more stable toward hydrolysis than conventional bonded silicas. This highly desirable feature of the new bonded phases not only reduces the need for frequent column replacement but also provides enhanced long-term reproducibility of retention data. The new bonded phases exhibit good separation of polycyclic aromatic hydrocarbons, basic solutes and polypeptides.

1. Introduction

Advances in the surface modification of sorbents, especially silica, have led to the development of HPLC into a powerful analytical and preparative separation technique. Alkyl-bonded silicas have had great popularity for HPLC separations of solutes ranging from low-molecular-mass organic compounds to biopolymers. Currently, the most common approach to prepare alkyl-bonded silicas involves organosilanization, a reaction between fully hydroxylated silica and dimethylalkylchlorosilane, as follows:

$$|Si{-}OH + ClSiMe_2R \rightarrow |Si{-}O{-}SiMe_2R + HCl \qquad (1)$$

This reaction produces a uniform monolayer of non-polar moieties covalently attached to the substrate's surface through a siloxane linkage, Si–O–SiC. In a related approach, "polymeric" bonded phases are prepared by reaction of trifunctional organosilanes of the type X_3SiR with silica in the presence of a measured amount of water and a suitable solvent

$$|Si{-}OH + X_3SiR \xrightarrow[\text{Solvent}]{H_2O} |Si{-}O{-}\underset{\displaystyle O\,Y}{\overset{\displaystyle Y\,O}{\overset{|}{\underset{|}{Si}}}}{-}R \qquad (2)$$

where X is an easily hydrolyzable group (e.g., halide, alkoxy, acyloxy, etc.) and Y represents –H or –Si≡. Although the thickness of the attached organic layer may vary according to the reaction conditions, it has been suggested that

* Corresponding author.

[1] On leave from Zadkine College, Rotterdam, Netherlands.

0021-9673/94/$07.00
SSDI 0021-9673(94)00964-3

most polymeric phases with surface coverages approaching those of materials made through reaction 2 are actually monolayer in nature [1].

Despite their wide utility, the bonded phases resulting from organosilanization suffer from two major drawbacks. Due to the steric hindrance of the R group, residual acidic silanols remain in varying degrees on the surface of alkyl-silicas. These unreacted species often result in strong interactions with certain basic solutes which lead to partial solute recovery, poor peak symmetry and non-reproducible retention. Perhaps the most stringent limitation of commercial alkyl-silicas lies in their unsatisfactory hydrolytic stability towards certain mobile phase compositions. Chemical deterioration of the bonded phase results in decreased retention and increased exposure of silanols, which in turn lead to poor long-term precision and degraded solute elution respectively.

To overcome the problems associated with the relatively poor hydrolytic stability of the siloxane linkage, alternate approaches involving the formation of direct Si–C linkages have been developed. The reaction of chlorinated silica with certain organometallic reagents has been used to accomplish this [2–4]

$$|\text{Si–Cl} + \text{RM} \xrightarrow[\text{ether}]{} |\text{Si–R} + \text{MCl} \qquad (3)$$

where M = MgBr or Li. Despite the hydrolytic advantage of the resulting Si–C linkage, bonded stationary phases prepared by this approach have not found widespread applicability, probably because the extreme reactivities of both the chlorinated silica and the organometallic reagent (Grignard or alkyl–lithium) make the process extremely cumbersome to carry out on a commercial scale.

We have recently developed a completely different approach for producing Si–C linkages on silica supports [5–7]. In this method, catalytic olefin hydrosilylation is used as the primary bonding reaction, according to

$$|\text{Si–H} + \text{CH}_2{=}\text{CH–R} \xrightarrow{\text{catalyst}} |\text{Si–CH}_2\text{–CH}_2\text{–R} \qquad (4)$$

The reaction involves the addition of surface silicon hydride to a terminal olefin. Silicon hydride groups are anchored to the silica surface by reaction with the hydrolysis products of triethoxysilane [7]

$$|\text{Si–OH} + (\text{EtO})_3\text{Si–H} \xrightarrow[\text{Dioxane}]{\text{HCl},H_2O} |\text{Si–O–}\underset{\displaystyle \begin{array}{c}\text{O}\\|\\\text{Y}\end{array}}{\overset{\displaystyle \begin{array}{c}\text{Y}\\\text{O}\\|\end{array}}{\text{Si}}}\text{–H} + 3\text{EtOH} \qquad (5)$$

where Y is defined as in reaction 2 above. While the bonded materials as well as the hydride intermediate have been previously evaluated by spectroscopic, thermal and chemical methods [5–7], there is still a need for an evaluation of the chromatographic performance of the new stationary phases. Such an evaluation is the subject of this work.

2. Experimental

2.1. Materials

Proteins and peptides, as well as 1-octadecene were obtained from Sigma (St. Louis, MO, USA). The standard mixture of polycyclic aromatic hydrocarbons (SRM869) was obtained from the National Institute of Standards and Technology (Gaithersburg, MD, USA). 1-Octene, dibenzo-18-crown-6, dibenzo-24-crown-8, trifluoroacetic acid (TFA), 1-phenylheptane, N,N-diethylaniline, N,N-dimethylaniline, aniline and phenol were purchased from Aldrich (Milwaukee, WI, USA). The barbiturate mixture was obtained from Alltech (Deerfield, IL, USA). A 100 m*M* hexachloroplatinic acid (37.5% as Pt, Aldrich) solution in 2-propanol was used as the catalyst for hydrosilylation. Bonded phases were prepared from a variety of commercially available silica sorbents whose physical properties are described in Table 1. LC-grade organic solvents were purchased from EM Science (Cherry Hill, NJ, USA). Deionized water was prepared on a

Table 1
Native silica sorbents used in this work.

Brand name	Lot	Particle diameter (μm)[a]	Pore diameter (nm)[b]	Specific surface area (m^2/g)[b]	Manufacturer
Vydac TP	890414	5.8	29.1	88.8	1
Vydac TP	900201	6.6	38.0	106.5	1
Vydac HS	900423	6.7	10.4	261.2	1
YMC-Gel	630212	10	13.8	314.0	2
Nucleosil	1021	7	30[a]	100[a]	3

Manufacturers: 1 = The Separations Group (Hesperia, CA, USA); 2 = Yamamura Chemical Laboratories Co., Ltd. (Kyoto, Japan); 3 = Macherey–Nagel (Düren, Germany).
[a] Data supplied by manufacturer.
[b] BET nitrogen adsorption method.

Millipore (Bedford, MA, USA) purification system.

2.2. Instrumentation

All chromatographic measurements were made with a Hewlett-Packard (Avondale, PA, USA) Model 1050 liquid chromatographic system equipped with quaternary gradient pump, automatic injector, variable-wavelength UV detector and computer data station. Columns were slurry-packed [10% (w/v) bonded silica in CCl_4–methanol (9:1, v/v)] into 15 cm × 0.46 cm I.D. stainless-steel tubes (Alltech) using a Haskel (Burbank, CA, USA) pneumatic pump at 40 MPa with methanol as the driving solvent. When required, column temperature was controlled by a Model CH-30 (Fiatron System, Oconomowoc, WI, USA) column heater. A Perkin-Elmer (Norwalk, CT, USA) Model 240C elemental analyzer equipped with a Perkin-Elmer Model 56 recorder was utilized for carbon determinations on bonded silicas. The specific surface area and mean pore diameter (Brunauer–Emmett–Teller, BET, nitrogen adsorption method) were determined at Chevron Research and Technology (Richmond, CA, USA) with a Micromeritics Model ASAP 2400. Data analysis and plotting were performed using RS/1 scientific spreadsheet software (BBN Research Systems, Cambridge, MA, USA).

2.3. Synthetic procedures

The C_8- and C_{18}-silicas were synthesized by olefin hydrosilylation as previously described [6]. The hydride intermediate was made according to a recently reported method [7]. Conventional octyl- and octadecyl-dimethylsilyl-silicas were prepared according to the procedures described by Berendsen et al. [8]. The concentration, α_R, of surface-bonded groups was obtained, as reported earlier [6] from the carbon content of the bonded material along with the BET specific surface area of the native silica substrate using the equation proposed by Berendsen and De Galan [9].

3. Results and discussion

3.1. Hydrolytic stability

The limited stability of the siloxane (Si–O–SiR) linkage has been recognized as the major source of hydrolytic instability of conventional silica-based stationary phases used in many HPLC bioseparations. The improved stability obtained through the formation of direct surface-to-carbon linkages strongly suggests that the siloxane and not the Si–C bond is the most hydrolytically labile portion of the organosiloxane structure. Short column lifetime, poor long-term precision and potential fraction contamina-

tion are the most evident deleterious effects arising from phase deterioration. Fraction contamination can be particularly disadvantageous in the case of preparative separations.

Recently, there has been a considerable activity aimed at evaluating stationary phase degradation [10–13]. Kirkland and co-workers [11,13], in their attempts to develop more stable silica-based separation materials, have studied degradation of bonded phases in a systematic way. The bonded phase degradation scheme used here was adapted from that developed by these authors. A mobile phase consisting of 0.10% (v/v) TFA in acetonitrile (solvent A) and 0.10% (v/v) TFA in water (solvent B) was passed at 1.00 ml/min through a packed column maintained at 50°C; the mobile phase composition cycle used is depicted in Fig. 1. The retention of 1-phenylheptane (10-μl injection of 0.1 mM solution in 50% solvent A) was used as an indirect measure of the alkyl coverage remaining on the bonded phase as it becomes degraded. This measurement was made during the initial isocratic period of the cycle and then repeated under the same conditions after subjecting the column to the entire mobile phase cycle. Column void volume was determined using KNO_3 (0.05 mM) as an unretained marker. Normalized retention data for 1-phenylheptane, in the form of fraction of remaining k', as a function of the number of column volumes passed through the bonded silica bed are shown in Fig. 2 for several columns tested. Clearly, all bonded phases undergo degradation under the test conditions, but the hydrosilylation product does so at a significantly slower rate. The loss of retention for the latter was only about 10% during the entire test period while, under the same conditions, conventional phases lost 35% or more. It is also apparent that lightly loaded phases (curve C of Fig. 2) are more rapidly degraded by the TFA-containing mobile phase, as expected. There does not seem

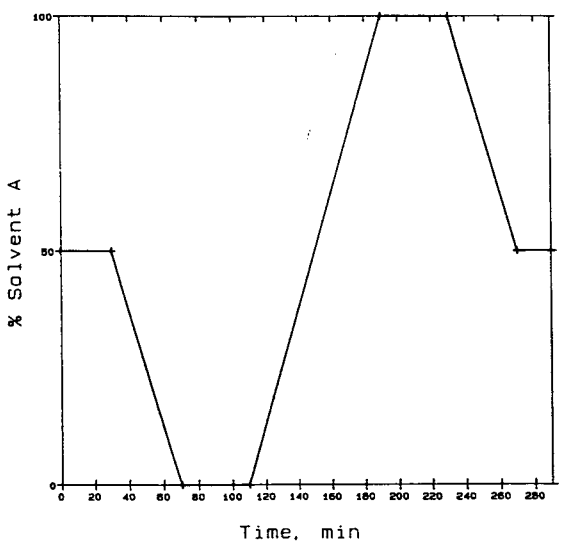

Fig. 1. Solvent composition cycle used for the long-term chromatographic hydrolysis test in TFA-containing mobile phase. Solvent A, 0.10% (v/v) TFA in acetonitrile; solvent B, 0.10% (v/v) TFA in water; flow-rate, 1.0 ml/min; column temperature, 50.0 ± 0.1°C.

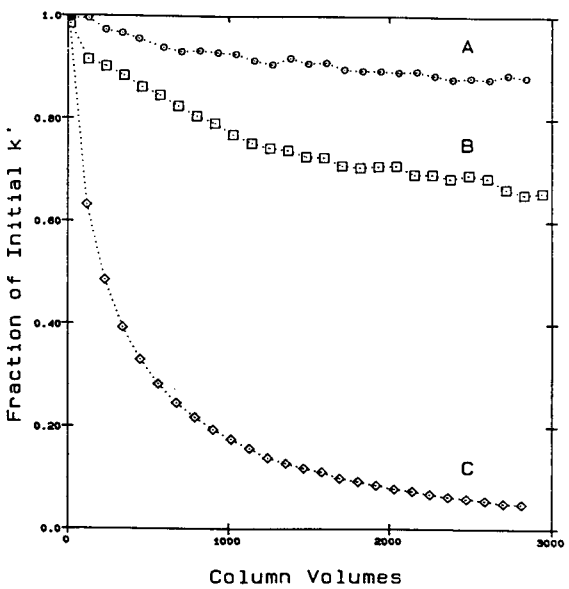

Fig. 2. Relative loss of retention for 1-phenylheptane on C_8-Vydac TP as a function of column volumes of mobile phase passed through the bonded phase during the long-term hydrolysis test. Retention (k') for 1-phenylheptane was measured during the initial isocratic period depicted in Fig. 1. Curves: A = hydrosilylation product (initial $\alpha_R = 3.2$ μmol/m^2, initial $k' = 5.9$, BET surface area $S_{BET} = 89$ m^2/g); B = conventional organosilanization product (initial $\alpha_R = 3.1$ μmol/m^2, initial $k' = 11.7$, $S_{BET} = 106$ m^2/g); C = low-coverage, conventional organosilanization product (initial $\alpha_R = 1.7$ μmol/m^2, initial $k' = 1.9$, $S_{BET} = 89$ m^2/g).

to be, however, a simple first-order rate function that fits any of the experimental data. Additionally, it should be noticed that, although the alkyl surface coverages for the upper and middle curves are comparable, the latter –the conventional phase– exhibits an unusually high retention towards the non-polar probe. One possible reason is that the organosilanization product was prepared from a silica having a higher surface area (106 versus 89 m^2/g). This observation alone, however, cannot account for the almost double retention shown by this phase. Neither can the presence of the two additional methyl groups at the base of the anchored octyl chain. The conventional octyl phases whose data are shown in Fig. 2 (curves B and C) correspond to the upper and lower hydrolytic stability limits found in similar phases prepared from the silica sorbents of Table 1; other conventional C_8 phases show stabilities which lie between the middle and lower curves.

Additional evidence that the bonded alkyl groups were actually lost from the tested sorbents can be obtained from carbon content and coverage data in Table 2. Again, it is quite evident that in the case of the conventional materials, a significant fraction of the bonded phase is lost as a result of the long-term elution with the TFA-containing mobile phase. In contrast, the bonded phase prepared by hydrosilylation via hydride maintains most of its carbon content upon the same hydrolysis regime. The present data also confirms the results from a previous non-HPLC study [6], in which elemental analysis was used to monitor the effects of phase degradation.

It seems clear that, compared to conventional organosilanization, olefin hydrosilylation on an SiH-containing substrate produces significantly more stable bonded phases. The superior stability of the new product is, very likely, a direct result of the greater hydrolytic strength of the Si–C linkage as compared to the siloxane Si–O–SiR linkage of conventional bonded phases. To some readers, the last statement may require further elaboration. While the necessity of representing pictorially the product of reaction 5 as

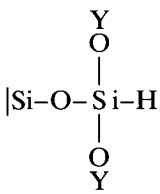

may lead to an apparent structural equivalence between the hydrosilylation product (reaction 4) and a polymeric phase (reaction 2), such a correspondence must not be taken literally. It should be emphasized that albeit the underlying siloxane layer in the new bonded phase is produced by a trifunctional (hydro)silane, it is far more efficiently attached to the silica surface than that of *any* trifunctional alkylsilane. This, naturally, is in virtue of the *minimal* size of the hydride group. By means of ^{29}Si cross-polarization (CP) NMR we have shown that about 90%

Table 2
Carbon, coverage and retention data for octyl-bonded silicas (Vydac TP) subjected to long-term hydrolysis test with TFA-containing aqueous acetonitrile mobile phases

Bonded phase[a]	Curve Fig. 2	Carbon content (%, w/w)[b]		Surface coverage ($\mu mol/m^2$) (initial)	k' for 1-phenylheptane		Column volumes
		Initial	Final		Initial	Final	
1	A	4.14	3.88	3.2	5.9	5.1	2842
2	B	4.22	3.24	3.1	11.7	7.6	2942
2	C	1.71	0.65	1.7	1.9	0.1	2813

[a] 1 = Product of 1-octene hydrosilylation; 2 = conventional octyldimethylsilyl product.
[b] Uncorrected.

of the hydride-bearing species in the intermediate are fully condensed (via formation of three siloxane linkages) whereas its presumably "analogue" polymeric C_8 phase exhibits only about 50% efficiency [7]. For steric reasons, this figure must be lower for a C_{18} phase. Thus, based on known NMR evidence, one can say that representing silica as |Si–OH (single silanol) is roughly 70% accurate [14], while representing the hydride intermediate as |Si–H is about 90% accurate and representing a "polymeric" phase as |Si–R is only 50% accurate if $R = C_8$ [7], or less if $R = C_{18}$. Another possible interpretation is that hydrosilanetriol, $HSi(OH)_3$, appears to be attached to the silica surface in the hydride intermediate more efficiently than silicic acid, $Si(OH)_4$, in native silica (not really surprising since a hydride group is smaller than a hydroxyl group). While this argument may seem like stretching the spectroscopic evidence, very few researchers would question the fact that the outermost layer of the silica surface is indeed an integral part of the substrate. Furthermore, if the new phase had been prepared through the much less attractive chlorination–reduction–hydrosilylation sequence [5,6], that is

$$|\text{Si–OH} \xrightarrow{SOCl_2} |\text{Si–Cl} \xrightarrow{LiAlH_4}$$
$$|\text{Si–H} \xrightarrow{CH_2=CH-R} |\text{Si–CH}_2\text{CH}_2\text{R}$$

neither the attachment of the underlying siloxane layer nor the monomeric nature of the final phase would likely be questioned. The only structural difference between this material and the current product is a higher population of unreacted SiH species underneath the anchored alkyl chains. Since the anchored SiH species in the hydride intermediate are an integral part of the silica surface, the formation of a true *surface*-to-carbon linkage (Si–C) via hydrosilylation should now be readily rationalized. Naturally, one can expect these materials to exhibit the hydrolytic stability of bonded phases prepared by a Grignard or a related method.

The practical importance of this hydrolytic advantage is evident:

(i) After several thousands of column volumes of a mobile phase containing aqueous TFA, a conventional bonded silica loses its anchored organic material to such an extent that the column has to be replaced by a new one. Because of the superior hydrolytic stability of the Si–C linkage (the predominant species in the new bonded packings) the useful lifetime of the column will be significantly increased. Obviously, the hydrolytic advantage means lower operating costs for HPLC separations.

(ii) From an analytical point of view, the long-term precision of retention is compromised in the case of a conventional bonded phase used under the conditions described above. Under the same conditions, the new bonded phases also degrade, but more slowly and therefore the long-term precision should be less limiting.

(iii) Another practical consequence of the loss of bonded phase during use is that significant organosiliceous material must be washed off the column during gradient elution. Elution of such hydrolytic degradation by-products would have deleterious consequences, particularly for preparative or process separations where fraction contamination may become a serious problem.

We also did some exploratory work on the hydrolytic stability of new and conventional bonded phases at basic pH by using neat acetonitrile as solvent A and replacing the aqueous TFA solution with 25 m*M* phosphate pH 9.0 in solvent B. The conventional C_8 phase (Vydac TP, initial $\alpha_R = 3.1$ μmol/m^2, initial $k' = 18.0$) virtually collapsed, as indicated by repeated pressure buildup and subsequent outlet frit clogging. This resulted in complete interruption of the test after only 1200 column volumes and an overall loss in retention for 1-phenylheptane of about 55% after that period. Although the C_8 phase prepared from hydrosilylation (Vydac TP, initial $\alpha_R = 3.2$ μmol/m^2, initial $k' = 4.7$) endured the whole test (about 2800 column volumes) without any abnormal pressure buildup, only about 50% of its retention remained by the end of the experiment. It is obvious that none of the bonded phases tested could withstand prolonged exposure to mobile phases containing aqueous high-pH buffers without undergoing unacceptable retention degradation in the case of our new

phase or disastrous phase collapse in the case of conventional bonded phases. Despite some advantage of the new bonded phases under the test conditions reported here, it seems clear that the inherently low hydrolytic stability of the siloxane linkages in the silica backbone is the primary limiting factor for this type of substrate.

3.2. Selectivity for polycyclic aromatic hydrocarbons

One very important application of reversed-phase (RP) chromatography is in the separation of polycyclic aromatic hydrocarbons (PAHs). Chemically bonded C_{18} phases are the most popular packings for the separation of PAHs. Although neutral solutes such as hydrocarbons do not exhibit elution problems such as peak tailing due to slow desorption kinetics, in some cases, particularly with structurally similar PAHs, separations are often difficult and sometimes impossible.

A simple empirical HPLC test has been developed by Sander and Wise [1,15–17] to assess the monomeric or polymeric nature of a reversed-phase material. The test mixture (known as SRM869) is an acetonitrile solution of three PAHs: benzo[*a*]pyrene (BaP), 1,2:3,4:5,6:7,8-tetrabenzonaphthalene (TBN) also known as dibenzo[*g*,*p*]-chrysene, and phenanthro[3,4*c*]-phenanthrene (PhPh). The elution order of the mixture is thought to be strongly dependent on the type of phase. Under isocratic conditions of acetonitrile–water (85:15, v/v) at 25 ± 2°C and 2.0 ml/min., monomeric C_{18} phases (see reaction 1) are expected to elute in the order BaP ≤ PhPh < TBN, while corresponding polymeric phases (see reaction 2) give the elution order PhPh < TBN ≤ BaP. Phases with intermediate properties (that is, heavily loaded monomeric or lightly loaded polymeric C_{18} phases) show elution order PhPh < BaP < TBN. Semiquantitative comparisons of different C_{18} phases have been made in terms of the selectivity factor of TBN with respect to BaP, that is, $\alpha_{TBN/BaP}$ (defined as the ratio k'_{TBN}/k'_{BaP}, where k' refers to the solute's retention factor). Polymeric phases show $\alpha_{TBN/BaP}$ values less than or equal to one, while monomeric phases have $\alpha_{TBN/BaP}$ greater than 1.7.

In order to avoid direct comparisons with literature figures derived from an empirical generalization, new and conventional bonded phases were prepared from the same silica substrate and the chromatographic tests were carried out under identical conditions. As shown in Table 3, it appears that, albeit the surface octadecyl densities of all phases were comparable and typical of monomeric C_{18}-silicas, the elution order of the mixture in four of the six phases corresponds to that of intermediate materials, that is, "heavily loaded monomeric" phases, according to the nomenclature used by Sanders and Wise. Additionally, the intermediate character of *all* phases shown is indicated by a selectivity of TBN/BaP consistently greater than 1 but smaller than 1.7. Notice also that while the new phases consistently exhibit α values slightly lower (average 1.34 ± 0.06, $n = 3$) than those for the corresponding octa-

Table 3
Retention and selectivity data for the three-component standard SRM869 mixture on octadecyl silicas

Silica	Bonded phase[a]	α_R (μmol/m^2)	k'_{BaP}	k'_{PhPh}	k'_{TBN}	$\alpha_{TBN/BaP}$
Vydac TP	1	2.35	3.35	3.35	5.27	1.57
Vydac TP	2	2.48	2.93	2.70	4.03	1.37
Nucleosil	1	2.60	4.11	4.31	6.82	1.66
Nucleosil	2	2.96	2.60	2.25	3.31	1.27
YMC-Gel	1	2.65	9.25	8.77	14.64	1.58
YMC-Gel	2	2.66	9.42	7.90	13.00	1.38

[a] 1 = Conventional octadecyldimethylsilyl product; 2 = product of 1-octadecene hydrosilylation.

than those for the corresponding octadecyldimethylsilyl products (average 1.60 ± 0.05, $n = 3$), none of the latter were ≥ 1.7 either. The important issue here is, nevertheless, that the selectivity data of the C_{18} phases prepared by hydrosilylation resemble those of the intrinsically monomeric conventional phases prepared by organosilanization, as expected. Fig. 3 illustrates typical separations of the test mixture in two silicas. It is interesting to note that the new phases appear to provide slightly but consistently weaker overall retention than the conventional ones.

Separations of a more complex mixture consisting of sixteen priority pollutant PAHs on several C_{18} phases (not shown) indicate that, in all cases, only partial separation of closely related isomers was achieved, a behavior which appears to be characteristic of monomeric phases [1,6]. It seems reasonable to conclude that selectivity of the octadecyl bonded phases prepared from olefin hydrosilylation is comparable to that exhibited by their conventional octadecyl-dimethylsilyl counterparts.

3.3. Mobile phase effects and silanophilic interactions

It has been proposed by Horváth and coworkers [18,19] that under regular RP conditions, (i.e., those with a mobile phase which is more polar than the stationary phase), retention

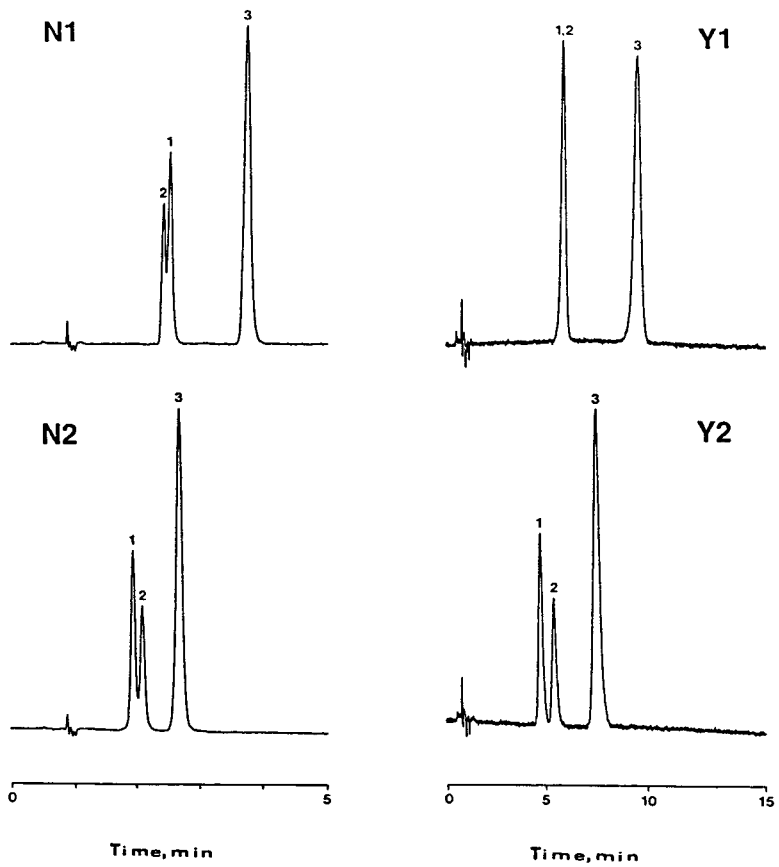

Fig. 3. Typical separation profiles for the SRM869 PAH mixture on C_{18} phases prepared from two brands of silica by two different methods. (N1) Nucleosil, conventional organosilanization product; (N2) Nucleosil, hydrosilylation product; (Y1) YMC-Gel, conventional organosilanization product; (Y2) YMC-Gel, hydrosilylation product. The mixture was chromatographed isocratically with acetonitrile–water (85:15, v/v) at 2.0 ml/min and UV detection at 254 nm. Peaks: 1 = PhPh; 2 = BaP; 3 = TBN.

is due to the superimposed contribution of two mechanisms, characterized by different modes of solute binding to the alkyl-derivatized silica surface: (i) regular solvophobic interactions and (ii) silanophilic interactions. The practical importance of the model is that it rationalizes the unusual behavior (non-linear logarithmic k' versus ψ plots, with ψ being the volume fraction of water in a binary mobile phase) observed with probes which are known to be particularly sensitive to silanophilic interactions. For instance, many biologically important solutes such as peptides having free amino groups exhibit this behavior [20,21].

There are several structural differences between conventional monomeric reversed phases (made via reaction 1) and those resulting from olefin hydrosilylation on hydride–silicas (reaction 4). Differences in the anchored moieties lie in the dimethylsiloxane linkages at the bottom of the attached group. In general, solute binding with these small groups should be rather weak and, therefore, from a solvophobic point of view the hydrocarbonaceous layers of the two alkyl-silicas are virtually equivalent. In conventional bonded phases at least 50% of the original silanols are left unreacted after their preparation. On the other hand, in the new bonded phase we find mostly SiH groups underneath the alkyl moieties. The low polarity of such SiH species should decrease even further the overall polarity of the bonded material. Thus, generally speaking, we expect to have a more hydrophobic bonded phase than the conventional one and, therefore, mostly solvophobic interactions should govern retention on these new bonded phases. This expectation, however, does not necessarily mean that silanols are absent from the new bonded phases. Although during the reaction of the silica with triethoxysilane (TES) (see reaction 5) most of the silanetriols formed upon hydrolysis are fully condensed, there are a few silanols that are not totally removed, as proved by IR and NMR [7].

In order to explore the possibility of obtaining some insight on the extent at which silanophilic and solvophobic interactions are present in both the conventional and the new RP phases, logarithmic k' versus ψ plots were developed for a series of octyl-bonded materials prepared from the same silica substrate. Crown ethers dibenzo-24-crown-8 (DB24C8) and dibenzo-18-crown-6 (DB18C6) were used as silanol-sensitive probes. Triplicate k' measurements at 30°C were made after prolonged column preconditioning, as described elsewhere [18,19]. A single lot of Vydac TP silica was used to eliminate any difference arising from any batch-to-batch substrate variation. Figs. 4 and 5 summarize the experimental results for DB24C8 and DB18C6, respectively. In addition to the C_8 phases, native and hydride sorbents are also included for comparison purposes. Although qualitatively the retention behavior of the crown ethers measured with C_8-Vydac TP silica resembles that found by Horváth and co-workers [18,19] with C_{18}-Partisil (i.e., k' increases with both low as well as high volume fraction of acetonitrile in water), simple analysis of the experimental data in terms of the dual

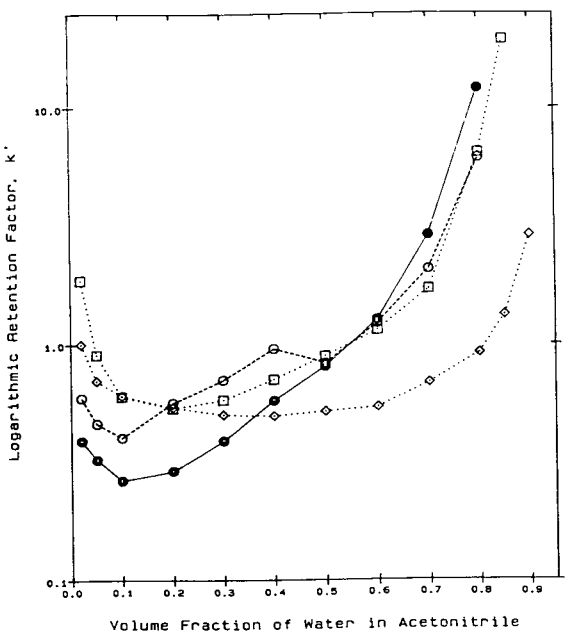

Fig. 4. Plots of the logarithmic retention factor of DB24C8 against the volume fraction of water in aqueous acetonitrile eluent, as a function of the surface chemistry of the sorbent. Curves: ◇ = bare silica; □ = hydride intermediate; ○ = conventional octyldimethylsilyl phase ($\alpha_R = 2.1$ μmol/m^2); ● = octyl phase from hydrosilylation ($\alpha_R = 3.2$ μmol/m^2). Conditions given in the text.

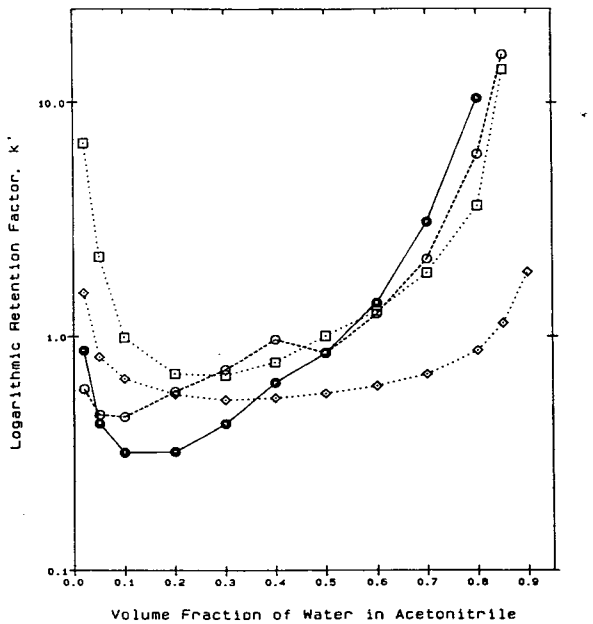

Fig. 5. Plots of the logarithmic retention factor of DB18C6 against the volume fraction of water in aqueous acetonitrile eluent, as a function of the surface chemistry of the sorbent. Curves as in Fig. 4.

retention equations [18,19] was not possible due to the lack of an acceptable fit. Retentions greater than those predicted by the dual model were consistently observed for mobile phase compositions where $0.1 < \psi < 0.6$. Both the conventional and the new C_8-bonded phases exhibit this behavior. These results suggest that, under the conditions used, additional or different binding modes may be operative and, as a consequence, the dependence of k' on eluent composition appears to be a more complex one. Despite this, some important qualitative observations can still be made about the data. Clearly, bare silica exhibits the lowest retention when water is the major component of the mobile phase ($\psi < 0.4$), in agreement with its essentially hydrophilic (silanol-populated) surface. On the other hand, surprisingly, the hydride and not the bare material shows the greatest retention at low water concentration in the mobile phase ($\psi < 0.1$), particularly in the case of DB18C6. Evidently, some very active sites are still present on the hydride surface and are readily accessible for interaction with the crown ring. If it is assumed that isolated silanols on bare silica are essentially removed during silanization with TES (reaction 5), partially condensed species of the type $\equiv$SiH(OH) might be responsible for the unusually high retention on the hydride material. Surprisingly again, at high water concentration in the eluent ($\psi > 0.8$) the hydride exhibits solvophobic retention for crown ethers as strong as that with the conventional C_8-bonded silica. Due to the greater alkyl coverage, larger k' values are shown by the new C_8 phase, as expected. It can be concluded that, although significant departure of the data from the dual model was observed, the general pattern exhibited by silanol-sensitive probes such as crown ethers is qualitatively followed in our case; that is, the logarithmic retention factor is larger at low as well as high water concentrations in the eluent, and a minimum is exhibited at intermediate compositions.

3.4. More on retention of basic solutes

Although crown ethers such as those tested above are sensitive probes for silanophilic interactions, a practical limitation of many RP sorbents lies in the separation of solutes containing basic nitrogen functionalities. These are frequently eluted with varying degrees of peak tailing depending on the accessibility of highly acidic silanol groups on the modified silica surface. To further compare the extent of silanophilic interactions in the new and conventional phases, an empirical HPLC test was utilized. The test, recently proposed by Engelhardt and coworkers [22,23], relies on the combined use of retention factors and peak asymmetries to characterize the chromatographic behavior of selected eluites, including basic solutes. The test solutes include, among others, toluene as a hydrophobic probe, aniline and N,N-dimethylaniline (N,N-DMA) as polar, basic probes and phenol as a neutral, weakly retained reference probe. The later compound has a polar, nonbasic group and therefore should not exhibit any strong acid–base interaction with the stationary phase. Consequently, any peak asymmetry arising from sources other than silanophilic interac-

tions will affect all solutes, while the later will affect only the basic probes. Under the conditions stipulated by the empirical test, isocratic elution with methanol–water [55:45, v/v (49:51, w/w)] at 1.5 ml/min., an RP phase is classified as "good" for the separation of basic solutes if the following requirements are fulfilled [22]: (i) $k'_{\text{aniline}} \leq k'_{\text{phenol}}$; (ii) $k'_{\text{N,N-DMA}} \leq k'_{\text{toluene}}$; and (iii) $A_{\text{s,aniline}}/A_{\text{s,phenol}} < 1.3$ (here A_s represents peak asymmetry as defined elsewhere [24]). Table 4 shows relevant data for two pairs of C_{18}-silicas modified by olefin hydrosilylation and conventional organosilanization. A detailed examination of the data reveals that, according to the empirical test, all bonded phases tested were "well behaved". It appears that the method of surface derivatization does not have a significant effect on the retention characteristics of the solutes under test. Any unfavorable retention of basic solutes in a given bonded phase can rather be attributed to the intrinsic adsorptivity of the native silica support [14,25]. Since it is the derivatization method and not the native silica support what is under study here, this hypothesis was not tested during this work. Furthermore, passing this empirical test does not constitute a sine qua non condition for a good bonded phase. In fact, based on statistical evidence, Schmitz et al. [26] have recently questioned the use of N,N-DMA as a truly silanol-sensitive probe. A cursory literature search reveals that virtually every research group establishes its own set of test compounds for evaluating chromatographic packings. Needless to say, all claim their selection is *the* test mixture, but an objective analysis always arrives at the conclusion that a really good LC column packing is one that gives narrow, symmetric peaks with reproducible retention characteristics for *all* solutes. Naturally, this observation is only a reminder of the many difficulties associated with the lack of standardization in the field of separations, which in turn reflects the complexity of the materials used. Generally speaking, pharmaceutical and related industries select their own product(s), either a basic drug, a peptide or a protein. More commonly, off-the-shelf reagents like simple amines containing a strong chromophore (e.g.: aniline and its derivatives) are the probes of choice. While the former approach responds to a "real world" situation, the second one involves a readily available, structurally simple and, perhaps, easy to model eluite. In our search for a sensitive probe for silanophilic interactions, we found that, compared to aniline and N,N-DMA, N,N-diethylaniline (N,N-DEA) shows a higher susceptibility, even though the latter compound seems intrinsically more hydrophobic than the other two. It must be clear that appropriate mobile phase conditions are required for this behavior to be exhibited. The water content in the mobile phase must be sufficiently high for convenient retention of the polar compounds to occur but not so great as to allow solvophobic interactions to cause the collapse of the anchored alkyl groups ("bristles"). In the absence of mobile phase additives, such a balance occurs at water contents ranging between 30–50% (v/v). At lower water content or with acetonitrile as the organic mobile phase component, retention

Table 4
Retention data for selected probes on octadecyl silicas

Silica	Type[a]	Phenol, k'	Aniline, k'	Aniline, rel. A_s [b]	N,N-DMA, k'	Toluene, k'
Vydac TP	1	0.90	0.82	1.1 ± 0.1	3.03	4.14
Vydac TP	2	0.84	0.86	1.2 ± 0.1	2.83	3.05
YMC-Gel	1	2.12	1.75	1.2 ± 0.1	10.15	14.69
YMC-Gel	2	1.94	1.88	1.4 ± 0.2	10.06	12.33

[a] 1 = Conventional octadecyldimethylsilyl product; 2 = product of 1-octadecene hydrosilylation.
[b] Relative asymmetry factor = $A_{\text{s,aniline}}/A_{\text{s,phenol}}$.

of basic solutes is weaker and with well-shaped elution profiles. We have compared the behavior of these and many other compounds, including basic drugs, peptides and proteins and found N,N-DEA to be one of the most sensitive solutes to these interactions, as evidenced by increased retention concomitant with considerable band tailing. When the four packings of Table 4 were tested with N,N-DEA, they all exhibited broad and asymmetric chromatographic profiles to varying degrees. In some cases this compound eluted with very low recovery, as evidenced by peak area comparisons. Additionally, the probe showed decreasing retention times along with improving peak shape upon consecutive injections. These observations suggest that this compound is strongly adsorbed on scarce but highly active sites which are still accessible on the silica surface. These tailing-producing sites are rendered inactive by strong binding with the organic amine upon consecutive injections. This phenomenon which is much less pronounced in the case of N,N-DMA, aniline and other basic probes, including basic proteins, has also been reported by Kirkland and co-workers [14,25]. It should be pointed out, however, that we were unable to find any correlation between the degree of retention of N,N-DEA and the method of preparing the bonded phase. It seems, nevertheless, that the intrinsic adsorptivity of the silica substrate plays a considerable role in the remarkably slow desorption kinetics of this sensitive chromatographic probe as suggested by this and previous studies [14,25]. When the hydride intermediate was also examined with respect to the elution of N,N-DEA, again, strong retention along with substantial tailing was observed in varying degrees, depending on the native silica as well as the hydride-producing reaction conditions (namely TES, HCl and water concentrations, see Ref. [7]). A more extensive study of the use of N,N-DEA as a silanol-sensitive probe is currently underway. It should be pointed out that this behavior could not be anticipated from our extensive spectroscopic characterization of the hydrosilylation product and its hydride intermediate. Chromatography appears to be considerably more sensitive in this respect than spectroscopy.

The basic probes were also used to evaluate the occasionally observed effect of darkening of the bonded silica product during olefin hydrosilylation [6]. Product darkening is more pronounced at relatively high reaction temperatures (above 110°C) and has been attributed to the reduction of the Pt(II) catalyst complex to elemental platinum by the surface SiH groups [27,28]. The catalytic activity of platinum is significantly decreased or completely lost as a result of this reaction. The test mixture was injected into columns containing darkened C_8- and C_{18}-silicas. The results (not shown) consistently indicate strong tailing for basic probes and, again, particularly for N,N-DEA. The effect of decreasing retention times of this solute (and to a lesser extent that of N,N-DMA) upon repeated injections with concomitant peak shape improvement was more pronounced in the case of darkened bonded phases, indicating a stronger adsorption of the organic amine(s). Clearly, product darkening must be avoided by careful choice of the catalyst and/or the reaction temperature.

The ability of a C_{18}-bonded silica (prepared via olefin hydrosilylation) for the separation of a mixture of alkaloids containing five barbital derivatives is shown in Fig. 6. Clearly, baseline separation of all sample components with good peak shape is obtained in about 10 min. This separation is a typical example of the applicability of the new bonded phases to pharmaceutical analysis.

Another important application involves certain macromolecular solutes such as proteins which, due to their structural complexities, appear to be particularly susceptible to being tenaciously adsorbed on many reversed phases. The incorporation of TFA or low pH phosphate buffers into aqueous acetonitrile or 2-propanol solvent mixtures has resulted in improved peak shapes. In some cases, particularly in preparative separations, TFA is preferred because is easily removed from the separated fraction by lyophilization. We have already demonstrated that the new

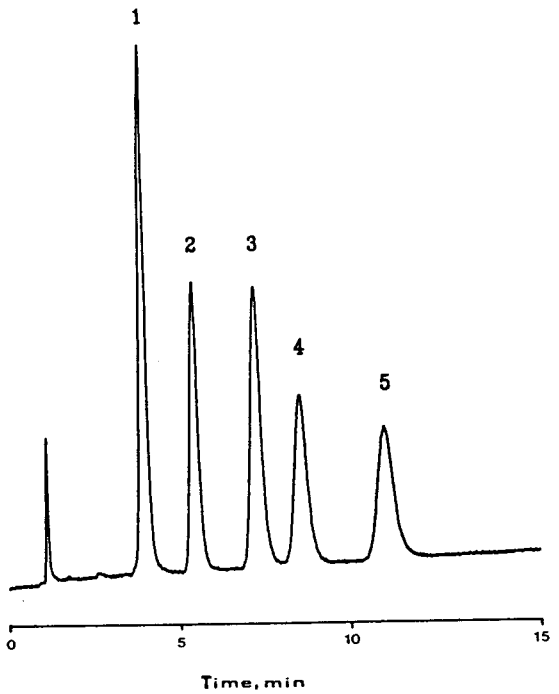

Fig. 6. RP separation of a commercial barbiturate mixture on a C_{18}-YMC-Gel prepared via hydrosilylation. Mobile phase: methanol–water (50:50) at 1.0 ml/min; sample injection: 10 μl; detection: UV at 220 nm. Peaks: 1 = butabarbital; 2 = amobarbital; 3 = secobarbital; 4 = phenobarbital; 5 = hexobarbital.

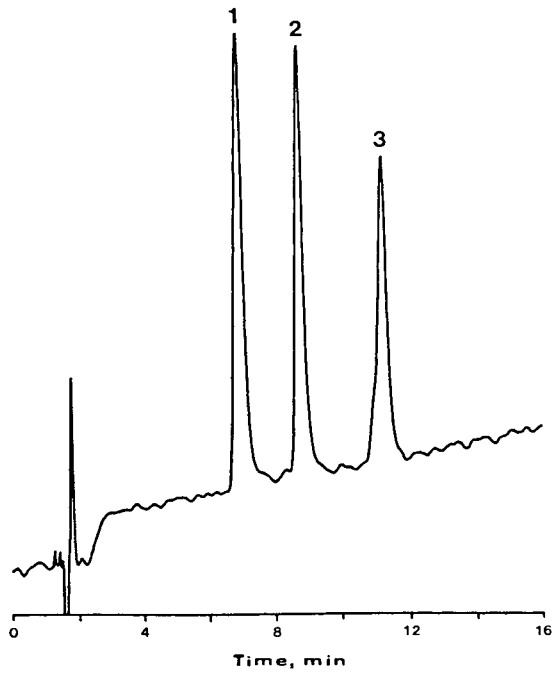

Fig. 7. RP-HPLC separation of peptides on C_{18}-YMC-Gel (10 μm, 13.8 nm) prepared via hydrosilylation. Mobile phase: solvent A: 0.10% (v/v) TFA in acetonitrile–water (75:25); solvent B: 0.10 (v/v) TFA in water. Linear gradient 25–45% A in 15 min. Flow-rate: 1.3 ml/min. UV detection at 214 nm. Injection: 5 μl of 0.5 mg/ml of each peptide. Peaks: 1 = bradykinin; 2 = angiotensin III; 3 = angiotensin I.

bonded phases which are the object of this study are very resistant to hydrolytic deterioration under these conditions. Gradient elution on C_4- and C_8-bonded, wide-pore silicas appears to provide satisfactory separation conditions for proteins. Smaller polypeptides are more commonly separated on narrow-pore C_{18} phases. The potential of C_{18}-YMC Gel (prepared also by olefin hydrosilylation) for the separation of three peptides is shown in Fig. 7. As illustrated in Fig. 8, a standard protein mixture of basic proteins can be separated with a C_8-Vydac TP phase. In all cases, similar chromatographic profiles (not shown) were obtained from columns packed with the same silica substrates modified in a conventional manner.

4. Conclusions

Evaluation of the alkyl-bonded phases prepared via olefin hydrosilylation on hydride-modified silica supports showed that, generally speaking, the selectivity of the new chromatographic phases resembles that of their conventional counterparts, alkyldimethylsilyl-bonded phases. Compared to conventional phases under particularly aggressive eluent conditions, more specifically those involving TFA-containing aqueous–organic solvents, the new bonded materials showed superior hydrolytic stability, as expected from a direct Si–C linkage formed upon olefin addition. Besides improving column longevity and long-term precision in retention,

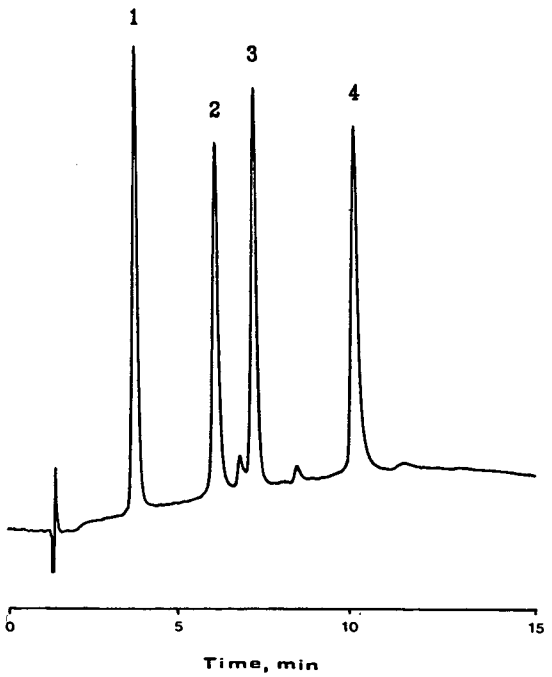

Fig. 8. Typical separation of a standard protein mixture on a C_8-Vydac TP (5.8 μm, 29.1 nm) prepared via hydride. Mobile phase: solvent A: 0.10% (v/v) TFA in acetonitrile–water (95:5), solvent B: 0.10% (v/v) TFA in water. Gradient: 25–100% A in 30 min at 1.5 ml/min. Sample injection: 5.0 μl of 0.4 mg/ml of each protein. Detection at 214 nm. Peaks: 1 = ribonuclease B; 2 = cytochrome *c*; 3 = lysozyme; 4 = myoglobin.

the hydrolytic advantage should reduce to a minimum the fraction contamination that might result from coelution of phase degradation by-products with the analyte(s) of interest.

The inherently deactivated surface underneath the anchored alkyl ligands provides for symmetric solute peaks. Nevertheless, darkening of bonded silicas during olefin silanization appears to have deleterious effect on the separation of organic amines, resulting in some cases in irreversible adsorption of certain solutes. Data presented here show that the irregular retention behavior of silanol-sensitive probes such as certain crown ethers cannot be described in the light of a dual-mechanism model.

Finally, the separating potential of C_8 and C_{18} phases prepared by the new method was demonstrated. Separation profiles of complex PAH mixtures indicate selectivity typical of monomeric stationary phases. Separation of alkaloids, polypeptides and proteins clearly confirmed the applicability of the new phases to the separation of a wide variety of samples.

Acknowledgements

This work was supported in part by The Separations Group, the National Science Foundation (CHE-9119933) and the Camille and Henry Dreyfus Foundation through a Scholar (J.J.P.) award. J. Fetzer and W. Biggs of Chevron Research and Technology are gratefully acknowledged for the BET analyses.

References

[1] L.C. Sander and S.A. Wise, *Adv. Chromatogr.*, 25 (1986) 139.
[2] D.C. Locke, J. T Schmermund and B. Banner, *Anal. Chem.*, 44 (1972) 90.
[3] K. Unger, W. Thomas and P. Adrian, *Kolloid Z. Z. Polym.*, 251 (1973) 45.
[4] J.J. Pesek and S.A. Swedberg, *J. Chromatgr.*, 361 (1986) 83.
[5] J.E. Sandoval and J.J. Pesek, *Anal. Chem.*, 61 (1989) 2067.
[6] J.E. Sandoval and J.J. Pesek, *Anal. Chem.*, 63 (1991) 2634.
[7] C. Chu, E. Jonsson, M. Auvinen, J.J. Pesek and J.E. Sandoval, *Anal. Chem.*, 65 (1993) 808.
[8] G.E. Berendsen, K.A. Pikaart and L. de Galan, *J. Liq. Chromatogr.*, 3 (1980) 1437.
[9] G.E. Berendsen and L. de Galan, *J. Liq. Chromatogr.*, 1 (1978) 561.
[10] J.L. Glajch, J.C. Gluckman, J.G. Charikofsky, J.M. Minor and J.J. Kirkland, *J. Chromatogr.*, 318 (1985) 23.
[11] J.L. Glajch, J.J. Kirkland and J. Köhler, *J. Chromatogr.*, 384 (1987) 81.
[12] J.N. Sagliano, T.R. Floyd, R.A. Hartwick, *J. Chromatogr.*, 443 (1988) 155.
[13] J.J. Kirkland, J.L. Glajch and R.D. Farlee, *Anal. Chem.*, 61 (1989) 2.
[14] J. Köhler, D.B. Chase, R.D. Farlee, A.J. Vega and J.J. Kirkland, *J. Chromatogr.*, 352 (1986) 275.
[15] L.C. Sander and S.A. Wise, *J. Chromatogr.*, 316 (1984) 163.
[16] L.C. Sander and S.A. Wise, *Anal. Chem.*, 56 (1984) 504.

[17] L.C. Sander and S.A. Wise, *Anal. Chem.*, 59 (1987) 2309.
[18] A. Nahum and Cs. Horváth, *J. Chromatogr.*, 203 (1981) 53.
[19] K.E. Bij, Cs. Horváth, W.R. Melander and A. Nahum, *J. Chromatogr.*, 203 (1981) 65.
[20] H. Engelhardt and H. Müller, *Chromatographia*, 19 (1984) 77.
[21] T. Hearn, in Cs. Horváth (Editor), *High Performance Liquid Chromatography —Advances and Perspectives*, Vol. 3, Academic Press, New York, 1983.
[22] H. Engelhardt and M. Jungheim, *Chromatographia*, 29 (1990) 59.
[23] H. Engelhardt, H. Löw and W. Götzinger, *J. Chromatogr.*, 544 (1991) 371.
[24] B.A. Bidlingmeyer and F.V. Warren, *Anal. Chem.*, 56 (1984) 1583A.
[25] J. Köhler and J.J. Kirkland, *J. Chromatogr.*, 385 (1987) 125.
[26] S.J. Schmitz, H. Zwanziger and H. Engelhardt, *J. Chromatogr.*, 544 (1991) 381.
[27] J. Chalk and J.F. Harrod, *J. Am. Chem. Soc.*, 87 (1965) 16.
[28] J.L. Speier, *Adv. Organomet. Chem.*, 17 (1979) 407.

ELSEVIER

Journal of Chromatography A, 688 (1994) 47–53

JOURNAL OF CHROMATOGRAPHY A

Determination of diethylenetriaminepentaacetic acid in pulp mill effluent by ion-interaction reversed-phase liquid chromatography

Desmond E. Richardson*, Gary H. Ash, Phillip E. Harden

Research Division, Australian Newsprint Mills Ltd., Boyer, Tasmania 7140, Australia

First received 3 March 1994; revised manuscript received 28 June 1994

Abstract

A method for analysing diethylenetriaminepentaacetic acid (DTPA) in pulp and paper mill effluent using ion-interaction reversed-phase liquid chromatography is presented. The analysis is based on formation of the iron(III) complex of DTPA and its separation on a C_{18} column using 4 m*M* octylamine in a water–acetonitrile mobile phase. A photodiode array detector is used in the analysis to enable peak purity of the Fe–DTPA peak to be compared between samples and standards. DTPA concentrations ranging from <1 to 200 mg l^{-1} may be measured using the technique. Elimination of the $FeCl_3$ reagent in the sample-preparation stage enabled the measurement of DTPA complexed to iron(III). This feature has been used to demonstrate that a significant proportion of the DTPA present in effluent is present in the iron form. The method has been applied to the analysis of DTPA in pulp and paper mill effluent at concentrations ranging from 1 to 20 mg l^{-1}. Recoveries of DTPA spiked into two sets of samples at levels of 2 and 4 mg l^{-1} averaged 102% with standard deviations of 12 and 16%, respectively. The use of the method to measure DTPA at various locations in the process has indicated that there was a major reduction in the DTPA concentration in pulp and paper mill effluent across the pulping and effluent treatment processes.

1. Introduction

Chelating agents are widely used in industrial processes and in detergents. Their use in the paper industry is primarily in association with hydrogen peroxide bleaching of pulp. One of the most efficient and widely used chelating agents is diethylenetriaminepentaacetic acid (DTPA) as it forms stable chelates with metals such as iron, manganese and copper, which are in pulp at concentrations of up to 100 mg kg^{-1}. In the absence of a chelating agent, these metals effect catalytic decomposition of hydrogen peroxide, thus reducing its efficiency and causing excessive usage of hydrogen peroxide to achieve a given level of brightness in the paper. Assuming no removal by chemical or biological means, DTPA concentrations in paper mill effluent could be as high as 100 mg l^{-1}. Chelating agents such as DTPA, nitrilotriacetic acid (NTA) and ethylenediaminetetraacetic acid (EDTA) have the potential to mobilise heavy metals from sediments [1,2], and to inhibit their removal by precipitation in effluent treatment processes [3]. While

* Corresponding author.

0021-9673/94/$07.00
SSDI 0021-9673(94)00874-4

these chelating agents are supposedly stable, there is evidence that in combination with iron(III), DTPA, NTA and EDTA may be photo degraded in sunlight [4].

Several methods are available for measuring the chelating agents NTA and EDTA in effluents by HPLC [5–7], GC [8,9] and polarography [10]. Methods published specifically for DTPA [11–14] include one where ion-interaction chromatography was used with Fe–DTPA formed in situ in the HPLC column [13].

This paper describes the formation of metal–DTPA complexes with the metal ions iron(III) and bismuth for determining DTPA in pulp and paper effluent using ion-interaction reversed-phase HPLC coupled with photodiode array UV detection for both qualitative and quantitative analysis. The metal–DTPA complex is formed prior to injection onto the HPLC so that, in the case of iron, exclusion of the metal reagent enables Fe–DTPA naturally present in the sample to be estimated. The method is applied to the analysis of effluents at various stages of the pulping and effluent treatment processes and show that DTPA is removed by either chemical, photochemical or biochemical degradation mechanisms.

2. Experimental

Water from a Waters Milli-Q apparatus was used to prepare all aqueous solutions. Analytical-reagent grade chemicals were used to prepare 0.1 *M* $FeCl_3$/0.1 *M* HCl and 0.1 *M* $Bi(NO_3)_3$/0.8 *M* HNO_3. A 50 m*M* octylamine (Aldrich) solution in acetonitrile (HPLC grade) was passed through an acetonitrile-rinsed C_{18} solid-phase extraction column (Analytichem Bondelut, part No. 607406). A 4 m*M* ion-interaction reagent (IIR) solution was prepared by diluting 160 ml of the 50 m*M* octylamine stock solution to 2 l with Milli-Q water. The IIR solution pH was then adjusted to 6 with 2 *M* H_2SO_4. The IIR solution made in this manner contained 8% CH_3CN. This solution was then filtered through a 0.2-μm nylon membrane filter and subjected to ultrasound for 10 min. A phosphate buffer was prepared by dissolving 65 g Na_3PO_4 in 1 l of water and adjusting to pH 8 with phosphoric acid.

A Varian 5060 HPLC system fitted with a Rheodyne 7126 injection valve (100-μl loop) and a Varian 9060 Polychrom photodiode array detector were used in this study. Two HPLC columns were used in this study, a 25 cm × 4 mm Econosil 10 μm C_{18} column (Alltech) and a 25 cm × 4 mm Alltima 5 μm C_{18} column, to each of which was fitted a Waters C_{18} precolumn. Samples were injected using a Varian 8050 autosampler and chromatographic data were processed with a Varian Star data system. The absorbance at 258 nm was used to detect the Fe–DTPA complex while Bi–DTPA was detected at 278 nm. The separations were performed isocratically at 2 ml min^{-1} using IIR solution and acetonitrile in proportions which caused the metal–DTPA solute to elute at about 4–6 min (usually 89% IIR solution and 11% CH_3CN).

The pH of either the DTPA standard (1–20 mg l^{-1} as the free acid) or an effluent sample was adjusted to 7. The metal–DTPA complexes were formed by adding either 2 ml of 0.1 *M* $FeCl_3$ or 0.2 ml of 0.1 *M* $Bi(NO_3)_3$ to 10 ml of sample. After standing for 15 min the solution was buffered to pH 7 by the addition of 2 ml of phosphate buffer to remove excess metal ions. The samples were then filtered through a 0.45-μm filter using an Alltech syringe filter device into an amber glass vial.

3. Results and discussion

3.1. Analytical method development

The newsprint mill at Albury in New South Wales (Australia) discharges its tertiary treated effluent into the River Murray. Environmental regulations require that the mill meet specific environmental licence limits in order to discharge effluent. The environmental licence regulation regarding DTPA required that it be measured as the total of free and chelated DTPA. It was therefore necessary to convert any metal–

DTPA complex to one where the conditional stability constant would be greater than that for any of the metals present in the effluent. Investigation of the effect of pH on conditional stability constants for iron and bismuth complexes of DTPA compared to those for other metals present in the paper mill effluent (Cu, Mn and Zn), clearly showed (Fig. 1) that formation of both bismuth and iron DTPA complexes is preferred over copper, zinc and manganese at pH < 6.5, while at pH > 8 the divalent metals have higher conditional stability constants. Alkaline earth cations such as magnesium and calcium, which form a significant proportion of the total cation content of the effluent being considered, have quite small stability constants relative to the heavy metals, and therefore do not compete in the chelation process. Formation of the appropriate complex (either iron or bismuth) was therefore thermodynamically favoured by keeping the pH at or below 7 in the sample preparation stage and by addition of an excess of the respective cation.

The chromatography of both iron(III)–and bismuth–DTPA complexes was quite similar with respect to retention and the effects of eluent strength and eluent pH upon retention. Using a mobile phase composition of about 89% IIR solution and 11% acetonitrile, Fe–DTPA eluted at $k' = 3.0$ ($N = 2220$) on the Alltech Econosil column, while Bi–DTPA eluted at $k' = 2.6$ ($N = 4040$). Fe–DTPA eluted on the Alltima column at $k' = 4.6$ with a much narrower peak width ($N = 14\,400$) than the Econosil column so the Alltima column was chosen as the preferred column for analysis of DTPA as the iron(III) complex. Fig. 2 shows chromatograms of 10 mg l^{-1} standards of the Fe–DTPA and Bi–DTPA complexes on the Alltima column.

The influence of eluent octylamine concentration on chromatographic performance was found to be significant. Increasing the octylamine concentration from 1 to 6 mM caused the retention time of both metal–DTPA complexes to increase in a linear fashion. This is consistent with the generally accepted mechanisms of ion-interaction chromatography [16]. The peak width at half height of the Fe–DTPA complex did not change significantly with the increased retention thus giving a marked improvement in column plate count with increase in IIR concentration.

The detection limit achieved by this technique was 0.2 mg l^{-1} when injecting a 200-μl sample and where iron was chosen as the complexing

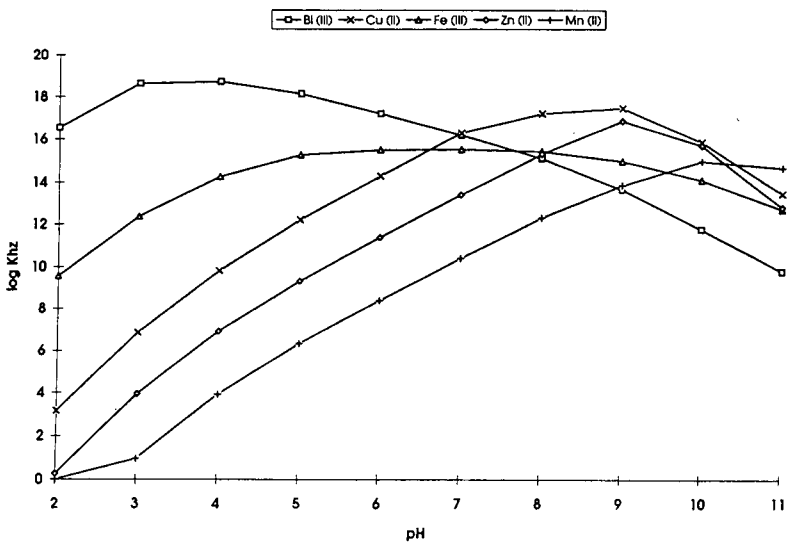

Fig. 1. Conditional stability constants of various metal–DTPA complexes as a function of pH. The curves were calculated from stability constant data supplied by Akzo Chemicals [15].

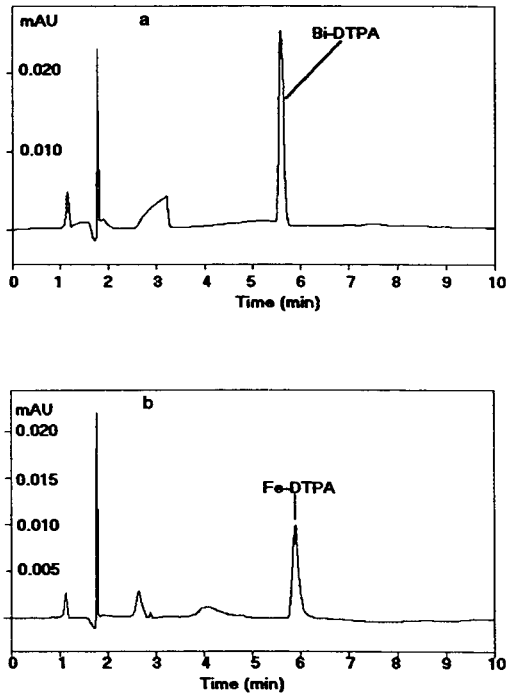

Fig. 2. Chromatogram of metal–DTPA complexes on 25 cm × 4 mm (5 μm) Alltech Alltima C_{18} column using 89% 4 m*M* octylamine (in acetonitrile–water, 8:92) and 11% acetonitrile at 2 ml min^{-1}, 100-μl injection loop: (a) 10 mg l^{-1} DTPA as Bi–DTPA, detection wavelength 278 nm; (b) 10 mg l^{-1} DTPA as Fe–DTPA, detection wavelength 258 nm.

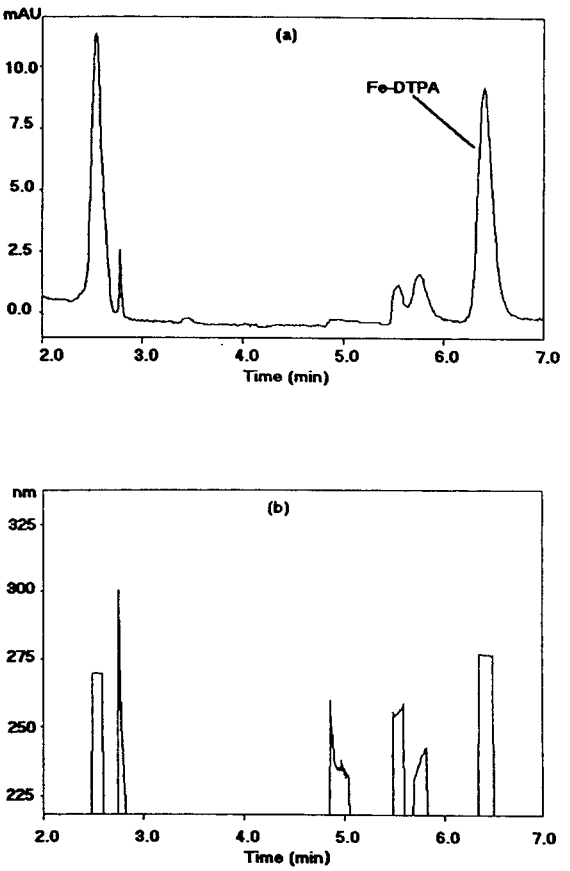

Fig. 3. Application of peak purity procedures to an effluent sample. (a) Chromatogram of effluent sample showing Fe–DTPA peak at 6.4 min. DTPA concentration 8.5 mg l^{-1}. Conditions as in Fig. 2. (b) Purity parameter profile across chromatogram.

metal. The greater plate count achieved for Bi–DTPA compared to Fe–DTPA would suggest that bismuth is a more suitable metal for achieving low detection limits. However the recovery rate in effluent samples for DTPA as Bi–DTPA was variable between 50 and 100% and therefore bismuth was considered an unsuitable chelating metal. The calibration curve for Fe–DTPA was linear over the range 2–40 mg l^{-1}, while the standard deviation in peak area associated with injections of standards was 4.6% ($n = 20$).

The ability to qualitatively determine an analyte adds an extra dimension to an analytical method. The use of photodiode array detection enabled this to be achieved in the case of Fe–DTPA. The chromatogram in Fig. 3a is of an effluent sample containing about 8.5 mg l^{-1} of DTPA, while directly underneath the chromatogram in Fig. 3b is the purity parameter profile for the chromatogram. The purity parameter is a measure of peak purity calculated from the absorbance-weighted mean wavelength for a specified wavelength range. For Fe–DTPA over the wavelength range 220–367 nm, the purity parameter averaged 276.776 ± 0.356 nm over the sample peak compared to a value of 276.933 ± 0.215 nm across a 10 mg l^{-1} standard peak. A level profile across a peak as shown in Fig. 3b is

also a visual indicator of the absence of any interfering compound.

The concept of peak purity was useful in this work to determine which of iron(III) and bismuth was the better metal to use as the chelating metal. It was observed for those samples in which bismuth was used as the chelating metal that the peak purity profile was not as level as for iron and that the peak purity parameter in a sample matrix was significantly different to that in the standard. These factors therefore precluded the use of peak purity as a qualitative tool in the case of Bi–DTPA. Although Bi–DTPA gave a narrower peak than Fe–DTPA, the fact that its peak purity profile was not level in standards and spiked samples, and that recovery of spiked DTPA in some sample matrices was not quantitative, lead to the conclusion that bismuth was less suitable than iron as the chelating metal for this analysis.

In contrast to methods based on ion chromatography in acidic eluents [13,14], our reversed-phase ion-interaction separation at pH 6 enables some speciation studies to be performed. DTPA present in the sample as Fe–DTPA was measured by leaving out the $FeCl_3$ reagent in the sample preparation stage. Examination of the UV spectrum and peak purity data for the Fe–DTPA peak in unfortified samples showed no differences to those of samples to which excess Fe^{3+} had been added.

3.2. Application of method to mill effluent samples

DTPA which is already complexed to metals other than the metal added in the sample preparation stage, must be released to form the more thermodynamically stable metal–DTPA chelate in order that total DTPA is measured. While the use of iron(III) as the metal ion was capable of this thermodynamically, it was necessary to ensure that this reaction was kinetically favourable. To demonstrate this, DTPA was added to two effluent samples for which the DTPA concentration had already been measured, after which the samples were left in the dark for 14 days to allow equilibration with metal ions present in the sample. A parallel sample containing no added DTPA was similarly stored. After 14 days, the spiked sample was analysed for DTPA and the unspiked sample was spiked with the same amount of DTPA just prior to addition of the $FeCl_3$ reagent. As the numbers in Table 1 show, the Fe–DTPA complex formed within the time allowed for in the method. The time that the sample was allowed to stand between addition of the chelating metal and the filtration step was

Table 1
Effect of equilibration time on metal–DTPA formation

	DTPA concentration (mg l^{-1})[a]	
	Untreated effluent	Treated effluent
Unspiked DTPA	20.0 ± 1.2	2.1 ± 0.1
Spiked (10 mg l^{-1}) DTPA (15 min equilibration)	32.7 ± 0.5	13.7 ± 0.5
Spiked (10 mg l^{-1}) DTPA (after 14 days equilibration)	31.0 ± 0.1	13.2 ± 0.3

[a]Untreated effluent is taken from a paper mill effluent prior to a biological treatment stage and contains higher amounts of DTPA than treated effluent which has undergone primary, secondary and tertiary treatment. Results are shown as mean ± one standard deviation.

also varied and 15 min was found to be sufficient to allow quantitative formation of the metal–DTPA complex.

The method based on iron(III) as the chelating metal has been applied to the analysis of DTPA in pulp and paper mill effluent over a period of some two years during which time the validity of the method has been assessed by spiking the sample with a known amount of DTPA. Samples from two locations at the mill were routinely analysed twice weekly. One was spiked at the rate of 2 mg l^{-1} while the other was spiked at the rate of 4 mg l^{-1}. The recovery of DTPA from these samples over a four month period was 102% (standard deviation 12%, $n = 32$) and 102% (standard deviation 16%, $n = 32$) respectively.

The technique has also been successfully applied to the analysis of DTPA in effluent from different stages in the pulping process and effluent treatment process, and has been instrumental in determining that DTPA is in fact degraded in these processes. Fig. 4 shows the mass discharge of DTPA at various points across the process calculated from the measured DTPA concentration and average effluent flow-rate. Compared to that used in the pulping process (an average of 217 kg day^{-1}), an average of 86 kg day^{-1} of DTPA is discharged from the pulping process, while an average of 16 kg day^{-1} is discharged in the final effluent. Clearly, DTPA is degraded in the pulping and effluent treatment process.

Measurement of DTPA as iron-bound DTPA in effluent samples has shown that the iron form of DTPA could account for anything from 2 to 100% of the total DTPA present, with the average being around 50% for the mills final effluent. Iron could therefore exert an important influence on the chemistry of DTPA, so it was necessary to consider a factor that leads to the degradation of DTPA, photooxidation in the presence of iron(III) [4], in sample handling. Samples were protected from exposure to light by collecting them into a light-protected black polyethylene container. Similarly samples prepared for chromatography were also stored in dark glass vials. The large proportion of DTPA normally present as Fe–DTPA also meant that photooxidation could play an important role in the degradation of DTPA in the mills effluent system in those areas where the effluent is exposed to light.

4. Conclusions

The use of ion-interaction reversed-phase liquid chromatography to determine DTPA as the iron(III) complex has enabled DTPA in pulp and

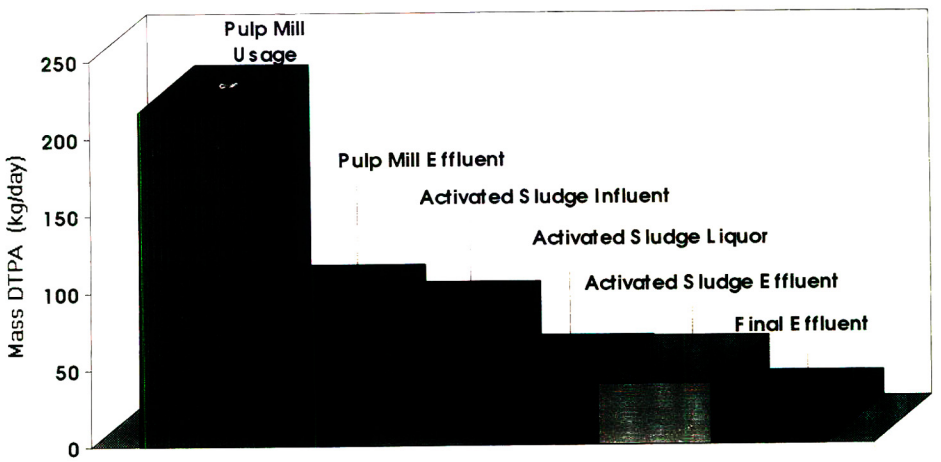

Fig. 4. Average mass daily discharge rates for DTPA at various locations in the mill effluent treatment system compared to daily usage.

paper mill effluent to be determined as both total and iron-bound forms. While bismuth was also found to chelate with DTPA, poor recoveries from some sample matrices and poor reproducibility of peak purity data excluded use of this metal from further investigation. The method has been used routinely to measure DTPA at different stages in the mill's effluent treatment process for over two years with the ability to qualitatively measure the peak purity of the Fe–DTPA peak as it elutes. The data shows that DTPA is significantly reduced in concentration within the mill's process water circuit prior to discharge to the mill's effluent treatment system. Some further reduction in concentration occurred across the biological stage and across the holding lagoon. The ability of the technique to analyse DTPA complexed to iron (Fe–DTPA) shows that the predominant form of DTPA in effluent samples is as Fe–DTPA, and this has implications in the study of degradation routes.

Acknowledgements

The permission of Australian Newsprint Mills Ltd. (ANM) to publish this work is gratefully acknowledged. Collection of samples by staff at the ANM Albury mill is also appreciated.

References

[1] J.L. Means, D.A. Crerar and J.O. Duguid, *Science*, 200 (1978) 1477–1481.
[2] V. Samanindou and K. Fytianos, *Water, Air Soil Pollut.*, 52 (1990) 217–225.
[3] R. Perry, P.W.W. Kirk, T. Stephenson and J.N. Lester, *Water Res.*, 18 (1984) 255–276.
[4] A. Svenson, L. Kaj and H. Bjorndal, *Chemosphere*, 18 (1989) 1805–1808.
[5] D.G. Parkes, M.G. Caruso and J.E. Spradling III, *Anal. Chem.*, 53 (1981) 2154–2156.
[6] J. Harmsen and A. van den Toorn, *J. Chromatogr.*, 249 (1982) 379–384.
[7] W. Buchberger, P.R. Haddad and P.W. Alexander, *J. Chromatogr.*, 546 (1991) 311–315.
[8] C. Schaffner and W. Giger, *J. Chromatogr.*, 312 (1984) 413–421.
[9] M.A. Ribick, M. Jemal and A.I. Cohen, *J. Pharm. Biomed. Anal.*, 5 (1987) 687–694.
[10] Z. Stojek and J. Osteryoung, *Anal. Chem.*, 53 (1981) 847–851.
[11] J. Dai and G.R. Helz, *Anal. Chem.*, 60 (1988) 301–305.
[12] M.M. Vora, S. Wukovnig, R.D. Finn, A.M. Emran, T.E. Boothe and P.J. Kothari, *J. Chromatogr.*, 369 (1986) 187–192.
[13] V. Huber, *Acta Hydrochim. Hydrobiol.*, 20 (1992) 6–8.
[14] C. Randt, R. Wittlinger and W. Merz, *Fresenius' J. Anal. Chem.*, 346 (1993) 728–731.
[15] P. Lenthe, Akzo Chemical Co., personal communication.
[16] P.R. Haddad and P.E. Jackson, *Ion Chromatography —Principles and Applications* (*Journal of Chromatography Library*, Vol. 46), Elsevier, Amsterdam, 1990.

ELSEVIER

Journal of Chromatography A, 688 (1994) 55–65

JOURNAL OF CHROMATOGRAPHY A

Application of the particle beam interface to high-performance liquid chromatography–thermal energy analysis and electron impact mass spectrometry for detection of non-volatile N-nitrosamines

Stanley M. Billedeau*, Thomas M. Heinze, Jon G. Wilkes, Harold C. Thompson, Jr.

Food and Drug Administration, National Center for Toxicological Research, HFT-230, 3900 NCTR Road, Jefferson, AR 72079, USA

First received 15 June 1994; revised manuscript received 12 September 1994

Abstract

Interest in the analysis of non-volatile N-nitrosamines has recently been renewed due to the development of several new reversed-phase HPLC interfaces to thermal energy analysis (TEA) or chemiluminescence detection. A new application of a counter flow gas diffusion cell (CFGDC)-based particle beam LC interface (Universal Interface, Vestec) is described for the HPLC–TEA analysis of the non-volatile N-nitrosamines, N-Nitrosodiethanolamine (NDELA) and N-nitrosomethyl-*p*-amino-2-ethylhexylbenzoate (NMPABAO). The interface incorporates a thermospray vaporizer, desolvation chamber, and CFGDC to reduce the LC effluent to a dry aerosol and a single-stage momentum separator to form a particle beam of the non-volatile analyte. Using this system, the LC–TEA response to NDELA was linear in the range 6–200 ng total amount injected. Several experiments are reported indicating the effect of thermospray tip temperature, He carrier flow-rate, and mobile phase composition on TEA response. Minimum detection limits (5 ng NDELA injected on column) are comparable to other LC–TEA interfacing methods. Several advantages over existing methodology which include ease of use, ruggedness and MS compatibility are discussed. Additional LC–particle beam MS data are reported indicating that full scan electron impact MS identification of the N-nitrosamine contaminants in cosmetics is possible for confirming TEA detection data.

1. Introduction

In recent years, the emphasis on analysis of non-volatile N-nitrosamines in foods, beverages, cosmetics and various other consumer products [1–4] has increased due to GC–thermal energy analysis (TEA) data confirming the presence of potentially carcinogenic volatile N-nitrosamines in such products. The lack of technology for interfacing reversed-phase HPLC with TEA, a detection method primarily used for GC analysis of N-nitroso compounds, has resulted in the development of two such interfaces, a KI/HOAc postcolumn reaction interface [5] and a UV photolysis-based interface [6]. Both of these interfaces are based on reactions which involve

* Corresponding author.

SSDI 0021-9673(94)00894-9

liberation of nitric oxide (NO gas) from the N-nitroso moiety rather than from pyrolysis as performed in the typical GC–TEA mode [7]. The liberated NO(g) and LC solvent is then swept by a flow of carrier gas into a series of cold traps which remove the LC mobile phase and residual vapors. The NO(g) survives the cold traps, enters the TEA detection cell, is mixed with ozone gas, and the resulting chemiluminescence detected using a sensitive photomultiplier tube. These two TEA interfacing techniques, although highly sensitive (1–10 ng total compound injected) and selective for a variety of N-nitroso compounds, are not suited to coupling with mass spectrometry (MS) due to the destructive reactions employed which alters the eluting compounds.

Recently, an US Food and Drug Administration (FDA) intra-agency collaboration was developed between the National Center for Toxicological Research (NCTR) and the Center for Food Safety and Applied Nutrition (CFSAN), Office of Cosmetics and Colors, Cosmetic Technology Branch, involving detection and identification of non-volatile N-nitroso compounds in cosmetics and their raw materials. The major objective of this project is to discover possible N-nitroso carcinogens in cosmetics for skin care, creams, lotions, or other long-term skin contact products, previously unreported in analytical tests. For identification of unknown non-volatile N-nitroso contaminants in these products, it was advantageous to perform HPLC–TEA analysis for flagging compounds of interest as possible N-nitroso carcinogens, as well as parallel HPLC–MS analysis on the intact compound to supply additional molecular mass, fragmentation, or functional group data for identifying TEA peaks of interest.

In this study, an HPLC–TEA interface is described utilizing a particle beam (PB) type of instrumentation developed initially for interfacing HPLC to MS [8]. The high solvent removal efficiency of this PB interface has made possible HPLC–TEA analysis with reversed-phase solvents (e.g. MeOH, water, CH_3CN,) without the need for solvent venting [9] or cryogenic trapping techniques [5,6] currently being used in alternative HPLC–TEA interfaces. The Vestec Model 702 B universal interface incorporates a thermospray vaporizer, desolvation chamber and counterflow gas diffusion cell (CFGDC) using a high counterflow (about 2 l/min) of helium to reduce the LC effluent to a dry aerosol of the intact non-volatile N-nitrosamine analyte. A single-stage momentum separator (specially designed for TEA) was used to form the particle beam which was directed into a 550°C pyrolysis tube of a Thermo Electron TEA Model 502 operated at 1.5 Torr vacuum (1 Torr = 133.322 Pa). To demonstrate the utility of the device, two non-volatile N-nitrosamines, N-nitrosodiethanolamine (NDELA) and N-nitrosomethyl-*p*-amino-2-ethylhexylbenzoate (NMPABA-O), were studied to test the sensitivity, reproducibility and linearity of response of the HPLC–PB-TEA system. An extraction method reported by Meyer and Powell [9] was modified for use in analysis of cosmetics by HPLC–PB-TEA. The application of this method for analysis of a skin care cosmetic product was successful in detecting NMPABAO contamination as well as several unknown TEA responding peaks.

2. Experimental

2.1. Standards and reagents

All solvents were distilled-in-glass HPLC grade or equivalent and all reagents were certified ACS grade or equivalent.

Non-volatile N-nitrosamine standards and cosmetic samples: the NDELA and NMPABAO standards and cosmetic samples in this study were obtained from the FDA, Center for Food Safety and Applied Nutrition, Cosmetics Section, Washington, DC, USA. The N-nitrosopyrrolidine (NPYR) and N-nitrosodibutylamine (NDBA) were obtained from Eastman Kodak (Rochester, NY, USA) The N-nitrosodiphenylamine (NDiPhA) was purchased from Sigma (St. Louis, MO, USA).

Nitrosation inhibitor: a solution containing 20 mg/ml hexyloxyaniline (HOA) in dichloromethane–hexane (1:9, v/v) was used to inhibit formation of N-nitrosamines during extraction. A 1-g quantity of HOA was dissolved in 5 ml

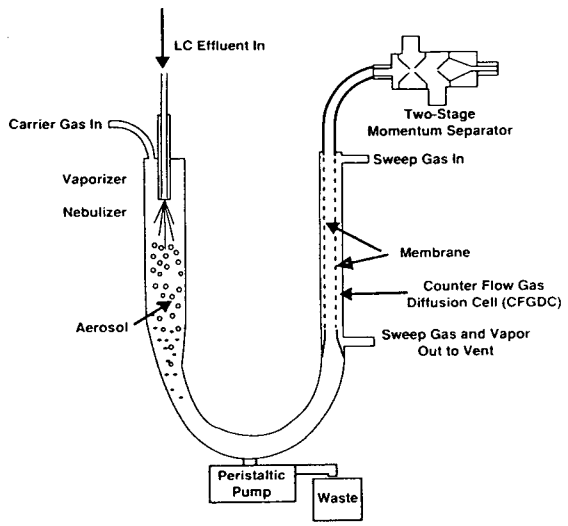

Fig. 1. Diagram of the Vestec separator, which includes the universal interface and a two-stage momentum separator.

dichloromethane and subsequently diluted to 50 ml total volume with hexane.

Ammonium acetate: the ammonium acetate used to make up HPLC mobile phase(s) was purchased from Fluka with a purity of >99%.

Safety note: N-nitrosamines are an extremely hazardous class of compounds and should be handled with the utmost caution.

2.2. PB-TEA

A diagram of the universal interface is shown in Fig. 1. Up to 1.5 ml/min flow of an HPLC mobile phase effluent is delivered to a heated capillary tube with a 0.75 mm thermospray vaporizer tip. The volatile mobile phase and non-volatile analyte(s) are nebulized into a heated desolvation chamber with a 2 l/min helium carrier. Larger droplets of solvent are removed to waste by a peristaltic pump connected to the bottom of a J-tube. The aerosol effluent from the J-tube is directed into the CFGDC where a PTFE membrane operated with a counterflow of He gas at 4.5 l/min removes most of the remaining solvent vapors to a waste receptacle. The resulting dry aerosol is passed through a 4 mm I.D. PTFE tubing into a stainless-steel single-stage momentum separator with a focusing nozzle (0.4 mm) impinging on a skimmer cone (0.6 mm). Residual solvent vapors are reduced further by diffusion of small molecules into the vacuum in the region between the nozzle and skimmer; the less volatile analyte, present as relatively large residual particles in the aerosol, is transmitted as a beam of high momentum particles past the skimmer orifice. As shown in Fig. 2, this particle beam of intact N-nitroso compound persisting through the skimmer is connected via a specially designed stainless-steel flange and delivery tube into the 550°C pyrolysis tube of a Thermo Electron Model 502 TEA operated at 1.5 Torr vacuum. A filter cartridge (CRT gas stream filter; Thermedics, Waltham, MA, USA) was used as a final filter to remove residual pyrolysis products. Following the filter, the pyrolysis product of the N-nitroso compound, nitric oxide (NO gas), is mixed with ozone electrically generated from an oxygen flow of 10 ml/min (on the flowmeter) in the TEA

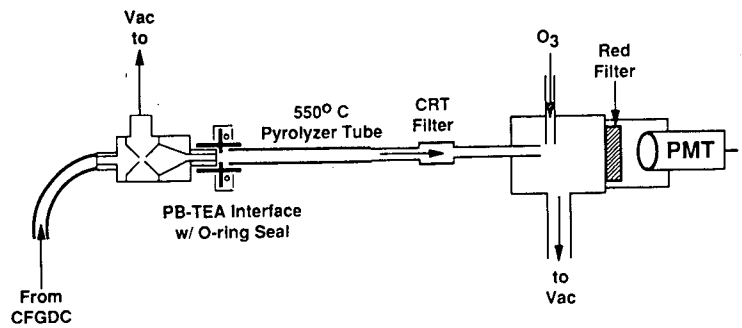

Fig. 2. Diagram of the PB-TEA interface with single-stage momentum separator and TEA detector. PMT = Photomultiplier tube; w/ = with; Vac = vacuum.

detector cell where the resulting chemiluminescence is detected by an extremely sensitive photomultiplier tube.

2.3. HPLC system

A Spectra-Physics Model 8800 ternary HPLC pump capable of operation in either isocratic or solvent programming mode was used to pump 1 ml/min of mobile phase into the appropriate HPLC column. An Altex Model 210 HPLC injector with a 50-μl loop was used for all standard and sample injections. A Supelcosil LC-18, 5 μm, 250 × 4.6 mm column operated isocratically at 1 ml/min of 5% MeOH–water (0.05 *M* ammonium acetate) was used to perform the initial NDELA experiments to test the feasibility of HPLC–PB-TEA analysis. A SynChropak SCD-100 (SynChrom, Lafayette, IN, USA), 250 × 4.6 mm column, solvent programmed at 1 ml/min of A–B (70:30) (start) to A–B (15:85) (final) in 8 min held for 5 min, was used for initial studies on TEA detection of NMPABAO. A MetaChem C_8, 5 μm, 250 × 4.6 mm column, with a solvent program of A–B (20:80) (start) to A–B (5:95) (final) in 2 min held for 13 min, was used for the analysis of cosmetic samples by electron impact (EI) MS. Mobile phase A = 100% aqueous 0.025 *M* ammonium acetate. Mobile phase B = 95% acetonitrile–water (saturated with ammonium acetate).

2.4. Mass spectrometers

A Vestec Model 201 quadrupole mass spectrometer was used to perform the initial PB-EI-MS experiments. The N-nitrosamine standards were flow injected into the PB-EI-MS system using MeOH–water (0.05 *M* ammonium acetate/1% acetic acid) (75:25) mobile phase flowing at 1 ml/min. The NDELA and NMPABAO were diluted in mobile phase to 100 ng/μl in separate flasks. A 70 eV EI mass spectrum, 150 μA emission, of 20-μl aliquots (2 μg total) of each compound was acquired by scanning the range from 46 to 400 u. The universal interface operating parameters were 60°C = T_1 (control temperature), 132°C = T_2 (thermospray tip temperature), 121°C = momentum separator temperature, 65°C = membrane separator temperature, and 2 l/min He carrier flow.

A Finnigan Model 4500 quadrupole mass spectrometer was used to perform the PB-EI-MS confirmational analysis on actual cosmetic extracts. A MetaChem C_8 250 × 4.6 mm column was used for cosmetic analysis. The MS conditions were 70 eV and 150 μA emission scanned from 50 to 350 u. The universal interface conditions were 112°C = T_2, 132°C = momentum separator temperature, 55°C = membrane separator temperature, and 2 l/min He carrier flow.

2.5. NDELA linearity

Standard solutions of NDELA containing 125, 250, 500, 1000, 2000 and 4000 ng/ml in MeOH–water (0.05 *M* ammonium acetate) (3.75:96.25) were prepared for HPLC–PB-TEA analysis for determining the minimum detection limit (MDL) and linearity. Triplicate 50-μl injections of these NDELA standards were analyzed on a Supelcosil C_{18} (previously described) using the diluent solution as an isocratic mobile phase at 1 ml/min. Interface parameters, T_2 and He carrier flow, were 140°C and 2 l/min, respectively. The retention for NDELA was 4.7 min on the HPLC–PB-TEA system.

2.6. Effect of variation of He carrier flow-rate upon response for NDELA using flow injection analysis–PB-TEA

The effect of varying the He carrier flow of the PB interface on the TEA response was determined by analyzing triplicate 50-μl injections of a 4 μg/ml NDELA standard solution (200 ng total injected) with He flow-rates of 1.0, 2.0, 3.0 and 4.0 l/min with all other variables remaining constant. A flow injection analysis method for HPLC–PB-TEA was used to reduce the time between assays and eliminate any variables which may be introduced by the HPLC column. The mobile phase and standard diluent were MeOH–water (0.05 *M* ammonium acetate) (3.75:96.25). The He counterflow on the

CFGDC was kept at twice the He carrier flow for each determination as recommended by the instrument manual for the interface.

2.7. Effect of ammonium acetate concentration in the mobile phase upon HPLC–PB-TEA response for NDELA

Duplicate injections of a 4 μg/ml NDELA standard were analyzed on the HPLC–PB-TEA system using concentrations of ammonium acetate 0, 0.01, 0.02 and 0.04 *M* in the mobile phase (MeOH–water, 3.75:96.25). A Supelcosil C_{18} column, 5 μm, 250 × 4.6 mm, was used with 1 ml/min flow of each mobile phase after equilibration with at least five column volumes of mobile phase prior to analysis.

2.8. Effect of thermospray tip temperature upon PB-TEA response for NMPABAO

A SynChropak SCD-100 column, 100 Å pore size, 250 × 4.6 mm, was used to perform HPLC separation of a NMPABAO standard (20 μl injected of 100 μg/ml). The mobile phase was acetonitrile–water (0.025 *M* ammonium acetate) (60:40) with 1 ml/min flow-rate. The tip temperature (T_2) of the thermospray was varied from 80 to 150°C in 10°C increments with the momentum and membrane separators kept constant at 130 and 60°C, respectively. Duplicate analyses were performed at each 10°C change in T_2.

2.9. Simplex optimization of TEA response for NMPABAO using flow injection–PB-TEA

The three interactive interface parameters, T_2, P_{ch} (desolvation chamber potentiometer setting), and He carrier flow-rate, were optimized using a Simplex optimization method [10,11]. Flow injection analysis was used to inject 50-μl aliquots of a 20 μg/ml NMPABAO standard for each experiment. Four different experiments were performed using different values for each of the interactive parameters listed. The TEA response (peak area) was used to rank the four experiments (BEST = highest TEA response, WORST = lowest TEA response). The average (P) of the top three values for each factor was the WORST (W) values to give $P - W$ values. A fifth experiment, R, was performed where $R = P + (P - W)$ and a sixth experiment, C_r, an example of variable-size Simplex optimization [11], where $C_r = P + (P - W)/2$. It should be pointed out that this is only an abbreviated example of Simplex optimization for PB-TEA and that several iterations of these experiments must be performed, discarding the W values and recalculating a new set of experiments to arrive at a comprehensive optimum.

2.10. Cosmetic extraction procedure

A 1.00-g sample of a skin cream, skin lotion or other cosmetic sample was weighed into a 15-ml tube with a PTFE-lined cap. A 50-μl aliquot of the HOA, nitrosation inhibitor, was added directly to the sample and vortexed thoroughly to mix. Sodium chloride (0.5 g) was added and vortexed again to reduce foaming. A 5-ml volume of hexane was added and vortexed and/or shaken for 5 min. The tube was centrifuged at 2000 *g* for 15 min at room temperature. The hexane extract (top layer) was transferred with a disposable pipet to a 15-ml graduated centrifuge tube with a PTFE-lined cap. The extract was concentrated by evaporating the hexane via nitrogen blowdown on a 60°C water bath. The oily residue was vortexed with exactly 1 ml of acetonitrile and centrifuged as before to separate the phases. A clear top layer with a slightly pink color due to the HOA was then analyzed by HPLC–PB-TEA and EI-MS.

2.11. Analysis of cosmetic extract using HPLC–PB-TEA

A 30-μl aliquot of the 1 ml acetonitrile extract was injected into a MetaChem C_8 HPLC column, 5 μm, 250 × 4.6 mm, using A–B (85:15) (6 min hold) to start and linear solvent programming to 100% A in 25 min. The HPLC flow-rate was 1 ml/min throughout the HPLC analysis. The interface conditions were T_2 = 124°C, momentum separator = 125°C and membrane

separator = 56°C. The TEA system was operated at 550°C pyrolyzer temperature, 1.5 Torr vacuum, and 10 ml/min ozone flow. Mobile phase A = acetonitrile–water (90:10), saturated ammonium acetate. Mobile phase B = 100% aqueous ammonium acetate (0.025 *M*).

3. Results and discussion

3.1. Initial PB experiments on N-nitrosamines using TEA and EI-MS

Standards of several N-nitrosamines, NDBA, NPYR, NDiPhA, NDELA, and NMPABAO, were subjected to EI-MS detection using flow injection analysis coupled with the universal interface. The volatile N-nitrosamines, NDBA and NPYR, showed no EI-MS response probably due to volatility losses during the desolvation steps prior to forming the aerosol particles. The NDiPhA, NDELA and NMPABAO were all successful in producing EI-MS spectra indicating good particle beam transport through the interface. The EI-MS spectra of NDELA and NMPABAO are shown in Fig. 3. The NDiPhA (M_r 198) spectra (not shown) identified the formation of some type of dimer ($M_r > 260$) apparently in the particle beam interface since an EI library 70 eV mass spectrum is available in our National Institute of Standards and Technology (NIST) database.

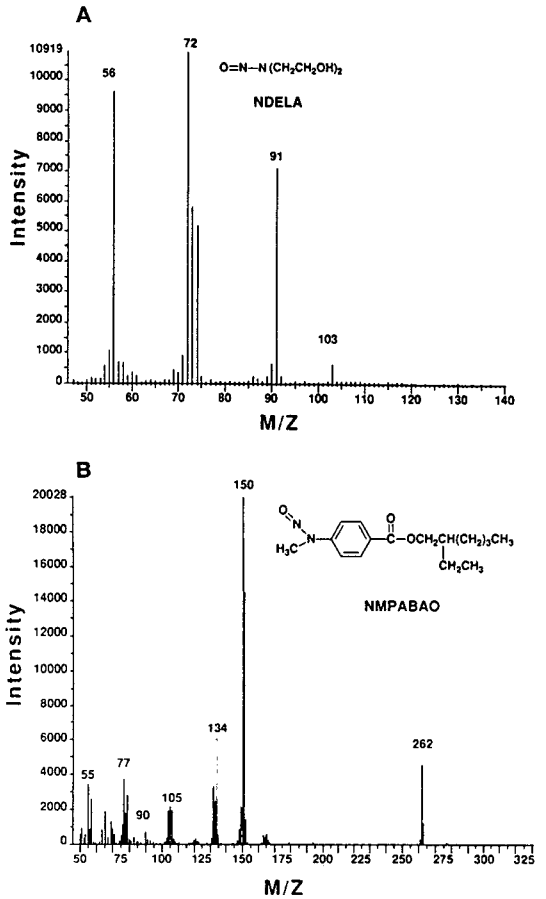

Fig. 3. Full-scan EI-MS of (A) NDELA and (B) NMPABAO using flow injection analysis coupled with PB-MS.

3.2. NDELA sensitivity and linearity study

After installation of the universal interface to the TEA system, flow injection analysis with 1 ml/min flow of MeOH–water (0.05 *M* ammonium acetate) (75:25) was used to test the response of the PB-TEA to NDELA standard injections.

The first HPLC column used to effect a separation of NDELA for HPLC–PB-TEA was a reversed-phase C_{18} which showed little retention of NDELA with the same flow injection mobile phase used previously. A MeOH–water (0.05 *M* ammonium acetate) (3.75:96.25) mixture eluted the NDELA in about 5 min at 1 ml/min from the C_{18} column (see Fig. 4). Using these HPLC conditions for PB-TEA analysis, the TEA response was shown to be linear for NDELA in the range 6–200 ng total compound injected with a correlation coefficient of 0.99901 and r^2 of 0.99802. The minimum detection limit for NDELA was 5 ng total injected on column.

3.3. Effects of thermospray tip temperature, He carrier flow, and ammonium acetate concentration on PB-TEA response to NDELA

Several experiments were performed to determine the effect of certain interface parameters on the sensitivity of response of the TEA. Data

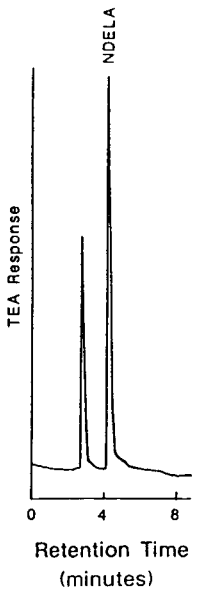

Fig. 4. HPLC–PB-TEA chromatogram of 750 ng NDELA standard injected on a Supelcosil LC-18, 5 μm, 250 × 4.6 mm column operated isocratically at 1 ml/min of MeOH–water (0.05 *M* ammonium acetate) (5:95).

presented in Fig. 5 and Table 1 has shown TEA sensitivity to be extremely dependent on thermospray tip temperature (T_2) and He flow with optimum response resulting at 110°C and 2.0

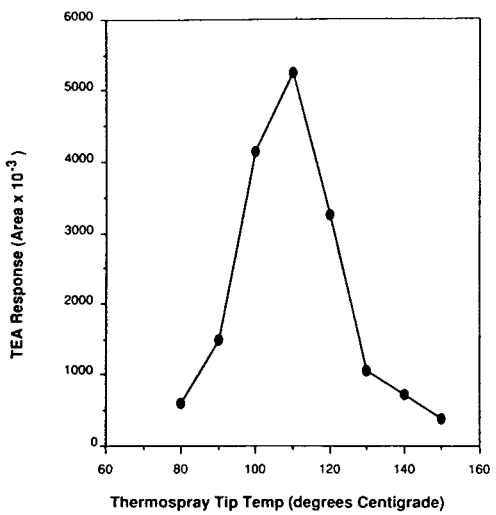

Fig. 5. Plot of TEA response versus thermospray tip temperature for HPLC–PB-TEA of NMPABAO.

Table 1
Effect of variation of flow-rate of helium carrier upon TEA response to NDELA (200 ng total amount injected) using flow injection analysis

He carrier flow (l/min)	NDELA response on TEA (mm peak height)			
	Inj 1	Inj 2	Inj 3	$\bar{x} \pm$ SD
1.0	84	83	87	85 ± 2
2.0	85	92	85	87 ± 4
3.0	74	74	71	73 ± 2
4.0	47	50	51	49 ± 2

Thermospray tip temperature (T_2) = 140°C; HPLC mobile phase = MeOH–water (0.05 *M* ammonium acetate) (3.75:96.25); spray chamber potentiometer setting (P_{ch}) = 2.80; momentum separator = 130°C; membrane separator = 60°C; He purge flow = 2 × carrier flow (l/min).

l/min, respectively, for NDELA at the prescribed HPLC conditions. The results shown in Table 2 indicated that a concentration in the range 0.02–0.04 *M* ammonium acetate must be present in the mobile phase for the best NDELA response on HPLC-PB-TEA. However, the smallest concentration of ammonium acetate giving optimum TEA response is recommended

Table 2
Relationship of ammonium acetate concentration in HPLC mobile phase to NDELA desolvation losses on universal interface as measured by TEA response using flow injection analysis

Ammonium acetate molarity (*M*)	TEA response (mm peak height)		
	Inj 1	Inj 2	$\bar{x} \pm$ S.D.
0	31	37	34 ± 4
0.01	64	64	64 ± 0
0.02	68	70	69 ± 1
0.04	71	70	71 ± 1
0.05	70	69	70 ± 1

Thermospray tip temperature (T_2) = 140°C; chamber (P_{ch}) = 2.80; momentum separator = 130°C; membrane separator = 60°C; He purge flow = 2 l/min. No TEA response was found for 50-μl injection of solvent blank (i.e. no NDELA present); all other injections were 50 μl of NDELA at 4 μg/ml in mobile phase (MeOH–water, 3.75:96.25) without ammonium acetate present.

to lessen the possibility of background response from low volatility impurities in the mobile phase. It should be noted that PB analysis of other analytes utilizing mobile phases containing higher percentages of organic solvents will exhibit very different optimum conditions for these interface parameters.

3.4. Simplex optimization of PB-TEA response to NMPABAO

Another N-nitrosamine contaminant, NMPABAO, found in some cosmetics containing the sunscreen ingredient, Padimate O, was studied. However, low sensitivity was first encountered in determining optimum PB parameters for NMPABAO. For different analytes and mobile phase ratios, these problems may be due to the interactive effects of T_2, P_{ch} and He carrier flow upon each other during aerosol transport. Simplex optimization [10] experiments were performed for these three interactive factors. The conditions from experiment R, $P + (P - W)$, which recorded the best TEA response, $5.19 \cdot 10^5$ area counts, for NMPABAO were 115°C tip temperature (T_2), 6.3 setting on the desolvation chamber potentiometer (P_{ch}) and 25 setting (1.2 l/min) on the He carrier flowmeter. However, these conditions will probably differ slightly for other analytes and substantially for other mobile phase mixtures. The TEA response using conditions for the sixth experiment, C_r, was $4.63 \cdot 10^5$ area counts or slightly less than the optimum response from the previous experiment R.

3.5. HPLC–PB-TEA analysis of cosmetic extract

For analysis of non-volatile N-nitrosamines in cosmetic samples, an extraction method previously reported by Meyer and Powell [9] was modified for applicability to HPLC–PB-TEA analysis. Several cosmetic samples could be extracted, centrifuged, evaporated and redissolved in 1 ml of acetonitrile and ready for HPLC–PB-TEA analysis within 1 h. A chromatogram of a 30-μl injection of a cosmetic sample (30 mg-equivalents of sample injected) is shown in Fig. 6A. NMPABAO was detected in the cosmetic at 8.5 ppm (w/w) (see Fig. 6A, at 8.0 min retention time) as compared to a NMPABAO standard (Fig. 7A). Upon UV irradiation of the sample at 365 nm for 16 h, the HPLC–PB-TEA chromatogram (Fig. 6B) indicated the loss of the NMPABAO peak due to photolysis as is typical for N-nitrosamines.

3.6. HPLC–PB-MS confirmation of NMPABAO in cosmetic extract

Full-scan EI-MS confirmation of NMPABAO in an actual cosmetic sample was performed by

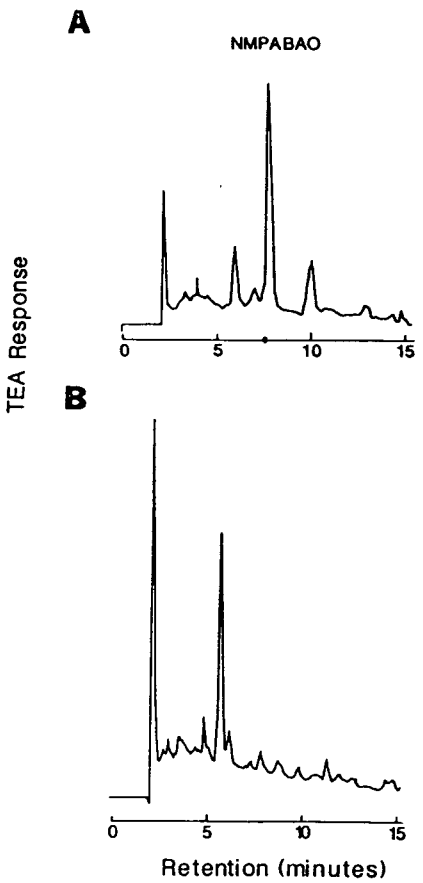

Fig. 6. HPLC–PB-TEA chromatograms of 30-μl injections of (A) a 1-g cosmetic skin cream sample in 1 ml extract and (B) the same extract after UV irradiation at 365 nm for 16 h.

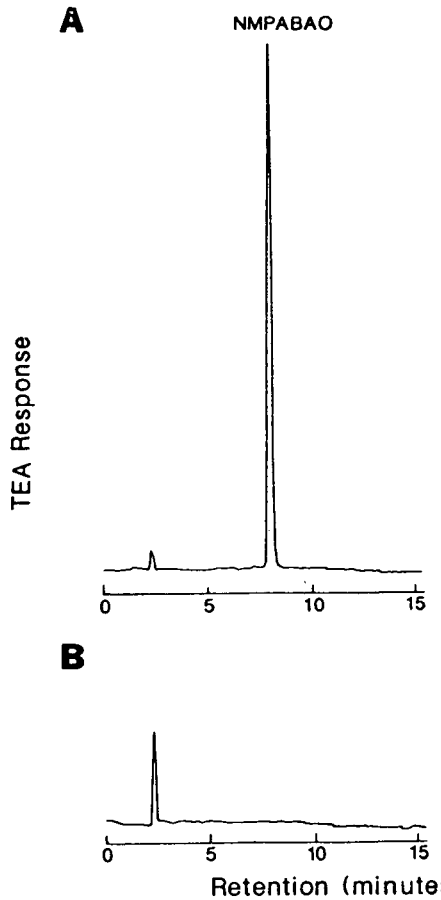

Fig. 7. HPLC–PB-TEA chromatogram of 30-μl injections of (A) 20 μg/ml of an NMPABAO standard solution and (B) reagent blank.

interfacing the HPLC–PB system to a mass spectrometer configured with a dual-stage momentum separator (as shown in Fig. 1). The reconstructed ion chromatogram (RIC) and ion scans at 262 and 263 m/z are shown in Fig. 8 using the same HPLC conditions (Fig. 6) for the cosmetic sample. Although numerous extraneous peaks appear in the RIC, a single-ion scan at 262 m/z and its EI-MS (Fig. 9, upper) has identified the peak at scan number 333 to be NMPABAO when compared to a NMPABAO standard. The peak in the 263 m/z ion scan (scan number 329, Fig. 8) was tentatively identified (no standard available) by EI-MS as MPABAO (Fig. 9, lower), the free amine of NMPABAO, since its spectra is consistent with the loss of NO (mass = 30) from NMPABAO (M_r 292) and addition of a hydrogen to give a molecular ion at 263 m/z. This further indicated that HPLC–PB-MS can be used to complement the HPLC–PB-TEA analysis of cosmetics by detecting the N-nitroso compound and the free amine, non-detectable by the TEA. However, most important for this application, HPLC–PB-MS has proven to be a very powerful, fast technique for identifying a N-nitrosamine contaminant found in a cosmetic product in a single HPLC separation without time consuming, peak collection procedures coupled with other MS introduction methods. Although for cosmetics containing lower levels of contaminants, a peak collection scheme can be used to increase detectability of this and other N-nitrosamine contaminants.

4. Conclusions

The first application of HPLC–PB-TEA for detection of non-volatile N-nitrosamines was successful in separating and detecting two compounds, NDELA and NMPABAO. Our modified cosmetic extraction method coupled with HPLC–PB-TEA was used to analyze for NMPABAO in a skin care cosmetic sample with confirmation by HPLC–PB-MS using EI ionization. Using the scenario of HPLC–PB-TEA analysis of cosmetics before and after UV photolysis, we hope to be able to screen several cosmetics for only TEA responding/UV degrading peaks. Other methods such as EI or CI-MS will then be applied to the identification of the most probable N-nitrosamine peaks.

The PB interface technology should be applicable to interfacing HPLC to TEA for detecting other low-volatility N-nitrosamines, N-nitroso derivatives, and TEA responding nitro-containing compounds in a number of different substrates. However, as with any new technique, additional research will be required to determine the scope and applicability of HPLC–PB-TEA to other analytical chemical problems.

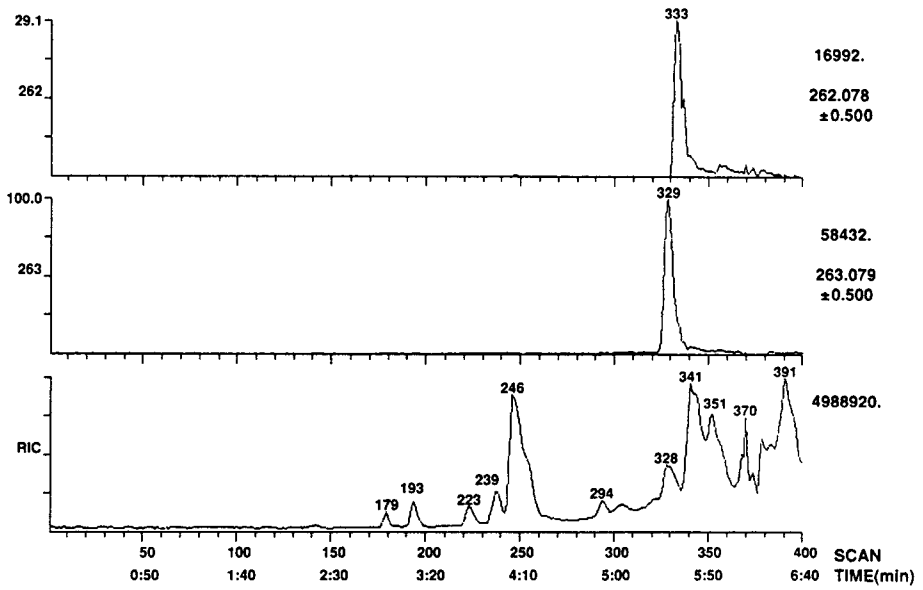

Fig. 8. RIC of HPLC–PB-MS analysis of a cosmetic skin cream extract with ion scans at 262 and 263 m/z.

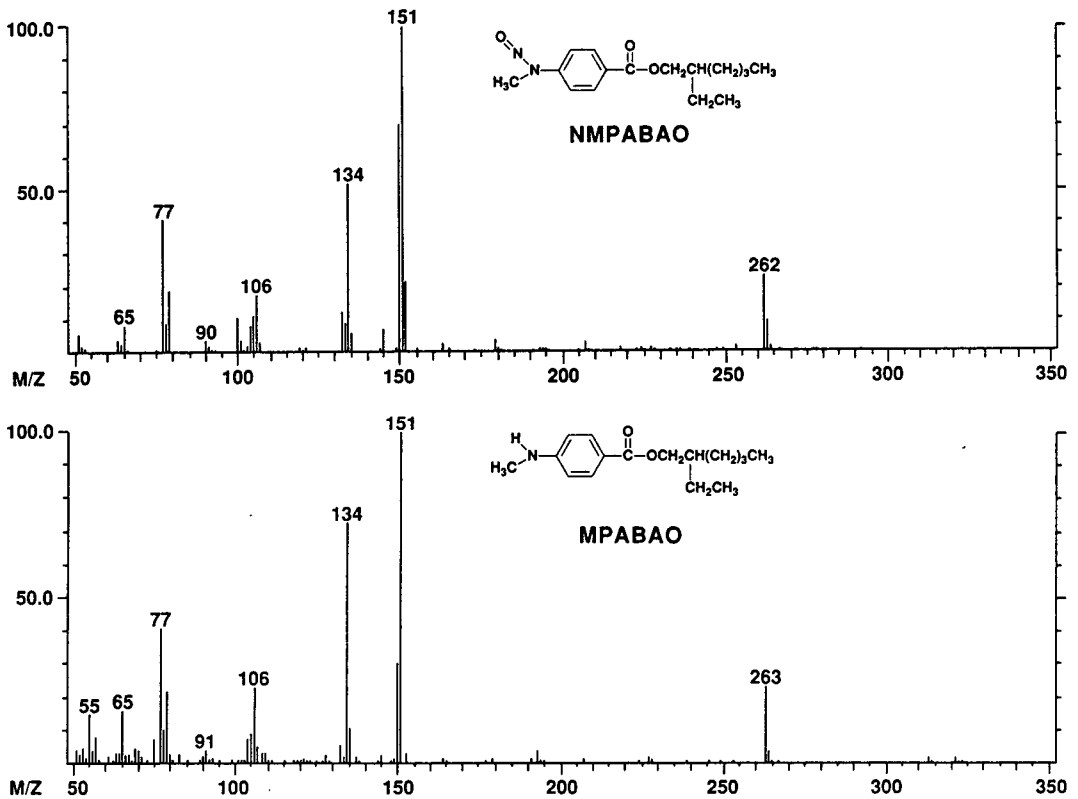

Fig. 9. EI-MS spectra of NMPABAO (upper, M_r 292) and MPABAO (lower, M_r 263) from scan numbers 333 and 329, respectively.

Acknowledgements

The authors would like to thank Don Havery and Hardy Chou of the Cosmetics Technology Section, Division of Colors and Cosmetics, CFSAN, Washington, DC, USA, for the NDELA and NMPABAO standards used in this study.

References

[1] B.J. Miller, S.M. Billedeau and D.W. Miller, *Food Chem. Toxicol.*, 27 (1989) 295–299.
[2] S.M. Billedeau, B.J. Miller and H.C. Thompson, Jr., *J. Food Sci.*, 53 (1988) 1696–1698.
[3] J.B. Morrison, S.S. Hecht and J.A. Wenninger, *Food Chem. Toxicol.*, 21 (1983) 69–73.
[4] H.C. Thompson, Jr., S.M. Billedeau, B.J. Miller, E.B. Hansen, Jr., J.P. Freeman and M.L. Wind, *J. Toxicol. Environ. Health*, 13 (1984) 615–632.
[5] D.C. Havery, *J. Anal. Toxicol.*, 14 (1990) 181–185.
[6] J.H. Hotchkiss and J.J. Conboy, *Analyst*, 114 (1989) 155–159.
[7] D.H. Fine, D. Lieb and R. Rufeh, *J. Chromatogr.*, 107 (1975) 351–357.
[8] M.L. Vestal, D. Winn, C.H. Vestal and J.G. Wilkes, in M.A. Brown (Editor), *LC/MS Applications in Agricultural Pharmaceutical and Environment Chemistry (ACS Symposium Series*, No. 421), American Chemical Society, Washington, DC, 1990, p. 215.
[9] T.A. Meyer and J.B. Powell, *J. Assoc. Off. Anal. Chem.*, 74 (1991) 766–771.
[10] J.G. Wilkes, *Dissertation*, University of Houston, Houston, TX, December 1991, pp. 127–131.
[11] A. Nelder and R. Mead, *Computer J.*, 7 (1964) 308.

ELSEVIER

Journal of Chromatography A, 688 (1994) 67–73

JOURNAL OF CHROMATOGRAPHY A

Determination of diquat and paraquat in water using high-performance liquid chromatography with confirmation by liquid chromatography–particle beam mass spectrometry

Indira Kambhampati[a], Kurt S. Roinestad[a,*], Thomas G. Hartman[a], Joseph D. Rosen[b], Elaine K. Fukuda[a], R. Lee Lippincott[c], Robert T. Rosen[a]

[a]*Center for Advanced Food Technology, Cook College, Rutgers University, New Brunswick, NJ 08903, USA*
[b]*Department of Food Science, Cook College, Rutgers University, New Brunswick, NJ 08903, USA*
[c]*Department of Environmental Protection and Energy, CN 409, 401 E. State Street, Trenton, NJ 08625, USA*

First received 17 May 1994; revised manuscript received 7 September 1994

Abstract

A method was developed for the extraction of diquat and paraquat from environmental water samples by ion-exchange column chromatography. Determinations were performed using high-performance liquid chromatography with diode array detection. The HPLC method was developed to be compatible with LC–MS techniques. Results were confirmed with LC–particle beam (electron ionization) MS, where a unique ionization process was observed.

Recoveries in drinking water were over 75% for both diquat and paraquat spiked at concentrations of 5–10 μg/l. The method presented is uniquely specific since a diode array UV spectrum is obtained as well as an particle beam mass spectrum, insuring correct identification and quantitation of diquat and paraquat.

1. Introduction

Since their introduction approximately 35 years ago, the bipyridinium compounds paraquat (1,1′-dimethyl-4,4′-bipyridinium dihalide, PQ) and diquat (1,1′-ethylene-2,2′-bipyridinium dihalide, DQ) have been extensively employed as rapid-acting herbicides. They are effective for terrestrial and aquatic weed control and as an aid in crop desiccation, pasture renovation and seed bed preparation [1,2].

Both herbicides are extremely soluble in water and essentially insoluble in organic solvents. They are thermally stable, non-volatile, and retain their identity in both acidic and neutral conditions. However, DQ is known to degrade slowly at pH greater than 9 [3] and PQ hydrolyses at pH above 12 [1].

A variety of analytical techniques have been developed to determine residues of PQ and DQ in various matrices. Previously developed methods have included utilization of gel-filtration and ion-exchange liquid chromatography (LC) [3], gas chromatography with nitrogen–phosphorous-specific detection (GC–NPD) [4], enzyme-linked immunoassay (ELISA) [5,6] and high-performance liquid chromatography (HPLC). An inherent disadvantage of many published methods is

* Corresponding author.

0021-9673/94/$07.00
SSDI 0021-9673(94)00889-2

lack of analytical specificity which may result in identification and quantitation difficulties, especially in complex matrices. The United States Environmental Protection Agency (EPA) prefers methodology where confirmation of identity by mass spectrometry (MS) is possible. Yoshida et al. [7] and Barcelo et al. [8] both in 1993, published work on the determination of PQ and DQ by HPLC using thermospray MS to confirm their presence. The thermospray spectra of Yoshida et al. showed a single ion, at m/z 186 for PQ and m/z 183 for DQ, but Barcelo et al.'s work showed major ions present at m/z 187 and 184. This indicates an instrument-specific spectrum. Both papers used the same solvents and modifiers in the mobile phase. Brown et al. [9] published a particle beam (PB; 70 eV) mass spectrum of PQ, identical to the one presented in this paper, as well as a calibration curve. Few details were presented in this paper concerning HPLC conditions or recoveries, but the work confirms that the particle beam mass spectrum can be consistently obtained.

Behymer et al. [10] of the EPA concluded that thermospray HPLC–MS, because of the relatively soft ionization process, did not provide the variety of structurally significant fragment ions characteristic of conventional electron ionization (EI) mass spectrometry. Therefore, thermospray mass spectra are not considered absolute confirmation of identity. However, HPLC–PB-MS, since it provides 70 eV EI library-searchable spectra, is useful in identifying target as well as additional analytes. Previously published works have explored the use of HPLC–PB-MS methods for the determination of less volatile organic environmental pollutants [11–13].

HPLC techniques have been developed for the determination of DQ and PQ in water, but these methods rely upon non-volatile ion-pairing reagents to facilitate chromatography. These reagents contain insoluble sodium and potassium salts, phosphates and sulfonates, which are not amenable to MS confirmation of DQ and PQ, since these salts quickly precipitate and clog the LC–MS interface.

In our study, we focused on developing a simple yet specific and sensitive method for determining DQ and PQ in drinking water. The method utilizes HPLC with a diode array UV detection. The mobile phase is MS compatible so that confirmation can be obtained via PB-MS (EI mode).

2. Experimental

2.1. Chemicals and reagents

Analytically pure paraquat dichloride and diquat dibromide were obtained from Chem Service (West Chester, PA, USA). Ethyl viologen was purchased from Aldrich (St. Louis, MO, USA). Caffeine was purchased from Sigma (St. Louis, MO, USA). Ammonium hydroxide, ammonium acetate, HPLC-grade acetonitrile and HPLC water were purchased from Fisher Scientific (Pittsburgh, PA, USA).

2.2. Standard solutions

PQ (100 mg) was dissolved in 100 ml HPLC-grade water to obtain a stock solution of 1 μg/μl and was further diluted to concentrations of 0.1 and 0.01 μg/μl. Standard solutions of DQ were prepared in the same manner. The concentration of both the DQ and the PQ solutions were recalculated to reflect the dissociation of the bromine and chlorine anions. The internal standard caffeine (50 mg) was dissolved in 100 ml of HPLC-grade water to obtain a concentration of 0.5 μg/μl.

2.3. Sample preparation

A 1–4-l sample of drinking water (pH adjusted to pH 8.5 with ammonium hydroxide) was decanted into a Millipore (Milford, MA, USA) 10-l stainless-steel pressure vessel, sealed and attached to a nitrogen tank. The vessel was then connected via PTFE tubing to a 30 cm × 1.5 cm glass column equipped with PTFE end fittings. The glass column was packed with 10 g of Dowex ion retardation resin (Sigma) which was previously conditioned by sequentially washing it with 100 ml of hexane, 100 ml of methanol and

100 ml of HPLC-grade water. The drinking water sample was then pumped through the ion-exchange column at a flow-rate of 25 ml/min. The DQ and PQ were eluted from the resin with 800 ml of 90% 0.2 *M* ammonium acetate and 10% acetonitrile. The eluate was collected in a 2000-ml round-bottom flask and rotary evaporated to 10 ml in a water bath at 70°C.

2.4. Instrumentation conditions

Analyses of DQ and PQ were performed by injecting a 200-μl aliquot of the sample into a Varian (Sunnyvale, CA, USA) Vista 5500 high-performance liquid chromatograph linked to a Varian Polychrome 9065 diode array detector and interfaced to a Techouse PC 386 DX data system. The column used for chromatographic separation was an Alltech (Deerfield, IL, USA) 250 mm × 4.6 mm, 100 Å mixed-phase C_{18}/cation-exchange column. The initial mobile phase consisted of 100% 0.05 *M* ammonium acetate (adjusted to pH 5.7 with glacial acetic acid). At 4 min, the mobile phase was switched to 90% 0.05 *M* ammonium acetate and 10% acetonitrile (adjusted to pH 4.5 with glacial acetic acid). The flow-rate of the system was 1 ml/min. The column temperature was held at 25°C. DQ and PQ were quantitated via diode array detection at 306 and 254 nm, respectively. Confirmation was obtained using the HPLC interfaced to a Vestec (Houston, TX, USA) Model 201 LC–MS system which was equipped with a PB (universal) interface. The mass spectrometer was operated in the EI mode. The filament voltage was 70 eV. The filament current was 200 μA. The source temperature was held at 220°C. The HPLC conditions were identical to those obtained off-line. A Teknivent (St. Louis, MO, USA) Vector/One MS data system was used for acquiring and processing data.

2.5. Internal standard

A 250-μg amount of caffeine (Sigma) was added to the final sample to obtain a 25 μg/ml concentration.

2.6. Quantitation

A calibration curve consisting of 14.5, 7.25, 1.45, 0.145 and 0.0725 μg standards (on-column, in triplicate) was constructed for PQ. A calibration curve consisting of 10.7, 5.35, 1.07, 0.107 and 0.0535 μg standards (on-column, in triplicate) was constructed for DQ. Caffeine was used as the internal standard (254 nm) and a response factor consisting of the area of the sample divided by the area of the internal standard was calculated for each level. The response factor for each standard was plotted against the on-column μg amount.

3. Results and discussion

3.1. Extraction procedure

Initial experiments to extract DQ and PQ from distilled water were conducted with various ion-exchange resins including a strong cation-exchange resin and a mixed-bed ion-exchange resin. Recoveries from these resins were below 30% for both DQ and PQ. However, extraction with Dowex ion retardation resin (50–100 mesh) resulted in acceptable recoveries (see Section 3.3) for both DQ and PQ in distilled water as well as drinking water, provided that the pH of the sample was adjusted to pH 8.5 with ammonium hydroxide before being pumped through the ion-exchange column.

3.2. HPLC conditions

An Alltech 250 mm × 4.6 mm, 100 Å mixed-phase C_{18}/cation-exchange column was used to separate DQ and PQ from other components of the drinking water matrix. A chromatogram of DQ and PQ displaying separation of these two components is presented in Fig. 1. Retention of analytes on the mixed-mode column that is used for our method is highly dependent on the pH of the mobile phase. Attempts to improve the resolution of DQ and PQ by increasing the pH of the mobile phase however, resulted in un-

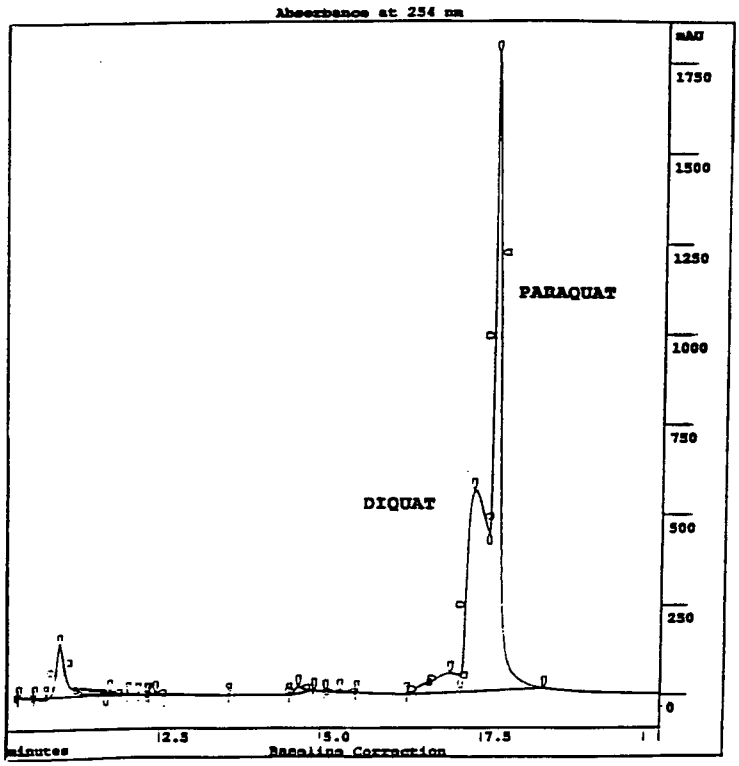

Fig. 1. Diquat and paraquat (20 μg each) chromatographed with LC–MS-compatible conditions.

acceptable chromatography. Lowering the pH of the mobile phase resulted in two very sharp peaks with identical retention times. In the case of coelution, however, it is still possible to quantitate each component as their diode array spectra are significantly different. DQ strongly absorbs at 306 nm while PQ exhibits virtually no absorbance at this wavelength. In systems where DQ and PQ coelute, diode array detection, as well as PB-MS, are useful in confirming the presence of PQ or DQ in the sample. The initial mobile phase to affect the separation of DQ from PQ consisted of 100% 0.05 *M* ammonium acetate (adjusted to pH 5.7 with glacial acetic acid). At 4 min, the mobile phase was switched to 90% 0.05 *M* ammonium acetate and 10% acetonitrile (adjusted to pH 4.5 with glacial acetic acid). This system contains only volatile buffers and is compatible with LC–MS, which is used to confirm the presence of DQ and PQ.

3.3. Internal standard, surrogate standard and recovery studies

Studies were conducted to choose an appropriate internal standard and surrogate standard for all subsequent analysis for DQ and PQ in drinking water. Caffeine was chosen as the internal standard whereas experiments conducted in our laboratory indicate that ethyl viologen (a homologue of PQ in which the methyl groups are replaced with ethyl groups) is a suitable surrogate standard since it is structurally very similar to DQ and PQ and is recovered from drinking water via our method for extracting DQ and PQ (recovery of surrogate

standard = 85.9% at the 1 μg/ml spiked level, average of duplicate analyses). A chromatogram of PQ and ethyl viologen is presented in Fig. 2. Recovery of DQ at 0.535 μg/ml in distilled water was conducted in triplicate and was determined to be 85.3% (R.S.D. = 2.8%). Recovery for PQ at 0.725 μg/ml was found to be 96.1% (R.S.D. = 0.9%). Recovery for DQ at the 5.3 μg/l level in distilled water was conducted in duplicate and was determined to be 86.3% (R.S.D. = 1.5%). That of PQ at the 7.3 μg/l level was 97.6% (R.S.D. = 4.0%). In drinking water, the same spiked levels were extracted and analyzed. Recoveries were determined to be 82.8% (R.S.D. = 2.4%) for DQ at the 0.535 μg/ml level, 84.2% (R.S.D. = 3.6%) for PQ at the 0.725 μg/ml level, 78.0% (R.S.D. = 2.0%) for DQ at the 5.3 μg/l level and 83.0% (R.S.D. = 4.8%) for PQ at the 7.3 μg/l level. All recovery studies were performed employing diode array as the detection system.

3.4. Mass spectrometry

EI (70 eV) particle beam mass spectra for DQ and PQ were generated and are presented in Figs. 3 and 4. The mechanism of ion formation of the compounds PQ and DQ is different than for non-ionic covalent molecules. With PQ and DQ, a singly charged mass spectrum results from a doubly charged species and must involve electron capture with subsequent charge elimination from one site, leaving an ion with a +1 charge state. With DQ, a $M^{2+} - H^{+}$ ion is also observed at m/z 183 and is larger than the M^{+} at m/z 184. We believe the mechanism of the formation of

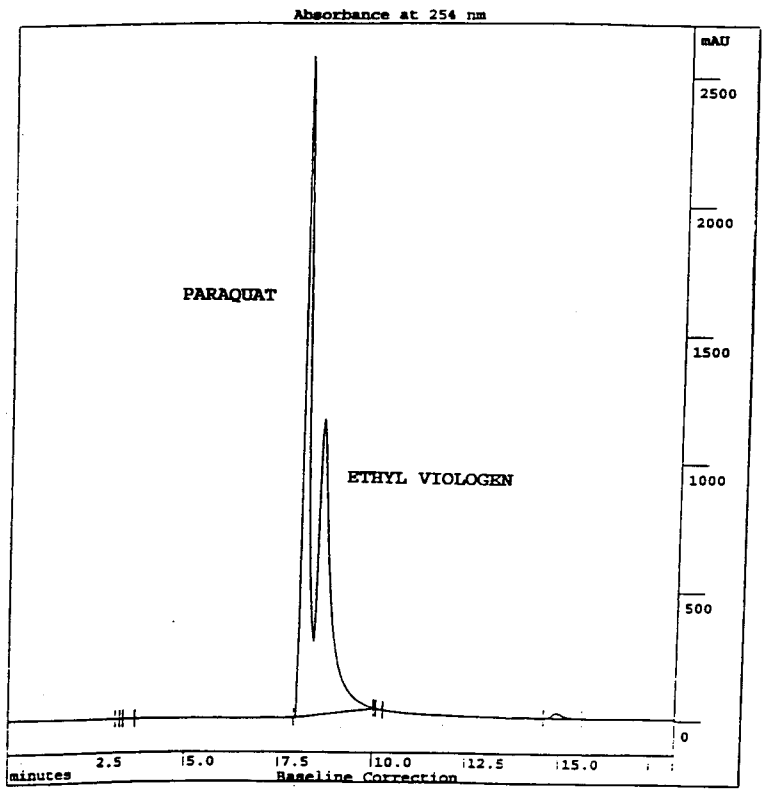

Fig. 2. Chromatogram of 25 μg of paraquat and 10 μg of ethyl viologen (surrogate standard).

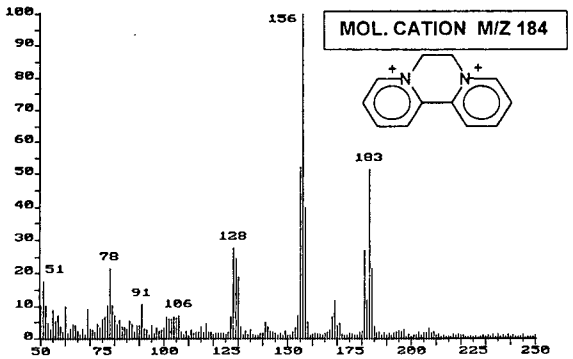

Fig. 3. Particle beam mass spectrum of diquat.

the ions for the above quats involves a disruption of the solvated particle (exiting from the PB interface) containing PQ and DQ with a subsequent release of the preformed molecular cations. This phenomenon is caused by the impact of electrons with the water particles containing the analyte. The observation supporting this hypothesis is that ions were not observed with the filament emission set to zero, no matter what changes were made in the focusing controls, and assuring that all other source voltages were indeed on. The observations described above support a secondary ionization process, i.e. desorption ionization. It was also observed that PQ does partially decompose with heat in the ion source of the mass spectrometer. While the mass chromatogram for the molecular ion shows a very sharp peak with no tailing eluting from the HPLC, the ions corresponding to the free base (m/z 156 and below) do show tailing.

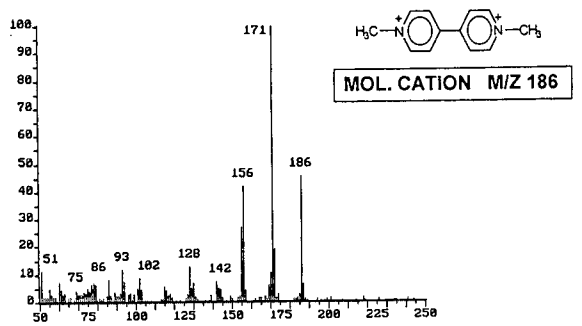

Fig. 4. Particle beam mass spectrum of paraquat.

This relates to material hitting the ion source walls.

In general, LC–PB-MS is not as sensitive as other HPLC methods of detection (this relates to electrostatic particle loss in the aerosol portion of the Vestec universal interface [13]) and absolute confirmation of these pesticides at low μg/l levels (<25 μg/l) may only be possible by selected ion monitoring (SIM). However, levels above 25 μg/l can be easily confirmed in the full scan mode.

The method presented allows the reliable identification of both DQ and PQ in drinking water samples. Work will continue and different water samples from other environmental sources will be tested to ascertain the ruggedness and uniformity of this method.

Acknowledgements

This research was supported by funds from the New Jersey Department of Environmental Protection and Energy. The Center for Advanced Food Technology is an initiative of the New Jersey Commission on Science and Technology. NJAES Publication No. D10570-1-94.

References

[1] E.V. Reed (Editor), *FDA Surveillance Index for Pesticides; PB82-913299*, National Technical Information Service, Springfield, VA, 1981.
[2] H.H. Funderburk, in P.C. Kearney and D.D. Kaufman (Editors), *Degradation of Herbicides*, Marcel Dekker, New York, 1969, pp. 283–298.
[3] I. Nakagiri, K. Suzuki, Y. Shiaku, Y. Kuroda, N. Takasu and A. Kohama, *J. Chromatogr.*, 481 (1989) 434–438.
[4] S.U. Khan, *Bull. Environ. Contam. Toxicol.*, 14 (1975) 745–749.
[5] J. Van Emon, J. Seiber and B. Hammock, *Anal. Chem.*, 58 (1986) 1866–1873.
[6] J. Van Emon, J. Seiber and B. Hammock, *Bull. Environ. Contam. Toxicol.*, 39 (1987) 490–497.
[7] M. Yoshida, T. Watabiki, T. Tokiyasu and N. Ishida, *J. Chromatogr.*, 628 (1993) 235–239.
[8] D. Barcelo and G. Durand, *J. Chromatogr.*, 647 (1993) 271–277.

[9] M.A. Brown, I.S. Kim, F.I. Sasinow, R.D. Stephens, in M.A. Brown (Editor), *Liquid Chromatography/Mass Spectrometry —Applications in Agricultural, Pharmaceutical, and Environmental Chemistry*, American Chemical Society, Washington, DC, 1990, pp. 198–214.
[10] T.D. Behymer, T.A. Bellar and W.L. Budde, *Anal. Chem.*, 62 (1990) 1686–1690.
[11] T.A. Bellar and W.L. Budde, *Anal. Chem.*, 60 (1988)
[12] L.B. Clark, R.T. Rosen, T.J. Hartman, J.B. Louis and J.D. Rosen, *Int. J. Environ. Anal. Chem.*, 45 (1991) 169–178.
[13] L.B. Clark, R.T. Rosen, T.G. Hartman, J.B. Louis, I.H. Suffet, R.L. Lippincott and J.D. Rosen, *Int. J. Environ. Anal. Chem.*, 47 (1992) 167–179.

ELSEVIER

Journal of Chromatography A, 688 (1994) 75–82

JOURNAL OF CHROMATOGRAPHY A

Liquid chromatographic determination of sulfonylurea herbicides in natural waters after automated sample pretreatment using supported liquid membranes

Göran Nilvé[1], Magnus Knutsson, Jan Åke Jönsson*

Department of Analytical Chemistry, University of Lund, P.O. Box 124, S-221 00 Lund, Sweden

First received 15 March 1994; revised manuscript received 23 September 1994

Abstract

Sample pretreatment for the determination of sulfonylurea herbicides in natural water samples is investigated. Both supported liquid membrane (SLM) extraction and solid-phase extraction (SPE) are used for enrichment of spiked samples. The liquid membrane technique is used on-line with liquid chromatography. The liquid chromatographic detection is by UV absorption at 240 nm. Enrichment with SLM gives a more selective extraction than SPE, resulting in much cleaner chromatograms. The detection limits for enrichment of 250-ml samples are 50–100 ng/l for SLM and around 1 μg/l for SPE.

1. Introduction

Sulfonylureas are a relatively new class of herbicides used for control of weed in crops. These herbicides are very potent weed killers and are used in doses that are substantially lower than for conventional herbicides. Since the mid-1970s, when the herbicidal activity of this class of compounds was discovered, the development has been very fast and in May 1989, 375 sulfonylurea herbicide patents had been issued [1]. The low doses used (ca. 4 g/ha; 1 ha = 10^4 m^2) make determinations of these compounds in recipient waters and in soils difficult. Apart from the requirements on the final analytical step (sensitivity and selectivity) the sample preparation step must be capable of large and, if possible, selective enrichments.

Solid-phase extraction (SPE), a technique well known for its large enrichment capacity, has been used for concentration and clean-up of sulfonylurea herbicides in aqueous samples in an off-line mode [2–4]. It is potentially possible to use this technique in an on-line mode as described by several authors [5,6]. This has, however, to our knowledge not been applied to sulfonylurea herbicides. Off-line SPE can be automated using several commercially available robotic instruments (i.e. ASPEC, Gilson).

Liquid–liquid extraction, probably still being the most commonly used sample preparation method for determination of non-volatile organics in aqueous samples, has also been used for sulfonylurea herbicides [7,8]. The general problems encountered when liquid–liquid extraction is used are however quite large and include

* Corresponding author.

[1] Present address: Astra-Draco AB, P.O Box 34, S-221 00 Lund, Sweden.

0021-9673/94/$07.00
SSDI 0021-9673(94)00918-X

factors like: time and labour intensive, emulsion formation, large consumption of organic solvents, evaporation of large volumes of solvents, and not easily automated

Sample preparation by means of liquid membrane extraction is a technique which in essence contains two liquid–liquid extractions in one step, whereby some of the problems mentioned above can be solved [9]. The technique can be used on-line with both gas [10–12] and liquid chromatography [13–15]. The set-up is easily automated and the sample preparation is performed in a closed system, thus minimizing the risks for contamination and losses during the process. As the extraction is made from one aqueous phase (donor) to a second, also aqueous phase (acceptor), further enrichment on a precolumn is possible, before injection into a liquid chromatograph. The supported liquid membrane method provides, in addition to high enrichment factors, also a high degree of clean-up. In complex matrices as urine [11], blood plasma [12,15] and manure [16] it has been demonstrated that chromatograms obtained from samples containing these matrices are very similar to chromatograms from standard solutions in distilled water. The technique can also be used for time integrating field sampling. The total leakage of phenoxy acids into recipient waters has thus been estimated [17,18].

In a previous paper [14] liquid membranes were used for enrichment of two sulfonylureas (metsulfuron methyl and chlorsulfuron) from clean aqueous samples. In the present paper the same approach is used for determinations of four sulfonylureas (thifensulfuron methyl, metsulfuron methyl, chlorsulfuron and tribenuron methyl) in natural water samples. The membrane method is also compared with SPE for the enrichment of the herbicides from these samples.

2. Experimental

2.1. Equipment

The flow system is shown in Fig. 1. Two peristaltic pumps (I) (Minipuls 2; Gilson Medical Electronics, Villiers-le-Bel, France) were used to independently control the flow-rates of the donor and acceptor phases. The pump tubings used in the peristaltic pumps were of the "acid flexible" type (Elkay Products, Shrewsbury, MA, USA). The various parts of the set-up were connected with 0.5 mm I.D. PTFE tubing and Alltech screw fittings. The confluence tees were made of PTFE or Kel-F and the channels meet at a 60° angle. The switching valves were pneumatically actuated four-way Kel-F slider valves (Cheminert; Laboratory Data Control, UK).

The membrane separator (see Fig. 1) consisted of two polyvinylidene difluoride (PVDF) blocks in which channels were machined so that when put together the channels face each other. The channels were 1.5 mm wide, 0.25 mm deep and 250 cm long, giving a volume in each channel of ca. 950 μl. The channels were arranged like Archimedes' spirals. The membrane was placed between the PVDF blocks, separating the donor from the acceptor channel and the set-up was clamped together with six screws.

The liquid membrane support was Fluoropore FG (PTFE membrane, average pore size 0.2 μm, total thickness 175 μm of which 115 μm is polyethylene backing, porosity 0.7; Millipore, Bedford, MA, USA). The liquid membrane was prepared by simply immersing the membrane support in the organic solvent mixture for about 15 min. After installation of the impregnated membrane in the separator both channels were flushed with water to remove excess of the solvent mixture on the surfaces of the membrane.

The chromatographic separations were performed with a Spectra-Physics (San José, CA, USA) SP 8800 liquid chromatographic pump. A pneumatically actuated Valco six-port valve in which the loop was replaced with a 20 mm × 2.1 mm I.D. precolumn (Upchurch Scientific, Oak Harbor, WA, USA) was used for injection. The packing used in the precolumn was pellicular C_{18} packing (Alltech, Deerfield, IL, USA). The analytical column was 150 mm × 2.1 mm I.D. filled with Spherisorb ODS-3 (3-μm particles) (Phase Separations, Queensferry, UK). The chromatographic eluent consisted in the SPE experiments of MeOH–1% aqueous acetic acid (1:1, v/v) and in the liquid membrane experi-

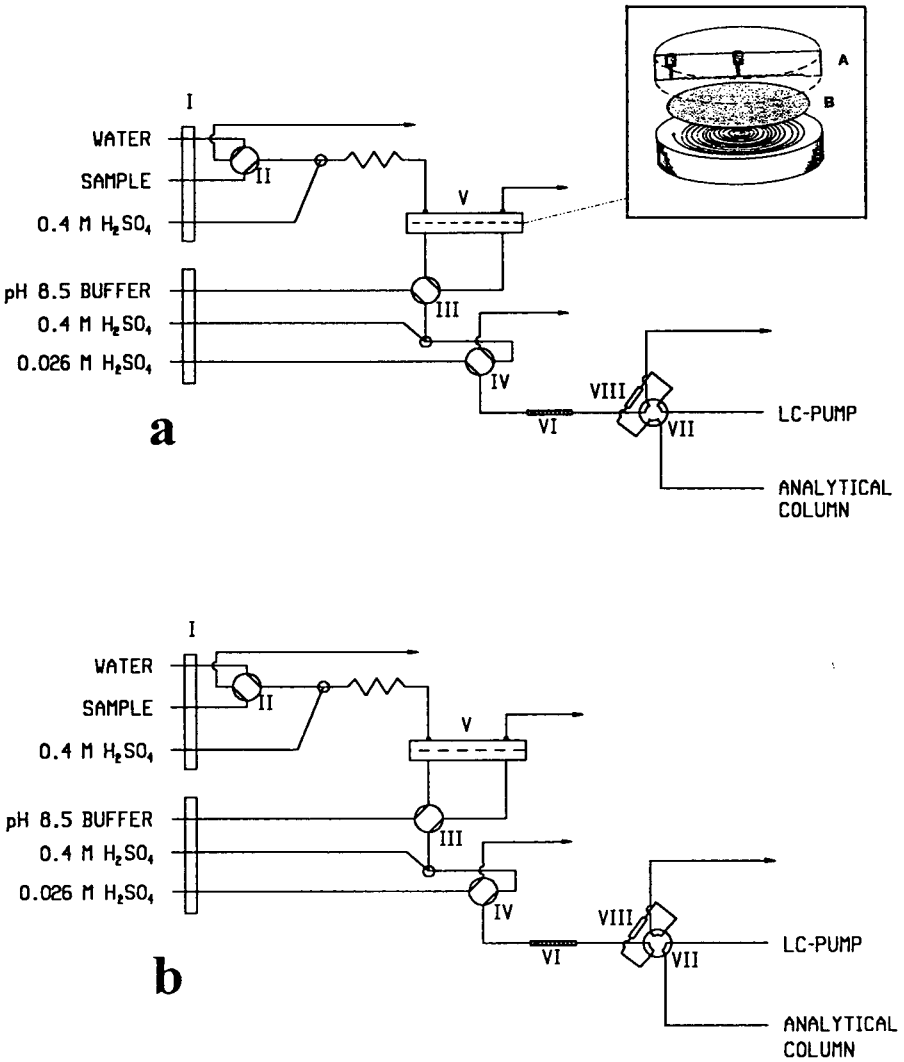

Fig. 1. Experimental setup. (a) Sample enrichment, (b) loading of the enriched sample onto the precolumn. Membrane separator (V): (A) PVDF blocks with grooves like Archimedes' spiral; (B) PTFE membrane with polyethylene backing. For more details on the set-up, see text.

ments of acetonitrile–water adjusted to pH 3 with acetic acid (3:7, v/v). The flow-rates were for the MeOH eluent 0.15 ml/min, and for the acetonitrile 0.2 ml/min.

Spectrophotometric detection was carried out at 240 nm with a LDC Spectromonitor III variable-wavelength UV detector (LDC, Riviera Beach, FL, USA). The chromatographic data were collected and handled with a personal computer (Model V386A; Victor Svenska, Stockholm, Sweden) using the JCL 6000 chromatography data system (Jones Chromatography, Hengoed, UK).

2.2. Operation of the liquid membrane flow system

Operation of the flow system used for liquid membrane sample pretreatment is shown in Fig. 1. Two peristaltic pumps (I) were used to pump

the different solutions. Fig. 1a shows positioning of the valves when the sample enrichment is performed. This can be made simultaneously with the LC analysis of the previous sample. The sample is injected through valve II. The sample volume is determined by the flow-rate through valve II and by the time this valve remains open. After mixing with acid in a mixing coil (100 cm × 0.5 mm I.D.) the acidified sample enters the membrane separation unit (V) on the donor side. The non-ionized solutes are extracted into the liquid membrane and diffuse through the membrane into the aqueous acceptor phase, which is kept stagnant by valve III. The acceptor pH is chosen so that the acidic analytes are ionized. The driving force of analyte mass transfer is thus the concentration gradient of non-ionized analytes between the donor and the acceptor phases. A detailed treatment of the mass transfer process is given elsewhere [19].

In Fig. 1b, loading of the enriched sample on the precolumn is described. Following the switching of valve III the enriched sample plug is mixed with acid in a pearl string mixer (VI), before it is loaded on the precolumn (VIII). After the loading, valve IV is switched to flush the precolumn with diluted acid. This prevents injection of the acceptor phase buffer in the liquid chromatographic system, which has previously been shown to give a large front peak in the chromatogram [11]. Finally, valve VII is switched, introducing the analytes on the column. The extraction efficiencies were calculated by comparison with injected standard solutions.

Typical flow-rates were: donor side: sample (or water) 0.8 ml/min, 0.4 *M* H_2SO_4 0.2 ml/min; acceptor side: pH 8.5 buffer 0.25 ml/min, 0.4 *M* H_2SO_4 0.05 ml/min and 0.026 *M* H_2SO_4 0.25 ml/min. All valves are controlled by the "timed event" facilities in the chromatography data system.

2.3. Solid-phase extraction

The SPEs were basically performed as described by Wells and Michael [2], using Supelclean LC-18 SPE tubes (Supelco, Bellefonte, PA, USA) (6 ml, 0.5 g). To 1 l of water were added 7.5 g KH_2PO_4 and 7.8 g K_2HPO_4 and the pH was then adjusted to 6 with H_2SO_4. The SPE cartridges were activated by flushing with 5 ml MeOH and conditioned with 5 ml water. Samples of 200 ml were extracted at a flow-rate of ca. 3 ml/min. After completed extraction the analytes were eluted with a 5-ml portion of MeOH. The methanol was evaporated to a final volume of <1 ml and subsequently the volume was adjusted to 1 ml with water. A 20-μl aliquot (unless stated otherwise) of this solution was injected into the liquid chromatograph. The extraction recoveries were calculated by comparison with injected standard solutions.

2.4. Chemicals

Thifensulfuron methyl (98.3%), metsulfuron methyl (99.7%), chlorsulfuron (99.7%) and tribenuron methyl (97.3%) (see Table 1) were all gifts from DuPont, Wilmington, DE, USA. The organic solvents used were *n*-undecane (Merck, Darmstadt, Germany) (analytical-reagent grade) and di-*n*-hexyl ether (Sigma, St. Louis, MO, USA). Apart from tri-*n*-octylphosphine oxide (TOPO) obtained from Fluka (Buchs, Switzerland), all other chemicals came from Merck and were of analytical-reagent grade. Reagent water was purified with a Milli-Q-RO-4 unit (Millipore). Natural water was collected from the Kävlinge river, 10 km north of Lund, southern Sweden.

3. Results and discussion

3.1. Solid-phase extraction

The recoveries of the four sulfonylureas (concentrations 10 μg/l), from spiked samples of natural water ($n = 4$), are given in Table 2.

A chromatogram of a 1 μg/l sample enriched by SPE (Fig. 2) shows that the analytes at that concentration are largely masked by interfering compounds. The injection volume was 20 μl. To increase the amount injected, larger volumes (up to 500 μl) of the enriched sample were (by syringe) injected on a small precolumn, 20 mm ×

Table 1
Sulfonylurea herbicides used in this study and their CAS numbers, dissociation constants and structures

Name	CAS No.	pK_a	Structure
Thifensulfuron methyl	79277-27-3	4.0[a]	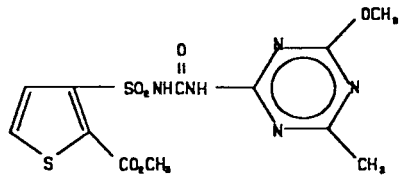
Metsulfuron methyl	74223-64-6	3.3[a]	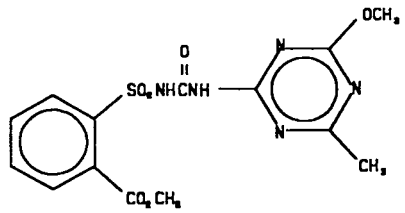
Chlorsulfuron	64902-72-3	3.6[a]	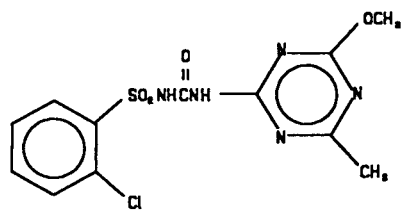
Tribenuron methyl	101200-48-0	5.0[b]	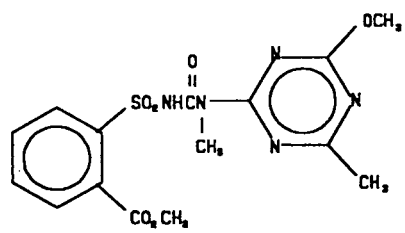

[a]From Ref. [20].
[b]From Ref. [21].

2,1 mm I.D., packed with pellicular C_{18}. The gain in the detection limit achieved by injection of larger volumes on a precolumn is negligible as the background absorption gets very large. Thus the clean-up selectivity of the SPE in this application, using C_{18} type stationary phase, is too low to permit the determination of low concentrations of the sulfonylureas (e.g. below 0.5–1 μg/l). The detection limit is largely governed by the amount of interfering compounds ex-

Table 2
Recoveries for the four sulfonylurea herbicides after SPE of 10 μg/l spiked natural water samples ($n = 4$) (95% confidence intervals)

Compound	Recovery (%)
Thifensulfuron methyl	100 ± 14
Metsulfuron methyl	102 ± 14
Chlorsulfuron	103 ± 13
Tribenuron methyl	103 ± 6

tracted. Wells and Michael [2] did not explicitly state detection limits for sulfonylureas in their paper, but a limit of 1 μg/l was mentioned for a similar compound.

A possible way to increase the selectivity in SPE would be to use an additional clean-up step, e.g. by elution of less-retained interfering compounds with water modified with a small amount of organic solvent [22]. This has not been carried out in this study. It is also possible to use more than one precolumn in series to increase the selectivity. Use of a C_{18} column in series with an ion-exchange column might be a possible route to a more selective enrichment. This has not been reported for sulfonylureas in the literature, but has been used for other pesticides [23].

As the enrichment factor can be made very large with SPE, the detection limit could probably be lowered by use of a more selective detection than UV detection at 240 nm, as

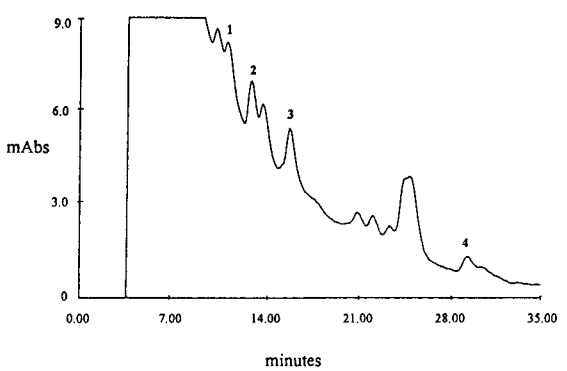

Fig. 2. A 1 μg/l concentration of the sulfonylureas enriched by SPE, 20-μl injection. Peaks: 1 = thifensulfuron methyl; 2 = metsulfuron methyl; 3 = chlorsulfuron; 4 = tribenuron methyl.

described in other papers, namely photoconductivity [24–26] and mass spectrometry [27–30]. For example, Zahnow [4] states a detection limit of 0.2 μg/l of sulfometuron methyl in river water, after SPE enrichment.

3.2. Liquid membrane extraction

The sulfonylureas are extracted from an acidified aqueous donor solution into an organic solvent in the liquid membrane and back extracted into a neutral/alkaline aqueous acceptor phase on the opposite side of the membrane.

The selectivity towards interfering substances is potentially larger when liquid membrane extraction is used for sample pretreatment than in the case of SPE. Only solutes that are non-ionized in the donor phase and ionized in the acceptor phase will be enriched in this system. Compounds which are neutral in both donor and acceptor solutions will simply equilibrate between the phases, while solutes being ionic in the donor will not be extracted into the liquid membrane at all. Furthermore, equilibrated non-ionized species in the acceptor solution may be washed out by pumping a clean solution through the donor channel, resulting in a back extraction of neutral compounds into the donor solution [9].

By changing the polarity of the organic solvent in the membrane, the selectivity may be controlled. Fig. 3 shows chromatograms after enrichment of blank natural water samples using three different solvent mixtures in the liquid membrane.

The least polar solvent used (*n*-undecane–di-*n*-hexyl ether, 1:1) gives the most efficient clean-up. A pure di-*n*-hexyl ether membrane gives a larger front peak in the chromatogram. With TOPO (a modifier that has been used in extractions of phenols and carboxylic acids [31–33]) in the membrane, the selectivity towards other substances in the water, possibly humic substances, is further decreased, reflected by the increased front peak seen after using this membrane.

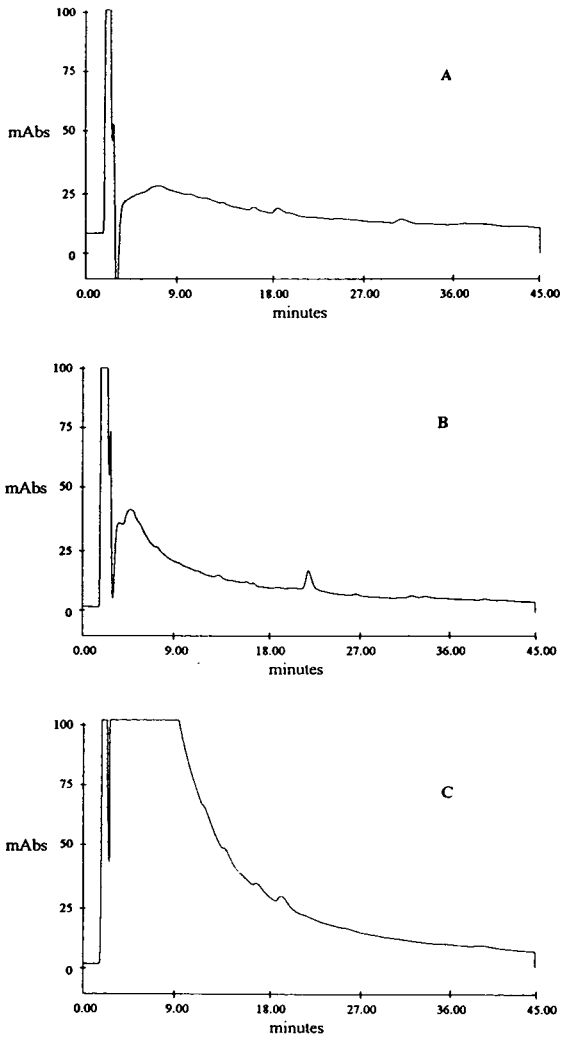

Fig. 3. Supported liquid membrane extraction of blank natural water samples. (A) *n*-Undecane–di-*n*-hexyl ether (1:1), (B) pure di-*n*-hexyl ether, (C) 5% TOPO in di-*n*-hexyl ether.

As the sulfonylureas are rather polar substances themselves, the recoveries in the extraction will also increase when using solvents of increasing polarity. The extraction efficiency for chlorsulfuron increased with a factor of nearly 2 using a di-*n*-hexyl ether compared to the 1:1 mixture [14]. Pure di-*n*-hexyl ether was choosen in the further work as a compromise between selectivity and extraction efficiency.

Table 3
Extraction efficiencies (%) with di-*n*-hexyl ether liquid membrane (concentrations 200, 400, 1000 and 2000 ng/l) ($n = 4$) (95% confidence intervals)

Compound	Extraction efficiency (%)	
	Standard solution	Natural water sample
Thifensulfuron methyl	24 ± 2	19 ± 2
Metsulfuron methyl	35 ± 3	33 ± 4
Chlorsulfuron	50 ± 4	43 ± 3
Tribenuron methyl	49 ± 5	39 ± 4

The extraction efficiencies for the sulfonylureas in standard aqueous solutions and in natural waters are given in Table 3. The R.S.D.s are in all cases in the range 4–7%. This includes both the extraction and determination steps. The extraction efficiencies are independent of the sample concentrations, leading to linear relationships between analytical response and analyte concentrations.

The extraction recoveries are lower in the natural water samples. For all compounds except metsulfuron methyl the difference is statistically significant (0.05 level). A possible explanation is that at the low pH in the donor, there may be some adsorption of the sulfonylureas on particles in the natural water samples. Thus the extraction efficiencies will have to be checked in the samples to be extracted.

The extraction efficiencies in Table 3 are considerable lower than 100%. With a enough low donor flow-rate, efficiencies close to 100% can be obtained on the expense on time. As was discussed elsewhere [9] a faster accumulation of analyte is obtained with high flow-rates, leading to lower, but constant, extraction efficiencies. This mode of operation can be applied when a large sample volume is available.

Fig. 4 shows a chromatogram after enrichment of 240 ml natural water sample containing 0.2 μg/l of the sulfonylureas, showing a higher degree of clean-up than with SPE (cf. Fig. 3). The detection limits are in the order of 50–100 ng/l.

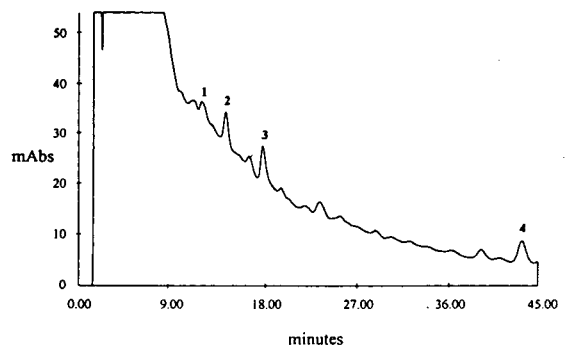

Fig. 4. Chromatogram after supported liquid membrane enrichment of a natural water sample containing 0.2 μg/l of each of the four sulfonylureas. Peaks as in Fig. 2.

4. Conclusions

The supported membrane technique has been shown to give a more selective enrichment of sulfonylurea herbicides than with solid phase extraction, leading to lower detection limits and adequate linearity and repeatability. It is likely that the SPE approach could be improved with some additional effort, for example involving several columns with different polarities. However, the inherent advantage of the supported liquid membrane technique, placing a barrier between the sample and the analytical instrument, remains. The analytes have to actively pass this barrier in order to be measured.

5. Acknowledgement

The financial support of the Swedish Council for Forestry and Agricultural Research is gratefully acknowledged.

References

[1] H.M. Brown, *Pestic. Sci.*, 29 (1990) 263.
[2] M.J.M. Wells and J.L. Michael, *J. Chromatogr. Sci.*, 25 (1987) 345.
[3] E.G. Cotterill, *Pestic. Sci.*, 34 (1992) 291.
[4] E.W. Zahnow, *J. Agric. Food Chem.*, 33 (1985) 479.
[5] R.W. Frei, M.W.F. Nielen and U.A.Th. Brinkman, *Int. J. Environ. Anal. Chem.*, 25 (1986) 3.
[6] M.W.F Nielen, R.W. Frei and U.A.Th. Brinkman, in K. Zech and R.W. Frei (Editors), *Sample Handling and Detection in High-Performance Liquid Chromatography*, Part A, Elsevier, Amsterdam, 1988, Ch. 1, p. 5.
[7] V. Leoni, C. Cremisini, A. Casuccio and A. Gullotti, *Pestic. Sci.*, 31 (1991) 209.
[8] I. Ahmad, *J. Ass. Off. Anal. Chem.*, 70 (1987) 745.
[9] J.Å. Jönsson and L. Mathiasson, *Trends Anal. Chem.*, 11 (1992) 106.
[10] G. Audunsson, *Anal. Chem.*, 58 (1986) 2714.
[11] G. Audunsson, *Anal. Chem.*, 60 (1988) 1340.
[12] B. Lindegård, J.Å. Jönsson and L. Mathiasson, *J. Chromatogr.*, 573 (1992) 191.
[13] G. Nilvé, G. Audunsson and J.Å. Jönsson, *J. Chromatogr.*, 471 (1989) 151.
[14] G. Nilvé and R. Stebbins, *Chromatographia*, 32 (1991) 269.
[15] B. Lindegård, H. Björk, J.Å. Jönsson, L. Mathiasson and A.-M. Olsson, *Anal. Chem.*, in press.
[16] L. Mathiasson, M. Knutsson, G. Bremle and L. Mårtensson, *Swed. J. Agric. Res.*, 21 (1991) 147.
[17] L. Mathiasson, G. Nilvé and B. Ulén, *Int. J. Environ. Anal. Chem.*, 45 (1991) 117.
[18] M. Knutsson, G. Nilvé, L. Mathiasson and J.Å. Jönsson, *J. Agric. Food Chem.*, 40 (1992) 2413.
[19] J.Å. Jönsson, P. Lövkvist, G. Audunsson and G. Nilvé, *Anal. Chim. Acta*, 277 (1993) 9.
[20] E.M. Beyer, M.J. Duffy, J.V. Hay and D.D. Schlueter, in P.C. Kearney and D.D. Kaufman (Editors), *Herbicides: Chemistry, Degradation and Mode of Action*, Vol. 3, Marcel Dekker, New York, 1988, Ch. 3, p. 117.
[21] *DPX L 5300 Herbicide; Technical Data Sheet*, DuPont, Wilmington, DE, 1985.
[22] R.B. Geerdink, C.A.A. Van Balkom and H.-J. Brouwer, *J. Chromatogr.*, 481 (1989) 275.
[23] V. Coquart and M.-C. Hennion, *J. Chromatogr.*, 585 (1991) 67.
[24] E.W. Zahnow, *J. Agric. Food Chem.*, 30 (1982) 854.
[25] R.V. Slates, *J. Agric. Food Chem.*, 31 (1983) 113.
[26] J.L. Prince and R.A. Guinivan, *J. Agric. Food Chem.*, 36 (1988) 63.
[27] A.C. Barefoot and R.W. Reiser, *J. Chromatogr.*, 398 (1987) 217.
[28] A.C. Barefoot, R.W. Reiser and S.A. Cousins, *J. Chromatogr.*, 474 (1989) 39.
[29] A.C. Barefoot and R.W. Reiser, *Biomed. Environ. Mass Spectrom.*, 18 (1989) 77.
[30] R.W. Reiser, A.C. Barefoot, R.F. Dietrich, A.J. Fogiel, W.R. Johnson and M.C. Scott, *J. Chromatogr.*, 554 (1991) 91.
[31] J.D. MacGlashan, J.L. Bixby and C.J. King, *Solv. Extr. Ion Exch.*, 3 (1985) 1.
[32] Y. Kuo and H.P. Gregor, *Sep. Sci. Technol.*, 18 (1983) 421.
[33] Y. Shen, L. Grönberg and J.Å. Jönsson, *Anal. Chim. Acta*, 292 (1994) 31.

ELSEVIER

Journal of Chromatography A, 688 (1994) 83–88

JOURNAL OF CHROMATOGRAPHY A

Preparative separation of naphthyltetrahydroisoquinoline alkaloids from *Ancistrocladus korupensis* by centrifugal partition chromatography☆

Yali F. Hallock[a], Jinrui Dai[b], Heidi R. Bokesch[b], Kaye B. Dillah[b], Kirk P. Manfredi[a,1], John H. Cardellina II[a], Michael R. Boyd[a,*]

[a]*Laboratory of Drug Discovery Research and Development, Developmental Therapeutics Program, Division of Cancer Treatment, National Cancer Institute, Building 1052, Room 121, Frederick, MD 21702-1201, USA*

[b]*Program Resources, Inc./DynCorp, National Cancer Institute–Frederick Cancer Research and Development Center, Frederick, MD 21702-1201, USA*

First received 2 July 1994; revised manuscript received 26 September 1994

Abstract

Crude extracts of *Ancistrocladus korupensis* contain a complex mixture of naphthyltetrahydroisoquinoline alkaloids, including the human immunodeficiency virus-inhibitory dimeric alkaloids michellamines A and B and the antimalarial monomeric korupensamines A–D. The efficient separation of michellamines A and B from these extracts has been accomplished by centrifugal partition chromatography. The chromatographic conditions used on a multi-channel cartridge unit (Sanki LLN) have been successfully scaled up with a newly developed, stacked-disk type centrifugal partition chromatography unit (Sanki NMF) for separating larger amounts of alkaloid mixtures with similar resolution. A refined, three-step process (solvent–solvent partitioning, centrifugal partition chromatography and HPLC) has been developed and applied to the scaled-up production of michellamine B for preclinical drug development.

1. Introduction

Recently, we disclosed [1,2] the isolation and identification of the unprecedented, human immunodeficiency virus (HIV)-inhibitory dimeric naphthyltetrahydroisoquinoline alkaloids, michellamines A and B (Fig. 1), from the tropical liana *Ancistrocladus korupensis*. We employed centrifugal partition chromatography as a key step in the initial analytical scale separation and purification of the michellamines. The selection of michellamine B by the US National Cancer Institute (NCI) for preclinical drug development has necessitated the development of suitable methods to provide much larger quan-

* Corresponding author.

☆ Part XIX in the series HIV-Inhibitory natural products. For Part XVIII, see J.B. McMahon, M.J. Currens, R.J. Gulakowski, R.W. Buckheit, Jr., C. Lackman-Smith, Y.F. Hallock and M.R. Boyd, *Antimicrob. Agents Chemother.*, submitted for publication.

[1] Present address: Department of Chemistry, University of Northern Iowa, Cedar Falls, IA 50614, USA.

0021-9673/94/$07.00
SSDI 0021-9673(94)00923-6

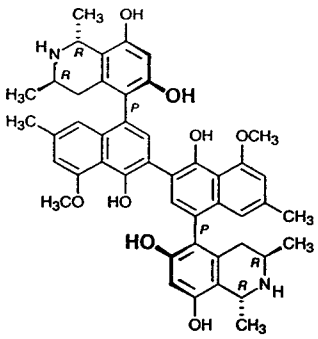

michellamine A

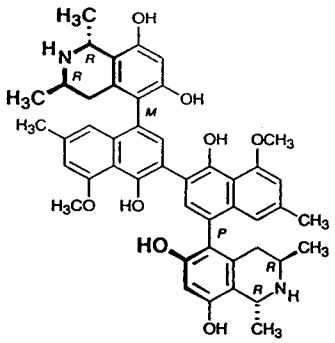

michellamine B

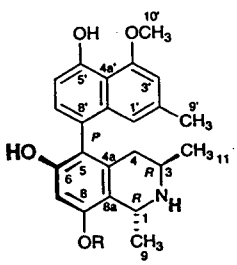

korupensamine A

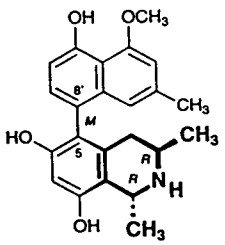

korupensamine B

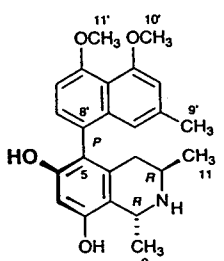

korupensamine C

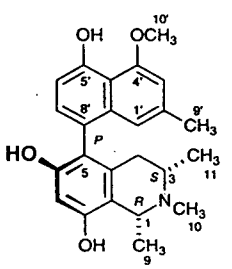

korupensamine D

Fig. 1. Structures of michellamines A and B and korupensamines A–D. The designators P (plus) and M (minus) refer to absolute configuration about the chiral biaryl axis [6].

tities (e.g., hundreds of grams) of michellamine B for investigational new drug application (IND A)-directed formulation, toxicology and pharmacokinetics studies. In this paper, we report results of our efforts to optimize and scale up the counter-current separation of these alkaloids.

2. Experimental

2.1. Reagents

All solvents, either analytical or HPLC grade, were purchased from Baxter Scientific. Mineral

and acetic acids were obtained from Aldrich. Precoated amino TLC plates (10 × 10 cm, 250 μm layer) were obtained from EM Science. McIlvaine buffer (0.025 *M* citrate and 0.05 *M* phosphate) [3,4] was adjusted to pH 4.5 with phosphoric acid. The two-phase solvent systems used for separation of the alkaloid mixture were prepared by mixing $CHCl_3$–MeOH–0.5% mineral acid or McIlvaine buffer (5:5:3, v/v/v) in a separatory funnel; the two phases were then allowed to equilibrate overnight prior to separation and use.

2.2. Crude extracts of Ancistrocladus korupensis

Samples of leaves and twigs of the tropical liana *Ancistrocladus korupensis* were collected in Cameroon under NCI contract by D. Thomas and J. Jato. Fresh plant material was air-dried, stored in the freezer for at least three days prior to processing, and then ground in a Wiley mill to a coarse powder. That powder was successively extracted with CH_2Cl_2, CH_2Cl_2–MeOH (1:1, 2 ×) and MeOH (2–3 ×). The CH_2Cl_2–MeOH and MeOH extracts thus obtained were enriched in alkaloid content by solvent–solvent partitioning; they were suspended in MeOH–water (9:1, 500 ml) and defatted by extraction with hexane (10 × 250 ml). The aqueous phase was concentrated under reduced pressure to give the alkaloid-rich extracts.

2.3. Centrifugal partition chromatography

Analytical-scale separations were performed at 24°C with a Sanki (Kyoto, Japan) cartridge CPC, Model LLN, which contained 12 (type 250W) interconnected multi-channel partition cartridges. Each cartridge has 400 channels or microcells with a net volume of 21.3 ml. The 12-cartridge setup gives a total of 4800 partition channels and a volume of 256 ml. Solvent and sample delivery was achieved using a Sanki FCU valve module fitted with a 3 ml sample loop and a constant flow pump (Sanki LBP-V). An ISCO V^4 absorbance detector (254 nm) and Foxy fraction collector were connected to the main Sanki CPC unit. The unit was operated at 400 rpm with a flow-rate of 2.8 ml/min.

Preparative-scale separations were carried out on a newly developed stacked-disk type Sanki CPC Model NMF instrument, which measures 177.8 mm in diameter and 144.5 mm in height, with a total volume of about 1.5 l. A Rainin SD-1 HPLC pump was used for solvent delivery and the direction of flow was controlled by a Sanki FCU valve module fitted with a 12-ml sample loop. The outlet of the CPC was connected to a Linear multi-wavelength UV detector (254 nm), chart recorder (Linear Instruments, NV, USA) and an ISCO Foxy fraction collector. The unit was operated at 300 rpm with a flow-rate of 16 ml/min.

2.4. High-performance liquid chromatography

A Rainin SD-1 pump and UV-1 detector were used. Separations were accomplished with a Rainin Dynamax-NH_2 column (25 × 4.1 cm), eluting with CH_2Cl_2–0.1% $(NH_4)_2CO_3$ in MeOH (22:3) at 60 ml/min and monitoring at 255 nm.

3. Results

The initial collections of *Ancistrocladus korupensis* were extracted by our standard protocol (sequential steeping in 1:1 CH_2Cl_2–MeOH and MeOH, combined to provide a crude organic extract). This material was then subjected to a multi-step, acid–base partitioning scheme. First, the extract was distributed between $CHCl_3$ and 5% HCl. The aqueous phase was then made basic with NH_4OH and extracted successively with $CHCl_3$–MeOH (3:1, then 1:1) to recover the alkaloids. We have developed a simpler method to obtain a comparable, alkaloid-rich fraction.

The plant material is first extracted with CH_2Cl_2, which effectively removes both fat and other lipids and most pigments. Subsequent extraction with CH_2Cl_2–MeOH (1:1) and MeOH then yields alkaloid-containing extracts. These extracts are further enriched by solvent

partitioning between hexane and MeOH–water (9:1). The aqueous methanol fraction is roughly equivalent to the alkaloid (basic) fractions obtained in the original approach. This method offers two important advantages when viewed from the perspective of preparative-scale production. First, the extraction step has become part of the separation process, considerably simplifying the overall task. Second, solvent can be recycled at both the extraction (CH_2Cl_2) and partition (hexane) steps, resulting in substantial cost savings.

NMR and TLC analyses of the alkaloid fraction from the *Ancistrocladus korupensis* extracts obtained from the acid–base partition from the initial protocol, or from the aqueous methanol fraction from the revised protocol, indicated a complex mixture of naphthylisoquinoline alkaloids. Michellamines A and B were initially separated from the alkaloid complex by centrifugal partition chromatography (Sanki LLN), using $CHCl_3$–MeOH–0.5% HBr (5:5:3) in the descending mode [1]. As shown in Fig. 2A, the dimeric michellamines were strongly retained in the stationary phase and partially resolved, while the accompanying monomeric alkaloids (korupensamines A–D, Fig. 1) eluted earlier.

The influence of the acid component on the separation was investigated by replacing HBr with different acids. $HClO_4$ and HI gave separations similar to that obtained with HBr, but with somewhat decreased resolution and retention (Fig. 2B and C). Substitution of HOAc (at 0.5, 2.5 or 5%) for HBr resulted in a dramatic loss of resolution and significant increase in retention. Only small amounts of non-polar constituents were eluted in the descending mode. These results might be related to acid strengths and the facility of ion pairing between the alkaloids and the acid modifiers.

The use of an aqueous buffer in place of an acid modifier for the counter-current separation of alkaloids has been reported [3,4]. We studied the separation with $CHCl_3$–MeOH–pH 4.5 McIlvaine buffer (5:5:3). Overall retention of alkaloids was increased relative to the HBr-containing solvent system (Fig. 2D); indeed, the dimeric michellamines were selectively retained

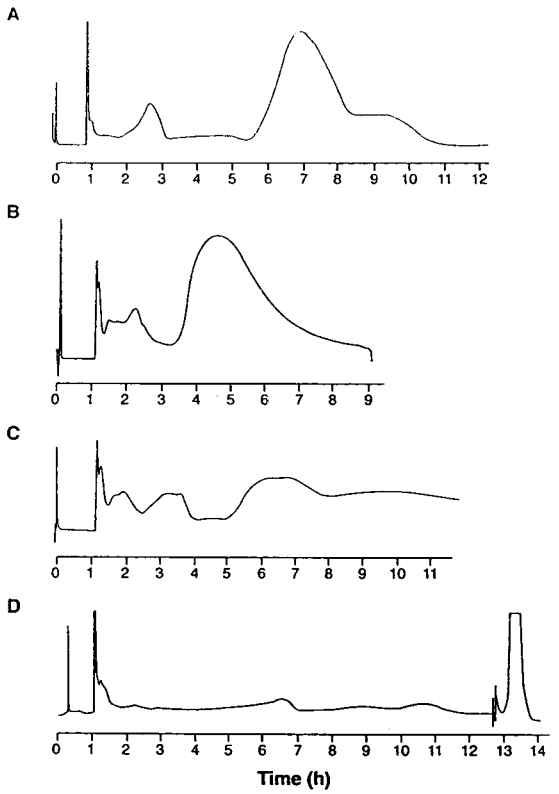

Fig. 2. Comparison of different centrifugal partition chromatography solvent combinations. All analyses performed on a Sanki CPC, model LLN with 12 analytical cartridges, with flow-rates of 2.8 ml/min at 400 rpm. Injections were 350–400 mg crude alkaloid mixture; descending mode was used in each case; detection by UV at 254 nm. (A) $CHCl_3$–MeOH–0.5% HBr (5:5:3); (B) $CHCl_3$–MeOH–0.5% $HClO_4$ (5:5:3); (C) $CHCl_3$–MeOH–0.5% HI (5:5:3); (D) $CHCl_3$–MeOH–pH 4.5 McIlvaine buffer (5:5:3).

in the stationary phase. Switching to the ascending elution mode resulted in coelution of michellamines A and B. Another disadvantage of the buffer system was the amount of salt (citrate and phosphate) in the fractions of interest; additional manipulations would be required prior to further purification (HPLC) of michellamines A and B. While it was likely that the retention and resolution of the michellamines could be modified by step gradient addition of counterions to the buffer [4], this would further complicate the separation by introducing even more salt to the fractions of interest.

Overall, the $CHCl_3$–MeOH–0.5% HBr (5:5:3) system evolved as the most advantageous of those examined, providing acceptable resolution of michellamine B and the other alkaloids as well as offering ease of workup, since no desalting step was necessary. A further advantage was the acquisition of the target compound as a hydrobromide salt, which proved to be a more stable form for storage than the free base.

In view of the requirement for multi-gram quantities of michellamine B for preclinical development, the analytical/semi-preparative-scale centrifugal partition chromatograph (Sanki LLN) was not a viable option for scale-up production of the compound. The maximum injection of crude alkaloid mixture which could be effectively resolved on this instrument was 350–400 mg.

A preparative-scale instrument (Sanki NMF) of 1.5 l capacity was expected to give a five- to six-fold increase in loading capacity with comparable resolution. Under similar operating conditions ($CHCl_3$–MeOH–0.5% HBr, 5:5:3, descending; 400 rpm; 16 ml/min flow-rate), virtually identical separations have been achieved (Fig. 3A). Reducing the spin rate to 300 rpm and the flow-rate to 15 ml/min reduced detector noise and improved resolution and, therefore, capacity

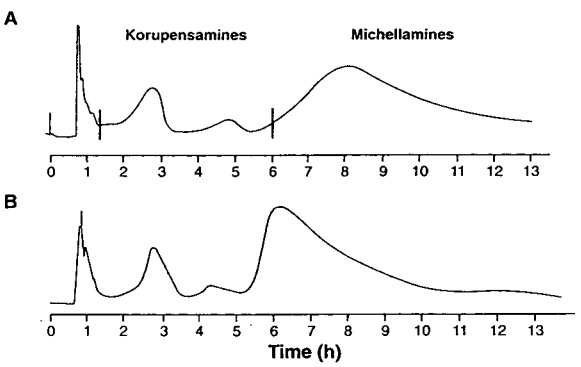

Fig. 3. Effect of spin rate on resolution in preparative-scale centrifugal partition chromatography. Analyses performed on a Sanki NMF (1.5 l capacity) with $CHCl_3$–MeOH–0.5% HBr (5:5:3) in the descending mode; detection by UV at 254 nm; (A) 2.1-g injection at 400 rpm, 16 ml/min; (B) 9.0-g injection at 300 rpm, 15 ml/min.

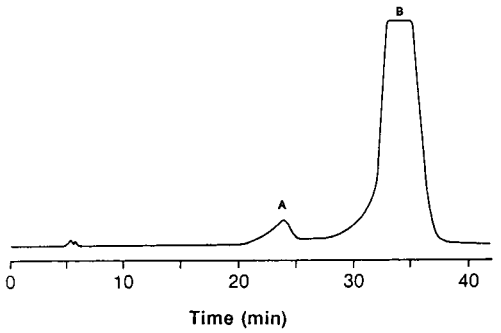

Fig. 4. Preparative HPLC purification of michellamine B. Conditions: Rainin Dynamax-Amino column (25 × 4.1 cm, 8 μm) eluted with CH_2Cl_2–0.1% $(NH_4)_2CO_3$ in MeOH (22:3) at 60 ml/min. Injection 100 mg, UV detection at 255 nm. Peaks: A = michellamine A; B = michellamine B.

(Fig. 3B). Currently, 8–9-g aliquots of crude alkaloid mixture are loaded and separated five times per week in our laboratory.

Final purification of michellamine B utilized normal-phase HPLC on an aminopropyl-bonded phase column (Rainin Dynamax-Amino, 25 × 4.1 cm). In the interests of cost reduction, environmental concern and health safety, we have been able to replace the $CHCl_3$ originally used at this stage [1] with CH_2Cl_2. Elution with CH_2Cl_2–0.1% $(NH_4)_2CO_3$ in MeOH (22:3) provides excellent separation (Fig. 4) of michellamines A and B with added loading capacity. This rapid and efficient, three-step process is currently providing 2.5 g per week of pure michellamine B for further preclinical investigation and drug development. In addition, this protocol has also facilitated access to the monomeric alkaloids (korupensamines), recently identified as antimalarial constituents of *A. korupensis* [5].

Acknowledgements

We thank Drs. G.M. Cragg, D. Thomas and J. Jato for the collections, T. McCloud for the extractions, J. Lind and C. Hughes for technical assistance and J. Cazes for many helpful suggestions.

References

[1] K.P Manfredi, J.W. Blunt, J.H. Cardellina II, J.B. McMahon, L.K. Pannell, G.M. Cragg and M.R. Boyd, *J. Med. Chem.*, 34 (1991) 3402.
[2] M.R. Boyd, Y.F. Hallock, J.H. Cardellina II, K.R. Manfredi, J.W. Blunt, J.B. McMahon, R.W. Buckheit, Jr., G. Bringmann, M. Schäffer, G.M. Cragg, D.W. Thomas and J.G. Jato, *J. Med. Chem.*, 37 (1994) 1740.
[3] A. Hermans-Lokkerbol and R. Verpoorte, *Planta Med.*, 45 (1986) 299.
[4] R. van der Heijden, A. Hermans-Lokkerbol, R. Verpoorte and A. Baerheim Svendsen, *J. Chromatogr.*, 396 (1987) 410.
[5] Y.F. Hallock, K.P. Manfredi, J.W. Blunt, J.H. Cardellina II, M. Schäffer, K.-P. Gulden, G. Bringmann, A.Y. Lee, J. Clardy, G. Francois and M.R. Boyd, *J. Org. Chem.*, (1994) in press.
[6] B. Testa, *Principles of Organic Stereochemistry*, Marcel Dekker, New York, 1979, pp. 68–71.

ELSEVIER

Journal of Chromatography A, 688 (1994) 89–95

JOURNAL OF CHROMATOGRAPHY A

Polyphosphate separations and chain length characterization using minibore ion chromatography with conductivity detection

Frederick S. Stover[a,*], Jo Ann Bulmahn[a], Janice K. Gard[b]

[a]*Industrial Products Group Technology, The Chemical Group, an operating unit of Monsanto Company, 800 N. Lindbergh Boulevard, St. Louis, MO 63167, USA*

[b]*Monsanto Corporate Research, 800 N. Lindbergh Boulevard, St. Louis, MO 63167, USA*

First received 2 August 1994; revised manuscript received 15 September 1994

Abstract

The separation of linear and cyclic polyphosphates with chain lengths of 1 to ca. 30, using 2 mm I.D. polymeric ion-exchange columns and suppressed conductivity detection, is described. The separations are characterized by good resolution of phosphate species and analysis times <30 min. To assess the accuracy of the chromatograms obtained, average chain lengths of sodium hexametaphosphate and glassy phosphates in the range 5–25 are determined and compared with results obtained by ^{31}P NMR and potentiometric titration. General agreement among the three techniques is seen. An example is presented using ion chromatography to follow the hydrolysis of sodium hexametaphosphate.

1. Introduction

One of the more challenging problems in the chemical analysis of phosphate salts is the total characterization of chain length distributions of polyphosphates. Common methods relying on end-group analysis for determining number-average chain lengths ($\bar{n}$) include ^{31}P NMR [1], pH titration [2], electrophoresis [3] and elemental analysis [4]. Polymeric phosphates with chain lengths (n) <50, such as industrially important sodium hexametaphosphate and sodium phosphate glasses, generally are not amenable to normal polymer characterization techniques such as viscosity and light scattering.

Separation methods which have been applied to determining polyphosphate chain length distributions include classical ion-exchange chromatography [5] and paper chromatography [6]. These methods are time consuming and are only partially successful in analyzing chain lengths >10.

While several systems for the HPLC determination of polyphosphates have been proposed [7,8], the most successful separations [9–12] used anion-exchange HPLC with post-column molybdate colorimetric detection to determine polyphosphates with chain lengths $<$ ca. 35. We have found that similar separations can be obtained on commercially available ion chromatography (IC) systems.

We report here the separation of linear (and cyclic) polyphosphates with chain lengths $<$ ca. 30 using minibore (2 mm I.D.) polymeric columns and suppressed conductivity detection. Advantages of this system, vs. strong anion

* Corresponding author.

0021-9673/94/$07.00
SSDI 0021-9673(94)00906-6

exchange with post-column reaction and colorimetric detection, include reduced analysis times and the ability to simultaneously detect non-phosphate anions. We also show that phosphate distributions obtained with this system give average chain lengths comparable to those obtained using other techniques.

2. Experimental

2.1. Apparatus

Polyphosphate separations were performed using IC components obtained from Dionex (Sunnyvale, CA, USA). The system consisted of a Model ASM autosampler, a Model AGP gradient pump with microbore heads, an ATC (50 × 2 mm) trap column, a CSI column stand/injector with a Rheodyne 9126 microbore valve and 25-μl sample loop, a 2-mm anion self-regenerating suppressor (ASRS) with controller module and a CDM-I conductivity detector and cell. The analytical column, a 250 × 2 mm Dionex PAX-100, contains 60-nm latex functionalized with quaternary alkanol amine and bonded to a microporous 8.5-μm ethylvinylbenzene–divinylbenzene resin substrate [13]. In certain cases, samples also were run on a standard-bore IC system, Model 4000i, using 50 × 4 mm AS5G and 250 × 4 mm AS5A columns, and a 4-mm ASRS suppressor. Data acquisition and instrument control was accomplished using a Dionex AI-450 data system.

Potentiometric titrations were performed using a Metrohm (Herisau, Switzerland) Model 636 automatic titrator equipped with a Fisher Scientific (Pittsburgh, PA, USA) Model 13-620-90 combination electrode and 20-ml buret.

^{31}P NMR spectra were collected on a Varian (Palo Alto, CA, USA) VXR-300S Fourier transform spectrometer with a phosphorus operating frequency of 121.42 MHz, at 25°C. A Varian robotic sample changer with a 50-sample tray was resident on the system. The spectrometer was equipped with a Sun Microsystems (Mountain View, CA, USA) Sparc 1+ computer, operating on Varian VNMR software, version 4.1a, and SunOS 4.1.3. Customized software developed by Monsanto was developed previously using specially designed operating environments [14].

2.2. Chemicals

Sodium hexametaphosphate was a commercial sample produced by Monsanto (St. Louis, MO, USA). Sodium phosphate glasses of nominal average chain lengths 5, 15 and 25 (type 5, type 15 and type 25) were obtained from Sigma (St. Louis, MO, USA). Sodium salts of ortho-, pyro-, tripoly- and trimetaphosphate and the hexammonium salt of tetrapolyphosphate also were obtained from Sigma. Potassium hydrogenphthalate (KHP) was a titrimetric standard obtained from NIST (Gaithersburg, MD, USA), and was dried at 105°C for 2 h. Deuterium oxide ($^2H_20$), 99.9%, was obtained from Cambridge Isotope Labs. (Woburn, MA, USA). Methanol was HPLC grade from Fisher Scientific. All water was deionized and obtained from a Millipore Milli-Q 4-bowl plus analytical purification system (Bedford, MA, USA). Other chemicals were reagent grade and used without further purification. Cation-exchange cartridges (OnGuard-H, 2 mequiv. capacity) in the acid form were obtained from Dionex.

2.3. Methods

For IC analysis, 25 ± 5 mg of sodium hexametaphosphate or sodium phosphate glass was dissolved in 100 ml deionized water. If the samples were not injected immediately, the pH was adjusted to 9.5 ± 0.5 with NaOH and stored at 4°C. Comparison of chromatograms from samples with and without pH adjustment showed no discernible effect of added base, other than minor NaOH impurity peaks eluting near the column void volume at 2 min. In certain cases, further dilution of samples was necessary to keep peaks on scale. Polyphosphate IC was performed at a flow-rate of 0.25 ml/min with a linear or No. 4 curved gradient (see Results) from 40 to 300

m*M* NaOH and a constant 5% (v/v) methanol content. The gradient was run from 0 to 20 min and held at the final eluent composition for 10 min. The suppressor was operated in the external water mode (deionized water supplied as suppressor regenerant) at a flow-rate of 3 ml/min. The conductivity detector output range was 30 μS full scale.

Conventional IC separations of ortho- through tetrapolyphosphates, when needed, were performed with linear gradients from 20 to 70 m*M* NaOH at 0 to 5 min and 70 to 100 m*M* NaOH at 5 to 15 min. Column flow-rate was 1.5 ml/min and the suppressor was operated in the recycle mode (eluent outflow supplied as suppressor regenerant).

Prior to pH titrations for determining polyphosphate chain length, sample solutions were passed through a cation-exchange resin to convert sodium salts to the acid form. Cation-exchange cartridges were prepared as per the manufacturer's instructions (4 ml water wash at 2 ml/min). A 50 ± 10 mg amount of sample was dissolved in 5 ml water, which was then passed through the cartridge at 2 ml/min using a disposable plastic syringe. Two subsequent washes of the cartridge with 5-ml aliquots of water were combined with the original eluate, and diluted to ca. 25 ml. Titrant was 0.05 *M* NaOH standardized in duplicate vs. KHP.

Samples for ^{31}P NMR analysis were prepared by adding 4 ml water and 0.5 ml $^{2}H_2O$ to 55 ± 5 mg sample, and the pH was adjusted to 9.5 ± 0.5 by addition of 0.1 *M* NaOH (ca. 0.7 ml) to minimize hydrolysis. Samples were analyzed in 5-mm NMR tubes using parameters optimized for aqueous polyphosphate solutions expected to contain significant amounts of ortho- and metaphosphates, species which have long relaxation times. Use of a 15° pulse, 7.0-s repetition rate, 40 000 data points and 0.8 s acquisition times have been shown [14] to result in >97.5% of the observable magnetization being determined for the longer-relaxing species and >99.5% for faster relaxing species such as tripoly- and pyrophosphate. Samples were signal averaged for 900 transients.

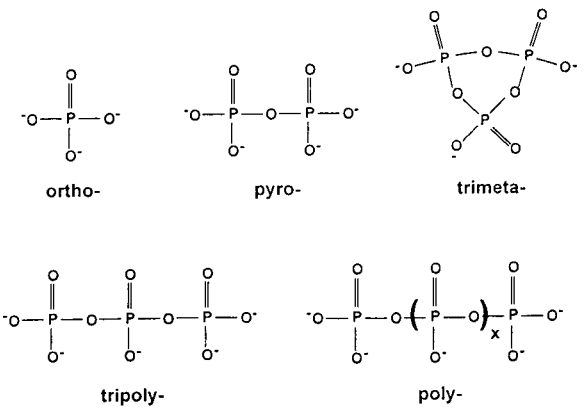

Fig. 1. Phosphate species separated by minibore ion chromatography.

3. Results

3.1. Polyphosphate separations

Phosphate species found in sodium hexametaphosphate (SHMP) and sodium phosphate glasses are shown in Fig. 1. A typical separation of SHMP using the minibore IC system is given in Fig. 2. The significant feature of this chromatogram is the improved speed of separation seen *vs.* previous analysis [9]. Comparison of

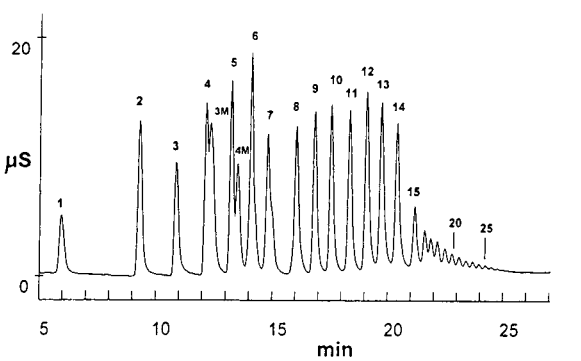

Fig. 2. Typical separation of polyphosphate species in sodium hexametaphosphate (SHMP). Peaks identified by number of phosphorous atoms for linear species, and by number of phosphorus atoms + "M" for meta-, or cyclic, phosphates. Concentration SHMP injected = 0.20 mg/ml. Gradient = linear.

peak areas with injections of standard materials indicates that minibore IC detection limits for smaller phosphates are on the order of 50 ng/ml, or ca. 1 ng by mass. Another feature of this separation is that the cyclic metaphosphates elute in order of their phosphorus numbers, instead of the inverse order seen previously [11].

Resolution acceptable for many applications is seen for phosphate species with chain lengths up to ca. 30. The poorest resolution is seen between the tetrapoly-/trimeta- and pentapoly-/tetrameta- peaks. Resolution of these pairs can be lost depending on sample loading and poly-/meta- ratios. Previous studies [9,11] indicated that an optimum separation of polyphosphates can be obtained using convex gradient elution. The effect of gradient curvature on separation quality of SHMP was tested by running the two least-curved convex and concave gradients available on the AGP pump. The most significant feature of these separations is changes in relative retention of meta- vs. linear polyphosates. While some flexibility in tailoring separations for specific samples is offered by the curved gradients, no single gradient gives complete baseline resolution of the phosphate species in SHMP. Convex gradient No. 4 is of the form $C = C_0 + [(t - t_0)/(t_f - t_0)]^a \cdot (C_f - C_0)$, where $a = 0.7$, C is the eluent concentration at time t, C_0 is the initial eluent concentration at time t_0, and C_f is the final eluent concentration at time t_f. This gradient shows improved tetrapoly-/trimeta- resolution but somewhat poorer pentapoly-/tetrameta- separation. Subsequent separations were performed with either linear or No. 4 gradient.

A typical application of the minibore IC system in our laboratory is assessment of hydrolytic stability of SHMP solutions under various conditions. The analysis of 40% SHMP solutions after 7 days storage at different temperatures is shown in Fig. 3. At room temperature, the original SHMP phosphate distribution remains intact. At 49°C, significant amounts of $n > 5$ polyphosphates are hydrolyzed. At 60°C, essentially all condensed phosphates are hydrolyzed to orthophosphate. Advantages of IC for this type of analysis include (1) obtaining a graphic description of changes in chain length distributions

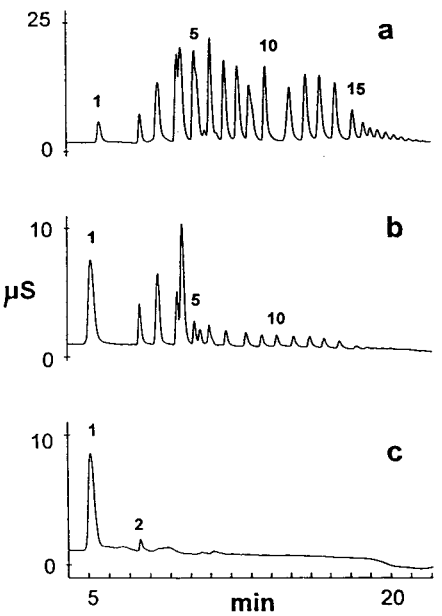

Fig. 3. Analysis of 40% SHMP solutions after 7 days storage at (a) room temperature, (b) 49°C and (c) 60°C. Peak labels as in Fig. 1. Gradient No. 4.

and (2) the capability of studying hydrolysis kinetics of individual P species.

The ability of the minibore IC to analyze other polyphosphates is shown in Fig. 4, where separations are shown for sodium phosphate glasses with different average chain lengths. The shift toward higher phosphate species with increasing chain length is clear, and reasonable separations are obtained for nominal $\bar{n}$ up to 25. Close inspection of the highest $\bar{n}$ sample shows that peaks for n approaching 40 can be detected.

3.2. Average chain length determination

The major difficulty in using suppressed conductivity detection for the quantitative analysis of polyphosphates involves the lack of standards for determining concentration-based response factors. For the chromatograms shown here, questions remain about how well IC peak area distributions correlate with actual chain length distributions. To assess the quantitative potential of the current IC system, comparisons were

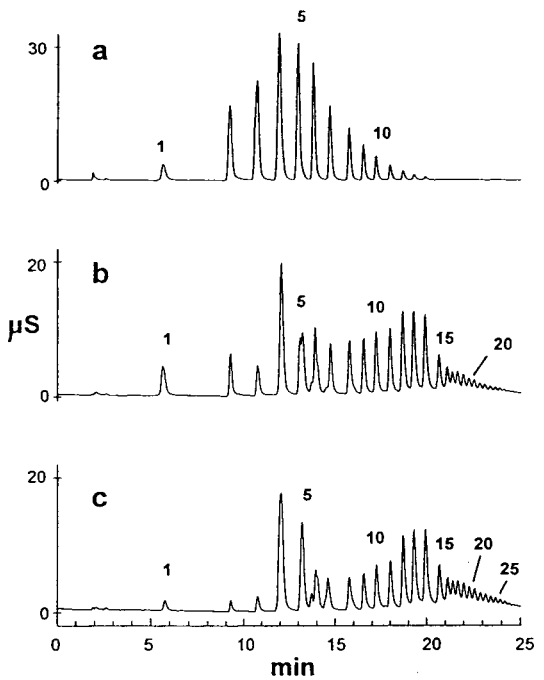

Fig. 4. Chromatograms of sodium phosphate glasses, (a) $\bar{n} \approx 5$, (b) $\bar{n} \approx 15$ and (c) $\bar{n} \approx 25$. Concentration injected = 0.25 mg/ml for (b) and (c), 0.125 mg/ml for (a). Peak labels as in Fig. 1. Gradient linear.

made between average chain lengths determined by IC and by other techniques.

Peak area-average chain lengths, $\bar{n}$(IC), were calculated from chromatograms shown in Figs. 2 and 4 using

$$\bar{n}(\mathrm{IC}) = \sum(\mathrm{area}_i \cdot n_i)/\sum(\mathrm{area}_i) \quad (1)$$

where n_i is the number of phosphorus atoms in the ith species. Average chain length calculations used all linear polyphosphate peaks (including ortho) but did not include metaphosphates. Trimetaphosphate content of the samples was verified by conventional 4-mm IC, where baseline separations of trimeta- and tetrapolyphosphate were obtained.

Typical determinations of average chain length by ^{31}P NMR and potentiometric (pH) titration are shown in Fig. 5. For NMR, the average chain length, $\bar{n}$(NMR), can be calculated from the integrated areas of the ortho (O), end-group (E) and internal (I) phosphorus resonances by

$$\bar{n}(\mathrm{NMR}) = (\mathrm{I} + \mathrm{E} + \mathrm{O})/(\mathrm{E}/2 + \mathrm{O}) \quad (2)$$

For pH titrations [2,3], the average chain length, $\bar{n}$(pH), can be calculated from the strong acid titer (A), weak acid titer (B), and an independent determination of the titers due to ortho (O) and meta (M), by

$$\bar{n}(\mathrm{pH}) = 2(\mathrm{A} - \mathrm{M})/(\mathrm{B} + \mathrm{O}) \quad (3)$$

A summary of the average chain lengths found for SHMP and sodium phosphate glasses is given in Table 1. M and O values used in Eq. 3 were taken from NMR data. Reasonable agreement among methods is seen for SHMP and the types 5 and 15 sodium phosphate glasses. Also, very good precision is seen for replicate analyses of SHMP by IC. This indicates that IC is well suited to comparative analysis of different polyphosphates. For type 25 glass, disagreement between IC/titration and NMR is pronounced. Investigations are continuing in order to assess the source of this bias. Potential sources of error include hydrolysis during sample preparation and unknown response factors for conductivity detection. However, the comparison in Table 1 shows that IC results correlate with chain lengths determined by other methods up to $\bar{n} = 15$, and gives an indication of the accuracy to be expected at different $\bar{n}$ values.

4. Discussion

End-group methods such as NMR and pH titration yield number-average, rather than mass-average, chain lengths. Polyphosphates with $n <$ 5 show roughly equal conductivity mass-response factors, as determined by injecting known amounts of standard compounds. However, if equal mass response is assumed over the entire chain length range, conversion from an area- (hence mass-) average chain length to a number-average chain length for SHMP gives $\bar{n} \approx 6$. Clearly, $\bar{n}$ values calculated from raw peak areas more closely approximate number average chain lengths.

From the known counterion binding properties

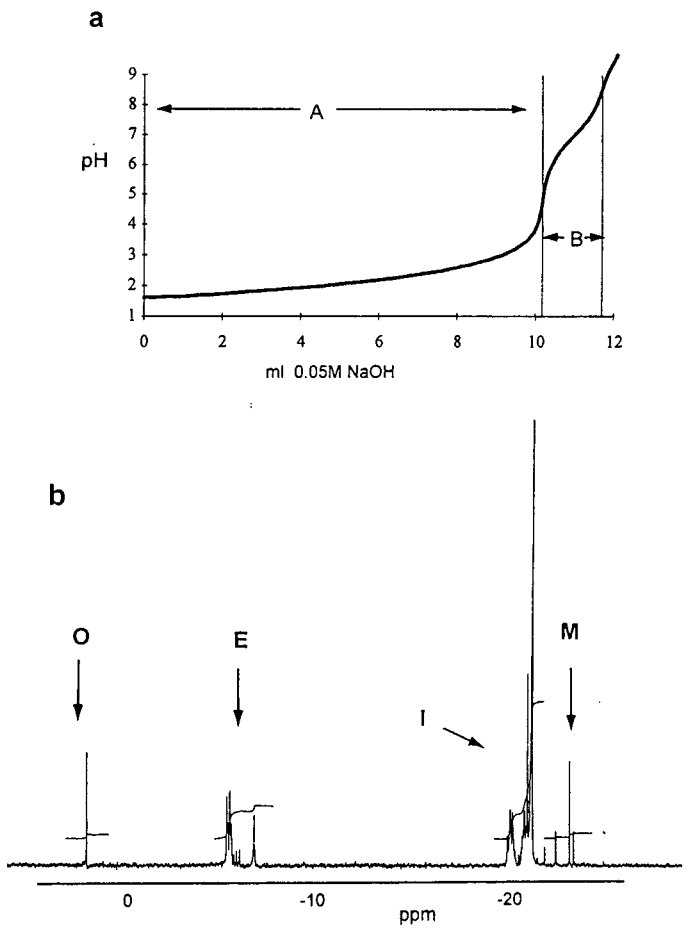

Fig. 5. Typical analysis for chain length by (a) pH titration and (b) ^{31}P NMR. (a) A = strong acid (internal, ortho and meta) region, B = weak acid (end-group and ortho) region. (b) O = ortho, E = end-group, I = internal and M = metaphosphate resonances.

Table 1
Comparison of average chain lengths obtained by different techniques

	$\bar{n}$(IC)	$\bar{n}$(pH)	$\bar{n}$(NMR)
SHMP	9.20 ± 0.06[a]	9.04 ± 0.11[a]	8.68 ± 0.26[a]
Sodium phosphate glasses			
Type 5	5.08	4.21	3.97
Type 15	11.6	12.6	10.1
Type 25	14.5	16.5	26.8

[a] Standard deviation, $n = 4$ for SHMP analyses.

of polyelectrolytes [15], counterion condensation and site-specific charge neutralization occur in longer-chain polyphosphates. Conductivity response factors for polyphosphates thus should decrease from a nearly equal-mass basis at low chain lengths to a more equal-molar response at higher chain lengths. Since standards are available for linear phosphates with $n < 5$, a preliminary assessment of response factors for $n \geq 5$ species was performed by calculating total masses and total areas of these species from SHMP chromatograms. The relative response factor (relative to $n < 5$) was found to average ca. 0.5 for all $n \geq 5$ components.

One unusual feature of the polyphosphate separations shown in Figs. 2–4 is the appearance of an almost bi-modal chain length distribution. Literature separations [9] of similar polyphosphates, using hydrolysis/colorimetry to give uniform P-based detection, have shown monomodal distributions. With conductivity detection, a minimum in the distribution appears near $n = 7$. It is likely that this is the point where conductivity response factors begin to decrease due to counterion binding. Consistent with this is the observation [3] that isotachophoretic response factors of polyphosphates show a change in the $n = 5–7$ region.

Despite the uncertainty in response factors discussed above, minibore IC with conductivity detection is shown to be a useful technique for rapid characterization of common polyphosphates. To develop the technique further as a quantitative tool, polyphosphate response factors for conductivity detection need to be determined. The most direct approach would be development of a polyphosphate standard that is well characterized by HPLC using post-column detection with constant-P response. Alternative approaches include (1) fraction collection, hydrolysis and P-content analysis by re-injection or colorimetry, and (2) solubility fractionation [16] of the polyphosphates to obtain narrow distributions for calibration.

Acknowledgements

The authors wish to thank David R. Gard, Helen M. Thompson and Edward E. Remsen for helpful discussions of polyphosphate chemistry and polymer characterization methods.

References

[1] J.C. MacDonald and M. Mazurek, *J. Magn. Reson.*, 72 (1987) 48.
[2] J.R. Van Wazer, E.J. Griffith and J.F. McCullough, *Anal. Chem.*, 26 (1954) 1755.
[3] I. Motooka, H. Nariai, K. Nakazaki and M. Tsuhako, *J. Chromatogr.*, 260 (1983) 377.
[4] J.R. Van Wazer, *Phosphorus and its Compounds*, Vol. I, Interscience, New York, 1958, p. 756.
[5] H.L. Rothbart, H.W. Weymouth and W. Rieman, *Talanta*, 11 (1964) 33.
[6] Y. Kiso, M. Kobayashi and Y. Kitaoka, in M. Halmann (Editor), *Analytical Chemistry of Phosphorus Compounds*, Wiley-Interscience, New York, 1972, Ch. 3, p. 124.
[7] R.S. Brazell, R.W. Holmberg and J.H. Moneyhun, *J. Chromatogr.*, 290 (1984) 163.
[8] W.R. Biggs, J.T. Gano and R.J. Brown, *Anal. Chem.*, 56 (1984) 2653.
[9] Y. Baba, N. Yoza and S. Ohashi, *J. Chromatogr.*, 350 (1985) 119.
[10] Y. Baba, N. Yoza and S. Ohashi, *J. Chromatogr.*, 348 (1985) 27.
[11] H. Yamaguchi, T. Nakamura, Y. Hirai and S. Ohashi, *J. Chromatogr.*, 172 (1979) 131.
[12] N. Yoza, H. Hirano, Y. Baba and S. Ohashi, *J. Chromatogr.*, 325 (1985) 27.
[13] *1994–1995 Product Selection Guide*, Dionex, Sunnyvale, CA, 1994, p. 64.
[14] J.K. Gard, J.C. Burquin, W.B. Wise and B.S. Herman, *Spectroscopy*, 7 (1992) 28.
[15] U.P. Strauss, D. Woodside and P. Wineman, *J. Phys. Chem.*, 61 (1957) 1353.
[16] J.R. Van Wazer, *J. Am. Chem. Soc.*, 72 (1950) 647.

ELSEVIER

Journal of Chromatography A, 688 (1994) 97–105

JOURNAL OF CHROMATOGRAPHY A

Analysis of colloids VII. ☆Wide-bore hydrodynamic chromatography, a simple method for the determination of particle size in the nanometer size regime

Ch.-H. Fischer*, M. Giersig

Hahn-Meitner-Institut Berlin, Department CK, Glienicker Strasse 100, D-14109 Berlin, Germany

First received 6 July 1994; revised manuscript received 6 October 1994

Abstract

Wide-bore hydrodynamic chromatography in a polyether ether ketone (PEEK) capillary (I.D. 0.7 mm, length 20 m) was used to determine the weight average diameter d_w of colloidal particles. The method was applied to cadmium sulphide and gold sols in the diameter range between 3 nm and 27 nm. The method is based on the radial distribution of the analyte in the capillary due to the hydrodynamic flow profile in the capillary and due to the diffusion coefficient of the particles, which is dependent on their diameter. The diameter was calculated from the ratio of the heights of convection peak and diffusion peak. The size-quantization effect of small semiconductor particles made it possible to visualise the separation inside of the capillary. One important advantage of the applied method is the very much reduced adsorption, which often causes serious problems in the HPLC especially of inorganic colloids. The results of wide-bore hydrodynamic chromatography, size exclusion chromatography and transmission electron microscopy were compared.

Introduction

The study of colloidal semiconductor and metal particles in the nanometer size regime is a steadily growing field in chemistry. Because ultra small particles exhibit unusual physical and chemical properties, e.g. blue-shifted absorption and fluorescence spectra with decreasing diameter and because of their possible application in solar energy technology and microelectronic devices they have become the focus of much recent physicochemical research [1,2]. However the investigation of size dependent properties requires good and reliable size analysis. The classical technique is transmission electron microscopy (TEM), where the particle diameters are measured directly. Nevertheless, problems can arise from radiation damage due to the high energy applied to the material [3]. If no expensive image processing system is available, the measurement of the sizes on the micrographs is also rather tedious and often quite subjective. Size exclusion chromatography (SEC) has also recently been shown to be a very convenient method for the size determination for inorganic colloids [4,5]. In the case of HPLC–SEC, the system measures

* Corresponding author.

☆ For part VI see Ref. [8], for part V Ref. [7] and for part IV Ref. [26].

0021-9673/94/$07.00
SSDI 0021-9673(94)00962-7

size distributions within a few minutes, once the initial calibration has been carried out [6,7]. Speed is important when kinetics of the growth of very unstable colloids is investigated [6]. Further advantages of the chromatographic method are the good statistics of the result, on-line coupling with diode array detectors for studies of size depending UV/Vis spectra [6] and the possibility of scaling-up the system for preparative separations [8]. However, with some kinds of colloids, e.g. PbS, adsorption or particle growth during the passage through the column causes difficulties even in the presence of the stabilisers in the eluent. The hydrodynamic chromatography in packed columns showed the same limitations [9]. In the classical hydrodynamic chromatography (HDC) in *narrow* capillaries or with other name capillary hydrodynamic fractionation (CHDF) organic particles could be separated according to the diameter with good resolution [10–13]. Silebi [11] described the analysis of latex particles with diameters down to 88 nm (diameter range of the inorganic particles under investigation: 3 nm–27 nm). Adsorption was less pronounced than in packed columns, but still a problem. Therefore a chromatographic technique could be helpful, where there is a smaller surface area than in a packed column or in a narrow capillary.

In 1978 Mullins and Orr [14] and in 1979 Noel et al. [15] reported the fractionation of micrometer-sized particles in a capillary with an internal diameter of 250 μm. Submicrometer particles could not be distinguished.

In 1984 Kelleher and Trumbore [16] described an easy method for the determination of the molar weight of biopolymers just by pumping a sample plug through a rather thick capillary. The internal diameter was some tenths of a millimetre and therefore much thicker than in classical hydrodynamic chromatography (capillary hydrodynamic fractionation) where the diameter is typically some microns. The experiment was carried out initially with a normal UV/Vis detector, but later with special RI detectors which measured the radial concentration gradient [17–19]. Unlike normal chromatography, it is the peak shape, rather than the retention time, which was used for the calculation of the molecular weight. The method is based on the dependence of the diffusion coefficient on the molecular weight. Conversely, diffusion coefficients of species with known molecular weight can be calculated from the peak width [20]. Vanderslice et. al. investigated the concentration profiles in such flow systems and calculated them under various conditions [21].

In the past the method in question has been contributed to the group of flow injection analysis (FIA). However, most often in FIA concentrations are measured by peak size either after mixing with special reagents or without mixing by the use of specific detectors. Though the described method has doubtless similarities with FIA, it is based on the hydrodynamic flow profile in the capillary, which is generated by the flow resistance of the walls. The species to be analysed interact dynamically with the flow medium and indirectly with the walls. This is typical for chromatography, though not a spectrum of various (particular) retention times is measured. Therefore we prefer the name *wide-bore* hydrodynamic chromatography (HDC) in order to stress similarities and differences to the *classical* HDC.

Experimental

Chromatography

Wide-bore HDC

The experimental set-up consisted of a Merck–Hitachi L6000 HPLC pump, a Merck Autosampler A2000 (sample volume 100 μl) and a Waters 990 diode array detector. Autosampler and detector were connected via a 20 m long, 0.7 mm I.D. polyether ether ketone (PEEK) capillary. The flow rate was 0.8 ml/min. The eluent for the cadmium sulphide sols was 10^{-3} *M* cadmium perchlorate (Ventron)/$6 \cdot 10^{-3}$ *M* sodium polyphosphate (based on the phosphate units, Riedel de Haen), and for gold sols 10^{-3} *M* sodium citrate was used.

SEC

Two 125 × 4 mm columns (Knauer Säulentechnik, Berlin, Germany) in series were used: For cadmium sulphide Nucleosil 500C4 (7 μm) and Nucleosil 1000C4 (7 μm) and for gold Nucleosil 500 (15–25 μm) and Nucleosil 1000C4 (15–25 μm). Eluents, pump and detector were the same as for HDC.

Preparation of the colloids

Cadmium sulphide sols

Hydrogen sulphide gas or aqueous sodium hydrogen sulphide solution was injected through a septum into an aqueous solution of 10^{-3} *M* $Cd(ClO_4)_2$ and $6 \cdot 10^{-3}$ *M* sodium polyphosphate, through which nitrogen had been bubbled for ten minutes. The solution was shaken prior to use. The particle size was controlled by the initial pH value of the solution before sulphide addition. A lower starting pH leads to smaller particles [22]. Aged samples containing larger colloids were also used in some experiments.

Gold sols

Gold sols were prepared by using a mixture of trisodium citrate and tannic acid (Mallinckrodt product no. 8835) as reducing agent [23]. $KAuCl_4$ (85 ml, 0.1%) was heated to 60°C and stirred rapidly. A second reducing solution was prepared by mixing trisodium citrate (4 ml, 1%) tannic acid (0–5 ml, 1%) and an equivalent amount of K_2CO_3 (0–5 ml, 10^{-2} *M* and making up to 25 ml. This solution was also heated to 60°C and then added rapidly to the chloroaurate solution. The colour of these sols developed almost instantly. The solution was then boiled for several minutes and allowed to cool. Tannic acid increases the rate of nucleation, thereby generating smaller particles. The higher the tannic acid:citrate ratio, the smaller the particle size. The lowest size limit achievable was found to be about 2–3 nm. The sols so prepared were stable for months, although sometimes a slow sedimentation was observed over time, which could be removed by centrifugation. The particle size distributions were measured from electron micrographs.

Electron microscopy

A small drop of sample was adsorbed onto a 400-mesh copper grid coated with a 50 Å thick carbon support film. After 10 seconds of contact time the fluid was blotted off. The grids were dried under argon and examined in a Philips CM 12 transmission electron microscope with an acceleration voltage of 120 kV. The microscope was equipped with a supertwin lens and an EDAX detector. For imaging, axial illumination was used as well as the "nanoprobe mode" with a beam spot size of 1.5 nm, to enable diffraction patterns of the individual clusters to be obtained. All images were made under conditions of minimum phase contrast and low electron dose with a magnification of 120 000 and 430 000 ×.

Results and discussion

Method

When a liquid passes through a capillary under laminar flow conditions, a parabolic flow profile is formed, i.e. fast flow in the centre and decreasing velocity towards the walls. Dissolved species are transported forward with the liquid flow, but they can also move in other directions by diffusion. Here the motion perpendicular to the flow direction is of particular importance. It brings the solute from the centre to the walls and vice versa, i.e. from faster streams to slower flowing parts of the cross-section. However, this motion is dependent on the diffusion coefficient of the sample. When a sample of very big colloidal particles or very large macromolecules is injected into such a flow system with appropriate flow rate, their diffusion is low compared to the speed of the forward stream. Therefore the radial movement is negligible. In Fig. 1a the axial and radial concentration distribution of sample species in the capillary is shown schematically, based on the calculations of Van-

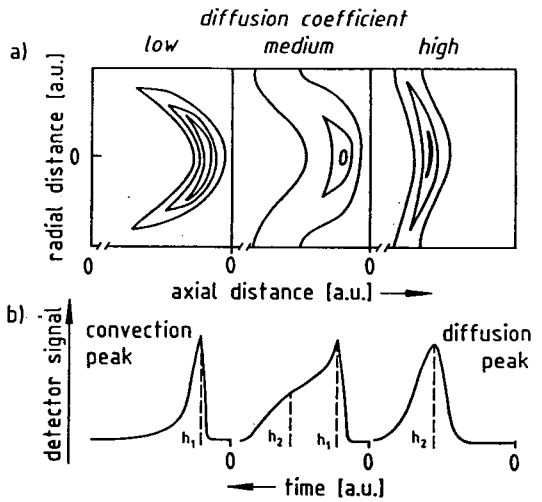

Fig. 1. Behaviour of material with small, medium and high diffusion coefficient during laminar flow through a "wide-bore" capillary. (a) Axial and radial concentration distribution expressed in equiconcentration lines, based on the theoretical calculations of Vanderslice et al. [21]. (b) Corresponding elution profiles.

derslice et al. [21]. The left part of Fig. 1 represents the situation just described for low diffusion coefficient. The analyte follows the laminar flow profile, apparently without any additional motion. On the other hand species with a very high diffusion coefficient exchange efficiently between slow and fast areas (Fig. 1, right part), and therefore the concentration is more uniform over the diameter and the average speed is slower than in the first case. Species with medium diffusion coefficient (Fig. 1, centre) show a behaviour between the extreme cases. These distributions cannot be easily visualised. But with a simple experimental set-up consisting of a pump, an injection valve with sample loop, the capillary and a detector with a through-flow cell, an elution profile can be obtained which is similar in principle to a chromatogram. The response gives the integral radial concentration at a certain axial distance from the injection point. Due to the flow, the whole distribution is pushed through the detector cell with time. The result is an early eluting, steeply increasing, but strongly tailing and therefore asymmetric convection peak for slowly diffusing species and a relatively symmetric late-eluting diffusion peak for material with a high diffusion coefficient. Materials with a medium diffusion coefficient show an elution profile with the elements of both kinds of peaks, the ratio depending on the size of the diffusion coefficient. Fig. 1b shows the elution profiles corresponding to the upper situations. The diffusion coefficient of dissolved organic polymers depends on the size of their coils which is proportional to the molecular weight. In the case of colloidal particles their diameter is the important parameter. The experimental set-up is very simple (Fig. 2). A pump delivers the eluent, and the sample is introduced by a sample valve and pumped through the capillary to the detector.

Application

Cadmium sulphide sols

For the first experiments cadmium sulphide sols were used. Much experience exists in SEC of these semiconductor colloids, so that the results could easily be compared. Stabilisers such as polyphosphates have to be added to these aqueous colloids in order to reduce particle growth. These molecules form complexes with the surface of the particles and protect it against direct contact with others and therefore against coagulation. On the other hand it also reduces adsorption on the surface of the column and the stationary phase.

A series of CdS sols of different particle size, 10^{-3} *M* each, were prepared, whereby the size was controlled via the pH value before the sulphide addition. These sols were injected simultaneously in the HDC capillary and onto the SEC column. The eluent compositions of both methods were the same: 10^{-3} *M* cadmium

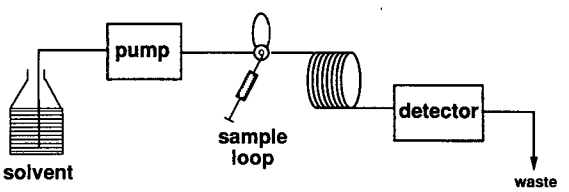

Fig. 2. Scheme of experimental set-up in wide-bore HDC.

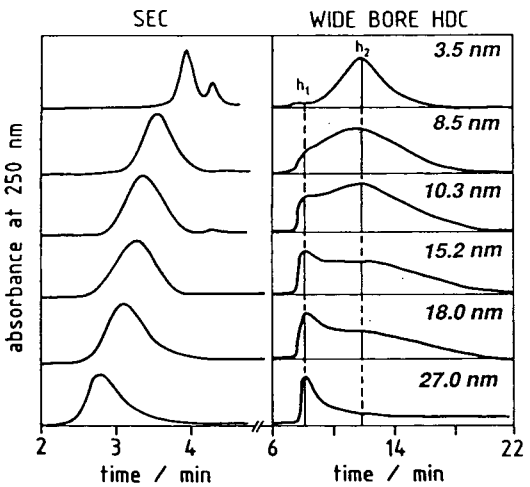

Fig. 3. Cadmium sulphide sols of different particle sizes analysed by SEC (left) and wide-bore HDC (right). The samples are sorted, the smallest particles on top, largest at the bottom. The weight average diameters d_w are given on the right hand side.

perchlorate/$6 \cdot 10^{-3}$ M sodium polyphosphate. Fig. 3 shows the results. On the left, the size exclusion chromatograms and on the right the corresponding hydrodynamic chromatograms. The samples are sorted with respect to increasing particle diameter. As the SEC peak shifted to shorter retention volumes, the HDC peak became less symmetric. In addition to the late diffusion peak, the early convection peak grew. Finally only the latter remained with a pronounced tailing.

For proof of the separation inside a wide capillary the size quantization effect (Q effect) of the nm-sized semiconductor particles could be used. For these particles, the onset of absorption shifts to shorter wavelengths with decreasing particle size [24,25]. When a CdS sol with a broader size distribution was analysed, different chromatograms were obtained depending on the observation wavelength. At shorter wavelengths (250 nm and below) all sizes are detected and have the same molar extinction coefficient, whereas at longer wavelengths smaller particles absorb less than larger ones. Consequently we found in Fig. 4a at 250 nm a large diffusion peak next to a small shoulder due to a convection peak. With increasing wavelength, the shoulder grew and at 500 nm the convection peak was pronounced, because smaller particles do not absorb any more in this wavelength range. The separation is also evident from the spectra taken with the diode array spectrometer during the run (Fig. 4b). The spectrum at 8.7 min had an onset

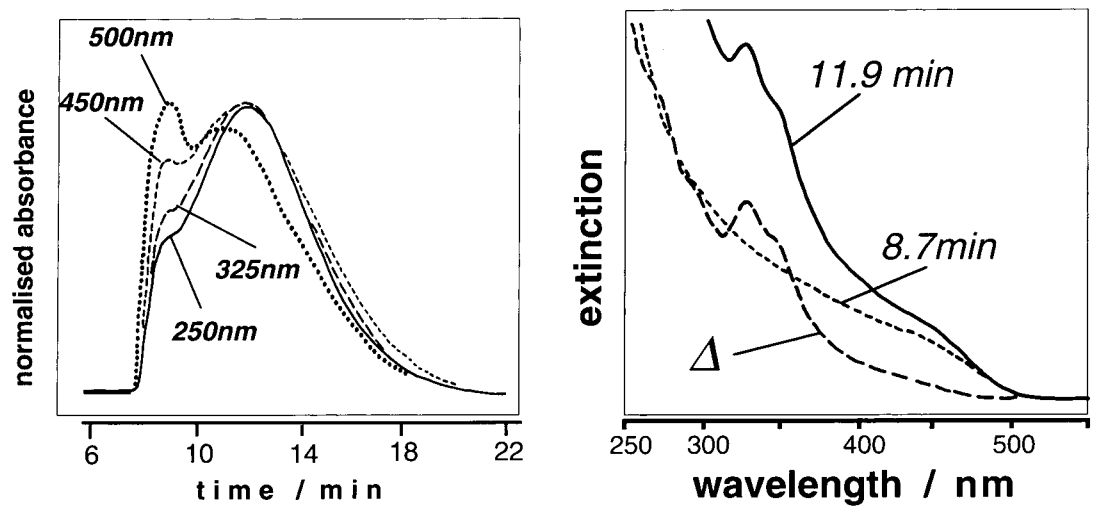

Fig. 4. Wide-bore HDC with diode array detection and the size quantization effect of a cadmium sulphide sol with a relatively broad size distribution. Left: Chromatograms obtained at different wavelengths. Right: UV–Vis spectra measured at 8.7 min (dotted line), at 11.9 min (solid line) and the difference Δ between both spectra (dashed line).

of absorption near 500 nm and no further fine structure, typical for rather large CdS particles. The spectrum obtained at 11.9 min showed a similar onset, but also a small maximum at 330 nm and a shoulder at 350 nm. This spectrum is a superposition of smaller and bigger particles, since the bigger particles of the sample are still eluting. As is evident from the chromatogram at 500 nm they are only of medium size with convection and diffusion peaks of about the same height. Therefore a spectrum with a pronounced maximum typical for particles below 3 nm is obtained, when the first spectrum is subtracted from the second (spectrum Δ in Fig. 4b). The maxima in this region are due to so-called magic agglomeration numbers, i.e. energetically very stable agglomerates [1,2].

Gold sols

Gold sols were prepared by the reduction of tetrachloroaurate with citrate in the presence of tannic acid [23]. Increasing concentration of the latter yields smaller particles. A series of these sols was also investigated by transmission electron microscopy (TEM). In the micrographs, the diameters of a sufficiently high number of particles, i.e. more than 150, was measured and the size distribution constructed (Fig. 5, left). Then SEC was carried out (Fig. 5, centre) on Nucleosil 500 and Nucleosil 1000 (15–25 μm) [26]. When smaller silica material was utilised, the gold sol was irreversibly adsorbed on the column. There are some samples with bimodal distribution in the SEC and only a single size population in TEM. It shows that sometimes in the TEM less frequent populations can be overlooked. For the wide-bore HDC of gold sols, a 1 m*M* sodium citrate solution was used as the eluent, the same as that used with SEC. Again, the same trend in the chromatogram shape from pure diffusion to pure convection peak was observed (sample a→e in Fig. 5, right). These parallel experiments allow a good comparison of all three methods.

Calculation

In the past different approaches have been used in the determination of the molecular weight from the obtained elution profiles. When a gradient detector was used, the molecular mass M_r was determined by means of the asymmetry ratio of the derivative signal [27]. Trumbore et al. [28] suggested for the normal elution profiles, the ratio R of the height of the convection peak h_1 to that of the diffusion peak h_2 (Eq. 1) for the determination of the molar weight M_n of a polymer by empirical correlation. When one of the both peaks is not sufficiently pronounced, the height of the chromatogram at the position in question is taken for the calculation.

$$R = h_1/h_2 \quad (1)$$

We also used the height ratio R, but as a function of the weight average *diameter* d_w, since colloid chemists prefer the use of diameter, considering that the solid particles are rigid and non-swelling as opposed to the organic polymer coils. For the calibration, a number of colloids were prepared and their weight average diameter was determined by computer evaluation of the SEC chromatograms or in the case of gold sols directly by TEM. In Fig. 6 the ratio R as a function of the diameter d_w is given for both colloids CdS and Au and there is a clear dependence. From these calibration plots the average particle size of unknown samples of the same material can easily be determined. The slopes of both curves are quite different. Two reasons can be given to explain this. Firstly, the eluent composition was different and secondly, the true size of the solid particles is different from the effective particle size due to the electrical double layer, which is formed at the solid–liquid interface by electrolytes of the solution. The thickness of this layer is dependent on the solid material but also on the particular electrolyte. Under the conditions of Fig. 6 the electrical double layer of the gold particles seems to be thicker and therefore diffusion plays a less important role than in the case of cadmium sulphide.

Finally it should be mentioned that the concentration of the colloid itself also has an effect on the diffusion rate and therefore on the result of size determination. The higher the concen-

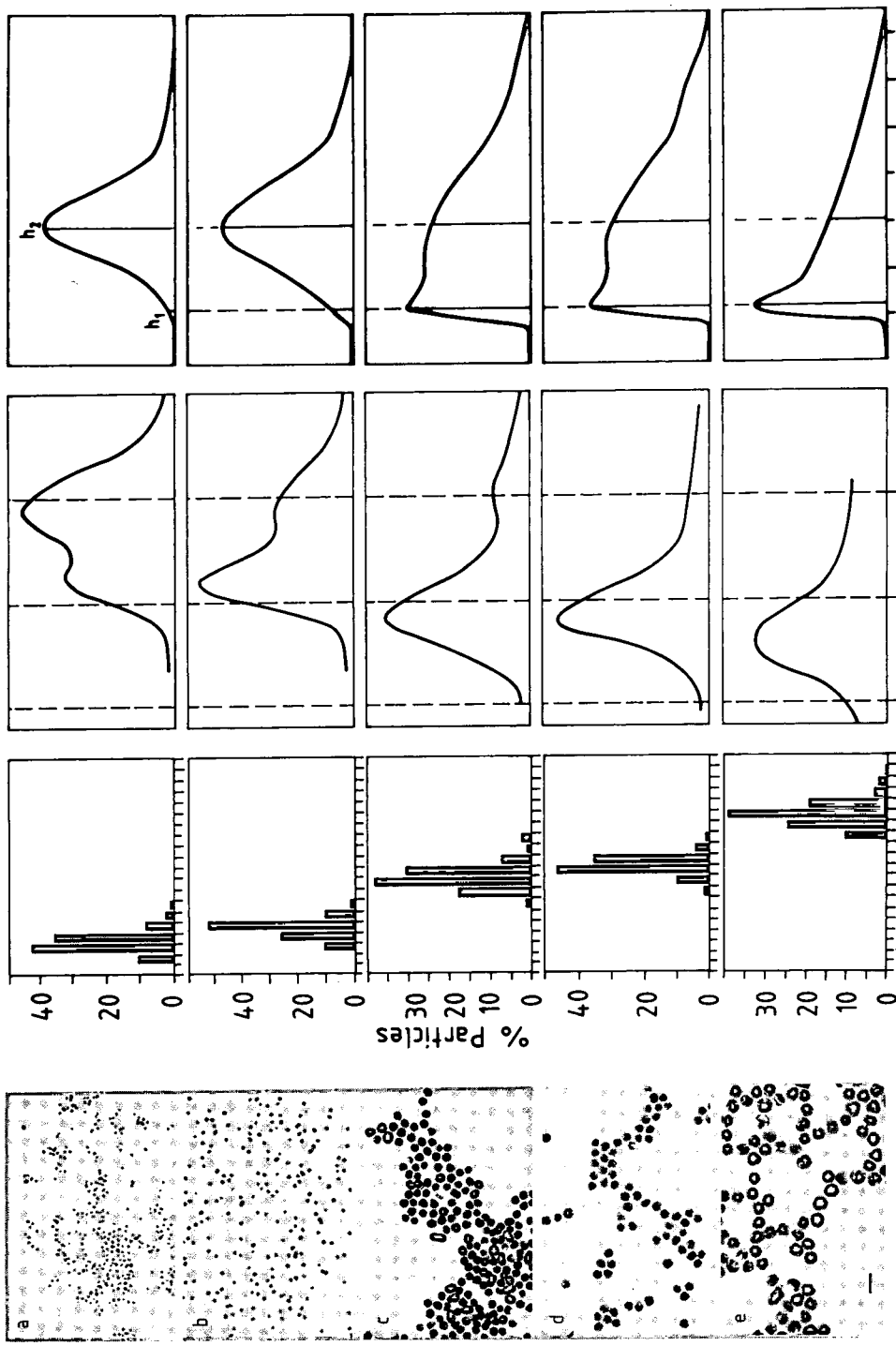

Fig. 5. Gold sols of various particle sizes. In the left part the electron micro graphs (scale bar 20 nm) and the corresponding histograms of the distribution of particle diameter are shown. In the centre the chromatograms of SEC and on the right side those of wide-bore HDC are given. Detection wavelength in both cases was 520 nm.

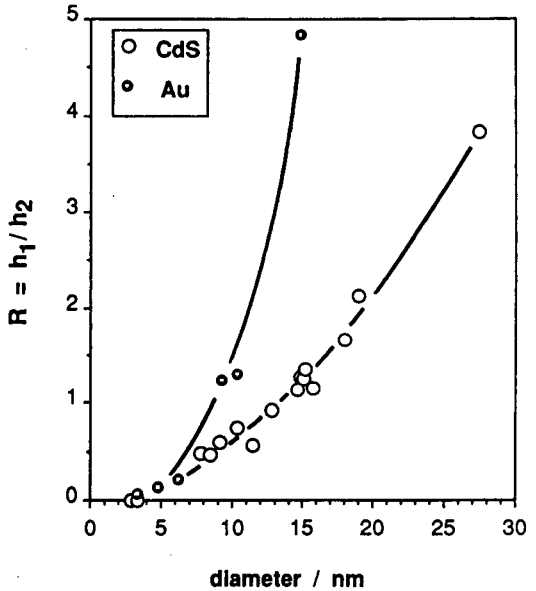

Fig. 6. Calibration plot for the wide-bore HDC of gold (●) and cadmium sulphide (○) sols. It shows the ratio $R = h_1/h_2$ of the height of convection peak over diffusion peak as a function of weight average particle diameter d_w, determined by SEC or electron microscopy, respectively. Experimental conditions are given in the text.

tration of the colloidal particles, the faster is their diffusion between slowly and fast flowing parts of the cross-section of the capillary and the more pronounced is the diffusion peak. This is demonstrated with a sol containing $5 \cdot 10^{-3}$ *M* CdS, which was diluted with water stepwise down to $1 \cdot 10^{-4}$ *M* (Fig. 7). From the particular height ratio *R* of the chromatogram and the calibration curve (Fig. 6) diameters between 89 nm and 104 nm were calculated. Although the influence of the concentration is not dramatic one should try to work always with identical colloid concentrations as those used for the calibration. For higher concentrations the effect is smaller than for more dilute ones. On the other hand highly concentrated colloidal solutions might become unstable, or particle growth may occur. A 10^{-3} *M* solution is recommended as a good compromise. Then a fivefold higher or a tenfold lower concentration would cause an error of only 7 or 8 percent, respectively.

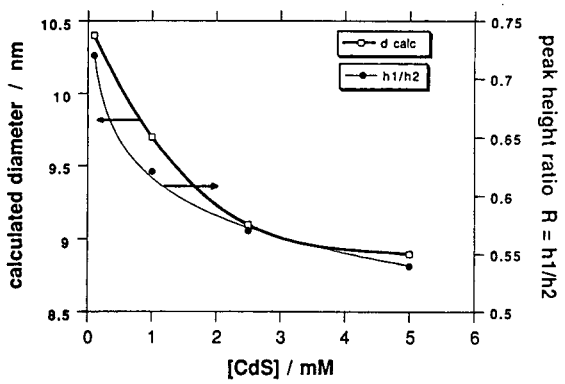

Fig. 7. Effect of concentration on the result of wide-bore HDC. A 5 m*M* cadmium sulphide sol was diluted stepwise down to 0.1 m*M*. Height ratio $R = h_1/h_2$ of convection peak to diffusion peak (●) and the particle diameter d_{calc} calculated from *R* as a function of CdS concentration (□).

Comparison of the methods and conclusion

TEM shows directly the size and shape of particles, but radiation damage can occur [3] and alter the original particle size. Furthermore, less frequent populations could be overlooked [26] and sometimes during sample preparation, smaller and larger particles separate to some extent by diffusion, so that the statistics in an observed part of the whole sample is not perfect any more. Without a digital analyser the analysis is time consuming and tedious. SEC gives a statistically more accurate view of the true size distribution as long as all colloidal material elutes. The analysis is very fast. However, the chromatography columns have a limited lifespan. A new column must then be calibrated again by TEM, because the colloids in question are not stable over long periods. Further drawbacks are that adsorption can occur with very active colloids and the equipment is relatively expensive. Wide-bore HDC cannot give direct information about the size *distribution*. However, in the case of small semiconductor or metal particles where the size-quantization effects allow an independent measure of the particle size, it can be done indirectly via the chromatograms at various detection wavelengths (see Fig. 3). But the wide-bore HDC has many advantages. Whereas in the

classic HDC equipment and handling are quite sophisticated and detection is difficult due to the small dimensions, the *wide-bore* HDC uses cheap, empty, standardised capillaries. Therefore one calibration can be directly transferred to any other capillary of the same type. Although this work was done with HPLC pumps, these sophisticated instruments are not necessary for this technique. A precise flow rate is not required because only the ratio of the peak *heights* is measured, and not the retention time. The method is fast and less calculation is necessary than in SEC. But most important is the lack of any packing material, the large surface of which often causes problems of reversible and irreversible adsorption. In a relatively wide capillary of 0.8 mm I.D. the surface does not play a significant role. Therefore the method is especially recommended for colloids with high surface activity.

Acknowledgement

The authors wish to express their thanks to Dr. Paul Mulvaney, Melbourne, for the preparation of the gold colloids as well as for fruitful discussions. The help with the laboratory work of Ms. U. Michalczik and the assistance of Ms. U. Bloek with the electron microscopy is gratefully acknowledged.

References

[1] A. Henglein, *Top. Curr. Chem.*, 143 (1988) 115.
[2] H. Weller, *Advanced Materials*, 5 (1993) 88.
[3] E. Zeitler (Editor), *Cryoscopy and radiation damages*, North-Holland Publ. Comp., Amsterdam, 1982.
[4] J.J. Kirkland, *J. Chromatogr.*, 185 (1979) 273.
[5] Ch.-H. Fischer, J. Lilie, H. Weller, L. Katsikas and A. Henglein, *Ber. Bunsenges. Phys. Chem.*, 93 (1989) 61.
[6] Ch.-H. Fischer, H. Weller, L. Katsikas and A. Henglein, *Langmuir*, 5 (1989) 429.
[7] Ch.-H. Fischer, M. Giersig and T. Siebrands, *J. Chromatogr.*, 670 (1994) 89.
[8] Ch.-H. Fischer, *J. Liq. Chromatogr.*, 17 (1994) 3593.
[9] A.W. Thornton, J.P. Olivier, C.G. Smart and L.B. Gilman, in T. Provder (Editor), *Particle Size Distribution Assessment and Characterization* (*ACS Symposium Series*, Vol. 332), American Chemical Society, Washington, DC, 1987, p. 256.
[10] C.A. Silebi and J.G. DosRamos, *J. Colloid Interface Sci.*, 130 (1989) 14.
[11] C.A. Silebi and J.G. DosRamos, *J. Colloid Interface Sci.*, 133 (1989) 302.
[12] J.G. DosRamos and C.A. Silebi, *J. Colloid Interface Sci.*, 135 (1989) 165.
[13] C.A. Silebi and J.G. DosRamos, *AIChE J.*, 35 (1989) 1351.
[14] M.E. Mullins and C. Orr, *Int. J. Multiphase Flow*, 5 (1979) 79.
[15] R.J. Noel, K.M. Gooding, F.E. Regnier, D.M. Ball, C. Orr and M.E. Mullins, *J. Chromatogr.*, 166 (1978) 373.
[16] F.M. Kelleher and C.N. Trumbore, *Anal. Biochem.*, 137 (1984) 20.
[17] J. Pawliszyn, *Anal. Chem.*, 58 (1986) 3207.
[18] D.O. Hancock and R.E. Synovec, *Anal. Chem.*, 60 (1988) 2812.
[19] D.O. Hancock, C.N. Renn and R.E. Synovec, *Anal. Chem.*, 62 (1990) 2441.
[20] G. Gerhardt and R.N. Adams, *Anal. Chem.*, 54 (1982) 2618.
[21] J.T. Vanderslice, A.G. Rosenfeld and G.R. Beecher, *Anal. Chim. Acta*, 179 (1986) 119.
[22] L. Spanhel, M. Haase, H. Weller and A. Henglein, *J. Am. Chem. Soc.*, 109 (1987) 5649.
[23] J.W. Slot and H.J. Geuze, *Eur. J. Cell. Chem.*, 38 (1985) 87–93.
[24] C.R. Berry, *Phys. Rev.*, 161 (1967) 611.
[25] A. Fojtik, H. Weller, U. Koch and A. Henglein, *Ber. Bunsenges. Phys. Chem.*, 88 (1984) 969.
[26] T. Siebrands, M. Giersig, P. Mulvaney and Ch.-H. Fischer, *Langmuir*, 9 (1993) 2297.
[27] V. Murugaiah and R.E. Synovec, *Anal. Chim. Acta*, 246 (1991) 241.
[28] C.N. Trumbore, M. Grehlinger, M. Stowe and F.M. Kelleher, *J. Chromatogr.*, 322 (1985) 443.

ELSEVIER

Journal of Chromatography A, 688 (1994) 107–116

JOURNAL OF CHROMATOGRAPHY A

Determination of inorganic Hg(II) and organic mercury compounds by ion-pair high-performance liquid chromatography

Yen-Sun Ho[1], Peter C. Uden*

Department of Chemistry, Lederle Graduate Research Tower A, University of Massachusetts, Amherst, MA 01003-4510, USA

First received 8 August 1994; revised manuscript received 27 September 1994

Abstract

The ion-pair chromatographic behavior of inorganic mercury(II) and organomercurials was investigated with tetra-*n*-alkylammonium bromides as ion-pair reagents and sodium halides in a methanol–water mixture as mobile phases. UV and three-electrode direct current argon plasma specific element detection were employed. The effects of the type and the concentration of sodium halide and ion-pair reagent, and the level of methanol on chromatographic behavior of mercury compounds were evaluated.

Both inorganic mercury(II) and benzylmercury species showed much greater UV response than other mercurials, while all analytes showed more consistent mercury-specific responses although there was some bias seen toward a greater response for the smaller organometallics.

1. Introduction

It is well known that inorganic mercury is introduced to the environment by various natural and pollutant processes and can be converted into more toxic alkyl mercury species by biological activity [1]. Also alkyl and aryl mercury compounds are frequently used in industrial manufacturing and in agriculture for mold and pest control [1]. The toxicity of mercury in environmental and biological systems has been evaluated differently according to the valence and the exact chemical form of the mercury.

High-performance liquid chromatography (HPLC) utilizing sensitive and selective detection is an efficient and rapid tool for the speciation and quantitation of mercury compounds. In 1974, normal-phase HPLC was first employed by Funasaka et al. [2] for the separation of organomercurials on Corasil I with *n*-hexane as eluent.

Reversed-phase HPLC is suited to separations of non-polar and moderately polar species while more polar and ionic species have been separated by utilizing secondary equilibria such as ion suppression, ion pair and ion exchange. A mode of reversed-phase HPLC termed on-column complexation or charge neutralization chromatography has proved particularly amenable to the determination of trace metal ions. The charged species injected are complexed on-column by a complexing agent added to the eluent and sepa-

* Corresponding author.

[1] Present address: Springborn Laboratories, Inc., Spencerville, OH 45887, USA.

0021-9673/94/$07.00
SSDI 0021-9673(94)00926-0

ration of inorganic mercury(II) and ionic organomercurials has been effected by the on-column formation of their neutral 2-mercaptoethanol complexes. This technique has been widely utilized for mercury speciation in drugs, fish, water and biological samples [3–9].

Several alternative detectors including electrochemical detection (ED) [4–7], inductively coupled argon plasma (ICP) [10] and graphite furnace atomic absorption (GFAA) [11] have been used for HPLC of mercury compounds with good sensitivity, linearity and/or selectivity.

ED may be sensitive and can monitor several different organometallics simultaneously, but is not highly selective and any interferent reducible species must be removed from solvent systems. The argon ICP provides continuous monitoring, low detection limits and simultaneous multielement monitoring but restrictions on the choice of mobile phase, peak broadening from nebulizer systems and high investment costs are drawbacks. ICP-mass spectrometry has been applied effectively for some organometallic compounds, its performance for arsenic compounds having been compared with hydrogen–argon flame atomic absorption spectrometry [12]. GFAA has been used for organometallics but discontinuous sampling and monitoring give decreased chromatographic resolution. The direct current argon plasma (DCP) is simple to interface and provides a convenient element-selective detector [13–15]

It has been shown [16–18] that quaternary ammonium halide salts are effective extractants for mercury compounds, both inorganic mercury(II) and organomercurials forming extractable anionic complexes in the presence of halide ions. The mechanism of extraction was expressed by Tajima et al. [19] who first applied the scheme shown in the following equations to analyze Hg(II) halides in the presence of counter ions such as tetra-*n*-butylammonium halides:

$$Hg^{2+} + 4X^- = HgX_4^{2-}$$

$$2R_4N^+ + HgX_4^{2-} = (R_4N)_2HgX_4$$

$$[2R_4NX + HgX_2 = (R_4N)_2HgX_4]$$

or

$$R'HgX + X^- = R'HgX_2^-$$

$$R_4N^+ + R'HgX_2^- = (R_4N)R'HgX_2$$

$$[R_4NX + R'HgX = (R_4N)R'HgX_2]$$

Gast and Kraak [20] also reported that in the separation of organomercurials by normal-phase HPLC, a significantly larger capacity ratio, good reproducibility and no decomposition of diphenylmercury were found upon addition of quaternary ammonium halide salts to the eluent.

2. Experimental

2.1. Instrumentation

An IBM Instruments (Danbury, CT, USA) Model LC/9533 ternary gradient liquid chromatograph equipped with Model LC/9522 ultraviolet detector set at 254 nm was used. Sample was introduced by a Rheodyne (Cotati, CA, USA) Model 7125 injector with a 10-μl loop. A Spectraspan IV (ARL, Sunland, CA, USA) DCP emission spectrometer was used with a Houston Instruments (Austin, TX, USA) Omniscribe chart recorder. A 5-μm Octadecyl column (250 × 4.6 mm I.D.) was used (IBM Instruments). A single-channel Model "Rabbit" peristaltic pump (Rainin, Woburn, MA, USA) and was used to pump standard solutions into the DCP.

2.2. Reagents and standards

Tetrabutylammonium bromide (TBABr) (Aldrich, Milwaukee, WI, USA), tetraethylammonium bromide (TEABr) (Fisher Scientific, Fairlawn, NJ, USA) and tetramethylammonium bromide (TMABr) (Eastman Kodak, Rochester, NY, USA) were used as received. HPLC-grade water was made from distilled water further purified using a NANOpure II system (Barnstead, Boston, MA, USA). Methylmercury chlo-

ride and ethylmercury chloride were obtained from Strem Chemical (Newburyport, MA, USA) and benzylmercury chloride was obtained from M.D. Rausch (Department of Chemistry, University of Massachusetts, Amherst, MA, USA); all were purified twice by recrystallization from methanol. Phenylmercury chloride (Alfa Inorganics, Beverly, MA, USA) was purified first by recrystallization from methanol and repurified by sublimation at 100°C and 0.5 Torr (1 Torr = 133.322 Pa). Mercuric chloride was obtained from Fisher Scientific and used as received. Each standard solution was prepared in HPLC-grade methanol, except the mercuric chloride, which was prepared by dissolution in a minimum amount of water and diluted with methanol. All the solutions were prepared weekly and stored in the dark at 2°C when not in use.

2.3. Sample preparation

A river water sample was obtained from the Connecticut River, sampled in Sunderland, MA, USA and spiked with appropriate amounts of mercury compounds. It was then filtered through a 0.45-μm membrane filter (Millipore, Bedford, MA, USA) prior to analysis.

2.4. Procedure

The mobile phases were prepared by dissolving the appropriate amount of tetra-*n*-alkylammonium bromide salts and sodium halide salts in a mixture of methanol and water. In order to achieve the maximum selectivity and sensitivity of DCP response, the position of the plasma and the wavelength setting needed to be optimized. First, the $HgCl_2$ aqueous solution was pumped directly into the DCP nebulizer through PTFE tubing by a peristaltic pump. Then the wavelength setting and orientation of the electrode assembly were adjusted appropriately. The interfacing of HPLC to DCP was accomplished by directly connecting PTFE tubing (50 cm × 0.25 mm I.D.) to the DCP nebulizer from the output of the UV detector.

3. Results and discussion

3.1. Separation of inorganic mercury(II) and organomercury compounds

Fig. 1B shows an isocratic separation of $HgCl_2$, CH_3HgCl, C_2H_5HgCl, C_6H_5HgCl and $C_6H_5CH_2HgCl$ on a C_{18} column with 0.01 *M* TBABr as the ion-pair reagent in methanol–water (60:40, v/v) used as the mobile phase. The amounts of mercury compounds injected were 62.5 ng for Hg(II) and benzyl, and 1250 ng for methyl, ethyl and phenyl species. The mercury compounds were well resolved and eluted with good peak shape, reproducibility and chromatographic efficiency. The elution order of organomercury compounds was methyl < ethyl < phenyl < benzyl, following the expected trend for homologues in reversed-phase HPLC for increasing elution volume as the number of methylene groups or the molecular mass increases.

3.2. Chromatographic behavior of mercury compounds under different mobile phase conditions

A number of experimental factors were investigated for effects on the chromatographic behavior.

Influence of the type and the concentration of sodium halide

Inorganic and organic mercury species can form stable charged bromide complexes, $HgBr_4^{2-}$ and $RHgBr_2^-$ respectively, with the bromide ion from the 0.01 *M* ion-pair reagent, TBABr. When sodium chloride was added to the eluent, the retention times decreased sharply. Fig. 1A shows the chromatogram obtained when 0.15 *M* NaCl was added to the eluent. This trend may be accounted for by the formation of the more soluble chloride complexes $HgCl_4^{2-}$ ($\log \beta_4 = 15.3$) and $HgCl_2^-$, even though they have lower stability constants than analogous bromide complex ions ($\log \beta_4 = 22.23$ for $HgBr_4^{2-}$) [21]. In addition to decreasing retention time, the addition of sodium chloride gave more symmetrical

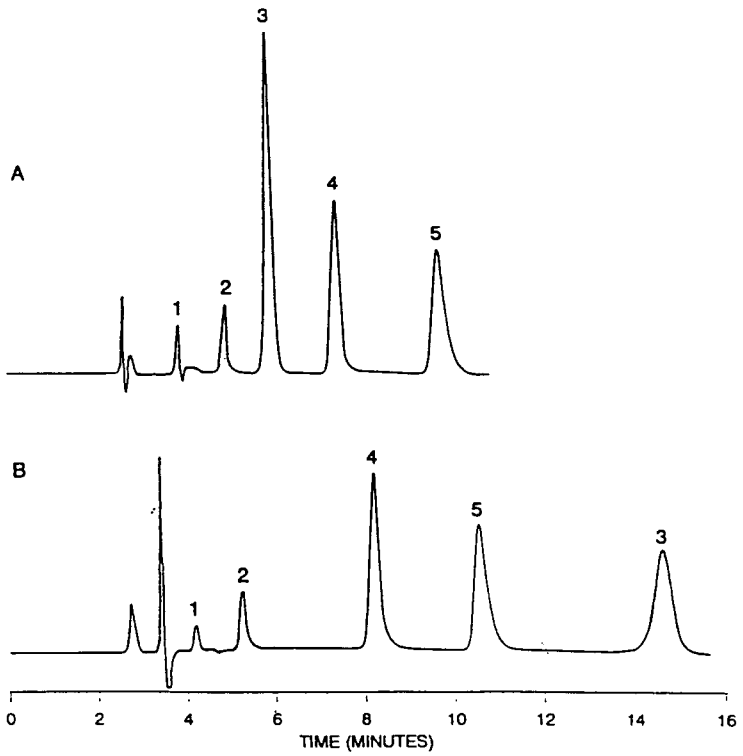

Fig. 1. Separation of inorganic mercury(II) and organomercurials on IBM C_{18} column, 5 μm, 250 × 4.6 mm I.D. Mobile phase: (A) 0.01 *M* TBABr and 0.15 *M* NaCl in methanol–water (60:40, v/v), (B) 0.01 *M* TBABr in methanol–water (60:40, v/v). Flow-rate: 1 ml/min. Detection: UV 254 nm. Peaks: 1 = CH_3Hg^+; 2 = $C_2H_5Hg^+$; 3 = Hg^{2+}; 4 = $C_6H_5Hg^+$; 5 = $C_6H_5CH_2Hg^+$.

and sharper peak shapes; thus in all further experiments sodium halide was always present in the eluent.

Fig. 2 shows graphically the effect of the concentration of chloride ion on the capacity factors of mercury compounds. Sodium chloride concentration was varied from 0.0 to 0.2 *M*. The drop in the capacity factor of inorganic mercury(II) with increase of chloride concentration can be attributed to the formation of more $HgCl_4^{2-}$, resulting in greatly increasing solubility. In contrast, the organomercury species only formed singly negative charged complexes and the capacity factors showed little change with increase of Cl concentration. A comparison of the influence of chloride and bromide concentrations on the capacity factors of the mercury compounds showed slightly larger values with Br^- than with Cl^-, consistent with the solubility order of the halides.

Influence of the level of organic modifier

The effect of the organic modifier concentration on the capacity factors of mercury compounds was investigated for methanol, the data being shown in Fig. 3. The logarithm of capacity factors decreases linearly with increase in the content of methanol in the eluent in the range of 50–70% as is commonly found for reversed-phase systems. However, the individual slopes are different, which indicates a change in selectivity when varying the methanol percentage. For organomercury compounds, the decrease in log k' almost parallels the increase in methanol content, which indicates no significant selectivity changes among them. In contrast to organomer-

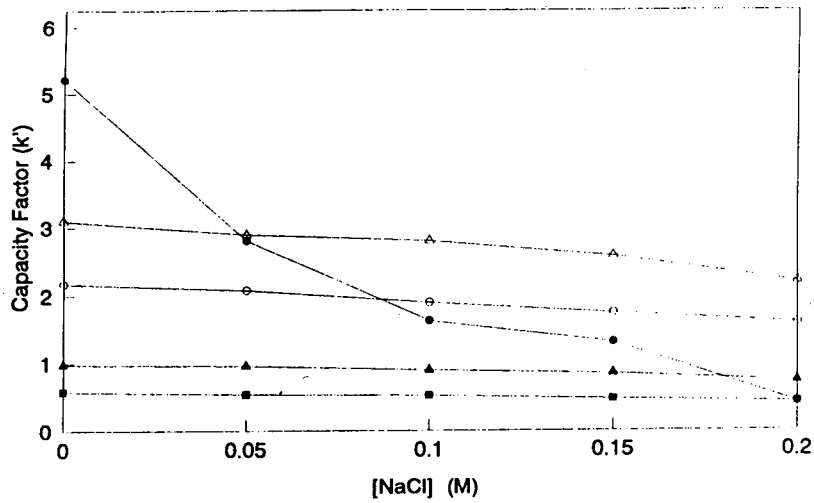

Fig. 2. Effect of sodium chloride concentration on the capacity factor, k', of mercury compounds. Chromatographic conditions as in Fig. 1A. ■ = CH_3Hg^+; ▲ = $C_2H_5Hg^+$; ● = Hg^{2+}; ○ = $C_6H_5Hg^+$; △ = $C_6H_5CH_2Hg^+$.

cury species, however, the capacity factor of inorganic mercury(II) drops markedly with increase in methanol content.

Influence of ion-pair reagent concentration

Fig. 4 shows the relationship between the capacity factor and the concentration of TBABr over the range 0.001 to 0.0316 *M*. As is typical in ion-pair chromatography, the capacity factors increase with the increase in ion-pair reagent concentration. The much larger slope for inorganic mercuric species corresponds to a higher stability constant for HgX_4^{2-}, which indicates that it requires a greater amount of ion-pair

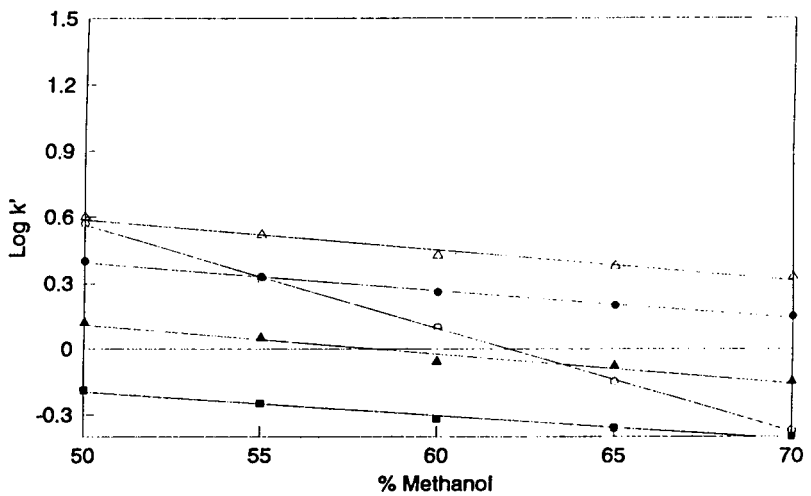

Fig. 3. Effect of methanol concentration on the capacity factor, k', of mercury compounds. Chromatographic conditions as in Fig. 1A. ■ = CH_3Hg^+; ▲ = $C_2H_5Hg^+$; ● = $C_6H_5Hg^+$; ○ = Hg^{2+}; △ = $C_6H_5CH_2Hg^+$.

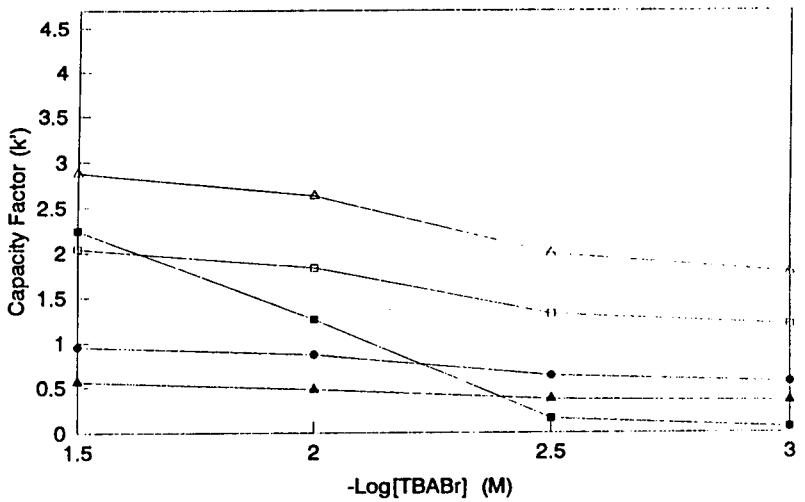

Fig. 4. Effect of ion-pair concentration on the capacity factor, k', of mercury compounds. Chromatographic conditions as in Fig. 1A. □ = Hg^{2+}; ▲ = CH_3Hg^+; ● = $C_2H_5Hg^+$; ○ = $C_6H_5Hg^+$; △ = $C_6H_5CH_2Hg^+$.

reagent for complete ion-pair formation. At lower TBABr concentrations, the inorganic mercury(II) species eluted close to the void volume, while at higher TBABr concentration, it was strongly retained. This indicates that the retention of Hg^{2+} is greatly dependent on the concentration of ion-pair reagent.

In contrast to the inorganic mercury(II), organomercury species show lower capacity factor slopes. In addition, the decrease in k' closely parallels the decrease in TBABr concentration suggesting similar structures for the ion pairs and similar stability constants of $RHgX_2^-$ species despite their differences in k'. This also indicates that the capacity factors for organomercury species are primarily dependent on their own chemical properties, rather than on the concentration of ion-pair reagent. For both Hg^{2+} and RHg^+ species, the peak shapes were found to be broader and less reproducible at higher TBABr concentrations; 0.01 *M* of TBABr was found optimal for HPLC.

Influence of the types of ion-pairing reagent

The effect of the different ion-pair reagents, TMABr, TEABr and TBABr, on the capacity factors of inorganic mercury(II) and organomercury species was examined The capacity factors of the organomercury species showed very little change with decreasing molecular size of ion-pair reagents, but the capacity factors for Hg^{2+} increased notably with increase in molecular size of the ion-pair reagents. This suggests that the more ionic complex ion species, HgX_4^{2-}, requires a larger counter-ion than the less ionic organomercury complex ions, $RHgX_2^-$ to pair effectively.

3.3. Calibration curves and detection limits with UV detection

Although alkylmercury compounds show a low molar absorption in the UV region [22], Hg^{2+} forms HgX_4^{2-} species which have a charge absorption band in the UV range [23]. Table 1 shows analytical data for UV detection for inorganic and organomercury species. Both Hg^{2+} and $C_6H_5CH_2Hg^+$ are detected with much greater sensitivity than the CH_3Hg^+, $C_2H_5Hg^+$ and $C_6H_5Hg^+$ species.

The detection limit of each mercury species was determined by measuring the minimum amount which had to be injected to provide a peak signal approximately twice the noise while the detector was at the most sensitive setting, AUFS 0.001. The detection limits were in the

Table 1
Analytical data for inorganic and organic mercury species by ion-pair HPLC with detection at 254 nm

Cation	Linear range (ng)	Slope	Correlation coefficient
CH_3Hg^+	8.0–200	0.0025	0.9989
$C_2H_5Hg^+$	3.8–200	0.0035	0.9987
Hg^{2+}	0.8–400	0.1260	0.9998
$C_6H_5Hg^+$	1.3–300	0.0060	0.9940
$C_6H_5CH_2Hg^+$	0.2–400	0.1300	0.9998

range of 0.2–8.0 ng which represents the range between the most sensitive benzylmercury and the least sensitive methylmercury species.

3.4. Mercury determination in a spiked river water sample

Fig. 5 shows the UV detection chromatogram of a river water sample "spiked" with Hg^{2+} (5 μg/ml) and CH_3Hg^+ (80 μg/ml) to illustrate the relative sensitivities of inorganic and organic mercury species. Recoveries were found to be $80.02 \pm 1.62\%$ and $96.71 \pm 2.32\%$ for Hg^{2+} and CH_3Hg^+, respectively, measured against aqueous standards. The lower percentage recovery

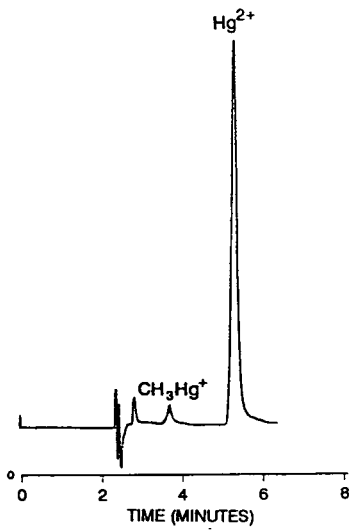

Fig. 5. Chromatogram of spiked water sample with inorganic mercury (5 μg/ml) and methylmercury (80 μg/ml). Column and conditions as in Fig. 1A.

for Hg^{2+} may be attributed to the matrix effects of the water sample whereby the ion reacted with any reactive substrate resulting in a low amount of "free" mercuric ion. In contrast the less ionic methylmercury species appeared without apparent loss in the system.

Although ion-pair chromatography with UV detection provides an improvement in the determination of Hg^{2+} through the formation of a highly UV absorbing HgX_4^{2-} species, the determination of Hg^{2+} may sometimes remain problematic in an environment where other relatively stable mercury(II) complexes may predominate.

3.5. DCP as a detection method

Fig. 6 shows a chromatogram of mercury compounds with both DCP and UV detection. The DCP plasma was found to be stable and no serious baseline noise was found when there was a high content of organic solvent (methanol) and the organic ion-pair reagent in the eluent. No substantial increase in retention times was observed upon incorporation of the 50 cm long interface tube. The UV trace shows response for each mercury species. However, in the DCP trace, inorganic mercury(II) and the benzylmercury species are missing from the chromatogram, while the methylmercury, ethylmercury and phenylmercury species show response. As noted previously, Hg^{2+} and $C_6H_5CH_2Hg^+$ show much higher UV sensitivity than the other three organomercury species. In order to bring the UV response to a comparable level for each mercury species, the amount of each injected was modified appropriately, only a very small amount (62.5 ng each) of Hg^{2+} and $C_6H_5CH_2Hg^+$ being injected on the column.

Fig. 7 shows another chromatogram also with UV and DCP detection, with equal amounts (4 μg) of each mercury species injected. The DCP trace shows similar response for each species, while in the UV trace, the response is off scale for the Hg^{2+} and $C_6H_5CH_2Hg^+$ species. The notable difference between the DCP and the UV responses occurs because the former is energetic

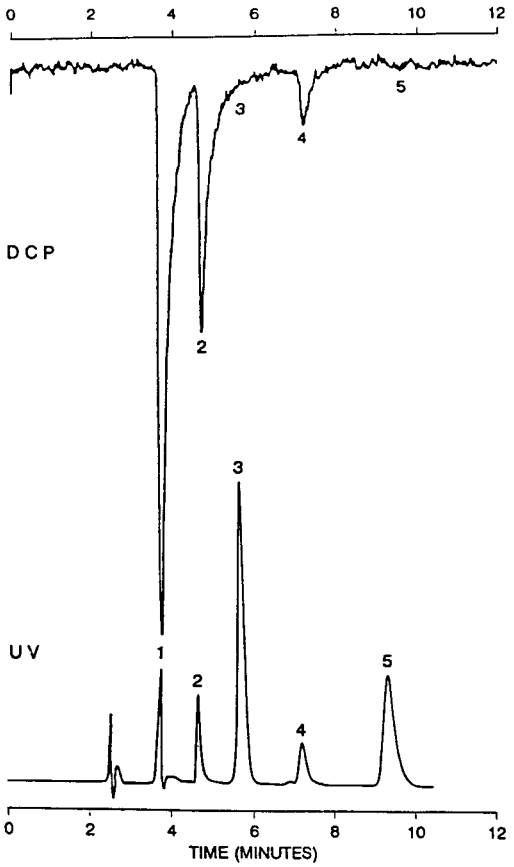

Fig. 6. Dual-detection chromatogram of mercury compounds. Column and conditions as in Fig. 1A. Lower chromatogram, UV detection at 254 nm; upper chromatogram, DCP emission detection at 253.6 nm. Peaks: 1 = CH_3Hg^+; 2 = $C_2H_5Hg^+$; 3 = Hg^{2+}; 4 = $C_6H_5Hg^+$; 5 = $C_6H_5CH_2Hg^+$.

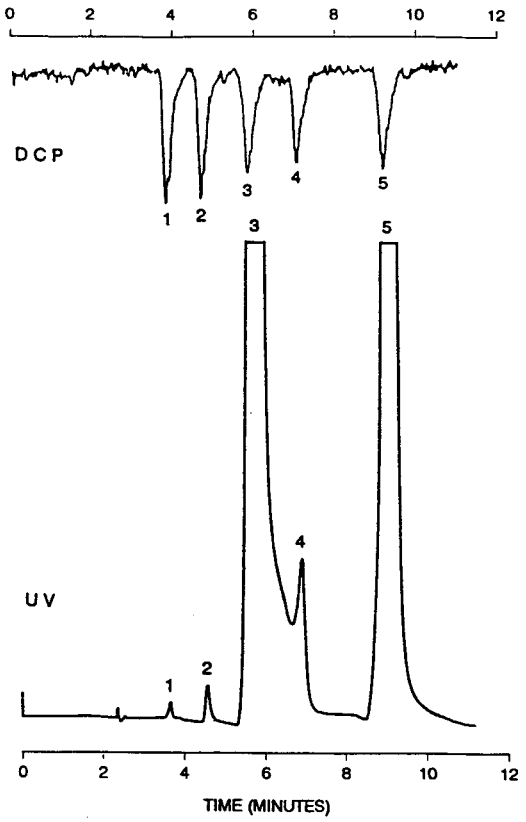

Fig. 7. Dual-detection chromatogram of mercury compounds (4 μg for each species). Column and conditions as in Fig. 1A. Lower chromatogram, UV detection at 254 nm; upper chromatogram, DCP emission detection at 253.6 nm. Peaks as in Fig. 6.

enough to completely atomize each molecule, thus its response is relatively independent of the matrix and chemical effects seen in the UV trace.

Fig. 8 shows the DCP calibration curves for the mercury compounds, the sensitivities decreasing in the order $CH_3Hg^+ > C_2H_5Hg^+ > C_6H_5Hg^+ > Hg^{2+} > C_6H_5CH_2Hg^+$. The sequence is the same order as volatility decrease, but is the reverse order of molecular size and UV responses. As is commonly found in atomic emission spectroscopy, the more volatile species will have the greater emission intensity. Also, the larger size of molecule may penetrate less efficiently into the DCP than the smaller one, resulting in decreased atomization efficiency and emission intensity.

The relatively high detection limits for mercury compounds, 175 ng (methyl)–255 ng (benzyl) may be attributed to the high content of carbon due to organic solvent and organic ion-pair reagent in the eluent which contributed to the noisy background. Another factor could conceivably be the formation of larger ion-pair species, which find it harder to penetrate into the DCP, resulting in low atomization efficiency.

ᐊᓕᓐᓂᐊᓪᓚᓂ ᑎᓐᓄᑕᓐᓂᒃ ᑲᓇᑕᒥᒃ
ᐊᓂᒍᓐᓇᓕᒃ ᑲᓇᑕᒥᒃ
ᐊᓂᒍᓐᓇᓕᒃ ᑲᓇᑕᒥᒃ

ต้นฉบับไม่มี

ELSEVIER

Journal of Chromatography A, 688 (1994) 117–123

JOURNAL OF CHROMATOGRAPHY A

Determination of second cross virial coefficients from gas–liquid chromatographic data
II. Dilute mixtures of water and brominated hydrocarbons

Brahim Khalfaoui*, D.M.T. Newsham

Chemical Engineering Department, UMIST, Sackville Street, Manchester M60 1QD, UK

First received 10 May 1994; revised manuscript received 9 August 1994

Abstract

Gas–liquid chromatographic measurements were carried out in the temperature range 298–323 K and were used to determine the second cross virial coefficients for each brominated hydrocarbon–carrier gas mixture studied. Measurements on mixtures of brominated compounds infinitely dilute in water were made using a gas–liquid chromatographic apparatus with a packed column under carrier gas inlet pressures up to 700 kPa and with water as the stationary phase. Nitrogen was used as the carrier gas. In addition, mixtures of water infinitely dilute in the brominated compounds were studied using an isopiestic apparatus. Henry's constants were also derived and group interaction parameters for the UNIFAC correlation were estimated using the experimental infinite dilution activity coefficients. The new group interaction parameters were used to predict activity coefficients for a range of brominated hydrocarbon–water mixtures.

1. Introduction

Brominated hydrocarbons are the second most important members in the class of halogenated hydrocarbons after the chlorinated hydrocarbons. The brominated compounds resemble the corresponding chlorinated compounds but their densities and boiling points are higher. In order to treat industrial waters containing chlorinated hydrocarbons we need to design equipment. A similar requirement exists for brominated hydrocarbon–water mixtures and in this work measurements were carried out on mixtures of water with tribromomethane, 1,2-dibromoethane and 1,1,2,2-tetrabromoethane.

Several workers [1–3] have given considerable attention to the use of gas–liquid chromatographic (GLC) retention volume measurements to obtain the activity coefficients (γ_i) of a volatile solute i in an involatile solvent, and second cross virial coefficients (B_{13}) of mixtures of solute vapour and carrier gas. Measurements of activity coefficients for very dilute mixtures of water and saturated chlorinated hydrocarbons, of water and unsaturated chlorinated hydrocarbons and of water and brominated hydrocarbons have been reported previously [4–6]. Also, measurements of second cross virial coefficients for unsaturated chlorinated hydrocarbon–nitrogen mixtures have been published [7]. This paper reports an exten-

* Corresponding author. On leave from the University of Constantine, Algeria.

0021-9673/94/$07.00
SSDI 0021-9673(94)00799-3

sion of the previous work [6]. In particular, second cross virial coefficients for brominated hydrocarbon (1)–nitrogen (3) mixtures were determined. Also, Henry's constants for brominated hydrocarbon (1)–water (2) mixtures were derived and an evaluation was made of the excess partial molar enthalpies at infinite dilution for brominated hydrocarbon–water mixtures in the temperature range 298–323 K. Further, new group interaction parameters were determined for Br–H_2O, CBr–H_2O, CBr_2–H_2O and CBr_3–H_2O interactions for the effective UNIFAC model using the experimental activity coefficients reported in an earlier paper [6]. These parameters were used to predict infinite dilution activity coefficients for several brominated hydrocarbon–water mixtures and these were compared with experimental values.

2. Experimental

The GLC apparatus used for measurements on brominated hydrocarbon infinitely dilute in water mixtures has been fully described previously [4–8]. The mixtures of water infinitely dilute in brominated hydrocarbons were studied using an isopiestic apparatus similar to that employed earlier [4–6].

2.1. Gas–liquid chromatograph

A schematic diagram of the apparatus [4] and a typical chromatogram from which the retention time is obtained [7] have already been published. In this technique, the chromatographic column is packed with a solid support phase that is uniformly coated with water. The chromatograph columns were made from 1.2 m lengths of soft annealed 7 mm I.D. copper tubing. They were prepared in a similar manner to those used previously [5–7]. However, a soap-bubble flow meter similar to that utilized by Cruickshank et al. [2] was used for the measurement of the carrier gas flow-rate. This is shown schematically in Fig. 1. The body of the flow meter was constructed entirely from Pyrex glass and was built to withstand a maximum pressure differential up to 1.2 MPa. The two tubes a and b of 3 mm I.D. serve as inlet and outlet ports respectively, for the carrier gas stream. The bottom section of the flow meter acts as a reservoir for the detergent solution (g) and serves to form the soap film necessary for flow measurement. The plug i, formed from a cylindrical magnet, could be raised and lowered smoothly by means of the annular magnet j. The top section (f) was domed to increase the mechanical strength of the assembly and serves as a soap film expander and breaker. Section c, which acts as a gas burette, was formed from glass tubing 50 cm long × 1.6 cm I.D. The two fiducial marks d and e were set approximately 40 cm apart to define the capacity of the burette, which was calibrated volumetrically by admission of water at a constant temperature of 298.15 K. Repetitive measurements showed the defined volume to be 74.40 cm^3. The flow-rate of the carrier gas was determined by measuring the time taken for a soap

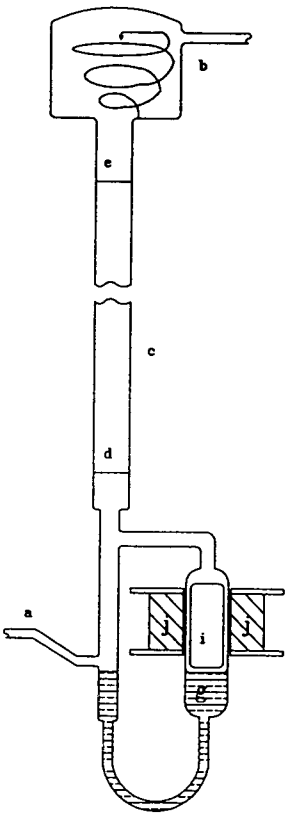

Fig. 1. Soap-bubble flow meter.

film to traverse the calibrated volume between the two marks d and e on the flow meter body. The measurement of the experimental quantities such as the solute retention time, nitrogen carrier gas flow-rate and column inlet and outlet pressures allows the calculation of the retention volume V_N which is related to the zero pressure partition coefficient k^0 as follows:

$$\ln V_N = \ln (k^0 V_2) + \beta P_o J_3^4 \quad (1)$$

where V_2 is the volume of solvent on the chromatograph column, J_3^4 is a correction for the pressure drop across the column, P_o is the pressure at the column outlet and β is a term related to gas-phase imperfection and partial molar volume of the solute in the solvent. The second cross virial coefficient B_{13} is in turn related to the term β:

$$\beta = (2B_{13} - \bar{v}_{12}^{\infty})/RT \quad (2)$$

where $\bar{v}_{12}^{\infty}$ is the partial molar volume of the solute infinitely dilute in the solvent (where this information is not available, then v_1^0 is used instead). As can be seen from Eq. 1, a plot of $\ln (V_N/V_2)$ against $P_o J_3^4$ gives a straight line with an intercept k^0 and a slope equal to β given in Eq. 2. This allows the calculation of the second virial coefficient of the solute and carrier gas.

2.2. Materials

The brominated hydrocarbons were all supplied by BDH and had purities in excess of 99%. The chromatograph columns were packed with diatomaceous earth (Diatomites 60–72 BSS mesh) supplied by JJ's Chromatography. Doubly distilled tap water was used throughout.

2.3. Determination of group interaction parameters

The UNIFAC (UNIQUAC functional group activity coefficients) method was originally developed by Fredenslund et al. [9]. In a multicomponent mixture the activity coefficient (γ_i) of component i is given by the sum of contributions depending on molecular size and shape (the combinatorial part) and molecular interactions (the residual part). The detailed form of the UNIFAC equation has been reported previously [4]. In this paper we report the results of one modification of the UNIFAC which is know' as the effective UNIFAC method. The effective UNIFAC method was developed by Nagata and Koyabu [10] and was described previously [7]. The group interaction parameters that occur in the residual contribution are given by

$$\Psi_{mn} = \frac{Q_m}{Q_n} \cdot \exp\left[- \frac{(U_{mn} - U_{nn})}{RT} \right] = \frac{Q_m}{Q_n} \cdot \exp\left(- \frac{a_{mn}}{T} \right) \quad (3)$$

where U_{mn} is a measure of the interaction energy between groups m and n. However, the group interaction parameters a_{mn} and a_{nn} ($a_{mn} \neq a_{nn}$) were estimated using both the activity coefficients of the solute at infinite dilution in the solvent (γ_1^{∞}) and of the solvent at infinite dilution in the solute (γ_2^{∞}).

3. Results and discussion

At each selected inlet pressure, the flow-rate of the carrier gas was adjusted according to the expected retention volume to give a convenient retention time. The net retention volumes were calculated at inlet pressure intervals of about 140 kPa over the range 275–700 kPa at three different temperatures (298.15, 308.15 and 323.15 K) for each brominated hydrocarbon. The measured values of column inlet pressure, 275–700 kPa, and column outlet pressure, 250–670 kPa, with corresponding column pressure drop 25–30 kPa, were used to calculate J_3^4. A typical set of results for the tribromomethane–water system at 298.15 K are shown in Fig. 2, where $\ln(V_N/V_2)$ is plotted against $P_o J_3^4$. Each point on the diagram represents the average and standard deviation of a set of up to seven measurements. The line of best fit with slope equal to β was found by a least-squares fitting procedure with a precision in $\ln(V_N/V_2)$ of ± 0.004.

The β values and the derived values of second cross virial coefficients (B_{13}) are given in Table

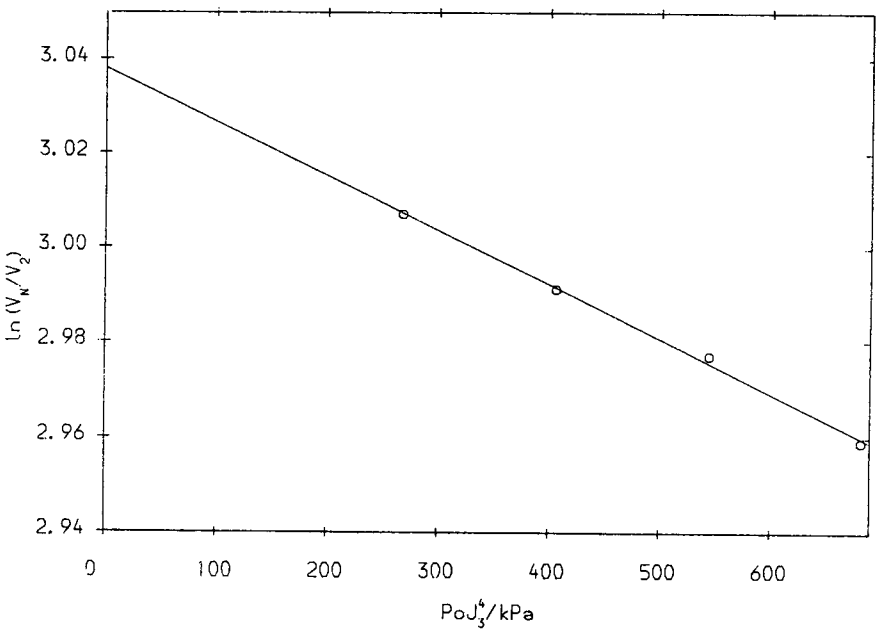

Fig. 2. Plot of $\ln(V_N/V_2)$ against $P_oJ_3^4$ for the tribromomethane–water system at 298.15 K.

1. Unfortunately, values of B_{13} are not available in the literature for any of the systems studied in this work and therefore no comparison with the values of B_{13} could be made.

Henry's law constants derived from activity coefficients ($k_i = \gamma_i^\infty P_i^0$) are given in Table 2 along with one value given by Kavanaugh and Rhodes-Trussell [11]. As can be seen from the very limited amount of data in the literature, an agreement seems to be achievable over a wider range of data, as was found in an earlier study [7] on unsaturated chlorinated hydrocarbon–water mixtures. As noted previously [7], the determination of the absolute accuracy of the experimental results is difficult. However, estimates of the likely experimental errors showed it to be similar to those obtained earlier [7] for chlorinated hydrocarbon–water mixtures. The pure component properties required for calculating these quantities were taken from a variety of

Table 1
The β values and second cross virial coefficients (B_{13}) for brominated hydrocarbon (1)–nitrogen (3) mixtures

Compound	T (K)	β (atm^{-1})	B_{13} (cm^3 mol^{-1})
Tribromomethane	298.15	−0.0114	−96.76
	308.15	−0.0096	−78.16
	323.15	−0.0068	−46.61
1,2-Dibromoethane	298.15	−0.0104	−85.50
	308.15	−0.0092	−74.42
	323.15	−0.0061	−37.09
1,1,2,2-Tetrabromoethane	298.15	−0.0073	−31.79
	308.15	−0.0065	−24.43
	323.15	−0.0059	−20.21

Table 2
Henry's law constants (k_i) for brominated hydrocarbon (1)–water (2) mixtures

Compound	T (K)	k_1 (MPa)	k_2 (MPa)
Tribromomethane	293.15	3.54[a]	
	298.15	6.60	1.06
	308.15	7.53	1.90
	323.15	9.62	3.16
1,2-Dibromoethane	298.15	4.44	0.74
	308.15	8.95	1.25
	323.15	9.92	2.11
1,1,2,2-Tetrabromoethane	298.15	5.46	0.98
	308.15	6.25	1.48
	323.15	6.78	2.87

[a] From Ref. [11].

sources (molar volumes [12–13]; virial coefficients [14]; vapour pressures [15,16]). One of the purposes of obtaining activity coefficients over a range of temperature [6] is to evaluate the excess partial molar enthalpy of solution at infinite dilution from the temperature dependence of the activity coefficient using the standard thermodynamic equation

$$\mathrm{d}\ln\gamma_i^{\infty}/\mathrm{d}(1/T) = (\bar{H}_i^{\infty} - H_i^0)/R = \Delta\bar{H}_i^{\infty}/R \qquad (4)$$

where $\bar{H}_i^{\infty}$ is the partial molar enthalpy of component i in the solution at infinite dilution and H_i^0 is the pure component molar enthalpy. This method requires activity coefficients of high accuracy and is usually slightly inferior to a direct measurement. As can be seen from Fig. 3, the expected linearity of the plot of $\ln\gamma_2^{\infty}$ against $1/T$ is obtained for tribromomethane–water mixtures. A similar linearity was obtained in the plots for the other two systems. The derived

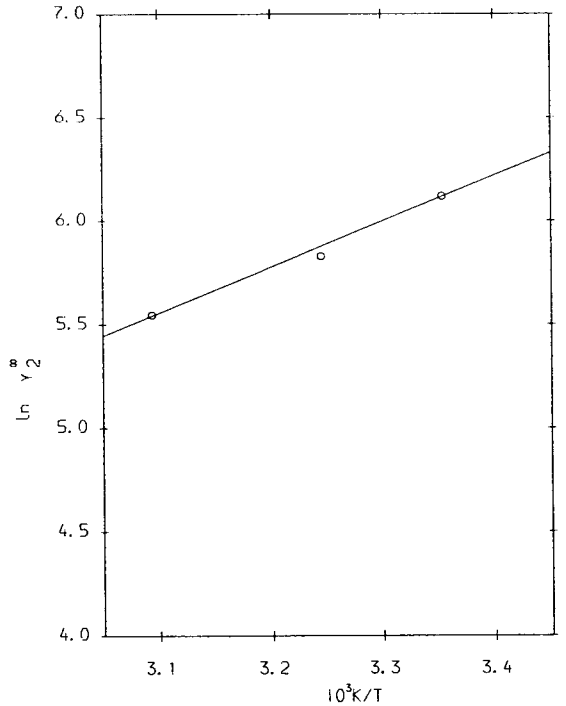

Fig. 3. Infinite dilution activity coefficients as a function of temperature for tribromomethane (1)–water (2) mixture.

values of $\Delta\bar{H}_i^{\infty}$ are given in Table 3. No comparison could be made owing to the absence of data in the literature. However, similar results for $\Delta\bar{H}_2^{\infty}$ were obtained for saturated chlorinated hydrocarbon–water mixtures [4].

A sample group assignment for the three brominated hydrocarbons is also given in Table 3. The group assignments and UNIFAC group volume (R_k) and surface area (Q_k) parameters have been reported previously [6]. It can be seen that each of these three organic compounds contains only one type of group and their mix-

Table 3
Sample group assignments and excess partial molar enthalpies at infinite dilution for brominated hydrocarbon (1)–water (2) systems for the temperature range 298–323 K

Compound	Sample group assignment	$\Delta\bar{H}_1^{\infty}$ (kJ mol^{-1})	$\Delta\bar{H}_2^{\infty}$ (kJ mol^{-1})
Tribromomethane	1$CHBr_3$	30.06	18.30
1,2-Dibromoethane	2CH_2Br	–	19.78
1,1,2,2-Tetrabromoethane	2$CHBr_2$	50.00	15.92

Table 4
Effective UNIFAC group interaction parameters for brominated hydrocarbon–water mixtures

	H_2O	Br	CBr	CBr_2	CBr_3
H_2O	0.0	297.2	554.0	1142.0	1576.0
Br	1100.0	0.0			
CBr	1263.0		0.0		
CBr_2	1391.0			0.0	
CBr_3	1513.0				0.0

The group parameters a_{mn} are in units of Kelvin; m is the row and n is the column of the matrix.

tures with water therefore constitute binary mixtures of groups. The group interaction parameters for the Br–H_2O interaction were calculated in a manner similar to that used previously [5,7], using a sequential search procedure developed by Nelder and Mead [17]. However, parameters for the CBr–H_2O, CBr_2–H_2O and CBr_3–H_2O interactions were obtained using a Newton–Raphson procedure as previously [4,6]. The values determined in this way for the effective UNIFAC model were obtained from experimental results at 298.15 K and are shown in Table 4. No comparison could be made because values of these new parameters are not available in the original table of Nagata and Koyabu [10].

Table 6
Errors in calculated activity coefficients of brominated hydrocarbons using the new effective UNIFAC parameters

Error range (%)	Data points in error range (%)
0–20	46.7
20–50	6.6
50–100	33.3
100–200	6.7
200+	6.7

The quoted errors are $[\gamma_i^{\infty}(\text{expt}) - \gamma_i^{\infty}(\text{calc})]/\gamma_i^{\infty}(\text{expt})$.

The values of the infinite dilution activity coefficients calculated using these new parameters and experimental values derived from liquid–liquid equilibria of Horvath [18] for many brominated hydrocarbon–water mixtures are compared in Table 5, which also includes the results for the mixtures previously reported [6]. Table 6 gives the percentage error ranges. These results are similar to those obtained for chlorinated hydrocarbon–water mixtures. It can be noted that as far as the brominated hydrocarbon systems are concerned, several more group interaction parameters need to be obtained so as to extend the application of the effective UNIFAC model to a wider range of systems. It can also be concluded that the B_{13} values obtained from the

Table 5
Comparison of experimental and calculated infinite dilution activity coefficients using new parameters for brominated hydrocarbon (1)–water (2) mixtures

Brominated hydrocarbon	T (K)	Source	$\gamma_1^{\infty} \times 10^{-4}$		γ_2^{∞}	
			Expt.	I	Expt.	I
Bromoform	298	VLE	0.9220	0.9230	454.5	454.3
1-Bromoethane	298	LLE	0.0670	0.0470	–	430.7
1,2-Dibromoethane	298	VLE	0.2340	0.2330	317.4	317.3
1,1,2,2-Tetrabromoethane	298	VLE	62.4500	62.4000	425.5	425.5
1-Bromopropane	303	LLE	0.2770	0.2920	–	489.3
2-Bromopropane	293	LLE	0.2130	0.3520	–	576.9
1,2-Dibromopropane	298	LLE	0.7840	1.4670	172.6	372.7
1,3-Dibromopropane	303	LLE	0.6670	1.3100	–	344.2
1-Bromobutane	289	LLE	1.3110	2.6940	–	721.4
1-Bromo-2-methylpropane	293	LLE	1.5000	2.4500	–	674.9
1-Bromo-3-methylbutane	293	LLE	4.3200	17.0600	–	764.1

The experimental values were determined either from vapour–liquid equilibria (VLE) or liquid–liquid equilibria (LLE) from Ref. [18], I effective UNIFAC.

slope β of the plots of $\ln(V_N/V_2)$ against $P_o J_3^4$ are subject to some errors which are difficult to evaluate. One of these errors in B_{13} values is the replacement of $\bar{v}_{12}^{\infty}$ by v_1^0 because values of $\bar{v}_{12}^{\infty}$ are not available. As has been pointed out previously [1], $\bar{v}_{12}^{\infty}$ and v_1^0 may differ by as much as 10 cm^3 mol^{-1}, and the B_{13} values obtained in this study are, therefore, subject to up to 10% error.

Symbols

a_{mn}	group interaction parameter
B_{13}	second cross virial coefficient
H_i^0	pure component molar enthalpy
$\bar{H}_i^{\infty}$	partial molar enthalpy at infinite dilution
$\Delta\bar{H}_i^{\infty}$	excess partial molar enthalpy at infinite dilution
J_3^4	pressure drop correction
k^0	zero pressure partition coefficient
k_i	Henry's law constant
P_o	outlet pressure
P_i^0	pure component vapour pressure
Q_k	group surface area parameter
R_k	group volume parameter
R	gas constant
T	temperature
U_{mn}	group interaction energy
v_i^0	pure component molar volume
$\bar{v}_{12}^{\infty}$	partial molar volume at infinite dilution
V_N	retention volume
V_2	solvent volume

Greek letters

β	coefficient in Eqs. 1 and 2
γ_i	activity coefficient
γ_i^{∞}	activity coefficient at infinite dilution
Ψ_{mn}	group interaction parameter

Subscripts

$i, 1, 2$	component identification
k, m, n	group identification
o	outlet

Superscripts

0	pure component or zero pressure
∞	infinite dilution

References

[1] D.H. Everett, *Trans. Faraday. Soc.*, 61 (1965) 637.
[2] A.J.B. Cruickshank, M.L. Windsor and C.L. Young, *Proc. R. Soc., London, Ser. A*, 295 (1966) 259.
[3] B.W. Gainey and C.L. Young, *Trans. Faraday. Soc.*, 64 (1968) 349.
[4] R.S. Barr and D.M.T. Newsham, *Fluid Phase Equilibria*, 35 (1987) 189, 207.
[5] R.M. Cooling, B. Khalfaoui and D.M.T. Newsham, *Fluid Phase Equilibria*, 81 (1992) 217.
[6] B. Khalfaoui and D.M.T. Newsham, *Fluid Phase Equilibria*, 98 (1994) 213–223.
[7] B. Khalfaoui and D.M.T. Newsham, *J. Chromatogr. A*, 673 (1994) 85.
[8] R.C. Pemberton and C.J. Mash, *NPL Report on Chemistry*, National Physical Laboratory, Teddington, 1974, p. 33.
[9] A. Fredenslund, R.L. Jones and J.M. Prausnitz, *AIChE J.*, 21 (1975) 1086.
[10] I. Nagata and J. Koyabu, *Thermochim. Acta*, 48 (1981) 187.
[11] M.C. Kavanaugh and R. Rhodes-Trussell, *Aqua Sci. Tech. Rev.*, 6 (1980) 0118.
[12] R.R. Dreisbach, *Adv. Chem. Ser.*, 15 (1955) 536.
[13] J. Timmermans, *Physico-chemical Constants of Pure Organic Compounds*, Vol. II, Elsevier, Amsterdam, 1965.
[14] J.H. Dymond and E.B. Smith, *Virial Coefficients of Pure Gases and Mixtures*, Clarendon Press, Oxford, 1980.
[15] T. Boublik, V. Fried and E. Hala, *Vapour Pressures of Pure Substances*, Elsevier, Amsterdam, 1973.
[16] S. Ohe, *Computer Aided Data Book of Vapour Pressure*, Data Book Publishing, Tokyo, 1976.
[17] J.A. Nelder and R. Mead, *Comput. J.*, 7 (1965) 308.
[18] A.L. Horvath, *Halogenated Hydrocarbons, Solubility–Miscibility with Water*, Marcel Dekker, New York, 1982.

ELSEVIER

Journal of Chromatography A, 688 (1994) 125–134

JOURNAL OF CHROMATOGRAPHY A

Comparison of uncorrected retention data on a capillary and a packed hexadecane column with corrected retention data on a packed squalane column

Michael H. Abraham[a,*], Jenik Andonian-Haftven[a], Chau My Du[a], Juliet P. Osei-Owusu[a], Panos Sakellariou[b], Wendel J. Shuely[c], Colin F. Poole[d], Salwa K. Poole[d]

[a]*Department of Chemistry, University College London, 20 Gordon Street, London WC1H 0AJ, UK*
[b]*ICI Paints, Wexham Road, Slough, Berks. SL2 5DS, UK*
[c]*US Army Chemical Research, Development and Standardisation Center, Aberdeen Proving Ground, MD 21010, USA*
[d]*Department of Chemistry, Wayne State University, Detroit, MI 48202, USA*

First received 22 November 1993; revised manuscript received 15 August 1994

Abstract

Retention data obtained previously at 25°C on a hexadecane capillary column by Zhang et al. and a packed hexadecane column by Abraham et al., both uncorrected for any effects due to interfacial adsorption, were compared with retention data obtained by Poole et al. on a packed squalane column at 120°C, with the latter fully corrected for such effects. It is shown that for most solutes, the capillary and packed column data are equally compatible with the squalene corrected data, but for the solutes dimethyl sulfoxide, dimethylformamide and dimethylacetamide the packed column data are in much better accord with the corrected data than are the capillary column data. It is further shown that both sets of results at 25°C for carboxylic acids are in error, owing to dimerization. Retention volumes on Chromosorb G AW DMCS are reported at 25 and at 93°C. It is shown that at 25°C, there could be some contribution to solute retention from adsorption on the support, but that this is almost impossible at 93°C.

1. Introduction

Some time ago [1], we defined a new solute descriptor, log L^{16}, where L^{16} is the solute Ostwald solubility coefficient, or gas–liquid partition coefficient, at 25°C on hexadecane. This solvent was chosen for two reasons, first because it is a well defined chemical, and second because L^{16} values can be combined with gas–water partition coefficients to give water–hexadecane partition coefficients that are useful in pharmaceutical and medicinal chemistry. We first determined L^{16} values for 140 solutes, using a gas–liquid chromatographic method (GLC) in which hexadecane was the stationary phase [1]. A packed column was used, with acid-washed, silanized Chromosorb G AW DMCS as the support. The log L^{16} values have subsequent-

* Corresponding author.

0021-9673/94/$07.00
SSDI 0021-9673(94)00819-1

ly proved to be very useful as a descriptor in linear free energy relationships (LFERs) and in quantitative structure–activity relationships (QSARs). Such LFERs have been used to analyse and to interpret processes including GLC retention [2–6], the solubility of vapors in soybean oil [7], polymer-probe interactions [8], the adsorption of gases and vapors on carbons [9] and on buckminsterfullerene [10] and the solubility of gases and vapors in organic solvents [11, 12]. A QSAR has been established for the effect of airborne chemicals on the upper respiratory tract irritation in mice [13]. Although the direct determination of log L^{16} values on hexadecane at 25°C is restricted to the more volatile solutes, the range of log L^{16} values can greatly be extended through the use of non-polar GLC phases at higher temperatures [14–16]. For example, the extensive data of Dutoit [17] on the stationary phase $C_{78}H_{158}$ at 130°C were fitted to an LFER of the form

$$I/10 = 6.669 + 8.918\,R_2 + 20.002 \log L^{16} \quad (1)$$

$$n = 138,\ \rho = 0.9995,\ \text{S.D.} = 0.449,\ F = 67\,450$$

where I is the retention index and the descriptor R_2 is the solute excess molar refraction [2]. In Eq. 1 and elsewhere, n is the number of data points, ρ is the correlation coefficient, S.D. is the standard deviation and F is the Fisher F-statistic. Once Eqn. 1 has been set up with solutes of known R_2 and log L^{16} values, then further log L^{16} values can be calculated from known values of I and R_2. In this way, around 1500 additional log L^{16} values have been obtained [14–16].

Although the original values [1] were obtained from retention data on conventional packed columns, the further log L^{16} values [14–16] were calculated from retention data on both capillary columns and conventional packed columns, usually at elevated temperatures. Recently, Zhang et al. [18], in a careful study, have re-determined log L^{16} values from data on hexadecane at 25°C, using a fused-silica open-tubular capillary column. For most of 85 common solutes, there was excellent agreement between the original values and those obtained using the capillary column, but for a number of solutes there were significant deviations (see Table 1). Zhang et al. [18] attributed these differences to interfacial adsorption in the packed column, rather than to any such effect in the capillary column. Certainly, adsorption effects will be expected to be larger at 25°C than at elevated temperature, but there is no direct evidence on exactly how large such effects are, with respect to the hexadecane packed column.

It is the purpose of this paper to present experimental data that will allow conclusions to be drawn on the possible effects of adsorption on the solid support and of interfacial adsorption, with respect to retention in packed columns with a low-polarity stationary phase. We hope in this way to obtain information on the actual origin of the discrepancies between retention data on the hexadecane capillary and packed columns.

2. Experimental

Specific retention volumes on the support Chromosorb G AW DMCS at the column temperature were obtained as set out before, with the usual corrections for the pressure drop across the column [1]. Data were obtained at 25°C, with the column immersed in a water-bath, and at 93°C using a conventional air oven. Specific retention volumes on squalane packed columns were obtained exactly as detailed before [19,20].

3. Results and discussion

Before dealing with new results, we give in Table 1 some log L^{16} values that we had re-determined before Zhang et al.'s paper [18] appeared. The new values for benzyl alcohol, phenol and butylbenzene go some way to resolving the discrepancies, but the new results for the cresols are essentially the same as our original values. The log L^{16} values for carboxylic acids obtained from either the capillary column or the packed column are incorrect, owing to dimerization of the acids. We have obtained log L^{16} values for the acids by an indirect, non-chro-

Table 1
Some discrepancies between log L^{16} values measured on capillary and packed columns

Solute	$C(25)$[a]	$A(25)$[b]	$A(HT)$[c]
Butylbenzene	4.714	4.686	4.730[d]
Benzyl alcohol	4.162	4.443	4.221
Phenol	3.641	3.865	3.766
o-Cresol	4.183	4.242	4.218
m-Cresol	4.187	4.329	4.310
p-Cresol	4.254	4.307	4.312
Acetic acid	2.331	3.290	1.750[e]
Propanoic acid	2.978	–	2.290[e]
Butanoic acid	3.427	–	2.830[e]
DMF	2.922	3.173	3.173[f]
DMA	3.357	3.717	3.717[f]
DMSO	3.110	3.437	3.459

[a] Capillary column data, Ref. [18].
[b] Packed column data, Ref. [1].
[c] Recent packed column data, at higher temperature, Ref. [16].
[d] Redetermined at 25°C.
[e] Indirect value, see text.
[f] Same as original values.

matographic, method, using gas–water partition coefficients [21] and water–hexadecane partition coefficients [22] that are corrected for dimerization. The calculated log L^{16} values are given in Table 1; we have confirmed that these indirect values reproduce GLC retention data at elevated temperatures, where the acids are monomeric in the gas phase. We are left with only three outlying solutes, viz., N,N-dimethylformamide (DMF), N,N-dimethylacetamide (DMA) and dimethyl sulfoxide (DMSO) where the new results are the same as our original results, and where there are considerable differences between the packed column and capillary data.

Possible effects of adsorption on the inert support can be studied through measurements of specific retention volumes on the support itself. Results at 25 and at 93°C are given in Table 2. We would have liked to obtain values at 120°C but the retention volumes were too small to measure conveniently. We can use these retention volumes to calculate the contribution made by adsorption on the support to the overall retention, by assuming that the support is, say, only 90% covered. The real contribution will be

Table 2
Values of log V_G on Chromosorb G AW DMCS at 25 and 93°C

Solute	Log V_G	
	25°C	93°C
Octane	−0.02	
Nonane	0.47	
Decane	0.95	−0.41
Undecane	1.36	−0.33
Dodecane		0.04
Tridecane		0.28
Tetradecane		0.56
Pentadecane		0.83
Hexadecane		1.13
Heptadecane		1.45
Octadecane		1.68
Nonadecane		1.94
Diiodomethane	0.49	−1.21
Dibutyl ether	1.11	−0.72
Tetrahydrofuran	0.79	
Pentan-2-one	0.75	
Heptan-2-one	1.41	
Octan-2-one		−0.18
Nonan-2-one		0.10
Nonan-5-one		−0.14
Decan-2-one		0.28
Butyl propanoate	1.25	−0.81
Pentyl acetate	1.32	
Methanol		−1.21
Ethanol	0.51	
Propan-1-ol	0.88	
Butan-1-ol	1.20	
Heptan-1-ol		−0.05
Octan-1-ol		0.22
Octan-2-ol		−0.13
Decan-1-ol		0.79
TFE		−0.73
HFIP	0.55	−1.19
Triethylamine		−0.47
DMF	[a]	0.05
DMA	[a]	0.17
DMSO	[a]	0.38
Benzene		−1.01
Toluene		−1.01
Ethylbenzene		−0.85
Propylbenzene	0.61	
Butylbenzene	1.19	
Chlorobenzene	0.27	
1,2-Dichlorobenzene	0.94	
3-Chlorotoluene		−0.99
4-Chlorotoluene	0.60	−0.99
Iodobenzene	0.93	
Acetophenone		−0.88

(Continued on p. 128)

Table 2 *(continued)*

Solute	Log V_G	
	25°C	93°C
Benzonitrile		−0.21
Aniline		−0.20
Phenol	2.23	
m-Cresol		0.37
2-Isopropylphenol		0.37
3-Isopropylphenol		0.66
3-Chlorophenol		0.80
Pyridine		−0.48

[a] These compounds were not eluted at 25°C.

some fraction of this, depending on the actual percentage covered. Results of calculations on these lines are given in Table 3. It is clear that for most solutes there will be a negligible contribution from adsorption on the support, but with alcohols, especially hexafluoropropan-2-ol (HFIP) and possibly also trifluoroethanol (TFE), there could be some contribution. In the event, there is good agreement between the packed column and capillary column results for HFIP. However, we observed that the three "key" solutes, DMF, DMA and DMSO, all failed to elute from the support at 25°C, so that it does seem possible that adsorption on the support could lead to log L^{16} values that are too large.

We cannot calculate possible support effects at 120°C in the same way, because the log V_G values were too small to determine. However, a rough estimate suggests that for 90% coverage, the contribution from adsorption on the support to retention on a squalane packed column is 0.8% and 0.4% for 5% and 10% loadings, respectively, with the solute DMSO. For DMF and DMA the contribution is even less, and for the other solutes studied it is also negligible. These results are in agreement with the study by Condor et al. [23], who showed that at low loadings of squalane on silanized Chromosorb P, adsorption of ethyl acetate at the support surface was substantial, but that this decreased with increasing temperature.

Table 3
Percentage contribution to retention volume by adsorption on Chromosorb G AW DMCS at 25°C assuming 90% support coverage

Solute	5% loading	10% loading
Octane	0.03	0.01
Decane	0.03	0.01
Pentan-2-one	1.46	0.69
Propan-1-ol	8.94	4.24
HFIP	21.10	9.98
Butylbenzene	0.04	0.02
Chlorobenzene	0.04	0.02
Phenol	3.38	1.60

Having to hand the log V_G values on Chromosorb G AW DMCS at 25 and 93°C, we can analyse them through our general solvation equation in the usual way [24]. The solute descriptors are those previously listed [24], and the found regression equations are

$$\log V_G(25) = -2.43 - 0.30R_2 + 0.35\pi_2^H + 2.13\Sigma\alpha_2^H + 2.05\Sigma\beta_2^H + 0.69 \log L^{16} \quad (2)$$

$n = 22$, $\rho = 0.9650$, S.D. $= 0.144$, $F = 43.3$

$$\log V_G(93) = -2.89 - 0.46R_2 + 0.59\pi_2^H + 1.18\Sigma\alpha_2^H + 0.66\Sigma\beta_2^H + 0.51 \log L^{16} \quad (3)$$

$n = 45$, $\rho = 0.9634$, S.D. $= 0.221$, $F = 100.7$

where π_2^H is the solute dipolarity/polarizability, $\Sigma\alpha_2^H$ is the solute overall or effective hydrogen-bond acidity and $\Sigma\beta_2^H$ is the solute overall or effective hydrogen-bond basicity. Although the equations are not very good, they are reasonable for gas–solid processes. The significant points are that (1) the support is considerably basic ($a = 2.13$ and 1.18) and is considerably acidic ($b = 2.05$ and 0.66), and (2) both basicity and acidity decrease markedly with increase in temperature. Thus any solute–support effects will also decrease with increase in temperature.

The problem of interfacial adsorption in packed columns is also less at elevated temperature, as found experimentally by Poole and coworkers [25–29], who determined the extent of interfacial adsorption in various systems

[19,20,25–30] using a well known procedure [31,32]. In this method, retention volumes for a given solute are obtained at several loadings of a particular stationary phase. Extrapolation of the retention volumes to infinite stationary phase volume yields the partition coefficient for the gas–stationary phase, free from any interfacial effects. The method requires (i) that the adsorption isotherm is linear, (ii) that the contribution from adsorption remains essentially constant as the loading is altered (constant surface area) and (iii) that the solute is at infinite dilution. Conditions (i) and (iii) can be fulfilled by the use of low solute concentration, and tested by the observation of symmetrical peak shape. Condition (ii) can be tested by the observation of a linear extrapolation of retention data against $1/V_L$, where V_L is the volume of the stationary phase. These conditions were always found to hold [19,20,25–30]. The procedure [31,32] used by Poole and co-workers will also eliminate effects from adsorption on the support, although as we have seen these will be very small at elevated temperature. In Table 4 we give the percentage contribution by adsorption to the total retention for DMSO, DMA and DMF, obtained as above, on a squalane packed column at 120°C. As found for adsorption on the support, above, these results show that at temperatures above about 100°C there is a negligible contribution from interfacial adsorption even for the three very polar solutes, DMSO, DMA and DMF, on the non-polar squalane phase.

A comparison of percentage contribution by adsorption for a number of solutes and solvents [29] is given in Table 5. Together with previous work [23], these results show that interfacial effects in non-polar packed columns can be eliminated by using high loadings of the non-polar phase and particularly by working at elevated temperatures.

In this way, we determined gas–squalane partition coefficients at 120°C that are corrected for any interfacial adsorption for a number of solutes common to the sets of Abraham et al. [1] and Zhang et al. [18], including the key solutes DMSO, DMA and DMF [33–35]. It is now possible to compare these fully corrected data at 120°C with the uncorrected data obtained on the packed and capillary columns at 25°C. The gas–squalane partition coefficients, as log K values, are given in Table 6, denoted as $P(120)$. Also in Table 6 are the log L^{16} values from the 25°C data on the capillary column, $C(25)$, and on the packed column, $A(25)$, and log L^{16} values obtained by the back-calculation method from retention data at higher temperatures, $A(HT)$. Finally, the best set of log L^{16} values from

Table 4
Percentage interfacial adsorption on squalane with Chromosorb W AW DMCS support

Temperature (°C)	Solute	Phase loading (%)			
		8.8	12.6	15.5	20.2
120	DMSO	1.6	0.9	1.2	0.6
	DMA	0.9	0.7	0.6	0.4
	DMF	1.9	1.2	1.0	0.8
100	DMSO	8.4	4.2	5.7	4.0
	DMA	8.2	4.2	5.5	4.0
	DMF	8.4	4.3	5.7	4.0
80	DMSO	17.3	11.3	8.7	7.9
	DMA	17.2	11.1	8.7	7.8
	DMF	17.3	11.2	8.8	7.8
60	DMSO	31.3	23.4	15.0	16.2
	DMA	31.3	23.2	15.7	16.0
	DMF	31.2	23.1	16.0	15.6

Table 5
Comparison of percentage interfacial adsorption for various solutes and stationary phases

Temperature (°C)	Solute	Stationary phase[a]				
		SQ	OV-17	CW-20M	TCEP	DEGS
121	Tridecane	1.5	0.6	4.5	21.7	26.9
	Oct-2-yne	2.1	0.6	5.9	7.1	11.2
	Methyl octanoate	0.9	0.4	3.7	1.9	7.3
	Benzonitrile	2.6	0.6	2.9	1.2	5.3
	Heptan-1-ol	2.6	0.6	1.9	2.0	6.6
	Heptan-2-one	1.0	0.8	1.8	3.3	7.0
	Ethylbenzene	2.8	0.8	4.7	12.5	11.4
	N,N-Dimethylaniline	2.5	0.5	2.1	2.8	12.5
	DMSO	1.2				
	DMA	0.6				
	DMF	1.0				
81	Tridecane	7.0	2.3	23.0	47.9	66.3
	Oct-2-yne	7.8	2.1	11.9	8.3	32.3
	Methyl octanoate	8.1	2.0	10.9	10.2	26.5
	Benzonitrile	7.8	2.1	7.2	16.0	37.1
	Heptan-1-ol	15.5	2.3	8.9	5.2	14.7
	Heptan-2-one	8.6	1.4	7.2	3.9	9.5
	Ethylbenzene	8.1	2.2	6.6	12.0	15.2
	N,N-Dimethylaniline	8.0	2.1	5.0	17.2	34.6
	DMSO	8.7				
	DMA	8.7				
	DMF	8.8				

Data from Ref. [29] and Table 4.
[a] SQ Squalane; OV-17 = poly(methylphenylsiloxane); CW-20M = poly(ethylene glycol); TCEP = 1,2,3-tris(2-cyanoethoxypropane); DEGS = poly(diethylene glycol succinate). The phase loading is 15–16% in all cases.

packed columns at 25°C and at higher temperatures is given as A(All).

We start by regressing the 40 values of $A(25)$ and the 33 values of $C(25)$ against R_2 and $P(120)$, exactly on the lines of Eq. 1, to yield

$$A(25) = 0.355 - 0.238R_2 + 1.719P(120) \quad (4)$$
$$n = 40,\ \rho = 0.9982,\ \text{S.D.} = 0.054,\ F = 5242$$

$$C(25) = 0.270 - 0.232R_2 + 1.734P(120) \quad (5)$$
$$n = 33,\ \rho = 0.9901,\ \text{S.D.} = 0.104,\ F = 750$$

There is no doubt that the uncorrected packed column data, $A(25)$, correlate better with the corrected packed column data than do the uncorrected capillary column data, $C(25)$. In both regressions, the difficult polar solutes DMSO, DMA and DMF are included (see Table 6). A referee pointed out that Eqs. 4 and 5 are not exactly matched, with respect to either the number or type of solutes. We therefore repeated regressions with the same 29 common solutes, including DMSO, DMA and DMF;

$$A(25) = 0.369 - 0.223R_2 + 1.710P(120) \quad (6)$$
$$n = 29,\ \rho = 0.9967,\ \text{S.D.} = 0.060,\ F = 1979$$

$$C(25) = 0.283 - 0.245R_2 + 1.731P(120) \quad (7)$$
$$n = 29,\ \rho = 0.9897,\ \text{S.D.} = 0.108,\ F = 620$$

As might have been expected, there is very little difference in the two sets of equations, and the conclusion remains the same: the uncorrected packed column data yield the better regression equation. The three solutes DMSO, DMA and DMF are not outliers in Eq. 4 (or Eq. 6), but

Table 6
Comparison of corrected log K values on squalane at 120°C with sets of log L^{16} values

Solute	$P(120)^a$	$C(25)^b$	$A(25)^c$	$A(HT)^d$	$A(ALL)^e$
Heptane	1.64	3.17	3.17		3.17
Octane	1.93	3.68	3.68		3.68
Nonane	2.22	4.18	4.18		4.18
Decane	2.52	4.69	4.69		4.69
Undecane	2.81		5.19		5.19
Dodecane	3.10		5.70		5.70
Tridecane	3.40		6.20		6.20
Nonanal	2.63		4.86		4.86
Butanone	1.14	2.27	2.29		2.29
Pentan-2-one	1.42	2.73	2.76		2.76
Hexan-2-one	1.71		3.26		3.26
Heptan-2-one	2.00		3.76		3.76
Octan-2-one	2.29		4.26		4.26
Nonan-2-one	2.57		4.74		4.74
Benzene	1.51	2.79	2.79		2.79
Butylbenzene	2.64	4.71	4.73		4.73
Butan-1-ol	1.26	2.54	2.60		2.60
Pentan-1-ol	1.62	3.06	3.11		3.11
Hexan-1-ol	1.91	3.55	3.61		3.61
Heptan-1-ol	2.21	4.07	4.12		4.12
Octan-1-ol	2.51	4.57	4.62		4.62
Nonan-1-ol	2.79		5.12		5.12
2-Methylpentan-2-ol	1.59		3.08		3.08
Sym-Tetrachloroethane	2.15		3.80		3.80
Toluene	1.80	3.34	3.33		3.33
Ethylbenzene	2.07	3.79	3.78		3.78
DMSO	1.89	3.11	3.44	3.46	3.46
DMF	1.70	2.92	3.17		3.17
DMA	2.02	3.36	3.72		3.72
Nitropropane	1.50	2.77	2.71	2.89	2.89
Pyridine	1.64	2.97	3.00	3.02	3.02
Aniline	2.23	3.93	3.99	3.93	3.93
N,N-Dimethylaniline	2.69	4.75	4.75	4.70	4.70
1,2-Dichlorobenzene	2.53	4.45	4.41	4.52	4.52
Chlorobenzene	2.01	3.63	3.64	3.66	3.66
Bromobenzene	2.26	4.02	4.04	4.04	4.04
Dioxane	1.50	2.79	2.80	2.89	2.89
Acetophenone	2.52	4.46	4.48	4.50	4.50
Phenol	2.05	3.64	3.86	3.77	3.77
p-Cresol	2.39	4.25	4.31	4.31	4.31
Benzonitrile	2.23	3.91		4.04	4.04
N-Methylaniline	2.55	4.49		4.48	4.48
Iodobenzene	2.56	4.51		4.50	4.50
Benzaldehyde	2.23	3.94		4.01	4.01
Dodec-1-yne	3.05			5.66	5.66
Oct-2-yne	2.06			3.85	3.85
cis-Hydrindane	2.54			4.64	4.64
Methyl heptanoate	2.34			4.36	4.36
Methyl octanoate	2.62			4.84	4.84
Methyl nonanoate	2.90			5.32	5.32
Methyl decanoate	3.18			5.80	5.80
Methyl undecanoate	3.46			6.29	6.29

(Continued on p. 132)

Table 6 *(continued)*

Solute	$P(120)^a$	$C(25)^b$	$A(25)^c$	$A(HT)^d$	$A(ALL)^e$
Nitrohexane	2.39			4.42	4.42
Nitrocyclohexane	2.66			4.83	4.83
Nitropentane	2.09			3.94	3.94
2,6-Dimethylaniline	2.84			5.03	5.03
Dihexyl ether	3.23			5.94	5.94
Benzodioxane	2.81			4.97	4.97
4-Chlorophenol	2.67			4.78	4.78
2,5-Dimethylphenol	2.66			4.77	4.77
2,6-Dimethylphenol	2.62			4.68	4.68
3,5-Dimethylphenol	2.71			4.86	4.86

[a] Corrected log K values on squalane at 120°C, Refs. [33,35].
[b] Uncorrected log L^{16} capillary values at 25°C, Ref. [18].
[c] Uncorrected log L^{16} packed column values at 25°C, Ref [1].
[d] Uncorrected, back-calculated log L^{16} values at higher temperature, Ref. [16].
[e] Taken log L^{16} values from previous two columns.

they are in Eq. 5 (or Eq. 7). If all three are excluded from Eq. 5, we find

$$C(25) = 0.340 - 0.242R_2 + 1.716P(120) \quad (8)$$
$$n = 30,\ \rho = 0.9986,\ \text{S.D.} = 0.039,\ F = 4987$$

There is almost no statistical difference between Eqs. 4 and 8, confirming the finding of Zhang et al. [18] that for most solutes there is little to choose between the packed column and the capillary column results on hexadecane at 25°C. Hence for solutes that are not too volatile, either a packed hexadecane column at 25°C or a capillary hexadecane column at 25°C will yield reasonable values of log L^{16}, as found by Zhang et al. [18]. Our conclusion regarding the outliers DMSO, DMA, and DMF is not the same as that of Zhang et al. however, because we have shown that the packed column results at 25°C are in essential agreement with the fully corrected values obtained at 120°C. Zhang et al. [18] warned against the use of calculations on the lines of Eq. 1 to obtain further log L^{16} values, but we can compare the back-calculated log L^{16} values, as $A(HT)$, with the corrected squalane values:

$$A(HT) = 0.372 - 0.239R_2 + 1.719P(120) \quad (9)$$
$$n = 34,\ \rho = 0.9993,\ \text{S.D.} = 0.031,\ F = 11\,281$$

The excellent correlation, eqn. 9, shows that calculation using data at elevated temperatures is probably the best method of determining log L^{16} values for polar solutes. Finally, we regressed the total set of log L^{16} values against the corrected log K values, as $P(120)$:

$$A(ALL) = 0.374 - 0.238R_2 + 1.716P(120) \quad (10)$$
$$n = 62,\ \rho = 0.9994,\ \text{S.D.} = 0.033,\ F = 22\,934$$

The regression Eq. 10 confirms that the set of log L^{16} values published [24] is entirely compatible with the corrected results on squalane at 120°C.

The data shown in Table 5 indicate that the use of heavily loaded packed columns with non-polar phases at elevated temperatures can lead to retention data essentially free from contributions due to interfacial adsorption. The situation with capillary columns is not so clear. First, a distinction must be made between capillary columns that have chemically bonded phases and capillary columns such as that used by Zhang et al. [18], which are deactivated by heating and which are coated from solution. The latter are not inert; indeed, Zhang et al. [18] specifically noted the problem of adsorption for DMSO, DMA, DMF, aliphatic amines, aniline and pyridine on the hexadecane capillary column. There seem to be a number of disadvantages in the use of capillary columns to obtain thermodynamic data, as follows. (i) It is very difficult to

obtain absolute retention data; Zhang et al. [18] overcame this problem by using data for alkanes on a packed hexadecane column, obtained by Abraham et al. [1] as standards for a hexadecane capillary column, but this stratagem is not usually available. (ii) The problem of interfacial adsorption still exists with capillary columns; Matisova et al. [36] examined a capillary column coated with the relatively non-polar OV-101 and Apiezon L. They showed that as the film thickness increased, the Kováts retention indices of methyl alkanoates reached limiting values, but for decan-1-ol no clear limiting value was obtained, at 100 or 110°C. Gvoliany and Rixiao [37] also examined a capillary column coated with OV-101, this time at 120°C. They showed that with a film thickness of 0.3 μm, interfacial adsorption makes a ca. 20% contribution to the total retention for solutes such as octan-1-ol and methyl hexanoate. Although we are concerned with non-polar phases, it is worth pointing out that Berezkin and Korolev [38] investigated a fused-silica open-tubular column coated with the polar phase SP-2380 and found that interfacial adsorption of alkanes was so large at 85°C that Kováts retention indices could not be determined. It seems, therefore, that interfacial adsorption in capillary columns is no less a problem than in packed columns. Zhang et al. [18] quoted Lichtenthaler et al. [39] as suggesting that the volume-to-area ratio for a capillary column could be more than two orders of magnitude larger than for a packed column, which, if correct, would indicate that interfacial adsorption should be very much less with capillary columns. We calculate that for a capillary column of length 20 m, of I.D. 0.053 cm and of film thickness 0.29 μm the volume to surface area is $2.90 \cdot 10^{-5}$ cm. For a packed squalane column of length 2 m, with a 15% loading (0.27 g of squalane and 1.53 g of support) and of support surface area 10^4 cm^2 g^{-1}, at 120°C where the density of squalane is 0.7278 g cm^{-3}, the volume to surface area is $2.43 \cdot 10^{-5}$ cm. The ratio between the capillary and packed columns is thus around 1.2, nowhere near the "two orders of magnitude" suggested. (iii) As clearly shown by Zhang et al. [18], the use of excessive amounts of solute can result in increased retention times through solute–solute association. Such use can also result in decreased retention times through non-equilibration of the solute with the stationary phase. A lack of linearity in the adsorption/absorption isotherm could lead to either an increase or a decrease in retention time. The overall effect will be compound specific and can result in an increase or decrease in retention time. We argue that these problems may be more severe with capillary columns as used by Zhang et al. [18] than with packed columns. In any case, it is clear that a calculated log L^{16} value could be larger or smaller on the hexadecane capillary column at 25°C than on the packed hexadecane column at 25°C.

Our conclusion is that there is no advantage to be gained through the use of capillary columns to measure thermodynamic data. With non-polar stationary phases it is reasonably clear that the use of heavily loaded packed columns at temperatures above about 100°C will yield retention data free from complications due to interfacial adsorption. As regards the determination of log L^{16} values for "difficult" polar solutes and for the less volatile solutes, we recommend that if packed columns are employed, then high loadings of non-polar stationary phases should be used. In any case, whatever the type of column, it is a marked advantage to work at elevated temperature.

References

[1] M.H. Abraham, P.L. Grellier and R.A. McGill, *J. Chem. Soc., Perkin Trans. 2*, (1987) 797.
[2] M.H. Abraham, G.S. Whiting, R.M. Doherty and W.J. Shuely, *J. Chem. Soc., Perkin Trans. 2*, (1990) 1451.
[3] M.H. Abraham, G.S. Whiting, R.M. Doherty and W.J. Shuely, *J. Chromatogr.*, 518 (1990) 329.
[4] M.H. Abraham, I. Hamerton, J.B. Rose and J.W. Grate, *J. Chem. Soc., Perkin Trans. 2*, (1991) 1417.
[5] M.H. Abraham, G.S. Whiting, R.M. Doherty and W.J. Shuely, *J. Chromatogr.*, 587 (1991) 229.
[6] M.H. Abraham, G.S. Whiting, J. Andonian-Haftvan, J.W. Steed and J.W. Grate, *J. Chromatogr.*, 588 (1991) 361.
[7] M.H. Abraham and G.S. Whiting, *J. Am. Oil Chem. Soc.*, 69 (1992) 1236.

[8] M.H. Abraham, G.S. Whiting, R.M. Doherty, W.J. Shuely and P. Sakellariou, *Polymer*, 33 (1992) 2162.
[9] M.H. Abraham and D.P. Walsh, *J. Chromatogr.*, 627 (1992) 294.
[10] M.H. Abraham, C.M. Du, J.W. Grate, R.A. McGill and W.J. Shuely, *J. Chem. Soc., Chem. Commun.*, (1993) 1863.
[11] M.H. Abraham, G.S. Whiting, R.M. Doherty and W.J. Shuely, *J. Chem. Soc., Perkin Trans.* 2, (1990) 1851.
[12] M.H. Abraham, J. Andonian-Haftvan, J.P. Osei-Owusu, P. Sakellariou, J.S. Urieta, M.C. Lopez and R. Fuchs, *J. Chem. Soc., Perkin Trans. 2*, (1993) 299.
[13] M.H. Abraham, G.S. Whiting, Y. Alarie, J.J. Morris, P.J. Taylor, R.M. Doherty, R.W. Taft and G.D. Nielsen, *Quant. Struct.–Act. Relat.*, 9 (1990) 6.
[14] M.H. Abraham, G.S. Whiting, R.M. Doherty and W.J. Shuely, *J. Chromatogr.*, 587 (1991) 213.
[15] M.H. Abraham and G.S. Whiting, *J. Chromatogr.*, 594 (1992) 229.
[16] M.H. Abraham, *J. Chromatogr.*, 644 (1993) 95.
[17] J.-C. Dutoit, *J. Chromatogr.*, 555 (1991) 191.
[18] Y. Zhang, A.J. Dallas and P.W. Carr, *J. Chromatogr.*, 638 (1993) 43.
[19] B.R. Kersten, S.K. Poole and C.F. Poole, *J. Chromatogr.*, 468 (1989) 235.
[20] S.K. Poole and C.F. Poole, *J. Chromatogr.*, 500 (1990) 329.
[21] J.A.V. Butler and C.N. Ramchandani, *J. Chem. Soc.*, (1935) 952.
[22] M.H. Abraham, H.S. Chadha, G.S. Whiting and R.C. Mitchell, *J. Pharm. Sci.*, 83 (1994) 1085.
[23] J.R. Condor, N.K. Ibrahim, G.J. Rees and G.A. Oweirmreen, *J. Phys. Chem.*, 89 (1985) 2571.
[24] M.H. Abraham, *Chem. Soc. Rev.*, 22 (1993) 73.
[25] S.K. Poole, K.G. Furton and C.F. Poole, *J. Chromatogr. Sci.*, 26 (1988) 67.
[26] C.F. Poole and S.K. Poole, *Chem. Revs.*, 89 (1989) 377.
[27] C.F. Poole, T.O. Kollie and S.K. Poole, *Chromatographia*, 34 (1992) 281.
[28] C.F. Poole and T.O. Kollie, *Anal. Chim. Acta* 282 (1993) 1.
[29] S.K. Poole, T.O. Kollie and C.F. Poole, *J. Chromatogr. A*, 664 (1994) 229.
[30] B.R. Kersten and C.F. Poole, *J. Chromatogr.*, 452 (1988) 191.
[31] J.A. Jonsson (Editor), *Chromatographic Theory and Basic Principles*, Marcel Dekker, New York, 1987, pp. 189–244.
[32] V.G. Berezkin, *Gas–Liquid–Solid Chromatography*, Marcel Dekker, New York, 1991.
[33] C.F. Poole, R.M. Pomaville and T.A. Dean, *Anal. Chim. Acta*, 225 (1989) 193.
[34] T.O. Kollie and C.F. Poole, *J. Chromatogr.* 550 (1991) 213.
[35] S.K. Poole and C.F. Poole, unpublished work.
[36] E. Matisova, J. Krupcik and J. Garaj, *Chromatographia*, 16 (1982) 169.
[37] Z. Gvoliany and C. Rixiao, *Chromatographia*, 29 (1990) 575.
[38] V.G. Berezkin and A.A. Korelov, *J. High Resolut. Chromatogr.*, 12 (1989) 617.
[39] R.N. Lichtenthaler, D.D. Liu and J.M. Prausnitz, *Macromolecules*, 7 (1974) 565.

ELSEVIER

Journal of Chromatography A, 688 (1994) 135–152

JOURNAL OF CHROMATOGRAPHY A

Pulsed discharge helium ionization detector Universal detector for inorganic and organic compounds at the low picogram level

W.E. Wentworth[a,*], Huamin Cai[a], Stanley Stearns[b]

[a]*Chemistry Department, University of Houston, 4800 Calhoun Road, Houston, TX 77204-5641, USA*

[b]*Valco Instruments Co., Inc., Houston, TX 77055, USA*

First received 22 June 1994; revised manuscript received 13 September 1994

Abstract

The pulsed discharge helium ionization detector is a universal ionization detector with sensitivity in the low picogram range. The response is approximately constant for saturated hydrocarbons on a per gram basis. Unsaturated and aromatic hydrocarbons have lower sensitivities, by about 10–20%. Heterocyclic substituents such as oxygen, chlorine and bromine tend to lower the response on a per gram basis. The dependence of the response on various parameters such as pulse interval and power, voltage, flow-rate and detector volume has been investigated. The response is linearly related to concentration over five orders of magnitude. The detector volume can be made small enough for high-speed microbore chromatography.

1. Introduction

In a previous publication the pulsed discharge helium ionization detector (PDHID) was introduced, and its capabilities in the analysis of permanent gases were demonstrated [1]. In other applications —air pollution analysis, for example— the simultaneous analysis of inorganic and organic compounds is desired; nitric oxide and sulfur dioxide need to be detected as well as formaldehyde, aromatic hydrocarbons and halogenated compounds. It is also important to analyze for trace water in organic streams, because water may be deleterious to the catalyst or process. In this paper we demonstrate the response of the PDHID to both inorganic and organic compounds.

Since the PDHID is sensitive and essentially non-destructive (ca. 0.01–0.1% ionization) it can be used in conjunction with more selective detectors of comparable sensitivity. For example, the pulsed discharge source can be adapted to the electron-capture mode, yielding sensitivities on the femtogram level [2]. Also various emission detectors such as microwave-induced plasma [3], alternating current helium plasma, [4] capacitively-coupled plasma [5], radio frequency plasma [6] and helium discharge [7,8], could be used in conjunction with the universal PDHID to detect various elemental compositions and functional groups. (For a general discussion of element-specific chromatographic detection by atomic emission, consult the text

* Corresponding author.

0021-9673/94/$07.00
SSDI 0021-9673(94)00913-9

which compiles the presentations given at a recent ACS symposium [9]).

To evaluate the performance of the PDHID in organic analysis, an appropriate basis for comparison is the flame ionization detector (FID). For inorganic analysis we compare it to the photoionization detector. In a subsequent publication we will demonstrate its use in high-speed chromatography with 0.05–0.10 mm I.D. microbore columns, comparing the results to those obtained with the micro-thermal conductivity detector.

2. Experimental

In the previous publication describing the analysis of permanent gases [1], we used a PDHID in which the sample passed through the reaction zone and then through the discharge region. This was satisfactory for the analysis of permanent gases, since decomposition of the inorganic compounds does not contaminate the electrodes. However, this configuration is unsuitable for organic analysis, since extensive analysis leads to contamination of the discharge electrodes. When trace analysis is being carried out with capillary columns, any contamination of the discharge electrodes is negligible.

A schematic diagram of the PDHID used in this study is shown in Fig. 1. The detector is divided into two sections: the discharge section (1.6 mm I.D.) and the reaction section (3 mm I.D.). The reaction section has two ring-shaped electrodes; a negative potential is applied to one, repelling electrons to the other for collection. Because we are demonstrating the use of the PDHID as a universal detector, we use a flow configuration in which only the helium makeup gas passes through the discharge region, minimizing the chance of discharge electrode contamination through contact with organic compounds. (However, if high concentrations of organic compounds are passed through the detector for extended periods of time, some organic material could still diffuse into the discharge region and contaminate the discharge electrodes. Under normal use with capillary

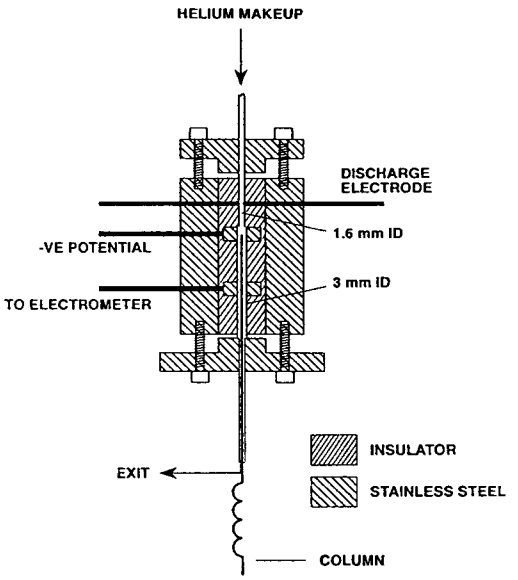

Fig. 1. Schematic diagram of the PDHID used in this study. -VE indicates bias potential.

columns, contamination of the electrodes is negligible even over extended periods of time). As makeup flow passes through the discharge region into the reaction zone, the analytes exit the GC capillary column directly into the reaction zone near the repelling electrode, flowing counter to the flow of the helium makeup. This configuration lends itself to miniaturization, making it more suitable for capillary column GC.

The analyte is ionized by high-energy photons as it moves through the 10-mm insulating section between the electrodes. The volume of this reaction zone is 113 μl; that is, the volume of a cylinder with a diameter of 3 mm and a length of 16 mm (3 mm for each electrode + 10 mm for the insulated spacer). A small portion of this volume is occupied by the capillary column. Since the column has an outside diameter ranging from 0.4 mm for microbore columns to 0.8 mm for megabore columns, the volume of the column in the reaction zone ranges from 1.75 to 7.0 μl, yielding an effective detector volume of approximately 106–111 μl. In this study we use an AT-5 (formerly RSL-200) bonded phase silica column, 30 m $\times$ 0.25 mm I.D., 1.0 μm film thickness (Alltech, Deerfield, IL, USA), installed in the

oven of a Varian (Walnut Creek, CA, USA) 1400 gas chromatograph.

Grade 5 (99.999%) helium gas (Trigas, Houston, TX, USA) is used as the capillary column carrier gas as well as the makeup gas that passes through the discharge region. The helium passes through a Valco (Houston, TX, USA) helium purifier, which uses a non-evaporable gettering alloy to remove all impurities except inert gases and nitrogen. (Although water is removed by the helium purifier, emission spectra generally show low levels of OH emission, probably arising from water which enters the helium from the stainless steel tubing connecting the purifier to the detector). The effects of various parameters such as makeup flow-rate, collecting potential and discharge frequency were evaluated using a Scotty II gas mixture of 100 ppm (v/v) of C_1–C_6 *n*-hydrocarbons in helium (Scott Specialty Gases, Houston, TX, USA).

The coil is charged with 20 V from a Heathkit 2718 tri-power supply unit (Heath, Benton Harbor, MI, USA). The duration of the charge and the pulse frequency are controlled by a 4001 ultravariable pulse generator (Global Specialties, New Haven, CT, USA). The negative potential that repels the electrons to the collecting electrode is supplied by a Keithley (Cleveland, OH, USA) Model 240A high-voltage power supply or a Kepco (Flushing, NY, USA) ABC d.c. supply.

The collection of electrons at the collecting electrode comprises the detector response. This signal is sent to the electrometer of the Varian 1400 GC system, but because the typical standing current for the PDHID (on the order of 1–5 nA) is much larger than the background current expected from an FID, the bucking current in the electrometer is increased to a maximum of 90 nA by changing a resistance from 10^{10} to 10^8 Ω.

The output of the electrometer is connected to a single-channel Houston Instrument (Austin, TX, USA) Omniscribe strip chart recorder Series B-5000 and to a Hewlett-Packard (Avondale, PA, USA) integrator 3390A. The total electrical quantity (Q) arising from the ionization of a given analyte can be calculated by integrating the GC peaks; thus, if we know the amount (mol) of analyte injected and assume that one molecule produces one electron after ionization, the ionization efficiency can be determined by the following equation

$$\%\ \text{ionization efficiency} = \frac{\text{current (C/s)} \cdot \text{time (s)}/F\ (96\,500\ \text{C/mol})}{\text{mol of analyte in detector (mol)}} \cdot 100\%$$

The product of current × time is the area under the GC peak, which was measured using a Hewlett-Packard integrator 3390A.

Injections are made by a Valco four-port sampling valve with an internal volume of 0.06 μl (determined by an engraving on the rotor), or by a Valco six-port sampling valve with external loops sized from 5–50 μl. A variety of gases and liquids (ca. 99% purity) were used to examine the relative response factors, with the liquids diluted in a solution of a high-boiling solvent such as *n*-decane (Sigma, St. Louis, MO, USA) before injection. The major peak is obvious from the chromatograms.

Measurements of the vacuum UV emission from the discharge source were carried out using a vacuum monochromator (Acton VM502) containing a holographic grating with 1200 grooves/mm. In order to obtain spectra below 120 nm, the pulsed discharge source was mounted directly to the monochromator body, without a window or entrance slit. The discharge is sufficiently narrow that it can serve as the optical image when placed vertically at the focal point of the monochromator. In order to have transparency down to ca. 60 nm, the monochromator was purged with pure helium. Below 60 nm the helium begins to absorb.

3. Results and discussion

The PDHID has several variable operating parameters that affect its sensitivity and the linearity of response with concentration. Two of these parameters are associated with the pulsed discharge: (1) the power transmitted to the primary coil of the pulsed high-voltage transformer, which in turn affects the voltage and

current of the discharge; and (2) the frequency or interval of the pulsed discharge. In most of our work we use a 20 V power supply. However, the power to the coil is a product of the duration as well as the voltage of the charge transmitted. The duration is varied by changing the width of the square wave pulse generated by the pulser. Charging times generally range from 15–100 μs, depending upon the pulse interval, which ranges from 200–1000 μs. The effects of the two pulse discharge parameters will be discussed shortly.

The other operating parameters that affect the PDHID are: (1) the potential applied to repel the electrons to the collecting electrode; and (2) the helium flow-rate through the discharge region. The effects of these parameters will also be discussed shortly.

3.1. Pulsed discharge: interval and power

In this study the electrode separation at the discharge is constant at ca. 1.6 mm; the diameter of the hole through which the helium flows is 1.6 mm (Fig. 1), and the electrodes are adjusted so that their tips are at the walls of this hole. The effect of the power applied to the discharge depends upon the electrode separation.

As explained previously, the power supplied to the discharge via the primary coil is changed by varying the charging time from a 20 V power supply. Fig. 2a shows the detector response to 0.89 ng of propane as a function of the charging time in μs. (The pulse interval was held constant at 300 μs). The response, expressed as the percent ionization, increases as the charging time is increased. However, it passes through a maximum of ca. 0.09% ionization at 45 μs and then decreases.

We also measured the standing current, which arises from the ionization of helium and impurities in the carrier gas, including column bleed. Fig. 2b shows the direct relationship between the percent ionization of propane and the standing current, which varies with the coil charging time. This suggests that the discharge power generates proportional amounts of ionization of the carrier gas (standing current) and of the analyte (detector response).

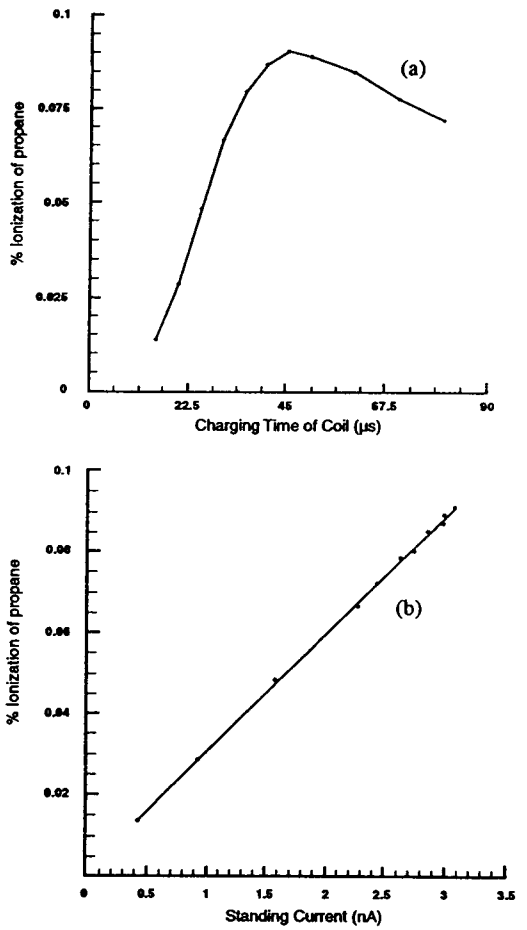

Fig. 2. Detector response in terms of percent ionization versus (a) coil charging time and (b) standing current (which changes with coil charging time); 5.0 μl of 100 ppm propane (0.89 ng); discharge flow-rate: 20 ml/min; pulse interval 300 μs.

The percent ionization of propane was also measured as a function of pulse interval, with the charging time constant at 40 μs. The results are shown in Fig. 3a. Note that the percent ionization remains somewhat constant from 200–50 μs but then decreases as the pulse period increases, as expected. However, the detector response goes through a second maximum of ca. 0.05% at ca. 500–600 μs. This behavior is probably related to the *LC* (inductance–capacitance) characteristics of the coil. The standing current was recorded as well; Fig. 3b shows a direct

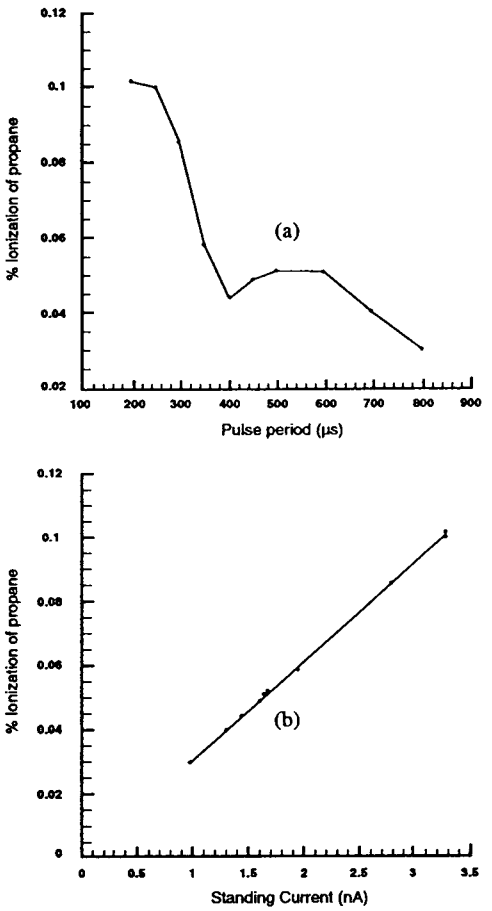

Fig. 3. Detector response in terms of percent ionization versus (a) pulsed discharge interval and (b) standing current (which changes with pulsed discharge interval); 0.89 ng propane, discharge flow-rate: 20 ml/min; charging time of the coil: 40 μs; d.c. voltage to the coil: 20 V.

relationship between the detector response as percent ionization and the standing current, which varies with the pulse interval.

Because detector response and standing current vary proportionally with the input pulse width and period, the effect of these parameters on detector response can be more readily ascertained by simply observing the standing current. More detailed observations of the dependence of the standing current on both the pulse width and period are shown in Fig. 4. Note that when pulse periods in the range of 200–1000 μs are used, the standing current goes through three maxima,

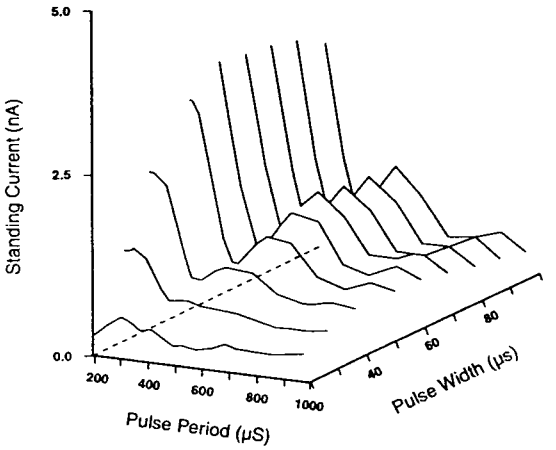

Fig. 4. Effects of pulse width and period on standing current.

regardless of pulse width. These maxima are around 225, 450 and 900 μs, values which correspond to integer multiples of the *LC* resonant frequencies of the discharge circuit. As the pulse period is increased, the three standing current maxima decrease rapidly. A similar relationship between standing current and input pulse width as in Fig. 2a under different pulse periods can also be observed in Fig. 4.

It appears from the data in Fig. 4 that if a higher energy pulse is desired, a charging time of 100 μs or more with a pulse interval of 500 μs is ideal. For the emission mode [12] it may be desirable to have a more energetic discharge at a wider pulse interval of, for instance, 500 μs. For the ionization mode a pulse interval of 200–300 μs with a charging time of 40–50 μs should be most satisfactory since the standing current and response are greater at these conditions. Since the discharge has a short duration (ca. 1 μs) and the pulse period is large (ca. 200–500 μs), the metal electrodes are exposed to the high current for only a small fraction of the time. Consequently, there is no apparent heating in the discharge region.

3.2. Bias voltage for electron collection

A constant negative bias voltage is applied to the electrode adjacent to the discharge, as shown in Fig. 1. Fig. 5 is a graph of the response to 0.89

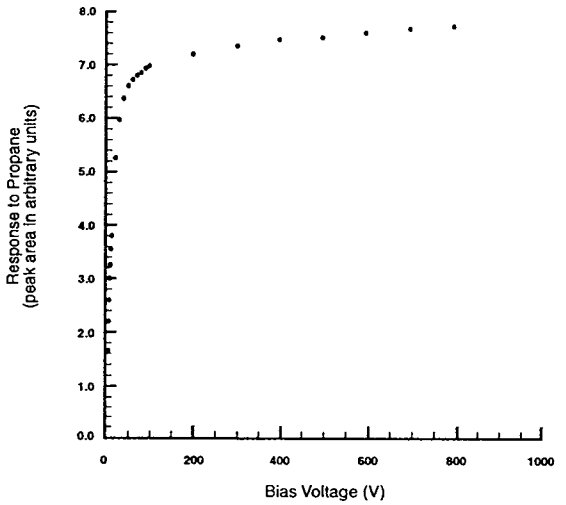

Fig. 5. Detector response (percent ionization) versus bias voltage; 0.89 ng propane; discharge flow-rate: 20 ml/min; pulse interval: 300 μs; charging time of the coil: 40 μs; d.c. voltage to the coil: 20 V.

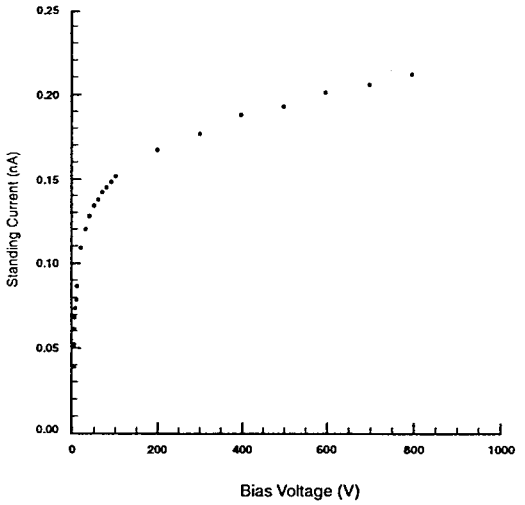

Fig. 6. Standing current versus bias voltage. Discharge flow-rate: 20 ml/min; pulse interval: 300 μs; charging time of the coil: 40 μs; d.c. voltage to the coil: 20 V.

ng of propane versus bias or repelling voltage. It appears that the response increases rapidly with increasing voltage, leveling off to a plateau. The region in which the response increases linearly with bias voltage is usually called the *collecting* region, and the region in which the response is independent of bias voltage is usually called the *saturation* region. The PDHID works in the saturation region, in which the noise level is lower. A similar curve is obtained for standing current versus bias voltage, shown in Fig. 6.

3.3. Helium flow-rate through the discharge region

The helium that passes through the discharge region has two purposes: (1) it keeps the discharge region clean so that helium excited species can be generated; and (2) it serves as makeup gas to reduce the residence time of the eluting analyte in the detector. The necessary residence time in the detector is a function of the chromatographic peak width. In order to maintain the integrity of the chromatography, the residence time in the detector should be as short as 10–20% of the peak width. Thus, if the peak width is 5 s the residence time should be 0.5–1 s, which requires a flow-rate of 6.8–13.6 ml/min through a cell with a volume of 113 μl. If the peaks are as sharp as 1 s width, then the helium flow-rate must be increased to 34–68 ml/min.

Generally as the flow-rate increases the eluting analyte becomes more dilute and the response decreases. If this were the only effect of the helium flow-rate, we would expect the response to vary linearly with the reciprocal flow-rate. Such a graph of the response to propane is shown in Fig. 7, and indeed, there is a linear dependence at high flow-rates. However, at lower flow-rates the curve breaks over and even appears to approach a plateau.

The decrease in response at higher analyte concentrations (lower flow-rates) could be due to saturation of the detector. To eliminate this possibility, response versus helium flow-rate was measured at two different analyte concentrations. This was accomplished using the six-port sampling valve and two sample loops (6 and 50 μl) to inject the 100 ppm propane mixture. The same shaped curves are obtained (Fig. 7), suggesting that the curvature is not related to concentration.

Further investigation indicated that the plateau in the response vs. 1/flow-rate curve is

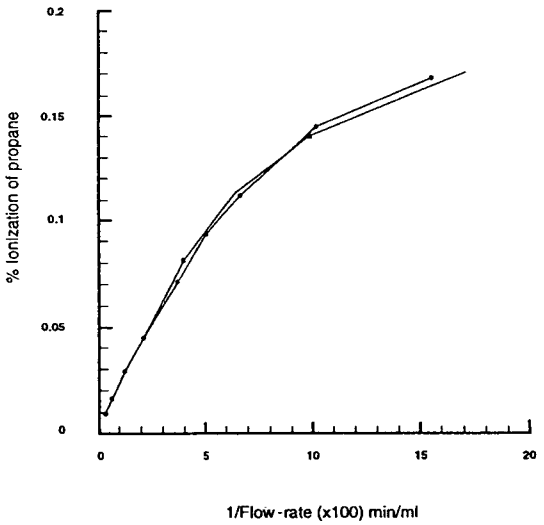

Fig. 7. Detector response (percent ionization) versus reciprocal flow-rate. Pulse interval: 300 μs; charging time of the coil: 40 μs; d.c. voltage to the coil: 20 V; bias voltage: 200 V; sample: 100 ppm propane; sample size: (●) 6 μl, (■) 50 μl; volume of detector: 113 μl.

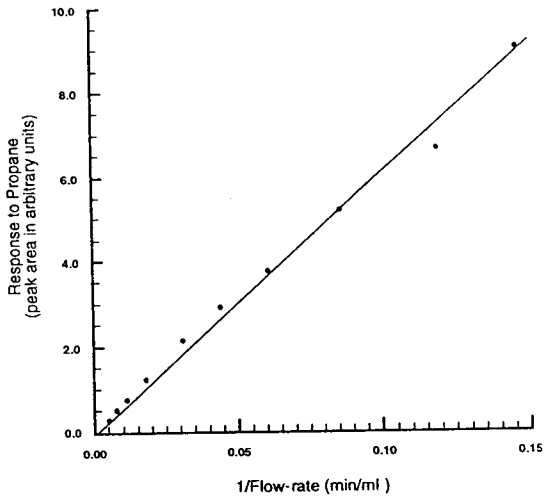

Fig. 8. Detector response (peak area in arbitrary units) versus reciprocal flow-rate under constant detector pressure (6 p.s.i.; 1 p.s.i. = 6894.76 Pa).

due to changes in detector pressure and in the amount of air back-diffusion as the flow-rate changes: the lower the flow-rate, the higher the air back-diffusion and the lower the detector pressure. Since both these factors contribute to decreased detector response, they offer a likely explanation for the plateau. To verify this, we measured and plotted the response vs. 1/flow-rate curve under constant detector pressure. As Fig. 8 shows, the response is linear, which verifies that the PDHID is essentially a concentration-dependent detector.

3.4. Detector volume

As calculated in the Experimental section, the effective internal volume of the detector is 113 μl when the diameter of the ionization region is 3 mm. The volume of the ionization region decreases to 50 μl if the diameter is 2 mm and increases to 314 μl with a diameter of 5 mm. The effect of this internal volume on the response of the detector was evaluated using a 100 ppm C_1–C_6 hydrocarbon mixture in helium.

The response of the detector to the hydrocarbon mixture was evaluated as a function of helium flow-rate, in a manner similar to that discussed previously. Fig. 9 is a graph of the response to propane versus the reciprocal flow-rate for the various ionization chambers. The general shapes of the curves for all detector sizes are similar to those in Fig. 7. Obviously the

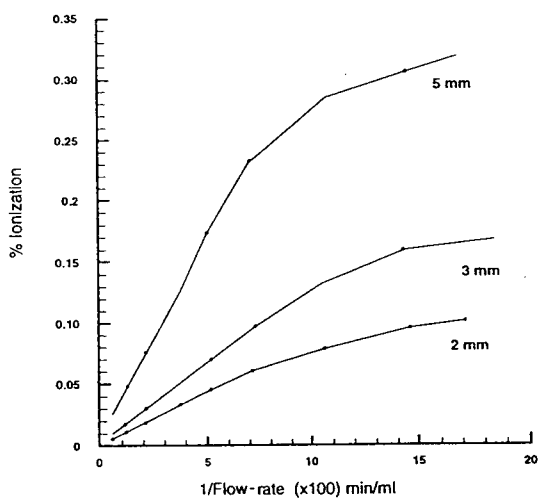

Fig. 9. Detector response (percent ionization) versus reciprocal flow-rate. Same conditions as Fig. 7 except different detector volumes, and only 6 μl sample size used (internal diameters are specified).

response for propane increases with increasing detector size. However, the increase in response is not directly proportional to the detector volume; in going from a 2 mm diameter to a 5 mm diameter the volume increases by a factor of ca. 6, whereas the response increases by a factor of ca. 4. But the standing current also increases with increasing detector volume, as shown in Fig. 10. An increased standing current increases the noise of the baseline, since a larger signal must be zeroed out by applying a larger bucking potential. This effectively negates any sensitivity gained from increased detector volume.

The factor of most concern to chromatographers is the effect of cell volume on the amount of flow required to yield a residence time which maintains the integrity of the chromatographic peak. Fig. 11 shows a chromatogram of the 100 ppm C_1–C_6 hydrocarbon mixture on the DB-5 column (30 m × 0.25 mm I.D., 1.0 μm film thickness). The chromatogram to the right in Fig. 11 was run with a faster chart speed to show the separation of the C_1–C_3 hydrocarbons. The methane and ethane are only just separated, but the C_3–C_6 hydrocarbons are well separated. However, note the water peak between C_3 and C_4 that tails into the C_4 peak. The water apparently comes from the sample loop, and could probably be reduced by heating.

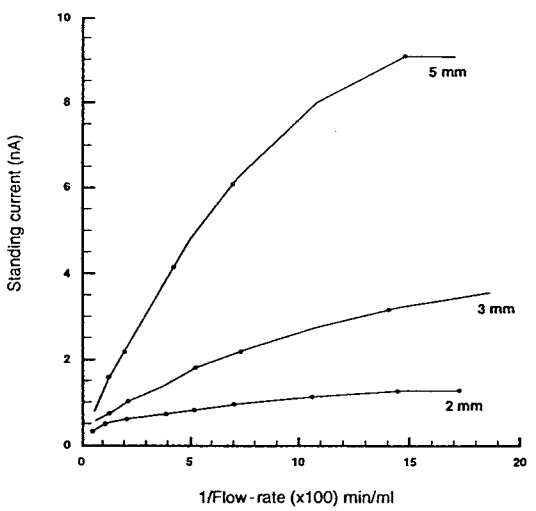

Fig. 10. Standing current versus reciprocal flow-rate. Same detector conditions as Fig. 7, except different detector volumes (internal diameters are specified).

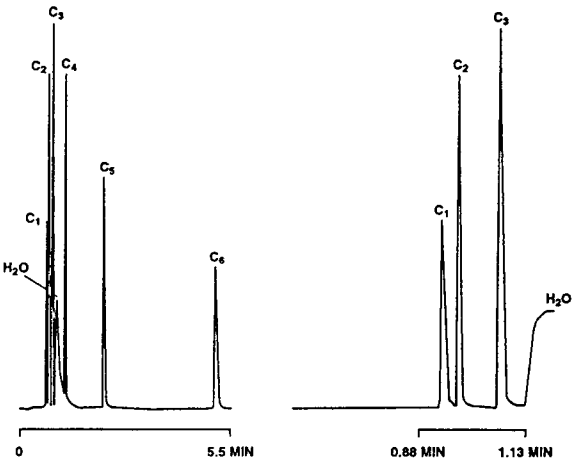

Fig. 11. Chromatograms of 100 ppm hydrocarbon mixture on the DB-5 column. Pulse interval: 300 μs; charging time of the coil: 40 μs; d.c. voltage to the coil: 20 V; bias voltage: 200 V; discharge flow-rate: 20 ml/min; sample size: 6 μl.

Because the C_1–C_6 hydrocarbon peaks have high resolution, this chromatogram gives a good test of detector performance. We measured both the peak area and the peak height for the C_3, C_4 and C_5 hydrocarbons, and determined the ratio of the area to the height as a function of the flow-rate through the detector. (The column flow-rate was kept constant, with only the helium flow through the discharge varied). This ratio should remain constant as long as the detector makes no contribution to peak broadening. A graph of the ratio versus reciprocal flow-rate shows a constant value at higher flow-rates, but a sharp increase at lower flow-rates, due to peak broadening from the increased detector residence time.

Fig. 12 shows the flow-rate at which each detector began to experience peak broadening for propane. As expected, the smallest volume detector (2 mm diameter/ca. 50 μl) could tolerate the lowest flow-rate, which was 11.4 ml/min ($8.7 \cdot 10^{-2}$ min/ml on the 1/flow-rate scale). This is probably the narrowest peak possible with this column. On the other hand, if the detector with the 5 mm diameter (ca. 314 μl) is used, the flow-rate must be 67 ml/min. For the 3 mm

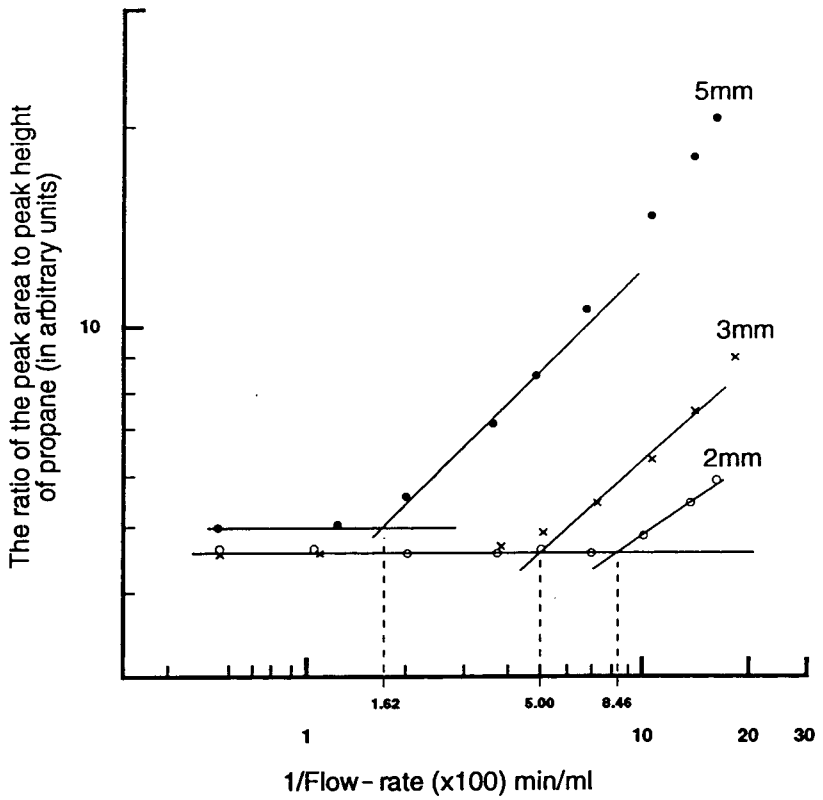

Fig. 12. Ratio of peak area to peak height of propane versus reciprocal flow-rate with different detector I.D. Pulse interval: 300 μs; charging time of the coil: 40 μs; d.c. voltage to the coil: 20 V; bias voltage: 200 V; discharge flow-rate: 20 ml/min.

detector (ca. 113 μl), a flow-rate of approximately 20 ml/min is required to prevent peak broadening for C_3. These requirements are consistent with a residence time of approximately 0.3 s, which seems adequate to resolve the C_3 peak with a base width of 1.4 s. Note that for the most part the required flow-rates fall on the linear portion of the curve, where the detector sensitivity is concentration-dependent. The required flow-rates and corresponding residence times for the C_3, C_4 and C_5 compounds for the three different detector diameters are shown in Table 1. Apparently a flow-rate of approximately 10 ml/min is sufficient for the 3 mm diameter detector. The 5 mm diameter detector requires an excessive flow-rate, on the order of 50 ml/

Table 1
Relationship between detector size and minimum flow-rate required

Diameter/volume of the ionization region	Minimum flow-rate (residence time) for		
	n-C_3H_8	n-C_4H_{10}	n-C_5H_{12}
2 mm/50 μl	11.8 ml/min (0.25 s)	8.5 ml/min (0.35 s)	–
3 mm/113 μl	20 ml/min (0.34 s)	13.6 ml/min (0.50 s)	9.0 ml/min (0.75 s)
5 mm/314 μl	62 ml/min (0.30 s)	35.6 ml/min (0.53 s)	27.4 ml/min (0.69 s)
Peak width	1.4 s	1.8 s	2.7 s

min, to adequately define the sharp peaks from a 0.25 mm I.D. column. However, the larger volume detector could be used successfully with megabore capillaries and packed columns where the gas chromatographic peaks are inherently broader.

3.5. Mode of ionization

In order to confirm the mode of ionization, the relative responses of numerous gases to the PDHID were measured and compared to those from a helium ionization detector (HID) [10] and a helium photo-ionization detector (HPID) [11]. As expected, the relative responses to the HID and HPID are quite different, since the ionization by helium-excited species should be quite different from ionization using photons from the helium resonance transition (58.4 nm). The data are shown in Table 2, where the responses are relative to methane. In general there is better agreement in the relative responses for the HID and the PDHID. (More than between the HID and the HPID). The greatest discrepancies are for H_2, CO_2 and SO_2.

Table 2
Detector response relative to methane on a per mol basis

Analyte	Type of detector		
	HID	PDHID	HPID
H_2	0.35	0.19	2.01
N_2	0.47	0.40	0.42
Ar	0.53	0.60	0.49
O_2	0.65	0.59	0.36
CO	0.71	0.51	0.42
CH_4	1.00	1.00	1.00
SF_6	1.11	0.89	0.22
C_2H_6	1.65	1.85	1.12
C_2H_4	1.94	1.40	0.78
C_3H_8	2.35	2.48	0.57
C_4H_{10}	2.65	3.23	–
CO_2	3.29	0.98	0.27
H_2S	3.06	1.65	–
N_2O	3.29	0.92	0.34
SO_2	3.29	1.61	0.75

3.6. Emission spectra from He_2

The emission spectrum from the discharge in helium was recorded using the monochromator described previously. The only helium emission spectra is the broad band in the vicinity of 70–90 nm. This is the well-known Hopfield emission which arises from the transition

$$He_2(A\,^1\Sigma_u^+) \rightarrow 2\,He(1\,^1S) + h\nu$$

The reason for the broad emission is the dissociative ground state. It would seem that this photoemission plays the dominant role in the ionization mechanism.

Since the PDHID response depends upon the He_2 continuum, with energies in the range 16–18 eV, it is understandable why the PDHID responses in Table 2 differ from the HPID responses, which depend upon the He resonance line at 21.2 eV. Of particular note is the low response of the HPID for C_3H_8 compared to the PDHID response. This might suggest that the HPID response to longer-chain hydrocarbons may be low, whereas with the PDHID, as we will see shortly, the molar response of the hydrocarbons increases with chain length.

The lower energy range of the vacuum UV emission spectra from the discharge consists of atomic emissions from other elements in the discharge. The background generally consists of atomic emission from N, O and H, which probably arise from air and water. The emission spectra from the pulsed discharge source can be used for specific element identification. The most useful emission spectra for the lighter atoms fall in the vacuum UV region from 100–200 nm. This is being investigated extensively and at the present time it appears to be effective for the detection of Cl, Br, I and S.

3.7. Percent ionization

The percent ionization for the PDHID has been determined for certain selected gases, with the results shown in Table 3. Generally the percent ionization increases with molecular size,

Table 3
Relative responses for various classes based on propane

Analyte	Molecular mass	Percent ionization	Relative response (to C_3)	
			per mol	per gram
n-Alkanes				
Methane	16.0	0.0099	0.404	1.11
Ethane	30.1	0.0184	0.751	1.10
Propane	44.1	0.0245	1.00	1.00
n-Butane	58.1	0.0320	1.31	0.99
n-Pentane	72.2	0.0423	1.73	1.06
n-Hexane	86.2	0.0503	2.05	1.05
n-Heptane	100.2	0.0579	2.36	1.04
n-Octane	114.2	0.0660	2.69	1.04
n-Nonane	128.3	0.0761	3.11	1.07
Branched alkanes				
2-Methylpropane	58.1	0.0341	1.39	1.06
2,2-Dimethylbutane	86.2	0.0555	2.27	1.16
3,3-Dimethylpentane	100.2	0.0592	2.42	1.06
3-Ethy pentane	100.2	0.0561	2.29	1.01
2,2,4,4-Tetramethylpentane	128.3	0.0711	2.90	1.00
Unsaturated and ring hydrocarbons				
Ethylene	28.1	0.0128	0.522	0.82
1-Propene	42.1	0.0217	0.885	0.93
1-Butene	56.1	0.0287	1.17	0.92
1-Pentene	70.2	0.0353	1.44	0.90
1-Hexane	84.1	0.0463	1.89	0.99
1,3-Butadiene	54.1	0.0270	1.10	0.90
Cyclohexane	84.2	0.048	1.96	1.03
Cyclohexene	82.1	0.038	1.55	0.83
Permanent gases				
Nitrogen	28.0	0.00400	0.163	0.26
Hydrogen	2.02	0.00187	0.076	1.67
Oxygen	32.0	0.00594	0.242	0.33
Argon	39.9	0.00594	0.242	0.27
Carbon monoxide	28.0	0.00510	0.208	0.33
Carbon dioxide	44.0	0.00980	0.400	0.40
Sulfur dioxide	64.1	0.01610	0.657	0.45
Sulfur hexafluoride	146.1	0.00883	0.360	0.11
n-Alcohols				
Methanol	32.0	0.0134	0.547	0.75
Ethanol	46.1	0.0222	0.906	0.87
n-Propanol	60.1	0.0312	1.27	0.93
n-Butanol	74.1	0.0375	1.53	0.91
n-Pentanol	88.2	0.0404	1.65	0.83
sec.-Alcohols				
2-Propanol	60.1	0.0308	1.26	0.92
2-Butanol	74.1	0.0397	1.62	0.96

(Continued on p. 146)

Table 3 (*continued*)

Analyte	Molecular mass	Percent ionization	Relative response (to C_3)	
			per mol	per gram
Aromatics				
Benzene	78.1	0.037	1.51	0.85
Toluene	92.1	0.044	1.80	0.86
Ethylbenzene	106.2	0.049	2.00	0.83
n-Propylbenzene	120.2	0.055	2.24	0.82
Chlorine compounds				
Dichloromethane	84.9	0.0286	1.17	0.61
Trichloromethane	119.4	0.0422	1.72	0.63
Tetrachloromethane	153.8	0.0535	2.18	0.62
Bromine compounds				
Dibromomethane	173.8	0.0353	1.44	0.36
Tribromomethane	252.7	0.0387	1.58	0.28

ranging from 0.002% for H_2 to 0.08% for nonane. Note that the C_4 compounds with different amounts of unsaturation and structure all have similar percent ionizations of 0.030–0.034%, whereas the one C_3 compound has a lower percent ionization of 0.025%.

Percent ionization is dependent on the parameters discussed previously: pulse discharge interval, pulse discharge power and helium flow-rate through the discharge region. The values used to obtain the data in Table 3 are somewhat typical: 300 μs interval between pulses, charging time of 40 μs at 20 V, and helium flow-rate of 40 ml/min. With the exception of a few permanent gases, the percent ionization falls in the range 0.01–0.08% for compounds of C_9 or less. This range of percent ionization can be compared to the typical percent ionization for other types of ionization detectors: 0.0005% for an FID, 0.3% for a helium photoionization detector [11] (which uses a microwave-induced discharge source and operates at low pressure), and 5% for a radioactive helium ionization detector. (Table 4)

Even though there is a great range in percent ionization among the detectors in Table 4, the background noise also varies considerably, gen-

Table 4
Ionization efficiency and relative sensitivity of some ionization detectors

	FID [10]	HPID [11]	HID [10]	PDHID (This work)
Apparent ionization efficiency (propane)	0.000005	0.003	0.05	0.0007
Noise level (A)	$1 \cdot 10^{-14}$	$4 \cdot 10^{-11}$	$2.5 \cdot 10^{-12}$	$1.2 \cdot 10^{-13}$
Percent ionization/noise	$5 \cdot 10^{8}$	$7.5 \cdot 10^{7}$	$2 \cdot 10^{10}$	$5.8 \cdot 10^{9}$
Relative sensitivity	1.0	0.15	40	12
Linear dynamic range	10^7	10^4	10^4	10^5
Carrier gas	Air/H_2	He	He	He
Substances	Most organics	Universal	Universal	Universal

erally increasing as percent ionization increases. Consequently, the sensitivity α (percent ionization/noise) varies by a factor of only 40 from FID to HID. The PDHID is more sensitive than the FID by a factor of ca. 12, but less sensitive than the HID by a factor of ca. 4. Note that the HID sensitivity is greatest; however, it is not a satisfactory detector for higher boiling organic compounds, since they would tend to absorb on the tritium foil. The PDHID sensitivity for propane is an order of magnitude greater than the FID and two orders of magnitude greater than the HPID. The linear dynamic range is greatest for the FID (10^7), but the range of 10^5 for the PDHID should be satisfactory in most cases. Of more importance is the fact that the PDHID response is universal, whereas the FID is restricted to organics.

3.8. Relative response for various classes of compounds

Table 3 shows the relative responses for several classes of compounds. As noted previously, the relative responses on a mole basis for the hydrocarbons increases with increasing carbon number. This is most apparent for the straight-chain hydrocarbons C_1–C_9, where the relative response changes from 0.50 to 3.11. Apparently the cross-section for ionization increases with increasing molecular size and the response increases in a manner similar to that for an FID. The last column of Table 3 shows the relative response on a per gram basis. Note that the responses for the *n*-C_2 to *n*-C_9 hydrocarbons vary by ca. 10%.

Also shown in Table 3 are the relative responses for branched hydrocarbons. On a per gram basis these values fall in the range 1.0–1.16. A few cyclic and unsaturated hydrocarbons, also given in Table 3, have relative responses ranging from 0.83 to 1.03. The relative responses for some aromatic hydrocarbons in Table 3 tend to be lower than those for saturated hydrocarbons, ranging from 0.82 to 0.86. The relative responses of the C_1–C_5 alcohols (Table 3) fall in the 0.75–0.93 range. Since these responses are below those for the saturated hydrocarbons, the OH is apparently less susceptible to ionization than a CH_3 group. With the exception of methane, the relative response per gram for all hydrocarbons and alcohols, regardless of structure, falls in the 0.75–1.16 range.

The relative responses of some chloro- and bromomethanes were also determined. The values for the chloro compounds are ca. 0.6 and for the bromo compounds ca. 0.3. One would expect the relative response for the halogenated compounds to be significantly less, because there are numerous electrons that are tightly held and probably not accessible for ionization. In the chloro compounds the 1s, 2s and 2p electrons are tightly held and probably do not contribute significantly to the ionization. Similarly, for the bromine atom the 1s, 2s, 2p, 3s and 3p electrons would not be ionized.

3.9. Concentration dependence

Concentration dependence was determined using the response to propane mixtures in helium. The detector with a 3 mm diameter was used, with a flow-rate of 20 ml/min. Six gas mixtures were prepared that ranged from $4.95 \cdot 10^{-5}$ to $9.13 \cdot 10^{-3}$ parts by volume. Three different sample volumes were used: 0.06, 5.0 and 50.0 μl. The 0.06-μl sample came from the sampling valve in which the sample is measured by an internal engraving on the rotor. (The volume of 0.06 μl is approximate, and should be calibrated with a larger, more accurately measured sample loop. In this study we assumed the 50-μl loop to be accurate and calibrated the 0.06-μl and 5.0-μl loops against it).

Fig. 13 shows a typical log–log plot of the response for propane versus the mass injected, using sample volumes of 0.6, 5.0 and 50.0 μl. The responses for the 0.6- and 5.0-μl volumes were corrected according to the calibration described previously. The straight line shows a slope of one, representing a linear relationship between response and concentration. Note that the data fit the straight line quite well until the concentration reaches $1 \cdot 10^5$ pg, shown by the dashed vertical line. The linear range in Fig. 13 extends over four orders of magnitude. Since the

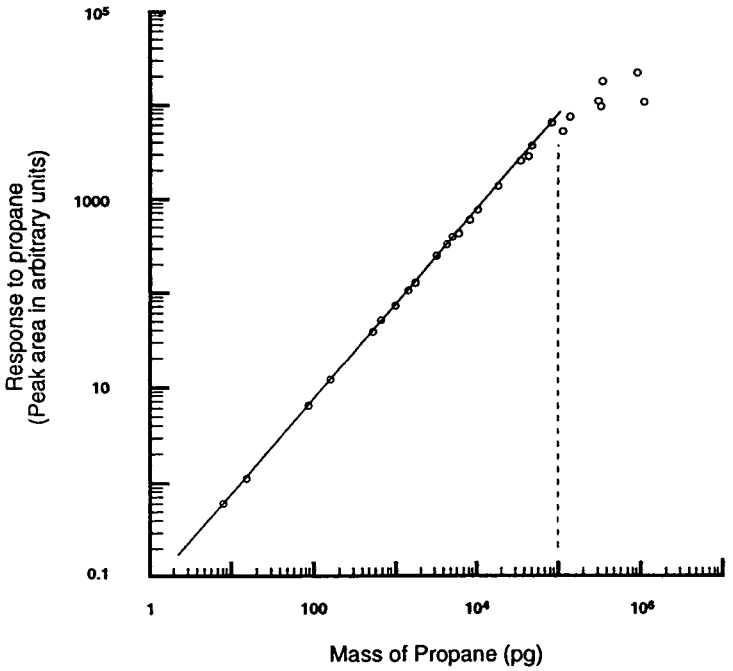

Fig. 13. Log relative response to propane versus mass of propane injected. Data using the 0.06-μl and 5.0-μl calibrated against the 50-μl loop. Same detector conditions as Fig. 11.

minimum detectable amount of propane is ca. 0.8 pg, the linear dependence could be extended by an additional order of magnitude. Consequently, the detector would be linear over a total range of five orders of magnitude.

The test of linearity is also shown in Fig. 14, where the percent ionization is graphed versus the logarithm of the injected mass of propane. In this type of graph a constant value of the percent ionization designates the linear concentration dependence of the detector. When the detector starts to become saturated there is a sharp decrease in percent ionization, as observed in Fig. 14 at approximately 10^5 pg = 100 ng.

3.10. Analysis of permanent gases

For many years helium ionization detectors have been used in conjunction with a 5A molecular sieve GC column to detect the so-called permanent gases (Ne, H_2, Ar, O_2, N_2, CH_4 and CO). Because of its importance to research and production in the solid-state industry, this analysis deserves special attention in our study of the PDHID. Although we reported on this analysis in a previous publication [1], that study involved a different flow configuration that allowed the analytes to pass through the discharge region. Because the current detector does *not* allow this we might expect a change in sensitivity, particularly toward gases like the permanent gases in which the ionization potentials range from 12.06 eV for O_2 to 21.564 eV for Ne.

The previous study used a packed 5A molecular sieve column, 5 ft. × 1/8 in. O.D. (1 ft. = 30.48 cm, 1 in. = 2.54 cm). This study employs a 5A molecular sieve porous layer open tubular (PLOT) column, 30 mm × 0.32 mm I.D. (Chrompack, Raritan, NJ, USA). Fig. 15 shows chromatograms of the permanent gases on this column at 25°C, where Ar and O_2 have separate

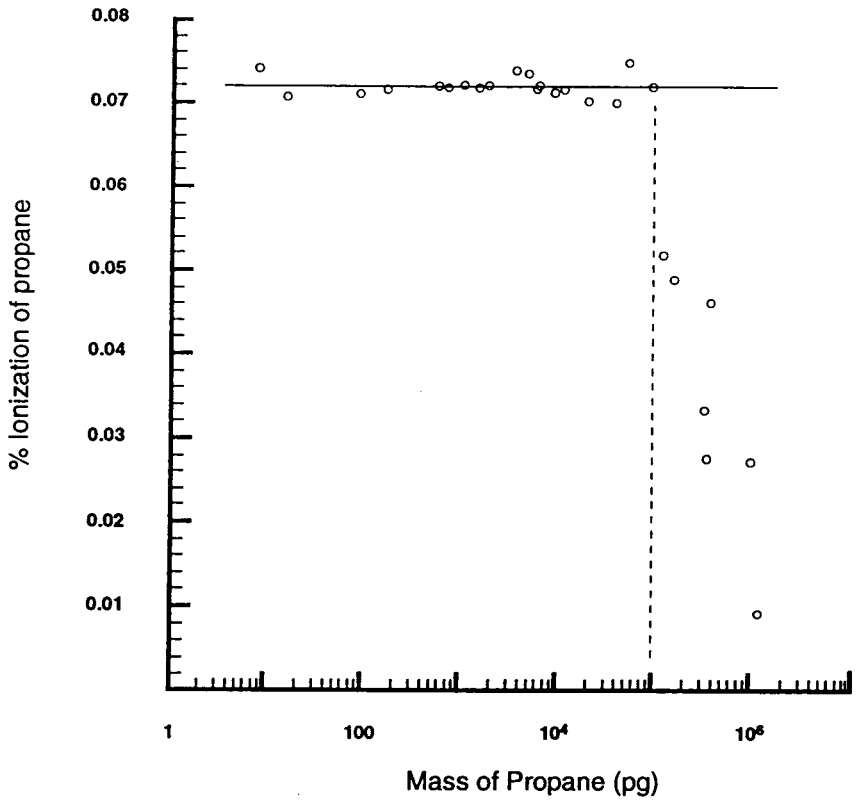

Fig. 14. Percent ionization versus log mass of propane. Same detector conditions as Fig. 13.

peaks, and at 100°C, where Ar and O_2 elute as one peak but the CO elutes in a reasonable length of time. The separation at 100°C is comparable to the results obtained in the previous study with the packed column at 95°C [1].

Because the Ar and O_2 were eluted simultaneously in the previous study we cannot compare the results with the current study in which a different Ar/O_2 concentration ratio was used. It is also risky to compare the sensitivity for N_2, since it is susceptible to possible air leakage into the sample. The sensitivities for the other permanent gases, expressed as minimum detectable quantity (MDQ), are given in Table 5, along with the values from the previous study [1]. In general it appears that the sensitivity of the PDHID used in this study is lower for these permanent gases by a factor of 5–10. Apparently the enhanced sensitivity realized in the first study arises from the direct ionization that occurs as the analytes pass through the pulsed discharge. As might be expected, the most dramatic difference between the sensitivities of the two configurations shows up with neon —its ionization potential of 21.564 eV makes it the most difficult of the permanent gases to ionize. The response from the PDHID used in this study is low because the energy of the He_2 emission responsible for analyte ionization (17.86–19.7 eV) is less than neon's ionization potential.

While this section demonstrates that greater sensitivity is realized when the analytes are allowed to pass through the discharge, this advantage is offset by the potential problems that may arise when a solvent or a large sample such as air disrupts the discharge.

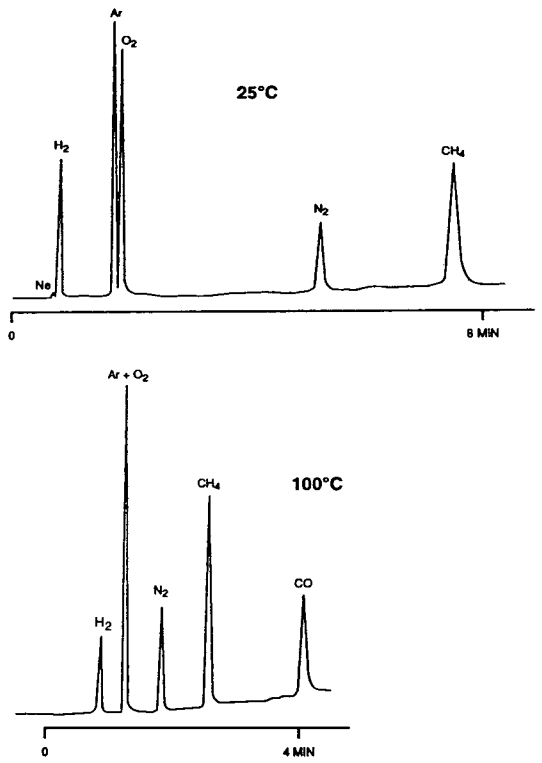

Fig. 15. Chromatograms of the permanent gases with column temperatures of 25 and 100°C. Column: Chrompack PLOT, fused-silica 5A molecular sieve, 25 m × 0.32 mm; detector: PDHID, flow-rate 20 ml/min, temperature 25°C; sample: 2 ppm, 50-μl sample loop.

3.11. Application to high-speed chromatography

As discussed previously, the analyte residence time in the PDHID is about 0.3 s with a 3 mm I.D. detector cell and 20 ml/min flow-rate. With a smaller I.D. detector cell and higher detector flow-rate the residence time is even briefer. This fast response feature makes it possible to apply the PDHID to high-speed chromatographic analysis. Fig. 16 illustrates one example of BTEX (benzene, toluene, ethylbenzene, xylenes) analysis with the PDHID and a microbore column (DB-1701, 10 m × 0.05 mm, 0.05 μm film thickness). The complete BTEX analysis in this example takes only 2.5 min, compared to ca. 20 min typical for normal GC analysis.

The sharp, symmetric BTEX peaks indicate that the PDHID gives a fast response to these components, but the technique has some limitations. A large sample loop cannot be used because the sample will be broadened under such a slow column flow-rate (0.1 ml/min). Consequently, the overall sensitivity of this method is not as high as normal GC analysis —a small amount of highly concentrated sample must be used to get significant response. This experiment used a valve with an 0.06-μl internal loop as an injector. Some other injection techniques, such as the cryogen concentration meth-

Table 5
Minimum detectable quantity (MDQ) of permanent gases

	MDQ (pg)		
	Column 25°C [a]	Column 100°C [a]	Column 95°C [b]
Neon	39.8	42.4	1.4
Hydrogen	0.23	0.31	0.04
Argon	1.68	2.48	0.8
Oxygen	2.46		
Nitrogen	3.28	1.58	1.9
Methane	2.47	1.02	0.1
Carbon monoxide	–	3.25	0.7

[a] This study.
[b] From Ref. [1].

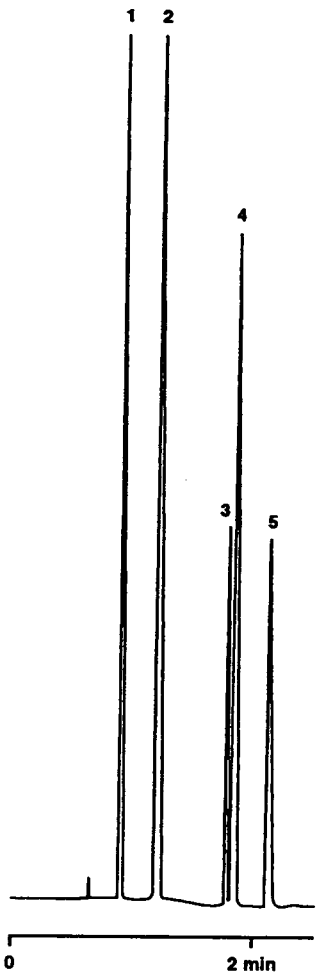

Fig. 16. Chromatogram of aromatics obtained by using PDHID and microbore columns. Column: J&W DB-1701, 10 m × 0.05 mm, film thickness 0.05 μm; detector: PDHID, flow-rate 20 ml/min; injector: split, 1:150 ratio. Peaks: 1 = benzene; 2 = toluene; 3 = ethylbenzene; 4 = *m,p*-xylene; 5 = *o*-xylene.

od, could help to increase the sensitivity of the high-speed gas chromatograph.

3.12. High-temperature operation

The results discussed before were obtained from a PDHID with Vespel as the insulation material. At high detector temperature, this detector has two major problems. First, the Vespel decomposes and produces compounds which enter the detector cell, resulting in reduced response. Consequently, the response of the detector continually decreases as the temperature increases. The response at 200°C is only half the response at 30°C. The other problem is electrical conductivity. The experiments show that the electrical leakage through the Vespel makes a measureable contribution to the standing current at about 150°C, and increases exponentially with increasing temperature. The maximum detector temperature at which the electrical leakage can be tolerated is about 200°C, which is not high enough for some applications.

At present, we are considering insulating materials that will allow the PDHID to operate at temperatures on the order of 350°C. Quartz, sapphire and high-density alumina have been shown to be satisfactory. The metal electrode poses an additional material consideration: at 350°C, there is a potential for it to act as a heterogeneous catalyst. The results of these studies will be reported in a future publication.

Acknowledgements

The authors would like to thank Larry Sims from the Electronics Shop (University of Houston) for his assistance in the design and repair of electronic components. We would also like to thank David Salge, technical writer at Valco Instruments, for his assistance in preparing the text and illustrations for this manuscript. This research was supported by a grant from Valco Instruments Co. Inc., Texas ATP grant 003652-108, and the Robert A. Welch Foundation, grant E-095.

References

[1] W.E. Wentworth, S.V. Vasnin, S.D. Stearns and C.J. Meyer, *Chromatographia*, 34 (1992) 219.
[2] W.E. Wentworth, E.D. D'Sa, H. Cai and S.D. Stearns, *J. Chromatogr. Sci.*, 30 (1992) 478.

[3] B.D. Quimby and J.J. Sullivan, *Anal. Chem.*, 62 (1990) 1027.
[4] R.B. Costanzo and E.F. Barry, *Anal. Chem.*, 60 (1988) 826.
[5] B.M. Patel, E. Heithmar and J.D. Winefordner, *Anal. Chem.*, 59 (1987) 2374.
[6] R.J. Skelton, P.B. Farnsworth, K.E. Markides and M.L. Lee, *Anal. Chem.*, 61 (1989) 1815.
[7] G.W. Rice, A.P. D'Silva and V.A. Fassel, *Appl. Spectros.*, 40B (1985) 1573.
[8] D.A. Ryan, S.M. Argentine and G.W. Rice, *Anal. Chem.*, 62 (1990) 1829.
[9] P.C. Uden (Editor), *Element-Specific Chromatographic Detection by Atomic Emission Spectroscopy*, American Chemical Society, Washington, DC, 1992.
[10] D.J. David, *Gas Chromatographic Detectors*, Wiley, New York, 1974.
[11] R.R. Freeman and W.E. Wentworth, *Anal. Chem.*, 43 (1971) 1987.
[12] S.V. Vasnin, W.E. Wentworth, S.D. Stearns and C.J. Meyer, *Chromatographia*, 34 (1992) 226.

ELSEVIER

Journal of Chromatography A, 688 (1994) 153–159

JOURNAL OF CHROMATOGRAPHY A

Holophotal flame photometric detection☆

Walter A. Aue*, Cecil G. Eisener, Jennifer A. Gebhardt, Nancy B. Lowery

Department of Chemistry, Dalhousie University, Halifax, Nova Scotia B3H 4J3, Canada

Received 1 June 1994

Abstract

A commercial flame photometric detector was modified such that a larger fraction of its luminescence would reach the photomultiplier tube. As tested with compounds of lead and osmium, these modifications resulted in up to fifty times enhanced light transmissions and —in rough accordance with the square-root dependence of quantum noise— typically sevenfold improvements in signal-to-noise ratio.

1. Introduction

A recent study by our group demonstrated that the noise of a flame photometric detector (FPD) was largely, if not exclusively, random in character and high in frequency [1]. Under these circumstances the signal-to-noise ratio (S/N) is proportional to the square root of light reaching the photomultiplier tube (PMT).

Improving the light throughput of the FPD should hence improve the S/N; provided the square-root relationship remains intact. The obvious question is how much improvement could be expected in theory, and how much of that could be realized in practice.

The conventional FPD used for this study has an acceptance cone of about 16°; i.e. approximately 0.5% of the light emitted by the flame reaches the photocathode of the PMT. (This percentage is obviously a rough estimate: it considers the flame an isotropically emitting point source and neglects such effects as light reflection off existing walls. It also disregards the significant absorption by the interference filter.) Yet, despite the coarseness of the estimate, there is no doubt that only a small fraction of the generated light reaches the PMT.

If all of it would, an S/N dominated by photon shot noise should improve by a factor of $2d/r$, where d is the distance between the flame and the photocathode and r the radius of the latter. [In our case, that turns out to be 14 times. This number can also be obtained from the given percentages, i.e. $(100/0.5)^{1/2} = 14$.]

Physical limitations make such a perfectly holophotal performance impossible to achieve. There will always be mechanical obstructions and optical imperfections; there will always be absorption, transmission and reflection losses.

Furthermore, shapes of luminescence differ for different elements and different flame conditions. It is also possible that the square-root law should be only partially applicable, or perhaps applicable only to certain flames. So, how much of that theoretical improvement can be translated into practice by a simple optical modi-

☆ Part of theses of J.A.G. and N.B.L.

* Corresponding author.

0021-9673/94/$07.00
SSDI 0021-9673(94)00901-5

fication (not a complete rebuilding) of the detector?

To provide an acceptable (i.e., a reasonable, reliable and relevant) answer to that question, two essentially identical instruments were tested by two different operators with two different types of test compound. Each worked under individually optimized conditions.

2. Experimental

This study used two Shimadzu gas chromatographs, both Models GC-8APFp with single-channel FPD. Modifications that had earlier been made to one or both units included the substitution of a variable PMT power supply, the provision of a larger bucking current, the removal of in-line flow restrictors, the installation of wider-range flow controllers and rotameters, the replacement of the detector cap by a differently shaped one, and the insertion of a PTFE gasket into the detector base (to keep gas exchange with the atmosphere to a minimum in that region of the detector).

Yet these earlier modifications are mentioned here *for the record only*. The two Shimadzu units performed to our full satisfaction as received. They were modified solely to accommodate a variety of research projects that demanded unconventional conditions, and we did not want to "unmodify" them for the present study. These earlier changes thus do not change the basic performance of the instruments. Nor —which is of crucial importance here— do they change the character of their noise.

Modifying the FPD for higher light throughput started by raising the flame, on a thinner jet, to the center of the light path (the optical axis). A parabolic mirror was installed with the flame at its focal point. It had been lathed into a 1-in. (1 in. = 2.54 cm) aluminum rod, which was then inserted through the (normally covered) second opening of the detector. The parabolic mirror was drilled —perpendicular to its optical axis and centered at its focal point— to accept the detector jet and its quartz chimney (both more slender than in the original FPD).

Since the two flames were of different size and shape, their centers (their visually observable locations of highest analyte emission intensity) were made to coincide with the focal point of the parabola. The Pb luminescence was relatively tall and lanceolate in shape; it therefore had to reside on a slightly (ca. 2 mm) shorter jet than the smaller and roughly spherical Os luminescence.

Instead of the conventional window, an inexpensive planoconvex lens of 50 mm focal length (Edmund Scientific, 101 East Gloucester Pike, Barrington, NJ 08007-1380, USA) was inserted and backed up by an aluminum tube. The tube was thin-walled to minimimize heat conduction, and had been internally polished to a mirror surface. Fig. 1 shows to-scale schematics of the optical components. It also indicates some light-paths used in the "conventional", "holophotal" and "comparative" FPD measurements. (Several "intermediate" configurations were tested as well, but these are easily described by reference to the displayed three archetypes.)

The "conventional" measurements were done with the detectors as received from the manufacturer —except for leaving in place the earlier listed but, in this context, inconsequential modifications, and except for removing the commercial quartz chimney. The removal of the chimney results, for reasons unknown, in a larger analyte signal.

The "holophotal" measurements were carried out on the detectors supplied with the most effective combination available of parabolic mirror, centered slender jet and chimney, reflecting tube, etc.

The "comparative" measurements were performed with the detectors using the light path of the conventional mode, but the jet and chimney of the holophotal mode. This hybrid version merely allowed reliable determination of the light throughput ratio.

All versions were tested under conditions optimized for the individual detector, analyte and analyst. For analytic relevance and academic expedience, the authors made use of ongoing thesis topics dealing with the FPD characteristics of organometallic compounds: J.A.G. tested her

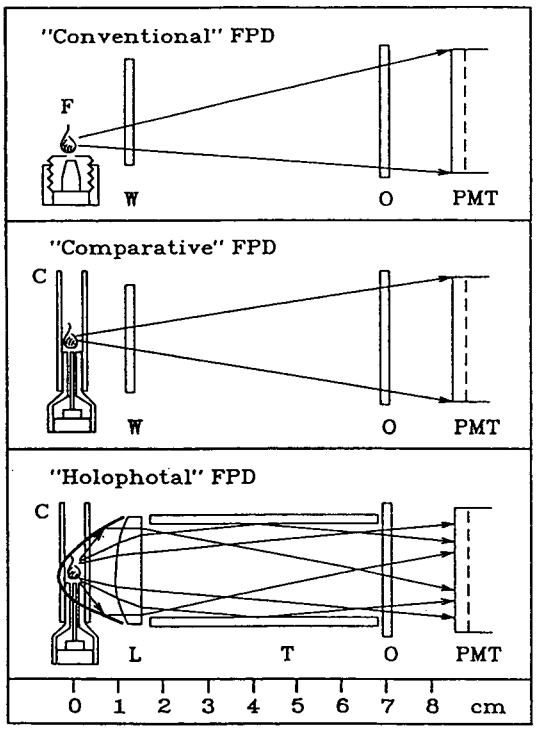

Fig. 1. Optical layout of "conventional", "comparative" and "holophotal" FPD configurations. C = Glass or quartz chimney; F = flame; L = planoconvex lens, focal length 5 cm; O = optical filter; PMT = photocathode; T = internally polished aluminum tube; W = quartz window. Not labelled but shown in bold line: aluminum parabolic mirror, focal length ca. 2.5 mm. In the holophotal configuration, the top of the jet is slightly lower than shown for Pb, and slightly higher than shown for Os (see text for explanation of the ca. 2 mm difference).

FPD versions with the σ-bonded tetraethyllead, N.B.L. hers with the π-bonded osmocene (dicyclopentadienyl osmium).

The tetraethyllead determination was carried out on a 100×0.3 cm I.D. borosilicate column packed with 5% OV-101 on Chromosorb W AW, 100–120 mesh (ca. 150–125 μm diameter particles) at 130°C. Flows were nitrogen 30, hydrogen 73 and air 13 ml/min (i.e., strongly hydrogen-rich). A Hamamatsu R-1104 PMT at −650 V was used behind a 665 nm longpass colored-glass filter (Oriel, 250 Long Beach Boulevard, Stratford, CT 06497, USA; item 51 330). The injected amounts of tetraethyllead were 10 ng for the "holophotal", 10 and 20 ng for various "intermediate", 50 ng for the "comparative" and 100 ng for the "conventional" configuration (all data are, however, reported "per 100 ng").

The osmocene determination was carried out on a 100×0.3 cm I.D. borosilicate column packed with 5% OV-101 on Chromosorb W AW, 100–120 mesh, at 180°C. Approximate flows were nitrogen 25, hydrogen 16 and air 40 ml/min (i.e., stoichiometric or close to it). A Hamamatsu R-2228 PMT was used at −900 V, behind a 630 nm longpass colored-glass filter (Oriel, item 51 320). The amount of osmocene injected was 5 ng for all configurations.

We shall distinguish these two independent sets of experiments by the symbols of the FPD-active elements involved, i.e. "Pb" and "Os".

3. Results and discussion

It is important to note that tetraethyllead and osmocene serve here only as two disparately behaved analytes, chosen to conduct two independent test series with similar optical objects but different analytical subjects. Some information on the FPD's response to the main-group element lead and the transition metal osmium can be found in earlier work from our group [2,3]; more will be reported in the forthcoming theses of two of the present authors (J.A.G. and N.B.L.).

The particulars of commercial detector construction, FPD response characteristics, and optical requirements for high light-throughput demanded —for reasons more of formal logic than of analytical practice— that a two-pronged experimental approach be employed in answering the central question of this study: Can light throughput and S/N be significantly improved?

If light throughput is to be the crucial parameter, then it should be measured —in both the conventional and the holophotal mode— with the *same* light source operating under *identical* conditions. In this study, close to holophotal conditions are obtained with a parabolic mirror. If that mirror is to intercept as much light as possible, its focal length must be very short.

Accordingly, it needs to approach the flame within a few millimeters. But if it does, the flame will become disturbed and develop flicker noise. Such disturbance can be avoided by a glass or quartz chimney separating mirror and flame.

The presence of a chimney would not seem to pose a problem: the commercial detector uses a quartz chimney as well. Yet several elements respond better in the FPD when that chimney is removed (e.g. [4]). Given that the parabolic mirror (the holophotal mode) cannot be rationally tested without a chimney, the question arises how then to test the conventional mode. *Without* a chimney the conventional response becomes stronger but the intended comparison with the holophotal mode becomes weaker; *with* a chimney the opposite occurs.

A similarly formal argument can be made about the circumference of the chimney (in the commercial detector it is wider) and about the fact that, for efficient light gathering, the flame needs to be in the center of the light tunnel (in the commercial detector configuration it is positioned near the bottom). Thus, the objectives of this study require that not just one but two questions be asked.

First the analytical question: Can a significant improvement in S/N be obtained when the best commercial configuration is changed to the best holophotal configuration, with each operating at individually optimized conditions?

Second the mechanistic question: If the light source —i.e. the flame and its conditions— do remain the same, will the increased light throughput achieved by the newly introduced optical elements lead to the square-root improvement in S/N that one expects for quantum-type noise?

Since both questions are important in their own right, this study will answer both. To do so, at least *three* detector configurations need to be tested. (We actually tested many more.)

To wit, the "conventional" measurements will represent the best the commercial detector can do, the "holophotal" measurements the best the fully modified detector can do. Additionally, the "comparative" measurements will represent a hybrid configuration in which the "flame jet and chimney" unit, as developed for the "holophotal" arrangement, is used in a detector environment otherwise resembling the "conventional" mode: this allows, first, direct measurement of the light throughput and, second, comparison of the theoretical with the experimental S/N improvement.

Table 1 shows the relative light intensity as measured from the baseline (baseline current minus dark current) and from a peak (peak apex current minus baseline current). Table 1 also shows the resulting S/N for both sets of five experimental configurations.

The increase in light throughput, from "conventional" to "holophotal" FPD configurations, is 31-fold (Pb) and 34-fold (Os) for the baseline, and 48-fold (Pb) and 37-fold (Os) for the analyte peak. If shot noise were the sole parameter to consider, S/N values should improve 5.6, 5.8, 6.9 and 6.1 times. The measured improvements are (Pb) 9.7 and (Os) 7.2 times.

The latter numbers provide a fair assessment of what can be achieved by a simple optical update: they document the success of the operation. Despite that success, a serious discrepancy appears to exist between calculated and measured S/N improvement factors. The main reason for this is the difference in light source —meaning different locations and conditions of the flame— in the two measurements.

That difference can, however, be removed. If the *same* jet-and-chimney is used for the comparison of the "comparative" with the "holophotal" configuration, the increase in light throughput for the *analyte peak* is (Pb) 51 and (Os) 33 times. That would predict S/N improvements of 7.2 and 5.7, respectively. The measured values, 7.1 and 6.2, are now in excellent agreement.

S/N values predicted on the *baseline* (8.2 and 4.8) show poorer agreement. That light throughput measured on a peak produces data of higher predictive ability than light throughput measured on the baseline should not come as a surprise.

It occurs most likely because the peak (= signal) enters directly, while the baseline enters only as the square root (= noise) into the S/N calculation. Also, the peak height determi-

Table 1
Comparison of different FPD configurations

FPD configuration	Baseline[a] current (A)	Peak current (A)	*S/N*
Tetraethyllead (100 ng)			
Holophotal[b,c,d]	$1.6 \cdot 10^{-7}$	$3.8 \cdot 10^{-7}$	340
Intermediate I[c,d]	$2.8 \cdot 10^{-8}$	$1.2 \cdot 10^{-7}$	210
Intermediate II[b,d]	$5.8 \cdot 10^{-8}$	$1.6 \cdot 10^{-8}$	114
Comparative[d]	$2.4 \cdot 10^{-9}$	$7.4 \cdot 10^{-9}$	48
Conventional[e]	$5.1 \cdot 10^{-9}$	$8.0 \cdot 10^{-9}$	35
Osmocene (5 ng)			
Holophotal[b,c,d]	$1.2 \cdot 10^{-7}$	$1.3 \cdot 10^{-7}$	230
Intermediate I[c,d]	$3.4 \cdot 10^{-8}$	$2.5 \cdot 10^{-8}$	87
Intermediate II[b,d]	$3.5 \cdot 10^{-8}$	$4.5 \cdot 10^{-8}$	160
Comparative[d]	$5.2 \cdot 10^{-9}$	$4.0 \cdot 10^{-9}$	37
Conventional[e]	$3.5 \cdot 10^{-9}$	$3.5 \cdot 10^{-9}$	32

[a] The typical dark current, $1.4 \cdot 10^{-9}$ A for Pb and $3 \cdot 10^{-10}$ A for Os, is not included.
[b] Parabola.
[c] Lens and light tube.
[d] Small, centered jet with chimney.
[e] Large, low jet without chimney.

nation is experimentally more robust, cancelling or minimizing contributions from the PMT dark-current, from room stray light, etc. It should also be noted that the eventual quantitative effect of all this may be influenced by the relative light levels of peak and baseline (which in practice means by the amounts of analyte injected).

From the agreement between calculated and measured *S/N* values we can safely assume —at least for our FPDs and their conditions— that the *S/N* increases with the square root of the light throughput from the flame. Detection limits and linear ranges should improve accordingly.

It is also obvious from Table 1 that Pb and Os —and the two instruments that process them— agree in the relative trends but differ in the absolute numbers. This is, again, not surprising. The working conditions for Pb and Os *are* very different —one reason we chose those particular analytes for testing. Besides, mirror surfaces lose reflecting power, chimneys get dirty, gas flows change with time, light leaks appear and vanish, etc.

Furthermore, a whole host of *non*-entropic circumstances —which, moreover, involve principle rather than practice, and are therefore much easier to describe and defend— can lead to apparent discrepancies in the observed *S/N* behavior. For instance:

(1) Baseline luminescence and peak luminescence often differ drastically in their intensity distributions in and around the flame —not to mention on the surface of the chimney.

(2) Because of their disparately shaped analyte —never mind baseline— luminescences, the Pb and Os flames differ in the beam divergence they cause, and in the slightly different jet heights used to center their maximum emission intensities. Differently sized jets, by virtue of being opaque, intercept different fractions of the light thrown forth by the parabola.

(3) The peak and baseline currents often show disparate dependencies on conditions, for instance the signal-to-background ratio often varies with flow-rates. Such effects may be moderated or exacerbated by the linear entry of the peak vs. the square-root entry of the baseline into the *S/N* calculation, and by the relative levels of peak and baseline.

(4) In that context, analyte peaks can depress

("eat into", "quench") the baseline on their run through the flame, just as the background can quench the analyte. (The latter phenomenon is readily apparent and has been widely researched [5,6]; the former remains obscure and has been nigh totally ignored.)

(5) The dark current of the PMT (which is normally considered part of the background, though not in this paper) remains essentially independent of (a moderate) light input. Configurations in which the dark current forms a sizeable fraction of the total PMT baseline current need therefore be treated with due caution.

(6) Although the FPD flame under our conditions produces mainly fundamental (i.e. photon shot) noise, the presence of minor contributions from "excess" (e.g. $1/f$) noise cannot be ruled out, particularly when narrow jets and chimneys are used, or when flames are run on the verge of extinction.

More types of S/N perturbations are possible and indeed probable. It is clear, however, that the anticipated S/N improvement could be successfully realized in this study. The largest credit for that goes to the parabolic mirror and to the aluminum tube with its internal mirror surface. As it turned out, the former was of greater relative benefit to the case of Os, the latter to the case of Pb. The parabolic mirror worked well even though it demanded the use of a chimney that depressed the response of both test compounds.

In other experiments, a commercial first-surface mirror of 10 mm focal length (Edmund Scientific, item 43 464) also worked well, with or without a chimney. So did two planoconvex lenses of 25 mm focal length (Edmund 45 098) that replaced the quartz window.

The choice of focal length (50 mm) for the planoconvex lens installed in the holophotal configuration represents a compromise. Its contribution to S/N improvement is small to start with, and it becomes almost negligible when the lens is used in conjunction with a parabolic or spherical mirror. On the other hand, why not use a lens instead of a window when the main task of either is merely to protect the PMT channel from the hot and humid atmosphere of the flame chamber?

Whether the achieved improvement in FPD performance is worth the trouble in FPD modification depends, inter alia, on laboratory priorities related to maximum analyte sensitivity vs. minimum instrument downtime. The hardware costs are negligible, but machining skill is definitely required for fashioning the parabolic mirror. In this context we should like to give special mention to one of the simplest, cheapest and yet most effective devices used in the FPD modification: the outside threaded, inside polished light propagation tube.

Beyond improving light propagation, such a tube serves other worthy causes as well: it shuts out room light, it allows the easy exchange of a window or lens, and it permits adjustment of the tension on the silicone rubber O-ring (thus helping to keep flame water from distilling into the PMT housing).

Because this tube is, furthermore, easily machined and installed on the commercial detector, we show its detailed blueprint in Fig. 2. Use of the internally reflecting tube (plus lens) alone —i.e. without the parabolic mirror— increased the S/N 4.4 and 2.4 times for Pb and Os, respectively. (The numbers seemed to differ too much among the two methods; however, a special cross-check in which lead was run on the Os instrument, and osmium on the Pb instrument, supported their validity.)

It may be noted in this context that optical improvements do not add up linearly: the tube, when added to an already installed parabola, is much less effective. So is, of course, the parabola when added to an already installed tube.

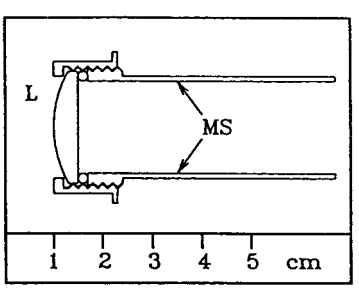

Fig. 2. Mechanical details of light-propagating tube and modified window holder. L = Lens; MS = mirror surface.

A simple, internally reflecting tube (or other type of light guide) may thus prove to be of minor cost but major benefit. It may also broaden the effective bandpass of the interference filter, owing to the wider angle of photon incidence. Fortunately the latter effect should be small and of little concern to most analytical methodologies.

The chosen "holophotal" modification is by no means the only or even the most effective one that can be envisioned. Moving a better-cooled PMT closer to the flame would, for instance, provide a —fairly obvious but in practice also fairly tricky— option. And a parabola is not necessarily the optically most efficient shape under the circumstances. One could, for instance, think of an ellipse, with the flame (enclosed by a gas-tight chimney) in one of its focal points, and with the plane of the PMT photocathode close to the other.

Such modifications would, however, have required more work on the detector body —work we considered unnecessary, both in terms of the argument being put forth by this paper and the performance already achieved by the two instruments.

Spherical mirrors and lenses have been used before in FPDs (e.g. [7–10]) —inspired, no doubt, by spectroscopic instrumentation (cf. [11]) in which their use is vital. Whether they yield the desired improvement in individual cases depends not only on the shape of the luminescence and the optical layout of the detector, but also on the nature of the baseline noise.

If the latter is dominated by flame flicker, the S/N will be independent of light throughput. If, on the other hand, it is dominated by PMT dark-current noise (i.e. if the background luminescence is at a negligible level), the S/N will be directly proportional to light throughput.

The two cases of this study, with their roughly square-root relationship between light throughput and S/N, are intermediate in their behaviour (and therefore in their potential for improvement). These cases —dominated as they are by photon shot noise— are, however, just the ones most typical of multi-element FPD methodology, and the ones most often encountered in routine chromatographic practice.

Acknowledgements

This study was supported by NSERC research grant A-9604. The most competent assistance of B. Millier in electronic design and J. Müller in quartz blowing are gratefully acknowledged.

References

[1] X.-Y. Sun, H. Singh, B. Millier, C.H. Warren and W.A. Aue, *J. Chromatogr. A*, 687 (1994) 259.
[2] W.A. Aue, X.-Y. Sun and B. Millier, *J. Chromatogr.*, 606 (1992) 73.
[3] X.-Y. Sun and W.A. Aue, *Mikrochim. Acta*, I (1990) 1.
[4] X.-Y. Sun, B. Millier and W.A. Aue, *Can. J. Chem.*, 70 (1992) 1129.
[5] S.O. Farwell and C.J. Barinaga, *J. Chromatogr. Sci.*, 24 (1986) 483.
[6] W.A. Aue and X.-Y. Sun, *J. Chromatogr.*, 641 (1993) 291.
[7] S.S. Brody and J.E. Chaney, *J. Gas Chromatogr.*, 4 (1966) 42.
[8] P.W. Grant, in D.H.Desty (Editor), *Gas Chromatography 1958 (Proc. Symp., Amsterdam, May 1958)*, Butterworth, London, 1958, pp. 153–163; as cited in D. Jentzsch and E. Otte, *Detektoren in der Gas-Chromatographie*, Akademische Verlagsgesellschaft, Frankfurt/Main, 1970, pp. 177–178.
[9] P.L. Patterson, R.L. Howe and A. Abu-Shumays, *Anal. Chem.*, 50 (1978) 339.
[10] B. Millier, X.-Y. Sun and W.A. Aue, *J. Chromatogr. A*, 675 (1994) 155.
[11] J.D. Ingle, Jr. and S.R. Crouch, *Spectrochemical Analysis*, Prentice Hall, Englewood Cliffs, NJ, 1988.

ELSEVIER

Journal of Chromatography A, 688 (1994) 161–170

JOURNAL OF CHROMATOGRAPHY A

Gas chromatography of Titan's atmosphere V. Determination of permanent gases in the presence of hydrocarbons and nitriles with a molecular sieve micropacked column and optimization of the GC parameters using a Doehlert experimental design

E. de Vanssay[a], S. Zubrzycki[a], R. Sternberg[a,*], F. Raulin[a], M. Sergent[b], R. Phan-Tan-Luu[b]

[a]*LISA, Centre Multidisciplinaire de l'Université Paris 12-Val de Marne, Avenue du Général de Gaulle, 94010 Créteil Cedex, France*

[b]*Laboratoire de Méthodologie de la Recherche Expérimentale, Centre de St Jérôme, Avenue Escadrille Normandie Niémen, 13397 Marseille Cedex 20, France*

First received 29 June 1994; revised manuscript received 18 August 1994

Abstract

An alternative for the GC determination of permanent gases in Titan's atmosphere, given the severe constraints of space instrumentation, is the use of a 100–120-mesh molecular sieve 5A micropacked column. Because of its high efficiency, small pressure drop and short analysis time, such a column is fully compatible with the experimental constraints of the Cassini–Huygens mission. In order to optimize the GC conditions associated with this column, a methodological approach was supported by a Doehlert experimental design. With such optimized conditions, the column provides a rapid separation of the selected products under isothermal conditions, with about 900 theoretical plates per metre at 70°C for most of the solutes studied.

1. Introduction

The composition and structure of the atmosphere of Titan, the largest satellite of Saturn, will be studied in detail by the Cassini–Huygens mission. The Huygens probe will carry a GC–MS experiment for analysing the chemical structure of Titan's atmosphere. As reported in previous papers [1–4], we are systematically studying GC columns that could provide the separation of most of the chemical constituents of Titan's atmosphere and of the pyrolysis products of its organic aerosols. We have shown that a Chrompack Molsieve 5A PLOT capillary column provides very good results for the separation of permanent gases, even in the presence of hydrocarbons and nitriles [4]. However, its mechanical strength seems too weak for space applications.

A literature survey indicated that molecular sieve 5A is one of the best materials for analyses for permanent gases. Because of the low head

* Corresponding author.

0021-9673/94/$07.00
SSDI 0021-9673(94)00796-9

pressure and low flow-rate imposed by space instrumentation, we chose the smallest internal diameter tubing compatible with the smallest particle size commercially available. We studied columns made of 0.8 mm I.D. stainless-steel tubing packed with 100–120-mesh (150–125-μm particle diameter) molecular sieve 5A.

In such a configuration, we assume that column temperature, column length and carrier gas column head pressure are the three main parameters that can affect the chromatographic performances. For this reason, to optimize these GC parameters, we applied a methodological approach, supported by a Doehlert experimental design [5,6], which takes into account the possible interactions between parameters. The studied response functions include both classical GC performance functions and space instrumentation constraints. In the case of the Huygens GC–MS instrument, the main chromatographic constraints are as follows: (i) low inlet pressure (i.e., about 0.5 bar), for efficient sampling; (ii) low outlet flow-rate (i.e., about 1 ml/min), for efficient GC–MS coupling; and (iii) column temperature between 30 and 100°C, at least slightly above ambient (about 30°C) but not exceeding 100°C, because of the limited power available on the probe.

The aim of this work was the development of a GC column able to determine the vertical profile of CO concentration in the atmosphere of Titan where N_2 is the major component. We therefore focused our attention on the determination of N_2 and CO, including the detection limit of CO in N_2 gas mixtures. We also studied the chromatographic behaviour of C_1–C_2 hydrocarbons and the effect of nitrile injection on the column efficiency.

2. Optimization

The joint action of column temperature, column length and carrier gas pressure on column performance can be studied through theoretical approaches [7]. However, this approach is generally very complex and often requires the use of parameters the values of which are not available. We propose here a multivariate experimental approach. The overall strategy is (i) definition of the most important experimental factors, (ii) choice of the experimental domain and (iii) adjustment of these factors, by a response surface technique, to an optimum chromatographic separation taking into account the range of parameters values imposed by space instrumentation. For analysing the results we consider both chromatographic separation and the constraints of space instrumentation.

The chromatographic functions measured for given chromatographic parameter values are called responses. For many reasons (particularly since it induces a loss of information) the use of a global chromatographic response function was considered unsuitable. We preferred the use of several complementary specific response functions, namely the height equivalent to a theoretical plate (HETP) to characterize the column efficiency, the capacity factor (k') for measuring the retention and the valley height (P) to characterize the chromatographic resolution. In addition, this study also included the use of parameters (head column pressure of carrier gas and column temperature) and of response (outlet column flow-rate of carrier gas) imposed by space instrumentation. The flow-rate must be around 1 ml/min, for a head pressure drop lower than 0.5 bar and a temperature range of 30–100°C without temperature programming if possible.

3. Experimental

3.1. Column and gas chromatography

Columns packed with molecular sieve 5A were prepared with 0.8 mm I.D. stainless-steel tubing. The column length is one of the experimental parameters: three values were chosen (0.5, 0.75 and 1 m). Each column was mounted on a Hewlett-Packard HP 5890 Series II gas chromatograph, equipped with a micro thermal conductivity detector, an electro-pneumatic six-port gas sampling valve (Valco) with a 0.25-ml sample loop and a Nelson OMEGA data acquisi-

tion system. A laboratory-made adaptation of a back-pressure regulator (0–2 bar) helps to derive a stable pressure with good precision in the direct injection mode because the column is directly connected to the gas sampling valve by a zero-dead-volume adapter.It is connected to the detector by uncoated fused-silica capillary tubing about 15 cm long. In order to cover a large range of pressure (0–7 bar) we added a three-port switching valve (Valco) which allows one to switch the carrier gas from the capillary column (0–2 bar) to the packed column (0–7 bar) modified injector system (Fig. 1). In the present study, owing to the range of carrier gas pressure used (0–0.5 bar), and to the highest possible accuracy of the associated manometer (about 0.02 bar), we used only the capillary column system.

The GC column was operated isothermally in the range 30–100°C. The temperatures of the detector, injector and gas sample valve were chosen as a function of the column temperature. Hydrogen was used as the carrier gas because for an equivalent column efficiency it can provide faster analyses. In addition, it is much more convenient for GC–MS space instrumentation,

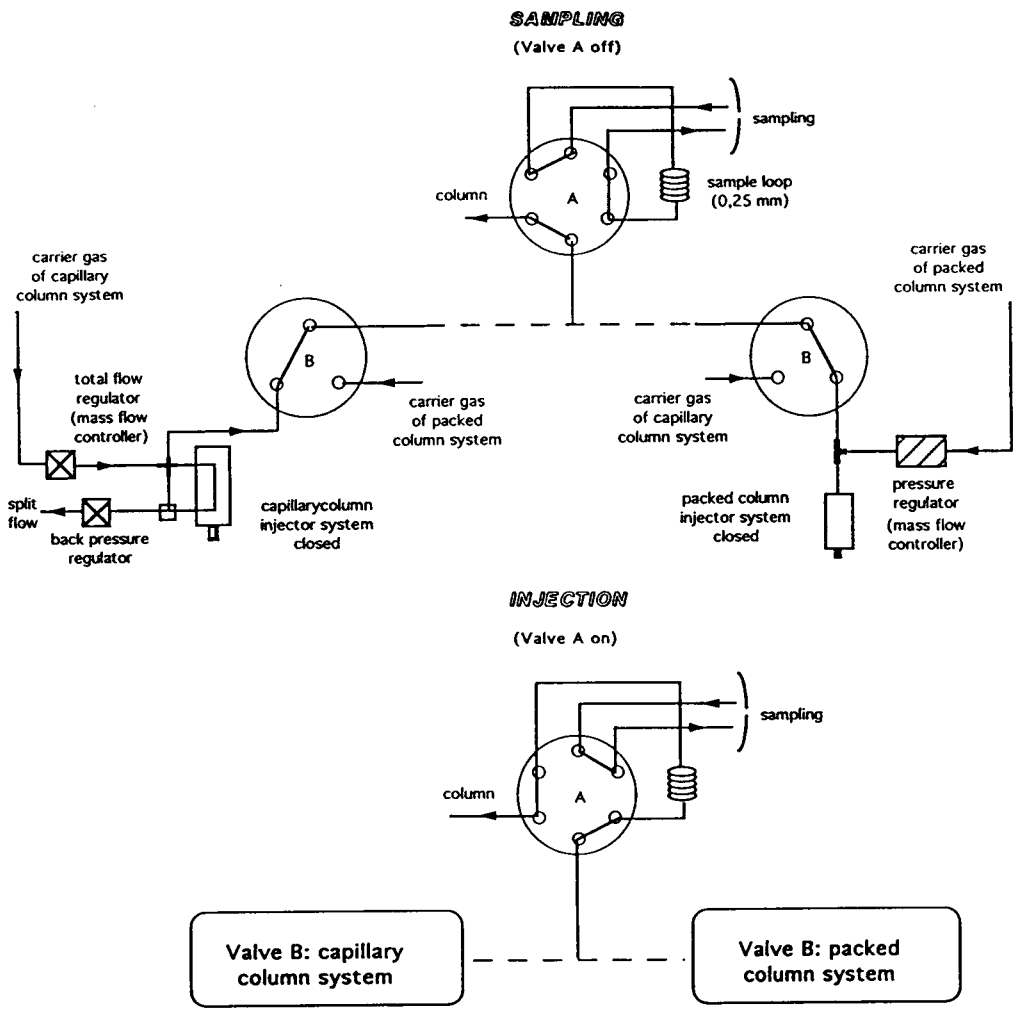

Fig. 1. Schematic representation of the laboratory-made injector adaptation with a gas sampling valve.

as it is much more easily pumped out than other carrier gases.

3.2. Sampling

Standard gas mixtures of known composition including CO, N_2, CH_4, C_2H_6 (with eventually other C_2 hydrocarbons) and noble gases (He, Ne, Ar, Kr and Xe) were prepared and stored in a sampling glass reservoir connected to a vacuum line and equipped with a high-vacuum stopcock (SVT, Ris Orangis, France). This reservoir was initially evacuated and then, except for CH_4 and Ar, each individual component was successively introduced by expanding a known volume of each gas at a known and precalculated pressure, as described previously [1]. CH_4 and Ar were introduced simultaneously by using a commercially available CH_4–Ar gas mixture (90:10). A similar method was followed to prepare the samples used to study the effect of CO dilution in N_2. The loop of the gas sampling valve was also connected to the vacuum line. It was directly sampled, at a known pressure, by expanding the content of the reservoir to the loop, initially evacuated.

The vacuum line, connected to a primary pump, was able to reach a vacuum as good as 10^{-2} mbar, checked with a Pirani vacuum gauge (MKS, Andover, MA, USA). Sample absolute pressures were measured with a manometer (Schlumberger, Montrouge, France) with a relative precision of better than 1%.

3.3. Reagents

Helium (grade C) was supplied by AGA (Toulouse, France). All other gases, i.e., argon–methane mixture (90:10, pure), nitrogen, neon and ethane (grade N30), krypton (grade N35), xenon, carbon monoxide and methane (grade N45) were supplied by Alphagaz–L'Air Liquide (Bois d'Arcy, France).

3.4. Selection of experimental factors and studied responses

The aim of this work was the GC study of CO when diluted in N_2. The effect of the column diameter and particle size on the detection limit are well known: the detection limit increases when these factors decrease. We therefore fixed the particle diameter at the lowest commercially available size, i.e., 100–120 mesh, corresponding to 150–125 μm mean particle diameter (d_p). We also used an optimum column diameter ($d_c = 0.8$ mm I.D.) corresponding to this particle diameter ($dc/dp \approx 5$) [7].

Table 1
Experimental domain

Real factor (natural variable)	Coded variable	Units	Centre	Step
U_1 = column temperature	*X1*	°C	75.00	50
U_2 = column pressure	*X2*	bar	0.40	0.69
U_3 = column length	*X3*	m	0.75	0.306

For each response, one can derive a model, and each response model is expressed using coded variables. In the following, *Xi* stands for the coded setting of real variable U_i. The column parameters, carrier gas head pressure, temperature and column length, which all have an effect on retention time and on chromatographic efficiency, were studied. The variation steps (ΔU_i) and centre values (U_i^0) of these experimental factors are specified in Table 1. The use of coded factor settings instead of the natural values (U_i) allows a quantitative comparison of the relative importance of each variable directly from the model.

The different response functions (η_i) used in this work are summarized in Table 2. The column capacity factor (k') was measured for

Table 2
Response functions (η_i) selected in this study

η_1	Flow-rate (ml/min)
η_2	*trmax*: maximum retention time (min)
η_3	HETP CO (mm)
η_4	HETP Xe (mm)
η_5	k'Ar: capacity factor
η_6	$k'N_2$: capacity factor
η_7	k'CO: capacity factor
η_8	k'Xe: capacity factor
η_9	$P(N_2 - CH_4) = P1$: valley height
η_{10}	$P'1 + P2$

Table 3
Theoretical values of coded variables (reduced coordinates of cuboctahedron)

No.	Coded variable		
	X1	*X2*	*X3*
1	0	0	0
2	1	0	0
3	−1	0	0
4	0.5	0.866	0
5	−0.5	−0.866	0
6	0.5	−0.866	0
7	−0.5	0.866	0
8	0.5	0.2887	0.8165
9	−0.5	−0.2887	−0.8165
10	0.5	−0.2887	−0.8165
11	0	0.5774	−0.8165
12	−0.5	0.2887	0.8165
13	0	−0.5774	0.8165

Ar, N_2, CO and Xe. Calculations of HETP were done only for CO because of its importance in Titan's photochemical models and Xe because it is the last solute eluted. For N_2, Kr, CH_4 and CO the height of valley (*Pi*), which varies within the range 0–1, was estimated for N_2 and CH_4 (*P1*), N2 and Kr (*P'1*) and CO and Xe (*P2*) because these pairs of peaks may be co-eluted (the total resolution between the peaks related to these compounds is rare). The other responses studied were the duration of the analysis (*trmax*) and the flow-rate of the carrier gas (*Fc*). In fact, after data retriveal, the *P'1* and *P2* responses appeared not to be sufficiently explicit for a good optimization. Therefore, we finally considered the sum of these two responses; this is the η_{10} response and it varies within the range 0–2.

3.5. Experimental design [5,6]

We used a "Doehlert uniform shell design [5,6]". It is derived from the theoretical example described below, starting from the theoretical coefficients presented in Table 3. Let us consider that the twelve sets of coefficients of this table (Nos. 2–13) correspond the reduced coordinates of the twelve vertices of a regular cubooctahedron. Such a geometrical figure offers a spatial representation of an experimental domain (covering the range of selected experimental parameters). The first set of coefficients (No. 1) corresponds to the reduced coordinates of the central point of this figure. From this experimental design, one can deduce an experimental plan, by converting coded variables *Xi* into the real variable (to be experimentally used) U_i, using the relationship $U_i = U_i^0 + X_i \Delta U_i$. Table 4 sum-

Table 4
Doehlert design: natural and coded variables[a] for each experiment (test)

Test	Natural variable			Coded variable		
	U_1 (°C)	U_2 (bar)	U_3 (m)	*X1*	*X2*	*X3*
1	75	0.4	0.75	0	0	0
2	100	0.4	0.75	1	0	0
3	50	0.4	0.75	−1	0	0
4	87	0.6	0.75	0.48	1	0
5	62	0.2	0.75	−0.52	−1	0
6	87	0.2	0.75	0.48	−1	0
7	62	0.6	0.75	−0.52	1	0
8	87	0.45	1	0.48	0.25	1
9	62	0.35	0.5	−0.52	−0.25	−1
10	87	0.35	0.5	0.48	−0.25	−1
11	75	0.5	0.5	0	0.5	−1
12	62	0.45	1	−0.52	0.25	1
13	75	0.3	1	0	−0.5	1

[a] The equation $U_i = U_i^0 + X_i \Delta U_i$ allows one to switch from coded variables to natural variables; U_i^0 = value of the natural variable, *i*, at the centre of the experimental domain; ΔU_i = step of variation of the natural variable, *i*, for a unit variation of the coded variable *Xi*.

marizes the values of the real variables used in this study and the corresponding derived coded variables.

3.6. Mathematical methods

Principles of response surface methodology [8,9]

It is reasonable to assume that the variation of the observed responses Y is functionally related to the detailed settings of the experimental factors. However, as the responses are experimentally determined, there will always be an experimental error component. We therefore write the functional relationship between the observed response and the experimental factors as

$$Y = f(X1, X2, \ldots, Xn) + e$$

where Xi are the coded variables and e is the experimental error component. It is not possible to derive an analytical expression for f from purely theoretical considerations. However, if we try to estimate f through a Taylor expansion, it will take the form of a polynomial in the independent factors:

$$Y = \beta_0 + \sum \beta_i x_i + \sum \sum \beta_{ij} x_i x_j + \sum \sum \sum \beta_{ijk} x_i x_j x_k + \cdots + e$$

A sufficiently good approximation can often be obtained if the Taylor development is truncated after the second-degree terms. The polynomial coefficients (which are in fact the model parameters) can be estimated by using the least-squares multiple regression of the polynomial to the observed response. The results (response surfaces) are obtained by the least-squares method. They are drawn up to 5% of the maximum experimental values, the lower variations being considered as non-significant.

All analytical treatments were supported by a specific software named NEMROD [10]. The principal analysis of the main components is included in the software.

Desirability function

In order to quantify our "desire", we used a specified function defined between 0 and 1. The nature of this function is related to the type and range of variation of each response.

The principle of this function is based on the search for a global optimum. To obtain this optimum, we build a desirability function $D = f(Y1, Y2, \ldots, Yn)$ defined by

$$D = \left(\prod_j d_j^{w_j} \right)^{1/w}$$

with $w = \Sigma_j w_j$, where dj is a partial desire function of D defined for each response η_i and w is a balancing empirical factor which improves the specific weight of each dj function.

The last step is the search for the optimum of the D function. For that purpose, we plot the surface response of D versus the Xi parameter. If D is equal to zero, the corresponding values of Xi variables are not considered. The result of this computation is expressed on a response surface graph. In addition, the software gives the maximum value of D corresponding to the optimum set of values of the Xi variables.

4. Results and discussion

The responses observed in these experiments are summarized in Table 5. In Table 6, we have calculated the ten coefficients bi of the experimental model for each response Yi. First, a response surface study was carried out on all responses in order to visualize their behaviour. The results show that factor $X3$, which corresponds to the length of the column, is generally the most important and that the column head pressure ($X2$) generally exhibits a very small influence (except for the flow-rate $Y1$). However, this factor is one of the main parameters constrained by space instrumentation, so it is not possible to rule it out. We tried to optimize this experiment within the domain of parameter values compatible with such constraints.

Then, for optimizing the three parameters $X1$, $X2$ and $X3$, we determined the partial desire function dj for the ten responses (all responses except $P'1$ and $P2$). Four types of such a function are presented in Fig. 2. They corre-

Table 5
Values of each response for all experiments (test)

Test	Flow-rate (ml/min)	Analysis time (min)	HETP (mm)		Capacity factor				Valley height	
	Y1	*Y2*	*Y3* (CO)	*Y4* (Xe)	*Y5* (Ar)	*Y6* (N_2)	*Y7* (CO)	*Y8* (Xe)	*P1* (*Y9*)	*P'1* + *P2* (*Y10*)
1	1.32	4.54	1.61	2.08	0.43	1.19	4.67	7.02	0.90	1.00
2	1.32	3.24	1.76	2.19	0.34	0.79	2.50	4.56	0.67	1.24
3	1.50	6.91	1.62	2.83	0.58	1.96	9.70	11.68	0.99	0.47
4	2.21	4.03	1.26	2.04	0.59	1.69	7.21	9.66	0.97	0.99
5	0.85	8.67	1.91	2.14	0.51	1.57	6.71	9.00	0.90	0.88
6	0.85	5.88	2.41	2.46	0.40	1.00	3.50	5.67	0.65	0.96
7	2.21	4.05	1.38	2.36	0.60	1.70	7.23	9.76	0.97	0.91
8	1.03	5.89	1.77	2.35	0.50	1.14	3.78	7.54	0.75	1.80
9	1.54	3.11	1.60	4.55	0.45	1.13	4.48	7.04	0.55	0.93
10	0.43	8.37	3.97	3.51	0.42	1.09	3.59	5.86	0.00	0.86
11	2.14	1.94	1.55	5.99	0.40	0.96	3.31	5.67	0.29	1.00
12	1.03	9.54	1.80	2.23	0.66	1.79	7.24	12.25	0.92	1.66
13	0.76	10.36	2.29	2.21	0.58	1.41	5.17	9.41	0.79	1.64

spond to the type of variation of *dj* (between 0 and 1) versus the value of the following responses: (a) flow-rate (*Y1*), (b) *trmax* (*Y2*), (c) HETP (*Y3* and *Y4*) and (d) capacity factor and valley height (*Y5* to *Y10*). The observed curves exhibits non-linear variations. From this *dj* the global desire function *D* as a function of *Xi* is derived. Then, the variation of *D* can be plotted against the value of *Xi*, as shown in Fig. 3. Fig. 3a represents the variation of *D* of *X1* and *X2* for a given *X3* value (*X3* = 0.657) fixed by the optimum *D* value. The projection of the volume thus defined on the *X1*, *X2* surface (along the *D* axis) is presented in Fig. 3b. The results of the computed optimization of the global *D* function allow one to define, in the first quadrant (Fig. 3b), a domain where the chromatographic parameters are optimum for the selected range of parameters values. In this domain, the point where the *D* function is optimum (top point) has the coordinates (0.223, 0.720, 0.657) corresponding to an 80°C column temperature (U_1), 0.55 bar column head pressure (U_2) and 0.9 m column length (U_3). To improve the reliability of these data, we studied the influence of small variations of the coordinates *Xi* on response *Yj*

Table 6
Coefficients *bi* of each experimental model response *Yi*

Coefficient	*Y1*	*Y2*	*Y3*	*Y4*	*Y5*	*Y6*	*Y7*	*Y8*	*Y9*	*Y10*
b0	1.3200	4.540	1.6100	2.080	0.4300	1.9000	4.6700	7.020	0.9000	1.0000
b1	−0.1838	−0.065	0.3750	−0.275	−0.0984	−0.4510	−2.7468	−2.945	−0.2013	0.2213
b2	0.7946	−2.330	−0.6149	0.251	0.0558	0.1640	0.8607	0.986	0.0931	0.0411
b3	−0.2633	2.527	−0.2572	−1.482	0.0966	0.2372	0.9831	2.169	0.3307	0.4715
b11	0.0900	0.537	0.0800	0.430	0.0300	0.1850	1.4300	1.100	−0.0700	−0.1450
b22	0.2500	1.311	0.1467	0.083	0.1167	0.3384	1.5134	1.637	−0.0133	0.0383
b33	−0.3325	2.533	0.7733	1.962	0.0716	−0.0354	−0.8469	0.727	−0.5042	0.5183
b12	0.0000	1.599	−0.3580	−0.370	0.0577	0.3233	1.8418	1.865	0.1443	0.0000
b13	0.6797	−6.016	−1.3431	0.841	−0.0982	−0.4866	−2.2213	−2.823	0.1817	0.1286
b23	−0.5691	1.093	0.5397	−1.452	0.0565	0.1999	0.7847	1.083	0.0412	0.0271

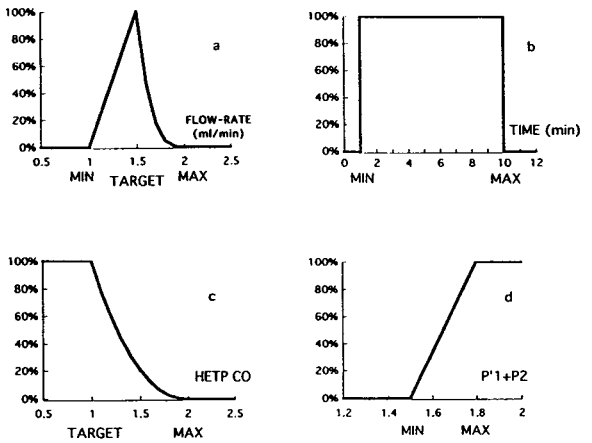

Fig. 2. Four typical partial desire function *dj* adapted for each experimental response function *Yi*: (a) represents flow-rate (*Y1*); (b) represents *trmax* (*Y2*); (c) represents HETP (*Y3* and *Y4*); (d) represents capacity factor and valley height (*Y5* to *Y10*).

and partial desire function *dj*. The results show only a slight variation of *Yj* and *dj* functions with *Xi*. This indicates that the range of parameter values corresponding to the optimum conditions is relatively wide.

A chromatogram obtained around the top point values is displayed in Fig. 4. Only one co-elution is observed, corresponding to He and Ne solute. This co-elution is also observed when a capillary column is used [4] excepted at low temperature (i.e., 20°C). The three solutes, N_2–Kr–CH_4, the GC resolution of which is characterized by the valley heights *P1* and *P'1*, are not fully separated, but this separation is sufficient for a quantitative GC–MS analysis.

4.1. CO dilution

Using the chromatographic values corresponding to the top point, we studied the limit of detection of CO in N_2 with a thermal conductivity detector. For 370 ppm of CO in N_2, the CO chromatographic peak is well separated from that of N_2 and its size and shape are compatible with a quantitative analysis. For 33 ppm of CO in N_2, the peak is still visible, but appears as a shoulder which does not allow a quantitative analysis.

4.2. Behaviour of light hydrocarbons and nitriles

Gas samples of Titan's atmosphere to be analysed will include light hydrocarbons and nitriles at noticeable concentrations. It is therefore of prime importance to know the chromatographic behaviour of these compounds on the GC columns which may be selected for the flight GC–MS instrument. If they are eluted with retention times short enough to be compatible with the GC analytical cycle, then the column dedicated to permanent gas analysis will also give information on these low-molecular-mass organics. If their retention time is longer than the duration of the GC analytical cycle, then it is important to know the shape of their GC peaks and to check whether there is any risk of interference between these "ghost" peaks and the others. Finally, if the compounds are not eluted at all, then it is necessary to check that their irreversible adsorption on the GC column does not induce any significant change in the chromatographic behaviour of the column.

The obtained results are the following. Hydrocarbons with more than two C atoms are not eluted from the molecular sieve 5A column at $T \leqslant 100$°C (even after 2.5 h). C_2H_2 and C_2H_4 show very long retention times with broad and irreproducible GC peaks. Because of their low concentrations in Titan's atmosphere, the corresponding GC ghost peak expected from these compounds on the flight gas chromatograph should not interfere with the analysis of permanent gases. Only ethane gives a GC peak of noticeable intensity with the molecular sieve column, but with a retention time which is about twice that of CO (at 100°C). Its elution will have to be taken into consideration in interpreting Titan's gas chromatograms: the C_2H_6 peak may appear as a ghost peak eluted during the chromatographic cycle of a sample corresponding to a later injection. However, the shape of this peak, much broader than those of peaks corre-

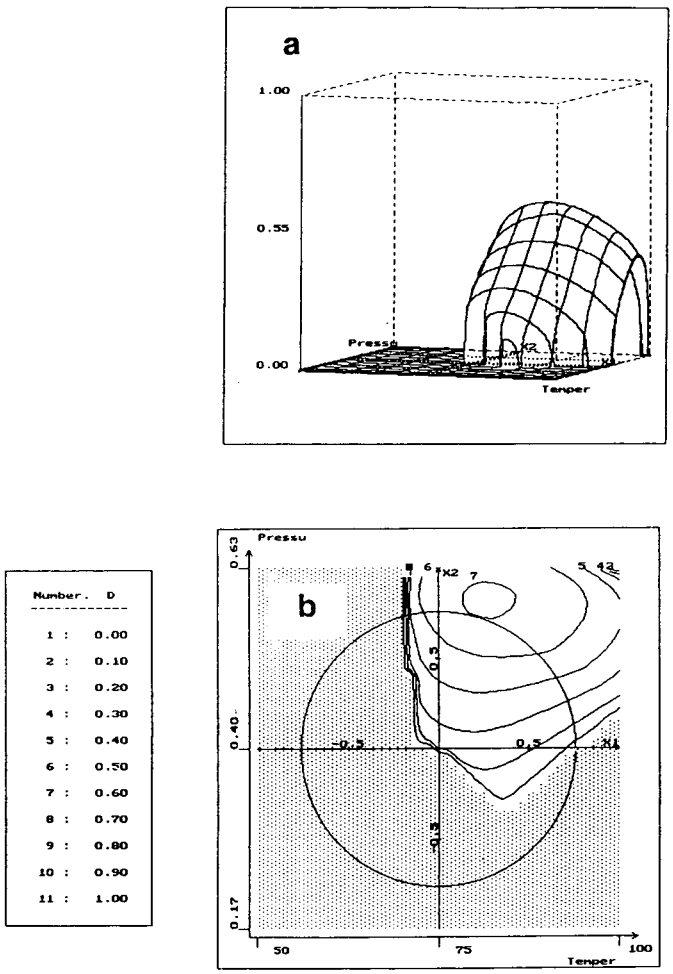

Fig. 3. (a) Response surface of the global desire function D versus $X1$ (temperature), $X2$ (pressure) and $X3 = 0.657$ (length). (b) Projection along the D axis of the surface defined in (a) on $X1$, $X2$ plan. Each curve represents an iso-D level. The values of each iso-D level are shown in the left column.

sponding to the last injection, may help to solve this problem.

Similar studies were carried out with nitriles (acetonitrile, cyanogen and butyronitrile). None of these compounds is eluted even at relatively high column temperatures (up to 100°C). The chromatographic behaviour of permanent gases was also studied after injecting various amounts of these nitriles (from 1 nmol to 2 μmol of each) into the molecular sieve 5A column. No significant changes in the retention times and peak shapes of the permanent gases were observed.

5. Conclusions

In this study, the experimental domain that we have defined a priori appears suitable for the space application we were looking for. However, we have not used the specific properties of the Doehlert experimental design. They consist in an easy displacement of the design into an unexplored portion of the experimental domain. Adding new variables that had not been previously studied is easy. Nevertheless, the small set of experiments that are derived from this method

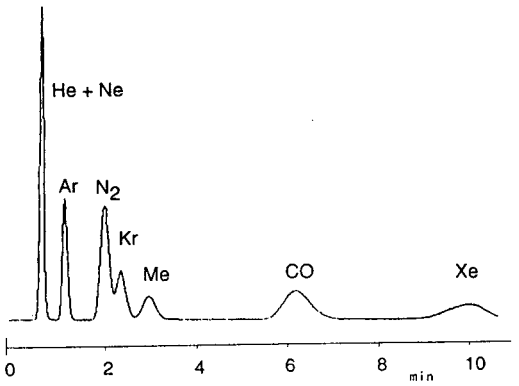

Fig. 4. GC analysis of a mixture of permanent and noble gases on a capillary column packed with molecular sieve 5A (1 m × 0.8 mm I.D.). Carrier gas, H_2; flow-rate, 1.3 ml/min; column head pressure, 0.45 bar; column temperature, 62°C.

allows a rapid overall study of the behaviour of the molecular sieve 5A packed column under relatively strong experimental constraints. With the optimum conditions obtained by this method (81°C, 0.55 bar and 0.91 m), which correspond to a flow-rate of 1.5 ml/min and an analysis time (*trmax*) shorter than 6 min, the molecular sieve 5A capillary column provides a sufficiently good separation of permanent and noble gases in the presence of hydrocarbons and nitriles for their determination in the atmosphere of Titan. The total amount of hydrocarbons and nitriles injected into the column during the descent of the Huygens probe in the atmosphere of Titan will still be one to two orders of magnitude [11,12] below the currently tested conditions. Hence it can be assumed that such a column will not be affected by the chemical conditions of Titan's environment. In addition, the chromatographic conditions are fully compatible with MS coupling and space instrumentation.

However, the determination of C_2 hydrocarbons does not seem possible with such a column. A study of capillary columns packed with other adsorbents such as molecular sieve 13X, Haysep A, carbon molecular sieve or mixed adsorbents is in progress. The experimental design used for these experiments will include new parameters such as the ratio of mixed adsorbents and CO concentration.

Acknowledgements

We thank E. Shiba for his help during the development of this work. This research was supported by a grant from the Centre National d'Etudes Spatiales.

References

[1] L. Do and F. Raulin, *J. Chromatogr.*, 481 (1989) 45.
[2] L. Do and F. Raulin, *J. Chromatogr.*, 514 (1990) 65.
[3] L. Do and F. Raulin, *J. Chromatogr.*, 591 (1992) 297.
[4] E. de Vanssay, P. Capilla, D. Coscia, L. Do, R. Sternberg and F. Raulin, *J. .Chromatogr.*, 639 (1993) 255.
[5] D.H. Doehlert, *Appl. Statist.*, 19 (1970) 231.
[6] D.H. Doehlert and V.L. Klee, *Discrete Math.*, 2 (1972) 309.
[7] G. Guiochon and C.L. Guillemin, *Quantitative Gas Chromatography* (Journal of Chromatography Library, Vol. 42), Elsevier, Amsterdam, 1988.
[8] G.E.P. Box and N.R. Draper, *Empirical Model-Building and Response Surfaces*, Wiley, New York, 1987.
[9] A.L. Sunesson, C.A. Nilsson and B. Andersson, *J. Chromatogr.*, 623 (1992) 93.
[10] D. Mathieu and R. Phan-Tan-Luu, *NEMROD Software*, LPRAI, Marseille, France, 1978.
[11] A. Coustenis, in *Proceedings of Symposium on Titan*, ESA Spec. Publ., SP-338, Estec, Noordwȳk, Netherlands, 1992, p. 53.
[12] D. Toublanc, J.P. Parisot, J. Brillet, D. Gautier, F. Raulin and C.P. McKay, *Icarus*, in press.

ELSEVIER

Journal of Chromatography A, 688 (1994) 171–180

JOURNAL OF CHROMATOGRAPHY A

Continuous monitoring of volatile organic compounds in water using on-line membrane extraction and microtrap gas chromatography system

Yong Hua Xu, Somenath Mitra*

Department of Chemical Engineering, Chemistry and Environmental Science, New Jersey Institute of Technology, Newark, NJ 07102, USA

First received 1 June 1994; revised manuscript received 30 September 1994

Abstract

A method for continuous monitoring of volatile organic compounds (VOCs) in water is presented. The aqueous sample containing VOCs is passed through a hollow fiber membrane. The VOCs selectively migrate across the membrane into an inert gas stream. The VOCs are trapped and concentrated by a microtrap in front of the GC column. The retained VOCs are desorbed from the microtrap by an electrically generated temperature pulse. Rapid heating generates a concentration pulse of analytes which serves as an injection for chromatographic separation. Continuous monitoring is achieved by making a series of pulses (or injections) and corresponding to each pulse a chromatogram is obtained. This system showed excellent results for VOCs monitoring at trace levels. Detection limits for most VOCs were at the low ppb (μg/l) level.

1. Introduction

The list of volatile organic compounds (VOCs) includes a variety of alkyl substituted aromatic hydrocarbons, as well as organic molecules containing different functional groups. Presence of VOCs in water is a public health concern because many of the VOCs are toxic and/or carcinogenic. VOC contamination may be encountered in ground water, surface water, industrial waste water as well as in drinking water. VOCs may come from industrial spills and emissions, leachate from municipal and industrial landfills, and can be formed as byproducts of chlorination during the water treatment process. Federal regulations require monitoring of effluent streams for the presence of VOCs.

The conventional Environmental Protection Agency (EPA) approved method of collection and analysis of VOCs in water consists of obtaining a grab sample, transporting the sample to a laboratory and analyzing the sample by purge and trap (e.g., EPA 502.2, 602 methods). In purge and trap, the VOCs are purged from the aqueous sample by bubbling an inert gas through it. The inert gas carries the VOCs into a sorbent trap where they are retained. Then the VOCs are thermally desorbed from the trap and analysis is done by GC or GC–MS. Head space analysis is another popular method where the sample is first allowed to equilibrate in a sealed sample vial. Then a small head space sample is withdrawn

* Corresponding author.

0021-9673/94/$07.00
SSDI 0021-9673(94)00944-9

and analyzed by GC or GC–MS. There are several inherent difficulties in the purge and trap procedure such as memory effect and incomplete desorption. The head space analysis has relatively poor accuracy and precision, and is usually used as a screening method. Direct injections of water samples have also been tried for analysis of VOCs, but the detection limits are usually quite high [1].

The limitation of the above mentioned techniques is that the sample has to be sent to the laboratory for analysis. These techniques can not be used for real-time, continuous monitoring. Real-time, on-line monitoring of VOCs in water offers several advantages. On-line techniques provide a more accurate analysis of VOCs by overcoming the problems associated with discrete sampling, sample preservation, transport, storage and laboratory handling of samples. Each of these steps may introduce errors such as sample loss and cross contamination. The grab samples are usually stable for a few days and the analysis has to be done within a few days. Very often samples have to be rejected just because the analysis could not be completed on time. Some of these problem can be solved using on-line monitoring techniques. Real-time VOC measurement devices can be used for continuous monitoring applications, such as monitoring ground water during clean up operations, drinking water supply, and waste water discharge from industries. Continuous monitoring can also be used in process control applications. Semicontinuous VOC monitoring systems for water have been developed based on purging of VOCs from water followed by IR or GC analysis [2]. At present there is a real need for a continuous monitoring technique which can separate and identify the different VOC components at trace level.

1.1. Membrane extraction of VOCs

In general, VOCs analysis in water involves an extraction/separation step where the VOCs are removed from the aqueous phase. The most common extraction method is purging with an inert gas as done in purge and trap. However, purging is a slow process and significantly increases the analysis time. The VOCs can be recovered from the aqueous phase via selective transport through a semi-permeable membrane. In this process, the aqueous sample is contacted with a membrane and the VOCs selectively permeate through the membrane into a gaseous phase on the other side. Membranes can be divided into two categories: nonporous and porous membranes. In nonporous membranes, the mechanism of VOCs permeation [3] involves the following steps. First the VOC components migrate from the aqueous phase to the surface of the membrane, and dissolve in the inside surface layer of membrane. Then the dissolved components migrate through the bulk membrane under a concentration gradient. This is followed by evaporation or stripping of the VOCs from the outer membrane surface into the stripping gas. On the contrary, in a microporous membrane (e.g. polypropylene membrane) the VOCs directly diffuse through pores. The nonporous, hydrophobic silicone membrane is more selective toward organic compounds, and it reduces the diffusion of water through the membrane. When the stripping gas is to be introduced directly into a GC column or GC–MS the elimination of water is an important consideration.

Measurement devices based on membrane separation have been developed for different type of applications [4–13]. VOCs from water sample have been directly introduced into mass spectrometers through a membrane without any GC separation [9–11]. An analysis system which combines membrane extraction followed by GC injection using a sampling valve has been reported [12,13]. Although gas sampling valves can automatically make injections into a GC column, they have certain limitations in trace analysis. Only a small volume (a few microliters to a milliliter) can be injected. A large injection causes excessive band broadening, while a small injection volume reduces sensitivity. As a result these systems have high detection limits and are not effective in monitoring at trace level.

1.2. On-line microtrap

The sample introduction device is the most important component in GC instrumentation

used for continuous, on-line monitoring. It should be able to make automatic, reproducible injections. Recently we have reported the development of an on-line microtrap (OLMT) for continuous monitoring of VOCs in air [14,15]. The microtrap is a short length of small diameter tubing containing an adsorbent. The microtrap is directly connected in front of the analytical column. A flowing gas stream containing the VOCs is introduced directly into a GC column through the OLMT. As the stream passes through the OLMT, the VOCs are retained by the adsorbent in the microtrap. A pulse of electric current rapidly heats the microtrap to desorb the trapped VOCs. Due to its low thermal mass, the microtrap can be heated (and cooled) very rapidly. This rapid desorption generates a concentration pulse of VOCs that serves as an injection for GC separation. So, the OLMT is not only an automatic injection device but also a sample preconcentrator. Consequently, low detection limits can be achieved using an OLMT.

In this investigation membrane extraction was combined with the on-line preconcentration cum injection by a microtrap. A membrane module consisting of a single hollow fiber membrane was used to extract the VOCs from the water sample into an inert gas stream. The VOCs in the gas stream were concentrated using an OLMT and then injected into GC for analysis. Continuous monitoring of the VOCs in water was achieved with this on-line membrane extraction microtrap system (OLMEM).

2. Experimental

The schematic diagram of the experimental system is shown in Fig. 1. Two different membrane module designs are possible using hollow fiber membrane: "flow-over" and "flow-through" [9,13]. In flow-through configuration, the aqueous sample is passed through a hollow fiber membrane while the stripping gas flows on the outside. While in flow-over configuration the water sample passes on the outside of the membrane. The membrane module here was operated in the "flow-through" configuration. The membrane used in this study was Dow Corning Silastic medical grade tubing (Dow Corning Corporation, Midland, MI, USA). The membrane size used was 0.012 in. I.D. × 0.025 in. O.D. (1 in. = 2.54 cm). The membrane module consisted of a single hollow fiber. The membrane was connected to narrow bore stainless steel

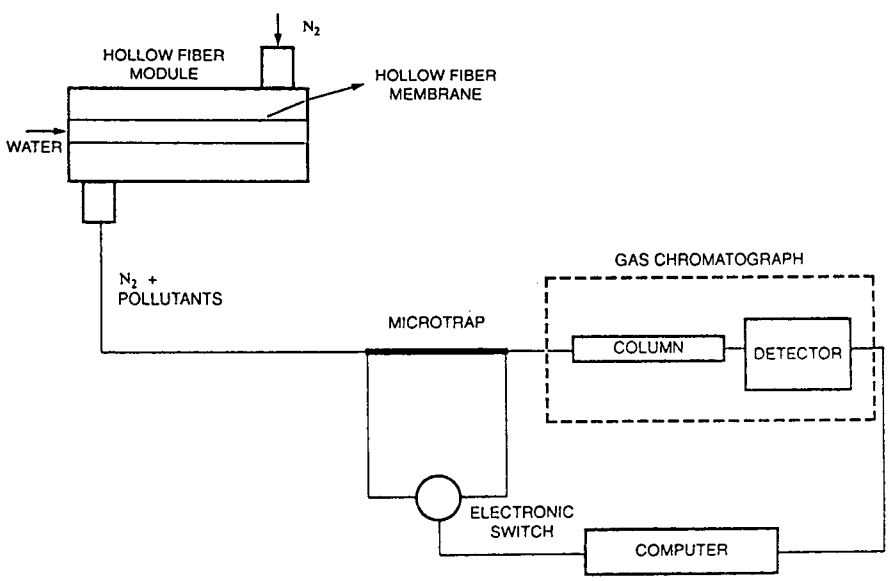

Fig. 1. Schematic diagram of the on-line membrane extraction microtrap system.

tubing of 0.015 inch outer diameter. To connect the hollow fiber membrane to the steel tubing, the end of the membrane was immersed in xylene for about 5 minutes. When it became swollen, 2 cm of the membrane was carefully slipped over the tubing. After the solvent evaporated, the membrane shrank to form a tight fit. The connection point was sealed by silicone glue. The active length of the fiber was approximately 20 cm.

A Hewlett-Packard 5890 Series II gas chromatograph (Hewlett Packard Company, Avondale, PA, USA) equipped with a conventional flame ionization detector was used for analysis. A 30 m long DB-1 fused-silica open-tubular column from J and W Scientific (Folsom, CA, USA) was used. The column inner diameter was 0.25 mm, and the stationary phase thickness was 1.0 μm. Typical flow rates were between 2 and 6 ml/min and the oven temperature was 95°C.

The microtrap was made by packing a length of 0.52 mm I.D. silica-lined stainless steel tubing with 60 mesh (0.25 mm) Carbotrap C. This microtrap had a resistance of 0.1 Ω/cm and its length was 14 cm. The microtrap was connected to a variable power supply (20–50 V AC). A computer-controlled electric switch was used to control the interval between pulses and also the time for which the microtrap current was turned on. Power resistors were put in series with the microtrap to limit the current through it. More detail of the microtrap and its operation are presented elsewhere [15].

2.1. System operation

The aqueous sample was pumped through the membrane module using an HPLC pump (Altex, Model 110A). Nitrogen (stripping gas) flowed counter-current around the membrane fiber and carried the permeated VOCs to the microtrap. The microtrap was pulsed (or heated) at regular intervals, and corresponding to each pulse a chromatogram was obtained. Interval between pulses were anywhere from a few seconds to several minutes. In a typical operation the microtrap was heated with a 5–10 A current for a duration of 500 to 1500 ms. All transfer lines were heated to 100°C to prevent any condensation of VOCs.

3. Results and discussion

The operation of the analytical system is demonstrated in Fig. 2 where a water stream containing 87 ppb (μg/l) each of benzene, toluene and ethyl benzene was continuously monitored. The water flowed continuously through the membrane module. Microtrap pulses were made at fixed intervals of time, and corresponding to each injection a chromatogram of the three compounds was obtained. In this example, analysis was done every two minutes. Excellent reproducibility of peak height, peak shape as well as retention time was obtained. For twenty-one consecutive injections, the relatively standard deviations of peak area for benzene, toluene and ethyl benzene were 1.4%, 0.41% and 0.44% respectively. In fact the relative standard deviation was lower than that obtained by making direct injections using a conventional GC injection port (R.S.D. was 2%). This shows that not only the microtrap injections, but also the membrane extraction process was quite reproducible. The heating–cooling cycle of the microtrap is very short (less than 5 seconds) and it is capable of making injections every few seconds. How often injections can be made depends upon the time required for GC analysis. Hence, it is advantageous to reduce the separation time as much as possible.

As mentioned before, the microtrap acts as a sample concentrator. It accumulates VOCs during the interval between two pulses (referred to as a pulse interval). So, the longer the interval, the greater is the amount of VOCs accumulated and larger is the detector response to a microtrap pulse. A typical detector response as a function of pulse interval is presented in Fig. 3. It is observed that as the time period increases, the response of the microtrap increases linearly until a maximum value is reached beyond which the response stays constant. The microtrap response can not be indefinitely increased because the

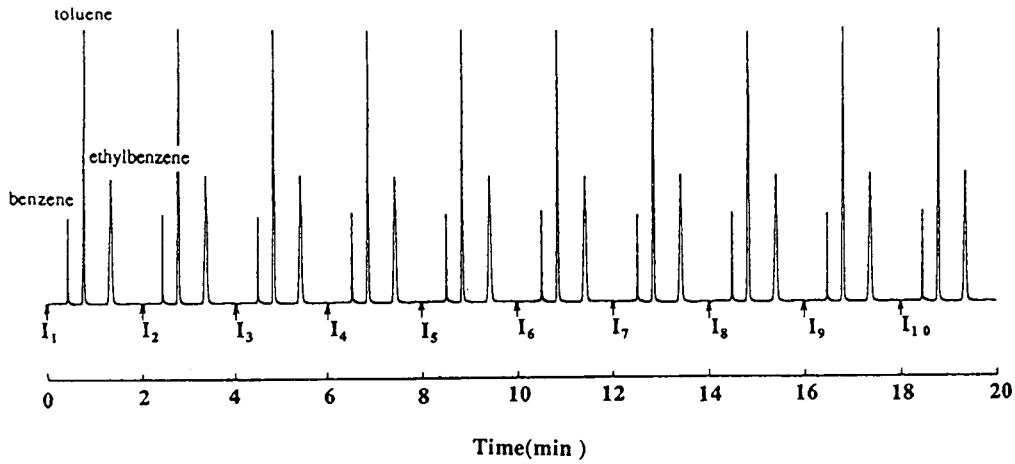

Fig. 2. Continuous monitoring of a water stream containing 87 ppb each of benzene, toluene and ethyl benzene. Microtrap pulses were made every two minutes at point I_1, I_2, I_3 . . . . Water flow rate was 1 ml/min, column temperature was 95°C, flow rate of stripping gas was 2 ml/min and temperature of membrane module was 80°C.

microtrap contains a small amount of adsorbent, and can retain the sample only for a short period of time before the sample breaks through. The analysis can be carried out quantitatively in the linear region or in the flat part of Fig. 3 [15].

3.1. Quantitative aspects of the analytical system

The calibration curves for several VOCs are presented in Fig. 4. The linear relationship between system response and concentration was observed in the low ppb to high ppm (mg/l) range. Detection limits (at signal to noise ratio of 3 [16]) for some VOCs is presented in Table 1. It is seen that this system showed low detection limits. For example, the detection limits for trichloroethane using this system was 0.28 ppb as compared to 30 ppb when a cryogenically cooled gas sampling value was used in another study [12]. The non-polar, hydrophobic molecules showed a detection limits in the low ppb levels, whereas the detection limit for the water soluble compounds such as acetone and ethanol was considerably higher.

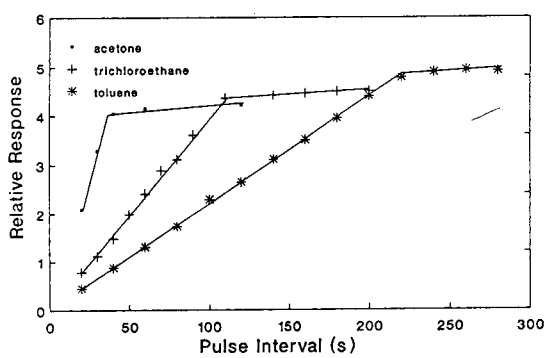

Fig. 3. Response of the analytical system as a function of interval between microtrap pulses. Water flow rate was 1 ml/min, flow rate of stripping gas was 5 ml/min, temperature of membrane module was 80°C.

The detection limit depends upon the extraction efficiency of the membrane as well as the preconcentration effect of the microtrap. By increasing the pulse interval, more analyte can be accumulated in the microtrap and consequently the detection limit can be lowered. The detection limits presented in Table 1 correspond to a pulse interval of 2 min. Detection limit could also be reduced by subambient cooling of the microtrap [15]. However, for a continuous monitoring device, subambient cooling is expensive and cumbersome, and was avoided in this application. It may be possible to further lower the detection limits by redesigning the membrane module with a longer hollow fiber or using

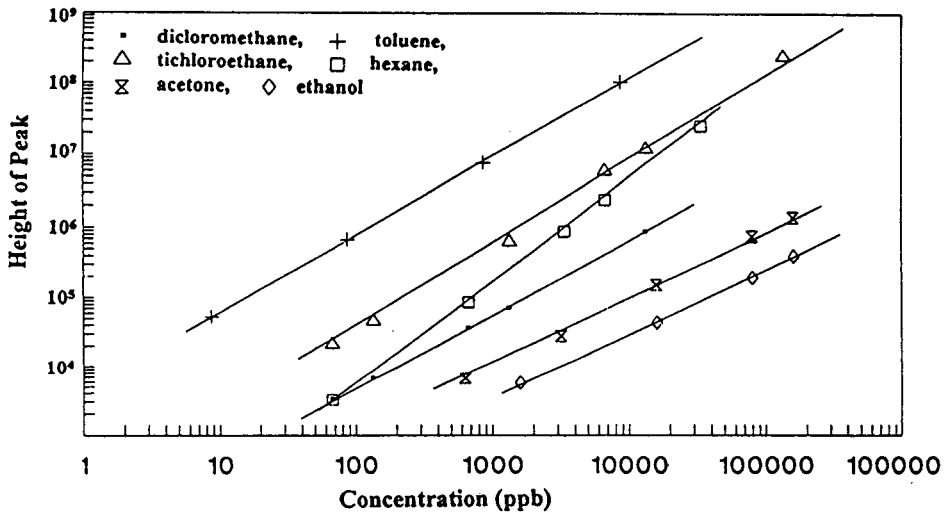

Fig. 4. Calibration curve for different VOCs. Water sample flow rate was 1 ml/min, pulse interval was 2 min, flow rate of stripping gas was 2 ml/min, membrane module was 80 C and column temperature was 70°C.

multiple hollow fibers so that higher extraction efficiency can be obtained.

The membrane extraction efficiency may be expressed as enrichment factor [4], E:

$$E = \frac{\text{mole fraction of analyte in stripping gas}}{\text{mole fraction of analyte in aqueous solution}}$$

The enrichment factor was experimentally determined by measuring the concentration of the VOCs at the inlet and the outlet of the membrane module and results are presented in Table 1. The enrichment factor was seen to vary between 4.1 and 65.1. As expected, the compounds with low enrichment factor have high detection limits, e.g., acetone and ethanol.

The membrane extraction process is analogous to liquid–liquid extraction and the partition coefficient of the VOCs between the membrane and aqueous phase determines the enrichment factor. Experimental values of the partition coefficient between the membrane and the aqueous phase are not available. So, the partition coefficients for these VOCs in the hexane–water

Table 1
Detection limits and enrichment factors for different VOCs

Compound	Detection limit (ppb) [a]	Enrichment factor [b]	Partition coefficient [17]	
			$\log P_{octanol}$	$\log P_{hexane}$
Toluene	0.042	65.1	2.11	2.85
Trichloroethane	0.28	61.8	2.31	NA [c]
Hexane	1.45	44.1	1.88	NA
Dichloromethane	7.75	42.4	1.68	NA
Acetone	61.1	7.5	−0.24	−0.92
Ethanol	212	4.1	−0.32	−2.26

The temperature of the membrane module was 80°C and the water flow rate was 1 ml/min.
[a] Pulse interval was 2 min.
[b] Water samples were analyzed by direct GC injection.
[c] NA = not available.

and octanol–water system [17] are listed in Table 1. Partition coefficient into the silicone membrane has been reported to be somewhat similar to the hexane–water system [5]. A correlation between enrichment factor and partition coefficient, and an inverse relation between partition coefficient and detection limits were seen. For example, acetone and ethanol have low partition coefficients, low enrichment factors, and high detection limits.

3.2. Optimization of membrane extraction conditions

To achieve high sensitivity it is desirable to transport as much of the VOCs as possible through the membrane into the GC. Two mechanisms control the transport of VOCs: (1) diffusion through the membrane; (2) mass transfer in the aqueous phase. The diffusion of VOCs through a membrane is governed by Fick's law of diffusion [18]. At steady state, the rate of diffusion per unit surface area per unit time is given as F:

$$F = -D\partial C/\partial X \quad (1)$$

where D is the diffusion coefficient of the VOCs in the polymeric membrane, and $\partial C/\partial X$ is the concentration gradient across the membrane. For a hollow fiber membrane:

$$\partial C/\partial X = (C - K_1 C_o)/L \quad (2)$$

where K_1 is the partition coefficient between the membrane and the aqueous phase, C_o is the concentration of VOCs in aqueous phase, C is the concentration of VOCs on outside surface of membrane and L is the membrane thickness.

When the flow rate of the stripping gas is high enough, C is close to zero. $K_1 C_o$ represents the concentration of the analyte on the inside membrane surface which is in contact with the aqueous sample. Under these conditions:

$$F = D\ K_1 C_o/L \quad (3)$$

According to this equation, F depends upon D and K_1 which in turn depend upon temperature. Thus, the temperature of the membrane module is an important factor which will effect the system response.

The flow rate of aqueous phase in the membrane is another important factor because the mass transfer in the aqueous phase depends largely upon it. The inorganic salt concentration (or ionic strength) and pH of the water sample are other parameters which can effect the system response.

Effect of flow rate

The effects of sample flow rate on the detector responses for dichloromethane and hexane at two different temperatures are shown in Fig. 5. As flow rate is increased, the system response increases because at higher flow rate there is more mixing at the water–membrane interface, and the formation of a boundary layer is reduced or eliminated. At higher flow rates, the rate limiting step is the mass transfer through the membrane rather than migration of the analyte through aqueous phase. Thus, increasing the flow rate beyond a certain value has negligible effect on system response.

For the components that permeate rapidly through the membrane, mass transfer in the aqueous phase is the rate limiting step. Mass transfer is better in a turbulent flow rather than in a laminar flow. Laminar flow turns turbulent at a Reynolds number between 2000 and 3000

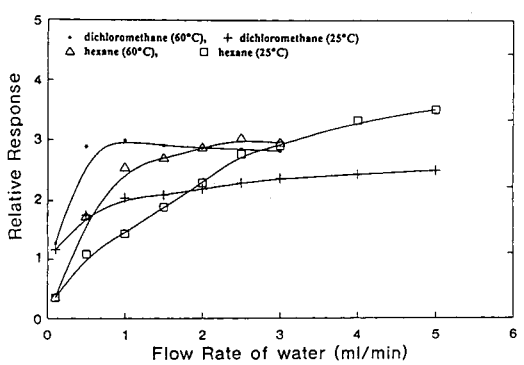

Fig. 5. Response of analytical system as a function of flow rate of water. Pulse interval was 2 min, flow rate of stripping gas was 2 ml/min and temperature of membrane module was 80°C.

[19]. The Reynolds number is calculated using the equation

$$N_{Re} = v\ d\ \rho/\mu \quad (4)$$

Here, d is the inner diameter of the membrane, v is the linear velocity of water stream, ρ is the density of the water stream, and μ is the viscosity of water stream. The membrane used here has an inner diameter of 0.012 in. and the N_{Re} reaches 2500 at a flow rate of 38 ml/min. At such a high flow rate, there is significant pressure drop across the narrow diameter hollow fiber. The silicone fibers are relatively delicate and are unable to withstand such pressure drops and can easily tear, especially at the connections. Another problem at high flow rate is that the residence time is short and only a small fraction of the analyte is extracted from the sample stream. To increase turbulence without increasing flow rate, the membrane tubing can be packed with glass beads [20]. However this method may increase the memory effect of the membrane module and will be addressed in future studies.

Effect of temperature

The effect of the water temperature on the system response is shown Fig. 6. It was seen that the responses initially increased with the increase in temperature. Beyond a temperature of 60°C for dichloromethane and 80°C for trichloroethane and chloroform, the responses decreased with increase in temperature. So, when response was plotted as a function of temperature the curve passed through a maximum point. The maximum point for all the compounds with the exception of acetone was in the temperature range studied here. The reason for such behavior is that permeability is a function of rate of diffusion (F) as well as the solubility of the analyte in the membrane [18,21]. The diffusion coefficient D increases with temperature and an Arrhenius type relationship exists:

$$D = D_o \exp(-E_d/RT) \quad (5)$$

where D_o is the diffusion coefficient at reference temperature, T is temperature and E_d is the activation energy for diffusion. However, solubility of the organic analyte in the membrane decreases with increase in temperature:

$$S = S_o \exp(-\Delta H/RT) \quad (6)$$

where ΔH is the apparent heat of solution, which has a negative value for organic liquid.

The initial increase of system response with increasing in temperature is due to the increased rate of diffusion. However, as temperature is further increased the decrease in solubility becomes the dominant factor and the system response begins to decrease.

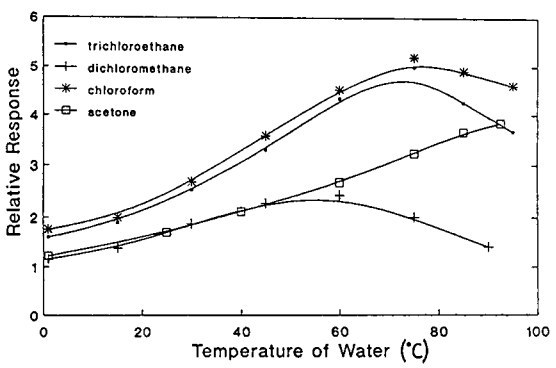

Fig. 6. Response of analytical system as a function of water temperature. Sample flow rate was 1 ml/min. Pulse interval was 2 min. Flow rate of stripping gas was 2 ml/min. Column temperature was 70°.

Effects of salinity

Environmental samples may contain inorganic ions such as Na^+, K^+, Cl^- etc. For example, in typical surface water and ground water, the total ionic strength may be of the order of 0.01 mol/l and 0.05 mol/l respectively, whereas in sea water the ionic concentration may be as high as 0.5 mol/l. The effect of ionic strength on the system response was studied in the concentration range of 0.0 to 4.0 mol/l using NaCl. The effect of salinity on ethanol, acetone, toluene and dichloromethane are shown in Fig. 7. In the low concentration range (0–0.4 mol/l), the response was unaffected by salt concentration. However, at higher concentrations (NaCl > 0.4 mol/l), the responses of toluene and dichloromethane de-

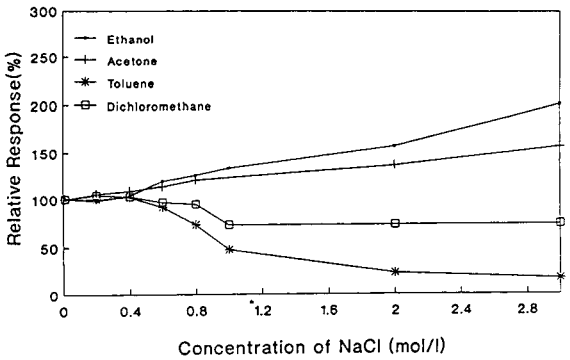

Fig. 7. Effect of ionic strength on system response for different VOCs. The sample response of zero ionic strength is considered 100%. The concentrations of toluene and dichloromethane were 1 ppm and the concentrations of acetone and ethanol 5 ppm.

creased with the increase of sodium chloride concentration, but the responses of acetone and ethanol increased with the increase of sodium chloride concentration. It seems that high ionic strength solutions, each component behaves differently. From a practical point of view, one seldom encounters ionic strength greater than 0.1 mol/l where the system response is not a function of ionic strength. At higher ionic strength recalibration of the system would be necessary.

Effect of pH

Usually the pH of environmental samples are in the range of 2.5 to 10.5. The response of two test compounds, toluene and ethanol, was studied in the pH range of 1.5 and 12.5. Both these compounds did not show any significant variation in response with pH. This is expected for most VOCs although pH may turn out to be an important factor for organic compounds that are acidic or basic [5].

4. Conclusion

The on-line membrane extraction microtrap system can be used to provide continuous, on-line monitoring of VOCs in water samples at ppb level. The microtrap is effective as an automatic, on-line, sample preconcentrator cum injector. As a result, the detection limits for most of VOCs were at the low ppb level. The detection limits for the water soluble, polar compounds was relatively higher than the nonpolar ones.

Acknowledgment

This research is partly supported by a grant from NSF/University Hazardous Substance Management Research Center at New Jersey Institute of Technology, Newark, NJ 07102.

References

[1] J.J. Ellington and C.D. Trusty, *J. High Res. Chromatogr. Chromatogr. Commun.*, 12 (1989) 470–473.
[2] B.C. Mcintosh, D.V' Vidrine and W.M. Doyle, *Am. Lab.*, Dec. (1991) 19–22.
[3] A. Lebovits, *Modern Plastics*, March (1966) 139.
[4] L.B. Westover, J.C. Tou and J.H. Mark, *Anal. Chem.*, 46(4) (1974) 568–571.
[5] R.G. Melcher, *Anal. Chim. Acta*, 214 (1988) 299–313.
[6] C.L. Arthur, L.M. Killam, S. Motlagh, M. Lim, D.W. Potter and J. Pawliszyn, *Environ. Sci. Technol.*, 26 (1992) 979–983.
[7] A.R.J. Andrews, A. Zlatkis, M.T. Tang, W. Zhang, and H. Shanfield, *Environ. Sci. Technol.*, 27 (1993) 1139–1145.
[8] J.A. Shoemaker, T.A. Bellar, J.W. Eichelberger and W.L. Budde, *J. Chromatogr. Sci.*, 31(7) (1993) 279–283.
[9] M.A. LaPack, J.C. Tou and C.G. Euke, *Anal. Chem.*, 62 (1990) 1265–1271.
[10] M.E. Bler and R.G. Cooks, *Anal. Chem.*, 59 (1987) 587–601.
[11] S.J. Bauer and R.G. Cooks, *Am. Lab.*, Oct. (1993) 36–51.
[12] K.F. Pratt and J. Pawliszyn, *Anal. Chem.*, 64 (1992) 2107–2110.
[13] R.G. Melcher and P.L. Morabito, *Anal. Chem.*, 62 (1990) 2183–2188.
[14] S. Mitra and J.B. Philips, *Anal. Instrument.*, 18(2) (1989) 127–145.
[15] S. Mitra and Y. Chen, *J. Chromatogr.*, 648 (1993) 415–421.
[16] D.A. Skoog and J.J. Leary, *Principles of Instrumental Analysis*, Saunders College Publishing, New York, 4th ed., 1992, Ch. 1, p. 7.
[17] A. Leo, C. Hansch and D. Elkins, *Chem. Rev.*, 71 (1971) 525.

[18] E. Baer, *Engineering Design for Plastics*, Robert E. Krieger Publishing Company, Huntington, NY, 1975, Chapter 9.
[19] R.B. Bird, W.E. Stewart and E.N. Lightfoot, *Transport Phenomena*, Wiley, 1974.
[20] T.S. Stevens, G.L. Jewett and R.A. Bredeweg, *Anal. Chem.*, 54 (1982) 1206–2106.
[21] R.M. Barrer, J.A. Barrie and N.K. Raman, *Polymer*, 3 (1962) 595–603.

ELSEVIER

Journal of Chromatography A, 688 (1994) 181–188

JOURNAL OF CHROMATOGRAPHY A

Determination of organic pollutants in small samples of groundwaters by liquid–liquid extraction and capillary gas chromatography

I. Harrison[a,*], R.U. Leader[a], J.J.W. Higgo[a], J.C. Tjell[b]

[a]*Fluid Processes Group, British Geological Survey, Kingsley Dunham Centre, Nottingham NG12 5GG, UK*

[b]*Institute of Environmental Science and Engineering, Technical University of Denmark, DK-2800 Lyngby, Denmark*

First received 22 June 1994

Abstract

A method is presented for the determination of 22 organic compounds in polluted groundwaters. The method includes liquid–liquid extraction of the base/neutral organics from small, alkaline groundwater samples, followed by derivatisation and liquid–liquid extraction of phenolic compounds after neutralisation. The extracts were analysed by capillary gas chromatography. Dual detection by flame ionisation and electron capture was used to reduce analysis time.

1. Introduction

The determination of organic pollutants in aqueous environmental samples is nowadays commonplace and numerous chromatographic methodologies have been established for this purpose, e.g. the US Environmental Protection Agency methods for drinking water (500 series) and municipal and industrial waste water (600 series). Typically, large volumes of water (ca. 1 l) are pre-concentrated by either purge-and-trap [1] or liquid–liquid extraction followed by concentration on a Kuderna–Danish apparatus [2]. Our experiments, into the organic degradative and sorptive processes occurring in different redox zones of the aquifers surrounding two landfill sites, generated only small aqueous samples (10 ml) containing up to 150 ppb (w/w) of individual organic compounds. In these experiments, a cocktail of organic compounds (see Table 1) mixed with the groundwater from a given site was pumped through undisturbed sediment isolated in stainless-steel microcosms [3,4]. Once loaded with the spiked groundwater the microcosms were left in situ and samples were withdrawn from time to time for analysis. The sample volume was constrained to 10 ml so that a reasonable number of samples could be taken from the limited volumes in the microcosms. This in turn meant that, in order to achieve a reasonable degree of pre-concentration, the volume of pentane used for liquid–liquid extraction had to be very small (100 μl) and an ad hoc device was designed to facilitate loading the syringe with the extracted sample.

The technique of rapid liquid–liquid extraction with pentane has already been critically evaluated [5]. In our study the samples withdrawn

* Corresponding author.

0021-9673/94/$07.00
SSDI 0021-9673(94)00902-3

Table 1
Boiling points, extraction efficiencies, water solubilities, log octanol–water partition coefficients, detection limits and relative response factors (R)

No.	Compound	B.p. (°C)	Extraction efficiency (%)	Solubility in water (ppm)	Log K_{ow}	Precision[a] (%)	Detection limit (ppb)	R
1	1,1,1-Trichloroethane	74.1	53	720	2.49	2.5 (ECD)	0.05	1.1[b]
2	Tetrachloromethane	76.5	56	800	2.83	4.5 (ECD)	0.01	4.2[b]
3	Benzene	80.1	30	1780	2.13	6.6 (FID)	1	0.99[c]
4	Trichloroethylene	87.0	58	1100	2.42	5.3 (ECD)	0.03	0.55[b]
–	BTCM (I.S.)	104.7	–	–	–	–	–	1.0[b]
5	Toluene	110.6	49	500	2.73	3.3 (FID)	1	1.0[c]
6	Tetrachloroethylene	121.0	65	150	3.40	1.8 (ECD)	0.015	1.9[b]
7	*o*-Xylene	144.4	53	175	3.12	2.2 (FID)	0.5	1.0[c]
8	1,1,2,2-Tetrachloroethane	146.2	–	2900	2.39	–	–	–
–	Cumene (I.S.)	159.2	–	–	–	–	–	1.0[c]
9	1,4-Dichlorobenzene	174.0	60	79	3.52	4.5 (FID)	1	0.47[c]
10	1,2-Dichlorobenzene	180.5	63	148	3.38	4.0 (FID)	1	0.49[c]
11	Phenol (Ester)	196.0	–	–	–	7.9 (FID)	1	–
12	Nitrobenzene	211.0	10	1900	1.85	4.0 (ECD)	2	0.26[b]
13	*o*-Cresol (ester)	–	–	–	–	4.9 (FID)	2	–
14	Naphthalene	218.0	73	30	3.30	6.1 (FID)	0.5	1.1[c]
–	2-Bromophenol (ester) (I.S.)	–	–	–	–	–	–	–
15	2,6-Dichlorophenol (ester)	–	–	–	–	6.9 (ECD)	1	–
16	2,4-Dichlorophenol (ester)	–	–	–	–	6.1 (ECD)	1	–
17	*o*-Nitrophenol (ester)	–	–	–	–	6.6 (ECD)	0.5	–
18	Biphenyl	255.9	75	7	3.90	2.2 (FID)	0.5	1.1[c]
19	*p*-Nitrophenol (ester)	–	–	–	–	5.3 (ECD)	0.5	–
	Hexadecane (I.S.)	287.0	–	–	–	–	–	–
20	Fluorenone	341.5	72	<1	3.58	5.8 (ECD)	0.05	–
21	Dibenzothiophene	333.0	102	<1	4.38	12.7 (FID)	0.5	0.95[c]
22	Pentachlorophenol (ester)	–	–	–	–	6.8 (ECD)	0.05	–
23	Phenanthrene	336.0	100	1	4.46	9.0 (FID)	0.5	1.1[c]

[a]Relative standard deviation ($n = 5$).
[b]Area relative to the area of BTCM (i.e. ECD).
[c]Area relative to the area of cumene (i.e. FID).

from the microcosms were preserved by being immediately made alkaline with sodium hydroxide [2]. In some groundwaters addition of NaOH produced turbid precipitates of metal hydroxides. These were found to interfere with the phase separation and were removed before proceeding. Centrifugation, in preference to filtration, was used to avoid loss of organics by sorption to filter media. Liquid–liquid extraction with pentane was performed on the clarified sample and the extract was analysed by capillary gas chromatography (GC) on a 5% phenylmethylpolysiloxane (DB-5) column. The phenolic constituents of the spiked groundwater were not extracted into the pentane because in aqueous alkaline medium they exist as ionic species (phenolates). Therefore, after GC analysis of the pentane extract, the alkaline aqueous phase was neutralised in order to liberate the phenols which were then selectively derivatised to their acetate esters with acetic anhydride. The esters were extracted into pentane–diethyl ether and determined using the same DB-5 column.

Our aim was to develop a simple and robust methodology that would allow the analysis of a large number of small samples, containing a wide range of organic compounds, in a short time. The method was found to produce reliable

results in terms of precision and detection limits —the technique and the instrumental set up were both simple and total analysis time was relatively short.

2. Experimental

The cocktail was produced by mixing together accurately weighed amounts (ca. 1 g each) of all the compounds in Table 1 except for phenanthrene, fluorenone and dibenzothiophene which, because of their low water solubilities, had their contribution to the mixture reduced to about 0.2 g each. For the liquid–liquid extraction of base/neutrals *n*-pentane, containing 4 ppm of each of the following internal standards; cumene (isopropylbenzene), hexadecane and bromotrichloromethane (BTCM), was used. The derivatisation of the phenols was performed using orthophosphoric acid, borax and acetic anhydride. For the extraction of the esterified phenols *n*-pentane, containing 1 ppm of 2-bromophenol as internal standard, and diethyl ether were used. All chemicals were pure (>99%) and obtained from Aldrich UK except for the pentane and the ether, which were glass-distilled GC grade, and obtained from Rathburns UK.

The determinations were made with a Pye Unicam PU 4400 gas chromatograph equipped with flame ionisation detection (FID) and ^{63}Ni electron-capture detection (ECD) systems, both maintained at 310°C. The volume of extract injected was 3 μl. The injector (250°C) was used in the splitless mode with a vent flow of 55 ml min^{-1} and it was held closed initially for 0.5 min.

A retention gap of deactivated silica tubing (5 m × 0.32 mm I.D.) was fitted before the DB-5.625 (J&W Scientific) capillary column (30 m × 0.32 mm I.D., 0.5 μm film thickness). A deactivated glass effluent splitter divided the column effluent into two streams. One stream was routed through a short length of PTE 5 (Supelco UK) capillary column (10 cm × 0.25 mm I.D., 0.25 μm film thickness) to the FID system and the other was directed through a longer length of deactivated silica tubing (2.5 m × 0.25 mm I.D.) to the ECD system. The helium carrier gas flow-rate was 2.6 ml min^{-1} (oven at 33°C). The make-up gas flow-rate to the FID system was 28 ml min^{-1} (helium) and that to the ECD system was 100 ml min^{-1} (nitrogen).

After an injection the oven was held at 33°C for 0.5 min, then raised at 0.2°C/min to 34°C and then at 15°C/min to 250°C. The chromatographic peaks were integrated using a Nelson 900 A/D interface and Nelson 2600 software (Perkin-Elmer UK). The same chromatographic conditions were used with either type of sample (base/neutral or phenolic esters) and a run was accomplished in 20 min.

Aqueous samples, taken in the field, were dispensed into 11-ml glass-stoppered test tubes (Quickfit MF24/1) each containing 50 μl of 3 *M* NaOH. The tubes were filled completely so that insertion of the stopper eliminated headspace. The samples, stored in ice were dispatched to the laboratory as quickly as possible. There the tubes were centrifuged and 10 ml of each supernatant transferred to a 10-ml graduated flask.

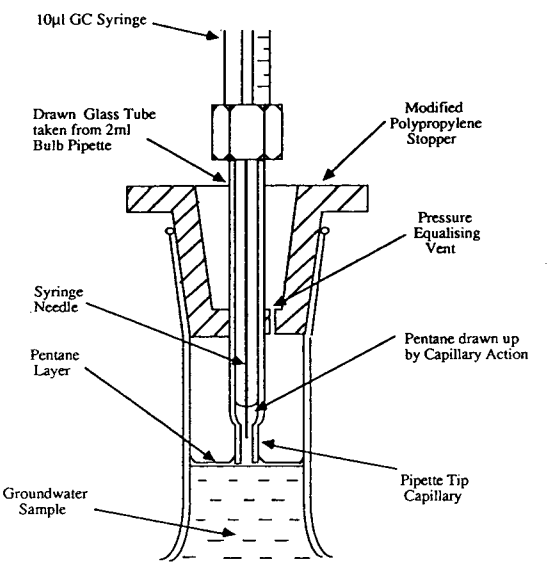

Fig. 1. GC syringe loading device. The glass tube of the device, which is a snug fit in the stopper, is gently lowered until the tip just contacts the thin layer of pentane extract which then rises by capillary action into the tip. The device is so constructed that when the GC syringe is fully inserted the needle's tip is completely immersed in the column of pentane extract.

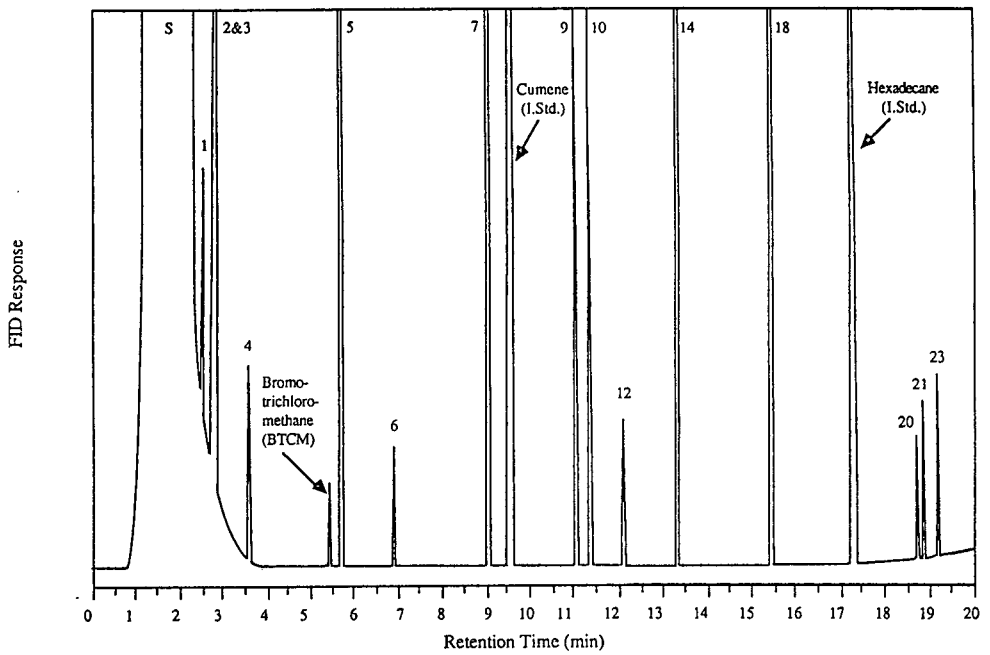

Fig. 2. Chromatogram (FID) of the pentane extract of spiked groundwater [1,1,2,2-tetrachloroethane (8) excluded]. Each component 37.5 ppb except for fluorenone (20), dibenzothiophene (21) and phenanthrene (23); these three each 7.5 ppb. I.Std. = Internal standard.

Using a 250-μl gas tight syringe, 100 μl of pentane containing internal standards was added to each flask. Glass stoppers, with PTFE sleeves, were inserted in the flasks and they were shaken vigorously for 1 min. This time had been found by experiment to be more than sufficient to establish extraction equilibrium. They were then stored bottom up in a refrigerator. To analyse, each sample was placed the right way up and allowed to stand for a few minutes to allow the phases to separate. The glass stopper was removed and replaced by an ad hoc device (Fig. 1) to facilitate loading of the GC syringe (Hamilton 701, 10 μl). A 3-μl volume of pentane extract was taken by syringe and injected into the gas chromatograph.

The remnants of the pentane layer, after the base/neutrals GC sample had been taken, were pipetted from the surface of the aqueous sample and discarded. Then 9 g of the aqueous sample were weighed out into a glass vial, provided with a PTFE-lined screw closure, ready for derivatisation and liquid–liquid extraction of the phenols as their acetate esters [6] which was carried out as follows: the pH was adjusted to 7.0 ± 0.2 with orthophosphoric acid and then 0.2 g borax were added and allowed to dissolve. From gas-tight GC syringes, 400 μl of 1 ppm 2-bromophenol in pentane and 40 μl of acetic anhydride were added. The vial was shaken on a mechanical shaker for 3 min before adding 400 μl of ether and shaking for a further 2 min. The organic layer was allowed to separate and 3 μl, taken by syringe, were injected onto the gas chromatograph.

3. Results and discussion

3.1. Separation

A slow injection technique was necessary with the system because of the small volume of the injection liner (76 mm × 2 mm I.D.). Fast injec-

tion of a 3-μl sample caused problems of solvent flooding and backflashing. Optimum performance was achieved when samples were injected at the rate of 3 μl in 10 s. Typical chromatograms of the pentane extract detected by FID and ECD are shown in Figs. 2 and 3, respectively. Those of the pentane–ether extract which contained the phenolic compounds are shown in Figs. 4 and 5. The peaks are numbered as in Table 1 and are referred to in the text by their numbers in parentheses.

The organic components of the spiked groundwaters eluted roughly in order of their boiling points [7,8] as expected on a relatively non-polar stationary phase like DB-5. Some low-boiling components appeared on the solvent tail (FID) viz. 1,1,1-trichloroethane (1), tetrachloromethane (2) and benzene (3). This did not matter for the two chlorinated aliphatics because they gave clear ECD peaks. For benzene the precision did not seem greatly affected even though its quantitation was complicated by the coelution of tetrachloromethane (a coelution compensation factor was derived by comparing the FID and ECD responses of tetrachloromethane). Cumene and hexadecane were used as internal standards for FID and since peaks for neither appeared in any of the groundwater blanks, variations in their area ratio could be used to warn of possible interference. One of the compounds, 1,1,2,2-tetrachloroethane (8), used initially in the cocktail was later excluded, because it was found to undergo rapid dehydrohalogenation to trichloroethylene (4) in alkaline aqueous medium. Its instability in neutral aqueous media has been noted by other workers [9,10].

3.2. Extraction efficiency

The extraction combines preconcentration with the transfer of the base/neutrals to the pentane phase. The transfer of low concentrations of components to small volumes of solvent has been shown to produce effects not expected from the known partition coefficients [5] which

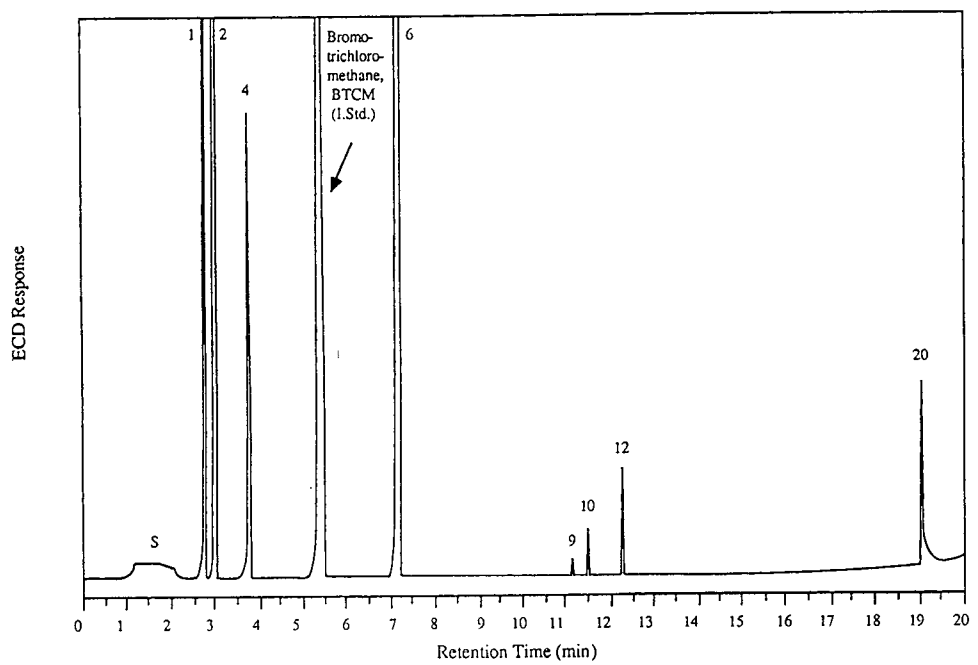

Fig. 3. Chromatogram (ECD) of the pentane extract of spiked groundwater [1,1,2,2-tetrachloroethane (8) excluded]. Each component 37.5 ppb except for fluorenone (20), dibenzothiophene (21) and phenanthrene (23); these three each 7.5 ppb.

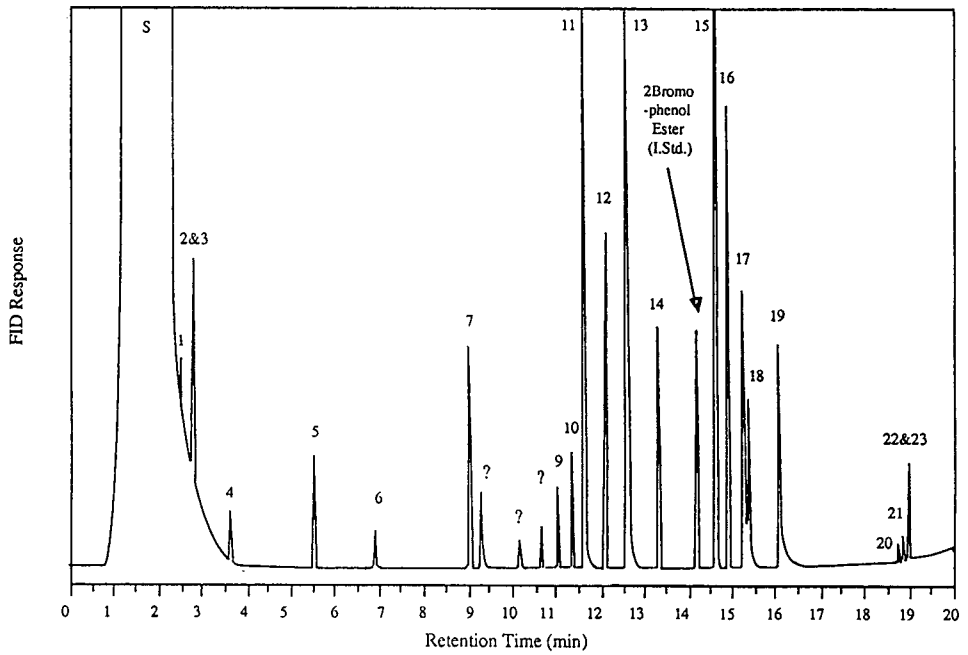

Fig. 4. Chromatogram (FID) of the pentane–ether extract of spiked groundwater [1,1,2,2-tetrachloroethane (8) excluded] following neutralisation and esterification of the aqueous phase remaining after initial pentane extraction. Each phenol 150 ppb. Peaks labelled "?" attributed to impurities and reaction products from the esterification. Note peaks due to re-extraction of base/neutrals remaining after pentane extraction.

influence the degree of preconcentration. Nevertheless, to some extent the observed extraction efficiencies correlate with the water solubility and K_{ow}, the octanol–water partition coefficient [11] (see Table 1). The calculation of extraction efficiency, which was based on comparing the response factors of the pure components in pentane with those obtained from extracted aqueous solutions, was not extended to the phenolic esters as only a few of the requisite acetates are available commercially. The remainder would require laboratory synthesis and purification [12] in order to obtain their extraction efficiencies.

3.3. Precision and detection limits

The precision (relative standard deviation, R.S.D.) was determined by analysing a spiked groundwater sample five times and was found to range from 1.8 to 12.7%. The values for each compound are shown in Table 1. Calibration curves, for compounds determined by FID, were all linear with correlation coefficients of 0.996 to 1.000. Calibration curves, for compounds determined by ECD were all non-linear.

The detection limits defined refer to the minimum concentrations of compounds in spiked groundwater that give clearly defined peaks (signal-to-noise ratio ca. 4). Lower levels could have been achieved by ECD by increasing the detector current level on the electron-capture amplifier. This, however, would have led to even greater calibration non-linearity, as a result of increased detector overload at high concentrations. The ECD sensitivity was, therefore, set at a compromise value appropriate to the range of concentrations of compounds encountered in the degradation experiments.

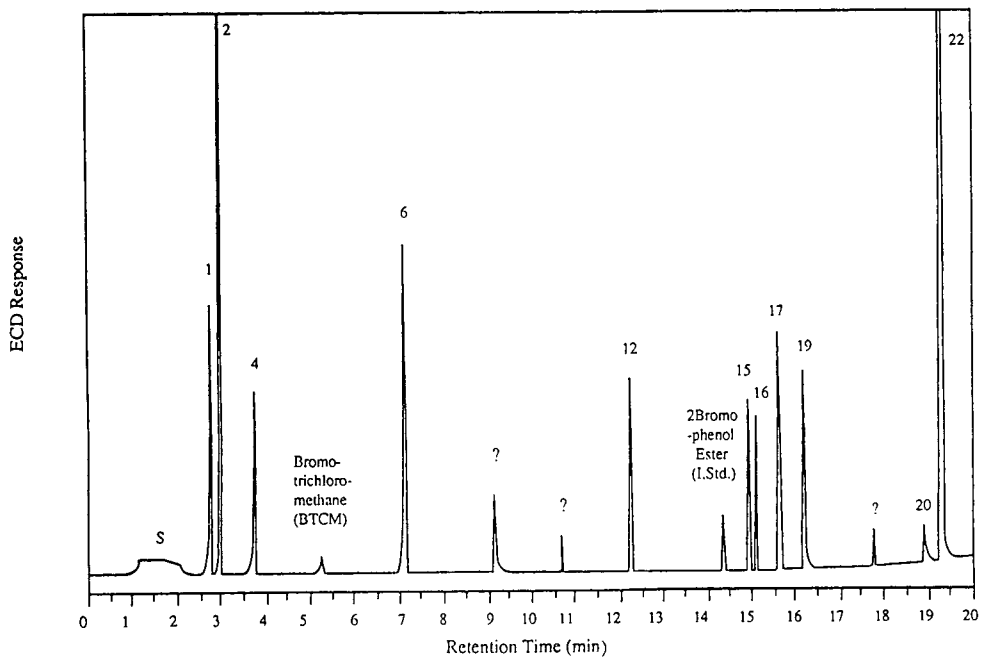

Fig. 5. Chromatogram (ECD) of the pentane–ether extract of spiked groundwater [1,1,2,2-tetrachloroethane (8) excluded] following neutralisation and esterification of the aqueous phase remaining after initial pentane extraction. Each phenol 150 ppb. Peaks labelled "?" attributed to impurities and reaction products from the esterification. Note peaks due to re-extraction of base/neutrals remaining after pentane extraction.

3.4. Sample stability studies and the effect of the precipitate

Experiments (using 50-ml samples and 500 μl pentane) showed that if the clarified samples were stored inverted and refrigerated after shaking with pentane they could be regarded as relatively stable. Thus plots of concentration against time over a 105-day period were smooth showing a slight downward trend corresponding to some loss of analytes (typically ca. 3%). There were, however, much greater variations in the response factors for the components of the pentane extract if the hydroxide precipitate was not removed. Possibly, random fluctuations in the amount of precipitate at the interface caused the poor reproducibility. The values obtained for the clarified sample were slightly lower than for samples containing precipitate, indicating some sorption to the precipitate, but the effect was reproducible and was included in the calculation of extraction efficiency.

Conversely, the esters of the phenols were found to be unstable in their aqueous ether–pentane matrix. Once derivatisation/extraction had been performed the ester sample needed to be analysed as soon as possible. Even when stored in a refrigerator there was a significant loss of analytes after only 12 h. However, storage of the alkaline groundwater (containing the unesterified phenols in their ionic form) for 14 days in a refrigerator resulted in no discernible loss of analytes. Accordingly, derivatisation, extraction and analysis were always carried out on the same day.

3.5. Application

The method described was formulated specifically for the analysis of organic compounds

containing a wide range of functional groups. It was designed to operate with small volumes of aqueous sample and the determination did not require sophisticated apparatus or instrumentation. A simple base/neutrals liquid–liquid extraction was first performed on spiked alkaline groundwater followed by derivatisation/extraction of the remaining aqueous phase to determine phenols. The method, successfully employed to analyse over 2000 samples, has proved to be reliable and should, in principle, be applicable to most situations where only small volumes of sample are available. Analysis time is short permitting a relatively high throughput of samples. Storage of the pentane extracts, inverted in a refrigerator, is permissible for short periods. The alkaline aqueous phase remaining, after discarding the pentane extract, may be stored similarly. Once derivatised however, the ester samples require prompt analysis.

Acknowledgements

We thank Clare Hughes and Dick Nicholson, of the Analytical Geochemistry Group at the British Geological Survey, for making available the GC system, and for their assistance. Funding for this work was provided by the Department of the Environment and the Commission of the European Communities. The results will be used in the formulation of Government Policy but do not necessarily represent that policy. This paper is published with the permission of the Director of the British Geological Survey (NERC).

References

[1] T.A. Bellar and J.J. Lichtenberg, *J. Am. Water Works Assoc.*, 66 (1974) 739-744.
[2] *US Environmental Protection Agency Method 625; Fed. Reg.*, 44, No. 233 (1979) 69 540–69 544.
[3] J.J.W. Higgo, P.H. Nielsen, T.H. Christensen, M.P. Bannon, I. Harrison, R.U. Leader and G.M. Williams, *Environ. Geol.*, (1994) submitted for publication.
[4] P.E. Holm, P.H. Nielsen, H.-J. Albrechtsen and T.H. Christensen, *Appl. Environ. Microbiol.*, 58 (1992) 3020–3026.
[5] K. Grob, K. Grob, Jr. and G. Grob, *J. Chromatogr.*, 106 (1975) 299–315.
[6] W. Krijgsman and C.G. van der Kamp, *J. Chromatogr.*, 131 (1977) 412–416.
[7] R.C. Weast, M.J. Astle and W.H. Beyer (Editors), *CRC Handbook of Chemistry and Physics*, CRC Press, Boca Raton, FL, 67th ed., 1986.
[8] K. Verschueren, *Handbook of Environmental Data on Organic Chemicals*, Van Nostrand Reinhold, New York, 2nd ed., 1983.
[9] M.P. Maskarinec, L.H. Johnson and C.K. Bayne, *J. Assoc. Off. Anal. Chem.*, 72 (1989) 823–827.
[10] R. Otsen and O.T. Williams, *J. Chromatogr.*, 212 (1981) 187–197.
[11] C. Hansch and A. Leo, *Medchem Project Issue No. 26*, Pomona College, Claremont, CA, 1985.
[12] A.S.Y. Chau and J.A. Coburn, *J. Assoc. Off. Anal. Chem.*, 57 (1974) 389–393.

ELSEVIER

Journal of Chromatography A, 688 (1994) 189–199

JOURNAL OF CHROMATOGRAPHY A

Determination of benzene, aniline and nitrobenzene in workplace air: a comparison of active and passive sampling

S.F. Patil[a,*], S.T. Lonkar[b]

[a]*Department of Chemistry and School of Environmental Sciences, University of Poona, Pune 411007, India*
[b]*Hindustan Organic Chemicals Ltd., Rasayani 410207, India*

First received 1 July 1994; revised manuscript received 10 August 1994

Abstract

There have been numerous investigations on methods for assessing the relative performance of pumped and diffusive sampling techniques for the determination of airborne contaminants. Diffusive sampling is a convenient and cost-effective analytical tool for measuring exposure to chemical hazards in air and has been available as a replacement for pumped sampling for around 20 years. In spite of the considerable amount of work put into their evaluation, diffusive samplers have only been partially successful in replacing pumps. Generally, evaluation studies on diffusive samplers have been concentrated primarily on their accuracy at high concentrations, neglecting the vital aspect of their applicability at lower concentrations (below mg/m^3) in the field. The present evaluation demonstrates that a Perkin-Elmer-type sampling tube, filled with Tenax TA and operated diffusively, provides a means of sampling that is sufficiently sensitive to measure benzene, aniline and nitrobenzene at concentrations as low as 0.10 mg/m^3. This method gives precise and accurate results that are well within the National Institute for Occupational Safety and Health (NIOSH) acceptability criteria of ±25% accuracy. No correlation is observed between active and diffusive sampling at concentration levels below 0.01 mg/m^3. Retention volumes, thermal desorption recoveries, sampling efficiencies, diffusive uptake rates and concentration effect on sampling performance were investigated. There are no previous reports, on determination of aniline and nitrobenzene in air by diffusive sampling and thermal desorption.

1. Introduction

The ability to achieve a safe workplace depends largely upon proper sampling techniques for the representative assessment of workplace exposure. Sampling is an integral and vital element of industrial hygiene in air pollution monitoring. Hence the sampling devices and analytical methods employed must be sufficiently sensitive and accurate to allow reasonable interpretation of the results, which are usually presented as time-weighted average exposure over a given period. The basic sampling techniques for the collection of substances in air using solid sorbents are active and passive sampling. The more popular and traditional active sampling utilizes volumetric pumps to draw a known volume of air through a bed of solid sorbent. The passive sampling techniques utilizes diffusion of compounds into a chamber containing solid sorbent. The diffusion of organic vapours

* Corresponding author.

0021-9673/94/$07.00
SSDI 0021-9673(94)00762-4

from the environment to the sorbent occurs according to Fick's first law of diffusion [1].

The traditional preconcentration of organic vapours used in most National Institute for Occupational Safety and Health (NIOSH) procedures utilizes charcoal or silica gel as the sorbent, followed by solvent extraction and gas chromatographic (GC) analysis [2]. A newer technique uses a porous polymer adsorbent and thermal desorption with cryofocusing into the gas chromatograph [3–8]. This technique offers better limits of detection than solvent extraction because the whole sample is injected into the chromatographic system as a narrow band, and it has become increasingly popular [9–14]. Further, this technique is perfectly amenable to complete automation of the analysis, which may become an important feature when a large number of samples have to be analysed and processed [15].

Some tube-type monitors can be used in the active or in the diffusive (passive) mode [16]. In workplace monitoring, it is highly desirable that each worker is monitored for his or her individual exposure in addition to measuring the general level of toxic vapours in workplace air. The drawback with pumped sampling, however, is the high cost involved in mass personal screening projects. Further, good-quality volumetric pumps are required for each person or for each location involved. It is also necessary to have spare pumps in case of breakdown and the pumps require calibration and servicing at regular intervals. Hence, in recent years, a cost-effective and simple sampling system has been developed in the form of "diffusive" (passive) samplers. Diffusive samplers are inexpensive, light, reusable and safe for use in flammable atmospheres.

Methods of comparing the performances of pumped and diffusive sampling have been widely investigated [17–21]. To date, there has been a mixed reception amongst occupational hygienists as to the acceptability and applicability of commercially available diffusive monitors. In order to allow the determination of air composition from the amount of analyte adsorbed, the exposure has to be done in a way that ensures a defined, diffusion-limited step that controls the rate of uptake from the atmosphere. The sampling rate of such diffusive samplers is low, owing to the slow rate-determining diffusion step. Consequently, at low atmospheric concentrations, the amount of sample is too small to analyse. To overcome this limitation, the exposure periods should be extremely long [22]. These problems of diffusive sampling have to be considered before taking into account their advantages such as simplicity of use and low cost.

An overview of several types of passive samplers and their performance was given by Brown and co-workers [23,24]. The important features of their studies include a diffusive sampler evaluation protocol (HSE protocol), effects of exposure variables on sampler performance and a method for comparison of the diffusive sampler with an independent pumped method. Most of the applications of passive samplers are in the monitoring of indoor pollution at fairly high levels (mg/m^3). There have been few measurements of organic pollutants below mg/m^3 levels by the diffusive sampling technique.

The organic pollutants benzene, aniline and nitrobenzene are known poisons with acute and chronic effects. The inhalation and absorption through the skin of these chemicals may lead to cyanosis with formation of methaemoglobin [25]. Benzene is also a known carcinogen, causing aplastic anaemia and leukaemia [26].

Nitrobenzene and aniline are the basic raw materials widely used in the polymer, rubber, agricultural and dye industries. It is estimated that nearly $3.5 \cdot 10^9$ lbs. (1 lb. = 0.4536 kg) of aniline and $2.5 \cdot 10^9$ lbs. of nitrobenzene are produced currently worldwide. It is interesting that about 300 chemical products are currently manufactured from aniline alone, involving thousands of workers exposed to these chemicals.

For the determination of aniline and nitrobenzene in air, there are validated methods (NIOSH and OSHA) using adsorption and solvent desorption [27,28]. Recently, we have reported the determination of trace levels (mg/m^3) of these pollutants at fixed locations in the workplace by adsorption and thermal desorption techniques making use of active sampling meth-

ods [29]. Many of the published assessments of passive samplers are from laboratory trials making use of exposure chambers. Such trials are a useful preliminary step in the evaluation of a new technique, but can in no way be considered a sufficient validation of a personal monitoring method, because it does not reproduce the conditions and variables that occur in real field use [30]. The aim of this study was to extend this work to personal monitoring by assessing the accuracy of the passive sampling technique in comparison with active sampling.

2. Experimental

2.1. Chemicals

Benzene, aniline and nitrobenzene were of analytical-reagent grade from Fluka (Buchs, Switzerland). Methanol used as a solvent was of analytical-reagent grade from S.D. Fine Chemicals (Bombay, India). Tenax TA of 60–80 mesh (180–250 μm) was obtained form Ohio Valley Specialty Chemicals (Marietta, OH, USA).

2.2. Apparatus

A Perkin-Elmer gas chromatograph equipped with an automatic thermal desorption system (ATD-50) was used. The ATD-50 was coupled with the heated transfer capillary to the gas chromatograph. GC analysis was carried out with a flame ionization detector and GP-100 printer–plotter. Stainless-steel sample tubes (Perkin-Elmer) 89 mm × 5 mm I.D. with stainless-steel wire gauges on both ends to hold the adsorbent and having metal sealing caps on both side for storage were used. During the determination of laboratory uptake rates and workplace air sampling, diffusion caps of 50-μm pore size, 0.2 cm^2 area and 1.5 cm path length were used on one side of tubes. The storage caps were replaced with analytical end-caps during analysis.

2.3. Determination of retention volumes

A glass chromatographic column (1 m × 2 mm I.D.) was packed with a known mass of Tenax TA (60–80 mesh). After packing, the column was conditioned at 25°C for 45 min. Thereafter, the temperature was increased at 2°C/min to a final temperature of 300°C, which was maintained for 24 h with a nitrogen flow of 20 cm^3/min. After conditioning of the column, a standard solution of benzene, aniline and nitrobenzene were injected separately at different column temperatures with a nitrogen flow-rate of 20 cm^3/min. The retention volumes were recorded along with the absolute column temperature.

2.4. Calibration of method by GC

Stock standard solutions (1%) of benzene, aniline and nitrobenzene were prepared in methanol. Working standard solutions to cover the range of interest (0.01–10 mg/cm^3) were prepared by serial dilution of the stock standard solution with the methanol. A 1-mm^3 volume of each standard solution was injected on to the GC column under the following optimum conditions: column, stainless steel (2.25 m × 2 mm I.D.); column packing, Tenax TA (60–80 mesh); injection port temperature, 250°C; flame ionization detector temperature, 290°C; oven temperature, 185°C for 1 min, then increased at 30°C min to 240°C, held for 6 min; carrier gas (nitrogen) flow-rate, 30 cm^3/min; and chart speed, 5 mm/min.

2.5. Thermal desorption recovery

Tenax TA (0.3 g) of 60–80 mesh was used to fill sample tubes, which were then conditioned under a flow of nitrogen (20 cm^3/min) at 300°C overnight in a specially made laboratory oven (Skylab, India). The conditioned sample tubes were fitted into the GC injection port maintained at 250°C with a nitrogen flow-rate of 20 cm^3/min. A set of five tubes were spiked with 1 mm^3 of each standard solution (0.01–10 mg/cm^3) at room temperature. The spiked tubes were disconnected after 2 min and thermally desorbed under the following optimum desorption conditions: desorption temperature, 250°C; desorption time, 10 min; transfer line temperature,

150°C; cold trap low, −30°C; cold trap high, 300°C; and cold trap adsorbent, Tenax TA (60–80 mesh). The analyses were performed using the optimized GC conditions used for calibration of the method.

2.6. Generation of test atmosphere

Test atmospheres for benzene, aniline and nitrobenzene were generated in the concentration range 0.12–8.34 mg/m^3 as described [31]. The test substance was fed as a liquid by means of an HPLC pump (880 PU, Jasco, Tokyo, Japan) and diluted with air stream with help of mass flow controllers (Porter Instrument, Hatfield, PA, USA). Provisions were made for water injection into the system to obtain atmospheres of controlled relative humidity. The air stream after appropriate dilution and thorough mixing was fed into the exposure chamber consisting of a 5-dm^3 glass vessel with an air-tight lid. The concentration in the exposure chamber was monitored at 30-min intervals using Tenax sampling tubes and were analysed by GC for control purposes.

2.7. Efficiency of active sampling

The efficiency of the active sampler was determined by drawing samples of test atmospheres through three samplers at a flow-rate of 20 cm^3/min for 2–8 h simultaneously, using precalibrated pumps (SKC, USA). During the sampling, the relative humidity was maintained at 50 and 90%, which was achieved by mixing dry air with the air that had been bubbled through deionized water. The exposure chamber was provided with two outlets for sampling and a third outlet was left in water to maintain the atmospheric pressure in the exposure chamber during sampling. Different concentrations were obtained by varing the flow-rate of the dilution air with the help of a mass flow controller.

2.8. Determination of laboratory uptake rate

After independent validation of the active sampling method, a set of three passive samplers with diffusive caps were exposed to test atmospheres for the determination of passive sampling rates. Samples were collected in the concentration ranges 0.12–8.34, 0.11–7.16 and 0.098–4.56 mg/m^3 for benzene, aniline and nitrobenzene, respectively, for 300 min. During the sampling, the relative humidity in the exposure chamber was maintained at 50 and 90%. The concentration in the exposure chamber was directly monitored by GC and was also checked by drawing sample actively over a Tenax TA sampling tube at a rate of 20 cm^3 min for 2–8 h for control purposes.

After the exposure, passive sampling tubes were analysed by GC with the thermal desorption system under the conditions specified above. Diffusive uptake rates for each compound were calculated as follows.

$$\text{uptake rate (cm}^3\text{/min)} = \frac{\text{mass of compound on diffusive tube (ng)}}{\text{concentration in exposure} \times \text{exposure time (min)}}$$

2.9. Workplace air sample analysis

Air samples were collected in chemical plants involving the processes of nitration of benzene to nitrobenzene and the reduction of nitrobenzene to aniline. When selecting the locations, emphasis was placed on the sources of potential exposure, such as manholes, drains, sampling points and the control room where the employee might be exposed to the process chemicals during the duty hours. Sampling tubes containing 0.3 g of Tenax TA of 60–80 mesh, conditioned as mentioned earlier, were used in the passive mode for sampling at each location. Samples were collected for 2–8 h in the passive mode. For the comparison of passive and active sampling results, a few sets of samples were also collected in the active mode at a distance of 10 cm from the passive sampling sets with the help of precalibrated pumps. The humidity and temperature of the workplace air during the period of investigation were found to vary between 50 and 90% and 20 and 40°C, respectively.

During thermal desorption and GC analysis of samples, the diffusion caps were replaced with

an analytical end-caps and the sampling tubes were placed on the turntable of the thermal desorption system for analysis. The tubes were thermally desorbed and analysed using the optimized conditions of thermal desorption and GC. The concentrations for the compounds of interest were determined as follows:

$$C \text{ (passive)} \ (\text{mg/m}^3) = \frac{\text{mass of compound found on tube (ng)}}{\text{uptake rate } (\text{cm}^3/\text{min}) \times \text{sampling time (min)}}$$

3. Results and discussion

3.1. Retention volumes

The retention volumes of each compound were recorded at different temperatures. The logarithm of the specific retention volume was plotted against the reciprocal of the absolute column temperature, which gave a linear relationship. The retention volumes of benzene, aniline and nitrobenzene were determined at 20°C and found to be 57, 2208 and 7331 dm^3/g, respectively.

3.2. Calibration of method by GC

The calibration graph for each analyte was obtained by plotting average peak area against known concentrations of the compounds injected. A linear graph passing through the origin was obtained for the investigated concentration range of 0.01–10.00 mg/cm^3 for each analyte. The pooled accuracy of the method was found to be better than 100% with relative standard deviations of 0.72–4.21, 0.95–7.14 and 0.94–7.5% for benzene, aniline and nitrobenzene, respectively. A regression coefficient of 0.999 was found for all the chemicals.

3.3. Thermal desorption recovery

The thermal desorption recovery of benzene, aniline and nitrobenzene on solid sorbent tubes packed with Tenax TA (60–80 mesh) was investigated at various concentrations. The tubes were spiked with different concentrations of standard solutions. After the spiking, each tube was connected to the pump and exposed to different relative humidities for 2–6 h in order to check for potential losses during field sampling. The thermal desorption recovery results are given in Table 1. The results indicate nearly quantitative recoveries of all the analytes at all levels of spiking in sample tubes. However, only at lower concentrations of spiking was a positive bias of up to 15% observed. This indicates that the adsorption of substances from the calibration mixture and subsequent thermal desorption were complete under the conditions used. The charged tubes can be stored at room temperature for 5 days with no significant change in recovery. The recoveries were almost complete within the relative standard deviation of the whole method (0.80–12%). This indicates that relative humidity has no effect on sampling over Tenax TA under the specified experimental conditions. Similar observations have been reported previously [3,32].

3.4. Sampling efficiency

The sampling efficiency for different concentrations of benzene, aniline and nitrobenzene was determined by analysing the sampling tubes exposed to known concentrations of test atmosphere. The results for the sampling efficiency with relative standard deviations are given in Table 2. Neither the concentration nor the relative humidity seems to affect seriously the sampling efficiency at a sampling rate of 20 cm^3/min. Three parallel samplings at a flow-rate of 20 cm^3/min were performed at 50 and 90% relative humidity. The overall sampling efficiency at the two relative humidities was found to be more than 98%, showing complete adsorption and thermal desorption of benzene, aniline and nitrobenzene from Tenax TA sampling tubes.

3.5. Laboratory uptake rate

The uptake rates for different concentrations of benzene, aniline and nitrobenzene were de-

Table 1
Thermal desorption recovery on Tenax TA (60–80 mesh)

Benzene		Aniline		Nitrobenzene	
Spiked	Recovery	Spiked	Recovery	Spiked	Recovery
0.010	0.011(110) [0.001]	0.010	0.011(114) [0.001]	0.011	0.012(114) [0.001]
0.040	0.041(103) [0.003]	0.040	0.048(115) [0.004]	0.040	0.041(102) [0.005]
0.400	0.411(103) [0.009]	0.404	0.382(95) [0.015]	0.403	0.401(100) [0.015]
2.000	2.033(102) [0.041]	2.020	1.849(92) [0.046]	2.013	1.936(96) [0.048]
3.600	3.644(101) [0.03]	3.636	3.646(100) [0.045]	3.623	3.698(102) [0.035]
5.200	5.237(101) [0.028]	5.252	5.237(100) [0.105]	5.239	5.248(100) [0.117]
8.000	7.907(99) [0.063]	8.080	8.012(99) [0.083]	8.052	8.060(100) [0.099]
10.000	9.867(99) [0.091]	10.100	10.243(101) [0.109]	10.065	10.064(100) [0.129]

Each value is average of five independent measurements (μg) with the recovery (%) in parentheses and the standard deviation (μg) in square brackets.

termined by analysing the passive sampling tubes exposed to known concentrations of test atmosphere. The results for passive sampling uptake rates for benzene, aniline and nitrobenzene are presented in Table 3 with standard deviations. The accuracy and precision of the uptake rate determinations were found to be excellent. In laboratory trials, the accuracy and precision of passive sampler were found to be better than those of the pumped sampler. A similar observation has been reported previously [33]. The overall precision of the uptake rate determi-

Table 2
Sampling efficiency of Tenax TA sorbent tube in active mode for different concentrations and relative humidity

Analyte	Test atmosphere concentration (mg/m^3)	Concentration found (mg/m^3)	Sampling volume (dm^3)	Sampling efficiency (%)	Precision (R.S.D.) (%)	Standard deviation (mg/m^3)
Benzene	0.120	0.126	5	105	2.38	0.003
	1.363	1.409	7.5	103	3.69	0.052
	8.347	8.221	8	99	2.74	0.226
Aniline	0.110	0.119	10	105	5.04	0.006
	1.481	1.444	9	98	3.04	0.044
	7.167	7.079	8	99	2.51	0.178
Nitrobenzene	0.098	0.103	8	105	7.77	0.008
	2.324	2.398	9	103	4.50	0.108
	4.563	4.489	10	98	3.54	0.159

Average of 4–6 determinations at 50 and 90% relative humidity.

Table 3
Laboratory determination of uptake rate in cm/min for different concentrations and relative humidity

Analyte	Test atmosphere concentration (mg/m^3)	Mass of analyte on diffusion tube (ng)	Uptake rate (cm^3/min)	Standard deviation (cm^3/min)	Effective uptake rate (cm^3/min)
Benzene	0.120	34	0.94	0.03	0.909
	1.363	373	0.911	0.018	
	8.347	2201	0.878	0.018	
Aniline	0.110	28	0.858	0.046	0.852
	1.481	379	0.853	0.020	
	7.167	1820	0.846	0.014	
Nitrobenzene	0.098	27	0.918	0.034	0.881
	2.324	601	0.862	0.010	
	4.563	1183	0.864	0.015	

Average of five independent measurements.

Table 4
Results of workplace air sample analyses for 5–8 h

Sample No.	Concentration (mg/m^3)					
	Passive sampling			Active sampling		
	Benzene	Aniline	Nitro-benzene	Benzene	Aniline	Nitro-benzene
1	0.100 (0.133)	0.384 (0.043)	0.311 (0.146)	0.040 (0.001)	0.157 (0.110)	0.124 (0.005)
2	0.030 (0.005)	0.046 (0.011)	0.154 (0.034)	0.028 (0.008)	0.074 (0.003)	0.102 (0.017)
3	0.026 (0.002)	0.245 (0.010)	0.041 (0.007)	0.043 (0.004)	0.265 (0.007)	0.021 (0.003)
4	0.027 (0.001)	0.669 (0.076)	0.045 (0.001)	0.012 (0.001)	0.738 (0.064)	0.031 (0.003)
5	0.066 (0.053)	0.229 (0.173)	0.122 (0.102)	0.018 (0.0004)	0.270 (0.013)	0.071 (0.004)
6	0.065 (0.005)	0.367 (0.033)	0.164 (0.131)	0.077 (0.003)	0.379 (0.048)	0.087 (0.008)
7	0.033 (0.055)	0.164 (0.041)	0.166 (0.011)	0.026 (0.005)	0.097 (0.019)	0.154 (0.007)
8	0.139 (0.066)	0.561 (0.023)	0.136 (0.007)	0.129 (0.004)	0.529 (0.029)	0.126 (0.005)
9	0.166 (0.003)	0.912 (0.035)	0.055 (0.008)	0.158 (0.006)	0.920 (0.018)	0.042 (0.004)
10	0.071 (0.009)	0.129 (0.003)	0.272 (0.017)	0.071 (0.004)	0.111 (0.011)	0.273 (0.008)

Each value is average of three independent measurements. Values in parentheses are standard deviations.

Table 5
Paired t-test of two independent methods (active and passive)

Analyte	No. of measurements	Paired t-test values	
		t (calculated)	t (tabulated)
Benzene	30	4.930	2.05
Aniline	30	13.489	2.05
Nitrobenzene	30	4.712	2.05

At the 95% confidence level.

nation was found to be in the range 1.00–5.36%. Neither the concentration nor the relative humidity seems to affect seriously the determination of uptake rates in the concentration range studied.

3.6. Workplace sample analysis

A field survey was carried out at nitrobenzene and aniline manufacturing plants performing nitration of benzene and subsequent reduction of nitrobenzene to aniline. Field measurements were made at four different locations at the workplace air for about 1 year in the passive mode. During the period of investigation, the temperature and relative humidity were found to vary between 20 and 40°C and 50 and 90%, respectively.

In the field evaluation of individual sampling techniques at fixed locations, the results of most of the measurements were within ±6% for active sampling and ±8% for passive sampling. It is generally believed that diffusive samplers are more reliable than pumped samplers because they eliminate pump failure. However, in our field trials with diffusive samplers, we found a variability of the results of 8–10%, wherein the results differed widely. Similar results have been reported previously [34].

The representative field sampling data are summarized in Table 4. The results of paired

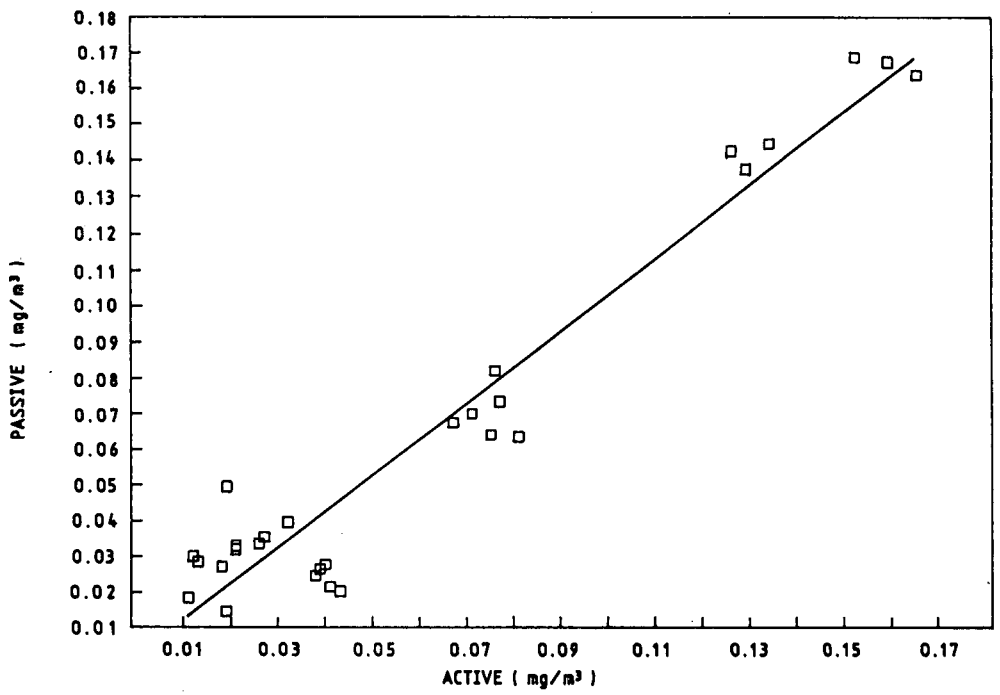

Fig. 1. Plot of concentration given by passive sampler versus active sampler for benzene in workplace air: $y = 1.009x + 0.002$; $R = 0.967$.

data sets for active and diffusive sampling for benzene, aniline and nitrobenzene were subjected to Students' *t*-distribution test for comparison. Table 5 gives results of the paired *t*-test of the two independent methods. According to the paired *t*-tests, the methods are comparable.

A correlation between the different results obtained from the two methods was also made using linear regression analysis. The data for 30 representative paired samples were evaluated by means of a point correlation diagram, wherein X and Y correspond to active and diffusive sampling values, respectively. The regression equations and correlation coefficients for benzene, aniline and nitrobenzene are given in Figs. 1, 2 and 3, respectively. The correlation is generally good for benzene, where the regression coefficient is 0.967. For aniline and nitrobenzene, relatively low correlation coefficients were obtained. Careful evaluation of the data indicates that the agreement between pumped and diffusive samplers is concentration dependent. No correlation was observed at concentration levels below 0.10 mg/m^3. At concentration levels above 0.10 mg/m^3, fairly good agreement was observed.

4. Conclusions

The results demonstrate that a Perkin-Elmer tube sampler, operated diffusively, provides a means of sampling that may be sufficiently sensitive for analysis at concentration levels of 0.1 mg/m^3 of benzene, aniline and nitrobenzene. Fairly good agreement between the results of pumped and diffusive sampling was observed as the correlation coefficient approached unity at concentration levels above 0.1 mg/m^3.

The tube-type diffusive sampler coupled with automatic thermal desorption offers the possibility of fully automated sample recovery. This, in combination with on-line GC chromatographic analysis, is very attractive when one is aiming for

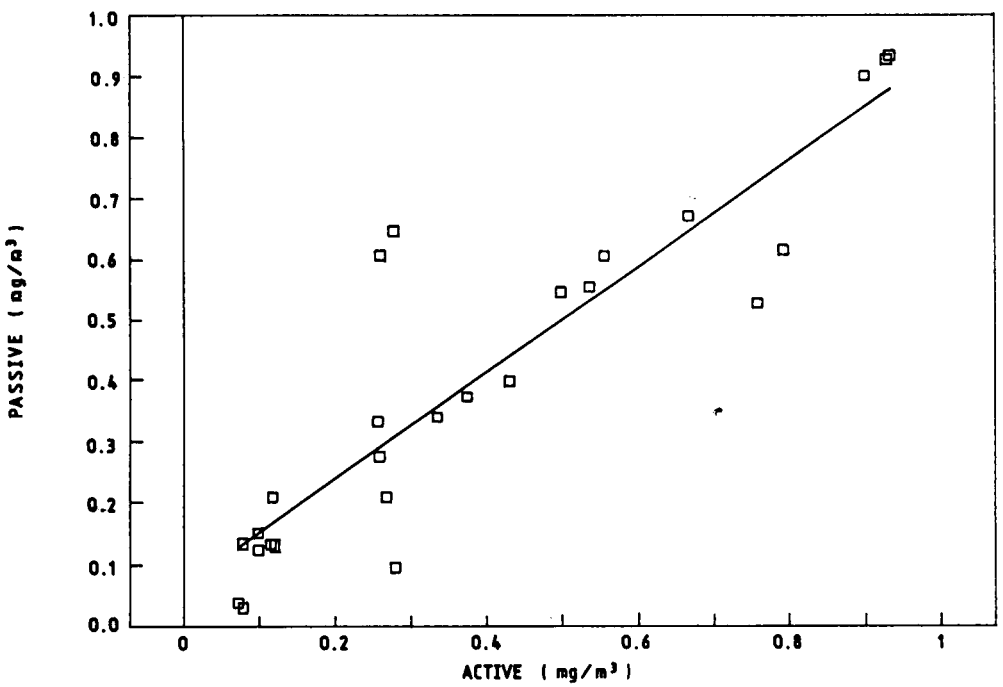

Fig. 2. Plot of concentration given by passive sampler versus active sampler for aniline in workplace air: $y = 0.873x + 0.064$; $R = 0.899$.

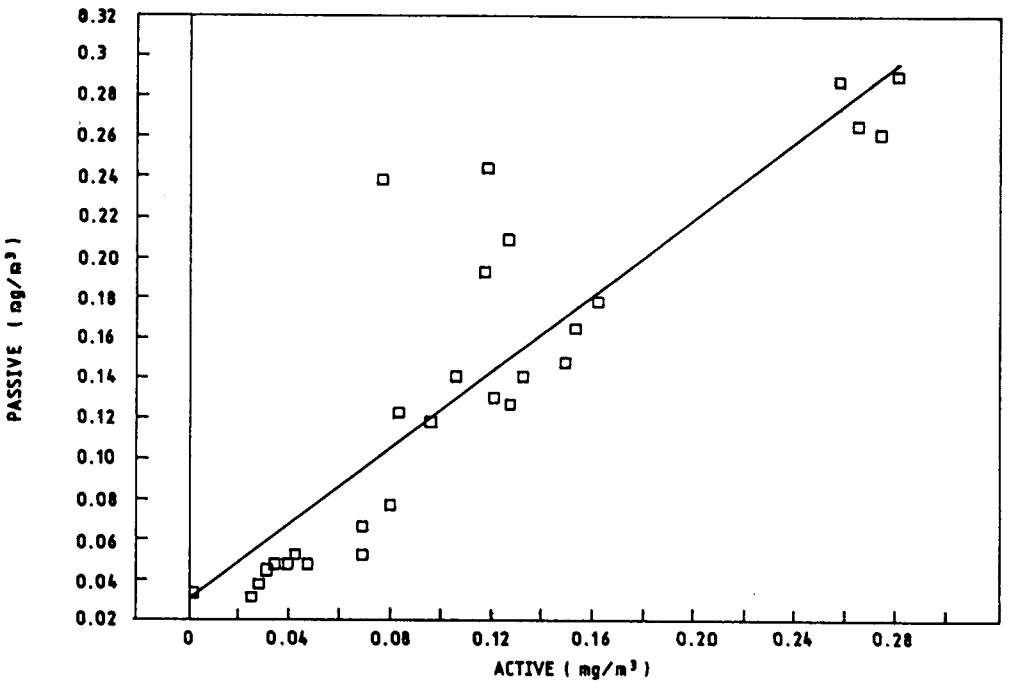

Fig. 3. Plot of concentration given by passive sampler versus active sampler for nitrobenzene in workplace air: $y = 0.947x + 0.029$; $R = 0.862$.

a convenient and cost-effective analytical procedure. Diffusive sampling and automated thermal desorption provide a convenient method for mass screening of workers exposed to organic vapours at a reasonable cost.

Acknowledgements

The authors thank Mr. V.K. Aundhe, Chairman and Managing Director, Hindustan Organic Chemicals, for permitting them to publish these results and Dr. P.D. Joshi, Chief Industrial Health Physician, for useful suggestions.

References

[1] M. Harper and C.J. Purnell, *Am. Ind. Hyg. Assoc. J.*, 48 (1987) 214.

[2] National Institute for Occupational Safety and Health (NIOSH), *Manual of Sampling Data Sheets*, Publ. 77-159, Department of Health, Education and Welfare (NIOSH), Cincinnati, OH, 1977.

[3] R.H. Brown and C.J. Purnell, *J. Chromatogr.*, 178 (1979) 79.

[4] J. De Greef., M. De Proft and F. De Winter, *Anal. Chem.* 48 (1976) 38.

[5] A. Zlatkis, J.W. Anderson and G. Holzer, *J. Chromatogr.*, 142 (1977) 127.

[6] P.J.H.D. Verkoelen and M.W.F. Nielen, *J. High. Resolut. Chromatogr. Chromatogr. Commun.*, 11 (1988) 291.

[7] C.V. Thompson, R.A. Jenkins and C.E. Higgins, *Environ. Sci. Technol.*, 23 (1989) 429.

[8] M. Termonia and G. Alaerts, *J. Chromatogr.*, 328 (1985) 367.

[9] A.H. Lawrence and L. Elias, *Can. Pat.*, CA 1 201 664 (1986).

[10] S. Coppi., A. Betti and M. Ascanelli, *J. Chromatogr.*, 390 (1987) 349.

[11] J.H. Raymer and E.D. Pellizzari, *Anal. Chem.*, 59 (1987) 1043.

[12] D.T. Coker., N.V. Hoed, K.T. Sanders and P.E. Tindle, *Ann. Occup. Hyg.*, 33 (1989) 15.

[13] T. Toy, P. Fabian, R. Borchers, F. Janssen, C. Cramers and J. Rijks, *J. Chromatogr.*, 393 (1987) 343.
[14] J.M. Thompson., W.I. Stepen and B.S. Adarajah, *Anal. Chim. Acta*, 178 (1985) 341.
[15] J. Kristensson, in A. Berlin, R.H. Brown and K.J. Saunders (Editors), *Proceedings of International Symposium on Diffusive Sampling, Luxembourg, September 22–26, 1986*, Royal Society of Chemistry, London, 1987, p. 333.
[16] L.L. Marsha and B.C. Linda, *Anal. Chem.*, 61 (1989) 128R.
[17] D.P. Coker, A.L. Jones and M.C. Simms, presented at *British Occupational Hygiene Society Annual Conference, Nottingham, 1981.*
[18] P. Tindle, *Inst. Occup. Hyg. Annu. Conf. Rep.* No. 4, 1983.
[19] S.B. Stockton, *Am. Ind. Hyg. Assoc. J.*, 46 (1985) 526.
[20] J.M. Thompson and R. Sithamparanadavajah, in A. Berlin, R.H. Brown and K.J. Saunders (Editors), *Proceedings of International Symposium on Diffusive Sampling, Luxembourg, September 22–26, 1986,* Royal Society of Chemistry, London, 1987, p. 22.
[21] C.N. Gray and J.N. Thompson, *Recent Advances in Occupational Health*, Vol. 2, Churchill Livingstone, Edinburgh, 1984, Ch. 15.
[22] D.W. Underhill, *Am. Ind. Hyg. Assoc. J.*, 45 (1984) 306.
[23] R.H. Brown, R.P. Harvey, C.J. Purnell and K.J. Saunders, *Am. Ind. Hyg. Assoc. J.*, 45 (1985) 67.
[24] R.H. Brown, J. Charlton and K.J. Saunders, *Am. Ind. Hyg. Assoc. J.*, 42 (1981) 865.
[25] N.I. Sax, *Dangerous Properties of Industrial Materials*, Van Nostrand Reinhold, New York, 4th ed., 1975.
[26] P. Eugenio, *Scand. J. Work Environ. Health.*, 15 (1989) 313.
[27] L.-K. Wu and W. Huang, *Sepu*, 7 (1989) 163; *C.A.*, 112 (1990) 239742m.
[28] V. Stransky, *Prac. Lek.*, 41 (1989) 195; *C.A.*, 113 (1990) 196789g.
[29] S.F. Patil and S.T. Lonkar, *J. Chromatogr.*, 600 (1992) 344.
[30] D.P. Coker, presented at *21st International Congress on Occupational Health, Dublin, Ireland, 1984.*
[31] N.V. Hoed and M.T.H. Halmans, *Am. Ind. Hyg. Assoc. J.*, 48 (1987) 364.
[32] T. Dublin and H.J. Thone, *J. Chromatogr.*, 456 (1988) 233.
[33] R. Pristas, *Am. Ind. Hyg. Assoc. J.*, 52 (1991) 297.
[34] D.T. Coker, presented at *Royal Society of Chemistry Conference, London, 1981.*

ELSEVIER

Journal of Chromatography A, 688 (1994) 201–209

JOURNAL OF CHROMATOGRAPHY A

Gas–solid chromatographic analysis of automobile tailpipe emissions as a function of different engine and exhaust system modifications

Daniel W. Armstrong*, Kang Le, George L. Reid, III, Shen C. Lee, Kevin K. Beutelmann, Mike Horak, Paul Tran

Departments of Chemistry and Mechanical Engineering, University of Missouri–Rolla, Rolla, MO 65401, USA

First received 14 June 1994; revised manuscript received 16 August 1994.

Abstract

A single, relatively short gas–solid porous-layer open-tubular chromatographic column was used to separate aliphatic hydrocarbons, aromatic hydrocarbons and some inorganic gases (O_2, CO and CO_2) found in automobile exhaust. The column's performance and longevity did not appear to be affected by the presence of water or carbon dioxide in the samples. The concentrations of the emission gases varied considerably with changes in air/fuel ratio, coil voltage and use of catalytic converters. The results of the analyses were compared with those obtained using a commercial emission analyser ("sniffer").

1. Introduction

Gas–solid chromatography (GSC) is a highly useful technique for separating gases and other volatile compounds. It is most often used for light hydrocarbons and a variety of inorganic gases. There are both packed and capillary GSC columns available. Useful GSC stationary phases are made from silica [1–4], aluminum oxide [5–14], porous polymers [15–18] zeolite-type molecular sieves [19–21] and most recently cyclodextrins [22–24]. Summaries of these approaches have been reported recently [22–24]. GSC alone or coupled with mass spectrometry may be the most viable analytical method to identify and determine a variety of individual components in automobile exhaust. The study of automobile tailpipe emissions is of increasing importance given social concerns about the environment and the resulting legislation and regulations [25–28].

Spark-ignition engines produce three general classes of tailpipe emissions that are unwanted and considered harmful: carbon monoxide (CO), hydrocarbons and nitrogen oxides (NO_x). Carbon monoxide results from the incomplete combustion (oxidation) of the fuel. Nitrogen oxides (largely NO and NO_2) form from the oxidation of N_2 in the air during high-temperature combustion. The hydrocarbons are a variety of organic compounds that come from uncombusted fuel. Vehicles produced for use in the USA after 1974 contain catalytic converters which, when functioning properly, decrease emissions of the aforementioned classes of compounds.

Currently, "tailpipe-sniffer" tests are used in cities that have air quality problems. Exhaust

* Corresponding author.

0021-9673/94/$07.00
SSDI 0021-9673(94)00784-5

samples are taken and the amounts of carbon monoxide (CO), carbon dioxide (CO_2) and total hydrocarbons are measured. Infrared analysis (IR) is used for CO and CO_2 while flame ionization detection (FID) without separation gives an approximate total hydrocarbon number. While the "sniffer" tests are relatively fast and inexpensive, nothing is learned about the speciation of the hydrocarbons or about the other gaseous components.

The aim of this work was to determine if the majority of gaseous automobile tailpipe emissions can be separated and identified using a single new GSC column. This is a capillary column that evolved from earlier packed column work [22–24]. Measurements were also made with several different engine and exhaust system configurations and the results were compared with those from a standard "tailpipe-sniffer test". Specifically, the effects of catalytic converters, air/fuel ratio, ignition system and various combinations of these were examined.

2. Experimental

2.1. Analytical methodologies

A Hewlett-Packard (Avondale, PA, USA) 5890 Series II gas chromatograph equipped with a split–splitless injection port, flame ionization and thermal conductivity detectors and a liquid nitrogen cryogenic coolant system was used. The injector and detector ports were set at 150 and 200°C, respectively. The oven temperature programs were as follows (a) for hydrocarbons, 85°C for 3 min, then increased at 7.5°C/min to 250°C, which was held for 20 min; (b) for oxygen and nitrogen, −65°C isothermal; (c) for carbon monoxide, −55°C isothermal; and (d) for carbon dioxide, 25°C isothermal. Data collection was accomplished with a Hewlett-Packard 3396B Series II integrator. Helium was used as the carrier gas for all experiments with flow-rates of approximately 2 ml/min. The column used in this study was a 15 m × 0.32 mm I.D. GasPro column produced by Advanced Separation Technologies (Whippany, NJ, USA). This commercial column is not identical with those we made and discussed in previous reports, although some of the selectivities are similar [22–24]. Quantification of aliphatic hydrocarbons and inorganic gases was effected by making calibration graphs using gas mixtures of known concentrations. All gas standards including 1000 ppm C_1–C_6 *n*-alkanes (can mix 236), 1000 ppm C_2–C_6 alkenes (can mix 223), 15 ppm branched alkanes (can mix 2) and 5% inorganic gas mixtures (can mix 234) were purchased from Alltech (Scott Specialty Gases; Plumsteadville, PA, USA). An aromatic hydrocarbon standard mixture (benzene, toluene and xylenes) was prepared by weighing the pure liquids, 19.8 mg of benzene, 19.2 mg of toluene, 18.6 mg of *o*-xylene, 21.0 mg of *m*-xylene and 19.6 mg of *p*-xylene in 1.0 l of methylene chloride, resulting in a standard mixture containing 19.8 mg/l of benzene, 19.2 of toluene, 18.6 mg of *o*-xylene, 21.0 mg of *m*-xylene and 19.6 mg of *p*-xylene. Quantification of samples was effected via peak-area measurements through the calibration graphs for the standards. Most components from C_1 to C_8 appeared to be resolved. The major compounds were identified via retention comparison with authentic standards and by GC–MS analysis with a Hewlett-Packard Model 5970 instrument.

For comparative purposes the exhaust samples were also evaluated with a Model MCA-3000 modular computer analyzer (Sun Electric, Crystal Lake, IL, USA). This "sniffer" gives a number (in ppm, v/v) for total hydrocarbon emissions (using FID) and also concentrations of CO and CO_2 (using IR) and O_2 (via an oxygen sensor). It is calibrated periodically by the manufacturer. According to the instruction manual this is done with gas samples containing 600 ppm (v/v) of propane, 11.0% of carbon dioxide and 1.6% of carbon monoxide. This instrument also measures the exhaust temperature, engine rpm and the air/fuel ratio.

2.2. Engine and exhaust configuration

The engine used in this study was a 1969 Oldsmobile 7.4-l (455-in^3; 1 in = 2.54 cm) V-8 power plant with dual exhaust (5.72 cm diameter) and a two-barrel Rochester carburetor. The bore was 10.48 cm and the stroke was 10.80 cm. This engine produces 310 hp (1 hp = 745.7 W) at 4700 rpm and a torque of 68 kg m (490 ft. lb.) at

2400 rpm. A large number of variables affect automobile exhaust emissions including the type of fuel, air/fuel ratio, intake manifold, engine speed, exhaust gas recirculation (EGR), valve timing, head/piston/port/valve design, spark timing, spark quality, exhaust manifold design, use of air injection reactors (AIR), use of catalytic converters and exhaust pipe length. It was beyond the scope of this project to study all of these factors. However, a few representative factors that can be easily and reproducibly controlled were chosen: the air/fuel ratio (specifically the effect of a lean burn system), spark quality, the use of an AIR and the use of catalytic converters. Each of these modifications is summarized below [27–29].

(1) The air/fuel ratio is the mass of air divided by the mass of fuel delivered to the engine. The stoichiometric air/fuel ratio is considered to be 14.7 parts air to one part of gasoline fuel. The equivalence ratio (ϕ) is used to describe whether an engine is operating with an excess of air or fuel. The equivalence ratio is defined as the fuel/air ratio (note that this is the inverse of the aforementioned air/fuel ratio) delivered to the engine divided by the stoichiometric fuel/air ratio. Consequently, if $\phi < 1$ the engine is said to run lean (or with excess air), when $\phi > 1$ the engine is said to run rich (or with excess fuel) and if $\phi = 1$ the engine is said to operate at the stoichiometric condition. The equivalence ratio is an important variable for engine operation because it affects the exhaust composition in addition to the engine's efficiency, power and smoothness of operation. In general, it is known that as ϕ increases the concentrations of carbon monoxide and hydrocarbons in the exhaust also increase (because of a lack of O_2 to burn the fuel). As ϕ decreases there is usually a corresponding decrease in the exhaust levels of carbon monoxide and hydrocarbons until misfire occurs. Maximum engine power occurs when $\phi = 1.1$. In order to make the intake mixture leaner, a Lean Power digital carburetion system was installed. It consisted of an air-intake system with filter and valve which feeds air into a baseplate that fits between the intake manifold and carburetor. The amount of air fed into the intake was regulated by a computer which read a crank sensor mounted near the flywheel. When the engine was operating with the "lean system" the equivalence ratio (ϕ) was approximately 0.85.

(2) A Jacobs Electronics ignition system (Energy Pak) was used to improve the ignition of the fuel–air mixture. This system uses a computer to read impedance changes in the coil. This is done in order to compute the best spark intensity, duration and phase angle for each engine condition. The coil included with this system was capable of a higher output voltage (56 000 V) than was provided by the baseline system (40 000 V). In order to simplify the ignition comparison all factors were kept constant except for variations in the coil voltage.

(3) Fig. 1A shows the basic exhaust configuration for the test vehicle. The catalytic converters used were from a 1994 Chevrolet Caprice containing a 5.7-l (350-in.^{3}) V-8 LT1 engine (i.e., AC wide oval part No. 25152589). They were installed as shown in Fig. 1B. The original exhaust pipes can be closed so that all of the emissions go through the catalytic converter. Stainless-steel sample tubes were connected to the front and rear of the converter in order to take exhaust gas samples (Fig. 2). Thermocouples were mounted in the exhaust pipe, 6 in. in front of the converter monolith. These were used to monitor the exhaust temperature, as temperature has a great effect on conversion efficiency. The so-called "light-off temperature" is the temperature at which the catalyst in the catalytic converter operates at 50% conversion efficiency with an excess of oxygen (i.e., conversion of carbon monoxide and the hydrocarbons to CO_2

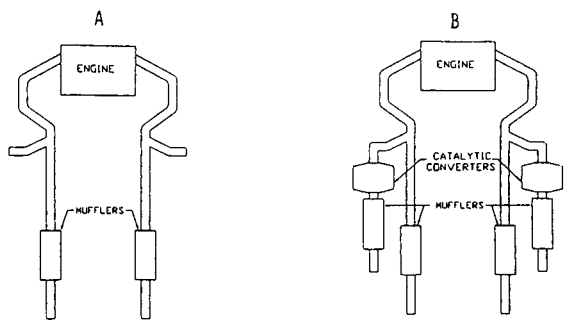

Fig. 1. (A) Unmodified exhaust system of original vehicle. (B) Modified exhaust systems showing the location of the two added catalytic converters (see Experimental for further details).

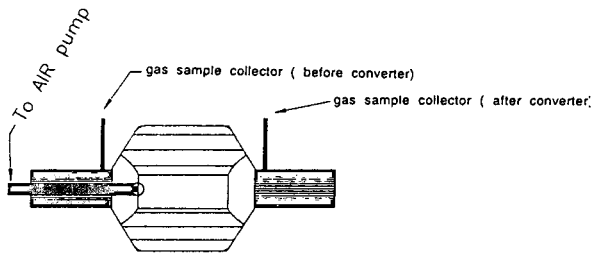

Fig. 2. Top view of an installed catalytic converter with "gas sample collection tubes" before and after the converter. Also shown is an additional AIR injection tube going directly into the catalytic converter (see Experimental for further details).

and water). The "light-off temperature" is in the range 250–300°C. Below this temperature the catalyst is considered ineffective for automotive purposes. There is also an upper temperature limit (ca. 500°C). This is the result of the sintering of the noble metal catalyst substrate at high temperatures, which lowers the surface area.

(4) The AIR pump was taken from a 1985 Oldsmobile Cutlass equipped with a 5-l (307-in.^{3}) V-8 engine. This is a rotary vane pump which forces additional O_2 (as air) into the catalytic converter in order to increase its effectiveness. The AIR pump was connected to brackets at the front of the engine in the same place where the air conditioning compressor is normally located. The supplemental air was injected into the front of the catalytic converter (see Fig. 2).

2.3. Sampling conditions

The following conditions were held constant for all samples. The engine was run on 87 octane unleaded gasoline. The engine was always run for 10 min at 1400 rpm allowing the exhaust gases to reach a steady-state temperature of 355 ± 20°C before any samples were taken.

All exhaust samples were taken with a 125-ml gas sampling bulb having PTFE stopcocks at both ends and a septum needle port on the side of the bulb (Supelco, Bellefonte, PA, USA). This bulb was attached to one or other of the previously described stainless-steel sample tubes. Approximately 30 "sample bulb volumes" of exhaust gas were passed through the sampling device before the stopcocks were closed (exit port first), thereby trapping the exhaust sample. Note that we did not dilute the samples ~14 to 1 with pure dry air as sometimes recommended by the EPA, in order to prevent condensation. This provided a more strenuous test of the column's relative inertness to injected water.

Samples were analyzed from seven different engine and/or exhaust configurations, as follows: (1) baseline engine (i.e., no catalytic converter, no AIR, no lean fuel mixture and the standard 40 000-V coil was used); (2) engine + coil (i.e., no catalytic converter, no AIR, no lean fuel mixture, but the special 56 000-V coil was used); (3) engine + lean + coil (i.e., no catalytic converter, no AIR, the lean carburetion system was used and the 56 000-V coil was used); (4) engine + converter (i.e., catalytic converter was used, no AIR, no lean fuel and the standard 40 000-V coil was used); (5) engine + converter + lean (i.e., the catalytic converter was used, the lean fuel carburetion system was used, no AIR and the standard 40 000-V coil was used); (6) engine + converter + lean + coil (i.e., the catalytic converter was used, the lean fuel carburetion system was used, the special 56 000-V coil was used, no AIR); (7) engine + converter + coil + AIR (i.e., the catalytic converter was used, the special 56 000-V coil was used, the AIR system was used, no lean fuel mixture).

3. Results and discussion

The ability to use a single, short (15 m) capillary column for the determination of aliphatic hydrocarbons, aromatic hydrocarbons and inorganic gases in automobile exhaust was convenient. However, because of different detection methods used [i.e., FID for the hydrocarbons and thermal conductivity (TCD) for the inorganic gases] and different column temperatures for the volatile analytes of interest, a minimum of two separate injections were required in order to determine all components. Fig. 3A shows the separation of the hydrocarbon components from the baseline engine exhaust (i.e., no catalytic converter or any other modifications; see Experimental). Note that most of the hydrocarbon

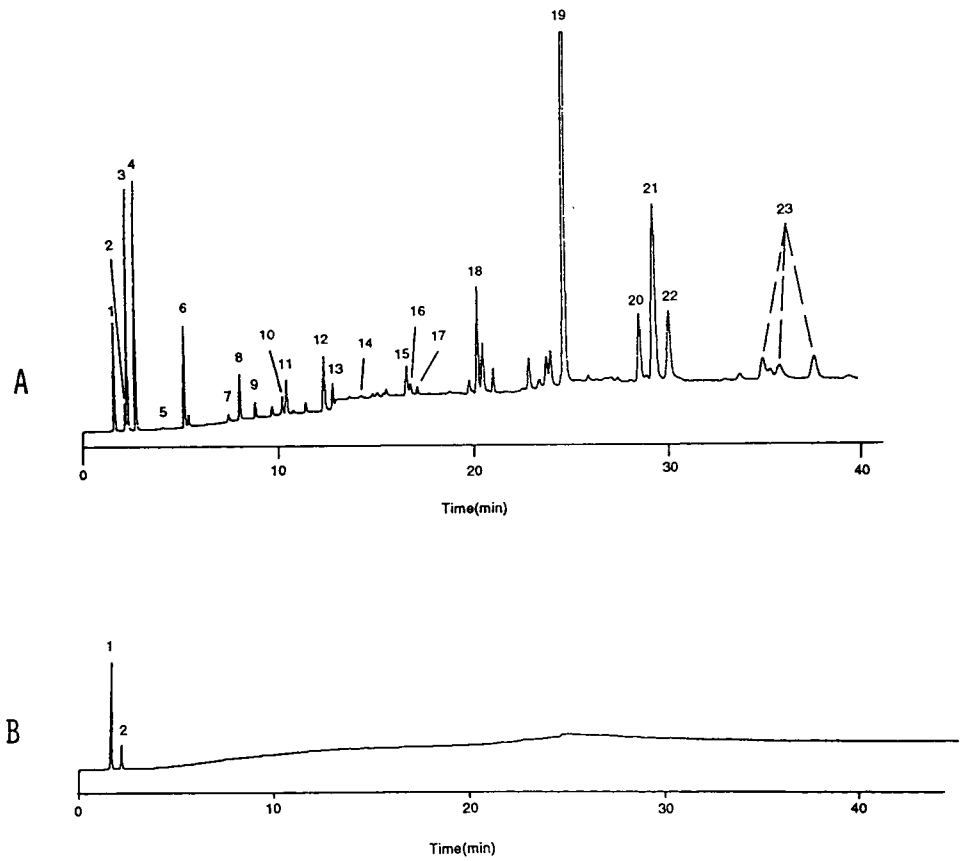

Fig. 3. (A) Gas–solid chromatogram showing the separation of a variety of aliphatic and aromatic hydrocarbon components in the exhaust of the baseline engine (i.e., an engine with no modifications to reduce unwanted emissions). This is characteristic for large pre-1975 engines in the USA. Peaks identified via GC–MS: 1 = methane; 2 = ethane; 3 = ethylene; 4 = acetylene; 5 = propane; 6 = propylene; 7 = isobutane; 8 = butane; 9 = propyne; 10 = butene; 11 = 1,3-butadiene; 12 = 2-methylbutane; 13 = pentane; 14 = pentene; 15 = 2-methylpentane; 16 = 3-methylpentane; 17 = hexane; 18 = benzene; 19 = toluene; 20 = ethylbenzene; 21 = *p*- and *m*-xylene; 22 = 0-xylene; 23 = alkylated benzenes. (B) Gas–solid chromatogram showing the effect of a catalytic converter in reducing hydrocarbon emissions in automobile exhaust (i.e., engine condition 5 in Table 1). The experimental conditions for (A) and (B) were identical (i.e., a 15 m × 0.32 mm I.D. GasPro column, flow-rate = 2.0 ml/min and a temperature program of 85°C for 3 min then ramped at 7.5°C/min to 250°C. See Experimental for further details.

species of interest appear to be easily resolved. An exception appears to be *m*- and *p*-xylene, which are co-eluted as peak 21. Fig. 3B is the analogous chromatogram generated under identical conditions except that the exhaust was run through a properly functioning catalytic converter (see Experimental). Fig. 4A shows the separation of oxygen, nitrogen and carbon monoxide on the same GSC column at subambient temperatures and Fig. 4B shows the separation of carbon dioxide at room temperature.

Table 1 lists the concentrations of many of the aliphatic hydrocarbons from the test automobile's exhaust under different conditions and Table 2 lists analogous data for the aromatic hydrocarbons. Table 3 gives the concentrations of several inorganic gases from the same samples. It was expected that the baseline engine emissions (with no control devices) would have the highest combustion product emissions. This was true except for case No. 3 (Tables 1–3), where the special carburetion system gave a lean air–fuel mixture to the engine. Ordinarily lean mixtures produce less hydrocarbon and carbon

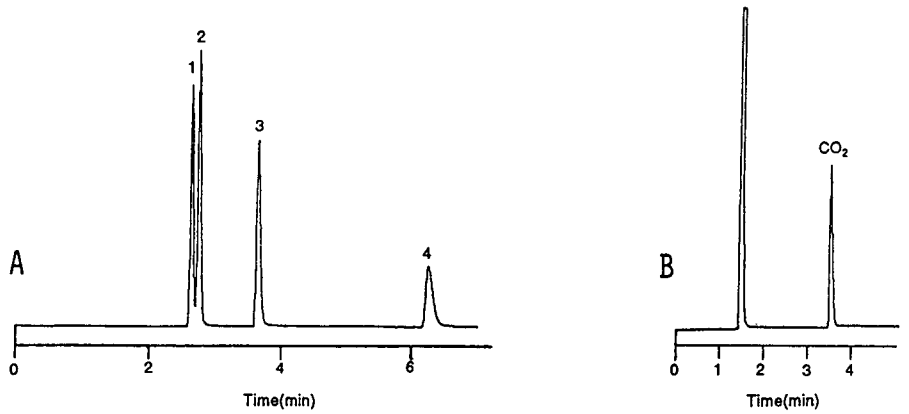

Fig. 4. GSC separation of (A) 1 = oxygen, 2 = nitrogen, 3 = carbon monoxide and 4 = methane on a 15 m × 0.32 mm I.D. GasPro capillary column at −65°C and (B) carbon dioxide on the same column at 25°C. When determining carbon monoxide (which is a very small peak in automobile exhaust) the separation is better at −55°C. The CO peak elutes faster and much sharper at this temperature (see Experimental).

monoxide emissions (owing to more complete oxidation processes). However, too lean a mixture will begin to cause engine misfire and an increase in uncombusted fuel products. That is what happened in this case. The chemical evidence for this is the increase in the exhaust concentrations of most hydrocarbons and oxygen (Tables 1–3). Clearly, when trying to improve fuel economy and emissions by having a lean air/fuel ratio, some caution must be exercised. An incorrect or inexpert modification that leads to misfires can make exhaust emissions worse rather than better. The two things in this study that seemed to give the greatest reductions in hydrocarbon and/or carbon monoxide emissions were the catalytic converter and the use of a higher coil voltage. In this test system the catalytic converter usually reduced the concentra-

Table 1
Concentrations of aliphatic hydrocarbons (ppm, v/v)[a] in the exhaust gas of the test vehicle

Engine conditions	Methane	Ethane	Ethylene	Propylene	Butane	Butene	2-Methyl-butane	Pentane	2-Methyl-pentane	3-Methyl-pentane	Total[b]
(1) Baseline engine	49.3	7.3	69.7	21.1	6.6	0.5	6.4	1.0	6.2	NC[c]	369.2
(2) Engine + coil	15.0	3.4	40.4	14.1	3.0	0.1	2.4	ND	2.3	ND	183.1
(3) Engine + lean + coil	19.4	5.1	69.7	29.4	13.9	2.1	10.7	5.3	10.2	UD	462.4
(4) Engine + converter	18.3	3.0	ND	ND	ND	ND	ND	ND	ND	ND	24.3
(5) Engine + converter + lean	46.3	6.7	ND	ND	ND	ND	ND	ND	ND	ND	59.7
(6) Engine + converter + coil + lean	16.8	2.3	ND	ND	ND	ND	ND	ND	ND	ND	21.4
(7) Engine + converter + coil + AIR	10.8	2.3	0.9	ND	ND	ND	0.1	ND	0.1	ND	18.3

[a] These concentrations are given in ppm by volume of gas.
[b] in order to obtain this "sum" for the total hydrocarbon mixture, the measured concentration of each component was multiplied by the number of carbons in that component. These numbers were then added together.
[c] ND = Not detected. This means that the concentrations of these compounds were below the limit of detection (LOD) for this particular system (see Experimental). The LODs for the instrumental conditions of this study are as follows: (in ppm, v/v): methane = 1.2, ethane = 0.8, ethylene = 0.9, propylene = 0.6, butane = 0.2, butene = 0.2, 2-methylbutane = 0.3, pentene = 0.2, 2-methylpentane = 0.3, 3-methylpentane = 0.3.

Table 2
Concentrations of aromatic hydrocarbons (mg/l)[a] in the exhaust gas of the test vehicle

Engine conditions	Benzene	Toluene	*m*- +*p*-Xylene	*o*-Xylene
(1) Baseline engine	0.045	0.35	0.14	0.057
(2) Engine + coil	0.025	0.095	0.045	0.017
(3) Engine + lean + coil	0.032	0.14	0.048	0.019
(4) Engine + converter	0.0086	0.014	ND[b]	ND
(5) Engine + converter + lean	ND	ND	ND	ND
(6) Engine + converter + coil + lean	ND	0.049	0.041	0.016
(7) Engine + converter + coil + AIR	ND	0.023	0.020	0.0057

[a] Note that these concentrations are not directly comparable with those of the aliphatic hydrocarbons in Table 1 because their units of concentration are different. The standards used to obtain these concentrations were made up as liquid solutions. Hence these concentrations are given as mg of aromatic compound per liter of solution (see Experimental).

[b] ND = Not detected. This means that the concentration of these compounds were below the limit of detection (LOD) for this particular system (see Experimental). The LODs for the instrumental conditions of this study are as follows (in ppm, w/v): benzene = 0.002; toluene = 0.002; *o*-, *m*- and *p*-xylene = 0.002.

tions of most of the hydrocarbons by one to two orders of magnitude. Methane and ethane were also reduced but only by about 60%. The catalytic converter also effectively oxidized carbon monoxide in all cases (Table 3).

While the quantification of individual components in automobile tailpipe emissions provides useful research information, it will not be done routinely for all vehicles because of time and cost restraints. Instead, a more rapid analysis of a few representative components with a computer-monitored set of sensors is used. All samples analyzed by GSC in this study were also evaluated with such a commercial modular emissions analyzer or "sniffer" (see Experimental). A comparison of the results obtained by GSC analysis and with the commercial analyzer for oxygen, carbon dioxide, "total hydrocarbons" and carbon monoxide are shown in Figs. 5–8. Except for carbon monoxide it appeared that both methods give similar relative results but slightly different absolute concentrations. For example, GSC analysis consistently gave higher results for hydrocarbons and oxygen. Converse-

Table 3
Concentrations of some inorganic gases (%, v/v) in the exhaust gas of the test vehicle

Engine conditions	Oxygen	Carbon monoxide	Carbon dioxide
(1) Baseline engine	3.7	0.6	10.7
(2) Engine + coil	4.0	0.7	6.1
(3) Engine + lean + coil	6.2	0.7	6.1
(4) Engine + converter	4.3	ND[a]	9.2
(5) Engine + converter + lean	4.3	ND	9.0
(6) Engine + converter + coil + lean	4.9	ND	7.9
(7) Engine + converter + coil + AIR	9.0	ND	3.1

[a] ND = Not detected. This means that the concentrations of these compounds were below the limit of detection (LOD) for this particular system (see Experimental). The LODs for this instrument (%, v/v) are as follows: $O_2 = 0.06$, $CO = 0.07$, $CO_2 = 0.08$.

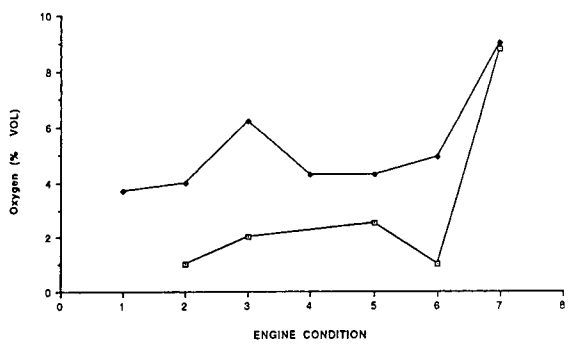

Fig. 5. Comparison of the oxygen levels measured in automobile tailpipe exhaust (◆) by GSC and (□) with the modular computer analyzer (see Experimental for details of the exact methodologies). The engine condition numbering convention is identical with that in Tables 1–3.

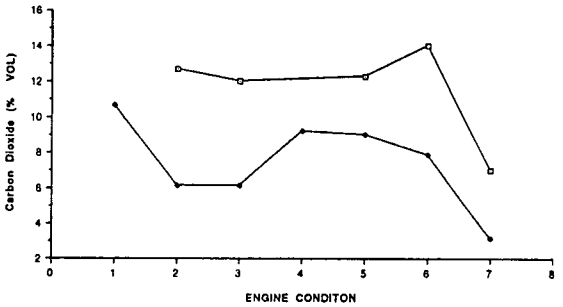

Fig. 6. Comparison of the carbon dioxide levels measured in automobile tailpipe exhaust (◆) by GSC and (□) with the modular computer analyzer (see Experimental for details of the exact methodologies). The engine condition numbering convention is identical with that in Tables 1–3.

ly, it always gave lower results for carbon dioxide. The fact that the GSC results for hydrocarbons were slightly higher than those given by the commercial emissions (modular) analyzer was surprising (Fig. 7). This was because the GSC results included only the normalized sum of the amounts of the aliphatic and olefinic hydrocarbons listed in Table 1. Hence significant amounts of aromatic hydrocarbons and a few other components were not included in the GSC hydrocarbon total (Table 1 and Fig. 7). As noted in the Experimental section, the quantitative GSC results were obtained using a calibration

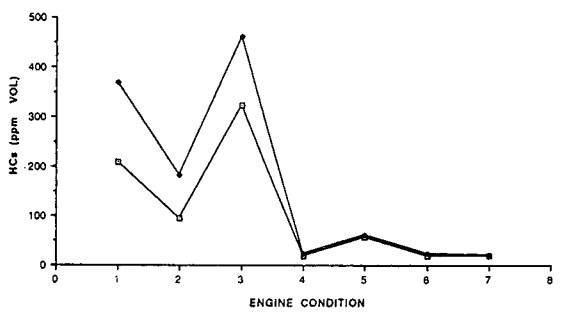

Fig. 7. Comparison of the total hydrocarbon levels measured in automobile tailpipe exhauts (◆) by GSC and (□) with the modular computer analyzer (see Experimental for details of the exact methodologies). Note that the "total hydrocarbons" for GSC include only the results for the aliphatic hydrocarbons (Table 1). If the results for the aromatic hydrocarbons were converted into comparable units and added to this total, there would be a larger discrepancy between the two methods. The engine condition numbering convention is identical with that in Tables 1–3.

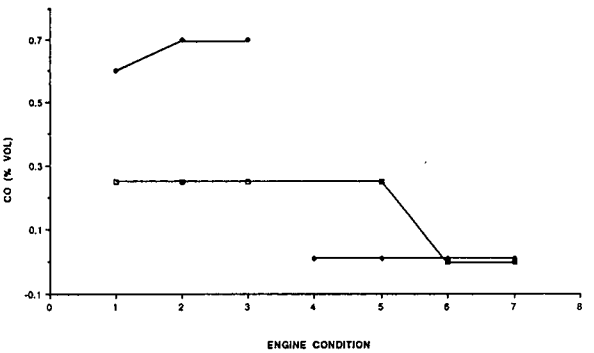

Fig. 8. Comparison of the carbon monoxide levels measured in automobile tailpipe exhauts (◆) by GSC and (□) with the modular computer analyzer (see Experimental for details of the exact methodologies). The engine condition numbering convention is identical with that in Tables 1–3.

graph for each component listed in Table 1. Conversely, the commercial analyzer was calibrated by the manufacturer every few months using a 600 ppm propane standard (i.e., a one-point calibration). The extent to which different hydrocarbon response factors and the matrix of the engine exhaust affect the modular emission analyzer's FID signal are not known to us. In view of these factors, it would be surprising not to find some differences in the two measurements of total hydrocarbons. Perhaps the worse correlation between the two methods was for carbon monoxide (Fig. 8). The modular emissions analyzer gave results over 50% lower in the first three tests, significantly higher for the fifth test and comparable results for the sixth and seventh tests (where the CO levels were lowest). This was the only case where there did not seem to be any correlation between the GSC results and the modular emissions analyzer results.

4. Conclusions

Both hydrocarbons and inorganic gases from automobile tailpipe emissions can be separated and determined on a single GSC capillary column. In the case of hydrocarbons, both aliphatic and aromatic components (up through alkylated benzenes) are measured in one run. Although subambient temperatures are needed for the

oxygen–nitrogen separation, they were easily resolved from each other and the other compounds present. It was easy to see the effects of different engine and exhaust system modifications by monitoring the level of compounds in the exhaust. The use of catalytic converters and a higher voltage coil tended to produce the most pronounced decreases in emissions of hydrocarbons. The catalytic converter produces the most significant decrease in carbon monoxide concentrations. With the exception of carbon monoxide, the emissions measured by GSC and by commercial emission analyzers showed similar trends and relative concentrations but different absolute concentrations. Some of the variations may have been due to differences in the calibration of these methods.

Acknowledgement

Support of this work by the Department of Energy (DOE FG02 88ER13819) is gratefully acknowledged.

References

[1] R.D. Schwartz, D.L. Brasseaux and G.R. Shoemake, *Anal. Chem.*, 35 (1963) 496.
[2] R.G. Mathews, J. Torres and R.D. Schwartz, *J. Chromatogr.*, 186 (1979) 183.
[3] M. Mohnke and W. Saffert, presented at the *4th International Symposium on Gas Chromatography, Hamburg, June 13–16, 1962*, preprints, p. 214.
[4] F.A. Bruner and G.P. Cartoni, *Anal. Chem.*, 36 (1964) 1522.
[5] J.J. Kirkland, *Anal. Chem.*, 35 (1963) 1295.
[6] D.L. Petitean and C.J. Leftault, Jr., *J. Gas Chromatogr.*, March 18 (1963) 18.
[7] S. Moriguchi, K. Naito and S. Takei, *J. Chromatogr.*, 131 (1977) 19.
[8] W. Schneider, J.C. Frohne and J. Bruderreck, *J. Chromatogr.*, 155 (1978) 311.
[9] R.C.M. de Nijs, *J. High Resolut. Chromatogr. Chromatogr. Commun.*, 4 (1981) 612.
[10] K. Naito, M. Endo, S. Moriguchi and S. Takei, *J. Chromatogr.*, 253 (1982) 205.
[11] R.C.M. de Nijs and J. de Zeeuw, *J. Chromatogr.*, 279 (1983) 41.
[12] N. Pelz, N.M. Dempster and P.R. Shore, *J. Chromatogr. Sci.*, 28 (1990) 230.
[13] L. Do and F. Raulin, *J. Chromatogr.*, 514 (1990) 65.
[14] J.Y.K. Lai, E. Matisová, D. He, E. Singer and H. Niki, *J. Chromatogr.*, 643 (1993) 77.
[15] G.E. Pollock, *J. Chromatogr. Sci.*, 24 (1986) 173.
[16] L. Do and F. Raulin, *J. Chromatogr.*, 481 (1989) 45.
[17] R.T. Talasek and K.E. Daugherty, *J. Chromatogr.*, 635 (1993) 265.
[18] O.L. Hollis, *J. Chromatogr. Sci.*, 11 (1973) 335.
[19] N.L. Soulages and A.M. Brieva, *J. Chromatogr.*, 101 (1974) 365.
[20] E. de Vanssay, P. Capilla, D. Coscia, L. Do, R. Sternberg and F. Raulin, *J. Chromatogr.*, 639 (1993) 255.
[21] J.V. Brunnock and L.A. Luke, *Anal. Chem.*, 40 (1968) 2158.
[22] G.L. Reid, III, C.A. Monge, W.T. Wall and D.W. Armstrong, *J. Chromatogr.*, 633 (1993) 135.
[23] G.L. Reid, III, W.T. Wall and D.W. Armstrong, *J. Chromatogr.*, 633 (1993) 143.
[24] G.L. Reid, III, and D.W. Armstrong, *J. Microcol. Sep.*, 6 (1994) 151.
[25] N. Pelz, N.M. Demster and P.R. Shore, *J. Chromatogr. Sci.*, 28 (1990) 230.
[26] S.K. Hoekman, *J. Chromatogr.*, 639 (1993) 239.
[27] J.R. Mondt, *History of the Internal Combustion Engine*, Vol. 8, Part A, American Society of Mechanical Engineers, New York, 1989.
[28] J.R. Mondt, *History of the Internal Combustion Engine*, Vol. 8, Part B, American Society of Mechanical Engineers, New York, 1989.
[29] M.H. Edison and C.F. Taylor, *Digital Calculations of Engine Cycles* (SAE Progress in Technology, Vol. 7), Society of Automotive Engineers, Warrendale, PA, 1964, pp. 65–81.

ELSEVIER

Journal of Chromatography A, 688 (1994) 211–219

JOURNAL OF CHROMATOGRAPHY A

Gas chromatographic–mass spectrometric, high-performance liquid chromatographic–UV and gas chromatographic–Fourier transform IR responses to an industrial mixture of diisopropylnaphthalenes

A. Sturaro*, G. Parvoli, R. Rella, L. Doretti

Ufficio Sicurezza e Prevenzione del CNR, Corso Stati Uniti 4, 35020 Padova, Italy

First received 28 July 1994; revised manuscript received 31 August 1994

Abstract

GC and HPLC parameters and mass spectrometric, ultraviolet and infrared responses of the diisopropylnaphthalene isomers are reported in order to allow their analytical determination. The interest in these compounds, widely used in the manufacture of special paper, is linked to their appearance as environmental and food pollutants due to recycling and waste processes.

1. Introduction

A recent GC–MS investigation showed the presence of a mixture of diisopropylnaphthalene (DIPN) isomers in some kinds of food (rice and pasta) and in their containers [1]. These naphthalene derivatives, with general formula $C_{16}H_{20}$, may give rise, theoretically, to ten positional isomers, i.e., 1,2-, 1,3-, 1,4-, 1,5-, 1,6-, 1,7-, 1,8-, 2,3-, 2,6- and 2,7-derivatives. Because of steric hindrances, their real number could be lower, considering that the isomers having adjacent substituents are not favoured under non-specific synthesis conditions [2].

These compounds are widely used in the manufacture of special paper, such as carbonless and thermal copy paper, ink for jet printers and similar commercial products [3–7]. There is a great deal of interest in these special papers because, being pure cellulose, they can be used as starting materials to obtain high-quality recycled paper. The recycling process does not involve any specific treatment for the removal of DIPN from the paper, therefore significant amounts of these compounds are put back into the environment as waste or in the form of material used in the production of container board. In this way the useless presence of diisopropylnaphthalenes may lead to environmental pollution and food contamination with, consequently, new implications even of a toxicological nature [8]. Samples of carbonless copy paper have shown that the average amount of these naphthalene derivatives is about 1% of their total mass. Until now, only some Japanese researchers have investigated the presence of these molecular species in the environment, realising their harmful effects due to their pos-

* Corresponding author.

0021-9673/94/$07.00
SSDI 0021-9673(94)00848-5

sible accumulation. Rivers, sea water and sediments have been investigated [9–12]. In spite of the widespread use and the large number of isomers, their analytical characteristics are almost unknown. Only two mass spectra of the 2,6-isomer, one obtained with an old spectrometer [11] and the other under 20 eV electron impact ionization conditions [13], have been reported. This paper reports the GC and HPLC parameters and UV, mass and Fourier transform (FT) IR spectra of the diisopropylnaphthalene isomers, as reference data for their analytical determination.

2. Experimental

2.1. Materials

All the chemicals, 1,3-, 1,6-, 1,4-, 1,5-, 2,6- and 2,7-dimethylnaphthalenes (DMN) and solvents of HPLC grade were purchased from Aldrich Chimica (Milan, Italy). 2,6-Diisopropylnaphthalene, 1- and 2-isopropylnaphthalene mixture (1:1) and 2-isopropylnaphthalene were supplied by Aldrich (Milwaukee, WI, USA). A sample of DIPN mixture was kindly furnished by a European manufacturer of carbonless copy paper.

2.2. Preparation of the samples

Mixtures of some diisopropylnaphthalene isomers were synthesized according to the literature procedure [14]. To a naphthalene solution (0.4 g) in 2-propanol (6 ml), used as the solvent and reagent, was added aluminium chloride catalyst. The mixture was maintained under agitation at room temperature for 5 h. After pouring off the crude reaction into water, the products were extracted with dichloromethane and injected into the GC–MS instrument. The analogous Friedel–Crafts reaction was also performed using separately the two monoisopropyl derivative samples (100 mg), isopropyl bromide (80 mg) in the presence of the same Lewis acid and light petroleum (10 ml) as a solvent [15]. The above reaction conditions and sample treatment were also applied to this second synthesis procedure.

An alternative Friedel–Crafts alkylation was carried out using naphthalene (150 mg) and 2-propanol (130 μl) in the presence of 80% sulfuric acid solution (1 ml) at 80°C for 3 h. Extraction of the products with *n*-hexane allowed the GC–MS analysis of DIPN obtained.

The complete DIPN mixture was obtained from carbonless copy paper (6.3 g) by extraction with CH_2Cl_2 (200 ml) by means of ultrasonic equipment for 30 min. Successive purification of the crude extract was performed applying flash chromatography on silica gel (Kieselgel 60, 70–230 mesh; Merck, Darmstadt, Germany) with *n*-hexane as the mobile phase. The compounds investigated showed an R_F value of 0.9. A further DIPN enrichment was obtained by the Bjorseth procedure by extraction with dimethylformamide–water (9:1) and back-extraction into cyclohexane to eliminate the aliphatic components of the sample [16]. The various steps of purification were checked with the available analytical techniques. All the data obtained from the DIPN extract were confirmed with an authenticated mixture used in carbonless copy paper production.

2.3. GC–MS apparatus and conditions

The GC–MS data were obtained with a Hewlett-Packard system consisting of a Model 5890 II gas chromatograph equipped with a PONA fused-silica capillary column (50 m × 0.2 mm I.D.; film thickness 0.5 μm) and a Model 5971 A mass spectrometer. An HP 59970 C data system was used for data acquisition and elaboration. Owing to the difficulty of isomer separation, the temperature programme chosen for the GC run was isothermal at 120°C for 0.5 min followed by a temperature increase of 3°C min^{-1} up to a final temperature of 260°C, maintained for 10 min. The helium flow into the column was constant at 0.528 ml min^{-1}.

The transfer line and injector temperatures were 280 and 250°C, respectively. The quadrupole conditions were electron energy 70 eV, emission current 300 μA and ion source tem-

perature 250°C. Mass spectra were recorded by cyclically scanning from 50 to 270 mass units with a cycle time of 0.51 s and a solvent delay of 9 min. A 1-μl volume from 150 ppm DIPN solution was injected into the GC–MS system under splitless conditions for 0.2 min.

2.4. HPLC apparatus and conditions

The measurements were performed using a Waters (Milford, MA, USA) HPLC system consisting of a Model 600 MS pump, a Model U6K injector, a Model 990 plus photodiode-array (PDA) detector and a Model 990 plotter. The acquisition and elaboration of the data were carried out with a NEC APC IV computer (Boxborough, MA, USA). The compounds under investigation were separated using a Delta-Pak RP-18 100 Å column (150 mm × 3.9 mm I.D. and spherical particles of 5 μm) and methanol–water (76:24) as the mobile phase at a flow-rate of 0.7 ml min^{-1}. The PDA detector recorded in the range 210–400 nm with a scan rate of 1 cycle s^{-1} and resolution of 1.4 nm. A 20-μl volume of 50 ppm DIPN solution was injected in the instrumental system.

2.5. GC–FT-IR apparatus and conditions

A Hewlett-Packard Model 5890 II gas chromatograph was coupled to a Model 5865 A FT-IR detector. The IR spectrometer recorded the transmittance/absorbance in the range 4000–750 cm^{-1} with a scan resolution of 4 cm^{-1}. The GC separation was performed by using an SPB-1 capillary column (Supelchem, Milan, Italy) (60 m × 0.32 mm I.D.; 1.0 μm film thickness) with a constant head pressure of 100 kPa. The oven temperature programme started from 150°C with a ramp rate of 5°C min^{-1} up to 230°C, maintained for 20 min. The flow-cell injector and transfer line were heated to 250°C. A helium

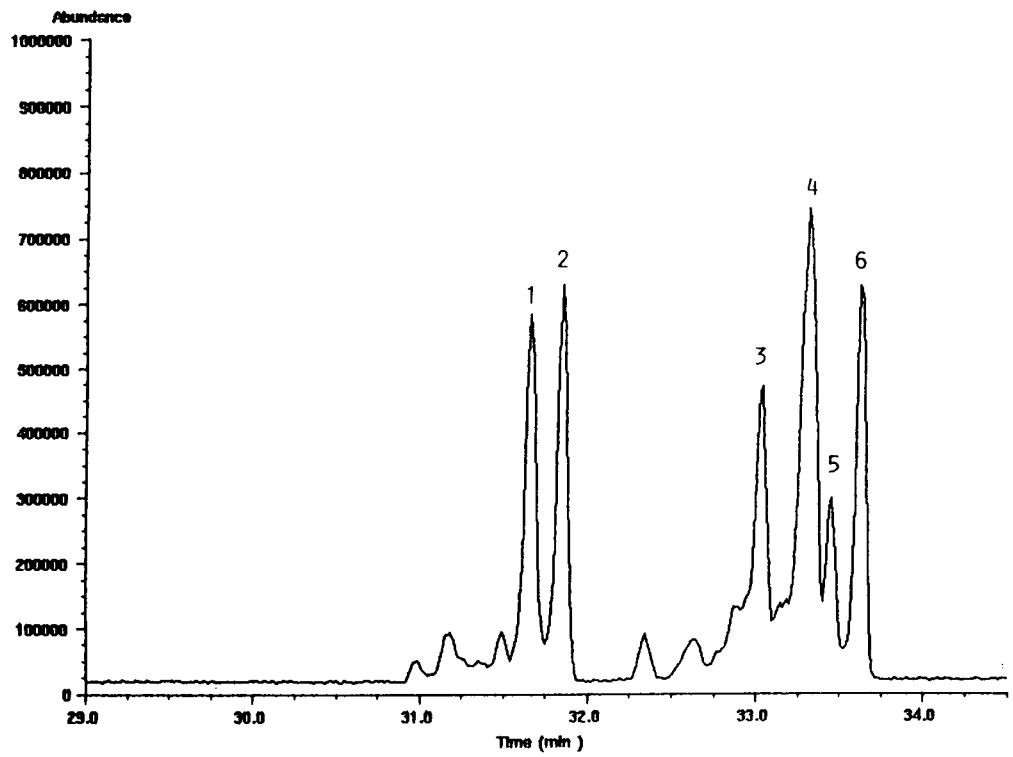

Fig. 1. GC–MS chromatograpic fingerprint of the industrial mixture of diisopropylnaphthalenes.

Table 1
Fragment ions and relative abundances (%) of six DIPN isomers, corresponding to GC peaks

Ion	m/z	Peak					
		1	2	3	4	5	6
$[M]^{+\cdot}$	212	57	52	43	54	63	45
$[M-CH_3^{\cdot}]^+$	197	100	100	100	100	100	100
$[M-C_3H_7^{\cdot}]^+$	169	12	9	10	8	9	7
$[C_{13}H_9]^+$	165	12	14	14	11	14	9
$[M-C_4H_9^{\cdot}]^+$	155	39	45	24	42	56	26
$[C_{12}H_9]^+$	153	18	23	18	20	25	14
$[M-C_5H_{11}^{\cdot}]^+$	141	14	13	13	12	15	8
$[C_{10}H_8]^{+\cdot}$	128	7	7	6	6	8	5
$[C_9H_7]^+$	115	7	5	6	5	6	5
$[C_7H_7]^+$	91	2	4	2	4	5	3
$[C_6H_5]^+$	77	3	3	3	2	4	2

pressure of 35 kPa was forced to feed the make-up flow. A 1-μl injection of a 2000 ppm DIPN solution was made in the splitless mode.

3. Results and discussion

All the samples containing the industrial mixture of diisopropylnaphthalenes showed by GC–MS analysis a characteristic total ion current distributed in six principal peaks as reported in Fig. 1. The lower peaks, recognized as DIPN, have not been attributed to any configuration owing to their low concentration in the mixture. The corresponding chromatogram may be considered as the fingerprint indicating the probable presence of such isomers. Under our experimental conditions the detection limit for the DIPN mixture was about 3.5 μg ml^{-1}.

The mass spectra corresponding to six peaks are reported in Table 1 and Fig. 2 shows the analog spectrum of the 2,6-isomer. The base peak for all was at m/z 197 due to CH_3 radical loss. The molecular ions (m/z 212) were very similar, in terms of relative intensity, for all the isomers. Another significant mass spectrometric peak was attributed to the loss of 57 and 59 mass units corresponding to the $[M-C_4H_9]^+$ and $[C_{12}H_9]^+$ fragment ions, leading to ionic species at m/z 155 and 153. All the other fragment ions had low relative intensities (<15%). The only mass spectrum found in the literature on these compounds was assigned to the 2,6-isomer [11], but it shows a significant difference in comparison with that above (see Fig. 2), as confirmed also by Peterman and Delfino [17]. In the old spectrum, the fragment ion at m/z 78 was probably due to the partial pyrolytic process, frequently occurring in old mass spectrometers. Therefore, this current MS response represents

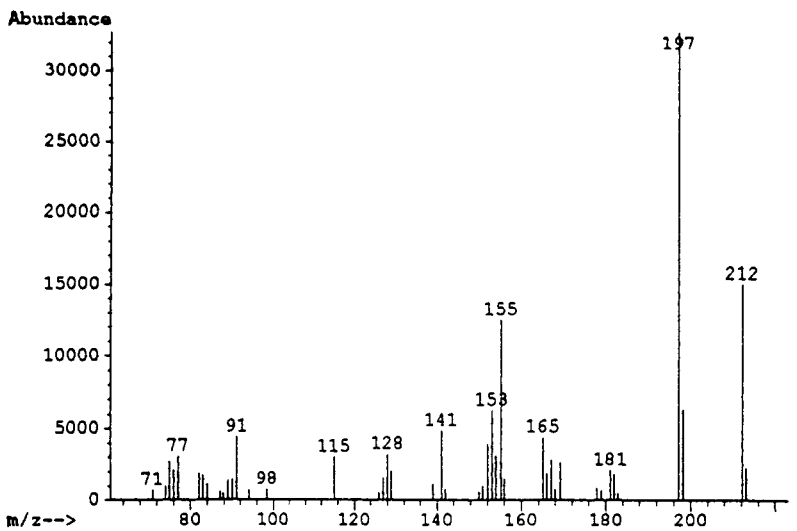

Fig. 2. Mass spectrum of 2,6-DIPN isomer.

an important update of the mass spectrometric behaviour of these naphthalene derivatives under the usual 70 eV electron impact ionization.

The HPLC analysis using PDA detection allowed the DIPN chromatographic peaks to be recorded together with UV information, as reported in Fig. 3. The UV spectra of all the HPLC peaks showed the same absolute absorption maxima at 227 nm, while lower absorption in the region 270–290 nm occurred at different wavelengths, probably owing to the positions of substituents on the naphthalene ring. The UV spectrum of the 2,6-isomer is reported in Fig. 4. Six isomers of dimethylnaphthalenes used as reference compounds were analysed separately with the HPLC–PDA system. These measurements highlighted three isomer pairs, having analogous positions of substituents with an absorption maximum at 279 nm for the α,β-, 286 nm for α,α- and 272 nm for β,β-configurations (Table 2). An analogous behaviour has been observed also for DIPN isomers where tentatively the maximum UV absorption at 280 nm was assigned to α,β-, 288 nm to α,α- and 271 nm to β,β-configurations. The comparison between the found values for DMN with respect to those for DIPN showed, in both instances, a red shift from β,β- to α,β- and α,α-substituted compounds. According to these data, the HPLC peaks of DIPN Nos. 1, 2 and 4 could be α,β-isomers, the third peak α,α- and the others (5 and 6) β,β-substituted (Table 2). The 2,6-isomer was confirmed by GC–MS and HPLC–PDA runs using an authenticated standard. This compound was eluted, under GC conditions, with the highest retention time, whereas in the HPLC sequence it occupied the fifth position (Table 3). From the relative abundance of each peak, obtained by both analytical techniques, a different position in the respective chromatogram was detected also for the other isomers, except for peaks 1 and 2 (Table 3).

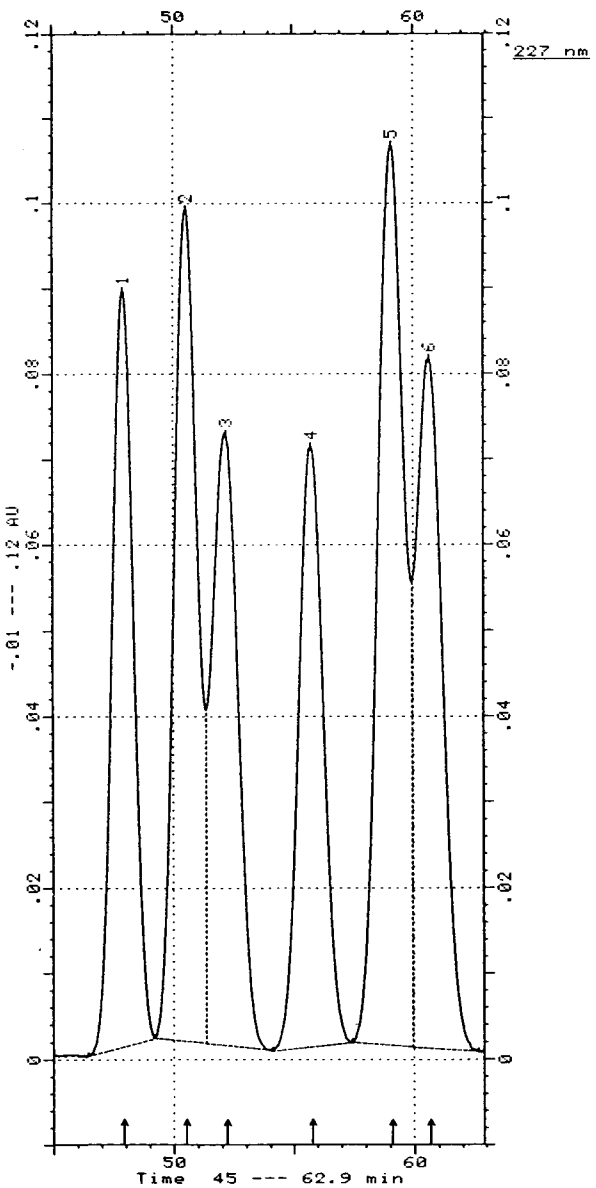

Fig. 3. HPLC fingerprint at 227 nm of the industrial mixture of diisopropylnaphthalenes.

The GC–FT-IR analysis confirmed the presence of CH_3 and =CH stretching in the range 3090–2880 cm^{-1} and specific bands in the 1000–700 cm^{-1} range, corresponding to CH bending out the plane due to different substituent positions (Table 4). Using the IR literature data for DMN isomers [18,19] the attribution of positions to the DIPN mixture was tried. The absorptions of chromatographic peaks 4, 5 and 6 in Fig. 1 were similar to those of 2,7-, 1,5- and 2,6-DMN, respectively (Table 4). Such a correspondence was not fully satisfied for the other peaks, but nevertheless the whole aspect of the spectra led

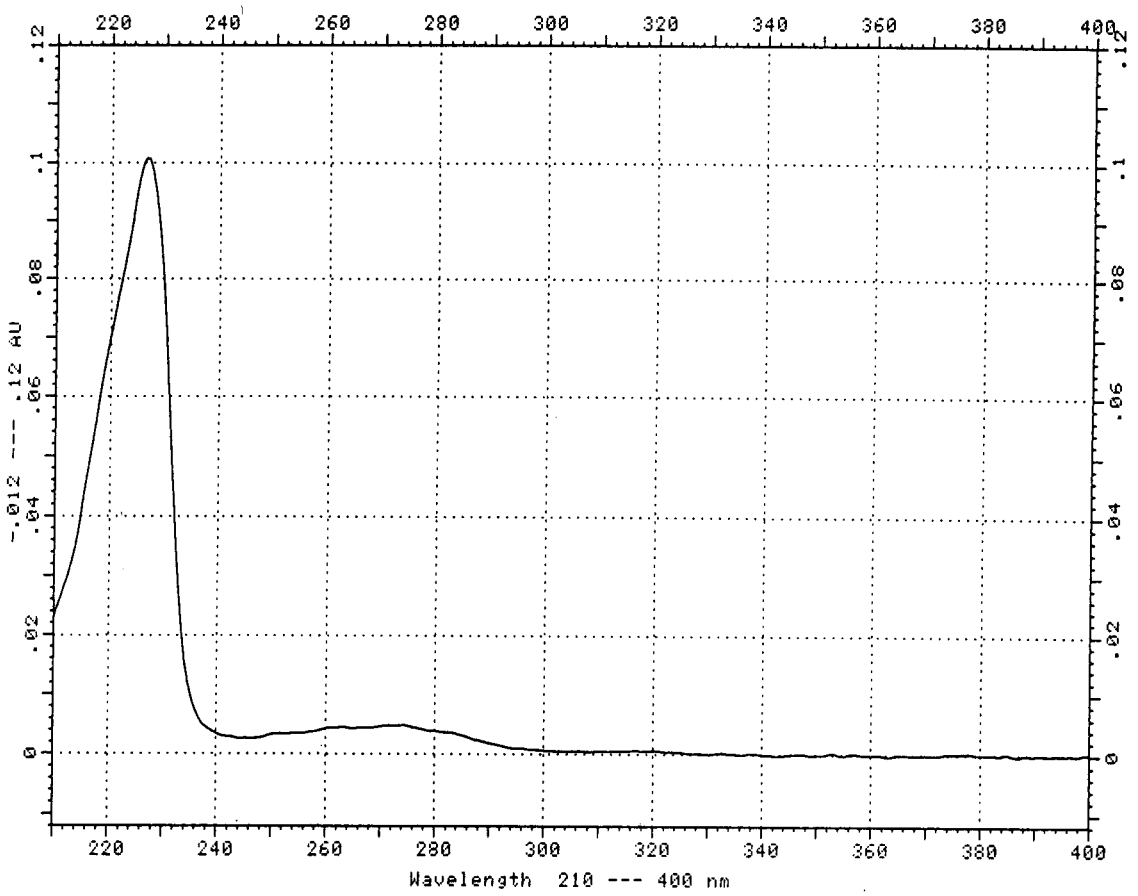

Fig. 4. UV spectrum of 2,6-DIPN isomer.

to the attribution of peaks 1, 2 and 3 to an α,β-configuration represented by the 1,3-, 1,6- and 1,7-isomers.

Friedel–Crafts synthesis was used to identify each isomer of the DIPN mixture. The products obtained starting from 2-isopropylnaphthalene and a 1- and 2-isopropylnaphthalene mixture showed the same isomers represented by the GC peaks 1, 2, 4 and 6 in Fig. 1. Probably this phenomenon is explained by an internal rearrangement due to the influence of aluminium chloride [15]. On the other hand, aromatic

Table 2
UV absorption wavelengths (nm) of six DMN isomers used as reference and the corresponding values found for DIPN isomer mixture

DMN isomer	Configuration	UV absorption (nm)	DIPN peak	UV absorption (nm)	Configuration
1,3-; 1,6-	α,β-	279	1,2,4	280	α,β-
1,4-; 1,5-	α,α-	286	3	288	α,α-
2,6-; 2,7-	β,β-	272	5,6	271	β,β-

Table 3
Elution sequence of DIPN isomers, from a commercial mixture, obtained by GC–MS, GC–FT-IR, HPLC and from synthesis, analysed by GC–MS

Method	Peak					
	1	2	3	4	5	6
GC–FT-IR GC–MS	1,3-	1,7-	1,6-	2,7-	1,5-	2,6-[a]
HPLC–PDA	1,3-	1,7-	1,5-	1,6-	2,6-[a]	2,7-
Synthesis	1,3-	1,7-	–	2,7-	–	2,6-[a]

Each chromatographic peak is assigned to a specific positional isomer.
[a] Confirmed by comparison with an authenticated reference compound.

substitution in the 2-position gives rise to the most stable alkyl derivative also under our experimental conditions. In fact, a similar synthesis procedure using naphthalene and 2-propanol as reagents produced the identical chromatographic pattern. Fig. 5 shows the HPLC trace of DIPN isomers obtained when Friedel–Crafts alkylation of naphthalene was carried out in presence of sulfuric acid as catalyst. The first evidence is the negligible amount of β,β-isomers (peaks 5 and 6) identified on the basis of their retention times and UV spectra as 2,6- and 2,7-derivatives, respectively. Moreover, as the naphthalene is first transformed into 1-naphthalenesulfonic acid,

Table 4
IR absorption wavenumbers in the region 1000–745 cm^{-1} of reference DMN isomers and the corresponding values detected from DIPN isomer mixture

DMN	IR absorption (cm^{-1})	DIPN peak	IR absorption (cm^{-1})
1,3-	745[a], 772, 859	1	780, 878[a], 942
1,7-	820[b]	2	830[a]
1,6-	748, 785, 812[a], 871	3	758[a], 835
2,7-	831[a], 890, 956	4	837[a], 899, 953
1,5-	787	5	778
2,6-	821[a], 889, 963	6	810, 884[a], 924

[a] More intense peak.
[b] The analog IR spectrum was reported by Schneider et al. [19].

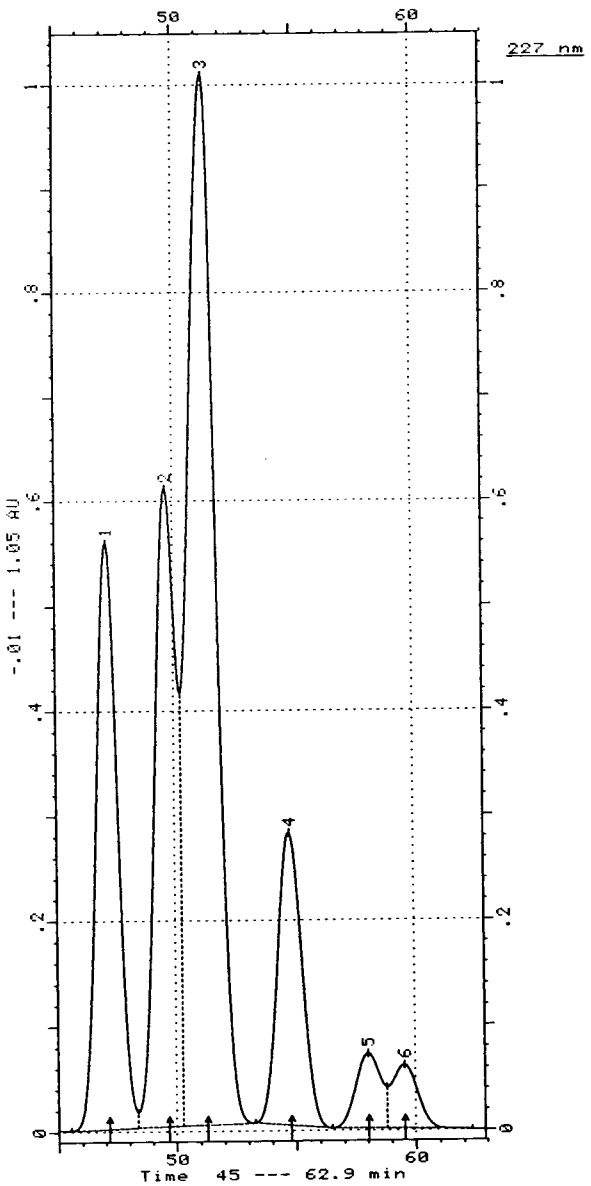

Fig. 5. HPLC of DIPN isomers obtained by Friedel–Crafts alkylation using sulfuric acid as catalyst.

the final products must be all considered 1-substituted [15]. The most abundant peak (3) having the α,α-configuration, is attributed to co-eluted 1,5- and 1,4-isomers. The presence of the 1,4-derivative is deduced by comparison of the relative abundances of GC and HPLC chromatographic peaks.

The GC–MS, HPLC–PDA and GC–FT-IR measurements together with reference compound and synthesis data allowed us to assign, with sufficient matching, the structures 2,7-, 1,5- and 2,6- to the last three GC peaks in Fig. 1, respectively (Tables 2, 3 and 4). Peak 1, having a α,β-configuration as emphasized by HPLC data, could be the 1,3- or 1,7-isomer. On the other hand, the GC–FT-IR and synthesis information led to the attribution of the 1,3-structure to this peak. This attribution was also supported by the analysis of the shape parameters [20]. In fact, the criteria used in the molecular shape determinations of DMN have been applied on a planar representation of DIPN (Table 5). These values were obtained by drawing the smallest rectangle enveloping the planar representation of each isomer which maximized the length-to-breadth ratio (L/B). Such data showing the lowest shape value for 1,3-compound confirmed our hypothesis, as this isomer is eluted first in both chromatographic techniques. Concerning the attribution of the GC peaks 2 and 3, the HPLC–PDA data (peaks 2 and 4) suggested an α,β-configuration. The IR information confirmed this, assigning the 1,7- and 1,6-structures, respectively.

NMR analysis constitutes a fundamental means to establish the certain configuration of substitution isomers. However, this technique requires for each isomer a few milligrams of pure sample, which could not be obtained for the studied DIPN mixture owing to insufficient HPLC resolution. Moreover, the selective synthesis of pure isomers was very difficult and with uncertain results. In contrast, the less specific HPLC–PDA technique supplied an unexpected and useful aid to assigning the positions of two isopropyl substituents in the naphthalene ring. The study of the UV spectra allowed us to distinguish the different isomers on the basis of the maximum absorption wavelength in the range 270–290 nm, working with analytical amounts. The responses of diisopropylnaphthalenes in the principal analytical techniques may be useful as references for their identification in different matrices and with respect to the choice of the most suitable analytical system.

Table 5
Molecular shape parameter values calculated for each DIPN isomer

Isomer	L/B (max)
1,3-	1.166
1,7-	1.237
1,5-	1.420
1,6-	1.443
2,7-	1.710
2,6-	1.867

Acknowledgements

The authors thank Dr. P. Pannocchia and Dr. D. Paolucci of Centro Ricerche dell'ENICHEM, Porto Marghera, Italy, for invaluable support in carrying out GC–FT-IR measurements and Dr. C. Tomaseth of CNR for the determination of molecular shape parameters.

References

[1] A. Sturaro, G. Parvoli, S. Bardati, R. Rella and L. Doretti, *Int. J. Food Sci. Technol.*, in press.
[2] J. Nieuwstad, P. Klapwijk and H. Van Bekkum, *J. Catal.*, 29 (1973) 404.
[3] Y. Okada, Y. Igarashi and K. Okubo, *Eur. Pat Appl.*, EP 56 177 (1982); *C.A.*, 97 (1982) 205802n.
[4] Kanzaki Paper Mfg., *Jpn. Kokai Tokkyo Koho*, JP 82 12 695 (1982); *C.A.*, 97 (1982) 101745e.
[5] Canon KK, *Jpn. Kokai Tokkyo Koho*, JP 82 03 872 (1982); *C.A.*, 96 (1982) 201403q.
[6] Fuji Photo Film Co., *Jpn. Kokay Tokkyo Koho*, JP 58 111 050 (1984); *C.A.*, 100 (1984) 200907w.
[7] Kureha Chemical Industry Co., *Jpn. Kokay Tokkyo Koho*, JP 58 38 246 (1983); *C.A.*, 99 (1983) 161227p.
[8] H. Hasegawa, M. Sato and H. Tsuruta, *Ind. Health*, 20 (1982) 283.
[9] T. Haga, K. Ozaki and Y. Tominaga, *Niigata Rikagaku*, 10 (1984) 43; *C.A.*, 102 (1985) 190609a.
[10] S. Tokuda, M. Kitamura, Y. Tomoyoshi and I. Shigeta, *Kyoto-shi Kogai Senta Nenpo*, 6 (1985) 44; *C.A.*, 105 (1986) 196859r.
[11] K. Sumino, *Arch. Environ. Contam. Toxicol.*, 6 (1977) 365.
[12] M. Sato, *Niigata Rikagaku*, 6 (1980) 43; *C.A.*, 93 (1980) 209979r.

[13] H. Kojima, H. Saito and T. Yoshida, *Chemosphere*, 11 (1982) 1003.
[14] I.P. Zukerwanik and I. Terentjewa, *Zh. Obshch. Khim.*, 7 (1937) 637.
[15] C.C. Price, *Org. React.*, 3 (1946) 1.
[16] A. Bjorseth, *Anal. Chim. Acta*, 94 (1977) 21.
[17] P.H. Peterman and J.J. Delfino, *Biomed. Mass Spectrom.*, 19 (1990) 755.
[18] C.J. Pouchert, *The Aldrich Library of FT-IR Spectra*, vol. 1. Aldrich, Milwaukee, WI, 1985.
[19] J.F. Schneider, L.A. Raphaellan, A.S. Boparai, M.C. Hansen and M.D. Erickson, *J. Chromatogr. Sci.*, 27 (1989) 592.
[20] R. Kaliszan, *Quantitative Structure–Chromatographic Retention Relationships*, Wiley, New York, 1987.

ELSEVIER

Journal of Chromatography A, 688 (1994) 221–230

JOURNAL OF CHROMATOGRAPHY A

Application of a two-dimensional chromatography system for gas-phase photodegradation studies of polychlorinated dibenzo-*p*-dioxins

L.D. Sivils[a], S. Kapila[a,*], Q. Yan[a], A.A. Elseewi[b]

[a]*Center for Environmental Science and Technology, University of Missouri–Rolla, 329 Schrenk Hall, Rolla, MO 65401, USA*
[b]*Environmental Affairs Division, Southern California Edison Company, P.O. Box 800, Rosemead, CA 91770, USA*

First received 24 May 1994; revised manuscript received 30 August 1994

Abstract

Gas-phase photodegradation of polychlorinated dibenzo-*p*-dioxins was studied with a two-dimensional gas chromatographic system consisting of two independently operated gas chromatographs interfaced to a photoreactor. Gas flow through the chromatographs and photoreactor were directed with two switching valves. This arrangement permitted isolation and irradiation of solute in the photoreactor for varied periods and under different atmospheres. The irradiation experiments revealed that different dioxin congeners degrade at different rates; e.g., a 20-min irradiation resulted in the degradation of approximately 80% of 2,3,7-trichlorodibenzo-*p*-dioxin, while only 30% of the 2,3,7,8-tetrachlorodibenzo-*p*-dioxin was found to degrade under the same conditions. As expected, photodegradation rates decreased with an increase in the number of chlorines. Degradation rates were also influenced by the position of chlorine substitutions. The results showed that, in contrast to solution-phase studies, congeners with peri chlorines photodegrade more rapidly than congeners with laterally substituted chlorines. These results indicate that, in the gas phase, more toxic (laterally substituted) congeners are more persistent than less toxic (peri substituted) analogues.

1. Introduction

Many sites in the USA and abroad are contaminated with polychlorinated dibenzo-*p*-dioxins (PCDDs) as a result of accidents or prolonged industrial activities. PCDDs, or dioxins (as these chemicals are generally known), are highly toxic unwanted byproducts of a number of chemical processes such as incineration and application of chlorine bleach in the pulp and paper industries [1–4]. The 75 PCDD homologues show varied physicochemical properties and toxicities depending on the degree and position of chlorine substitutions. Analogues with four or more chlorines are practically insoluble in water, resistant to biodegradation and exhibit a high degree of environmental persistence [5,6].

Photodegradation, i.e., destruction (transformation) achieved through exposure to the near-UV components of sunlight, is reported to be the most significant natural mechanism for removal of dioxins in the environment [7]. The degradation proceeds through a free radical

* Corresponding author.

0021-9673/94/$07.00
SSDI 0021-9673(94)00847-7

mechanism and, under suitable conditions, leads to the formation of analogues with fewer chlorines. Depending on the substitution, the elimination of chlorine can result in analogues with higher or lower toxicities [8]. A number of studies dealing with photodegradation of dioxins and related polychlorinated dibenzofurans (PCDFs) in the solution phase have been reported in literature [9–15]. However, the mechanism of photoreaction for these compounds has not been fully elucidated. It has been observed that both the rate of degradation and the nature of photoproducts are affected by the physical state of the matrix. Significant differences have been reported in the types of dechlorination products formed in solution phase and on solid particles [16,17]. A preferential loss of chlorines from the lateral positions (2,3,7,8) has been reported in a number of solution phase studies. However, Kieatiwong et al. [18] have observed that dechlorination of octachlorodibenzo-*p*-dioxin (OCDD) adsorbed on soil occurs preferentially at the peri positions (1,4,6,9). Similar results have been obtained by Tysklind et al. [19] with PCDD bearing fly ash samples. Surprisingly, dechlorination of PCDFs, in the same study [19], was shown to occur preferentially at the lateral position. Since the toxicity of PCDD is dependent on the chlorine substitution, the dechlorination route can have significant effect on toxicity. A review of literature revealed that one of the most overlooked areas has been photodegradation in the vapor phase.

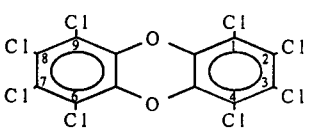

The primary reason for the lack of information in this area is related to the low ambient vapor pressure of these compounds. However, it is quite evident that despite their low vapor pressure, substantial portions of PCDDs in the troposphere exist in the vapor phase; e.g., according to one estimate, ca. 20–60% of TCDD is present in the vapor form [20]. Furthermore, one of the major sources of widespread distribution of dioxins in the environment is incineration which releases these contaminants into the atmosphere [21–23]. These facts, coupled with the observation that bioavailability of dioxins through pulmonary uptake is nearly 100% [24], make gas-phase photochemistry of dioxins an important and interesting area of research.

The objective of the study was to investigate the vapor-phase photodegradation of PCDDs in the gas phase. The emphasis was placed on degradation kinetics of variously substituted dioxins and characterization of photoproducts obtained under different atmospheric conditions. These objectives were met with the application of a dual-column chromatographic system interfaced to a photoreactor.

A number of studies on gas-phase reactions with dual-column gas chromatographic systems have been reported in literature [25–27]. A few of these studies have been dedicated to the gas-phase photolysis of organic compounds [28,29]. The advantages of such chromatographic arrangement for gas-phase photolysis have been discussed by Aue and Aigner-Held [28]. The system used in the present study permitted a convenient means of discerning the photodegradation rate for PCDDs and permitted characterization of hydrodehalogenation products.

2. Experimental

The chromatographic system was constructed around a thermostated aluminum block. The block served as the housing for the photoreactor, two switching valves, and an externally mounted cryogenically cooled trap consisting of a thin-wall 1/8-in. (1 in. = 2.54 cm) stainless-steel tube with a nichrome wire wound around it. The low mass cryogenic trap was rapidly cooled by passing liquid nitrogen through it and rapidly heated by passing an electrical current through the nichrome resitive wire. The gas chromatographs, photoreactor and the cryotrap were interconnected through the switching valves. A schematic of the system is shown in Fig. 1. The analytes of

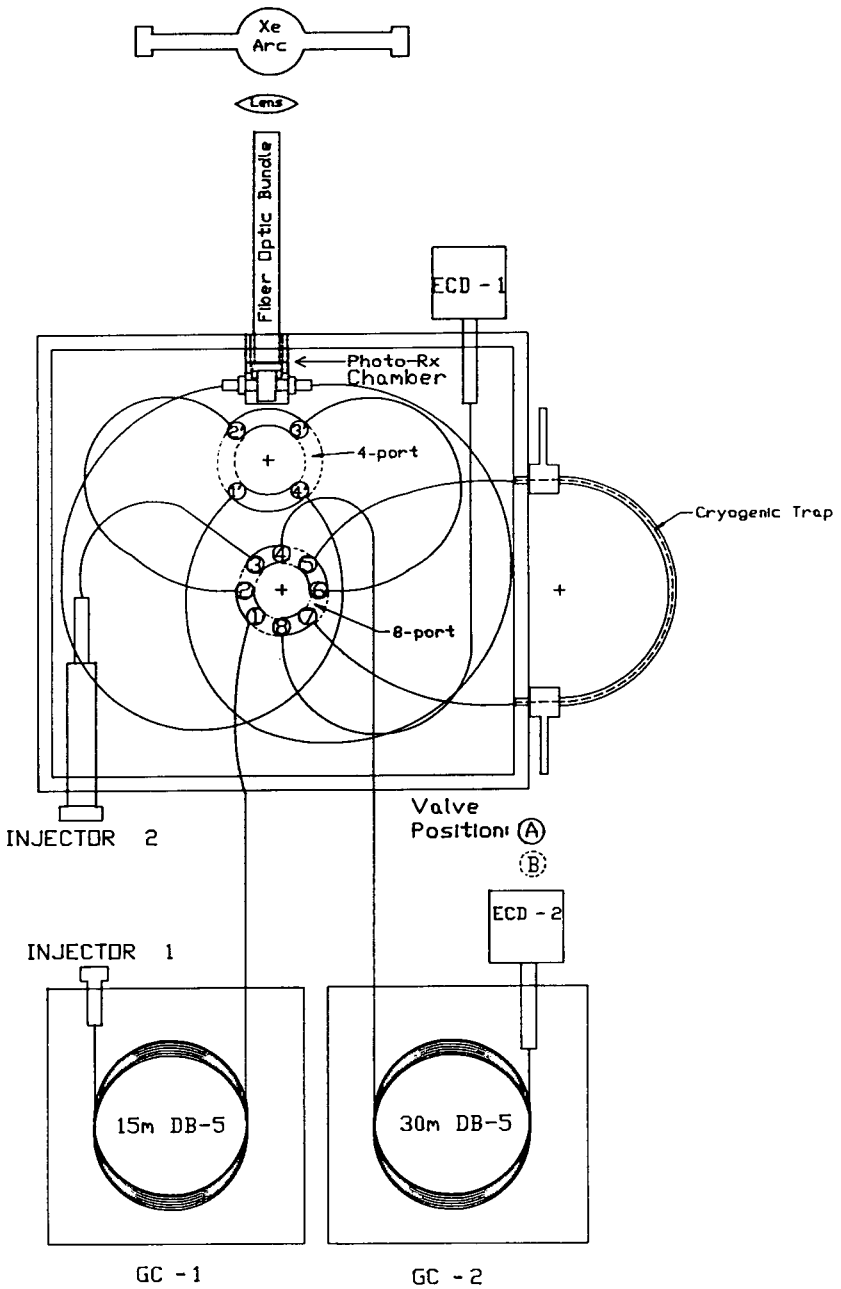

Fig. 1. Schematic diagram of two-dimensional reaction gas chromatography system. Broken lines denote valve positions B.

interest were introduced into the system via the first gas chromatograph (GC-1) equipped with an electron-capture detector (ECD-1). The detector served as a monitor for eluting components and facilitated in switching the appropriate component. The component transfers were accomplished with an eight-port valve (V1; VICI 4C8WT). A four-port valve (V2; VICI 4C4WT)

was also incorporated into the system to permit transfer and entrapment of the selected analyte in the photoreactor. The low-dead-volume valves were obtained from Valco (VICI, Houston, TX, USA). This feature allowed variation of irradiation time over a wide range. After irradiation, the residual analytes and photoproducts were transferred to the cryotrap and standard analytes were added to the second injector to facilitate product peak confirmation through co-chromatography. All components of the system were interconnected with 0.25 mm I.D. aluminum clad fused-silica tubing.

The photoreactor consisted of a 500-μl quartz cell placed in gas-tight stainless casing. The broadband-UV excitation used for irradiation was obtained from a xenon arc lamp. The light from the xenon lamp was passed through a water filter (Oriel 61945) to absorb IR radiation. The filtered light was collected and focused with a fiber optic coupler (Oriel 77800) onto a high-grade fused-silica fiber optic bundle. The optic bundle was obtained from Fiberguide Industries (SFS320/385T). The bundle was designed to withstand temperatures up to 325°C for extended periods of time.

Initially, both valves were switched to position A. This permitted passage of effluent from GC-1 to ECD-1 while bypassing the photoreactor. All valve-switching operation timing began with the appearance of the solvent front at ECD-1. The change of V2 to position B allowed the sample band to pass into the photoreactor. After a set time interval, V2 was switched to position A, trapping the sample band in the photoreactor. The analyte in the reactor was irradiated with broadband radiation in the UV–visible region. After the desired exposure period, the reactor contents were transferred to the cryogenically cooled trap by switching V2 to position B. V1 was switched to position B, and the trapped residual analyte and photoproduct were flash vaporized and introduced into the second column. The separated components were monitored by the second electron-capture detector (ECD-2) or a quadrupole mass spectrometer. An example of the timing sequence for the photoanalysis of hexachlorobenzene is given in Fig. 2. The initial separation of the analyte was carried out with a 15 m × 0.25 mm fused-silica capillary column coated with 95% methyl-/5% phenylpolysiloxane. This column was installed in GC-1, a benchtop gas chromatograph (Tracor Model 560) equipped with a split/splitless injector. Separation of the residual and photoproducts was accomplished with a 30 m × 0.25 mm fused-silica capillary column coated with 95% methyl-/5% phenylpolysiloxane that was installed in GC-2 (Shimadzu MiniGC-3). The column oven parameters and chromatographic conditions were optimized for the analyte of interest.

3. Results and discussion

The overall objective of the present study was to investigate photoinduced disappearance (dechlorination) of PCDDs in the gas phase. The specific objectives of the study were to determine the correlation between rate of disappearance (degradation) and chlorine substitution and to characterize neutral photoproducts. A two-dimensional gas chromatography system with a photoreactor was selected as the apparatus of choice for the study. Although similar systems have been used for photochemical and analytical studies in the past [26–29], the present system provided better resolution, permitted a higher degree of flexibility in the irradiation time and allowed for condition modification in the photoreaction chamber.

Prior to its use in PCDD studies, the performance of the system was evaluated with hexachlorobenzene (HCB). This polychlorinated compound was selected because of its high response with both ECD and MS as well as its good chromatographic properties. Chromatographic profiles of HCB obtained through peak transfer to GC-2 are shown in Fig. 3. The peak in profile A shows HCB transferred without irradiation whereas profile B depicts two peaks obtained after 5 min irradiation. One of the peaks in profile B eluted with the same retention time as HCB while the other eluted 2.94 min earlier than HCB. The retention time of the early peak matched that of pentachlorobenzene.

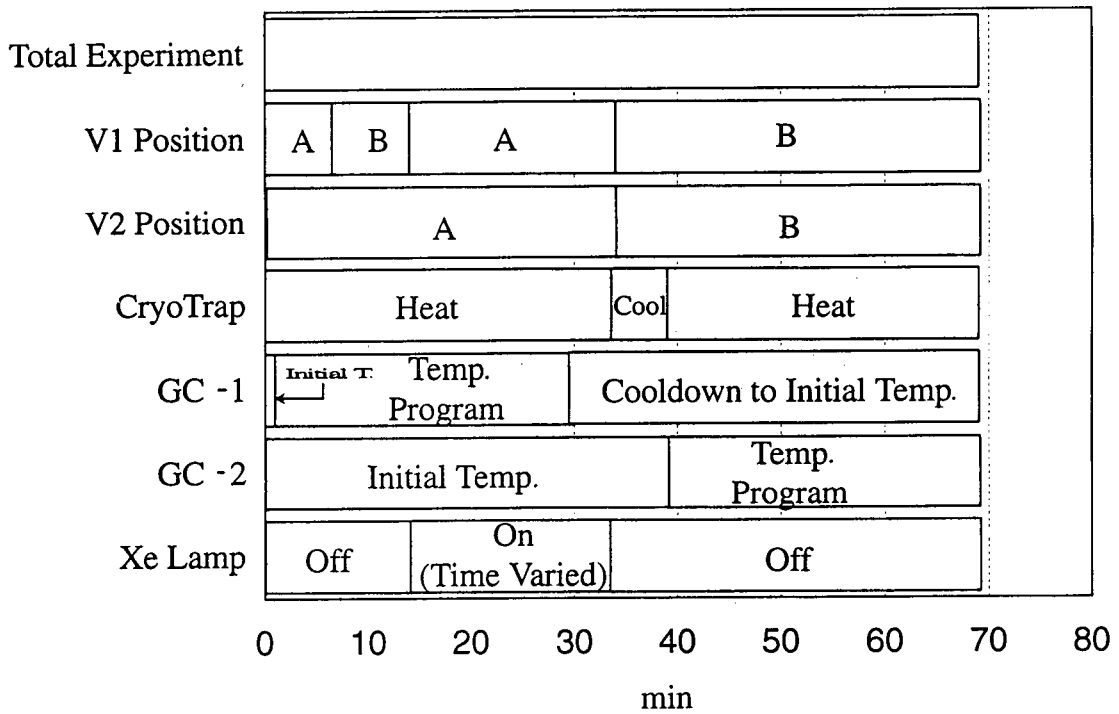

Fig. 2. An example of a timing sequence used for the gas-phase photodegradation of a typical analyte. Initial injection was at $T = 0$.

This observation was confirmed by co-chromatography. For this purpose, a standard solution of pentachlorobenzene was injected into the second injector and pentachlorobenzene was trapped in the cryotrap. The residual HCB and photoproduct obtained after irradiation was also trapped in this same trap. The contents of the trap were heat desorbed and chromatographed on the second column. The photoproduct and standard pentachlorobenzene were found to co-elute, thus establishing the identity of the photoproduct. A quantitative assessment of the photoreaction revealed that, under the experimental condition, approximately 5% of HCB was converted to pentachlorobenzene. Similar replacement of chlorine with hydrogen upon irradiation of chlorinated benzenes has been reported by Aue and Aigner-Held [29]. The photoproduct yields in the mercury sensitized system used by Aue appears to be appreciably higher than the pentachlorobenzene yields obtained with the present system with "pure" He. However, an increased yield of photoproducts was obtained when a hydrogen donor such as hexane was added to the gas stream. The products obtained with the carrier gas doped with hexane are shown in Fig. 4. The degradation kinetics of HCB degradation was studied in a limited set of experiments by irradiating a known amount (500 pg) of HCB for varied time periods. The results yielded first-order degradation kinetics (Fig. 5). The successful evaluation of the system with HCB led us to its use with the PCDDs. The system can be used to study vapor-phase phototransformation of other environmental pollutants such as polychlorinated biphenyls.

In order to delineate a correlation between dioxin structure and photodegradation, a number of trichloro- through pentachloro- dioxins were subjected to photoirradiation. The congeners selected for the study included 2,3,7-trichlorodibenzo-*p*-dioxin (TriCDD); 1,2,3,4-

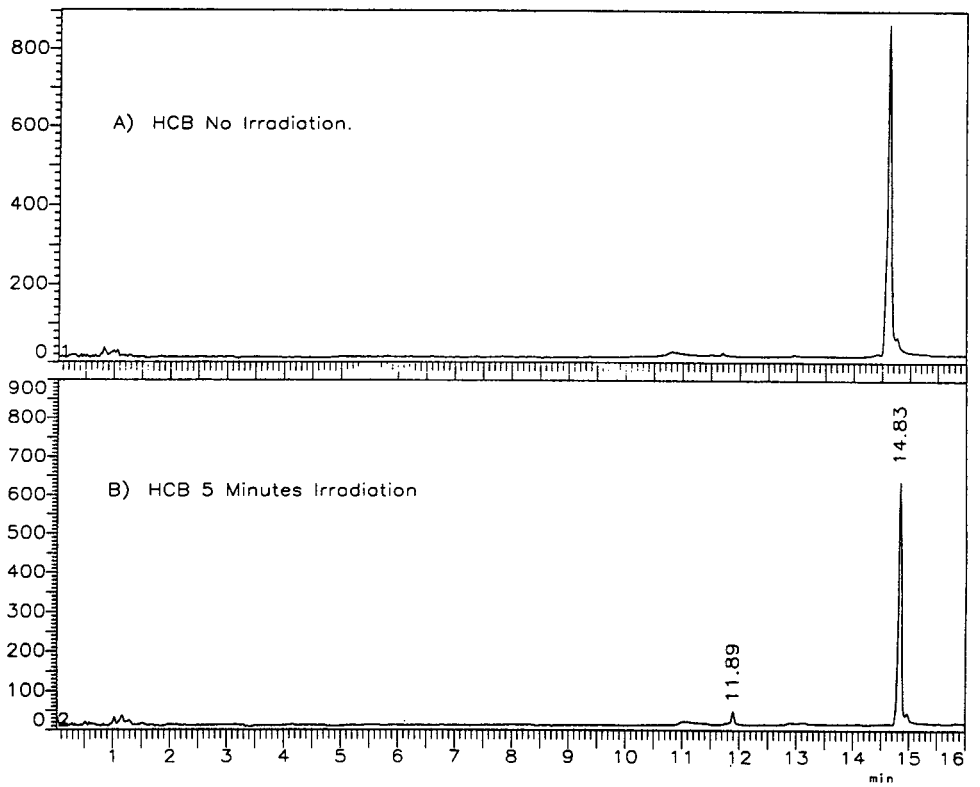

Fig. 3. Chromatographic profiles of HCB. Chromatographic output in this figure, and subsequent figures, were obtained with ECD-2. The peak at 11.89 min in trace B is pentachlorobenzene resulting from hydrodehalogenation of HCB.

tetrachlorodibenzo-*p*-dioxin (1,2,3,4-TCDD); 2,3,7,8-tetrachlorodibenzo-*p*-dioxin (2,3,7,8-TCDD); 1,2,4,7,8-pentachlorodibenzo-*p*-dioxin (1,2,4,7,8-PentaCDD); and 1,2,3,7,8-pentachlorodibenzo-*p*-dioxin (1,2,3,7,8-PentaCDD).

The irradiation experiments revealed that different dioxin congeners degrade at different rates; e.g., a 20-min irradiation resulted in degradation of as much as 80% of TriCDD while only 30% of the 2,3,7,8-TCDD was found to degrade under the same conditions. The results also showed that, in contrast to HCB, none of the dioxin congeners yielded a hydrodehalogenation photoproduct. The chromatographic output for 1,2,3,4-TCDD is shown in Fig. 6. The upper trace represents non-irradiated analyte and the bottom trace depicts the residual analyte after 20 min of irradiation. These chromatographic results are typical of the profiles obtained with the other congeners. The rate of disappearance for different congeners was determined. An examination of the data revealed an inverse relationship between the degree of chlorination and the rate of disappearance. The results are shown in Fig. 7. The data also shows that the trichloro congener degraded at a faster rate than the tetrachloro which, in turn, degraded faster than the pentachloro congeners. The data also showed that degradation followed first-order kinetics.

As discussed earlier, the differences in the stability of laterally and peri substituted congeners is an important toxicity criterion. Significant differences have been shown to exist in photo-induced dechlorination of PCDD in the solution phase and on solid surfaces. Preferential loss of lateral chlorines in solution-phase photolysis has been reported by a number of researchers. The

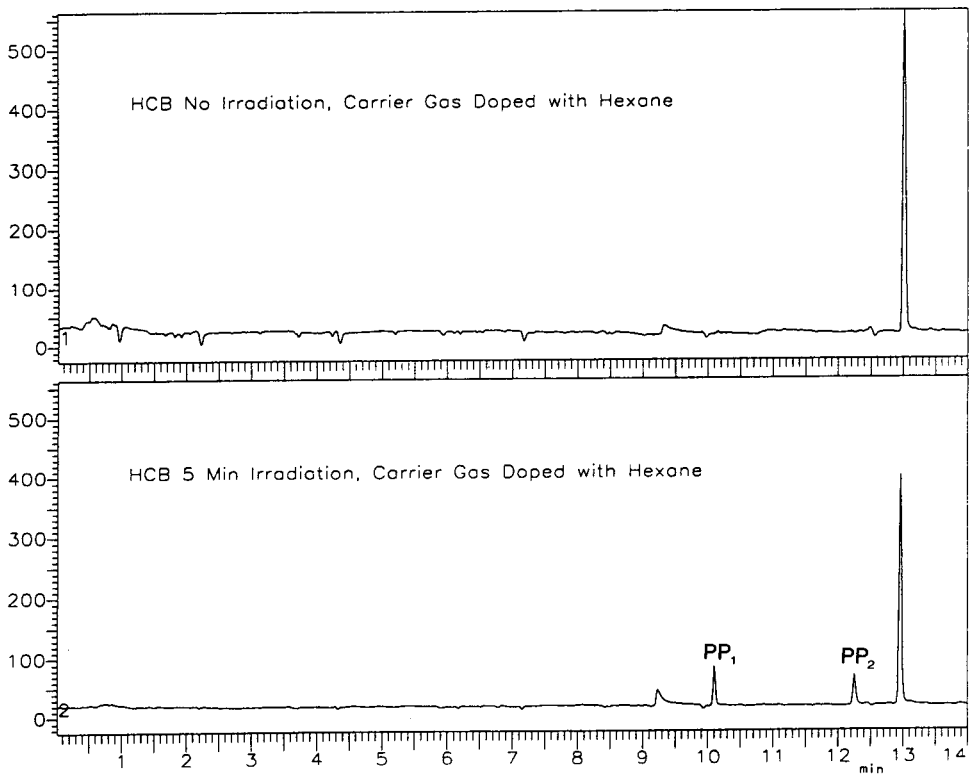

Fig. 4. Chromatographic profiles of residual HCB and photoproduct obtained in the presence of hexane (dopant) in the carrier gas. PP = Photoproduct.

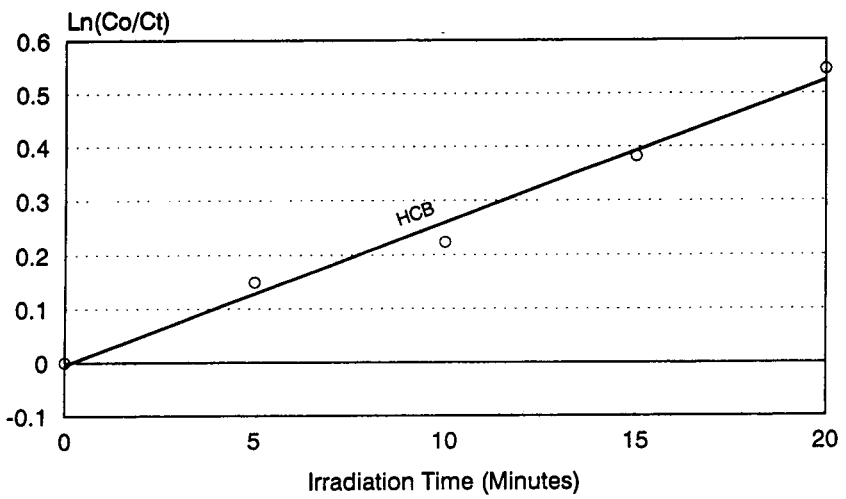

Fig. 5. Plot of HCB photodegradation vs. irradiation time. Co = Initial concentration; Ct = concentration at time t.

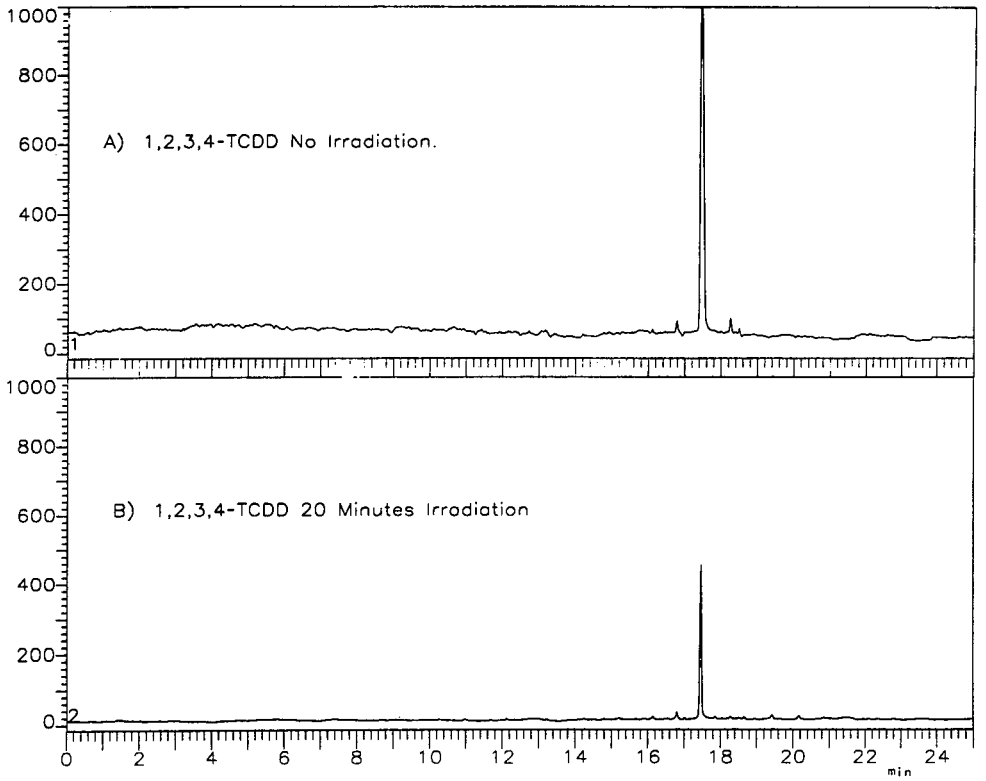

Fig. 6. Chromatographic profile of 1,2,3,4-TCDD.

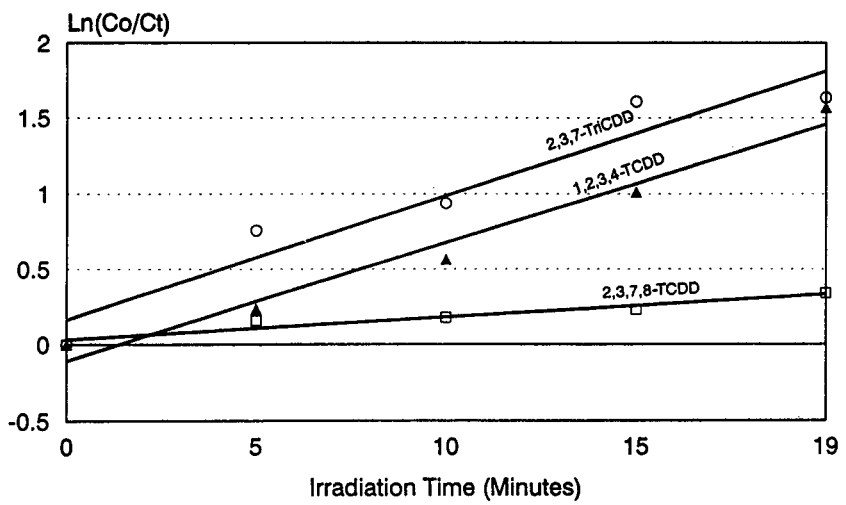

Fig. 7. Plot of PCDD degradation vs. irradiation time.

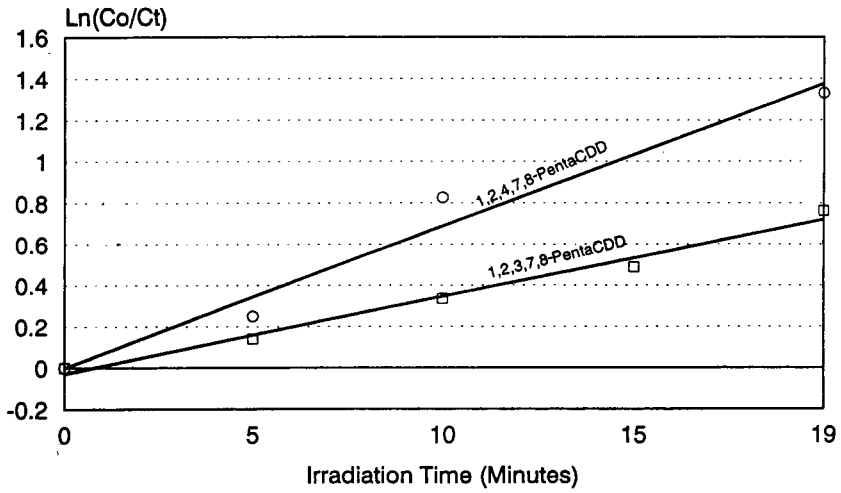

Fig. 8. Plot of PentaCDD degradation vs. irradiation time.

loss of chlorine has been shown to occur from the peri positions on adsorbent surfaces. The data obtained from the present studies indicated that photodechlorination occurred preferentially from the peri position, and the lack of photoproducts prevented an independent confirmation of the preferential loss mechanism. Therefore, this conclusion was drawn only on the basis of the relative rates of disappearance of the analyte peak. The degradation rate for 2,3,7,8-TCDD (which possesses no peri chlorines) was measurably slower than all trichloro through pentachloro congeners. Clear differences were also obtained between the two pentachloro isomers. 1,2,4,7,8-PentaCDD with two peri (1 and 4) chlorines degraded faster than 1,2,3,7,8-PentaCDD which contains only one peri chlorine. These results are summarized in Fig. 8. The data seem to indicate that the more toxic laterally substituted congeners degrade at a slower rate than the peri-substituted congeners.

Acknowledgement

These studies were supported in part through a co-operative agreement with the US Environmental Protection Agency Hazardous Substances Research Center, Region 7 and 8, Kansas State University, Manhattan, KS, USA. The study was also supported through a research contract with the Environmental Affairs Division of the Southern California Edison Company, Rosemead, CA, USA.

References

[1] O. Hutzinger and H. Fiedler, *Chemosphere*, 18 (1989) 23–32.
[2] A. Heindl and O. Hutzinger, *Chemosphere*, 15 (1986) 2001.
[3] H. Fiedler, *Organohalogen Compounds*, 11 (1993) 221–228.
[4] G. Amendola, D. Barna, R. Blosser, L. LaFleur, A. McBride, F. Thomas, T. Tierman and R. Whittemore, *Chemosphere*, 18 (1989) 1181–1188.
[5] S. Kapila, A.F. Yanders, C.E. Orazio, J.C. Medows, S. Cerlesi and T.E. Clevenger, *Chemosphere*, 18 (1989) 1079–1085.
[6] A.F. Yanders, C.E. Orazio, R.K. Puri and S. Kapila, *Chemosphere*, 18 (1989) 841–844.
[7] J.R. Plimmer, M.I. Klingebiel, D.G. Crosby and A.S. Wong, in E.H. Blair (Editor), *Chlorodioxins—Origins and Fate, (Advances in Chemistry Series*, Vol. 120), American Chemical Society, Washington, D.C., 1973, pp. 44–54.
[8] G. Miller, V. Herbert, M. Miille, R. Mitzel and R. Zepp, *Chemosphere*, 18 (1989) 1265–1274.
[9] D.G. Crosby, A.S. Wong, J.R. Plimmer and E.A. Woolson, *Science*, 173 (1971) 748–749.

[10] D.G. Crosby and A.S. Wong, *Science*, 195 (1977) 1337–1338.
[11] G.G. Choudhry and G.R. Webster, *Toxicol. Environ. Chem.*, 14 (1987) 43–61.
[12] J.R. Plimmer and U.I. Klingebiel, *Science*, 174 (1971) 407–409.
[13] Q. Yan, L.D. Sivils, S.D. Palepu, S. Kapila, A.F. Yanders and A.A. Elseewi, *Chemosphere*, in press.
[14] M. Koshioka, I. Masumi, T. Yamada, J. Kanazawa and T. Murai, *J. Pesticide Sci.*, 15 (1990) 39–45.
[15] G.G. Choudhry and G.R. Webster, *Chemosphere*, 14 (1985) 9–26.
[16] M. Tysklind, A. Carey, C. Rappe and G. Miller, *Organohalogen Compounds*, 8 (1992) 293–296.
[17] M. Dung and P. O'Keefe, *Organohalogen Compounds*, 8 (1992) 233–236.
[18] S. Kieatiwong, L.V. Nguyen, V.R. Hebert, M. Hackett, G.C. Miller, M.J. Miille and R. Mitzel, *Environ. Sci. Techno.*, 24 (1990) 1575–1580.
[19] M. Tysklind, K. Lundgren, C. Rappe, L. Erikson and M. Sjostrom, *Organohalogen Compounds*, 8 (1992) 173–175.
[20] T.F. Bidleman, *Environ. Sci. Technol.*, 22 (1988) 361–367.
[21] H. Ballschmiter, H. Buchert, R. Niemczyk, A. Munder and M. Swerev, *Chemosphere*, 15 (1986) 901–915.
[22] J.R. Visalli, *J. Air Pollut. Control Assoc.*, 37 (1987) 1451–1463.
[23] H.Y. Tong, S. Arghestani, M.L. Gross and F.W. Karasek, *Chemosphere*, 18 (1989) 577–584.
[24] C. Nessel, M. Amoruso, T. Umbreit, R. Meeker and M. Gallo, *Chemosphere*, 25 (1992) 29–32.
[25] C.R. Hastings, T.R. Ryan and W.A. Aue, *Anal. Chem.*, 47 (1975) 1169–1175.
[26] S. Kapila and W.A. Aue, *J. Chromatogr.*, 108 (1975) 13–21.
[27] W.A. Aue, V. Paramisigamani and S. Kapila, *Mikrochim. Acta*, I (1978) 193–200.
[28] W.A. Aue and R. Aigner-Held, *J. Chromatogr.*, 189 (1980) 119–125.
[29] W.A. Aue and R. Aigner-Held, *J. Chromatogr.*, 189 (1980) 127–138.

ELSEVIER

Journal of Chromatography A, 688 (1994) 231–242

JOURNAL OF CHROMATOGRAPHY A

Thermal decomposition characterization of explosives by pyrolysis–gas chromatography–mass spectrometry

Jehuda Yinon[a,*], Richard A. Yost[a], Suryanarayana Bulusu[b]

[a]*Department of Chemistry, University of Florida, Gainesville, FL 32611, USA*

[b]*US Army Armament Research, Development and Engineering Center (ARDEC), Picatinny Arsenal, NJ 07806, USA*

First received 30 June 1994; revised manuscript received 29 August 1994

Abstract

Pyrolysis–GC–MS was used to study the thermal decomposition products of a series of explosives, including 1,3,5-trinitro-1,3,5-triazacyclohexane (RDX), 1,3,5,7-tetranitro-1,3,5,7-tetrazacyclooctane (HMX), 2,4,6,N-tetranitro-N-methylaniline (tetryl), monoaminotrinitrobenzene (MATB), diaminotrinitrobenzene (DATB) and triaminotrinitrobenzene (TATB). Pyrolysis products were determined as a function of temperature in the range of 400–1000°C. Decomposition products were found to be in the low-molecular-mass range, resulting mainly from the cleavage of the C–C ring structure in the trinitroaromatic compounds and the C–N ring structure in the nitramines. Decomposition pathways and processes were determined for the various explosives.

1. Introduction

Chemical mechanisms, kinetic parameters and thermodynamic properties are key topics in the understanding of the ignition/combustion process and product distribution of explosives. A structural analysis of the fragments and intermediates resulting from controlled heating of energetic compounds can yield important information relevant to the understanding of the thermal processes. Moreover, the characterization of the individual products resulting from the combustion process can provide important data pertinent to the use of incineration of explosives as a way of disposing of obsolete explosives and ammunition. Identification of these products is important in order to single out those which are toxic, so as to avoid environmental pollution.

Pyrolysis in combination with various analytical techniques has been used to study thermal decomposition of explosives. Pyrolysis–thin layer chromatography (Py–TLC) has been used to study the thermal decomposition of 2,4,6-trinitrotoluene (TNT) [1]; pyrolysis–gas chromatography (Py–GC) has been used to identify smokeless powders and their residues [2] and to investigate the thermal decomposition of 1,3,5-trinitro-1,3,5-triazacyclohexane (RDX) and 1,3,5,7-tetranitro-1,3,5,7-tetrazacyclooctane (HMX) [3]; pyrolysis–atmospheric pressure ionization tandem mass spectrometry (Py–API-MS–MS) has been used to study the thermal decomposition of RDX and HMX [4–6]. Thermal decomposition of RDX and HMX has also been largely studied by mass spectrometry itself [7–10], and more

* Corresponding author. On sabbatical leave from the Weizmann Institute of Science, Department of Environmental Sciences and Energy Research, Rehovot 76100, Israel. Correspondence should be addressed to the Weizmann Institute of Science.

0021-9673/94/$07.00
SSDI 0021-9673(94)00827-2

recently by simultaneous thermogravimetry and modulated beam mass spectrometry [11–15].

The Py–GC–MS technique provides unique advantages for the identification of the pyrolysate products. It incorporates the gas chromatograph for the separation of the various products and the mass spectrometer as an identification tool.

GC, MS and GC–MS and their applications in the analysis of explosives have been extensively reviewed [16]. Pyrolytic methods and instrumentation [17] and Py–GC and Py–MS techniques [18] have also been described.

In order to determine the thermal decomposition products and contribute to the understanding of the decomposition pathways and processes, a Py–GC–MS study of a series of explosives was undertaken. The explosives studied were RDX (**1**), HMX (**2**), tetryl (**3**), monoaminotrinitrobenzene (MATB, trinitroaniline) (**4**), diaminotrinitrobenzene (DATB) (**5**) and triaminotrinitrobenzene (TATB) (**6**).

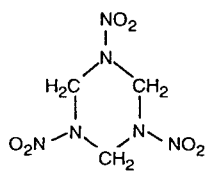

1

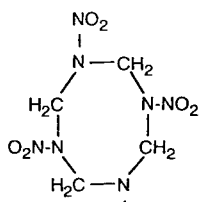

2

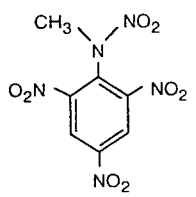

3

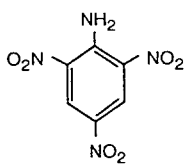

4

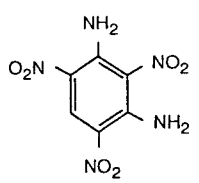

5

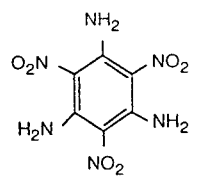

6

2. Experimental

Thermal decomposition of the explosives was carried out with a Pyroprobe 100 solids pyrolyser (Chemical Data Systems, Oxford, PA, USA) equipped with a platinum coil desorption probe. Pyrolysis was carried out with the temperature ramp (rise time) in the off position; the final temperature was set at 400–1000°C and held for 2 s. The sample (approximately 100 μg) was placed in a quartz tube in the form of an acetone solution. After complete drying, the quartz tube was positioned in the platinum coil of the pyrolysis probe. The actual temperatures of the samples in the pyrolysis experiments are uncertain. Therefore, the temperatures set on the pyrolyser should be considered as nominal temperatures. The pyrolyser was interfaced to a Finnigan MAT ITS 40 ion-trap GC–MS system. GC columns used were a 27.5 m × 0.53 mm I.D. PoraPLOT Q fused-silica capillary column with a film thickness of 20 μm (Chrompack, Middelburg, Netherlands) and a 30 m × 0.545 mm I.D. GC-Q porous polymer fused-silica capillary column (J&W Scientific, Folson, CA, USA). A split–splitless injector was used.

Pyrolysis was performed with a flow of helium at a pressure of 20 p.s.i. The flow-rate of helium through the GC column, at 10 p.s.i., was 1 ml/min, which was passed into the ion-trap mass spectrometer. As both GC columns were megabore columns, in order to obtain low flow-rates (necessary for the ion trap), a 0.5-m piece of microbore fused-silica capillary column was connected between the GC column and the ion trap.

The GC conditions were as follows: injector temperature, 175°C; initial column temperature, 35°C (hold time 5 min); heating rate, 15°C/min; final temperature, 200°C (hold time 20 min). The ion trap was operated in the electron impact (EI) mode at a temperature of 220°C and a helium pressure of about $3 \cdot 10^{-4}$ Torr (the gauge reading of the housing pressure was $3 \cdot 10^{-5}$ Torr). Explosive samples were obtained from the US Army Armament Research Development and Engineering Center, Picatinny Arsenal, NJ, USA.

3. Results and discussion

3.1. RDX and HMX

Figs. 1 and 2 show the Py–GC–MS reconstructed ion chromatograms (RIC) (total ion chromatograms) of RDX and HMX, respectively, at 1000°C. One can observe the typical similarity of the two chromatograms.

Fig. 3 shows an example of a mass spectrum of a decomposition product of RDX from pyrolysis at 1000°C. The m/z of this product is 70 and is probably due to $C_3H_6N_2^+$. The full list of the molecular ions obtained is given in Table 1.

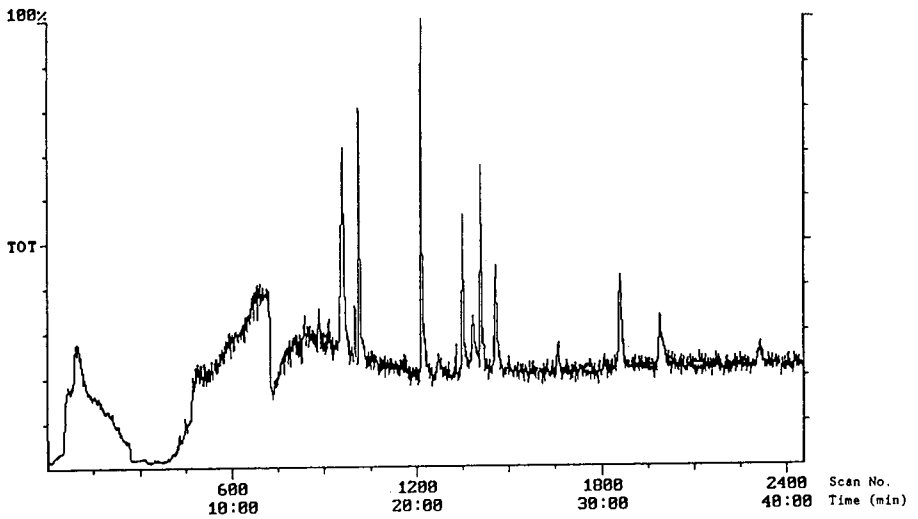

Fig. 1. Py–GC–MS: reconstructed ion chromatogram of RDX at 1000°C.

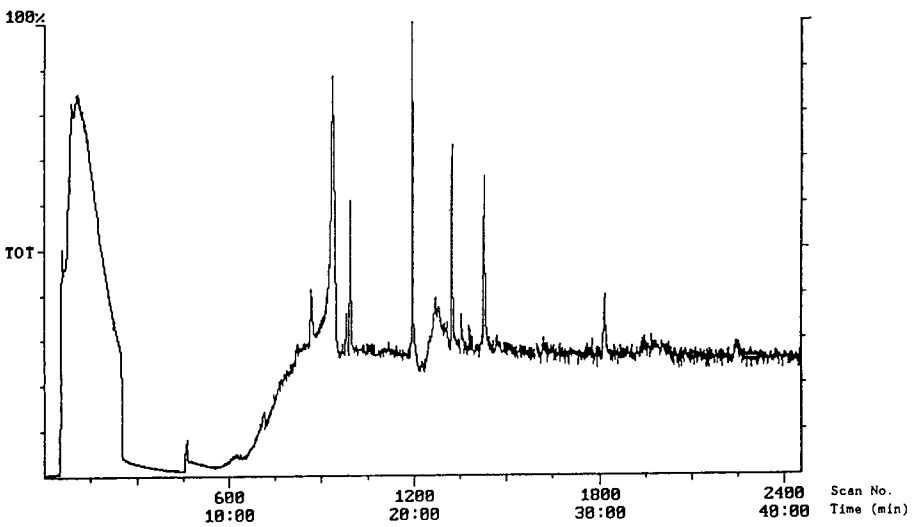

Fig. 2. Py–GC–MS: reconstructed ion chromatogram of HMX at 1000°C.

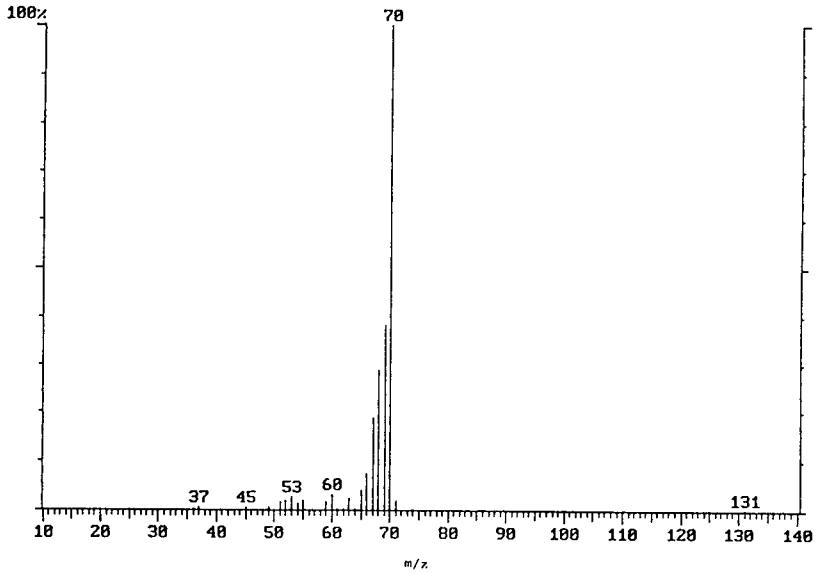

Fig. 3. Py–GC–MS: Py–GC–MS mass spectrum of a decomposition product of RDX from pyrolysis at 1000°C.

Fig. 4 shows an example of a mass spectrum of a decomposition product of HMX from pyrolysis at 1000°C. The m/z of this product is 81 and is probably due to $C_3H_3N_3^+$.

As the ion trap is operated at a high pressure of helium, ion–molecule reactions might occur resulting in MH^+ ions. These MH^+ ions should not be confused with the molecular ions. One way to differentiate between them is to look at the mass chromatographic peak shapes. An example is given in Fig. 5, showing the mass chromatograms of m/z 74 and 75 ions in the

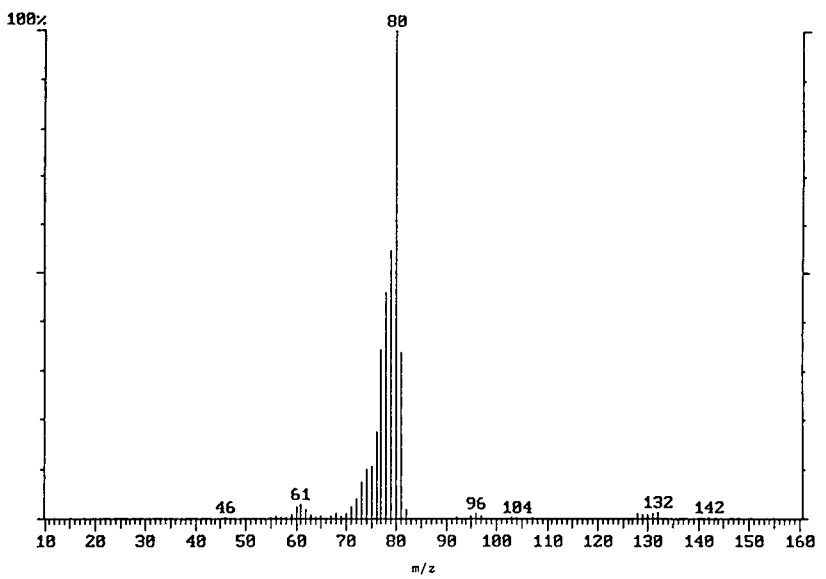

Fig. 4. Py–GC–MS: mass spectrum of a decomposition product of HMX from pyrolysis at 1000°C.

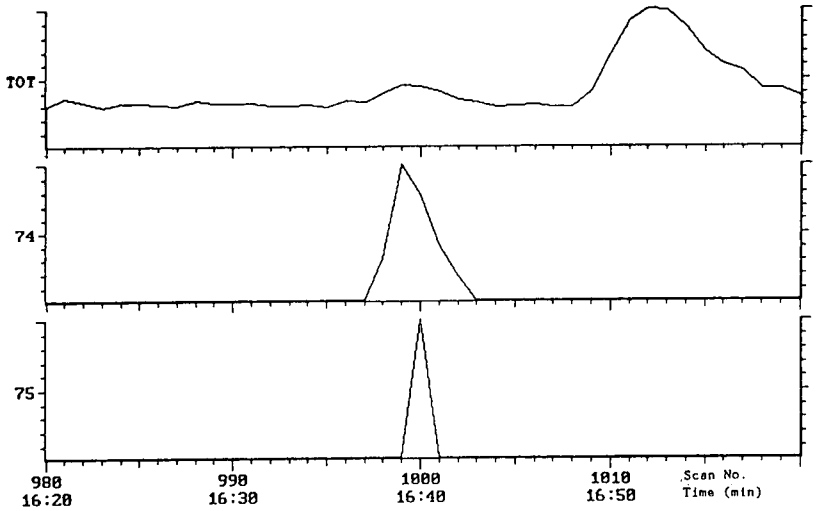

Fig. 5. Mass chromatograms of m/z 74 and 75 ions in the Py–GC–MS of RDX.

Py–GC–MS of RDX. The peak of m/z 75 is much narrower than that of m/z 74, indicating that it is formed through an ion–molecule reaction, when its concentration reached an optimum level.

Table 1 shows the molecular ions obtained in the Py–GC–MS of RDX and HMX and their suggested interpretation. The reproducibility of the pyrograms over an extended period of time was about ±20%. Under these conditions no distinct temperature effect was found in the range 500–1000°C (at 100°C intervals). At 400°C several ions were observed which did not appear at higher temperatures. Table 1 also shows the ions observed in the Py–MS of RDX and HMX by Snyder and co-workers [4,6]. When trying to identify some of the thermal decomposition products, we could only rely on the EI mass spectra and on previously published work [4–6]. The suggested species are shown in Table 2. To obtain positive identification it is necessary to compare the mass spectra with the mass spectra of standards and to carry out MS–MS of both with collision-induced dissociation.

Some of the species listed in Table 1 do not seem to have been observed before, either in pyrolysis studies [4–6] or in thermal decomposition studies [11–15]. Examples are the ions at m/z 100, 105 and 106, which probably represent residues containing the original RDX ring. The ion at m/z 97 (oxy-*s*-triazine) was previously observed as an important intermediate in the decomposition of RDX [12].

In order to determine the decomposition processes in RDX and HMX, as a first step, mainly the ions observed in both compounds were taken into consideration, as the decomposition processes in both compounds are expected to be similar. The pattern of thermal decomposition will therefore be shown here only for the case of RDX.

The thermal fragmentation pathways of the RDX molecule are depicted in Fig. 6. There is an initial loss of most NO_2 groups as a result of the cleavage of the N–N bond, followed by cleavage of two C–N bonds. Some of these fragments decompose further to produce the lower molecular mass fragments $C_2H_2^+$, CN^+, CH_2N^+, CO^+, NO^+, CH_2O^+, $CHNO^+$ and CH_2NO^+.

It is assumed that the thermal fragmentation pathways of HMX are similar, as most of the ions obtained in the Py–GC–MS of HMX are identical with those of RDX.

Table 1
Molecular ions obtained in the Py–GC–MS of RDX and HMX

m/z	RDX	HMX	Suggested formula	Refs. [4] and [6]		
				RDX	HMX	Formula
26	+	+	$C_2H_2^+$ or CN^+			
28	+	+	CH_2N^+ or CO^+			
30	+	+	NO^+ or CH_2O^+			
43	+[a]	+[a]	$CHNO^+$ or $C_2H_5N^+$		+	C_2H_5N
44	+	+	CH_2NO^+ or $C_2H_6N^+$			
45	–	+[a]	CH_3NO^+	+	+	CH_3NO
53	+	+	$C_3H_3N^+$ or $C_2HN_2^+$			
57	+[a]	–	$C_2H_3NO^+$ or $C_2H_5N_2^+$		+	C_2H_3NO
58	+	+	$C_2H_4NO^+$ or $C_2H_6N_2^+$			
59	+	+	$C_2H_5NO^+$ or $CH_3N_2O^+$	+	+	C_2H_5NO
60	–	+[a]	$CH_4N_2O^+$			
70	+	+	$C_3H_6N_2^+$		+	$C_3H_6N_2$
71	–	+[a]	$C_2H_3N_2O^+$ or $C_3H_5NO^+$			
72	+	–	$C_3H_6NO^+$			
73	+	+	$C_3H_7NO^+$	+	+	C_3H_7NO
74	+[a]	+[a]	$C_2H_6N_2O^+$	+	+	$C_2H_6N_2O$
75	–	+[a]	$CH_3N_2O_2^+$ or $C_2H_7N_2O^+$			
81	+	+	$C_3H_3N_3^+$			
82	+	–	$C_3H_4N_3^+$		+	$C_4H_6N_2$
96	+	–	$C_3H_2N_3O^+$			
97	+	+	$C_3H_3N_3O^+$	+	+	$C_3H_3N_3O$
98	+	–	$C_3H_4N_3O^+$			
99	+	–	$C_3H_5N_3O^+$			
100	–	+	$C_3H_6N_3O^+$ or $C_4H_8N_2O^+$			
105	+[a]	–	$C_2H_5N_2O_3^+$			
106	–	+[a]	$C_2H_6N_2O_3^+$ or $C_2H_8N_3O_2^+$			

+ = Obtained; – = not obtained.
[a] Obtained only at a low temperature of 400°C.

Table 2
Suggested thermal decomposition species in RDX and HMX

m/z of molecular ion	Suggested species	Formula	Also seen in Ref.
43	Ethylenimine		[13]
	N-Methylmethyleneimine	$H_3CN{=}CH_2$	
45	Formamide	$HCONH_2$	
59	Acetamide	CH_3CONH_2	[12]
	Methylformamide	$HCONHCH_3$	
70	–	$CH_2{=}NCH_2N{=}CH_2$	[3]
73	N,N-Dimethylformamide	$HCON(CH_3)_2$	[12,15]
74	N-Nitrosodimethylamine	$(CH_3)_2NNO$	
81	Triazine	$C_3H_3N_3$	

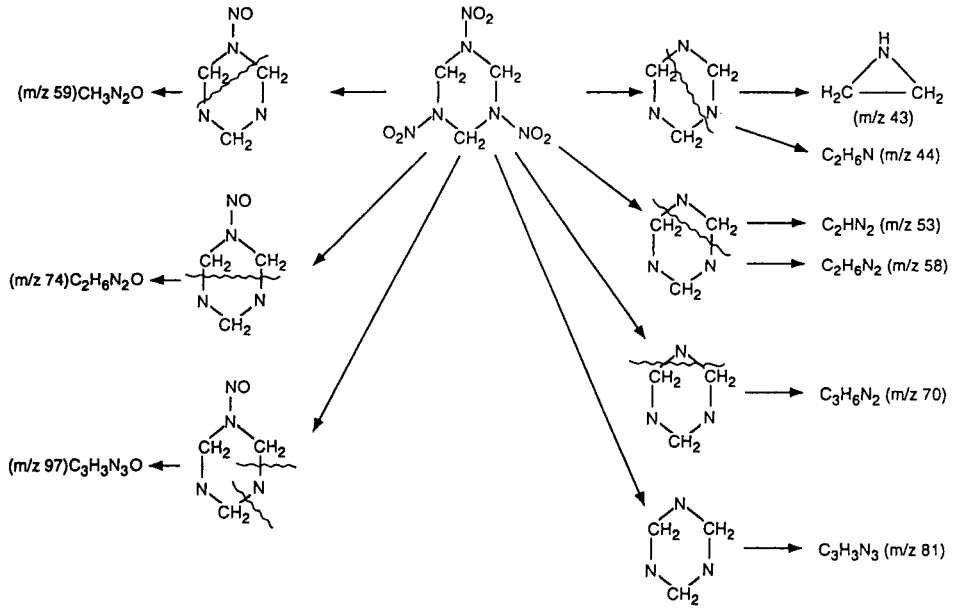

Fig. 6. Thermal fragmentation pathways of RDX.

3.2. *MATB, DATB and TATB*

Fig. 7 shows the Py–GC–MS RIC of MATB at 800°C. Fig. 8 shows an example of a mass spectrum of a decomposition product of MATB from pyrolysis at 800°C. This product is probably due to $C_4H_3N_2^+$.

Table 3 shows the molecular ions obtained in the Py–GC–MS of MAT, DATB and TATB and their suggested interpretation. No major tem-

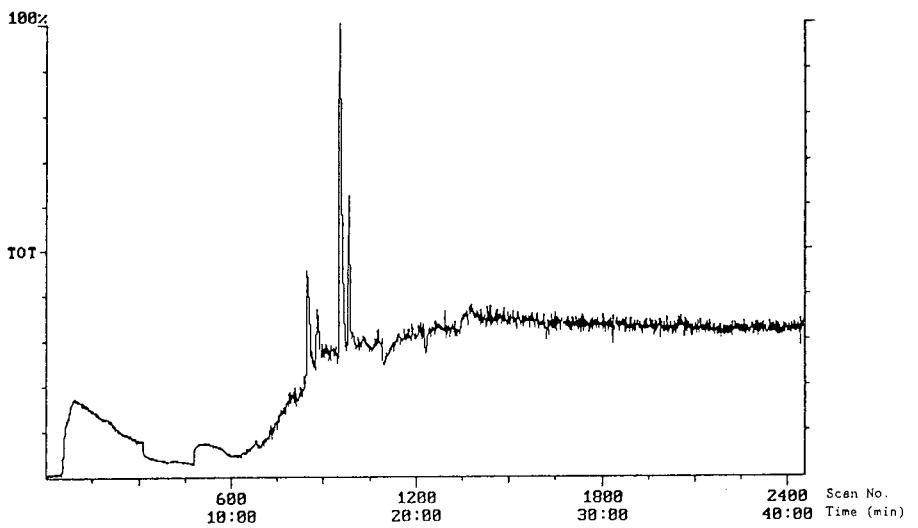

Fig. 7. Py–GC–MS: reconstructed ion chromatogram of MATB at 800°C.

Table 3
Molecular ions obtained in the Py–GC–MS of MATB, DATB and TATB

m/z	MATB	DATB	TATB	Suggested formula
26	+	+	+	CN^+
28	+	+	+	CH_2N^+ or CO^+
30	+	+	+	NO^+
43	−	+	+	$CHNO^+$
44	−	+	+	CH_2NO^+ or CO_2^+
45	+	−	−	CH_3NO^+ or HCO_2^+
51	+	−	−	C_3HN^+
53	+	−	−	$C_2HN_2^+$
54	+	−	−	$C_2H_2N_2^+$
57	−	−	+	$C_2H_3NO^+$
58	+	+	+	$C_2H_4NO^+$ or CNO_2^+
59	−	+	+	$CHNO_2^+$ or $C_2H_5NO^+$
63	−	−	+	$CH_5NO_2^+$
78	−	+	−	$C_4H_2N_2^+$
79	+	−	−	$C_4H_3N_2^+$
82	−	+	−	$C_4H_4NO^+$
87	−	−	+	$C_2H_3N_2O_2^+$
91	+	−	−	$C_5H_3N_2^+$
96	−	−	+	$C_4H_4N_2O^+$
98	+	−	−	$C_3H_2N_2O_2^+$
104	+	−	−	$C_2H_4N_2O_3^+$

+ = Obtained; − = not obtained.

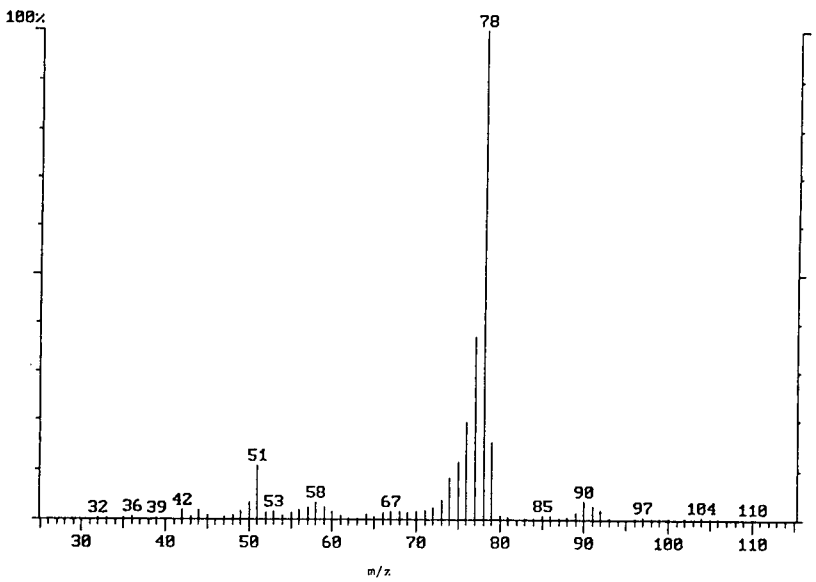

Fig. 8. Py–GC–MS: mass spectrum of a decomposition product of MATB from pyrolysis at 800°C.

perature effect was found in the range 400–1000°C. No published information was found on the decomposition species of MATB and DATB. Land et al. [19] investigated the thermal decomposition of TATB by thermogravimetric modulated beam mass spectrometry. They found that the major decomposition products formed were the lower molecular mass species: H_2O, HCN, CO, NO, HNCO, CO_2 and C_2N_2, although significant amounts of high-molecular-mass species in the range m/z 210–256 were also formed and assigned to furoxan and furazan derivatives. Apparently these compounds were not stable at the pyrolysis temperature used, which was 340°C. TATB seems to form significant amounts of cyanogen (m/z 26 in Table 3). We could not find any correlation between the low-molecular-mass decomposition products and the number of NH_2 groups in the molecule.

Fig. 9 shows suggested decomposition pathways of MATB. The main fragmentation pathway is through cleavage of two C–C bonds. In some instances this occurs while keeping part or all of the NH_2 and NO_2 groups still bonded to the C atoms. A typical example is the fragment ion in MATB at m/z 98, due to $C_3NH_2NO_2$. These fragments then decompose further, producing the low-molecular-mass species CNO_2, HCO_2, CO, NO and CN.

3.3. Tetryl

Tetryl is both a nitroaromatic and a nitramine compound. Fig. 10 shows the Py–GC–MS RIC of tetryl at 1000°C and Fig. 11 shows an example of a mass spectrum of tetryl at that same temperature. Decomposition species from tetryl have not been previously reported.

Table 4 shows the molecular ions obtained in the Py–GC–MS of tetryl in the range 400–1000°C. No major temperature effect was found in this range. Table 4 shows the fragments also found in RDX, HMX, MATB, DATB and TATB. Fig. 12 shows suggested thermal decomposition pathways of tetryl. Most of the fragments are produced through cleavage of the bond between the carbon atom of the nitroaromatic ring and the nitraminic nitrogen atom.

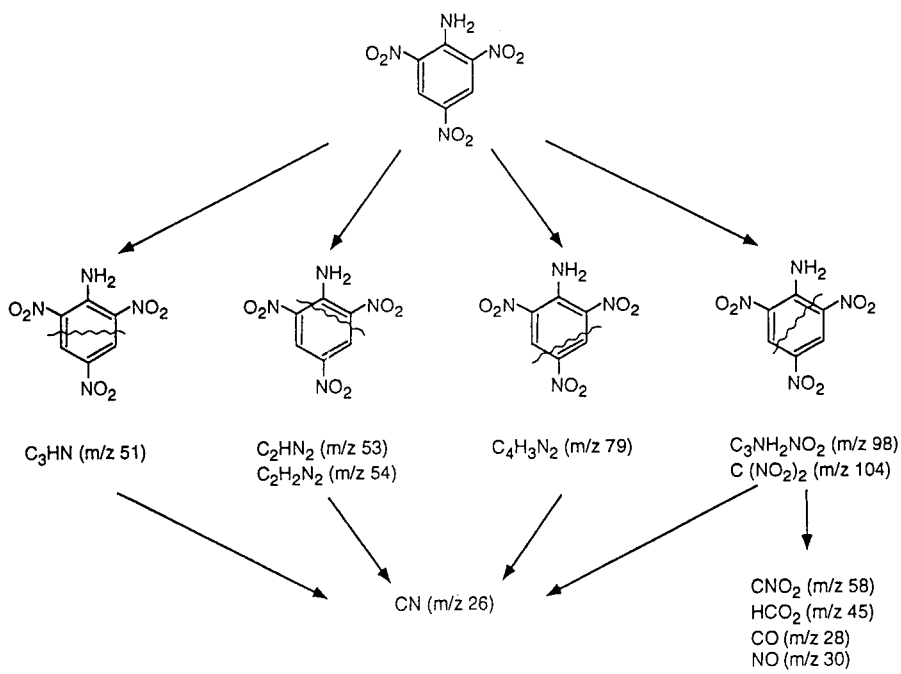

Fig. 9. Thermal fragmentation pathways of MATB.

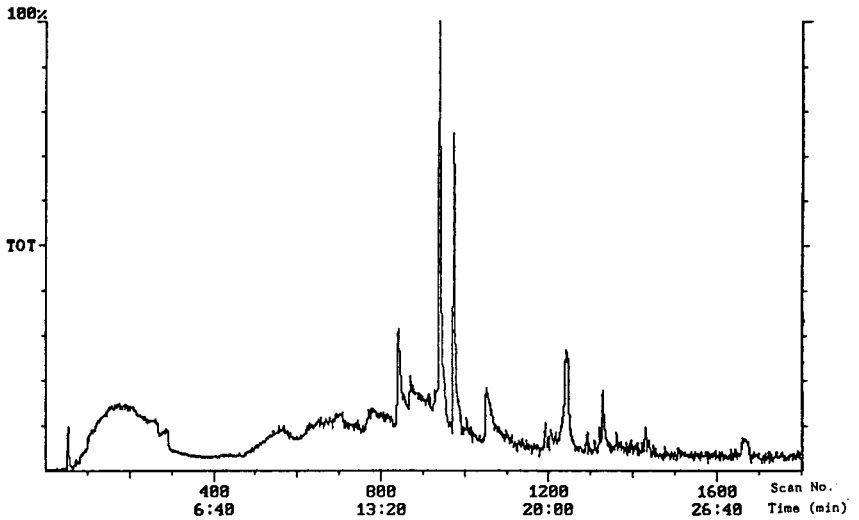

Fig. 10. Py–GC–MS: reconstructed ion chromatogram of tetryl at 1000°C.

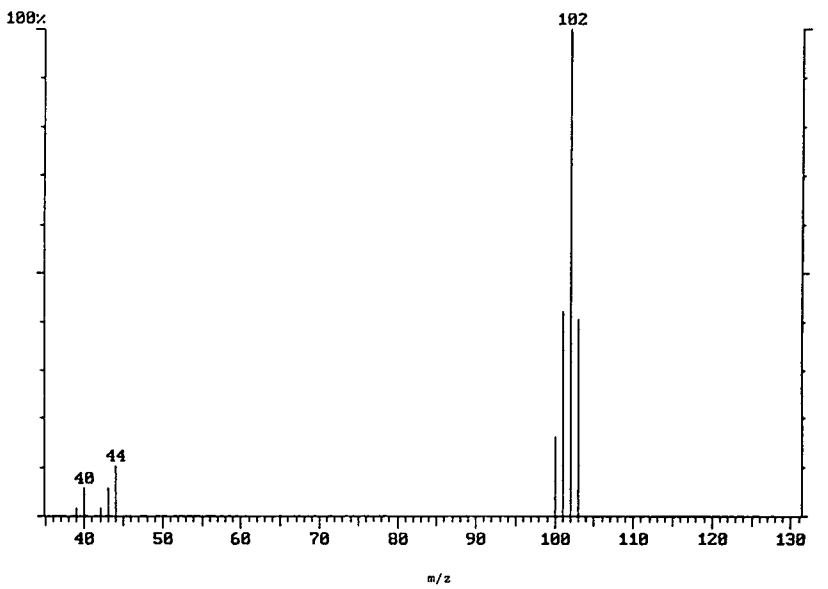

Fig. 11. Py–GC–MS: mass spectrum of a decomposition product of tetryl from pyrolysis at 1000°C.

Table 4
Molecular ions obtained in the Py–GC–MS of tetryl

m/z	Suggested formula	Also found in				
		RDX	HMX	MATB	DATB	TATB
28	CH_2N^+ or CO^+	+	+	+	+	+
29	CH_3N^+	−	−	−	−	−
30	NO^+	+	+	+	+	+
43	$CHNO^+$	+	+	−	+	+
44	CH_2NO^+	+	+	−	+	+
45	CH_3NO^+	−	+	+	−	−
52	$C_3H_2N^+$	−	−	−	−	−
53	$C_3H_3N^+$ or $C_2HN_2^+$	+	+	+	−	−
57	$C_2H_3NO^+$ or CHN_2O^+	+	−	−	−	+
58	$CH_2N_2O^+$ or CNO_2^+	+	+	+	+	+
59	$CH_3N_2O^+$ or $CHNO_2^+$	+	+	−	+	+
60	$CH_2NO_2^+$	−	+	−	−	−
65	$C_3NH_2^+$	−	−	−	−	−
77	$CH_5N_2O_2^+$ or $C_4NH_2^+$	−	−	−	−	−
103	$C_2H_3N_2O_3^+$ or $CHN_3O_3^+$	−	−	−	−	−

+ = Obtained; − = not obtained.

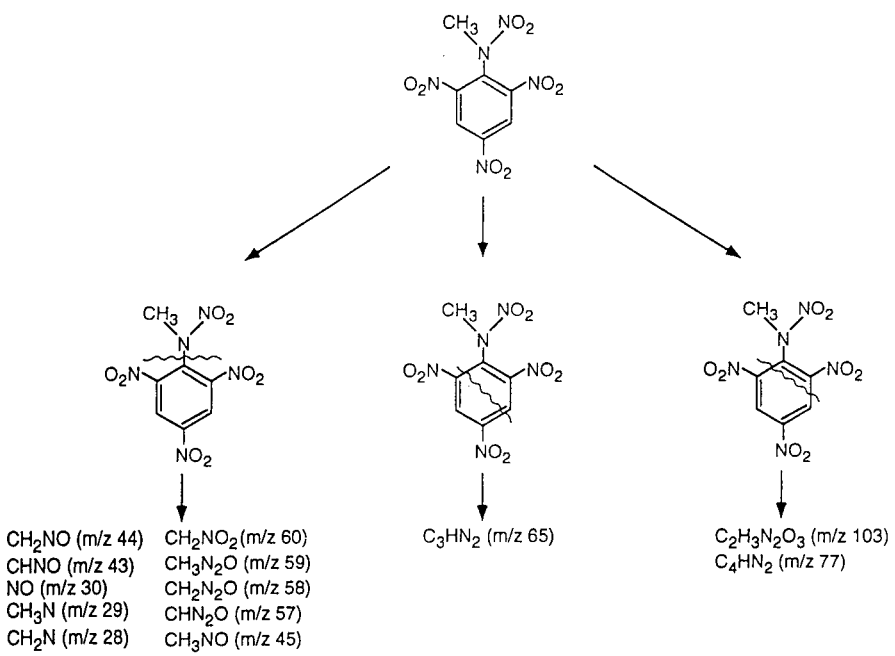

Fig. 12. Thermal fragmentation pathways of tetryl.

This fragmentation produces the species having low molecular mass up to m/z 60. Higher molecular mass fragments are formed through cleavage of two C–C bonds of the nitroaromatic ring.

4. Conclusions

Important chemical species were observed in the pyrolysis of several explosives in the temperature range of 400–1000°C, consisting of mostly low-molecular-mass species. These products resulted mainly from the cleavage of the C–C ring structure in the nitroaromatic compounds and the C–N ring structure in the nitramines. As expected, many of the higher molecular mass species, formed under thermal decomposition conditions at much lower temperatures, were not found. In several explosives, toxic species were formed during pyrolysis.

Acknowledgement

We thank Dr. Dean D. Fetterolf of FBI Laboratory in Quantico, VA, USA, for the loan of the pyrolyser.

References

[1] R.N. Rogers, *Anal. Chem.*, 39 (1967) 730.
[2] N.A. Newlon and J.L. Booker, *J. Forensic Sci.*, 24 (1979) 87.
[3] L. Huwei and F. Ruonong, *Thermochim. Acta*, 138 (1989) 167.
[4] A.P. Snyder, J.H. Kremer, S.A. Liebman, M.A. Schroeder and R.A. Fifer, *Org. Mass Spectrom.*, 24 (1989) 15.
[5] A.P. Snyder, S.A. Liebman, M.A. Schroeder and R.A. Fifer, *Org. Mass Spectrom.*, 25 (1990) 61.
[6] A.P. Snyder, S.A. Liebman, S. Bulusu, M.A. Schroeder and R.A. Fifer, *Org. Mass Spectrum.*, 26 (1991) 1109.
[7] B. Suryanarayana, R.J. Graybush and J.R. Autera, *Chem. Ind. (London)* 52 (1967) 2177.
[8] J.N. Bradley, A.K. Butler, W.D. Capey and J.R. Gilbert, *J. Chem. Soc., Faraday Trans. 1*, 73 (1977) 1789.
[9] M. Farber and R.D. Srivastava, *Chem. Phys. Lett.*, 64 (1979) 307.
[10] M. Farber and R.D. Srivastava, *Chem. Phys. Lett.*, 80 (1981) 345.
[11] R. Behrens, Jr., *J. Phys. Chem.*, 94 (1990) 6706.
[12] R. Behrens, Jr., and S. Bulusu, *J. Phys. Chem.*, 95 (1991) 5838.
[13] R. Behrens, Jr., and S. Bulusu, *J. Phys. Chem.*, 96 (1992) 8877.
[14] R. Behrens, Jr., and S. Bulusu, *J. Phys. Chem.*, 96 (1992) 8891.
[15] R. Behrens, Jr., and S. Bulusu, presented at the *29th JANNAF Combustion Meeting, NASA Langley Research Center, Hampton, VA, October 1992.*
[16] J. Yinon and S. Zitrin, *Modern Methods and Applications in Analysis of Explosives*, Wiley, Chichester, 1993.
[17] R.F.C. Brown, *Pyrolytic Methods in Organic Chemistry*, Academic Press, New York, 1980, Ch. 2.
[18] W.J. Irwin, in J.D. Winefordner (Editor), *Treatise on Analytical Chemistry. Part I. Thermal Methods*, Vol. 13, by Wiley, New York, 1993.
[19] T.A. Land, W.J. Siekhaus, M.F. Foltz and R. Behrens, Jr., in *Proceedings of the 10th International Detonation Symposium, Office of Naval Research, Arlington, VA, 1993*, in press.

ELSEVIER

Journal of Chromatography A, 688 (1994) 243–250

JOURNAL OF CHROMATOGRAPHY A

Synthesis and use of pentadeuteroethyl ethofumesate as an internal standard for the determination of ethofumesate and its metabolites in water by gas chromatography–mass spectrometry

M. Terreni[a,b,*], E. Benfenati[b], M. Natangelo[b], G. Facchini[b], G. Pagani[a]

[a]*Dipartimento di Chimica Farmaceutica, Università di Pavia, via Taramelli 12, Pavia, Italy*

[b]*Istituto di Ricerche Farmacologiche "Mario Negri", Via Eritrea 62, 20157 Milan, Italy*

Received 2 August 1994

Abstract

Pentadeuteroethyl ethofumesate (ETO-d_5) was synthesized starting by acid hydrolysis of ethofumesate to 2,3-dihydro-2-hydroxy-3,3-dimethylbenzofuran-5-yl methanesulfonate (ETO-OH) and successive ethylation with iodoethane-d_5. This deuterated compound was used as an internal standard for the determination by gas chromatography–mass spectrometry in the selected-ion monitoring mode of ethofumesate (ETO) and its chief metabolites, ETO-OH and 2,3-dihydro-2-oxo-3,3-dimethylbenzofuran-5-yl methanesulfonate (ETO-K). The recovery of these substances by solid-phase extraction from drinking water was comparable to those with C_{18}-bonded silica and Carbopack B phases. The recoveries of ETO and ETO-K were virtually complete, compared with 66% extraction for ETO-OH.

1. Introduction

Mass spectrometry is important in the analysis of pesticides and has been proposed as a validating technique on account of its high sensitivity in determining compounds on the basis of their chemico-physical characteristics [1]. GC–MS and LC–MS in the selected-ion monitoring (SIM) mode permit compounds labelled with stable isotopes to be used as internal standards (I.S.), providing good accuracy and reproducibility. The choice of a suitable I.S. is always difficult in pesticide analysis, not only for MS.

We were interested in the MS of ethofumesate (ETO) (**I**) (Fig. 1), a pesticide [2,3] widely used in Europe [1], and its chief metabolites [4] 2,3-dihydro-2-hydroxy-3,3-dimethylbenzofuran-5-yl methanesulfonate (ETO-OH) (**II**) and 2,3-dihydro-2-oxo-3,3-dimethylbenzofuran-5-yl methanesulfonate (ETO-K) (**III**) [5,6], as part of a more extended research programme including other pesticides [7]. A library search [8] found only five reports considering ethofumesate analysis, three dealing with HPLC analysis [9–11] and two with GC [12,13]. Two studies considered water analysis, one by GC–MS [12] and the other by HPLC [9]. Legrand et al. [12] measured

* Corresponding author. Address for correspondence: Istituto di Ricerche Farmacologiche "Mario Negri", Via Eritrea 62, 20157 Milan, Italy.

0021-9673/94/$07.00
SSDI 0021-9673(94)00871-X

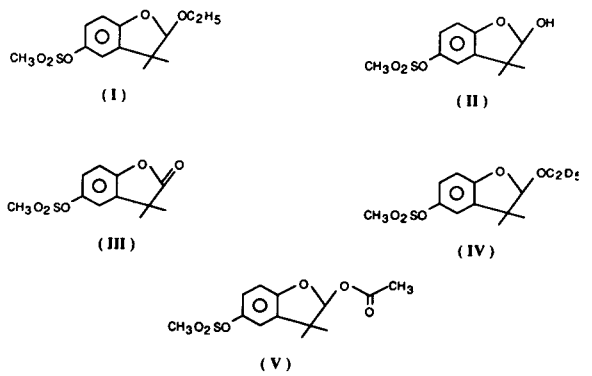

Fig. 1. Formulae of the compounds analysed.

this and 37 other pesticides in French surface and ground waters at or below a concentration of 100 ng l^{-1} and reported a recovery of around 80% for ETO, with liquid–liquid extraction (LLE). They used a moving-needle injector and an MS detector in the SIM mode employing electron ionization (EI) without the use of an I.S. No data were reported regarding reproductibility, linearity and limit of detection.

We present here the synthesis and use of deuterated ethofumesate (**IV**) as an I.S., with the aim of improving the accuracy and reproducibility of analysis. We preferred to use solid-phase extraction (SPE) to recover the compound from water, comparing different extractive materials (Carbopack B and C_{18}-bonded silica), as SPE may offer advantages over LLE [14,15]. The simultaneous extraction and determination of the metabolites of ETO, ETO-OH and ETO-K by GC–MS-SIM were considered using the same I.S.

2. Experimental

2.1. Chemicals and materials

Ethofumesate was purchased from Riedel-de Haën (Seelze, Germany). [$^2H_5$]Iodoethane (iodoethane-d_5), silver nitrite and all other synthesis reagents were obtained from Aldrich (Milwaukee, WI, USA). Preparative and analytical TLC (Kieselgel 60 F_{254}) and silica (Kieselgel 60, 70–230 mesh ASTM, 0.062–0.21 mm) were purchased from Merck (Darmstadt, Germany). C_{18}-bonded silica phase (Bondesil C_{18}, 40 μm) was purchased from Analytichem International (Harbor City, CA, USA). Carbopack B (120–400 mesh, 0.037–0.125 mm) was purchased from Supelco (Bellefonte, PA, USA). The solvents used for synthesis and residue analysis were obtained from Merck. Other reagents for extraction were ascorbic acid (Carlo Erba, Milan, Italy) and trifluoroacetic acid (Merck); acetic anhydride and pyridine for derivatization were purchased from Aldrich.

2.2. Instrumental analysis

Direct inlet system (DIS) MS was performed on a VG TS 250 instrument by EI at 70 eV. For GC–MS analysis we used a Hewlett-Packard HP 5890 Series II gas chromatograph coupled with an HP 5971 mass-selective detector at 70 eV. The chromatographic columns were OV-1701 (10 m × 0.25 mm I.D.) and SE 52 (15 m × 0.25 mm I.D., both with a film thickness of 0.25 μm, from Mega (Legnano, Italy). The injector temperature was 240°C. The oven temperature was programmed from 120 to 180°C at 10°C/min, then to 200°C at 5°C/min and finally to 270°C at 10°C/min. The carrier gas was helium, the head pressure 30 kPa and the source temperature 180°C.

Three ions for each pesticide and metabolite were chosen for screening analysis by SIM (Table 1).

The 300 MHz ^1H NMR spectrum was recorded on a Bruker ACE-300 spectrometer in deuterochloroform using tetramethylsilane as an internal standard; chemical shifts are in δ (ppm) and the signals are reported as s (singlet), bs (broad singlet), d (doublet) and m (multiplet).

2.3. Synthesis of ETO-OH and pentadeuteroethylethofumesate (I.S.)

Pentadeuteroethylethofumesate (**IV**) was obtained from ethofumesate (**I**) by acidic hydrolysis to 2,3-dihydro-2-hydroxy-3,3-dimethylbenzofuran-5-yl methansulfonate (**II**) and further ethylation with iodoethane-d_5 [16] (Fig. 2).

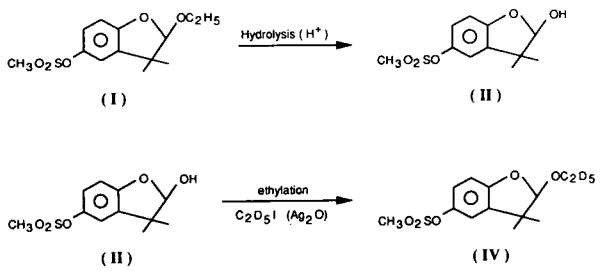

Fig. 2. Scheme of synthesis of pentadeuteroethyl ethofumesate (**IV**).

2.4. 2,3-Dihydro-2-hydroxy- 3,3-dimethyl benzofuran-5-yl methansulfonate (II)

A 100-mg amount of ethofumesate (**I**) was dissolved in 10 ml of acetone and added to 10 ml of water acidified to pH 1 with sulfuric acid. The acidic solution was stirred, heating at reflux for 16 h to complete reaction, analysed by GC–MS, then cooled to room temperature. After evaporation of the acetone under reduced pressure, the aqueous residue was extracted three times with 20 ml of ethyl acetate; the organic phase was washed twice with 20 ml of water and dried over anhydrous sodium sulfate. After evaporation of the organic solvent under reduced pressure, the crude product was purified on a silica gel column (Kieselgel 60, 70–230 mesh ASTM) and eluted with hexane–ethyl acetate (7:3), obtaining 83 mg of pure product (**II**) (yield 92%), m.p. 69–71°C. The product was identified by DIS-MS and its purity was ascertained by GC–MS and TLC (Kieselgel 60 F_{254}), eluting with hexane–ethyl acetate (7:3).

Mass spectrum: *m/z* [relative abundance (%)]: 258 (M^+, 36%); 229 (38%); 201 (14%); 179 (100%); 161 (36%); 137 (45%); 105 (33%); 79 (56%).

^1H NMR (δ): 1.30 and 1.35 (2s, 6H, $2CH_3$); 3.13 (s, 3H, SO_2CH_3); 3.25 (bs, 1H, OH); 5.58 (d, 1H of CH); from 6.80 and 7.03 (m, 3H Ar).

2.5. Pentadeuteroethylethofumesate (IV)

A 140-mg amount of product **II** was dissolved in 15 ml of acetone and 500 mg of silver(I) oxide, previously prepared from silver nitrite with sodium hydroxide solution and dried in an oven at 110°C. Then 400 μl of iodoethane-d_5 were added and the black suspension was heated at reflux for 6 h with vigorous stirring, until complete disappearance of **II**, confirmed by GC–MS, then cooled to room temperature. After evaporation of the solvent under reduced pressure, the pale oil obtained was dissolved in ethyl acetate, the solution was washed twice with 20 ml of distilled water and then dried over anhydrous sodium sulfate. Then the ethyl acetate was removed under reduced pressure and ETO-d_5 (**IV**) was purified on a silica column (Kieselgel 60, 70–230 mesh ASTM) and by preparative TLC (Kieselgel 60 F_{254}) and eluted with hexane–ethyl acetate (7:3), obtaining 73 mg (47% yield) of pure ETO-d_5 (**IV**). The product was identified by DIS-MS and its purity was evaluated by GC–MS and TLC (Kieselgel 60 F_{254}), eluting with hexane–ethyl acetate (7:3). The mass spectrum of compound (**IV**) is reported in Fig. 3B.

Mass spectrum: *m/z* [relative abundance (%)]: 291 (M^+, 38%); 241 (7%); 212 (100%); 180 (20%); 161 (43%); 138 (20%); 105 (18%); 79 (45%).

2.6. Derivatization of ETO-OH

ETO-OH was derivatized by acetylation [17], dissolving in the solvent–reagent mixture acetic anhydride–pyridine (4:1) for 60 min at room temperature to obtain the acetylated derivative ETO-OAc (**V**). After this time the sample was dried under a stream of nitrogen and dissolved in ethyl acetate for analysis.

2.7. Calibration graphs

Calibration graphs were plotted by injecting 1 μl of a solution of ETO and its metabolites (ETO-OH and ETO-K) at six different concentrations (0, 25, 50, 100, 500 and 1000 pg μl^{-1}) obtained by successive dilutions from a solution at 2 ng μl^{-1} concentration, against a fixed concentration of the labelled I.S. (200 pg μl^{-1}). Calculations were made on the basis of the compound/I.S. peak-area ratios using the ions at *m/z* reported in Table 1 and Fig. 6.

2.8. Recovery

Recovery studies of ETO, ETO-OH and ETO-K were made by extracting drinking water solutions of the compounds, at different concentrations and in different volumes, by SPE in quadruplicate. After elution, the sample was dried under a stream of nitrogen and derivatized as reported below to obtain acetylated ETO-OH. After dissolution of the sample in ethyl acetate, to obtain a theoretical concentration of 250 pg μl^{-1}, ETO-d_5 (I.S.) was added to each to achieve a final concentration of 200 pg μl^{-1} for GC–MS analysis by injection of 1 μl of final solution.

SPE was carried out in an all-glass apparatus [15,18] with Carbopack B and C_{18} phases. The extraction procedure for the different phases were as follows.

(i) The C_{18} phase (500 mg) was washed with 10 ml of ethyl acetate, activated with 10 ml of methanol and eluted with 10 ml of ethyl acetate.

(ii) Carbopack B (400 mg) was washed with 10 ml of methylene chloride–methanol (8:2), activated with 5 ml of methanol and 20 ml of ascorbic acid solution (10 mg ml^{-1} in 0.01 *M* HCl). Elution was effected with 10 ml of methylene chloride–methanol (8:2) for the neutral and basic fractions, or 10 ml of methylene chloride–methanol (8:2) containing trifluoroacetic acid (0.2%, v/v) for the acidic fraction [19].

3. Results

3.1. GC–MS analysis

The mass spectrum of unlabelled ETO, shown in Fig. 3A, shows the molecular ion at *m/z* 286. Loss of $CH_3SO_2^{\cdot}$ gives the ion at *m/z* 207, which by further elimination of ethylene produces the ion at *m/z* 179. This gives rise to the ion at *m/z* 161 through loss of water. The ion at *m/z* 79 corresponds to the $CH_3SO_2^{+\cdot}$ ion.

The mass spectrum of ETO-d_5 (Fig. 3B) differs from that of the unlabelled compound in the ions with the ethyl chain or derived from its fragmentation. Thus, the molecular ion is at *m/z* 291; at *m/z* 212 there is the ion corresponding to the ion at *m/z* 207 of ETO. Similarly, the ion at *m/z* 180, due to the loss of ethylene-d_4, is shifted 1 u compared with the ion at *m/z* 179 of

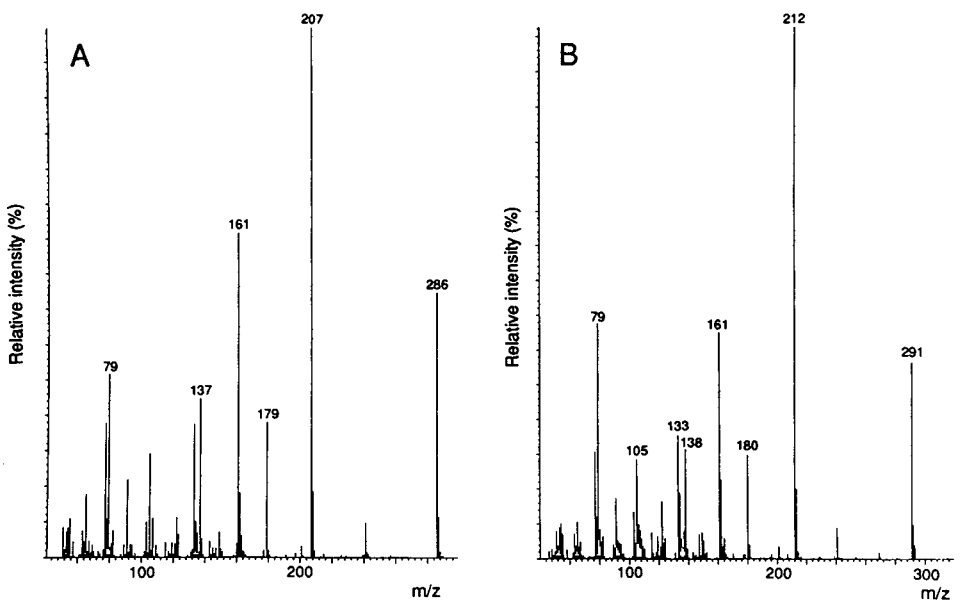

Fig. 3. Mass spectra of (A) ETO and (B) its pentadeuterated derivative ETO-d_5.

ethofumesate, on account of the presence of one deuterium.

This spectrum confirms the identity of the deuterated I.S., and supports the fragmentations indicated for ETO. ETO-d_5, determined by SIM, was found to contain about 1% of unlabelled ETO. Hence this deuterated I.S. does not cause significant interference when less than 500 pg are injected. The mass spectrum of ETO-K is reported in Fig. 4A, and Fig. 4B and C show the mass spectra of ETO-OH and ETO-OAc.

Only ETO and ETO-K can be determined by GC–MS using an SE-52 column, so an OV-1701 column was employed for the simultaneous determination of ETO-OH and the other compounds. The sensitivity for ETO-OH was higher with acetylation (Table 1) and, in this way, both columns can be employed to determine ETO and its metabolites together. GC–MS of the mixture before and after acetylation indicated no decomposition of ETO-K and ETO during derivatization.

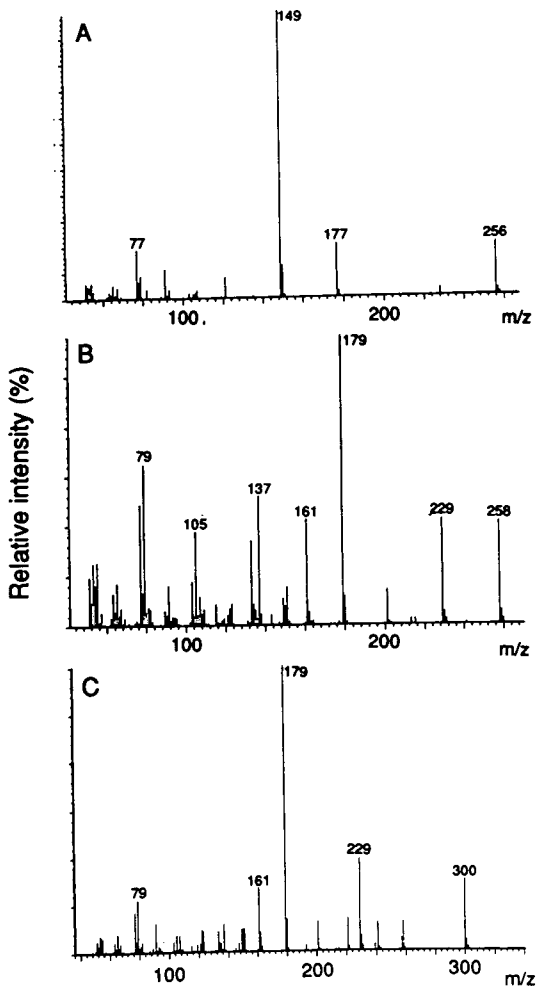

Fig. 4. Mass spectra of (A) ETO-K, (B) ETO-OH and (C) its acetylated derivative, ETO-OAc.

The ions reported in Table 1 were chosen for SIM analysis. For ETO, the ions at m/z 286 (molecular ion) and 161 were selected, the ion at m/z 207 not being considered because of its possible interference with column bleeding. For ETO-d_5, the parent ion at m/z 212 was chosen with the molecular ion at m/z 291. For ETO-K, ions at m/z 149 and 177 were chosen, whereas m/z 179 and 229 were selected for both ETO-OH and its acetylated derivative. Examples of SIM chromatograms for ETO, ETO-d_5, ETO-K and ETO-OAc are presented in Fig. 5.

The calibration graphs are shown in Fig. 6A and B, with the analytes-to-ETO-d_5 (ion at m/z 212) peak-area ratio on the abscissa. Each point is the mean of three injections of the same standards. The correlation coefficients (r^2) were >0.999 for ETO and ETO-OH as acetylated derivative, whereas for ETO-K it was lower (0.996).

The instrumental limits of detection (LOD) (Table 1) were at the picogram level for ETO, ETO-K and ETO-OAc, but considerably higher (1000 pg) for underivatized ETO-OH than for its acetylated derivative.

Table 1
SIM ions chosen for each analyte, in order of relative abundance, and the corresponding limit of detection (LOD)

Compound	Ions (m/z)	LOD (pg) (ion)[a]
ETO	161, 286, 179	3 pg (286)
ETO-K	149, 177, 256	10 pg (149)
ETO-OH	179, 229, 258	1 ng (179)
ETO-OAc	179, 229, 300	3 pg (179)
ETO-d_5	212, 291, 180	1 pg (212)

[a] In parentheses are the ions (m/z) chosen for establishing the LOD.

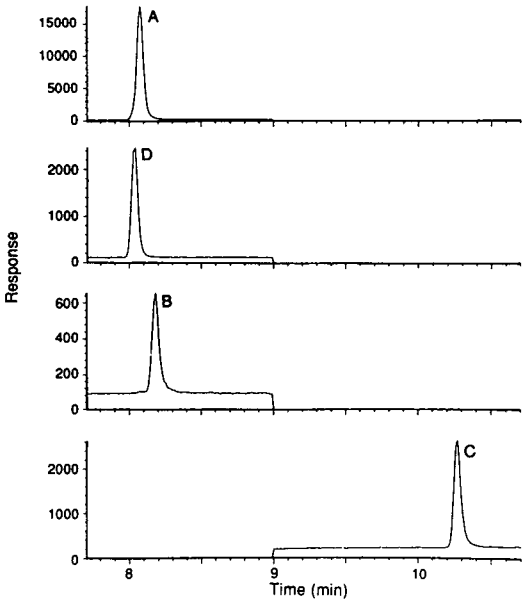

Fig. 5. SIM chromatograms of the compounds analysed, using an OV-1701 column as reported under Experimental. (A) ETO (*m/z* 286); (B) ETO-K (*m/z* 256); (C) ETO-OAc (*m/z* 179); (D) ETO-d_5 (*m/z* 212).

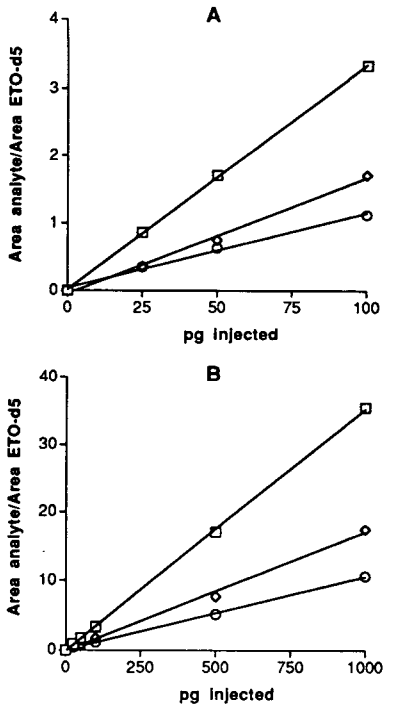

Fig. 6. Calibration graphs for ETO and its metabolites in different amounts with 200 pg of I.S. for each point, using an OV-1701 column. Experimental conditions are reported in the text. (A) Low-range curves (0–100 pg); (B) full-range curves (0–1000 pg). □ = ETO (*m/z* 286), regression equation $y = 0.035x - 0.138$; ◇ = ETO-K (*m/z* 149), regression equation $y = 0.017x - 0.156$; ○ = ETO-OH, after acetylation (*m/z* 179), regression equation $y = 0.010x + 0.038$.

Table 2 reports the day-to-day reproducibility for the ETO calibration graph. The reproducibility was good, as shown by the relative standard deviations, which with the exception of the 100-pg injections (18.4%), were always less than 15%.

3.2. Water recovery

The water extraction recoveries for ETO using Carbopack B under different conditions are reported in Table 3. Carbopack B provided high recoveries in the neutral fraction, but ETO was not found in the acidic fraction. The recovery was always higher than 80% with this SPE procedure, studying different concentrations and water volumes, and was complete (103%) at a concentration of 0.1 $\mu g\ l^{-1}$, which is the limit set by many European regulations regarding pesticides and related compounds. The standard deviation was low even when the recovery was measured in a day-to-day evaluation (Table 3).

The recovery was also good with Carbopack B for metabolites (Table 4), particularly ETO-K, but was less complete for ETO-OH.

Table 2
Day-to-day reproducibility for GC–MS analysis of the ETO calibration samples

Day	ETO concentration (pg/μl)				
	25	50	100	500	1000
1	3.06	5.44	10.70	47.19	94.25
2	2.42	4.26	7.80	36.52	74.24
3	2.52	4.33	7.96	36.98	73.59
Mean	2.66	4.67	8.82	40.22	80.69
R.S.D. (%)	12.7	14.1	18.4	14.9	14.5

Each value represent the ratio of the ETO peak area (*m/z* 161) to the ETO-d_5 peak area (*m/z* 212), and is the mean of three injections of the same solution, using an OV-1701 column, as described under Experimental.

Table 3
Recovery (±S.D.) by Carbopack B extraction of ethofumesate, with different procedures, and day-to-day reproducibility

Extraction	n[a]	Recovery (%)	
		Cpb N[b]	Cpb A[c]
50 ml, 100 μg/l	4	81.2 ± 6.3	0
500 ml, 1 μg/l	4	82.7 ± 5.9	0
500 ml, 0.1 μg/l	4	103.1 ± 3.7	0
Day-to-day[d]	10	101.2 ± 8.5	0

Extraction procedure and analysis by GC–MS, using an OV-1701 column, were as described under Experimental.
[a] No. of replicates.
[b] Carbopack B neutral fraction.
[c] Carbopack B acidic fraction.
[d] Samples consisting of extractions of 500-ml portions of water spiked with 0.1 μg/l, on three different days.

Comparable results were obtained with SPE using the C_{18} phase (Table 4) and the standard deviations were generally lower than 10%, except for ETO-OH extraction with Carbopack B (18%).

4. Conclusions

ETO-d_5 can be easily and quickly prepared and conveniently used in the determination of ETO by GC–MS-SIM, increasing the accuracy of the method. This pesticide can be completely extracted from water samples with the SPE procedure, using Carbopack B, improving the previously reported recovery by LLE [12].

Table 4
Recovery of extraction (±S.D.) for ETO and metabolites from 500 ml of mineral water spiked with 0.1 μg/l, using C_{18}-bonded silica and Carbopack B

Analyte	Recovery (%)	
	Cpb N[a]	C-18[b]
ETO	103 ± 3	94 ± 5
ETO-K	109 ± 8	95 ± 10
ETO-OH	66 ± 18	66 ± 11

[a] Carbopack B neutral fraction; No. of replicates = 4.
[b] C_{18}-bonded silica; No. of replicates = 4.

These results, and the sensitivity and accuracy of the instrumental technique, show that this procedure, using the deuterated I.S., can be successfully employed for the determination of ethofumesate in water as required by European regulations.

A further application of this I.S. and the analytical procedure is the determination of two major ETO degradation products, ETO-OH and the related ETO-K. ETO and its chief degradation products (ETO-OH and ETO-K) can alternatively be extracted by SPE using C_{18}, achieving a comparable performance. These results could be usefully exploited for multi-residue or on-line water analysis.

Acknowledgement

This work was supported by the European Commission (EV5V-CT92-0061).

References

[1] M. Fielding, D. Barcelò, A. Helweg, S. Galassi, L. Torstensson, P. Van Zoonen, R. Wolter and G. Angeletti, *Pesticides in Ground and Drinking Water* (*Water Pollution Research Reports*, No. 27), Commission of the European Communities, Brussels, 1992.
[2] J.F. Harris, *Ger. Offen.*, 2 537 891 (1976); *C.A.*, 84 (1976) 180028f.
[3] R.J. Whiteoak, M. Croft, R.J. Harris and K.C. Overton, *Anal. Methods Pestic. Plant Growth Regul.*, 10 (1978) 403.
[4] R.J. Whiteoak, M. Crofts and R.J. Harris, *Pesticide Analytical Manual*, Vol. II, Food and Drug Administration, Washington, DC, 1984, Pesticide Reg. Sec. 180, 345.
[5] P.S. Gates, J. Gillon and D.T. Saggers and D. Thomas, *US Pat.*, 3 689 507 (1972); *C.A.*, 77 (1972) 139791s.
[6] P.S. Gates, J. Gillon and D.T. Saggers, *Ger. Offen.*, 1 926 139 (1969); *C.A.*, 72 (1970) 100487u.
[7] E. Benfenati, D. Barceló, A. Helveg, S. Galassi, G. Stella, K. Levsen and B. Rindone, presented at the *4th Workshop on Chemistry and Fate of Modern Pesticides and Related Pollulants, Prague, 8–10 September, 1993.*
[8] M. Terreni, E. Benfenati, V. Pistotti and R. Fanelli, presented at the *4th Workshop on Chemistry and Fate of Modern Pesticides and Related Pollutants, Prague, 8–10 September, 1993.*
[9] M.A. Alawi, *J. Chromatogr.*, 393 (1990) 1695.

[10] R.T. Krause, *J. Chromatogr.*, 255 (1983) 497.
[11] T.H. Byast, *J. Chromatogr.*, 134 (1977) 216.
[12] M.F. Legrand, E. Costentin and A. Bruchet, *Environ. Technol.* 12 (1991) 985.
[13] W.L. Saxton, *J. Chromatogr.*, 393 (1987) 175.
[14] D. Barceló, *Analyst*, 116 (1991) 681.
[15] E. Benfenati, S. Garofani, G. Facchini, A. Cantù and M. Terreni, in L.C. Wrobel and C.A. Brebbia (Editors), *Water Pollution II —Modelling, Measuring and Prediction*, Computational Mechanics, Southampton, 1993, p. 341.
[16] R. Hansel, J. Shulz and A. Pelter, *Chem. Ber.*, 108 (1975) 1482.
[17] R. Vilceanu, P. Schulz, R. Draghici and P. Soimu, *J. Chromatogr.*, 82 (1973) 285.
[18] E. Benfenati, S. Garofani, M. Natangelo, S. Mangiapan and R. Fanelli, presented at the *4th Workshop on Chemistry and Fate of Modern Pesticides and Related Pollulants, Prague, 8–10 September, 1993.*
[19] A. Di Corcia and M. Marchetti, *Anal. Chem.*, 63 (1991) 580.

ELSEVIER

Journal of Chromatography A, 688 (1994) 251–259

JOURNAL OF CHROMATOGRAPHY A

Identification by headspace gas chromatography–mass spectrometry of in vitro degradation products of homo- and copolymers of L- and D,L-lactide and 1,5-dioxepan-2-one

Sigbritt Karlsson, Minna Hakkarainen, Ann-Christine Albertsson*

Department of Polymer Technology, Royal Institute of Technology (KTH), S-100 44 Stockholm, Sweden

First received 1 November 1993; revised manuscript received 2 September 1994

Abstract

Poly(L-lactide) (PLLA), poly(D,L-lactide) (PDLLA), poly(1,5-dioxepan-2-one) (PDXO) and six different types of copolymers of L-LA–DXO and D,L-LA–DXO (80:20, 50:50 and 20:80) were hydrolysed in vitro in phosphate buffer (pH 7.4) at 37°C for periods of up to 20 months and the degradation products were identified by headspace gas chromatography–ion trap mass spectrometry. A suitable method to identify the decarboxylic acids and hydroxy acids formed was developed using derivatization with N-*tert.*-butyldimethylsilyl-N-methyltrifluoroacetamide reagent. The derivatives gave a single chromatographic peak with no tailing in the mass spectra. The main products identified in the in vitro buffers are lactic acid and 2-hydroxyethoxypropionic acid, which are the linear forms of the monomers D,L- or L-lactide and 1,5-dioxepan-2-one. The amount of degradation products formed depends on the copolymer composition and the degradation time.

1. Introduction

The detection and identification of low-molecular-mass compounds formed in aged inert and degradable polymers are means of determining the interaction of polymers with the environment. By headspace gas chromatography–mass spectrometric Hs-GC–MS, GC–MS and LC techniques, different natural and synthetic polymers have been studied. Natural polyhydroxyalkanoates are interesting polymeric materials for application in packaging and in biomedical materials and considerable research efforts are being made to explore their characteristics and long-term properties mainly due to their source, a renewable carbon source in contrast to the traditional oil-based bulk polymers. Alkaline hydrolysis products of poly(β-hydroxybutyrate) (PHB) and poly(β-hydroxybutyrate–co-β-hydroxyvalerate) (PHB/PHV) have been detected using LC [1]. Monomers, oligomers and some of their derivatives, mainly produced by dehydration at the OH terminus, were present in the hydrolysed samples. In thermally oxidized PHB samples the amount of crotonic acid formed increases as the molecular mass decreases [2].

In another study of thermally oxidized inert low-density polyethylene (LDPE), we identified hydrocarbons, ketones, aldehydes and alcohols in various amounts and patterns [3]. Degradable polymers using PE as the matrix and different additives promoting degradation are also materi-

* Corresponding author.

0021-9673/94/$07.00
SSDI 0021-9673(94)00859-O

als under study in our department [4]. LDPE with corn starch and a pro-oxidant is one formulation which gives an increased susceptibility to photo-oxidation and thermolysis and also to biodegradation. Using GC–MS we have analysed the subsequent degradation products formed after photo-oxidation, thermolysis and biodegradation of the samples [5–7]. Inert LDPE was degraded in an accelerated environment (water at 95°C), resulting in the formation of 2-butanol, propionic acid, 1-pentanol, butyric acid, valeric acid, caproic acid, *n*-octane, *n*-nonane, *n*-decane, *n*-dodecane, *n*-tridecane and *n*-tetradecane as monitored by GC–MS [8]. Similar types of compounds (butane, ethanol, pentane, formic acid, butanal, 2-butanone, 1-butanol, 3-hexanone and higher alkanes) were also identified in LDPE containing starch filler [5].

Environmental interaction was also demonstrated in connection with the "sick building" syndrome, where we discovered a problem experienced in connection with the use of self-levelling floor-covering material [9]. The bad odour was related to emission of volatile mono-, di- and polyamines formed during putrefactive degradation of casein, a natural polymer present in floor covering material [10]. GC and LC techniques were adapted to this special application, resulting in detection of ppm–ppb levels of amines and organic acids in the degraded casein-containing concrete [9–11].

Many synthetic polymers used inside the body are subject to biodegradation (generally a simple hydrolysis reaction). In many instances these polymers are deliberately designed to be degradable to meet specific end-uses. Aliphatic polyesters are the largest group of biodegradable polymers, and poly(lactic acid) (PLA) and poly(glycolic acid) (PGA) are the most widely studied of these synthetic biodegradable polymers. The PLAs have been investigated for controlled-release devices [12], degradable sutures [13], absorbable fibres [13] and implants for bone fixation [14]. There is also increasing interest in using PLA for disposable packages and table-ware and techniques are under development to produce PLA from renewable resources.

High-molecular-mass PLA is normally obtained by ring-opening polymerization of the lactide monomer. The polymer stereochemistry is controlled by the original lactide stereochemistry. The resulting stereopolymer has widely different physical characteristics, e.g. poly(L-lactide) (PLLA) is a semicrystalline polymer with a glass transition temperature (T_g) of 67°C, while poly (DL-lactide) (PDLLA) is amorphous (T_g = 58°C). High-molecular-mass copolymers of glycolic and lactic acid have T_g values above body temperature [15] and usually a crystalline character with little elasticity.

Copolymerization of lactide with monomers with different values of T_g and crystallinity creates opportunities for designing polymers with widely different properties. One interesting monomer is 1,5-dioxepan-2-one, synthesized by Albertsson and co-workers [16,17] in ongoing studies focused round the design of new monomers used in ring-opening polymerization for creating degradable biomedical materials. 1,5-Dioxepan-2-one (DXO) copolymerized with lactide yields materials with an amorphous character and interesting properties for new degradable biomedical polymers [18].

The aliphatic polyesters all belong to a group with hydrolytically unstable linear aliphatic ester bonds which is very useful for in vivo degradation in the body. From the literature it is difficult to determine the precise mechanism of degradation of polyesters in the body. It has been proposed that chain scission occurs through simple hydrolysis, although the presence of cations or anions and also enzymes may influence the kinetics [19]. The kinetics of chain scission are indicative of an autocatalytic process in which the carboxylic acid and groups generated by ester hydrolysis participate in the transition state. Water preferentially penetrates the amorphous parts, but crystalline domains are also affected [20].

The increased use of polyesters in a variety of implant devices and drug-release systems has resulted in the need to develop analytical methods to identify the degradation products. All implants cause a foreign body reaction due to the surgical trauma and most often also due to differences in mechanical properties in comparison with the tissue surrounding the implant. For

degradable polymers, especially those with short service times, leakage of degradation products may be significant and contribute to the local tissue response at the implantation site.

The objective of this work was to find suitable methods to identify low-molecular-mass compounds formed by hydrolysis of new degradable biomedical polymers. Degradable homopolymers of 1,5-dioxepan-2-one (DXO), L-dilactide, D,L-dilactide and DXO–LLA and DXO–DLLA copolymers were made by ring-opening polymerization and subsequently hydrolysed in vitro. The degradation products were identified by Hs-GC with detection by ion trap mass spectrometry (ITD-MS). Molecular mass changes were monitored by size-exclusion chromatography (SEC).

2. Experimental

2.1. Polymerization and copolymer compositions

Simplified reactions for the formation and subsequent hydrolysis of (a) PDXO, (b) PLA and (c) the hydrolysis of LA–DXO copolymer are shown in Fig. 1. PLLA, PDLLA, PDXO and three different compositions of both L-LA–DXO and D,L-LA–DXO copolymers were hydrolysed in vitro. The copolymer compositions (molar ratios) were 80:20, 50:50 and 20:80 LA:DXO in both instances. All the polymers were synthesized by ring-opening polymerization. The detailed synthesis and characterization of these polymers have been described previously [21,22].

2.2. In vitro degradation

In vitro degradation was performed in phosphate buffer at 37°C and pH 7.4 using melt-pressed films of 0.5 mm thickness. Circular discs with a diameter of 13 mm were punched from the films. The discs were immersed in serum bottles with 20 ml of phosphate buffer consisting of 7.57 g of Na_2HPO_4, 1.61 g of NaH_2PO_4 and 4.4 g of NaCl in 1000 ml of water. The buffer was filtered (0.46 μm) before use. Aliquots were withdrawn after different periods of time and subsequently analysed.

2.3. Solvent extraction and TBDMS derivatization

MTBSTFA (N - *tert.* - butyldimethylsilyl - N-methyltrifluoroacetamide) (98%; Aldrich), iso-octane (99%; Aldrich), diethyl ether (99.9%;

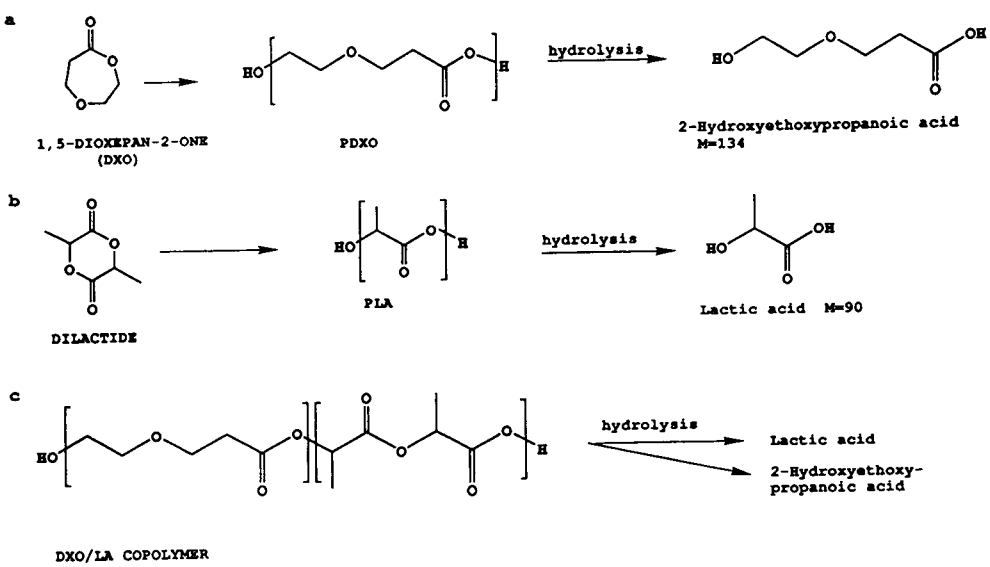

Fig. 1. Reactions for formation of aliphatic polyesters and tentative hydrolysis. (a) PLA; (b) PDXO; (c) PDXO–PLA.

Merck) and chloroform (99.0–99.4%, Riedel-de Haën) were used as received. Acidified (pH 2–3) in vitro buffer solutions were extracted three times with diethyl ether (analytical-reagent grade). The extracts were combined and evaporated with a stream of nitrogen. The derivatization reactions were carried out in 4-ml glass vials with PTFE-lined plastic screw-caps. MTBSTFA was added to the dry residue from solvent extraction and the solution was diluted with 0.1 ml of isooctane. When too little reagent was used, one of the reagent peaks was missing in the chromatograms and the unreacted acid was retained in the column. By injecting mixture of isooctane and MTBSTFA it was possible to elute the retained acids. Therefore, the influence of the amount of reagent and the reaction temperature and time were studied and optimum conditions were found to be 20 μl of MTBSTFA with reaction at 60°C for 30 min. After derivatization the samples were stored in a refrigerator or injected directly into the GC system. Fig. 2 shows the formation of *tert.*-butyldimethylsilyl (TBDMS) derivatives of acids and alcohols with MTBSTFA reagent.

2.4. Gas chromatography–mass spectrometry

The gas chromatograph used was a Perkin-Elmer Model 8500 with a split–splitless injector. It was connected to a Perkin-Elmer ITD mass spectrometer with the ITD 4.10 data handling program (Finnegan). The gas chromatograph was equipped with a WCOT fused-silica CP-Sil-43 CB or CP-Sil-19 CB capillary column from Chrompack (25 m × 0.32 mm I.D.). Helium was used as the carrier gas. Samples were introduced in the splitless injection mode at 250°C. The oven temperature was initially held at 40°C for 1 min, programmed to 200°C at 10°C/min and then held at 200°C for 8 min. The operating conditions for ITD are given in Table 1. All TBDMS derivatives were separated in the CP-Sil-19 CB column.

Table 1
Operating conditions for ITD

Mass range	20–500
Seconds per scan	1.0
Multiplier voltage	1600 V
Transfer temperature	250°C
Peak threshold	1
Mass defect	30 mmu/100 amu
Scan mode	Full

2.5. Headspace gas chromatography–mass spectrometry

The above equipment was connected to a Perkin-Elmer HS 101 headspace autosampler and a WCOT fused-silica CP-Sil-19 CB column from Chrompack (25 m × 0.32 mm I.D.). Samples were thermostated at 90°C for 12 min. The oven temperature was held at 40°C for 1 min, then programmed to 200°C at 10°C/min and held

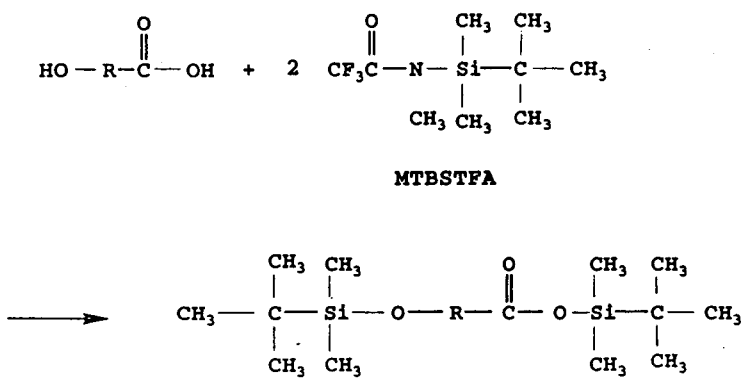

Fig. 2. Derivatization of acids and alcohols with MTBSTFA.

there for 8 min. The operating conditions for ITD are given in Table 1.

2.6. SEC analysis

SEC was used for monitoring molecular mass changes in the residual polymer. The measurements were made at 30°C with five μStyragel columns (10^5, 10^4, 5000, 1000, 100 Å). A Waters Model 510 instrument Waters Model 410 with a refractive index detector and tetrahydrofuran (THF) as solvent at a flow rate of 1.0 ml/min was used. Polystyrene standards were used for calibration.

3. Results and discussion

3.1. Development of analysis

Two different type of columns were tested (CP-Sil-43 CB and CP-Sil-19 CB) in the Hs-GC–MS analysis. The capacity to separate polar compounds was higher with the latter column. Using the CP-Sil-43 CB column no degradation products were detected in the extract from the in vitro solutions. CP-Sil-19 CB was better but part of the polar compounds were retained in the columns and peak tailing was observed for the remaining compounds. It can also be expected that underivatized compounds of low concentrations would be absorbed in the injection port line or in the column. Aliquots from the in vitro solutions were therefore derivatized in order to improve the separation and to avoid retention in the GC system.

N-*tert.*-Butyldimethylsilyl-N-methyltrifluoroacetamide (MTBSTFA) was chosen because it can be applied to all components with proton donor capacity (e.g., decarboxylic acids and hydroxy acids) and the subsequent *tert.*-butyldimethylsilyl (TBDMS) derivatives have high hydrolytic stability and superior GC and MS properties [23–25].

A single chromatographic peak with no tailing was usually obtained for TBDMS derivatives separated in the CP-Sil-19 CB column. It is typical of mass spectra of TBDMS derivatives that the molecular ions and $[M-15]^+$ ions are absent or of low intensity. The characteristic $[M-57]^+$ ions, due to the loss of a *tert.*-butyl group, are, however, very intense, and thus permitted the easy identification of acids. The ion at m/z 73 corresponding to $(CH3)_3Si^+$ is of high intensity, as is expected for the bis-TBDMS derivatives of dicarboxylic acids and hydroxy acids. Other prominent ions were observed at m/z 75, 115, 147 and 189, corresponding to $HO^+ = Si(CH_3)_2$, $[(CH_3)_3C](CH_3)_2Si^+$, $(CH_3)_3SiO^+ = Si(CH_3)_2$ and $[(CH_3)_3C](CH_3)_2SiO^+ = Si(CH_3)_2$, respectively. All the derivatives are stable for at least 3 months, as shown when freshly derivatized standards were compared with those kept in a refrigerator for that time. GC and MS data are summarized in Table 2.

3.2. In vitro degradation

Immediately after placing the amorphous PLA–PDXO polymer in the in vitro phosphate buffer, absorption of water could be observed as the transparent appearance of the samples changed to opaque. PLA–PDXO (20:80) also changed its shape, whereas PLA–PDXO (80:20) showed a smaller water uptake and very small changes in dimension, which can be attributed to the higher crystallinity of this copolymer.

Fig. 3 shows the Hs-GC–MS of derivatized degradation products of PDXO hydrolysed for three different periods of time. Prolonged degradation leads to a continuous increase in the amount 2-hydroxyethoxypropanoic acid formed. The monomer DXO was also identified in the in vitro solutions of PDXO. The amount of DXO is, however, the same irrespective of the degradation time and hence this DXO is a residual monomer originating from the polymerization. For biomedical application the amount of residual compounds must be minimized by careful purification steps, otherwise the in vivo behaviour will be affected. In the chromatograms unidentified peaks also appear, and the amounts of these products tend to increase with the exposure time, which is an indication that these are degradation products of the polymer, or

Table 2
Retention times and prominent ions from the mass spectra of *tert.*-butyldimethyl (TDMS) derivatives of lactic acid, dimer of lactic acid and 2-hydroxyethoxypropanoic acid.

Compound	Retention time (min)	*m/z*	Relative intensity (%)	Fragment
Lactic acid	12.4	318		M
	(43 CB)[a]	303	5	M − 15
		261	72	M − 57
		233	71	
		189	38	
		147	99	
		133	24	
		75	22	
		73	100	
Dimer of	17.5	380		M
lactic acid	(43 CB)[a]	375	10	M − 15
		333	100	M − 57
		285	51	
		261	69	
		159	83	
		103	68	
		75	43	
		73	83	
2-Hydroxy-	18.0	362		M
ethoxy-	(43 CB)[a]	347	8	M − 15
propanoic		305	92	M − 57
acid	17.4	187	60	
	(19 CB)[a]	159	40	
		103	48	
		99	41	
		89	78	
		75	21	
		73	100	

[a] CP-Sil-43 CB or CP-Sil-19 CB column.

products of further reaction of the initial degradation products.

Fig. 4 shows GC–MS analyses of PLLA and LLA–DXO copolymers hydrolysed for 20 months. Lactic acid and 2-hydroxyethoxypropanoic acid were identified. In the 50:50 composition the dilactide was also identified, which is the dimer of the lactic acid.

The molecular mass decrease of the samples starts as soon as they are incubated in the in vitro solution [26]. Table 3 gives the initial and final molecular masses (M_r) after 20 months for

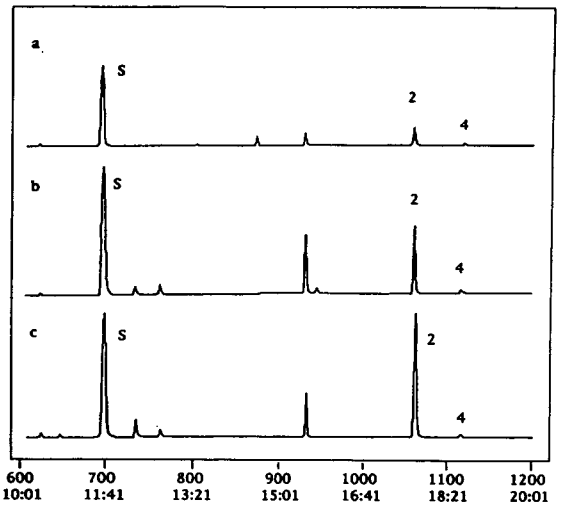

Fig. 3. Hs-GC–MS analysis of degradation products of PDXO. Polymers were hydrolysed in phosphate buffer (pH 7.4) at 37°C for (a) 7, (b) 13 and (c) 27 weeks. S = system peak; TBDMS derivatives of (2) 2-hydroxyethoxypropanoic acid and (4) DXO. Upper scale: scan; lower scale: time in min:s.

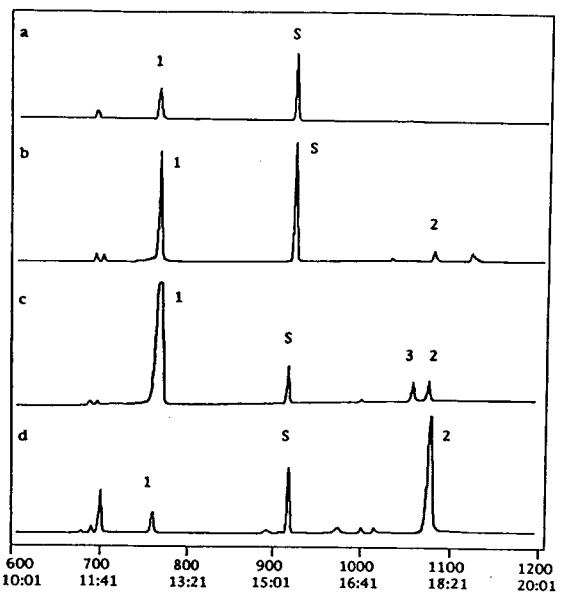

Fig. 4. GC–MS of degradation products of (a) PLLA and (b)–(d) L-LA–DXO copolymers with molar ratios (b) 80:20, (c) 50:50 and (d) 20:80. Samples were hydrolysed in phosphate buffer (pH 7.4) at 37°C for 20 months. S = system peak; TBDMS derivatives of (1) lactic acid, (2) 2-hydroxyethoxypropanoic acid and (3) dilactide. Upper scale: scan; lower scale: time in min:s.

Table 3
Molecular masses (M_r) of copolymers of (D), L-LA and DXO before and after 20 months of hydrolysis in vitro

Copolymer	Composition	M_r (g/mol)	
		Initial	Final
PLLA–PDXO	80:20	68 000	7 000
	50:50	70 500	13 000
	20:80	76 000	23 000
PDLLA–PDXO	80:20	68 100	7 000
	50:50	66 700	11 000
	20:80	70 300	20 000

the PLLA–PDXO and PDLLA–PDXO copolymers as obtained by SEC analysis. The amount of L-LA influences the molecular mass changes; thus the molecular mass of the 80:20 PLLA–PDXO decreased from 68 000 to 7000 after exposure for 20 months whereas that of the 20:80 copolymer decreased from 76 000 to 23 000 during the same period. Many aliphatic polyester show a phenomenon where the initial degradation is slow, indicating a bulk hydrolysis where the induction period is associated with a lack of significant mass loss. This induction period has been observed to range from 5 to 9 weeks depending on the composition of the copolymer [18]. This mass loss behaviour occurs simultaneously with a broadening of the molecular mass distribution (MMD). This can be explained by an initial chain cleavage after water absorption, which produces shorter chains and broadens the MMD. When the molecular masses of the chain are sufficiently small, the oligomers can diffuse through the bulk and dissolve, causing mass loss.

Fig. 5 shows GC–MS of hydrolysed PDLLA and the copolymer of DLLA with DXO. The same type of products could be identified as in Fig. 4, although the absence of a dilactide (the dimer) for the 50:50 DLLA–DXO copolymer must be noted.

The same type of behaviour with maximum lactic acid formed in the 50:50 copolymer can be observed for both PLLA–PDXO and PDLLA–PDXO (Figs. 4c and 5c). The molecular mass changes in the PDLLA–PDXO are generally

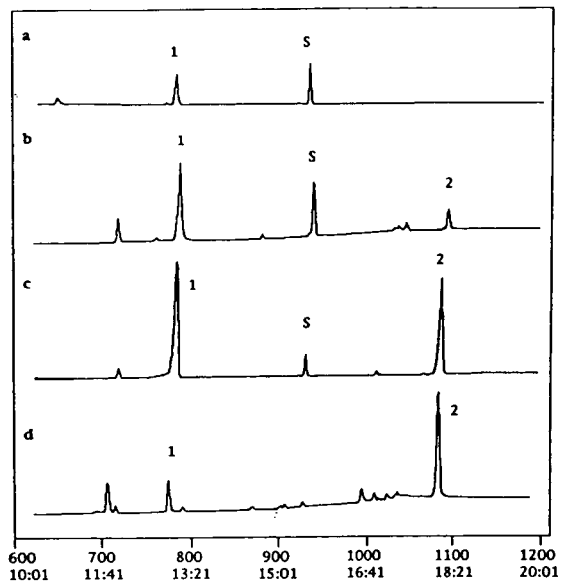

Fig. 5. GC–MS of degradation products of (a) PDLLA and (b)–(d) D,L-LA–DXO with molar ratios of (b) 80:20, (c) 50:50 and (d) 20:80. Samples were hydrolysed in phosphate buffer (pH 7.4) at 37°C for 20 months. S = system peak; TBDMS derivatives of (1) lactic acid and (2) 2-hydroxyethoxypropanoic acid. Upper scale: scan; lower scale: time in min:s.

larger than those observed in the PLLA–PDXO samples, although the same induction period was experienced [26]. Mass spectra for the lactic acid, dilactic acid and 2-hydroxyethoxypropanoic acid are shown in Fig. 6.

The pH of the buffer solutions was monitored continuously and a constant pH was observed during the first 2 weeks in all samples. The rapidly degrading lactide-rich copolymers produced acidic degradation products, in excess of the buffer capacity, and lowered the pH to 6.4 for the 80:20 PDLLA–PDXO, which is the largest pH change observed. The pH change correlates well with the molecular mass changes and the total amount of degradation products in the most degraded D,L-LA-rich copolymer.

The higher the content of lactic acid units in the copolymer, the faster is the degradation. Pitt and Gu [27] investigated the kinetics of the hydrolysis and derived two equations based on uncatalysed and autocatalysed hydrolysis. Albertsson and Löfgren [18] showed that the co-

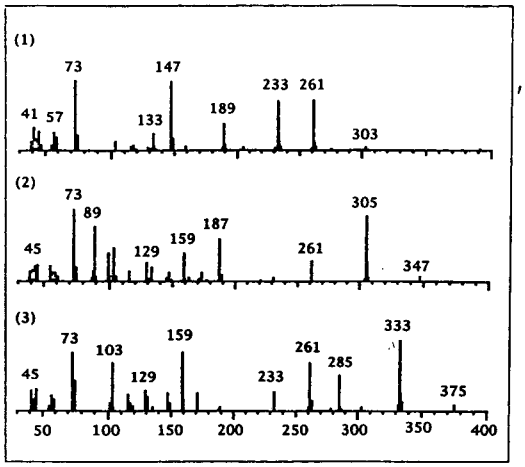

Fig. 6. Mass spectra of TBDMS derivatives of (1) lactic acid, (2) 2-hydroxyethoxypropanoic acid and (3) dilactic acid. Scale: m/z.

polymers with a high content of L-LA have almost identical fits to both models, whereas for the 50:50 and 20:80 PLLA–PDXO and PDLLA–PDXO the uncatalysed mechanism fits slightly better. Fig. 7 shows the hydrolysis mechanism for the two copolymers. The degradation products of the copolymers as identified by GC–MS are consistent with the ester hydrolysis mechanism, although deviations were observed in the chromatograms.

The in vivo reaction to biomedical implants is a major issue determining the usability of the materials. A significant difference in tissue response has been demonstrated between the semicrystalline L-LA–DXO copolymer and the amorphous D,L-LA–DXO copolymer. The amorphous D,L-LA–DXO (77:23) degraded at a faster rate, causing a less pronounced foreign body reaction than the corresponding L-LA–DXO (80:20) [28]. This investigation provides a means to predict the long-term properties of the degradable biomedical homo- and copolymers as manifested by the type of degradation products formed and a starting point for the discussion of in vivo reactions to new biomedical degradable polyesters.

4. Conclusions

Hs-GC–MS and GC–MS techniques were developed that allow the identification of hydrolysis products of new degradable biomedical aliphatic polyesters. By Hs-GC–MS, N-*tert.*-

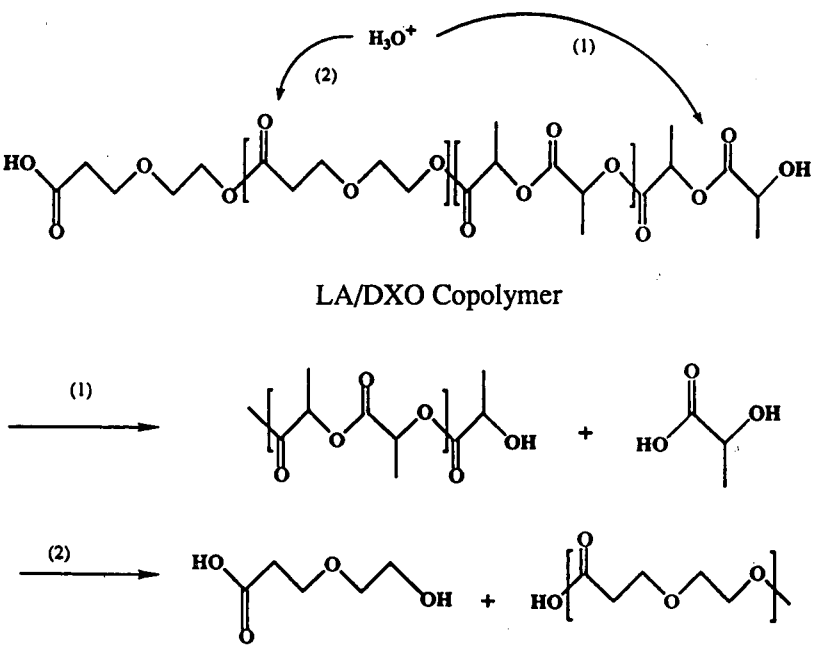

Fig. 7. Hydrolysis mechanism of PLLA–PDXO copolymer.

butyldimethylsilyl-N-methyltrifluoroacetamide derivatives were demonstrated to give a single chromatographic peak with no tailing when separated in a CP-Sil-19 CB column. This method proved to be suitable for the separation and identification of the highly polar degradation products of homo- and copolymers of L- or D,L-lactide and 1,5-dioxepan-2-one. The main products formed in amounts depending on composition and degradation time were lactic acid and 2-hydroxyethoxypropionic acid. We could also demonstrate a higher amount of lactic acid formed in the 50:50 copolymers of PLLA–PDXO and PDLLA–PDXO than in the 80:20 copolymers.

Acknowledgement

Financial support by NorFa is gratefully acknowledged.

References

[1] S. Karlsson, C. Sares and A.-C. Albertsson, in H.G. Schlegel and A. Steinbüchel (Editors), *International Symposiun on Bacterial Polyhydroxyalkanoates—ISBB '92*, Goltze-Druck, Göttingen, 1993, p. 455.
[2] S. Karlsson, C. Sares, R. Renstad and A.-C. Albertsson, *J. Chromatogr. A*, 669 (1994) 97.
[3] A.-C. Albertsson and S. Karlsson, in G. Glass and G. Swift (Editors), *Agricultural and Synthetic Polymers (ACS Symposium Series*, No. 433), American Chemical Society, Washington, DC, 1990, p. 60.
[4] A.-C. Albertsson and S. Karlsson, *Makromol. Chem., Makromol. Symp.*, 48/49 (1991) 395.
[5] A.-C. Albertsson, C. Barenstedt and S. Karlsson, *Polym. Degrad. Stab.*, 37 (1992) 163.
[6] A.-C. Albertsson, C. Barenstedt and S. Karlsson, *J. Appl. Polym. Sci.*, 51 (1994) 1097.
[7] A.-C. Albertsson, C. Barenstedt and S. Karlsson, *Acta Polym.*, 45 (1994) 97.
[8] A.-C. Albertsson and S. Karlsson, *Polym. Mater. Sci. Eng.*, 62 (1990) 976.
[9] S. Karlsson and A.-C. Albertsson, *Mater. Struct.*, 23 (1990) 352.
[10] S. Karlsson, Z.G. Banhidi and A.-C. Albertsson, *J. Chromatogr.*, 442 (1988) 267.
[11] S. Karlsson, Z.G. Banhidi and A.-C. Albertsson, *Mater. Struct.*, 22 (1989) 163.
[12] J. Heller, *Biomaterials*, 1 (1980) 51.
[13] J.P. Pennings, H. Dijkstra and A. Pennings, *Polymer*, 34 (1993) 942.
[14] M. Vert, P. Christel, F. Chabot and J. Leray, in G.W. Hastings and P. Ducheyne (Editors), *Macromolecular Biomaterials*, CRC Press, Boca Raton, FL, 1984, p. 120.
[15] H. Fukuzaki, M. Yoshida, M. Asano and M. Kumakura, *Eur. Polym. J.*, 25 (1989) 1019.
[16] T. Mathisen, K. Masus and A.-C. Albertsson, *Macromolecules*, 22 (1989) 3842.
[17] A.-C. Albertsson and R. Palmgren, *J. Macromol. Sci., Pure Appl. Chem.*, A30 (1993) 919.
[18] A.-C. Albertsson and A. Löfgren, *J. Appl. Polym. Sci.*, 52 (1994) 1327.
[19] T.G. Park, S. Cohen and R. Langer, *Macromolecules*, 25 (1992) 116.
[20] T. Mathisen and A.-C. Albertsson, *J. Appl. Polym. Sci.*, 39 (1990) 591.
[21] S. Lundmark, M. Sjöling and A.-C. Albertsson, *J. Macromol. Sci. Chem.*, A28 (1991) 15.
[22] A.-C. Albertsson and A. Löfgren, *Makromol. Chem., Makromol. Symp.*, 53 (1986) 221.
[23] K.R. Kim, M.K. Hahn, A. Zlatkis, E.C. Horning and B.S. Middleditch, *J. Chromatogr.*, 468 (1989) 289.
[24] Y. Ghoos, B. Geypens, M. Hiele, P. Rutgeerts and G. Vantrappen, *Anal. Chim. Acta*, 247 (1991) 223.
[25] S. Steffenrud, P. Borgeat, H. Salari, M.J. Evans and M.J. Bertrand, *J. Chromatogr.*, 416 (1987) 219.
[26] A.-C. Albertsson and A. Löfgren, *J. Macromol. Sci., Pure Appl. Chem.*, A32 (1995) 41.
[27] C.G. Pitt and Z. Gu, *J. Controlled Release*, 4 (1987) 283.
[28] A. Löfgren, A.-C. Albertsson, Y. Zhang and L.-M. Bjursten, *J. Biomater. Sci., Polym. Ed.*, 6 (1994) 411.

ELSEVIER

Journal of Chromatography A, 688 (1994) 261–271

JOURNAL OF CHROMATOGRAPHY A

Separation of homologous aromatic alcohols and carboxylic acids by packed column supercritical fluid chromatography

Roger M. Smith*, David A. Briggs

Department of Chemistry, Loughborough University of Technology, Loughborough, Leics, LE11 3TU, UK

First received 1 November 1993; revised manuscript received 6 October 1994

Abstract

The retention behaviour of the members of homologous series of polar analytes on supercritical fluid chromatography has been investigated on different stationary phases; octadecylsilyl- amino- and cyano-bonded silicas and polystyrene divinylbenzene. The changes in the relative retentions of homologous phenylalkanols and phenylalkanoic acids with changes in temperature and pressure of the mobile phases were determined. The results suggested that in each case there was a mixed mode of separation in which the retention could be related to a combination of the vapour pressure of the analytes and of polarity interactions, whose importance increased with the polarity of the stationary phase.

1. Introduction

Many of the early studies of the retention of analytes in supercritical fluid chromatography (SFC) were carried out using relatively non-polar stationary phases in capillary columns and the work usually concentrated on the relationship between pressure and/or temperature and the solute solubility in the mobile phase [1]. It was found that the retention of homologues, such as the alkyl benzenes [2] and alkyl aryl ketones [3], increased with carbon number and that there was little change in selectivity with temperature [2]. Although, it was recognised that interactions with the stationary phase played a part in retention, this was frequently regarded as a problem and considerable effort was devoted to preparing inert surfaces free from strong interactions [1].

In contrast, the effect of the stationary phase has been studied more closely in packed column supercritical fluid chromatography. Upnmoor and Brunner [4,5] examined the separation of xanthines, fat-soluble vitamins and carboxylic acids on a range of different columns and suggested that, with carbon dioxide as the eluent, the separations were determined by a normal-phase type mechanism. Retentions were influenced primarily by interactions between the analytes and polar silanol groups on the surface

* Corresponding author.

0021-9673/94/$07.00
SSDI 0021-9673(94)00966-X

of the silica gel. If methanol was added as a modifier, it reduced retentions for both bonded and non-bonded silica stationary phases confirming that alkyl-bonded chains on the surface played little part in retention, other than to shield some silanol groups from the analytes.

Recently the use of packed columns in SFC has been reviewed by Taylor and Chang [6], Petersen [7], Schoenmakers et al. [8] and by Poole et al. [9]. These reviews noted the significance of silanol interactions and that as a consequence numerous studies have been devoted to devising phases in which the silanols are fully masked, or to investigating the potential of non-silica based polymeric stationary phases. A different approach has been to use modified eluents in which a polar additive, such as methanol, was included in the mobile phase. This was considered to interact preferentially with the active sites on the stationary phase. Alternatively the effective area of silica can be reduced by using pellicular beads or wide-pore materials [10]. In most of these studies, the aim has been to reduce or to eliminate the normal-phase type interactions rather than use the interactions to increase the selectivity of the separation.

At constant density, eluent strength on both types of columns is considered to be dependent on the solubility of the analyte in the mobile phase [11]. Solubility differences between analytes are governed mainly by their vapour pressure and only secondarily by solute–solvent interaction with the supercritical phase. However, under conditions of constant eluent pressure, the significance of the volatility changed with temperature. On increasing the temperature the separation passed initially through a "LC-like region" in which the density and hence the solubility strength of the eluent decreased and hence retention increased. At higher temperatures retentions decreased as analyte volatility became more important and the separations occurred in a "GC-like region". Berger has recently emphasised that these changes do not imply a change from one mechanism of retention to another but that both mechanisms are always operating and it is the sum of these effects that is observed [12]. The influence of vapour pressure even on solid analytes was observed in an earlier separation of three sterols [13] by SFC. Although they had negligible volatilities, they were still eluted in the order of their vapour pressures.

Thermodynamic models of retention in SFC, such as those described by Schoenmakers [14] and more recently the detailed treatment based on a lattice–fluid model by Martire and Boehm [15] (Eq. 1) describe retention as combination of a mobile phase contribution [$F(T_R, \rho_R)$] dependent on the reduced temperature and density of the eluent and an analyte–stationary phase interaction, which can be expressed as the retention factor (k^0) at zero density corresponding to ideal gas chromatography. This latter term is closely related to vapour pressure and for a homologous series increases systematically with chain length corresponding to increased retention [16].

$$\ln k = \ln k^0 + F(T_R,\rho_R) \quad (1)$$

These changes with chain length are reflected in direct solubility studies. *n*-Heptane and *n*-dodecane were miscible in liquid carbon dioxide at 22–24°C. but *n*-hexadecane is only 5% soluble and *n*-tetracosane 1–2% soluble [17].

Despite many studies of the effect of the physical and stationary phase effects on retention in SFC, little work has systematically compared the effects of analyte structure or the presence of different functional groups on the retention. Wheeler and McNally [18] compared the retention of various compounds of agricultural interest in capillary packed column SFC with retention on reversed-phase HPLC. However, as with many similar studies the analytes had different sizes, polarities and ionisation differences so that the influence of the individual effects could not easily be isolated. King and Friedrich [19] examined the potential of solubility parameter theory to predict solubilities and hence retention in SFC. They found a reasonable correlation between the reduced solubility parameter $\Delta = \delta_1 / \delta_2$ and retention. The solubility parameter of the mobile phase (δ_1) was derived from standard equations. The solubility parameter for the analyte (δ_2) was calculated using a method proposed by Fedors [20] as the ratio of the energy of

vaporisation (ΔE_v) and the corresponding molar volume. Each of these values was derived by the accumulation of terms for the carbon skeleton and functional groups. Low values of δ_2 and hence high values of the reduced solubility parameter Δ corresponded to non-polar analytes and could be correlated with low retentions on SFC.

Previously, we have examined the separation of homologous analytes on packed columns by SFC. When the relatively non-polar alkyl aryl ketones or alkylbenzenes were examined on an octadecylsilyl(ODS)-bonded silica column, there was a linear relationship between log k of the homologues and their carbon number [21]. A similar general relationship was also found for a PS-DVB column, which lacks silanol groups [22]. Although these relationships resembled those found for similar homologues on reversed-phase high-performance liquid chromatography (HPLC) and could have been attributed to a "hydrophobic" effect, this comparison would probably be misleading and a better model would be with the influence of analyte volatility in gas–liquid chromatography (GLC). Supercritical carbon dioxide has a low polarity with relatively weak intermolecular forces so that the size of the analyte should not have the same importance as in reversed-phase chromatography.

However, when the alkyl aryl ketones were examined on a polar cyano-bonded silica column material by SFC, the retentions of the smaller and more polar homologues increased with decreasing carbon number, although the higher homologues showed a linear relationship between log k and carbon number [23]. A similar effect was observed on cyano-bonded columns from different manufacturers. The separations were compared with normal-phase liquid chromatographic separations on the same columns and from the results it was proposed that the retentions of the alkyl aryl ketones in SFC were determined by the summation of a volatility effect, which increased the retentions systematically with carbon number, and a normal-phase polar–polar interaction between the analytes and active sites on the stationary phase. This latter effect became less important with increasing carbon number but was dominant for the smallest homologues.

The present study extends the examination of the relationship between chain length and retention on polar and non-polar stationary phases by packed column SFC to determine the influence of different functional groups. Homologous phenylalkanols and phenylalkanoic acids are separated on polar and non-polar stationary phases to compare the relative effects of polar interactions and analyte volatility. Little previous work has examined the influence of carbon chain length or carbon skeleton on the retention of analytes containing the same functional groups. By examining homologues in which the polarity or ionisation of any functional group is the same the polarity effects can be normalised and the differences caused by size and methylene selectivity can be compared.

2. Experimental

2.1 Chemicals and samples

The phenylalkanols, phenylalkanoic acids and alkyl aryl ketones were of laboratory grade from a range of supplies. Carbon dioxide was laboratory grade from British Oxygen Company and solvents were HPLC grade from Fisons Scientific Equipment.

2.2 Equipment

The supercritical fluid separations were carried out using a JASCO system (Japanese Spectroscopic Company, Tokyo, Japan), consisting of a 880 PU pump with cooled pump head for the delivery of carbon dioxide at 2 ml min^{-1}, a PU-980 pump for the delivery of modifier into a SP8500 dynamic mixer (Spectra Physics), an 860-CO column oven, an 875-UV ultraviolet detector fitted with a high-pressure flow cell and a 880-81 back-pressure regulator. The chromatograms were recorded using Jones JCL6000 chromatographic data system software on an Elonex 386SX computer. Samples (5 μl) were injected

using a 7125 Rheodyne valve (Cotati, CA, USA) fitted with a 20-μl loop.

The separations were carried out on a cyano Capcell column (4.6 × 150 mm, Shiseido, Yokohama, Japan), a Spherisorb ODS-B column (5 μm, 4.6 × 250 mm, Phase Separations, Queensferry, UK), aminopropyl-Spherisorb (5 μm, 4.6 × 250 mm, Phase Separations), or a PLRP-S column (5 μm, 4.6 × 160 mm, Polymer Laboratories, Church Stretton, UK).

3. Results and discussion

Two series of homologues, the phenylalkanols from benzyl alcohol to 5-phenylpentanol and the phenylalkanoic acids from benzoic acid to 5-phenylhexanoic acid were chosen to represent different polar interactions. These analytes and phenol were chromatographed on both nominally non-polar, ODS-silica and PS-DVB columns, and on polar cyano- and amino-bonded silica columns. Similar pressures and hence densities of carbon dioxide were used on each column to permit comparisons. Under selected conditions the results were also compared with the separations of the alkyl aryl ketones.

3.1 ODS-Silica column

Although a ODS-bonded silica column should behave as a non-interactive non-polar stationary phase, because of the number of uncapped silanol groups that are present on the silica surface, it will still possess significant polar activity. This is clearly reflected in many SFC studies as the addition of even very low proportions of methanol as a modifier usually has a significant effect on retention.

In the present study, a base-deactivated silica, Spherisorb ODS-B, was chosen as a typical low-silanol alkyl-bonded silica column. The retentions of the phenylalkanols on elution with carbon dioxide at about 150 bar and 60°C showed a systematic increase with increasing chain length except for the longest member, phenylpentanol, which decreased slightly (Table 1). These changes along the homologous series can be correlated with increases in the vapour pressures of the analytes: benzyl alcohol, b.p. 204°C; 2-phenylethanol, 219°C; 3-phenylpropanol, 235°C [24]. Phenol was more rapidly eluted than the phenylalkanols in agreement with its lower boiling point (182°C) [24]. All the retention times were reduced markedly on the addition of 1.0% *v/v* methanol as a modifier (Table 1) and little difference was then found between the homologous phenylalkanols suggesting that at least part of the original retention was due to interactions with the stationary phase.

Table 1
Retention of phenylalkanols on ODS-bonded silica column

Compound	Retention factor	
Pressure (bar)	155	162
Modifier (% methanol)	0.0	1.0
Phenol	2.11	-
Benzyl alcohol	2.48	1.72
2-Phenylethanol	3.76	1.66
3-Phenylpropanol	4.33	1.92
4-Phenylbutanol	5.32	2.18
5-Phenylpentanol	5.08	2.26

Conditions: column, ODS-B Spherisorb; eluent, carbon dioxide; flow rate, 2 ml min^{-1}; temperature, 60°C, column pressure as given.

Under similar elution conditions, the phenyl weak alkanoic acids showed a very different behaviour and no elution occurred with carbon dioxide alone. A similar problem was found for benzoic acid on ODS-silica by Smith and Sanagi [21]. Geiser et al. [25] found that it was often necessary to add water to the mobile phase to obtain good peak shapes for the free fatty acids. Nomura et al. were able to elute the fatty acids with carbon dioxide alone but only from a specially prepared highly endcapped column material [26].

On the addition of 1.96% *v/v* methanol as a modifier, most of the acids were eluted. However, they had virtually the same retention times, except phenylacetic acid, which was much more highly retained, and benzoic acid, which was totally retained. (Table 2). On further increasing the proportion of methanol to 4.76%, the re-

Table 2
Retention of phenylalkanoic acids on ODS-bonded silica column.

Compound	Retention factor	
Pressure (bar)	156	156
Modifier (% methanol)	1.96	4.76
Benzoic acid	retained	5.70
Phenylacetic acid	20.77	6.15
Phenylpropanoic acid	10.78	3.31
Phenylbutanoic acid	9.39	2.74
Phenylpentanoic acid	10.19	2.95
Phenylhexanoic acid	10.31	3.02

Conditions as in Table 1. None of the acids were eluted with carbon dioxide alone.

tentions decreased and benzoic acid was eluted. The retentions of phenylpropanoic acid to phenylhexanoic acid were again very similar (Table 2) but the shorter acids were again more highly retained. It appeared that there was a strong interaction between the carboxylic acids and the stationary phase and this effect was strongest for benzoic and phenylacetic acids. For the higher homologues the similarity of their retention times suggested that under these conditions the polarity effects were dominant and that the influence of the analyte vapour pressure was much smaller. This can be correlated with their boiling points, which were much higher than the phenylalkanols (benzoic acid, b.p. 249°C; phenylacetic acid, 248°C and phenylpropanoic acid 279°C [24]) and hence they would have lower volatilities.

The increased retention of benzoic and phenylacetic acids could also be because they were partially ionised, however, although they are the stronger acids their pK_a values of 4.19 and 4.28, respectively, are not very different from those of the larger homologues, phenylpropanoic acid, 4.37, and phenylbutanoic acid, 4.76 [27]. Berger and Deye [28] have reported that for a number of strong acids the inclusion of an acidic additive to the modifier, such as citric, trifluoroacetic or dichloroacetic acid, improved the retention and peak shapes. The added acid apparently acted by ion suppression of the analytes. However, under their conditions benzoic acid was virtually unretained in both the absence and presence of modifier so that the potential influence of ionisation on weak acids was unclear.

The separations of both these homologous series were markedly different from the separation of the alkyl aryl ketones at 153 bar and 60°C (Fig. 1). For the same carbon number the retentions of the ketones were much shorter reflecting their lower polarities even though the boiling points of the ketones and alcohols were similar: acetophenone, b.p. 202°C; propiophenone, 218°C and butyrophenone, 220°C [24]. The ketones showed a nearly linear relationship between carbon number and logarithm of the retention factor with a very different slope to the alcohols. Thus even though this is a well-capped column, polarity effects are apparently dominating the separation of polar analytes.

The solubility parameters for these sets of analytes were calculated using the methods of Fedors [20]. The resulting δ_2 values (Table 3) decreased systematically with carbon chain length and were smaller for the alkyl aryl ketones than for the phenylalkanols or phenylalkanoic acids. For any eluent conditions, the

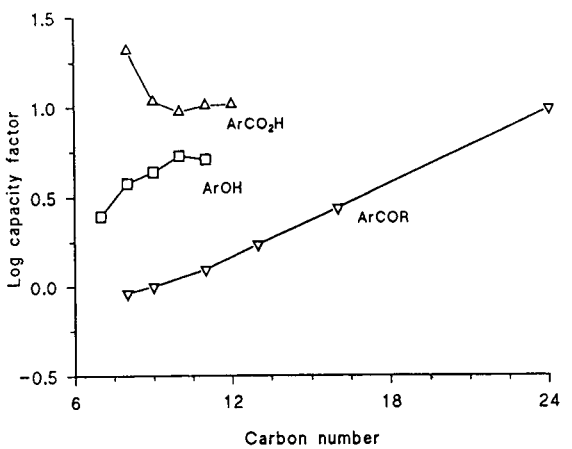

Fig. 1. Comparison of retention factors of homologues on an ODS-bonded silica column at 60°C. Compounds: ▽ = alkyl aryl ketones with carbon dioxide as eluent at 153 bar; □ = phenylalkanols with carbon dioxide at 155 bar; △ = phenylalkanoic acids with carbon dioxide plus 1.96% methanol at 156 bar.

Table 3
Solubility parameters (δ_2) for homologues

Carbon number	Solubility parameter (δ_2)		
	Alkyl aryl ketones	Phenylalkanoic acids	Phenylalkanols
7		11.93	12.78
8	9.90	11.53	12.27
9	9.76	11.21	11.88
10	9.65	10.95	11.56
11	9.56	10.74	11.29
12	9.48	10.56	11.07

Values calculated according to Fedors [20].

reciprocals of these solubility parameters will be directly related to the corresponding reduced solubility Δ values so that greater solubility (and hence shorter retentions) would be predicted for the alkyl aryl ketones than the other groups. This is in agreement with the present study. However, the changes in the solubility parameters with increased chain length predicts that the solubility should increase and hence retentions should decrease with carbon number. As already noted the opposite change is observed for homologues in SFC and retention increases with chain length (Fig. 1). The experimental changes also agree with the reported changes in solubility in supercritical fluid noted earlier for the alkylbenzenes [17].

The changes in solubility parameters were also compared with a recent report of the separation of homologues on a diol column using normal-phase conditions [29]. In that case there was a systematic decrease in retention factors with chain length in agreement with the predictions: *n*-alkanols on elution with hexane changed from ethanol $k = 3.40$ to dodecanol $k = 2.41$; alkan-2-ones using hexane–diethyl ether 99.2:0.8; from pentan-2-one, $k = 2.82$, to 2-undecanone, $k = 2.37$; and similar changes were observed for homologous methyl and ethyl esters.

Thus the results from this study appear to agree with the model proposed by Martire and Boehm [15] in which the solubility of sample in a supercritical fluid depends on a solute–stationary phase interaction. This is represented by a k^0 term for the retention in an eluent with zero density, which would be directly related to volatility (or carbon number of a homologue). The validity of this approach is further confirmed by a recent report by Wang et al. which reported a linear relationship between retention values and boiling points of homologues in SFC [30].

3.2 PS-DVB columns

In order to determine the extent of the effect of the residual silanol groups on the ODS-silica columns, the homologues were separated on a polystyrene-divinylbenzene (PS-DVB) column at 151 bar and 60°C (Table 4). The retentions of the phenylalkanols were similar to those on the ODS column under similar conditions and the alcohols were again eluted with a systematic increase in retention with increasing carbon number from benzyl alcohol to phenylpentanol. Surprisingly, phenol was now more highly retained than benzyl alcohol even though they have similar boiling points. This effect is probably caused by π–π interactions between the phenolic ring and the aromatic polystyrene stationary phase and similar interactions have been reported for naphthols and PS-DVB columns [31].

However, on adding methanol as modifier to the mobile phase there was a much smaller effect than on the ODS-bonded silica column. Increasing proportions of methanol, 1.23%, 2.76% and 4.76%, caused a systematic decrease in retention

Table 4
Retention of phenylalkanols on PS-DVB column

Compound	Retention factor							
Pressure (bar)	151	151	152	153	157	207	247	153
Temperature (°C)	40	60	60	60	60	60	60	80
Modifier (% methanol)	0.0	0.0	1.23	2.76	4.76	0.0	0.0	0.0
Phenol	3.13	3.79	2.57	2.57	1.44	2.74	2.01	4.72
Benzyl alcohol	2.13	2.87	2.10	-	1.39	1.55	1.45	4.22
2-Phenylethanol	2.36	3.37	2.37	1.97	1.48	1.44	1.53	4.97
3-Phenylpropanol	3.37	5.19	3.08	3.02	1.83	2.54	2.05	7.64
4-Phenylbutanol	4.10	6.44	3.82	3.45	2.34	3.04	2.46	10.08
5-Phenylpentanol	4.72	7.67	4.60	4.11	2.57	3.57	2.74	13.16

Conditions: column, PL-RPS; eluent, carbon dioxide plus modifier as indicated; flow rate, 2 ml min^{-1}.

for all the analytes. For example, the retention of 5-phenylpentanol changed from $k = 7.67$ to 4.60 to 4.11 to 2.57. In contrast, on the ODS-bonded silica column (Table 1), the addition of 1.0% modifier reduced the retention factor for 5-phenylpentanol from $k = 5.08$ to 2.26. The smaller change with modifier for the PS-DVB column suggested that the effect of the methanol was to alter the solubilising properties of the eluent rather than by altering strong surface interactions as with the surface silanols on the silica based column.

If the column temperature was changed from 40° to 60° to 80°C, which would decrease the density of the carbon dioxide from 0.79 to 0.60 to 0.43 g ml^{-1}, the retentions of the phenylalkanols increased (Table 4) suggesting that the separations were being carried out in the "LC region" of the temperature vs. retention relationship [2] in which the decrease in eluent density is more important than the increase in analyte volatility. The corresponding effect was observed on increasing the column pressure from 151 bar to 207 bar and then to 247 bar at 60°C (Table 4). The reductions in the retentions of each of the alcohols can be attributed to the increases in the density of the eluent from 0.60 to 0.73 and to 0.79 g ml^{-1}.

The differences in retention on comparison with the ODS-bonded silica column were equally marked for the phenylalkanoic acids. None of the acids was eluted with carbon dioxide alone but the addition of even a small proportion of methanol (1.23%) was sufficient to elute all the acids (Table 5). Unlike the ODS-bonded silica column, the acids showed a marked increase in retention with carbon number corresponding to the changes in boiling points. Thus it appeared that there was only a small polar interaction with the stationary phase and the elution of the analytes was primarily determined by their relative volatilities. Further addition of methanol decreased the retention times in each case but caused no change in relative retentions (Table 5). Taylor and Chang [6] described a separation by Yang which showed a similar relationship between chain length and retention for the separation of the free fatty acids on a PS-DVB column.

Table 5
Retention of phenylalkanoic acids on PS-DVB column. Conditions: as Table 4; temperature, 60°C. None of the acids were eluted with carbon dioxide alone

Compound	Retention factor		
Pressure (bar)	156	169	163
Modifier (% methanol)	1.23	2.44	4.76
Benzoic acid	4.52	2.43	1.65
Phenylacetic acid	4.46	2.41	1.52
Phenylpropanoic acid	4.89	2.75	1.69
Phenylbutanoic acid	6.12	3.33	2.05
Phenylpentanoic acid	7.21	4.01	2.52
Phenylhexanoic acid	8.88	5.46	2.90

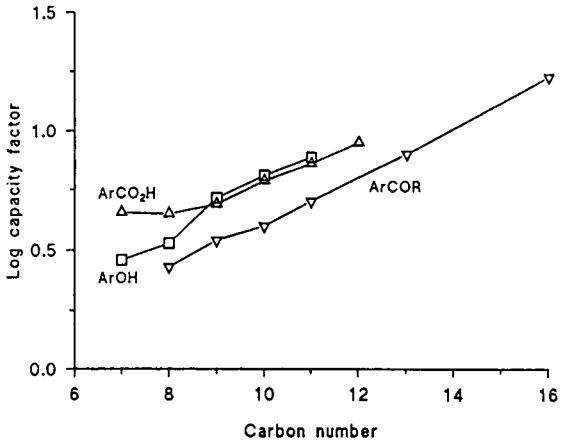

Fig. 2. Comparison of retention factors of homologues on a PS-DVB column at 60°C. Compounds: ▽ = alkyl aryl ketones with carbon dioxide as eluent at 147 bar; □ = phenylalkanols with carbon dioxide as eluent at 151 bar; △ = phenylalkanoic acids with carbon dioxide plus 1.23% methanol as eluent at 156 bar.

The retentions of the phenylalkanols were compared with the separation of a series of homologous alkyl aryl ketones (Fig. 2) under similar conditions with carbon dioxide as the eluent and with the phenylalkanoic acids in the presence of 1.25% methanol. The alcohols and ketones with similar boiling points, such as benzyl alcohol and acetophenone, had almost identical retentions suggesting that vapour pressure was playing a major part in the solubility of the analyte in the mobile phase. In each case the slope of the relationship between log k and carbon number for the higher homologous was similar suggesting that in each case there was a common systematic methylene increment corresponding to the changes in volatility. For the smaller acids there were deviations from linearity so that some polarity effects may still be present.

3.3 Cyano-bonded silica column

From earlier studies [23], it would be expected that analytes would experience stronger polar interactions on a cyano-bonded column. The separation of the homologues was therefore examined using a cyano-Capcell stationary phase. This material is coated with a polymeric layer and should show little silanol activity [32,33].

Under similar conditions to those used to achieve separations on the ODS-bonded silica and PS-DVB columns, the phenylalkanols were eluted with shorter retention times (Table 6). This suggests that in this case the retention may be resulting from the very few remaining free silanol groups rather than from interactions with the cyano groups themselves. In a previous study large differences between cyano-bonded columns were observed which could be attributed to variation in silanol activity [23]. Reports from HPLC studies also suggest that the retentive activity of cyano-bonded silica columns results primarily from uncapped silanol groups [34]. The retentions increased if the column temperature was raised to 80°C but decreased if the pressure was raised to 201 bar (Table 6), which can be attributed to changes in the density of the eluent. Under these conditions phenol was more highly retained than both benzyl alcohol and 2-phenylethanol, in contrast to its more rapid elution on ODS-bonded silica, suggesting that in the present case its higher polarity was more significant than its higher volatility and that it was interacting more strongly with the stationary phase.

The alkyl aryl ketones were only weakly retained on this column [23]. The difference between the two series of homologues (Fig. 3) suggested that for compounds with similar boiling points, e.g propiophenone, $k = 0.55$ com-

Table 6
Retention of phenylalkanols on cyano-bonded silica column

Compound	Retention factor			
Pressure (bar)	156	156	157	201
Temperature (°C)	40	60	80	60
Phenol	1.42	1.65	2.61	1.04
Benzyl alcohol	1.27	1.43	1.99	0.86
2-Phenylethanol	–	1.59	2.38	0.93
3-Phenylpropanol	1.99	2.19	3.30	1.24
4-Phenylbutanol	2.12	2.38	3.93	1.32
5-Phenylpentanol	2.13	2.58	4.36	1.33

Conditions: column, cyano-Capcell; eluent, carbon dioxide; flow rate, 2 ml min^{-1}.

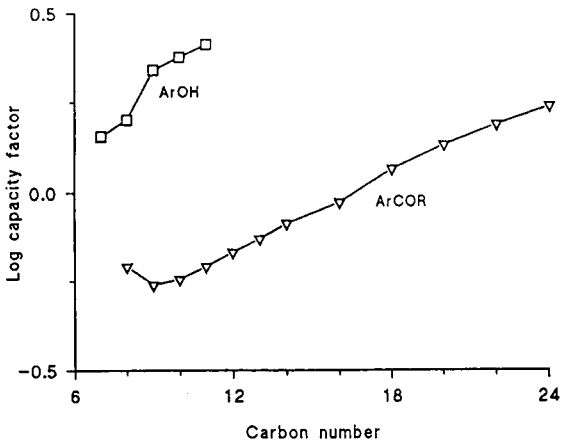

Fig. 3. Comparison of retention factors of homologues on cyano-bonded silica phase at 60°C with carbon dioxide as eluent. Compounds: ▽ = alkyl aryl ketones at 156 bar [data from Ref. 23]; □ = phenylalkanols. Conditions as in Table 6.

pared to 2-phenylethanol, $k = 1.59$, the higher polarity of the phenylalkanols significantly increased their retention. As with the ODS-bonded silica column the slopes of the two sets of homologues differed and the phenylalkanols showed a greater change with increasing chain length. Unlike the other two columns, it was not possible to elute the phenylalkanoic acids even on the addition of methanol to the mobile phase. Again this suggest the presence of strong polar–polar interactions with this stationary phase. This would agree with the observation by Karlsson et al. [35] using cyanosilicone-coated capillary columns that increasing the proportion of methanol in the eluent (up to 20%) decreased the retention of benzoic acids and sharpened the peak shape. Like Berger and Deye [28] they also examined the effect of the addition of citric acid to the eluent but it had little influence on retention or peak shape. However, the cyano stationary phase was unstable and degraded markedly over a period of three weeks use so the effective chemical nature of the column material used in the study is uncertain.

3.4 Amino bonded silica

A brief study was also carried out to examine the retention of the phenylalkanols on an amino-propyl-bonded silica column. Addition of methanol (0.5%) as a modifier was required to elute the phenylalkanols and the retention factors showed a typical polar effect with benzyl alcohol being retained more than 2-phenylethanol (Table 7). However, unlike the separations on the cyano-bonded column, the retentions then increased markedly with chain length so than analyte vapour pressure effects were important. The phenylalkanoic acids were not eluted even with a modified eluent.

Table 7
Retention of phenylalkanols on aminopropyl bonded silica column

Compound	Retention factor
Benzyl alcohol	8.59
2-Phenylethanol	7.66
3-Phenylpropanol	10.14
5-Phenylpentanol	12.06

Conditions: column, S5NH$_2$-Spherisorb; eluent, carbon dioxide plus 0.5% methanol; flow rate, 2 ml min^{-1}; temperature, 60°C; pressure, 150 bar.

In order to separate the effects of the amino groups and underlying silanols, a trial run was also carried out using an amino-bonded vinyl alcohol copolymer column but problems were experienced and it appeared that the column was not suitable for SFC work. Although a study on this type of column has recently been reported by Berger and Deye, the results were not good [36].

4. Conclusion

It has often been claimed that the primary influence on retention in SFC is the solubility of the analyte in the supercritical fluid mobile phase and it has frequently been demonstrated that this model can explain changes in retention with the temperature and pressure of the eluent. However, few studies have examined the influence of analyte structure on retention. The present work has demonstrated the inadequacy of the concept that the solubility in supercritical fluids can be

solely defined by using reduced solubility parameters in an analogy of solubility effects in organic solvents. This method predicts that higher members of a homologous series would be less polar and hence they would be more soluble in supercritical carbon dioxide leading to shorter retentions.

However, the retention of homologues generally increases with chain length. The present studies have shown that the volatility of the analyte, which decreases with increasing chain length, plays a significant contribution, and can be used to predict the changes in the retention of homologues. This is in agreement with theoretical studies on retention in SFC which include an element for the retention factor in ideal gas chromatography. In addition the effect of the different stationary phases on the homologous series provides evidence that stationary phase interactions also play an important role.

Thus separations in SFC are controlled primarily by two factors. Polar–polar interactions are present similar to those found in normal-phase chromatography. Secondly, there is a vapour pressure effect which causes the larger less volatile members of homologous series to be more highly retained by reducing their solubility in the mobile phase.

The nature of the stationary phase in the SFC column determines which of these effects is the more important. On non-polar PS-DVB columns, in which polar–polar interactions are minimal, volatility is important, although $\pi-\pi$ interactions can have an effect. Under these conditions the principal effect of a modifier is to increase the solubility of the analytes in the eluent. On a ODS-silica column volatility plays a role but polar interactions with the underlying silanols have a more significant effect which can be largely eliminated by the addition of even small amounts of a polar modifier. In contrast, on a cyano-bonded silica, polarity effects dominate and volatility plays only a small part in determining retention. Even significant additions of modifier may not be sufficient to eliminate strong polar interactions, such as those with carboxylic acid groups. However, this group of analytes may also be partially ionised.

Acknowledgements

The authors thank the Science and Engineering Research Council for a research grant and Phase Separation Ltd, Polymer Laboratories, and Shiseido Co. Ltd for columns.

References

[1] M.L. Lee and K.E. Markides (Editors), *Analytical supercritical fluid chromatography and extraction*, Chromatography Conferences, Provo, UT, 1990.
[2] T.L. Chester and D.P. Innis, *J. High Resolut. Chromatogr.*, 8 (1985) 561.
[3] C.R. Yonker and R.D. Smith, *Anal. Chem.*, 59 (1987) 727.
[4] D. Upnmoor and G. Brunner, *Ber. Bunsenges. Phys. Chem.*, 93 (1989) 1009.
[5] D. Upnmoor and G. Brunner, *Chromatographia*, 28 (1989) 449.
[6] L.T. Taylor and H-C.K. Chang, *J. Chromatogr. Sci.*, 28 (1990) 357.
[7] M. Petersen, *J. Chromatogr.*, 505 (1990) 3.
[8] P.J. Schoenmakers, L.G.M. Uunk and H-G. Janssen, *J. Chromatogr.*, 506 (1990) 563.
[9] C.F. Poole, J.W. Oudsema, T.A. Dean and S.K. Poole, in B. Wenclawiak (Editor), *Analysis with Supercritical Fluids: Extraction and Chromatography*, Springer, Berlin, 1992.
[10] T.A. Dean and C.F. Poole, *J. Chromatogr.*, 468 (1989) 127.
[11] K.P. Johnston, S. Kim and J. Combes in K.P. Johnston and J.M.L. Penninger (Editors), *Supercritical Fluid Science and Technology* (*ACS Symposium Series*, Vol. 406), American Chemical Society, Washington, DC, 1989, p. 52.
[12] T.A. Berger, *J. Chromatogr.*, 478 (1989) 311.
[13] K.P. Johnston, in K.P. Johnston and J.M.L. Penninger (Editors), *Supercritical Fluid Science and Technology* (*ACS Symposium Series*, Vol. 406), American Chemical Society, Washington, DC, 1989, p. 1
[14] P.J. Schoenmakers, *J. Chromatogr.*, 315 (1984) 1.
[15] D.E. Martire and R.E. Boehm, *J. Phys. Chem.*, 91 (1987) 2433.
[16] D.E. Martire, *Abstracts 5th International Symposium on Supercritical Fluid Chromatography and Extraction*, Supercritical Conferences, Baltimore, January 1994, p. 5.
[17] J.A. Hyatt, *J. Org. Chem.*, 49 (1984) 5097.
[18] J.R. Wheeler and M.E. McNally, *Fresenius' Z. Anal. Chem.*, 330 (1988) 237.
[19] J.W. King and J.P. Friedrich, *J. Chromatogr.*, 517 (1990) 449.

[20] R.F. Fedors, *Polym. Eng. Sci.*, 14 (1974) 147.
[21] R.M. Smith and M.M. Sanagi, *J. Chromatogr.*, 505 (1990) 147.
[22] R.M. Smith and M.M. Sanagi, *Chromatographia*, 26 (1988) 77.
[23] R.M. Smith, S. Cocks, M.M. Sanagi, D.A. Briggs and V.G. Evans, *Analyst*, 116 (1991) 1281.
[24] *Aldrich Catalogue Handbook of Fine Chemicals*, Gillingham, 1990-91.
[25] F.O. Geiser, S.G. Yocklovich, S.M. Lurcott, J.W. Guthrie and E.J. Levy, *J. Chromatogr.*, 459 (1988) 173.
[26] A. Nomura, J. Yamada, K. Tsunoda, K. Sakaki and T. Yokochi, *Anal. Chem.*, 61 (1989) 2076.
[27] *Handbook of Chemistry and Physics*, Chemical Rubber Co., Cleveland, OH, 49th ed., 1968.
[28] T.A. Berger and J.F. Deye, *J. Chromatogr.*, 547 (1991) 377.
[29] M. Lübke and J-L. Le Quéré, *J. Chromatogr.*, 646 (1993) 307.
[30] F. Wang, Y. Guo, T. Cao and Y. Wang, *Shiyou Huagong*, 22 (1993) 825; *Chem. Abs.*, 120 (1994) 314901.
[31] A. Villermet, D. Thiébaut, M. Caude and R. Rosset, *J. Chromatogr.*, 557 (1991) 85.
[32] Y. Ohtsu, H. Fukai, T. Kanda, K. Nakamura, M. Nakano, P. Nakata and Y. Fujiyama, *Chromatographia*, 24 (1987) 380.
[33] O. Shirata, Y. Ohstu, and O. Nakata, *J. Chromatogr. Sci.*, 28 (1990) 553.
[34] E.L. Weiser, A.W. Salotto, S.M. Flach and L.R. Snyder, *J. Chromatogr.*, 303 (1984) 1.
[35] L. Karlsson, T. Buttler and L. Mathiasson, *J. Microcol. Sep.*, 4 (1992) 423.
[36] T.A. Berger and J.F. Deye, *J. Chromatogr. Sci.*, 31 (1993) 127.

ELSEVIER

Journal of Chromatography A, 688 (1994) 273–282

JOURNAL OF CHROMATOGRAPHY A

Effects of pH and hydroxypropyl β-cyclodextrin concentration on peak resolution in the capillary electrophoretic separation of the enantiomers of weak bases

Yasir Y. Rawjee[1], Robert L. Williams, Lisa A. Buckingham[2], Gyula Vigh*

Chemistry Department, Texas A & M University, College Station, TX 77843-3255, USA

First received 28 June 1994; revised manuscript received 12 September 1994

Abstract

Weak base enantiomers were separated by capillary electrophoresis using hydroxypropyl β-cyclodextrin-containing background electrolytes. The multiple equilibria-based electrophoretic separation selectivity model (DID model) of enantiomers was used to analyze the results and determine the model parameters. The extended peak resolution equation of capillary electrophoresis has been applied to calculate the peak resolution surfaces as a function of the pH and the hydroxypropyl β-cyclodextrin concentration of the background electrolyte, the dimensionless electroosmotic flow coefficient, and the effective portion of the applied potential. Combination of the DID selectivity model and the extended peak resolution equation allows the rational optimization of the operating conditions and the realization of separations previously deemed impossible.

1. Introduction

By considering the pertinent multiple equilibria, an equation has been derived [1,2] to express selectivity in the CE separation of the enantiomers of weak bases as a function of the pH and the chiral resolving agent (hydroxypropyl β-cyclodextrin, HP-β-CD) concentration of the background electrolyte (BGE):

$$\alpha_{R/S} = \frac{\mu^0_+ + \mu^0_{HRCD^+} \cdot K_{HRCD^+}[CD]}{\mu^0_+ + \mu^0_{HSCD^+} \cdot K_{HSCD^+}[CD]} \cdot \frac{1 + K_{HSCD^+}[CD] + \frac{[OH^-]}{K_b} \cdot (1 + K_{SCD}[CD])}{1 + K_{HRCD^+}[CD] + \frac{[OH^-]}{K_b} \cdot (1 + K_{RCD}[CD])} \quad (1)$$

where subscripts R and S describe the two enantiomers, + is shorthand notation for the dissociated weak base enantiomers, HR^+ and HS^+, which are not complexed with HP-β-CD, RCD and SCD, and $HRCD^+$ and $HSCD^+$ stand for the non-dissociated and dissociated weak base enantiomers which are complexed with HP-β-CD, μ^0_+, $\mu^0_{HRCD^+}$ and $\mu^0_{HSCD^+}$ are the ionic mobilities of the free and the complexed enantiomers, K_b is the base dissociation constant of the enantiomers, and K_{RCD}, K_{SCD}, K_{HRCD^+} and

* Corresponding author.

[1] Present address: Smith-Kline Beecham, King of Prussia, PA 19406, USA.

[2] Present address: Department of Chemistry, Sweet Briar College, VA 24595, USA.

0021-9673/94/$07.00
SSDI 0021-9673(94)00888-4

K_{HSCD^+} are the formation constants for the respective enantiomer–HP-β-CD complexes, and [CD] and [OH^-] are the molar concentrations of HP-β-CD and hydroxyl ion in the BGE. If the analytical concentration of the analyte is much smaller than that of the HP-β-CD, [CD] can be considered identical to the analytical concentration of HP-β-CD. (For the sake of discussion, it is assumed that in the presence of cyclodextrin the mobility of the *S* enantiomer is smaller than that of the *R* enantiomer.)

The model parameters (K_b, μ^0_+, $\mu^0_{HRCD^+}$, $\mu^0_{HSCD^+}$, K_{RCD}, K_{SCD}, K_{HRCD^+} and K_{HSCD^+}) can be easily calculated from the electroosmotic flow-corrected effective mobilities of the enantiomers, measured in three sets of BGEs. The first set of measurements is carried out in the absence of CD: the pH of the BGE is varied, but the ionic strength is kept constant at a preselected value [3]. In the second set, pH is kept constant at least 1 (preferably, 2) pH units below the pK_a of the conjugate acid enantiomers, and [CD] is varied while the ionic strength is kept constant at the preselected value. Finally, in the third set of experiments, pH is kept constant at about 0.5 pH units above the pK_a of the conjugate acid enantiomers, and [CD] is varied while the ionic strength is kept constant at the preselected value. In each run, the coefficient of the electroosmotic flow is also determined by simultaneous injection of a non-charged component (e.g. benzyl alcohol). The effective mobility data are then analyzed using a non-linear least square approach.

It was recognized in Refs. [1] and [2] that three different types of CE enantiomer separations exist, depending on the numeric values of the model parameters. The separation in which only the non-charged forms of the analytes interact selectively with the resolving agent (i.e. $K_{RCD} \neq K_{SCD}$), has been called a *Type I* separation. In order to have a more descriptive name, it is suggested that such separations be called *desionoselective* CE separations. The separation in which only the charged forms of the analytes interact selectively with the resolving agent (i.e. $K_{HRCD^+} \neq K_{HSCD^+}$), has been called a *Type II* separation. It is suggested that such separations be called *ionoselective* CE separations. Finally, the separation in which both the charged and the non-charged forms of the analytes interact selectively with the resolving agent (i.e. $K_{RCD} \neq K_{SCD}$ and $K_{HRCD^+} \neq K_{HSCD^+}$), has been called a *Type III* separation. The recommended term for such a separation is *duoselective* CE separation. The selectivity model itself will be referred to as DID selectivity model.

An equation has been introduced [3,4] to express peak resolution in the CE separation of enantiomers as a function of the separation selectivity, α, the dimensionless electroosmotic flow coefficient, β, and the effective charge of the enantiomers, z_R^{eff}, z_S^{eff}:

$$R_s = \sqrt{\frac{Ele_0}{8kT}} \cdot \frac{\text{abs}(\alpha - 1) \cdot \sqrt{\text{abs}(\alpha + \beta)} \cdot \sqrt{\text{abs}(1 + \beta)} \cdot \sqrt{z_R^{eff}} \cdot \sqrt{z_S^{eff}}}{\sqrt{\text{abs}[(\alpha + \beta)^3] z_R^{eff}} + \sqrt{\alpha\ \text{abs}[(1 + \beta)^3] z_S^{eff}}} \quad (2)$$

where E is the field strength, l the length of the capillary from injector to detector, e_0 the electric charge, k the Boltzman constant and T the absolute temperature. In this expression, the dimensionless coefficient of the electroosmotic flow, β, is defined as:

$$\beta = \frac{\mu_{eo}}{\mu_S^{eff}} \quad (3)$$

with

$$\mu_S^{obs} = \mu_S^{eff} + \mu_{eo} \quad (4)$$

where μ_S^{obs} is the observed mobility of the *S* enantiomer, μ_S^{eff} is the effective mobility of the *S* enantiomer and μ_{eo} is the coefficient of the electroosmotic flow. According to Refs. [1] and [2], μ_S^{eff} is:

$$\mu_S^{eff} = \frac{\mu^0_{HS^+} + \mu^0_{HSCD^+} K_{HSCD^+}[CD]}{1 + K_{HSCD^+}[CD] + \frac{[OH^-]}{K_b} \cdot (1 + K_{SCD}[CD])} \quad (5)$$

while according to Refs. [3] and [4], the effective charge of the S enantiomer, z_S^{eff}, is:

$$z_S^{eff} = \frac{z^0_{S^+} + z^0_{HSCD^+}K_{HSCD^+}[CD]}{1 + K_{HSCD^+}[CD] + \frac{[OH^-]}{K_b}\cdot(1 + K_{SCD}[CD])} \quad (6)$$

with $z^0_{HS^+}$ and $z^0_{HSCD^+}$ as the ionic charges of the fully dissociated enantiomers, non-complexed and complexed, respectively. Similar expressions exist for the R enantiomer.

The objective of this paper is to show that peak resolution for the enantiomers of weak bases is an explicit function of both the pH and the HP-β-CD concentration of the background electrolyte, as well as the dimensionless electroosmotic flow. Knowledge of the unique resolution surfaces that belong to the ionoselective, desionoselective and duoselective separation types allow the rational optimization of the separation conditions and the realization of the CE separations of weak base enantiomers which were previously considered impossible.

2. Experimental

A P/ACE 2100 system (Beckman Instruments, Fullerton, CA, USA) was used for all measurements, with its UV detector set at 200 nm and the thermostatting liquid bath temperature maintained at 25°C. The electrode at the injection end of the capillary was kept at high positive potential; the electrode at the detector end of the capillary was at ground potential. The field strength was varied between 150 and 750 V/cm to keep the power dissipation at 95 mW. The 0.1–0.2 mM samples (which also contained benzyl alcohol as electroosmotic flow marker) were injected electrokinetically. Untreated, 45.5 cm (39.5 cm from injector to detector) × 25 μm I.D. × 150 μm O.D. fused-silica capillaries (Polymicro Technologies, Phoenix, AZ, USA) and 39.7 cm (33.2 cm from injector to detector) × 75 μm I.D. × 375 μm O.D. fused-silica capillaries with a neutral coating (Beckman Instruments) were used.

HP-β-CD (average degree of substitution of 7 [3]) was synthesized according to the modified procedure of Rao et al. [5] from β-cyclodextrin (American Maize Products, Hammond, IN, USA). BGE components 3-[tris(hydroxymethyl)-methylamino]-1-propanesulfonic acid (TAPS) and 3-(cyclohexylamino)-2-hydroxy-1-propanesulfonic acid (CAPSO) were obtained from Sigma (St. Louis, MO, USA), methanesulfonic acid (MSA) from Aldrich (Milwaukee, WI, USA), Jeffamine ED-600 from Texaco (Houston, TX, USA), and 250MHR PA hydroxyethyl cellulose (HEC) from Aqualon (Wilmington, DE, USA). Test solutes atropine, chloroamphetamine, propranolol and benzyltrimethylammonium bromide (BTM^+) were obtained from Sigma. α-(Hydroxymethyl)benzyltriethylammonium chloride ($HBTEA^+$) was synthesized in our laboratory according to Ref. [6].

All solutions were freshly prepared using deionized water from a Milli-Q unit (Millipore, Milford, MA, USA). Irrespective of the pH of the BGE, the anion concentration was maintained constant at 100 mM. The anion-concentration balanced background electrolytes [3] were prepared by adding an accurately measured volume of the concentrated stock solution of the buffer, accurately weighed amounts of Jeffamine ED-600, HP-β-CD, ionic strength controlling agent MSA and an accurately measured volume of the concentrated stock solution of HEC to a volumetric flask [3]. The flask was filled to 95% of its capacity with deionized water and the contents mixed thoroughly. The pH of the solution was then adjusted using a concentrated solution of lithium hydroxide or 40% tetrabutylammonium hydroxide solution. Subsequently, the volume was made up to the mark with deionized water. The BGE was degassed prior to loading into the electrolyte reservoirs. Before each series of measurements, the capillary was washed with 0.1 M NaOH, rinsed by deionized water and equilibrated with the background electrolyte (5 min, 5 min and 15 min,

respectively). Each run was repeated in at least triplicate.

The parameters in Eqs. 1, 5 and 6 were estimated from the measured, electroosmotic flow-corrected effective mobilities using the Table Curve 3D software package (Jandell, San Raffael, CA, USA) running on a 486DX2 66 MHz 16M RAM personal computer (Computer Access, College Station, TX, USA). Eq. 5 was rewritten as user defined function in the *·udf format of the Table Curve 3D software package and the μ^0 and K values were obtained as parameters. Once the parameters were determined, the three-dimensional surfaces were calculated using the Origin Version 3.0 software package (MicroCal, Northampton, MA, USA).

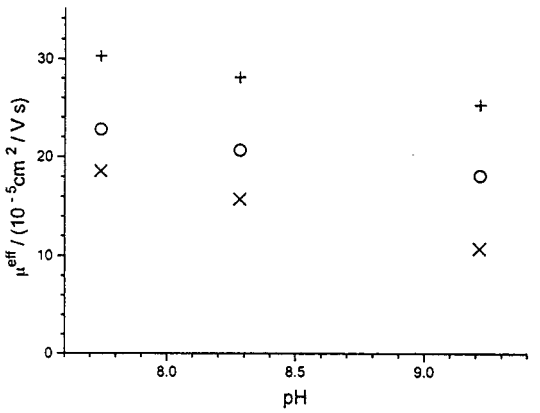

Fig. 1. Effective mobility of propranolol (+), $HBTEA^+$ (○), and BTM^+ (×) in 100 mM TAPS buffers as a function of the BGE pH, adjusted by tetrabutylammonium hydroxide.

3. Results and discussion

3.1. Determination of the model parameters

In order to determine the base dissociation constant and ionic mobility of a weak base, one can change the pH of the BGE around the expected pK_b value and measure the effective mobilities of the solute [7]. To obtain correct pK_b values, the observed effective mobility change must be due to the change in the solute charge only. One can ascertain that this premise is fulfilled by adding a permanent cation probe, such as BTM^+ or $HBTEA^+$, to the sample. If the effective mobilities of the permanent cation remain constant while the pH of the BGE is changed, the effective mobility values of the simultaneously electrophoresed weak base can be used for the pK_b determinations. If one prepares the BGE in the conventional way, e.g. starting with a 100 mM TAPS ($pK_a = 8.4$) solution and varying its pH from 7.5 to 9.5 by adding increasing amounts of tetrabutylammonium hydroxide, and then uses these BGEs to determine the effective mobilities, one obtains results similar to those shown in Fig. 1. Clearly, the effective mobilities of both the weak base solute (propranolol, symbol +) and the permanent cations (BTM^+, symbol × and $HBTEA^+$, symbol ○), decrease significantly. This large mobility decrease is due to the fact that the anion concentration (counter-ion concentration) increases drastically as pH is increased (from about 2 mM at pH 6.75 to about 99 mM at pH 10.5). Therefore, to keep the anion concentration constant, a non-hydrolyzing anion, e.g. methanesulfonate (MSA^-), must be added to the BGE in decreasing concentrations as the pH is increased. Such BGEs are called counter-ion concentration-balanced BGEs [3] and can be prepared as described in the Experimental section for weak base analytes, and in Ref. [3], for weak acid analytes.

The K_b and μ_+^0 values of the weak base test solutes were determined using counter-ion concentration-balanced BGEs. In the $7.1 < pH < 9.5$ range these BGEs contained 100 mM TAPS and 20 mM Jeffamine ED-600; in the $9.3 < pH < 10.1$ range they contained 100 mM CAPSO ($pK_a = 9.6$) and 20 mM Jeffamine ED-600. The final pH adjustment was made with a small amount of tetrabutylammonium hydroxide solution. BTM^+ and $HBTEA^+$ were added to the samples as permanently cationic mobility markers. As an example, the effective mobilities of atropine are plotted in Fig. 2a as a function of the pH of the BGE. With counter-ion concentration balancing [3], the mobilities of the permanent cation, $HBTEA^+$, indeed become constant. The calculated K_b and μ_+^0 values of the weak base test

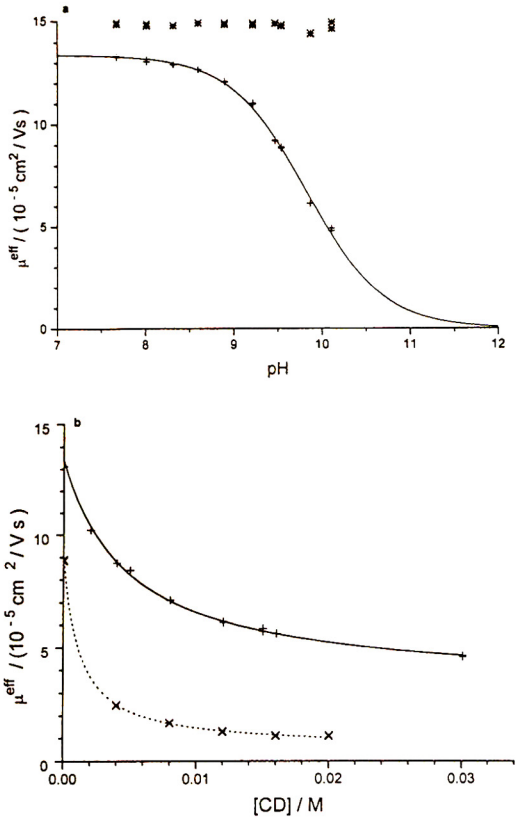

Fig. 2. Effective mobility of atropine (+) and $HBTEA^+$ (*) in counter-ion concentration balanced 100 m*M* TAPS buffers as a function of (a) the pH of the BGE, (b) the HP-β-CD concentration of the BGE at pH 7.63 (top curve), and at pH 9.5 (bottom curve). Solid lines: best fit curves calculated with the constants listed in Table 1.

solutes determined from these measurements are listed in Table 1.

Next, the effects of the HP-β-CD concentration were tested in a low-pH TAPS background electrolyte, in which the weak base analytes are almost completely dissociated (pH 7.63). Again, as an example, the effective mobilities of atropine are plotted in Fig. 2b as a function of [CD] in the BGE. Finally, the effects of the HP-β-CD concentration were tested in a high-pH TAPS background electrolyte, in which the weak base analytes are about 50% dissociated (pH 9.5). Again, as an example, the effective mobilities of the less mobile enantiomer of atropine are plotted in Fig. 2b as a function of [CD]. The calculated $\mu^0_{HRCD^+}$, $\mu^0_{HSCD^+}$, K_{HRCD^+}, K_{HSCD^+}, K_{RCD} and K_{SCD} values of the weak base test substances are listed in Table 1.

Since the complex formation constants of the protonated atropine enantiomers are identical, i.e. $K_{HRCD^+} = K_{HSCD^+} = 211$, this separation represents a desionoselective separation (a Type I separation, in the old nomenclature [1–3]). Since the complex formation constants of the nonprotonated chloroamphetamine enantiomers are identical within the experimental error ($K_{RCD} = 1000$ and $K_{SCD} = 1006$), this separation represents an ionoselective separation (a Type II separation, in the old nomenclature). For propranolol, none of the complex formation constants are identical, $K_{HRCD^+} \neq K_{HSCD^+}$ and $K_{RCD} \neq K_{SCD}$. Therefore, this separation represents a duoselective separation (a Type III sepa-

Table 1
Estimated model parameter values for the chiral week bases

Parameter	Atropine	Chloroamphetamine	Propranolol
μ^0_+ (10^{-5} cm^2/V s)	13.40 ± 0.06	17.5 ± 0.1	12.4 ± 0.1
10^5 K_b	6.62 ± 0.03	5.65 ± 0.05	2.9 ± 0.1
pK_a	9.82	9.75	9.47
$\mu^0_{HRCD^+}$ (10^{-5} cm^2/V s)	3.3 ± 0.1	3.3 ± 0.1	3.2 ± 0.1
$\mu^0_{HSCD^+}$ (10^{-5} cm^2/V s)	3.3 ± 0.1	3.4 ± 0.1	3.2 ± 0.1
$K^0_{HRCD^+}$	211 ± 8	140 ± 4	108 ± 3
$K^0_{HSCD^+}$	211 ± 8	148 ± 4	116 ± 3
K_{RCD}	2140 ± 60	1000 ± 40	148 ± 5
K_{SCD}	2320 ± 60	1000 ± 40	163 ± 5

ration, in the old nomenclature). Since all the parameters used in the effective mobility, effective charge, separation selectivity and peak resolution equations are known, the respective surfaces for the three separation types can be calculated and studied.

The general appearance of the z^{eff} and μ^{eff} surfaces are similar for all test solutes, except that the curvature of the surfaces along the HP-β-CD concentration axis varies, depending on the magnitude of the K_{HRCD^+}, K_{HSCD^+}, K_{RCD} and K_{SCD} constants: the greater the constant values, the sharper the initial decrease as [CD] is increased. As examples, the effective charge surface and the effective mobility surface of the less mobile enantiomer of atropine as a function of pH and [CD] are shown in Fig. 3a and b.

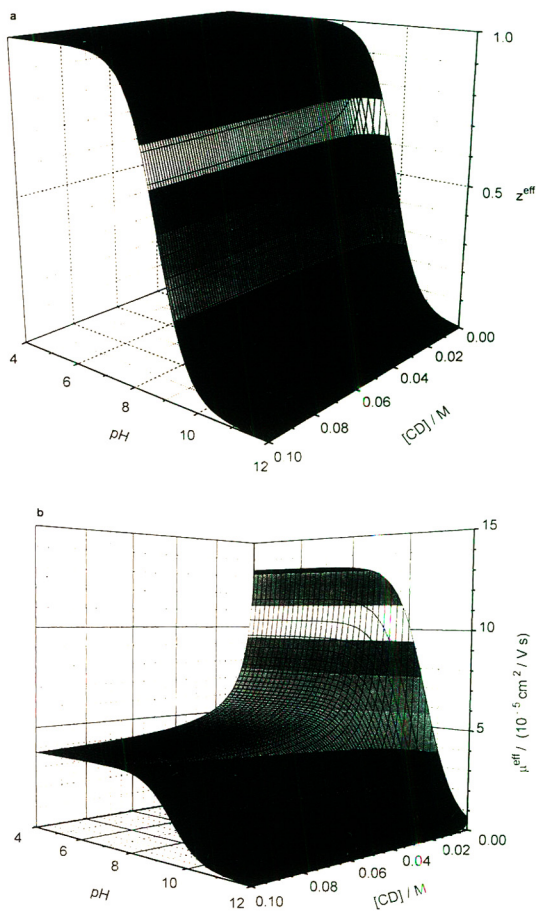

Fig. 3. The dependence of the (a) effective charge and (b) effective mobility of the less mobile enantiomer of atropine as a function of the HP-β-CD concentration and the pH in counter-ion concentration balanced 100 mM TAPS BGEs. The surfaces were calculated with Eq. 6 (charge), Eq. 5 (mobility) and the constants in Table 1.

3.2. Separation selectivity surfaces

The three-dimensional separation selectivity surfaces for atropine, chloroamphetamine and propranolol are shown in Fig. 4 (with the contour plots on the bottom plane) as a function of pH and [CD]. For atropine, selectivity increases from unity at low pH and low [CD] to a limiting high value at high pH and high [CD]. This behavior is typical of desionoselective weak base enantiomer separations (Fig. 4a). For chloroamphetamine at low pH, α increases rapidly as [CD] is increased (Fig. 4b), passes a maximum at about [CD] = 15 mM, then slowly decreases as [CD] is increased further. Along the pH axis, at [CD] $\approx$ 15 mM, α remains a constant high value as long as pH $<$ pK_a $-$ 2, then decreases rapidly, crosses the $\alpha = 1$ plane and continues to decrease as pH is increased further. This means that the migration order of the enantiomers can be reversed by selecting the right combination of pH and [CD]. This behavior is typical of ionoselective separations of weak base enantiomers. For propranolol (Fig. 4c), α again passes a maximum as [CD] is increased at both low and high pH, then drops below unity at low pH as [CD] is increased further. This means that the migration order of the enantiomers can be reversed at low pH by greatly increasing [CD]. This behavior is typical of duoselective separations. Along the pH axis, at [CD] $\approx$ 15 mM, α remains constant as long as pH $<$ pK_a $-$ 2, then increases to a limiting value in the pH $>$ pK_a + 1 range.

3.3. Peak resolution surfaces

The peak resolution surfaces can be calculated with Eq. 2. However, since R_s depends on pH, [CD] and β, the dimensionless electroosmotic flow coefficient, one of these variables must be

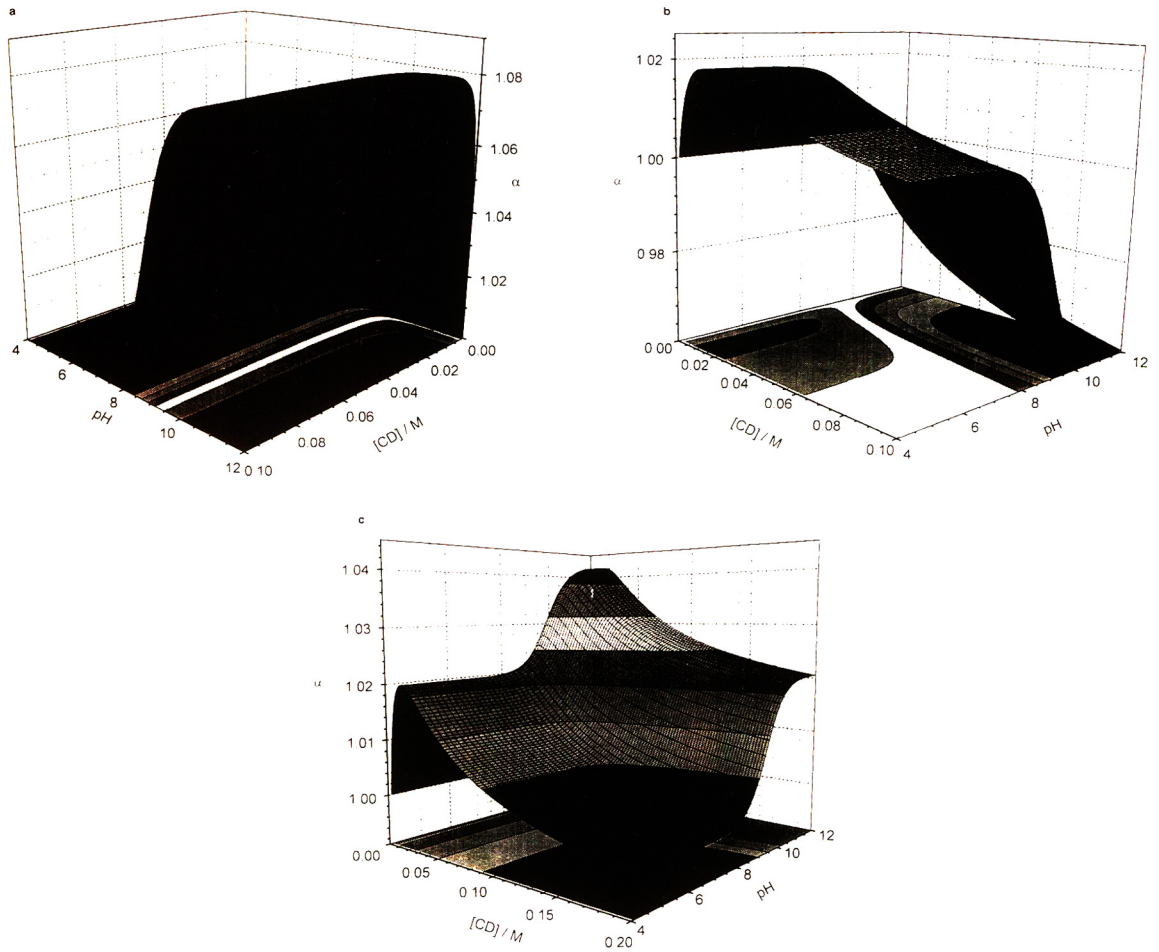

Fig. 4. Selectivity surfaces for the separation of the enantiomers of (a) atropine (desionoselective separation), (b) chloroamphetamine (ionoselective separation) and (c) propranolol (duoselective separation) as a function of the HP-β-CD concentration and the pH in counter-ion concentration balanced 100 mM TAPS BGEs. The surfaces were calculated with Eq. 1 and the constants in Table 1.

held constant if the surfaces are to be visualized. For Fig. 5, where R_s is shown as a function of pH and [CD] for atropine, chloroamphetamine and propranolol, we selected $\beta = 0$ (i.e. no electroosmotic flow). This condition can be realized easily by using capillaries with a hydrophilic, neutral coating. For the desionoselective separation shown in Fig. 5a (atropine), resolution can only be achieved over a narrow pH range, about 2 pH units wide, in the vicinity of the pK_a value. This means that desionoselective separations are not rugged in terms of the pH variable. This may be the main reason why previous attempts to separate the enantiomers of atropine [8] proved unsuccessful. On the [CD] axis, resolution barely changes once the HP-β-CD concentration exceeds 20 mM, i.e. the separation is quite rugged in terms of the [CD] variable.

For the ionoselective separation shown in Fig. 5b (chloroamphetamine), the resolution surface has two lobes. The primary lobe is at low pH, where the separation is rugged in terms of the pH variable (as long as it is at least 1.5 units below the pK_a), and not rugged in terms of

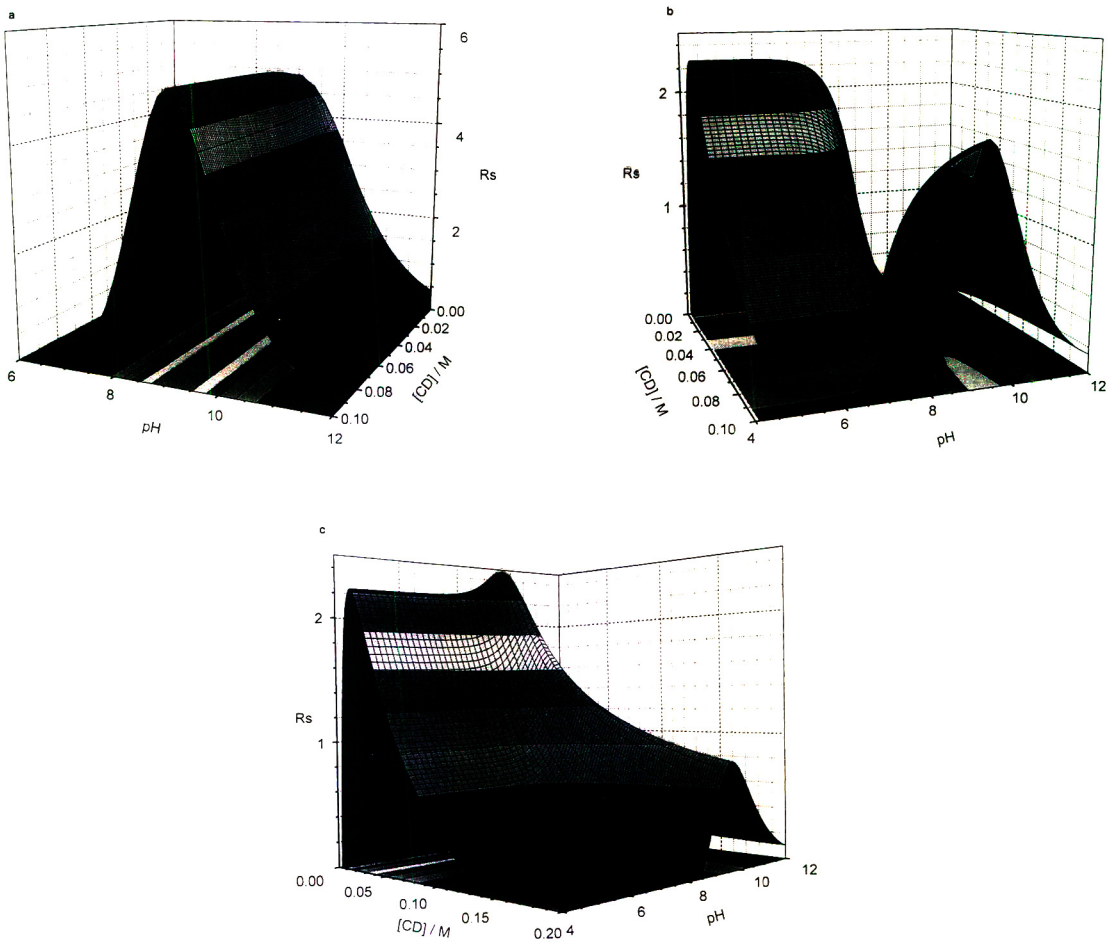

Fig. 5. Peak resolution surface for the separation of the enantiomers of (a) atropine (desionoselective separation), (b) chloroamphetamine (ionoselective separation) and (c) propranolol (duoselective separation) as a function of the HP-β-CD concentration and the pH in counter-ion concentration balanced 100 mM TAPS BGEs. The surface was calculated with Eq. 2 and the constants in Table 1 for $\beta = 0$ and $E = 329$ V/cm, $T = 298$ K and $l = 38.65$ cm.

[CD]. From a practical point of view, one is better off selecting a [CD] value that is slightly above the maximum point, because R_s changes here less rapidly than below the maximum point. The secondary lobe is at high pH. The migration order of the enantiomers on the secondary lobe is opposite to the one on the primary lobe. The separation is not rugged either in terms of pH or [CD].

For the duoselective separation shown in Fig. 5c (propranolol), the resolution surface again has two lobes. The primary one is at low [CD] and spans the entire pH range. The separation is rugged on the primary lobe in terms of pH, as long as it is about 1.5 units below the pK_a. Both the charged and the non-charged forms of the enantiomers of propranolol contribute to the separation cooperatively, because $K_{HRCD^+} < K_{HSCD^+}$ and $K_{RCD} < K_{SCD}$. Since K_{HSCD^+}/K_{HRCD^+} is smaller than K_{SCD}/K_{RCD} (1.07 vs. 1.10), R_s increases as pH is increased towards the pK_a value at [CD] ≈ 2 mM. A global R_s maximum is passed, then the resolution decreases rapidly due to the loss of charge at even

higher pH. The secondary lobe can be accessed more easily at low pH by increasing [CD] to high values. Just as in an ionoselective separation, the migration order of the enantiomers is opposite on the primary and the secondary lobes.

To show how closely the loci of the predicted and measured Rs maxima agree, and also, to demonstrate the importance of pH in a desionoselective separation, the electropherograms of atropine were determined at $E = 267$ V/cm using a 39.2/46.2 cm × 75 μm I.D. capillary with an experimental neutral coating (Beckman). The background electrolytes had a constant, 50 mM HP-β-CD concentration, and their pH was varied between 7.4 and 9.6. The measured (symbol ×) and the predicted (symbol +) R_s values are plotted as a function of pH in Fig. 6. The predicted R_s values were calculated with the constants in Table 1. The measured R_s values are only a third as high as the predicted ones, because electromigration dispersion leads to peak distortion. However, a baseline–baseline separation, shown in the inset in Fig. 6, can be achieved by simultaneously increasing the field strength to 378 V/cm and dynamically matching

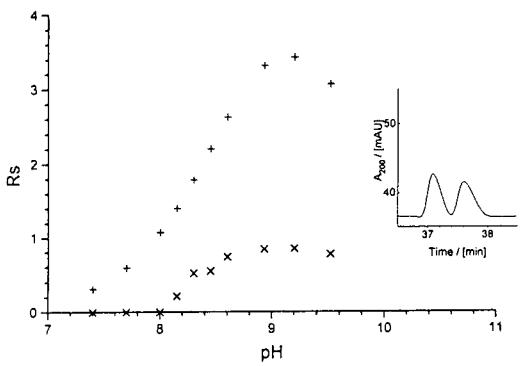

Fig. 6. Comparison of the predicted (+) and measured (×) R_s values for atropine as a function of pH in counter-ion concentration balanced 100 mM TAPS, [CD] = 50 mM BGEs. The measured values were obtained using a 33.2/39.7 cm × 75 μm I.D. capillary with a neutral coating (Beckman), $E = 267$ V/cm. Inset: partial electropherogram of a racemic mixture of atropine obtained in a counter-ion concentration balanced BGE with 50 mM TAPS, pH 8.6, [CD] = 50 mM, $E = 378$ V/cm, $T = 298$ K, $\beta < 0.1 \cdot 10^{-5}$ cm^2/V s, using a 33.2/39.7 cm × 75 μm I.D. capillary with an experimental neutral coating (Beckman).

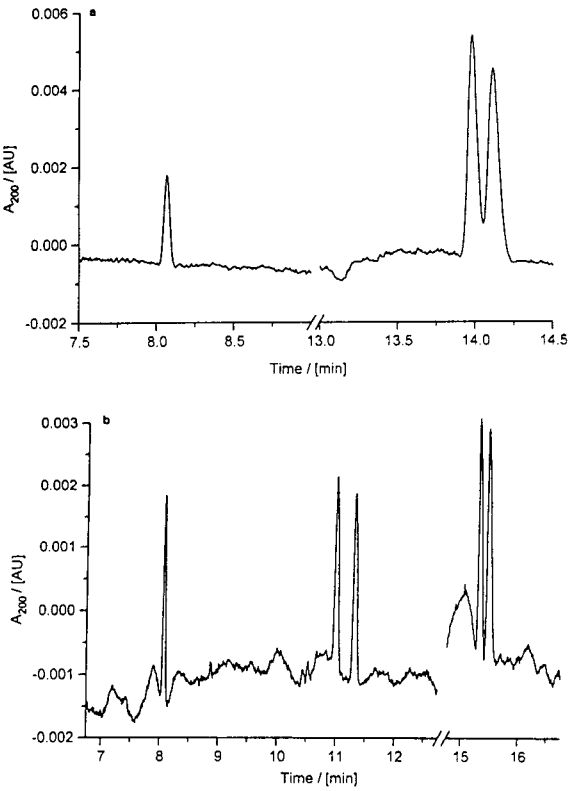

Fig. 7. Electropherograms of (a) BTM^+ and a racemic mixture of chloroamphetamine, and (b) BTM^+, racemic mixtures of $HBTEA^+$ and propranolol, obtained in a counter-ion concentration balanced 100 mM TAPS, pH 7.6, [CD] = 15 mM BGE, $E = 267$ V/cm, $T = 298$ K, $\beta < 0.1 \cdot 10^{-5}$ cm^2/V s, using a 33.2/39.7 cm × 75 μm I.D. capillary with a neutral coating (Beckman).

the mobilities of the solutes and the BGE components (as described in Ref. [9]).

Finally, the electropherogram of a sample containing BTM^+ and a racemic mixture of chloroamphetamine is shown in Fig. 7a, while that of BTM^+ and racemic mixtures of $HBTEA^+$ and propranolol is shown in Fig. 7b.

4. Conclusions

The multiple equilibria-based DID selectivity model and the extended peak resolution equation of CE were used to analyze the possibilities of electrophoretic enantiomer separations for

chiral weak bases, using HP-β-CD as resolving agent. The existence of all three separation types predicted by theory has been verified experimentally for chiral weak bases. In a desionoselective separation (exemplified by atropine), only the non-dissociated enantiomers complex selectively, and resolution is possible only in a narrow pH range in the vicinity of the pK_a value. These separations are rugged in terms of the concentration of the resolving agent. In an ionoselective separation (exemplified by chloroamphetamine), only the dissociated enantiomers complex selectively. Resolution, displaying a local maximum as a function of the resolving agent concentration, is possible at any pH value that is at least two units below the pK_a. Resolution is also possible in the vicinity of the pK_a value, albeit at high resolving agent concentrations, and with a reversed migration order. Finally, in a duoselective separation (exemplified by propranolol), both the dissociated and the non-dissociated forms of the enantiomers complex selectively with the resolving agent. The resolution surface again has two lobes, affording different migration orders at different pH and resolving agent concentration combinations. The resolution equation explicitly shows the impressive resolution gains that can be realized by a judicial choice of the magnitude of the dimensionless electroosmotic flow coefficient. Combination of the extended peak resolution equation and the DID selectivity models permit the development of chiral CE separations in a methodical fashion, rather than by trial-and-error. Further work is under way in our laboratory to extend the model to other analytes and resolving agents as well.

Acknowledgements

Partial financial support by the National Science Foundation (CHE-8919151 and an NSF-REU fellowship to L.A.B.), the Texas Coordination Board of Higher Education Advanced Research Program (Project No. 010366-016), Beckman Instruments (Fullerton, CA, USA), the W.R. Johnson Pharmaceutical Research Institute (Springfield, PA, USA), and the Dow Chemical Company (Midland, MI, USA) is gratefully acknowledged. American Maize Products Corporation (Hammond, IN, USA) and the Aqualon Corporation (Wilmington, DE, USA), respectively, are acknowledged for the donation of the β-cyclodextrin and HEC samples. The authors are indebted to I. Cruzado for assistance with the atropine measurements.

References

[1] Y.Y. Rawjee, D.U. Staerk and Gy. Vigh, *J. Chromatogr.*, 635 (1993) 291.
[2] Y.Y. Rawjee, R.L. Williams and Gy. Vigh, *J. Chromatogr. A*, 652 (1993) 233.
[3] Y.Y. Rawjee and Gy. Vigh, *Anal. Chem.*, 66 (1994) 619.
[4] Y.Y. Rawjee, R.L. Williams and Gy. Vigh, *J. Chromatogr. A*, 680 (1994) 599.
[5] C.T. Rao, B. Lindberg, J. Lindberg and J. Pitha, *J. Org. Chem.*, 56 (1991) 1327.
[6] J.N. Kanazawa and N.S. Nishinomiya, *US Pat.*, 3 135 788 (1964).
[7] J.L. Beckers, F.M. Everaerts and M.T. Ackermans, *J. Chromatogr.*, 537 (1991) 407.
[8] M. Heuermann and G. Blaschke, *J. Chromatogr.*, 648 (1993) 267.
[9] Y.Y. Rawjee, R.L. Williams and Gy. Vigh, *Anal. Chem.*, 66 (1994) 3777.

ELSEVIER

Journal of Chromatography A, 688 (1994) 283–292

JOURNAL OF CHROMATOGRAPHY A

Capillary electrokinetic chromatography with a suspension of chromatographic particles

K. Bächmann*, B. Göttlicher, I. Haag, K.-Y. Han, W. Hensel, A. Mainka

Technische Hochschule Darmstadt, Fachbereich Chemie, Hochschulstrasse 10, 64289 Darmstadt, Germany

Received 8 June 1994

Abstract

The use of a suspension of chromatographic particles as a pseudo-stationary phase in capillary electrokinetic chromatography is demonstrated. The separation of nine phenol derivatives is presented to demonstrate the influence of the particles. Reversed-phase particles with a diameter of 1.5 μm were chosen. These particles were coated with a surfactant to form a stable suspension. The capacity factor of the chromatographic separation can be varied by changing the particle concentration, independent of other parameters. To avoid light scattering at the particles, a discontinuous set-up was developed.

1. Introduction

As it is not possible to separate uncharged analytes or analytes with equal mobilities in capillary zone electrophoresis (CZE), new analytical techniques such as micellar electrokinetic chromatography (MEKC) [1–3], cyclodextrin-modified electrokinetic chromatography (CD-EKC) [4] and microemulsion electrokinetic chromatography (MEEKC) [5,6] have been developed. In MEKC and MEEKC it is not possible to increase the amount of the organic modifier beyond a certain limit, otherwise the stability of the microemulsion can no longer be guaranteed and, in the case of micelles as a pseudo-stationary phase, inverse micelles are formed. A possible solution is the use of a suspension of chromatographic particles.

Although the plate numbers in CZE are very high owing to the plug profile (up to 1 000 000), the selectivity may be the limiting factor. It can be improved, however, by the addition of a pseudo-stationary phase. Velocity differences of the analytes are enlarged according to the distribution between a pseudo-stationary phase and the buffer solution.

Chromatographic and especially reversed-phase (RP) particles show different selectivities (known in HPLC) compared with MEKC and MEEKC, so separation problems may be solved more easily. The selectivity of chromatographic particles is high, so the versatility of the EKC systems is increased by the incorporation of chromatographic particles as a pseudo-stationary phase. The capacity factor in the new method is influenced by the content of organic modifier and by the concentration of the particles. Particles with charged functional groups form stable suspensions in aqueous buffers. Particles with apolar surfaces have to be coated dynamically to

* Corresponding author.

0021-9673/94/$07.00
SSDI 0021-9673(94)00853-1

form a stable suspension. In this study, we adapted a well known CZE separation of nine selected phenols to discontinuous SEKC. As in chromatography the separation of phenols is made with RP particles, we chose RP-18 particles with a diameter of 1.5 μm. Dynamic coating was achieved by the addition of sodium dodecyl sulfate.

2. Experimental

2.1. Chemicals

All phenols were purchased from Supelco (Bad Homburg, Germany) and sodium dodecylsulfate (SDS) from Merck (Darmstadt, Germany). Toluene and Sudan III were used as received from Fluka (Neu-Ulm, Germany).

Buffer solutions were prepared from analytical-reagent grade chemicals (Merck) used for electrophoresis: sodium tetraborate and sodium phosphate, pH adjusted with NaOH. Samples for hydrodynamic injection were prepared in water.

Non-porous Chromspher UOP RP-18 particles with a size of 1.5 μm were provided by Chrompack (Frankfurt, Germany).

2.2. Preparation of suspensions (dynamic particle coating)

The particle suspensions are manufactured ultrasonically. SDS is added to the buffer as a surfactant to achieve a charged surface. This suspension remains stable for more than 1 h. Subsequently, significant sedimentation of the particles is observed, leading to a decrease in particle concentration and to a lower reproducibility of retention times. To achieve maximum reliability, the suspension is treated in an ultrasonic bath for several minutes before each injection.

Particle concentrations of more than 10% (w/v) often result in a blocked capillary, so this concentration seems to be the limit for easy handling. It is possible to regenerate blocked capillaries by using an ultrasonic bath or pressure.

2.3. Instrumentation

The modular electrophoresis instrument used consisted of a Lambda 1000 variable-wavelength UV detection system (Bischoff, Leonberg, Germany), an HCN 6M-30000 high-voltage power supply (FUG, Rosenheim, Germany) and a PRINCE basic electrophoresis apparatus with autosampler (Lauer Labs., Netherlands). Fused-silica capillary tubes with an I.D. of 75 μm were purchased from Chromatographieservice (Düsseldorf, Germany). Detection was achieved on-column.

2.4. Separation conditions

For the separation of phenols, different amounts (0.1–0.9 g) of Chromspher UOP RP-18 particles were suspended in 10 ml of buffer consisting of 10 m*M* sodium tetraborate–5 m*M* sodium phosphate–4 m*M* SDS (pH 10). Detection was carried out at 206 nm.

3. Theory

3.1. Suspension of chromatographic particles

The use of chromatographic particles as a pseudo-stationary phase can be regarded as a combination of electrophoresis and chromatography and represents the latest method in the field of EKC. In analogy with MEKC, electrokinetic chromatography using suspensions of chromatographic particles as a pseudo-stationary phase will be termed suspension electrokinetic chromatography (SEKC).

The separation of the analytes will be achieved according to the distribution between the buffer and the particle surface. This process leads to a change in the velocity of the separated species. For uncharged species it is necessary to create a relative velocity between the buffer and the particles, otherwise there will be no influence on the analyte velocity and consequently no sepa-

ration. The separation of charged analytes can be influenced either by using charged particles (with their own mobility) or uncharged particles (without their own mobility). In the latter instance the mobility of the charged analyte is decreased by the adsorption process. The greatest influence on the retention time will be found for particles showing an opposite migration direction to the analyte. This effect increases with increasing velocity differences between the analyte and the particles. Charged particles based on classical stationary phases known from pressure-driven chromatography [normal-phase (NP) and reversed-phase (RP) particles are mostly used] with sufficient mobility can be formed according to pH (NP) by the use of surfactants interacting with the polar surface (RP-18), or by synthesizing particles with a certain degree of charged groups.

3.2. Comparison to CZE and related techniques with other pseudo-stationary phases

To achieve a sufficient resolution of the analytes it is necessary to have a large migration-time window. This is defined as the possible range of the migration time of a neutral analyte and is limited between the migration times of the bulk solution (t_0) and that of the pseudo-stationary phase (t_q).

In EKC, the velocities of the analytes and the pseudo-stationary phases such as micelles were described by Hückel [7]. The basis of this application is the fact that the thickness of the diffuse double-layer, δ, (Stern model) is larger than d_p, which is correct for ions and micelles. For the chromatographic particles that we use as the pseudo-stationary phase δ is always smaller than d_p. In this case the particle velocity is described by the equation developed by Smoluchowski [8]:

$$v = \frac{\varepsilon E \zeta}{\eta} \quad (1)$$

where v = velocity of the particle, E = electrical field strength, η = shear viscosity of the buffer, ε = dielectric constant and the zeta potential (ζ) characterizes the electrical potential at the particle surface. As the velocity of the particles increases with increasing zeta potential, it is necessary to chose particles with a high zeta potential. If the particle itself shows only a low potential, it is possible to create a higher one on its surface by coating, e.g. with SDS. The coated particles we use show a zeta potential of 43 mV.

It is unknown whether the influence of a coated particle is caused by the apolar RP phase or by the polar outside. Therefore, only the net effect will be considered. Amphiphilic analytes may be incorporated in the surface layer as described for micelles by Terabe et al. [9]. Usually the concentration of the surfactant used is higher than the critical micellar concentration (cmc), so the effect of micelles, which influence the separation, also has to be considered.

The resolution for uncharged species in EKC is described by the following equation according to Terabe et al. [3]:

$$R_s = \frac{\sqrt{N}}{4}\left(\frac{\alpha - 1}{\alpha}\right)\left(\frac{k_2}{1 + k_2}\right)\left[\frac{1 - t_0/t_q}{1 + (t_0/t_q)k_1}\right] \quad (2)$$

where $k_{1,2}$ = capacity factors of analytes 1 and 2, t_0 = retention time of the electroosmotic flow (EOF), t_q = retention time of the pseudo-stationary phase and α = separation factor = k_2/k_1.

The last term on the right-hand side is due to the contribution of the limited migration-time window between the boundaries t_0 and t_q. To obtain an improved resolution it is necessary to decrease the ratio t_0/t_q. Two principal approaches are obvious [9].

From Eq. 2, a relationship among retention times and migration velocities can be developed:

$$v = L/t_r \quad (3)$$

where L = effective length of the capillary, t_r = retention time of the analyte,

$$t_0/t_q = v_q/v_{eof} \quad (4)$$

and v_q = velocity of the pseudo-stationary phase.

It is possible to decrease the electroosmotic flow or to increase the electrophoretic mobility. The electrophoretic mobility may be increased dramatically using particles as the pseudo-stationary phase which show higher velocities

than micelles. As a consequence, the resolution will be improved for a given separation factor. This is obviously an advantage of SEKC over MEKC. The resolution may be optimized by varying either the velocity of the particles or their concentration.

3.3. Peak broadening compared with other electrokinetic techniques

The H/E dependence for MEKC was discussed in detail by Terabe et al. [2] and Sepaniak and Cole [10]. The total band broadening (H_{tot}) is described as the sum of five independent parameters:

$$H_{tot} = H_l + H_m + H_{aq} + H_T + H_{ep(m)} \quad (5)$$

where H_l = longitudinal diffusion, H_m = adsorption/desorption kinetics, H_{aq} = intermicelle mass transfer, H_T = radial temperature gradient and $H_{ep(m)}$ = dispersion due to different mobilities of the micelles. Among these five factors, H_l, H_m and $H_{ep(m)}$ are found to contribute significantly to band broadening in MEKC. The analogous discussion can also be applied to SEKC.

The longitudinal diffusion decreases with increasing applied voltage. The influence of H_m and $H_{ep(m)}$ depends on the capacity factor. They both increase with increasing velocity (increase in the applied voltage). For a larger k' and a high v_{eof}, $H_{ep(m)}$ shows the greatest influence, whereas H_m contributes significantly to a medium k' and high v_{eof}. An analogous equation may be derived for SEKC.

For the discontinuous set-up an additional parameter, H_i, has to be considered (see Eq. 6) due to the inhomogeneity of the particles. The parabolic flow profile which results from pumping the particles into the capillary leads to differences in concentrations at the end of the zone. A cross-sectional concentration gradient of the particles is observed. Therefore, the desorption process leads to peak broadening which is serious for large k' and high v_{eof}. $H_{ep(p)}$ is used instead of $H_{ep(m)}$ for the micelles to describe the influence of different particle velocities. For SEKC the total peak broadening is composed of

$$H_{tot} = H_l + H_m + H_T + H_{ep(p)} + H_i \quad (6)$$

where $H_{ep(p)}$ = dispersion due to different particle velocities and H_i = dispersion due to flow profile. For a mixed system (MEKC and SEKC due to the need to suspend the particles), the following equation results:

$$H_{tot} = H_l + H_m + H_{aq} + H_{ep(m)} + H_T + H_{ep(p)} + H_i \quad (7)$$

4. Results and discussion

4.1. Particles suspended in a buffer system containing SDS as surfactant

Particle coating

The main disadvantage of SEKC is the necessity to suspend the particles in the buffer. A more or less stable suspension (according to sedimentation and, therefore, to the size of the particles) may be formed using ultrasonication. As RP particles are not moistened by water, the addition of surfactants such as SDS to the buffer solution and to the suspension is necessary to form a stable suspension. SDS covers the surface of the particles, forming a charged exterior.

The minimum amount needed to form a suspension was found to be the cmc of the buffer solution. The surface tension of this system was measured using the Wilhelmy plate method. The determination of the cmc is made with a Gibbs diagram (plotting σ versus concentration of SDS), where the cmc is indicated as the minimum of the curve. For the aqueous buffer we used, the cmc was found to be 4 mM for SDS. The resulting suspension remains stable for more than 1 h. The drawback of this method is that the used surfactant acts as an eluent, resulting in low capacity factors.

Assuming about 40 A^2 [11] as the space required for one SDS molecule, only 0.1% of the 4 mM SDS involved is needed to cover all particles in the suspension (0.9 g per 10 ml of

buffer). Therefore, the amount of SDS can be considered to be independent of the particle concentration.

To check this assumption, the amount of SDS left in the buffer was measured. As the electrolyte we used 5 m*M* sodium molybdate. Indirect UV detection was achieved at 211 nm. Fig. 1 shows an electropherogram of 1 m*M* SDS in water. Calibration was carried out with SDS in water in the range 0–2.5 m*M*. The remaining SDS concentration in the particle suspension was measured in the solution after sedimentation of the particles. For the quantification of SDS the solution was diluted (four-fold) to suppress the formation of micelles. The calibration and the amount of SDS found in the solution are given in Fig. 2. This experiment shows that the concentration of SDS in the buffer can be regarded as constant in the presence of the particles.

Particle velocity

The EOF and the mobility of the particles show opposite directions. The velocity of the particles is 17.7 cm/min (at 20 kV) and is larger than the EOF. To avoid problems arising with optical detection (light scattering of the particles), a discontinuous experimental set-up is

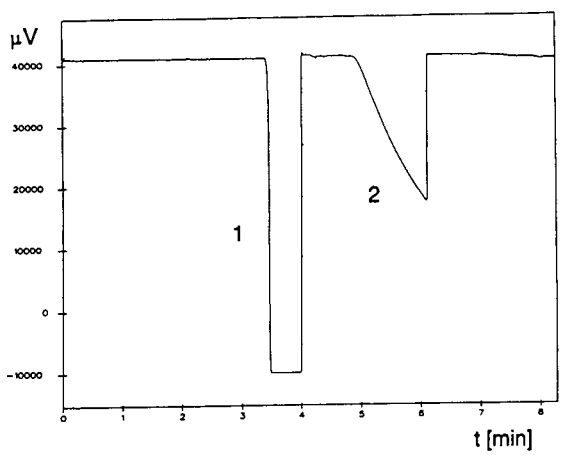

Fig. 1. Electropherogram of SDS. Conditions: electrolyte, 5 m*M* sodium molybdate; capillary, total length 83 cm, effective length 63 cm, 75 μm I.D.; detection, UV at 211 nm, indirect; separation, 30 kV; sample, 1 m*M* SDS; injection, 150 mbar, 0.4 min. Identification: 1 = EOF; 2 = SDS.

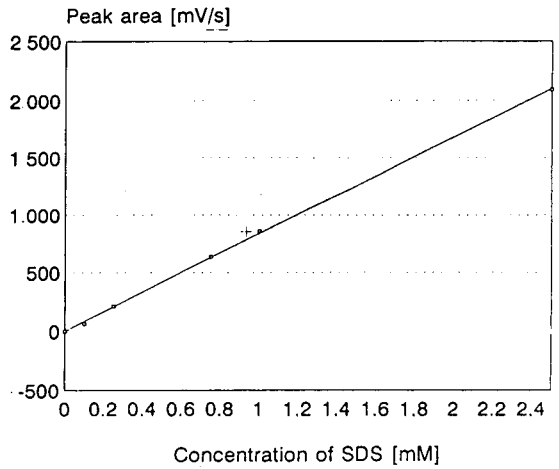

Fig. 2. Concentration of free SDS. □ = Calibration; + = 1.5 μm.

used. The capillary is filled with the suspension up to the detection window. The buffer for electrophoresis consists of the electrolyte and contains the same SDS concentration as the suspension to allow a constant particle velocity. The sample is injected hydrodynamically. The particles which have a higher mobility than the EOF move out of the capillary during the separation while the EOF transports the analytes towards the detection window. The phenol derivatives we used are slower than the EOF in any observed case. Separation is achieved with positive voltage at the injection end. The velocity parameters observed in this SEKC are shown schematically in Fig. 3. This experimental set-up is limited to low capacity factors. Analytes that have a high capacity factor or a high mobility compared with the EOF may be removed from the capillary.

As the degree of coverage of the surface with SDS is high in an aqueous buffer, the influence of the particles on the separation has to be seen as a competition of surfactant, acting as an eluent, and analyte. An additional influence will be found for bifunctional analytes. These analytes may additionally interact with the polar surfactant at the surface or may also be incorporated in the surface layer of SDS comparable to micelles [9].

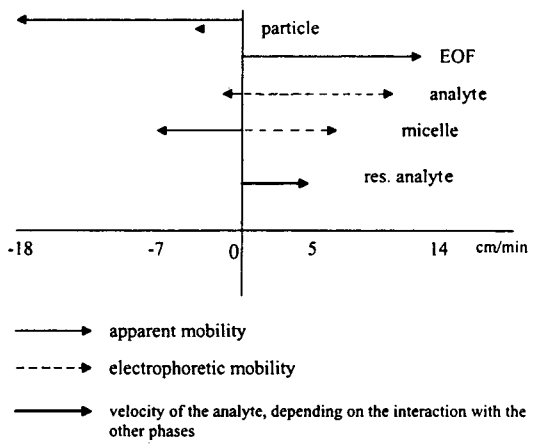

Fig. 3. Velocities of the different phases in SEKC.

Influence on the separation of phenol derivatives

To obtain an impression of the influence of the particles on plate height and to compare the results with those of MEKC and the predictions drawn from theory, we measured the H/E dependence for three phenolic compounds. The resulting data for MEKC compared with SEKC for 4-nitrophenol are given in Fig. 4. A decrease in plate height is found for larger voltages. This may be due to the limited heat dissipation in the particle zone. It is therefore necessary to work at lower voltages compared with MEKC to obtain the best resolution.

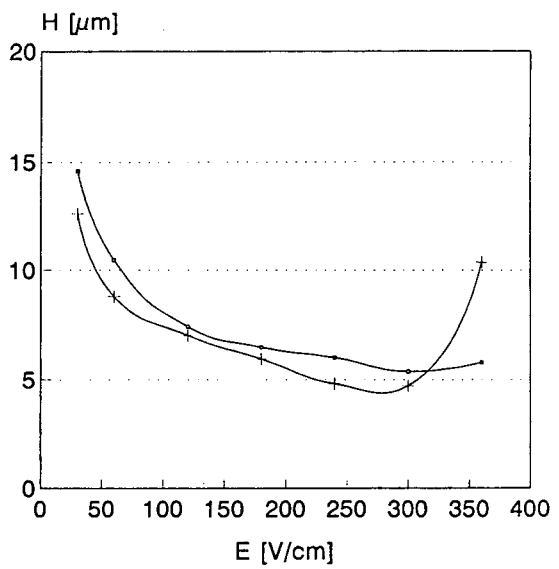

Fig. 4. H versus E curves for 4-nitrophenol. □ = Without particles; + = with particles.

In a further investigation, the influence of different particle concentrations (the buffer contains 4 mM SDS) on the separation of nine phenol derivatives was measured.

Generally, it is possible to separate phenolic compounds according to their own mobility [12–14] or by the use of MEKC [15,16]. We used a buffer system that will not lead to a complete separation. The aim of our work was to show the influence of the particles on a simple separation problem. Phenols were chosen as an example of analytes with low capacity factors. Under the given separation conditions (buffer of pH 9.5), most of the phenols are negatively charged. The pK_a values of the phenols involved are given in Table 1. All the systems investigated consisted of the same buffer and SDS concentration. Fig. 5A shows the separation of nine phenol derivatives in free-flow CZE without SDS. All phenol derivatives are slower than the EOF, so they can be detected in the EOF direction. Some of the phenols are already partly separated.

The influence of SDS needed for the preparation of the suspension was examined. Fig. 5B shows the same separation with an additional content of 4 mM SDS. The resolution of the separation is only slightly affected. As described above, the amount of the micelles is not changed even at increased particle concentrations because

Table 1
pK_a values of the phenols studied

Phenol	pK_a
4-Chloro-3-methylphenol	9.54
2-Chlorophenol	4.50
2,4-Dichlorophenol	7.89
2,4-Dinitrophenol	4.07
2-Methyl-4,6-dinitrophenol	4.70
2-Nitrophenol	7.23
4-Nitrophenol	7.16
Phenol	10.00
2,4,6-Trichlorophenol	6.23

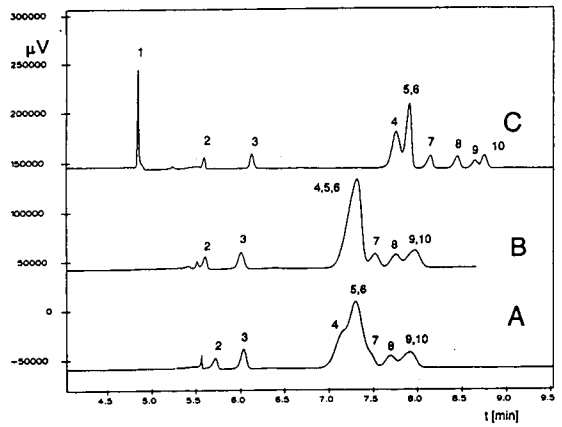

Fig. 5. Comparison of the separation of nine phenols using (A) buffer, (B) SDS and (C) 0.1 g of particles in 10 ml of buffer. Conditions: buffer, 10 m*M* sodium tetraborate–5 m*M* sodium phosphate (pH 9.5); SDS concentration, 4 m*M*; particle amount, 0.1 g of RP-18 (1.5 μm) in 10 ml of buffer with SDS; capillary, 59 cm to detector, 77 cm total length, 75 μm I.D.; injection, hydrodynamic, 50 mbar, 12 s; analyte concentration, 0.9 m*M* of each phenol; separation, 20 kV; detection, UV at 206 nm.

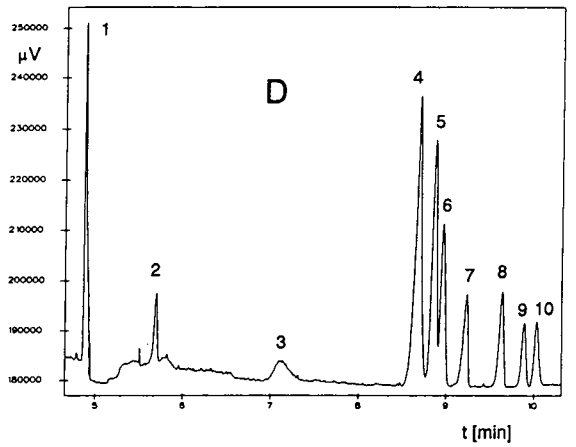

Fig. 6. Identification of the phenol deivatives (separation with 0.9 g of particles in 10 ml of buffer). Peaks: 1 = EOF; 2 = phenol; 3 = 4-chloro-3-methylphenol; 4 = 2,4,6-trichlorophenol; 5 = 2,4-dichlorophenol; 6 = 2-chlorophenol; 7 = 2-methyl-4,6-dinitrophenol; 8 = 2,4-dinitrophenol; 9 = 4-nitrophenol; 10 = 2-nitrophenol.

SDS is used in a large excess. Hence it is possible to compare this electropherogram with the results of the influence of a particle suspension. In Fig. 5C a separation with the aid of a suspension containing 0.1 g of particles in 10 ml of buffer is shown. In Fig. 6 the identification for a particle amount of 0.9 g in 10 ml of buffer for the separation of phenols is given. Analytes adsorbed at the particle surface (independent of the discussed SDS/RP mechanism) show an increased retention time according to the higher mobility of the particles compared with the analytes showing no adsorption. In the case of phenol derivatives an increased resolution is observed. An increase in particle concentration results in longer retention times (Fig. 7).

Calculation of the capacity factor for SEKC

For the calculation of capacity factors for discontinuous SEKC using SDS for particle coating, a simple model was developed. As described above, Eq. 3 gives the relationship between retention time and the velocity of the analyte.

The total velocity of the analyte in MEKC (Eq. 8) and continuous SEKC (Eq. 9) is composed of the velocity present on or in the different phases (micelles, buffer or particle) weighted with the molar fraction ($X_i = n_i/n_{tot}$ where n_i and n_{tot} are the analyte amount in

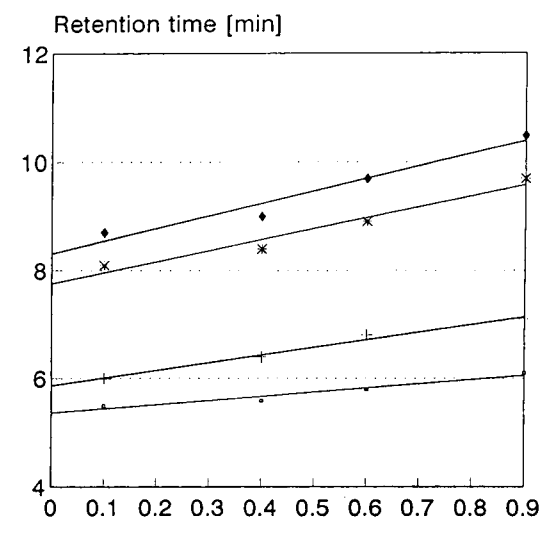

Fig. 7. Influence of the particle concentration on retention time. □ = Phenol; + = 4-chloro-3-methylphenol; * = 2-methyl-4,6-dinitrophenol; ◆ = 2-nitrophenol.

phase i and the total amount, respectively) plus the velocity of the EOF.

$$v_{tot1} = X_1 v_m + X_2 v_a + v_{EOF} \quad (8)$$

where v_{tot1} = velocity of the analyte in MEKC and v_a = velocity of the analyte.

$$v_{tot2} = X_3 v_m + X_4 v_a + X_5 v_p + v_{EOF} \quad (9)$$

where v_{tot2} = velocity of the analyte in continuous SEKC and v_p = velocity of the particles.

The velocity measured for discontinuous SEKC consists of two parts, first the behaviour of the analyte in the particle zone and second of the analyte in the zone without particles (Eq. 10), both weighted with the time fraction they spend in each zone (Eq. 11).

$$v_{tot3} = (v_{tot1})Z_1 + (v_{tot2})Z_2 \quad (10)$$

$$Z_i = \frac{t_i}{t_{tot}} \quad (11)$$

where v_{tot3} = velocity of the analyte in discontinuous SEKC, Z_i = time ratio ($i = 1$, without particles; $i = 2$, particle zone), t_i = time spent in zone i and t_{tot} = retention time of the analyte.

Additionally, two more equations for the mass balance of each system are available for MEKC (Eq. 12) and SEKC (Eq. 13).

$$X_1 + X_2 = 1 \quad (12)$$

$$X_3 + X_4 + X_5 = 1 \quad (13)$$

Further, the balance for the time fractions is

$$Z_1 + Z_2 = 1 \quad (14)$$

As the micelle concentration is not changed by the addition of the particles, which could be proved by the calculation given earlier, the capacity factor of the micelle is constant, leading to

$$k_m = \frac{n_a}{n_m} = \frac{X_1}{X_2} = \frac{X_3}{X_4} \quad (15)$$

where n_a = moles of the analyte in the buffer, n_m = moles of the analyte in the micelles and k_m = capacity factor of the micelles.

The time spent in each zone (Eq. 16) is a consequence of the relative velocity among the analyte and the particles (Eq. 17).

$$t_2 = \frac{v_{rel}}{L_p} \quad (16)$$

$$v_{rel} = v_{tot2} - v_P \quad (17)$$

where v_{rel} = relative velocity and L_p = length of the particle zone. This leads to

$$Z_2 = \frac{L_P}{t_{tot}(v_{tot2} - v_P)} \quad (18)$$

If all values for the different velocity parameters are known, at least seven equations are necessary to obtain the solution due to the seven unknown molar and time fractions.

The velocity of the particles, the micelles, the EOF and the velocity of the analyte are known from direct measurements. According to Terabe et al. [3], Sudan III is used as a tracer for the micelle velocity (for the electrolyte we use a velocity of the micelles of 6.5 cm/min). Hence the calculation of all molar fractions is possible. As the capacity factor k_p is the ratio of the total moles of analyte on the particle surface to those in the surrounding buffer, it is derived as the ratio of the mole fractions of the particle and of the buffer:

$$\frac{X_5}{X_4} = k_p \quad (19)$$

where k_p = capacity factor of the particles. Therefore, it is necessary to calculate both molar fractions. X_1 and X_2 may be calculated first. Using Eqs. 8 and 12, it is possible to obtain

$$X_2 = \frac{v_{tot1} - v_m - v_{EOF}}{v_a - v_m} \quad (20)$$

X_1 is derived from Eq. 12. Combining Eqs. 10 and 18 leads to

$$V_{tot2} = \frac{t_{tot} v_p (v_{tot3} - v_{tot1}) - L v_{tot1}}{t_{tot}(v_{tot3} - v_{tot1}) - L} \quad (21)$$

The combination of Eqs. 10, 13 and 15 leads to

$$X_5 = \frac{(v_a - v_m) - (k_m + 1)(v_{tot2} - v_{EOF} - v_m)}{(v_a - v_m) - (k_m + 1)(v_p - v_m)} \quad (22)$$

Table 2
Capacity factors of the phenols studied at different particle concentrations

Phenol	Capacity factor	
	0.1 g per 10 ml of buffer	0.9 g per 10 ml of buffer
4-Chloro-3-methylphenol	0.03	0.62
2-Chlorophenol	0.17	0.84
2,4-Dichlorophenol	0.17	0.79
2,4-Dinitrophenol	0.21	0.98
2-Methyl-4,6-dinitrophenol	0.19	0.89
2-Nitrophenol	0.25	1.01
4-Nitrophenol	0.20	0.99
Phenol	<0.01	0.18
2,4,6-Trichlorophenol	0.13	0.75

Table 2 summarizes the capacity factors derived from Eq. 19 for the phenol derivatives at given particle amounts of 0.1 and 0.9 g in 10 ml of buffer. As predicted, the capacity factors increase with increasing particle concentration. For the phenols involved they are low. This is caused mainly by two effects: first, SDS acts as a strong eluent, and second, the charged phenol derivatives show little tendency to adsorb on the particles.

For a different system where SDS is not necessary to form a suspension, we expect higher capacity factors and therefore a larger influence of the particles on retention time.

4.2. *Reproducibility*

The reproducibility for SEKC is found to be comparable to or slightly lower than that for MEKC or CZE. For the retention time and peak area reproducibilities of 1–5% are found.

5. Conclusions

This is the first stage of an investigation concerning the use of SEKC. The aim was to demonstrate some of the possibilities and difficulties resulting from this experimental set-up. It was shown that using SEKC it is possible to influence a separation based on CZE and MEKC. The capacity of the system is controlled by the particle concentration. Therefore, we are able to vary this parameter without affecting others. As the capacity factors are small, it will be a major task to increase the capacity factors in order to obtain increased effects on resolution. An increased effect on the resolution will be found for particles having an opposite migration direction compared with the analytes. This can perhaps be achieved in the case of anionic species such as phenolates by the use of, e.g. tetradecyltrimethylammonium bromide instead of SDS as a surfactant. There is a strong need for the development of particles optimized for SEKC. These particles have to have a partly charged surface and functional groups to interact with the analyte.

The use of other detection methods such as amperometric or fluorescence detection, which are not affected by particles, will help to realize continuous SEKC in the future. This will lead to increased effects on retention and resolution.

Acknowledgement

We are grateful to Chrompack for providing the particles.

References

[1] P. Gareil, *Chromatographia*, 30 (1990) 195.
[2] S. Terabe, K. Otsuka and T. Ando, *Anal. Chem.*, 61 (1989) 251.

[3] S. Terabe, K. Otsuka and T. Ando, *Anal. Chem.*, 57 (1985) 834.
[4] J. Szejtli, B. Zsadon and T. Cserhati, in W.L. Hinze and D.W. Armstrong (Editor), *Ordered Media in Chemical Separations* (*ACS Symposium Series*, Vol. 342), American Chemical Society, Washington, DC, 1987, p. 200.
[5] H. Watarai, *Chem. Lett.*, (1991) 391.
[6] H. Watarai, *Anal. Sci.*, 7, Suppl. (1991) 245.
[7] E. Hückel, *Phys. Z.*, 25 (1924) 204.
[8] M. v. Smoluchowski, *Bull. Int. Acad. Sci. Cracovie*, 8 (1903) 182.
[9] S. Terabe, N. Matsubara, Y. Ishihama and Y. Okada, *J. Chromatogr.*, 608 (1992) 23.
[10] M.J. Sepaniak and R.O. Cole, *Anal. Chem.*, 59 (1987) 472.
[11] J. Kloubek and A.W. Neumann, *Tenside*, 6 (1969) 4.
[12] K. Bächmann, B. Göttlicher, I. Haag, M. Hannina and W. Hensel, *Fresenius' J. Anal. Chem.*, 350 (1994) 368.
[13] C.D. Gaitonde and P. Pathak, *J. Chromatogr.*, 514 (1990) 389.
[14] M.G. Khaledi and S.C. Smith, *Anal. Chem.*, 65 (1993) 193.
[15] H.K. Lee, S.F.Y. Li, C.L. Ng and C.G. Ong, *J. Chromatogr.*, 542 (1991) 473.
[16] L.K. Goebel, H.M. McNair and H.T. Rassmusen, *J. Chromatogr.*, 517 (1990) 549.

ELSEVIER

Journal of Chromatography A, 688(1994) 293–300

JOURNAL OF CHROMATOGRAPHY A

Separation of water-soluble *p*-sulfonated calixarenes 4, 6 and 8 and 4-hydroxybenzene sulfonate by use of capillary zone electrophoresis

Yuling Zhang, Isiah M. Warner*

Department of Chemistry, Louisiana State University, Baton Rouge, LA 70803, USA

First received 6 June 1994; revised manuscript received 25 August 1994

Abstract

A method for the separation of sulfonated calixarenes 4, 6 and 8 and the 4-hydroxybenzene sulfonate monomer by capillary zone electrophoresis with direct UV absorbance detection is described. The electroosmotic flow (EOF) decreases with addition of K^+ and reverses with addition of Mg^{2+}. The suppression of the EOF upon the addition of K^+ slightly improves the separation of the calixarenes and the monomer. However, the elution times of those compounds increase almost 35 min. The reversal of the EOF by addition of Mg^{2+} reduces the migration time and also improves the separation efficiency. The calixarenes are baseline separated in less than 14 min by use of a borate buffer with the addition of 4.0, 6.0 or 12.0 m*M* $MgCl_2$ at pH 8.3.

1. Introduction

Calixarenes are a class of cyclic phenols linked by methylene groups. These compounds can form a variety of host–guest type inclusion complexes [1–3]. Although the complexation properties of calixarenes have not been examined as extensively as those of cyclodextrins [4–6], calixarenes [1,2] have been used in the recovery of cesium and uranium, ion selective electrodes and field effect transistors. Other applications, such as phase transfer agents, hydrolysis catalysts and separation of organic molecules have also been reported. The most common forms of calixarenes are slightly soluble in several organic solvents, but are essentially insoluble in water. Therefore, experimental efforts have been directed toward enhancing the aqueous solubility of calixarenes. Several water-soluble derivatives of sulfonato- [7], amino- [8], nitro- [9], carboxyl- [10] and phosphonato- [11] calixarenes have been synthesized. The sulfonated calixarene derivatives are highly soluble in water and can be potentially useful as mimics of enzyme–substrate complexes [12].

Water-soluble sulfonated calixarenes are similar to cyclodextrins [4–6] and cyclophanes [13], in that they can form complexes with a variety of guests in aqueous solution [1,2] according to their size and hydrophobicity. Thus, the inclusion complexation abilities of calixarenes are often compared to those of cyclodextrins. The cavities of α-, β- and γ- cyclodextrins have inner

* Corresponding author.

0021-9673/94/$07.00
SSDI 0021-9673(94)00816-7

diameters of 5.7, 7.8 and 9.5 Å, respectively [6]. In contrast, those of calixarene 4, calixarene 6 and calixarene 8 are 3.0, 7.6 and 11.7 Å, respectively [1]. The sizes of the calixarenes play important roles in their complexation capabilities.

In contrast to cyclodextrins, the calixarenes must be synthesized. The procedures for syntheses of calixarenes 4, 6 and 8 [14] are quite similar. Thus, it is sometimes difficult to obtain calixarenes with a specific number of phenol units. Since calixarenes have the same empirical formulas, it is also not possible to distinguish the differences by chemical analysis. Although NMR can provide some structural information about calixarenes, the low sensitivity of this technique is a problem for calixarene analysis. Therefore, separation methods can be very useful for detection and purification of calixarenes.

Capillary electrophoresis (CE) is a powerful separation technique for many compounds, especially charged compounds [15,16]. There are many advantages for the use of CE as a separation technique. These include high separation efficiency, high speed and low consumption of electrolytes and/or samples. The CE method has been used as a separation technique in many areas of research, including biological systems [17–20] to separate proteins, peptides, drugs and chiral compounds. It has also been employed to separate diverse species [21–23] such as inorganic acids, metal ions and surfactants.

In capillary zone electrophoresis (CZE), charged particles can be separated on the basis of differences in their electrophoretic mobilities (μ_{ep}) [16]. At pH 2–11, the inner walls of fused-silica capillaries are usually negatively charged. In the presence of an electric field, the electrolyte migrates toward the cathode as a flat flow profile with mobility μ_{eo}. The electroosmotic flow (EOF) forces all solutes (anionic, cationic, neutral) to migrate toward the cathode ends of the capillaries. In most instances, at high pH values μ_{eo} is larger than μ_{ep}. Therefore, anionic compounds are also carried to the cathode and detected [15,17]. The higher EOF gives shorter migration time, but poorer resolution. Cations, such as Ca^{2+}, Ba^{2+}, Mg^{2+}, Sr^{2+}, K^+ and Na^+, are often added to suppress the EOF and improve the separation efficiencies of anions [22]. The disadvantage of cation additives is that the migration times of the analytes in the capillaries are lengthened. To overcome this difficulty, cations are often used to reverse the electroosmotic flow at a certain pH.

In this manuscript, a procedure is described for separation of calixarenes and the phenol monomer by use of reversed electroosmotic flow CZE with UV absorbance detection. The electropherograms of calixarenes and the monomer as a function of different concentrations of Mg^{2+} also provide information about complex formation between the calixarenes and Mg^{2+}.

2. Experimental

2.1. Materials

Synthesis of water-soluble p-sulfonated calixarenes

The *p*-sulfonatocalixarenes 4, 6 and 8 (SCX4, SCX6 and SCX8) were synthesized by use of previously developed procedures of Gutsche et al. [14] and Shinkai et al. [7]. The synthesis is a three-step process to obtain the water-soluble sulfonated calixarenes. In the first step, *p-tert.*-butylcalixarenes are prepared according to the method of Gutsche et al. [14]. The second step involves debutylation of *p-tert.*-butylcalixarenes [24]. The last step involves sulfonation of the calixarenes in concentrated sulfuric acid (fuming sulfuric acid and 96% sulfuric acid) [7], producing the water-soluble sulfonated calixarenes. The structures of the calixarenes used in this study are provided in Fig. 1.

The sodium salt of the *p*-hydroxybenzene sulfonate monomer was purchased from Aldrich. The compounds $Na_2B_4O_7$, H_3BO_3, KCl and $MgCl_2$ were purchased from Fisher. All buffer solutions and samples were prepared by use of double ion-exchange deionized water and then passed through a 45-μm membrane filter.

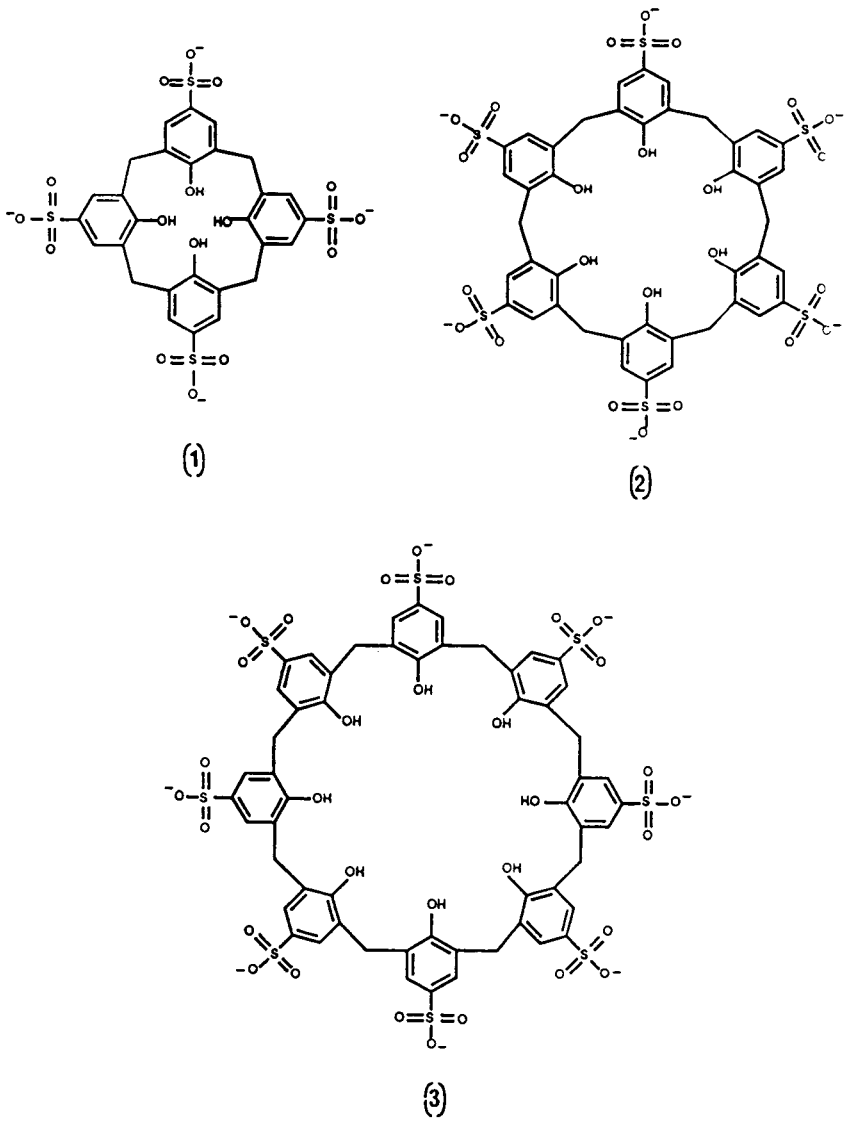

Fig. 1. Structures of *p*-sulfonated calixarenes: 1 = SCX4; 2 = SCX6; 3 = SCX8.

2.2. Apparatus

The CE instrument (CES1) was purchased from Dionex (Houston, TX, USA). Detection was by UV absorbance at 215 nm. Fused-silica capillaries (64 cm × 75 μm I.D.) were used. The distance between injection and detection was 60 cm. The applied electric field was 20 kV. All analyses were conducted at room temperature (21°C).

3. Results and discussion

For each separation buffer used in this study, the samples of calixarenes (about $1.0 \cdot 10^{-5}$ *M*):

SCX4, SCX6, SCX8, monomer (about $5 \cdot 10^{-5}$ *M*) and their mixtures were run at least three times, or until results were reproducible. The migration order of the mixture was assigned by testing the migration time of each component alone. The buffer was a combination of 50 m*M* H_3BO_3 and 10 m*M* $Na_2B_4O_7$. The pH of the buffer was 8.3. In this case, positive potential was employed. In other words, the anode was on the injection side. The electropherogram of the mixture of calixarenes and monomer under these conditions is shown in Fig. 2. The migration time of the monomer is about 8.3 min, which is far from the calixarenes (ca. 17 min). Although the calixarenes cannot be separated under these conditions, the elution order of the four analytes can still be determined, which is monomer, SCX4, SCX6 and then SCX8. This elution order can be explained by recalling that the inner surface of the capillaries contains $\equiv$Si–OH groups which are ionized to $\equiv$Si–O^- in alkaline and slightly acidic media (pH > 2). When an electric field is applied to the capillary, the positive counterions in the buffer migrate toward the cathode. Since the cations are solvated, the solvent flows with them, resulting in EOF. The direction of the EOF is identical for ionic and neutral molecules, despite their electric charges [16].

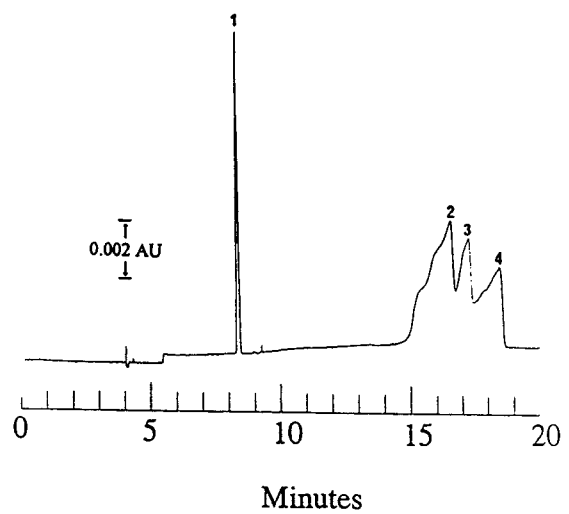

Fig. 2. Electropherogram of the calixarenes and phenol monomer; buffer: 50.0 m*M* boric acid and 10.0 m*M* sodium borate; pH 8.3. Peaks: 1 = monomer; 2 = SCX4; 3 = SCX6; 4 = SCX8.

It should also be noted that hydrolysis of the analytes and the pH of the buffer affects the separation efficiency and the elution order [25]. The pK_a values of the hydroxyl groups of the monomer unit, SCX4 and SCX6 have been reported. The pK_a values of SCX8 have not been found in the literature. Therefore, the discussions here regarding pK_a values are limited to monomer, SCX4 and SCX6. The pK_a values of SCX8 may be inferred from the trend observed relative to the three other analytes. As reported, for the monomer, the pK_a is 8.7 [26]; for SCX4: $pK_{a1} = 3$–4, $pK_{a2} = 11$ [27]; for SCX6: $pK_{a1} < 1$, $pK_{a2} = 3$, $pK_{a3} = 4$ and $pK_{a4} > 11$ [28]. The low pK_a values of the calixarenes are due to the formation of intramolecular hydrogen bonds which have been discussed previously [27,28]. Thus, at the buffer pH 8.3, the ionic forms of the analytes in the buffer solution is expected to be $[S]^-$; SCX4 as $[SCX4]^{5-}$; SCX6 as $[SCX6]^{9-}$. The charge-to-mass ratio for these three analytes are $5.78 \cdot 10^{-3}$, $6.76 \cdot 10^{-3}$ and $8.11 \cdot 10^{-3}$, respectively. If electrophoretic mobilities of ions are proportional to the values of charge to mass ratio [29], the mobilities of the analytes should be in the order of monomer < SCX4 < SCX6. Since all analytes are negatively charged, the electrophoretic mobilities of the analytes would be opposite to the direction of EOF. However, due to the dominant contribution of the EOF, the migration order of the analytes will be monomer, SCX4, SCX6 and then SCX8. The detection order in Fig. 2 agrees with this prediction. However, the separation of the calixarenes is not satisfactory. In the electropherogram, the peaks of calixarenes are very broad. To improve the separation of calixarenes, some manipulations of the buffer were undertaken.

3.1. K^+ and Mg^{2+} effects

The addition of cations in CE has been shown to decrease the EOF and improve the separation of many compounds such as sulfonate and sulfate surfactants [22]. Therefore, different amounts of

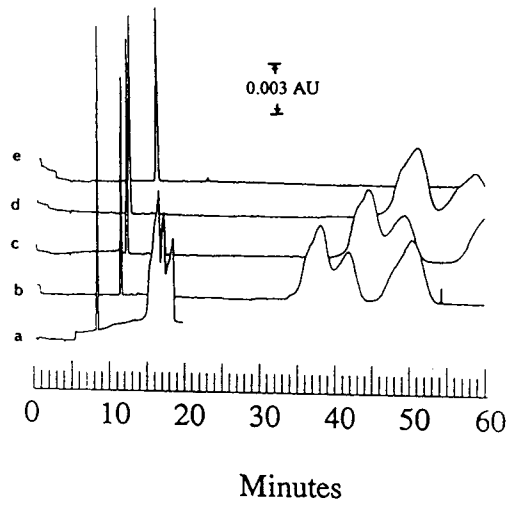

Fig. 3. Electropherograms of the calixarenes and monomer; buffer: borate buffer (as in Fig. 2) in presence of KCl: (a) 0.0; (b) 0.25 m*M*; (c) 0.5 m*M*; (d) 1.0 m*M*; (e) 2.0 m*M*.

K^+ and Mg^{2+} were used as additives to examine the effects of cations on the separation of the calixarenes. Fig. 3 provides the electropherograms of the mixtures of calixarenes and monomer under the condition of borate buffer with various amounts of KCl. The retention times of all four analytes increase by the addition of K^+. The retention time of the monomer increases from 8.3 to 16.1 min, while those of the calixarenes increase from 16 to 50 min. With 0.25 m*M* KCl, SCX8 can be separated from SCX6 and SCX4. By addition of 1.0 m*M* KCl, SCX6 and SCX4 can be barely separated. However, the migration times for the calixarenes are as long as 50 min. In addition, the peaks are broad and poorly resolved. Thus, this would not be an acceptable separation method for calixarenes.

Another cation, Mg^{2+}, was also investigated as an additive to the buffer. Initially, the injection was on the anode side and migration time was monitored for 100 min. No peaks appeared during this long period time, indicating that the EOF was reversed. The polarity of the electric field was then switched. Then, the cathode was placed on the injection side. The electropherograms of the analytes are shown in Fig. 4. Several details can be noted in these figures:

(1) As the amount of Mg^{2+} increases from 2.0 to 12.0 m*M*, the migration times of all the analytes were reduced. The separation by use of 4.0, 6.0 or 12.0 m*M* Mg^{2+} is satisfactory.

(2) The migration time of the monomer is very much a function of the concentration of Mg^{2+}.

(3) In all buffers with Mg^{2+}, the elution order for calixarenes is SCX4, SCX6 and SCX8.

At pH > 2.0 and in alkaline solution, the EOF is toward the negative electrode. By addition of Mg^{2+} at pH 8.3,

$$\equiv Si\text{–}O^- + Mg^{2+} \rightleftharpoons \equiv Si\text{–}OMg^+$$

is formed on the inner wall of the capillary [30]. Then the diffuse layer of solvent is negatively charged. Under an applied potential, the diffuse layer migrates toward the anode. The EOF is reversed under these conditions. Higher concentrations of Mg^{2+} in the buffer solution produces a greater amount of $\equiv Si\text{–}OMg^+$ on the wall. Thus, the reversed EOF is enhanced. This produces a shortening of the migration times for all analytes.

Reversed EOF usually results in a reversal of elution order of the analytes [31] unless there are other interactions between the analytes and the buffer components. As we discussed earlier, the order of electrophoretic mobilities of the calixarenes at pH 8.3 should be SCX8 > SCX6 > SCX4. The phenol monomer has the smallest mobility and is expected to be the last component to elute. In the electropherogram (Fig. 4a), the monomer is the last to elute. However, the elution order of calixarenes is not reversed because of the reversed EOF.

The characteristics of calixarenes should be considered to explain the above observations. Calixarenes are cyclic compounds, which can form complexes with metal ions. A number of studies on solid-state complexation of calixarenes have been reported [32]. The *p-tert.*-butylcalixarene amides have been used to extract metal ions from aqueous solution [33]. This suggests that the calixarenes may be capable of complexing Mg^{2+} ion. If water-soluble calixarenes can complex with Mg^{2+}, the positive Mg^{2+} would neutralize a corresponding number of negative

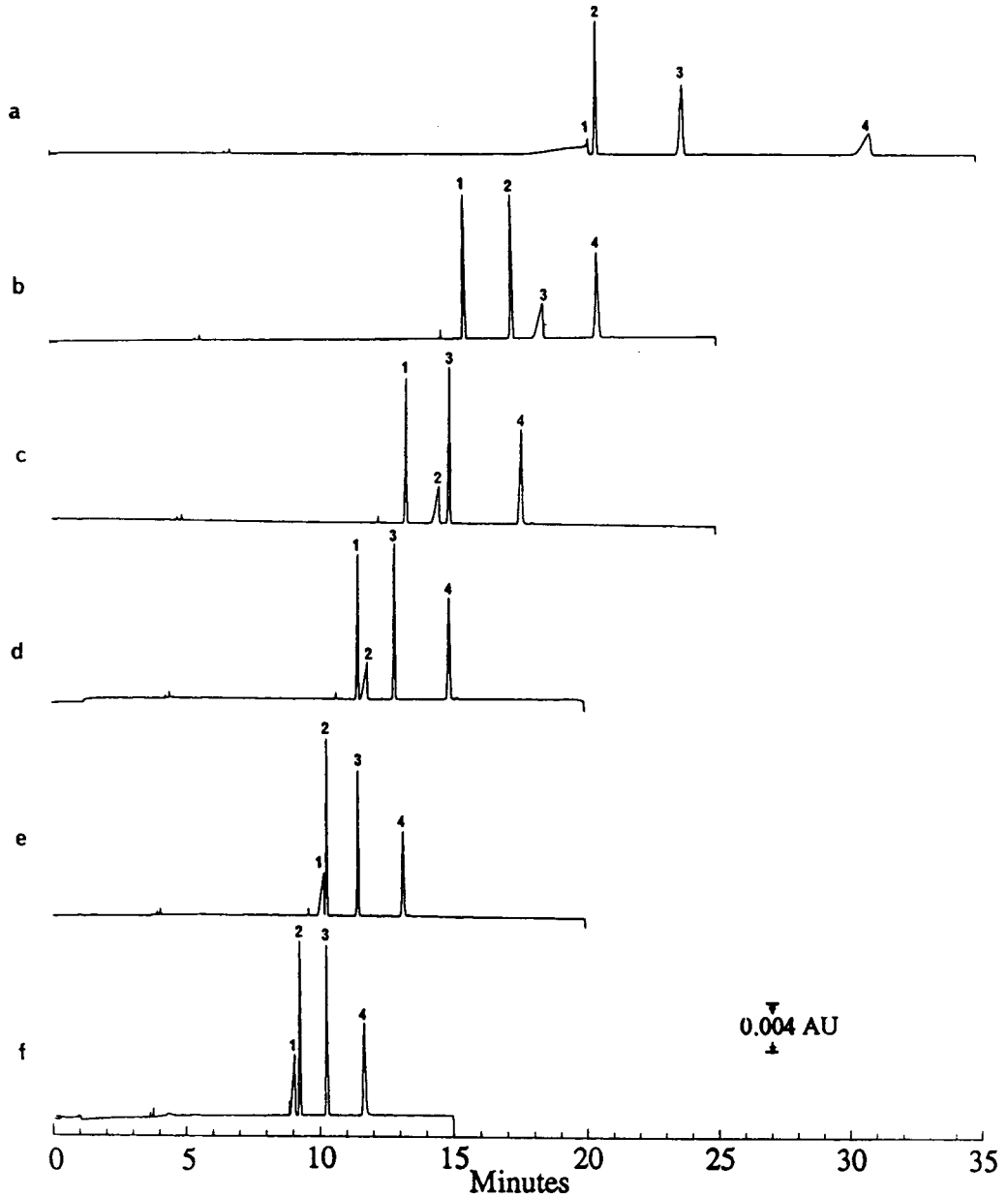

Fig. 4. Electropherograms of the calixarenes and monomer; buffer: borate buffer (as in Fig. 2) in the presence of (a) 2.0 m*M* $MgCl_2$ (peaks: 1 = SCX4; 2 = SCX6; 3 = SCX8; 4 = monomer), (b) 4.0 m*M* $MgCl_2$ (peaks: 1 = SCX4; 2 = SCX6; 3 = monomer; 4 = SCX8), (c) 6.0 m*M* $MgCl_2$ (peaks: 1 = SCX4; 2 = monomer; 3 = SCX6; 4 = SCX8), (d) 8.0 m*M* $MgCl_2$ (peaks: 1 = SCX4; 2 = monomer; 3 = SCX6; 4 = SCX8), (e) 10.0 m*M* $MgCl_2$ (peaks: 1 = monomer; 2 = SCX4; 3 = SCX6; 4 = SCX8) or (f) 12.0 m*M* $MgCl_2$ (peaks: 1 = monomer; 2 = SCX4; 3 = SCX6; 4 = SCX8).

charges on the calixarenes. Thus, the net negative charge density of calixarenes decreases and this suppresses the mobilities of the calixarenes. In other words, the more Mg^{2+} complexed by the calixarenes, the smaller the electrophoretic mobilities of the calixarenes. The phenol monomer does not complex with Mg^{2+} and does not change with the addition of Mg^{2+}. Thus, the net change in migration for the monomer, due to the increase of EOF, is larger than those for calixarenes. This results in the observed drastic changes in elution order of the monomer.

It is well known that calixarenes are size-selective host molecules [1,2]. It has been reported that extraction efficiencies (%) of *p-tert.*-butylcalixarene amides 4, 6 and 8 (non-water-soluble) for Mg^{2+} are less than 1.0, 11.8 and 14.2%, respectively. This suggests that the complexation capability with calixarene amide 8 is the strongest, followed by 6 and then 4. In Fig. 4, the elution order of the water-soluble calixarenes is SCX4, SCX6, SCX8. This is opposite to what was observed without Mg^{2+} in Fig. 2. This suggests that SCX8 may complex with the greatest amount of Mg^{2+}, followed by SCX6 and then by SCX4. This is the same trend observed for the calixarene amides.

3.2. Detection limit

For UV detection, the detection limit is typically on the order of 10^{-5} to 10^{-6} *M* depending on the absorptivities of the analytes [34]. The detection limit of the calixarenes and monomer can be as low as $10^{-7}M$. Fig. 5 shows an example of the electropherogram of SCX6 ($2.5 \cdot 10^{-7}$ *M*). With this low detection, CZE can be used to detect the impurities in the calixarene samples. Fig. 6 is an electropherogram of one batch of SCX8. The retention times of SCX4, SCX6 and SCX8 are 13.75, 15.25 and 18.43 min, respectively. In Fig. 6, there are two peaks whose retention times are about 15 and 18 min. The small peak is assigned to SCX6 and the larger one is SCX8. Thus, the appearance of a small amount of SCX6 can be noted in that SCX8 sample.

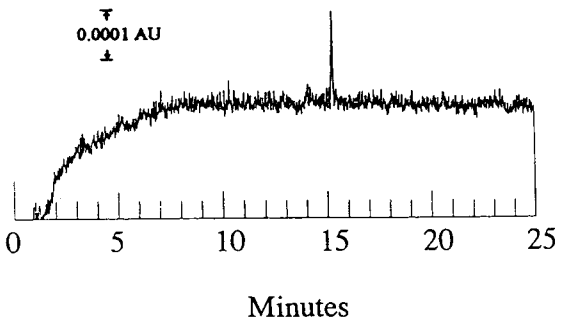

Fig. 5. Electropherogram of SCX6 at $2.5 \cdot 10^{-7}$ *M*.

4. Conclusions

CZE is a very effective method for separation of the calixarenes. The borate–boric acid buffer with 4.0, 6.0 or 12.0 m*M* Mg^{2+} is recommended for separation of these compounds. In addition, CZE is useful for examining the purity of the calixarene samples. CZE is also a potential

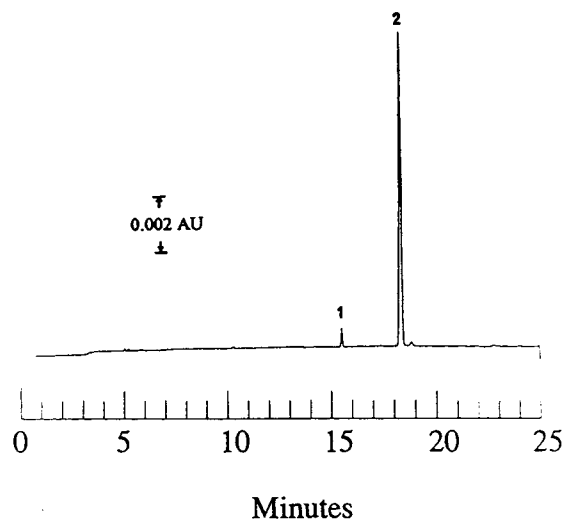

Fig. 6. Electropherogram of one batch of SCX8 sample which includes a small amount of SCX6. Peaks: 1 = SCX6; 2 = SCX8.

technique for studying the complexation abilities of calixarenes with cations and neutral compounds. However, the disadvantage of CZE is that it cannot be used as a preparative method. HPLC would be a better method in this regard.

Acknowledgements

This work was supported by the Division of Chemical Sciences, Office of Basic Energy Sciences, Office of Energy Research, US Department of Energy (Grant DE-FG05-91ER14219). The authors are grateful to Mr. J. Wang for technical assistance.

References

[1] C.D. Gutsche, *Calixarene*, Royal Society of Chemistry, Cambridge, 1989.
[2] J. Vicens and V. Böhmer, *Topics in Inclusion Science: Calixarenes, a Versatile Class of Maerocyclic Compounds*, Kluwer, Dordrecht, 1991.
[3] C.D. Gutsche and R. Muthukrishnan, *J. Org. Chem.*, 43 (1978) 4905.
[4] M.L. Bender and M. Komiyama, *Cyclodextrin Chemistry*, Springer, Berlin, 1978.
[5] J.M. Schuette, T.T. Ndou and I.M. Warner, *J. Phys. Chem.*, 96 (1992) 5309.
[6] J. Szejtli, *Cyclodextrins and their Inclusion Complexes*, Akademia Kiadio, Budapest, 1982.
[7] S. Shinkai, S. Mori, H. Koreishi, T. Tsubaki and O. Manabe, *J. Am. Chem. Soc.*, 108 (1986) 2409.
[8] C.D. Gutsche, J.A. Jevine and P.K. Sujeeth, *J. Org. Chem.*, 50 (1985) 5802.
[9] S. Shinkai, T. Tsukabi, T. Sone and O. Manabe, *Tetrahedron Lett.*, 26 (1985) 3343.
[10] *A. Arduini, A. Pochini, S. Reverberi and R. Ungaro, J. Chem. Soc., Chem. Commun.*, (1984) 981.
[11] T. Arimura, T. Nagasaki, S. Shinkai and T. Matsuda, *J. Org. Chem.*, 54 (1989) 3766.
[12] S. Shinkai, H. Kawabata, T. Arimura, T. Matsuda, H. Satoh and O. Manabe, *J. Chem. Soc., Perkin Trans. I*, (1989) 1073.
[13] F. Diederich, *Angew. Chem., Int. Ed. Engl.*, 27 (1988) 362.
[14] C.D. Gutsche, B. Dhawan, M. Leonis and D. Stewart, in J.D. White (Editor), *Organic Syntheses*, Vol. 68, Wiley, New York, 1990, pp. 238–242.
[15] J.W. Jorgenson and K.D. Lukacs, *Anal. Chem.*, 53 (1981) 1298.
[16] A.G. Ewing, R.A. Wallingford and T.M. Olefirowicz, *Anal. Chem.*, 61 (1989) 292A.
[17] J.S. Green and J.W. Jorgenson, *J. Chromatogr.*, 478 (1989) 63.
[18] D.A. McGregor and E.S. Yeung, *J. Chromatogr. A*, 652 (1993) 67.
[19] K.C. Chan, C.W. Whang and E.S. Yeung, *J. Liq. Chromatogr.*, 16 (1993) 1941.
[20] S. Terabe, K. Otsuka and H. Nishi, *J. Chromatogr. A*, 666 (1994) 295.
[21] M. Aguilar, X. Huang and R.N. Zare, *J. Chromatogr.*, 480 (1989) 427.
[22] S. Chen and D. Pietrzyk, *Anal. Chem.*, 65 (1993) 2770.
[23] X. Huang, J.A. Luckey, M.J. Gordon and R.N. Zare, *Anal. Chem.*, 61 (1989) 766.
[24] C.D. Gutsche and L.G. Lin, *Tetrahedron*, 42 (1986) 1633.
[25] M.A. Hayes, I. Kheterpal and A.G. Ewing, *Anal. Chem.*, 65 (1993) 27.
[26] A.E. Martell and R.M. Smith, *Critical Stability Constants*, Plenum Press, New York, 1977, p. 3.
[27] G. Arena, R. Cali, G. Giuseppelobardo, E. Rizzarelli, D. Sciotto, R. Ungaro and A. Casnati, *Supramolecular Chem.*, 1 (1992) 19.
[28] S. Shinkai, *Pure Appl. Chem.*, 58 (1986) 1523.
[29] S.F.Y. Li, *Capillary Electrophoresis*, Elsevier, Amsterdam, 1992, p. 203.
[30] H.B. Oldham and J.C. Myland, *Fundamentals of Electrochemical Science*, Academic Press, San Diego, CA, 1994, p. 322.
[31] Y. Liu and S. Sheu, *J. Chromatogr. A*, 663 (1994) 239.
[32] J.L. Atwood, G.W. Orr, F. Hamada and S.G. Bott, *Supramolecular Chem.*, 1 (1992) 15.
[33] S.K. Chang, S.K. Kwon and I. Cho, *Chem. Lett.*, (1987) 947.
[34] A.G. Ewing, J.M. Mesaros and P.F. Gavin, *Anal. Chem.*, 66 (1994) 527A.

ELSEVIER

Journal of Chromatography A, 688 (1994) 301–316

JOURNAL OF CHROMATOGRAPHY A

Development of a capillary electrophoresis method for the characterization of enzymatic products arising from the carbamoylase digestion of paralytic shellfish poisoning toxins☆

A. Buzy, P. Thibault*, M.V. Laycock

Institute for Marine Biosciences, National Research Council, 1411 Oxford Street, Halifax, Nova Scotia B3H 3Z1, Canada

First received 30 June 1994; revised manuscript received 31 August 1994

Abstract

A sample stacking procedure is presented for the capillary electrophoretic (CE) separation of paralytic shellfish poisoning (PSP) toxins dissolved in high ionic strength buffers. The application of such a stacking procedure prior to the zone electrophoretic separation is demonstrated for the analysis of decarbamoyl toxins arising from the digestion of PSP toxins by an hydrolytic enzyme from little neck clams (*Protothaca staminea*). Improvements in separation efficiency facilitated identification and quantitation of substrates and enzymatic products present in the digest using CE. The separation conditions developed were found to be entirely compatible with electrospray mass spectrometry, which permitted the analysis of PSP toxins and their decarbamoyl derivatives present in the low micromolar range in crude enzyme digests. The products released during the enzymatic digestion were identified using CE combined with tandem mass spectrometry.

1. Introduction

The toxins associated with paralytic shellfish poisoning (PSP) constitute a group of potent marine phycotoxins produced by certain strains of dinoflagellates such as *Alexandrium* spp. [1,2]. Blooms of these dinoflagellates are unpredictable and constitute a serious public health hazard in view of the rapidity with which toxins can accumulate in the filter-feeding shellfish. Consequently, the exploitation and development of coastal shellfish resources and aquaculture can also be severely threatened in areas where such toxic blooms are encountered.

The toxin composition and profile vary considerably between species of toxic dinoflagellates. This feature has been used previously with some success to study the distribution of dinoflagellate species [3]. Toxins produced by the phytoplankton include compounds such as saxitoxin (STX) and neosaxitoxin (NEO), and a complex suite of sulfate and N-sulfonate analogues (Fig. 1). These toxins also vary in terms of their specific toxicities to mammals. The most potent are the carbamate toxins such as STX, NEO and gonyautoxins 1 and 4 ($GTX_{1,4}$), with specific toxicities (with respect to LD_{50} for intraperitoneal injection in mice) ranging from 400 to 550 μg of STX equivalent per μmol. In

* Corresponding author.

*NRCC No. 38060.

SSDI 0021-9673(94)00850-7

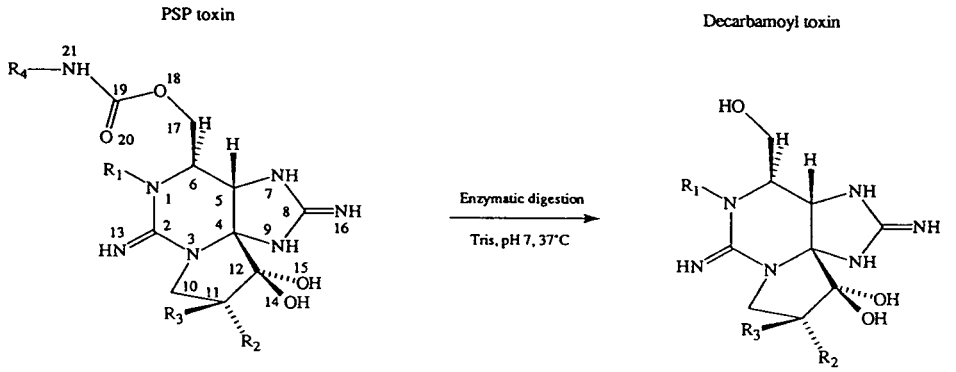

R_1	R_2	R_3	R_4	Toxin	M_r	
H	H	H	H	STX	299	Carbamate toxins
OH	H	H	H	NEO	315	
H	OSO_3H	H	H	GTX_2	395	
H	H	OSO_3H	H	GTX_3	395	
OH	OSO_3H	H	H	GTX_1	411	
OH	H	OSO_3H	H	GTX_4	411	
H	H	H	SO_3H	B_1	379	N-sulfocarbamoyl toxins
OH	H	H	SO_3H	B_2	395	
H	OSO_3H	H	SO_3H	C_1	475	
H	H	OSO_3H	SO_3H	C_2	475	
OH	OSO_3H	H	SO_3H	C_3	491	
OH	H	OSO_3H	SO_3H	C_4	491	

Fig. 1. Paralytic shellfish poisoning toxins: structures, molecular masses and decarbamoyl derivatives.

contrast, the N-sulfocarbamoyl derivatives (B_1, B_2, C_{1-4}) are much less toxic (5–70 μg STXeq./μmol).

The bioaccumulation and transformation of the PSP toxins in shellfish are extremely complex processes. The toxin profiles depend not only on the phytoplankton species on which they have been feeding, but also on the shellfish and the organs examined [4]. In controlled experiments where toxic *Alexandrium* cultures were fed to bivalves, earlier studies have demonstrated that toxin profiles found in a given shellfish species can exhibit significant differences from those of the dinoflagellates [5–9]. Such variations in toxin profiles were found to be species-specific while also displaying a time dependence. Evidence of such variability was also noted in the PSP toxin profiles observed for different populations of wild shellfish species collected from the same geographic location [4,10].

The differences in toxin profiles observed between shellfish and ingested toxic dinoflagellates can be accounted for by a selective retention/elimination of specific toxins and/or by metabolic processes within tissues [4]. One of the stronger pieces of evidence supporting the latter mechanism is the appearance of new toxin components in shellfish that were not present in the original toxic dinoflagellates. Such transformations have been documented for the reduction of

NEO to STX in scallop tissues [11] and for the conversion of $GTX_{1,4}$ to $GTX_{2,3}$ plus STX, and of NEO to STX, by marine bacteria [12]. Although it was originally assumed [11] that such reductions could be mediated enzymatically, recent evidence suggests that these processes could be effected by naturally occurring chemical reductants such as glutathione and cysteine [13]. Formation of de novo toxins was also reported for the conversion of N-sulfocarbamoyl and carbamoyl PSP toxins to their corresponding decarbamoyl derivatives in little neck clams (*Protothaca staminea*) [14] and in two species of Japanese clams [13]. Decarbamoyl toxins have been detected only in a few clam species, and have not been found in most shellfish [13,14].

Evidence accumulated thus far concerning the formation of these decarbamoyl derivatives suggests that loss of the carbamate side chain could be catalysed by hydrolytic enzymes from the bivalve digestive glands. Sullivan et al. [14] indicated that a rapid hydrolysis of PSP toxin substrates (STX, $GTX_{2,3}$, B_1 and $C_{1,2}$) to their corresponding decarbamoyl derivatives (Fig. 1) was observed for homogenates obtained from the viscera of *P. staminea* whereas extracts prepared from the mantle, muscle and siphon yield only limited conversion. An enzymatic process was also indicated by the fact that the conversion was inactivated when the homogenates were exposed to heat, organic solvent (methanol) or low pH [14].

In spite of the numerous studies describing the observation of carbamoylase activity in shellfish, no report has been presented thus far on the isolation and purification of the enzyme(s). This is partly due to the complex nature of the digestive gland extracts and to the lack of a fast, sensitive and efficient chemical-based assay capable of screening fractions obtained during the purification steps. To date, previous studies documenting this specific carbamoylase activity in shellfish extracts have typically used an HPLC–fluorescence detection (FLD) method whereby the separated PSP toxins are converted into fluorescent derivatives using a post-column oxidation procedure [15]. Although this method provides excellent sensitivity (typically 4 ng/ml for STX [15]), the monitoring of carbamoylase activity using this method is difficult in view of the lack of resolution between the substrate and its corresponding decarbamoyl derivative [15]. Improvements in resolution can be achieved using alternate HPLC columns and buffer systems [16], but this is very time consuming since the characterization of all PSP toxins requires a set of three different HPLC conditions, one for each of the toxin groups (STX and NEO, GTXs and C toxins).

In the present study we report the development of a rapid capillary electrophoresis-based method that can be used both for the monitoring of crude enzyme fractions and for the characterization of digestion products. Capillary zone electrophoresis (CZE) with both UV and mass spectral detection has been described previously for the analysis of PSP toxins [17,18]. More recently, enhanced sample loadings for the analysis of PSP toxins was demonstrated using capillary isotachophoresis (cITP) prior to CZE separation [19]. This cITP preconcentration step has provided an improvement of concentration detection limits of at least two orders of magnitude over those obtainable using the conventional CZE format, and facilitated the identification of PSP toxins in biological extracts [19]. This type of sample preconcentration is best effected using coated capillaries to minimize the electroosmotic flow during the cITP step. Unfortunately, the injection of a large number of crude sample extracts can result in irreversible modification of the capillary surface coating, and thus a decrease in the separation performance. Alternate electrophoretic separation procedures capable of handling samples with high salt concentrations or shellfish extracts, with relatively little sample clean-up, were therefore developed for the present application. The judicious choice of electrolyte systems for use with uncoated capillaries enabled proper focusing of the analyte bands even in the presence of highly mobile salts. Mobilization of the PSP toxins was achieved using an acidic buffer, acting as a temporary terminator during the stacking step prior to the zone electrophoresis separation. For purposes of simplicity, the term "capillary electrophoresis"

(CE) will be used here to refer to the combined stacking/zone electrophoresis separation. Such a CE analysis was found to be entirely compatible with the operation of electrospray mass spectrometry (ES-MS), and permitted the monitoring of toxin derivatives formed during the incubation of PSP toxin substrates with crude enzyme extracts from *P. staminea*. Identification and characterization of products released during the enzymatic digestion are demonstrated using on-line CE–ES-MS, and CE with tandem mass spectrometry.

2. Experimental

2.1. Isolation of PSP toxins

Samples of STX, NEO, GTX_{1-4} and $C_{1,2}$ were purified from cultured algal cells of *Alexandrium excavatum* and *A. minutum* according to a procedure described earlier [20]. All toxins were dissolved in 0.1 *M* acetic acid. PSP toxins such as STX, NEO and GTX_{1-4} can also be obtained through the Marine Analytical Chemistry Standards Program (Institute for Marine Biosciences, Halifax, Canada) as individual calibration solutions. The B_1 toxin was obtained following reduction of the $C_{1,2}$ toxins in 0.1 *M* dithiothreitol (Sigma, St. Louis, MO, USA) at 40°C for 1 h. Purification of the reaction products was achieved using a Bio-Gel P-2 column (Bio-Rad Labs., Richmond, CA, USA), eluting the toxin with 0.1 *M* acetic acid [20]. Prior to the enzymatic reaction all PSP standards were dissolved in Tris–HCl to a final buffer concentration of 0.1 *M* and pH 7.

2.2. Preparation of enzyme extracts

Little neck clams (*P. staminea*) were collected from beaches at Bamfield Research Station, Vancouver Island, Canada. All samples were kept frozen at −20°C prior to their extraction. A crude enzyme extract was obtained by dissecting the digestive glands from two clams (5 g wet mass) and grinding in a cold mortar with glass. The homogenized tissues were suspended in 3 ml of 0.1 *M* Tris–HCl, pH 7, and centrifuged at 15 000 *g* for 20 min. The supernatant was concentrated 6 times by ultrafiltration using an Amicon PM-10 membrane (Amicon Canada, Oakville, Canada), and filtered through a 0.22-μm nylon membrane (Millipore, Bedford, MA, USA).

2.3. Toxin incubation

Unless otherwise specified, enzymatic digestions were performed at 37°C using a 40-μl aliquot of PSP toxin solution to which was added 160 μl of the concentrated enzyme extract in Tris buffer pH 7, to give a final toxin concentration between 160 and 240 μg/ml. Aliquots of the reaction mixture (typically 10 μl) were removed at different times, and the digestion process stopped by adding an equal volume of 0.1 *M* HCl. The reaction solution was then neutralized and centrifuged at 10 000 *g* for 5 min to remove those proteins which had precipitated upon the addition of acid. The supernatant was then analyzed directly by CE–UV and CE–MS.

2.4. Capillary electrophoresis

All experiments were performed using a Beckman P/ACE 2100 system (Beckman Instruments, Fullerton, CA, USA). Uncoated fused-silica columns were obtained from Polymicro Technologies (Phoenix, AZ, USA). Unless otherwise specified, dimensions were typically 97 cm (90 cm to UV detector) × 50 μm I.D. × 360 μm O.D. columns. Separations were conducted in constant voltage mode by applying + 30 kV at the injector end of the capillary. Samples were introduced by pressurizing the vial with a low (0.5 p.s.i.; 1 p.s.i. = 6894.76 Pa) pressure injection for typically 20 s, resulting in the injection of 20 nl. The CE separation buffer was 100 m*M* morpholine in water adjusted to pH 4.0 with formic acid. Between each run the capillary was washed with 1 *M* NaOH. UV detection was monitored at 200 nm. All concentration measurements were calculated from corrected peak areas (peak area/migration time) to compensate for variation of the electroosmotic flow. All buffer chemicals were purchased from Sigma.

2.5. Mass spectrometer and interface

All MS experiments were performed using a PE/SCIEX API/III$^+$ triple quadrupole mass spectrometer (PE/SCIEX, Thornhill, Canada) equipped with an atmospheric pressure ionization (API) source operated in nebulizer-assisted electrospray (ionspray) mode. The interface was constructed from a fully articulated IonSpray source and is based on a co-axial column arrangement [21] which was subsequently modified in our laboratory [18].

CE–ES-MS analyses used the same CE system as that described above except that the current monitoring function of the Beckman P/ACE 2100 instrument was disabled to permit normal CE operation once the cathodic end of the capillary was connected to the CE–ES-MS interface. In order to minimize the length of the CE column the cartridge was modified so that the capillary exited from the top left corner of the cartridge. Mass spectral acquisition was performed using dwell times of 3 ms per step of 1 u in full mass scan mode, or 100 ms per channel for selected ion monitoring experiments. Fragment ion spectra obtained from combined CE–ES-MS–MS analyses were achieved by selecting the appropriate precursor m/z values in the first quadrupole, and using collisional activation with argon target gas in the high-pressure radio frequency (rf)-only quadrupole collision cell. Collision energies were typically 25 eV in the laboratory-frame of reference, and the collision gas thickness was $3.80 \cdot 10^{15}$ atoms $\cdot$ cm^{-2} deduced from the pressure measured by a Baratron capacitance manometer upstream of the cell. Tandem mass spectra were acquired using dwell times of 3 ms per step of 0.5 u. A MacIntosh Quadra 950 computer was used for instrument control, data acquisition and data processing.

3. Results and discussion

In a series of preliminary experiments different buffer systems were investigated for the analysis of PSP toxin standards. Best separation performance was generally obtained using morpholine at pH 4 in order to minimize the adsorption of PSP toxin on the bare fused-silica surface of the capillary wall, a phenomenon more often observed for NEO and other N^1-hydroxy toxin derivatives. The choice of separation buffer was also motivated by considerations affecting the sensitivity for MS detection. Suitable buffers for CE–ES-MS operation must also carry relatively low currents, be sufficiently volatile to prevent accumulation of residue on the orifice plate, and have low proton affinity to minimize the level of chemical background noise. Amongst the different buffers investigated previously [19] morpholine offered the most accommodating properties.

The separation of PSP toxins on bare fused-silica capillaries was found to be substantially affected by the sample buffer. In particular, the separation performance could not be maintained when the toxins were dissolved in high-ionic-strength buffers such as those used for the enzymatic digestion. An example of this effect is presented in Fig. 2 for the CE–UV analysis of a mixture of the epimeric pair GTX_1 and GTX_4 at a concentration of 360 and 100 μM, respectively, in either 0.1 M acetic acid or Tris buffer at pH 7. When the PSP toxins were prepared in 0.1 M acetic acid, baseline separation of the CE peaks was achieved using a 100 mM morpholine buffer pH 4 on a 57 cm $\times$ 50 μm I.D. capillary (Fig. 2A). Separation efficiencies, calculated from peak widths at half height, were 64 000 and 123 000 theoretical plates for GTX_1 and GTX_4, respectively. The lower number of theoretical plates observed for GTX_1 is due only to the higher concentration of this toxin, and not to adsorption of the toxin on the capillary walls. In the present case, the fact that the sample matrix has a lower conductivity than the running buffer provides an ideal situation for sample stacking. Since a higher field strength will be imparted to the sample zone, ionic analytes will be focused at the boundary of the running buffer. Such stacking conditions also enable the injection of larger sample sizes with minimal zone distortion. Previous studies[19] have demonstrated that using similar electrophoretic systems, sample loadings can be increased to 10% of the capillary volume with negligible degradation of the resolution of the PSP toxins.

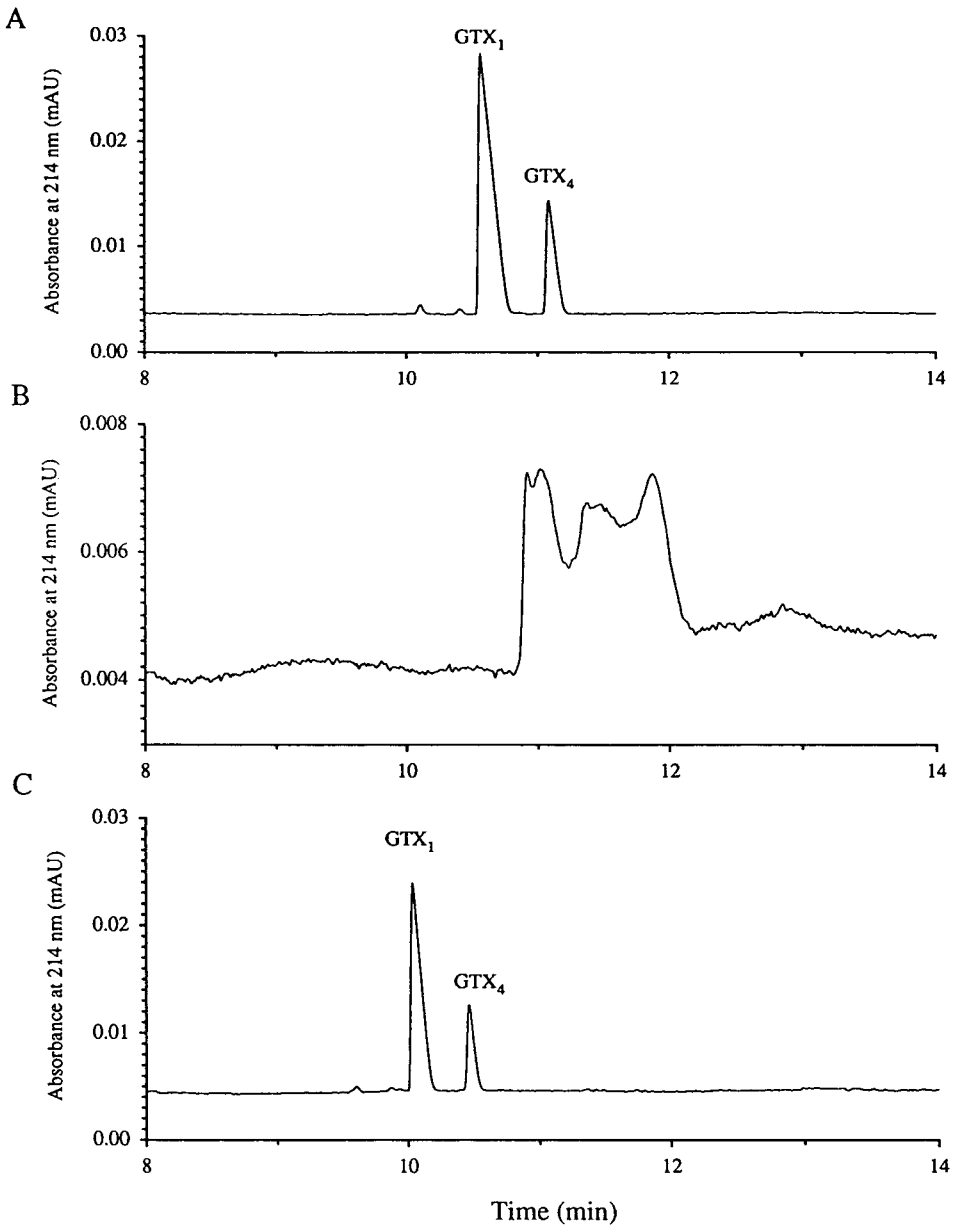

Fig. 2. CE–UV analysis of a mixture of GTX_1 and GTX_4 toxins dissolved in 0.1 *M* acetic acid (A), 50 m*M* Tris pH 7 (B) and 50 m*M* Tris pH 7 with stacking using a terminating electrolyte of 0.1 *M* acetic acid (C). Conditions: 10-nl injection of a standard solution containing GTX_1 (360 μM) and GTX_4 (100 μM), 100 m*M* morpholine pH 4 buffer, bare fused-silica column 57 cm × 50 μm I.D. column for all separations.

In contrast, the CE–UV analysis of the same two toxins dissolved in Tris pH 7 (Fig. 2B) shows very poor separation of GTX_1 and GTX_4, a situation clearly not satisfactory for identification purposes. It is noteworthy that under the same experimental conditions STX and NEO were

resolved (data not shown) owing to their larger electrophoretic mobilities. Sulfated PSP toxins such as GTXs have electrophoretic mobilities ranging from $15 \cdot 10^{-9}$–$17 \cdot 10^{-9}$ m^2 V^{-1} s^{-1} in a morpholine buffer pH 4, whereas the values for STX and NEO are $34 \cdot 10^{-9}$ and $32 \cdot 10^{-9}$ m^2 V^{-1} s^{-1}, respectively.

The difficulty in focusing the GTX toxins is partly attributed to the high conductivity of the Tris sample buffer, and to the low mobilities of these toxins compared to that of the electroosmotic flow ($10 \cdot 10^{-9}$ m^2 V^{-1} s^{-1}, as determined using mesityl oxide). Such conditions are naturally ineffective in providing proper mobilization of the analytes, and lead to anti-stacking effects. In order to alleviate such difficulties, it is possible to focus the sample ions using a discontinuous buffer system in which the separation buffer has a composition different from that of the stacking buffer. The composition of the latter electrolyte is chosen such that it is of a low pH, and possesses a conductivity lower than that of any of the sample or separation buffers. This procedure is similar to that of cITP, except that only 2% of the capillary is filled with the sample and the analyte bands are mobilized in an uncoated capillary with appreciable electroosmotic flow.

Fig. 2C shows the separation of a mixture of GTX_1 and GTX_4 under conditions similar to those used to obtain Fig. 2B, except that a stacking period of 1.5 min using 0.1 *M* acetic acid (pH 3) preceded the zone electrophoresis separation. As observed, resolution of GTX_1 and GTX_4 is now clearly achieved, with separation efficiencies in excess of 100 000 plates for both toxins. The improvement in separation performance is thought to arise from sample stacking where the highly mobile H^+ ions form a temporary leading zone behind the morpholine buffer. Ionic species present in the sample focus into sharp bands behind this leading zone, before the separation is allowed to proceed in a zone electrophoresis format by changing the terminating electrolyte to morpholine.

Separation conditions originally developed with UV detection were also investigated using ES-MS. The CE–ES-MS analyses (20-nl injection) of products released during the enzymatic digestion of a 285 μM solution of NEO, are shown in Fig. 3. In this case, a total of 5 pmol of toxin was injected on the capillary column. The reconstructed ion electropherograms (RIEs) corresponding to the sums of intensities of MH^+ ions of NEO (*m/z* 316) and decarbamoyl (dc)-NEO (*m/z* 273) extracted from the full mass scan acquisition, are presented in Fig. 3A-C for aliquots taken at incubation times of 0, 3 and 6 h, respectively. For purposes of convenience, the analyte signals have been normalized with respect to the intensity of the MH^+ ion of NEO prior to incubation (Fig. 3A). As indicated by the RIE profiles of Fig. 3, the intensity of NEO progressively decreased over the 6-h incubation period. Similarly dc-NEO toxin, which migrates just before NEO, shows a corresponding increase of intensity over the same time period, and is of almost equal abundance to that of NEO at 6 h (Fig. 3C). The identities of the substrate and enzymatic reaction product were confirmed from their full mass spectra, as illustrated in Fig. 4 for the CE peaks migrating at 11.8 and 12.2 min in Fig. 3C. The mass spectra of dc-NEO (Fig. 4A) and NEO (Fig. 4B) both show an abundant ion corresponding to the protonated molecule (MH^+) together with a sodiated adduct (MNa^+).

In a separate series of experiments, the temporal profile of the enzyme digestion of NEO was also monitored by CE–UV detection to ensure that no other product was released during the digestion. Fig. 5 compares the results of the CE–UV analyses with those of CE–ES-MS acquired in selected ion monitoring acquisition mode for *m/z* 273 and 316. In view of the fact that no standard of known concentration was available for dc-NEO, the response factors of this toxin for both UV and ES-MS detection were assumed to be the same as those for NEO. This assumption was justified on the basis that the two guanidino groups of the perhydropurine skeleton are the major chromophores absorbing at 200 nm, and are thus not likely to be affected by substitution taking place on the C-17 side chain. Similarly the same two basic functionalities are the most likely sites of protonation on

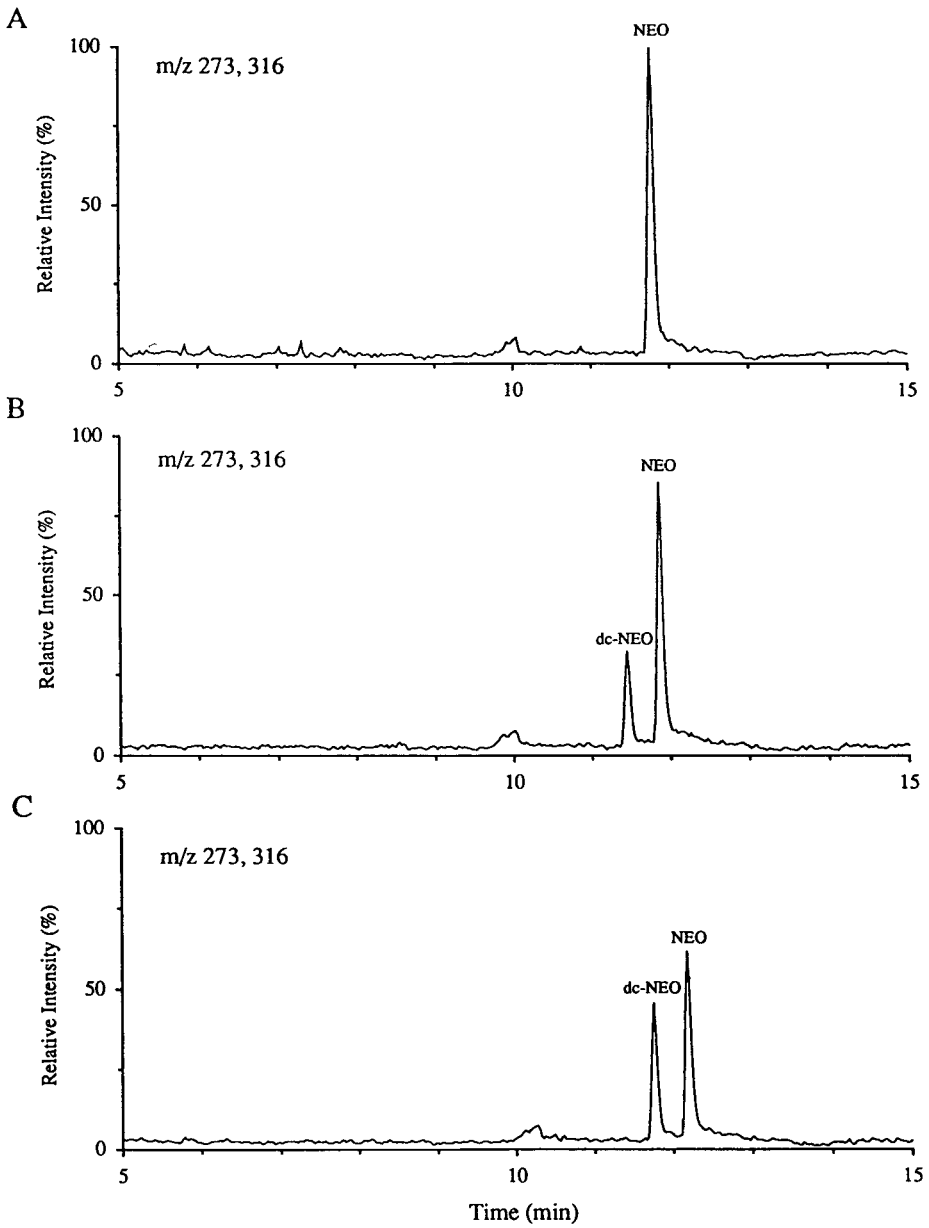

Fig. 3. Reconstructed ion electropherogram for the composite signals at m/z 273 and 316 extracted from the CE–ES-MS analysis (m/z 200–500) of an enzyme digest of NEO toxin. Ion current profiles taken after an incubation period of 0 (A), 3 (B) and 6 h (C). Conditions: 20-nl injection of NEO solution (285 μM) incubated with 140 μl of a crude clam homogenate extract; 35 mM morpholine pH 4 separation buffer, 0.1 M acetic acid terminating electrolyte, bare fused silica column 97 cm × 50 μm I.D. column.

the molecule and electrospray ionization would be therefore expected to yield similar responses for dc-NEO and NEO.

Hydrolysis of NEO to the dc-NEO toxin was found to proceed readily, and a dc-NEO peak corresponding to an intensity of 5% of the

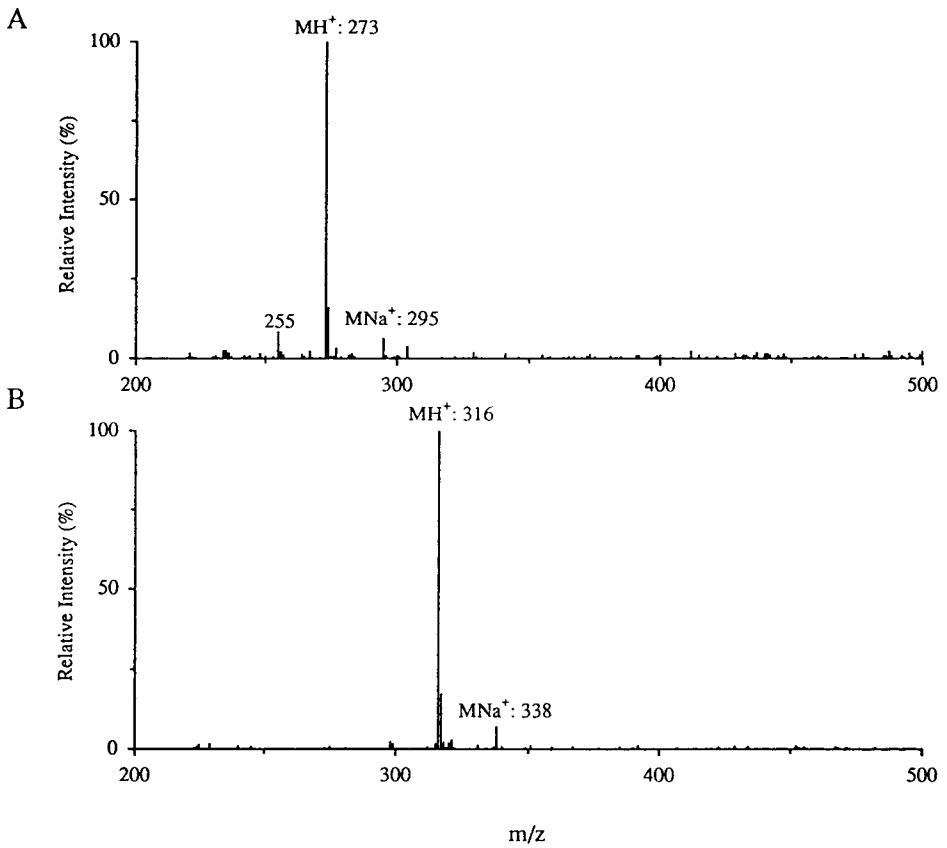

Fig. 4. Extracted mass spectra for peaks migrating at (A) 11.8 and (B) 12.2 min in Fig. 3C.

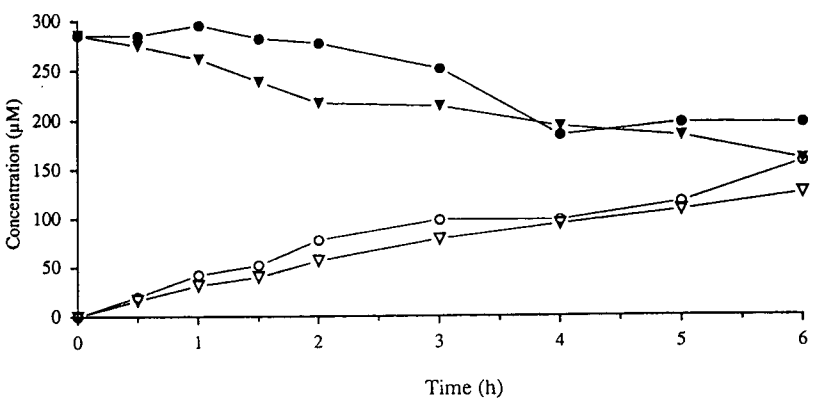

Fig. 5. Comparison of concentration profiles for the digestion of NEO by a *P. staminea* carbamoylase using CE–UV (triangles) and CE–ES-MS with selected ion monitoring (circles). NEO and dc-NEO are represented by filled and open symbols, respectively.

original NEO peak area was observed within the first 30 min of the reaction. Using both CE–UV and CE–ES-MS a decrease in NEO concentration of approximately 50% was detected after 6 h of incubation (Fig. 5), and more than 90% conversion was observed for incubation times longer than 15 h. The decrease in NEO concentration was paralleled by a concurrent increase of the dc-NEO peak area. In fact the sum of the two corrected areas observed in CE–UV experiments was found to be constant and equal to the original NEO peak area to within experimental uncertainties ($\pm 8\%$). No other major components were observed on the corresponding CE–UV electropherograms. The CE–ES-MS analyses performed on the same fractions using selected ion monitoring (Fig. 5) were consistent with these observations, and showed excellent correlation with data obtained independently using CE–UV. Furthermore, CE–ES-MS analyses performed in full mass scan acquisition mode confirmed that the reaction product was indeed dc-NEO, and that no other major products were detected in the chosen mass range (m/z 200–500). Evidence accumulated thus far indicated that the decarbamoyl toxin is the only product released from the incubation with the crude clam extract. However, further studies were required to address this point as the enzyme specificity and affinity might vary depending on the type of substrate investigated.

Incubation of both N-sulfocarbamoyl and carbamoyl toxins in homogenates of *P. staminea* resulted in hydrolysis of the carbamate ester bonds of all PSP toxins. The rate at which this conversion took place was found to be highly dependent on the structure of the toxin. Previous studies [14] using HPLC–FLD indicated that formation of the decarbamoyl toxin was significantly faster for the N-sulfocarbamoyl toxins than for substrates such as STX, GTX_2 and GTX_3, although no measurements of activity were reported. A comparison of CE–ES-MS profiles obtained for different PSP toxins, following incubation periods of 15 h in all cases, is shown in Fig. 6. Each electropherogram represents the RIE profile corresponding to the MH^+ ions of the substrates and their corresponding decarbamoyl derivatives extracted from the full mass scan acquisition (m/z 200–500). The concentrations of the PSP toxins prior to the CE–ES-MS analysis were approximately 250 μM in all cases with the exception of GTX_3, C_1 and C_2 for which the concentrations were 60, 180 and 110 μM, respectively. An aliquot of 160 μl of the crude clam extract was added to each substrate solution.

Consistent with previous investigations [14], faster rates of enzymatic hydrolysis were observed for N-sulfocarbamoyl toxins such as B_1 (Fig. 6C) and $C_{1,2}$ (Fig. 6E) toxins. Amongst all toxins investigated, the formation of decarbamoyl toxin appears to proceed fastest for the sulfocarbamoyl toxin B_1, which was entirely converted to the dc-STX after 15 h of digestion (Fig. 6C). No signal was detected for B_1 which migrates at 25 min. under these conditions. In contrast, carbamate toxins such as STX (Fig. 6A) and NEO (Fig. 6B) displayed much slower reaction rates, and abundant MH^+ ions were observed for both the reaction products and the substrates after the same period of incubation.

Slower enzymatic activity was observed for the $GTX_{2,3}$ toxins (Fig. 6D) for which only a small fraction (typically less than 25%) was converted into the dc-$GTX_{2,3}$ toxins even after 15 h of incubation. In contrast, the formation of dc-$GTX_{2,3}$ toxins from the $C_{1,2}$ toxins (Fig. 6E) proceeded more rapidly, although the latter toxins differ from the $GTX_{2,3}$ toxins only by an extra sulfonate functionality at the N-21 position. It is noteworthy that the $GTX_{2,3}$ toxins observed in Fig. 6E correspond to residual impurities which were not totally separated from the C toxins during purification by column chromatography on Bio-Gel P-2. Interestingly, the hydrolysis of the $C_{1,2}$ toxins also gave rise to two additional peaks at 20.5 and 21.0 min. Abundant ions at m/z 353 were observed in the extracted mass spectra for these two components suggesting that these compounds could be isomers of dc-$GTX_{2,3}$. Fragment ions characteristic of dc-$GTX_{2,3}$, such as those corresponding to losses of H_2O and/or SO_3 (m/z 335, 273 and 255) were also observed for these two minor peaks in CE–ES-MS analyses conducted in selected ion moni-

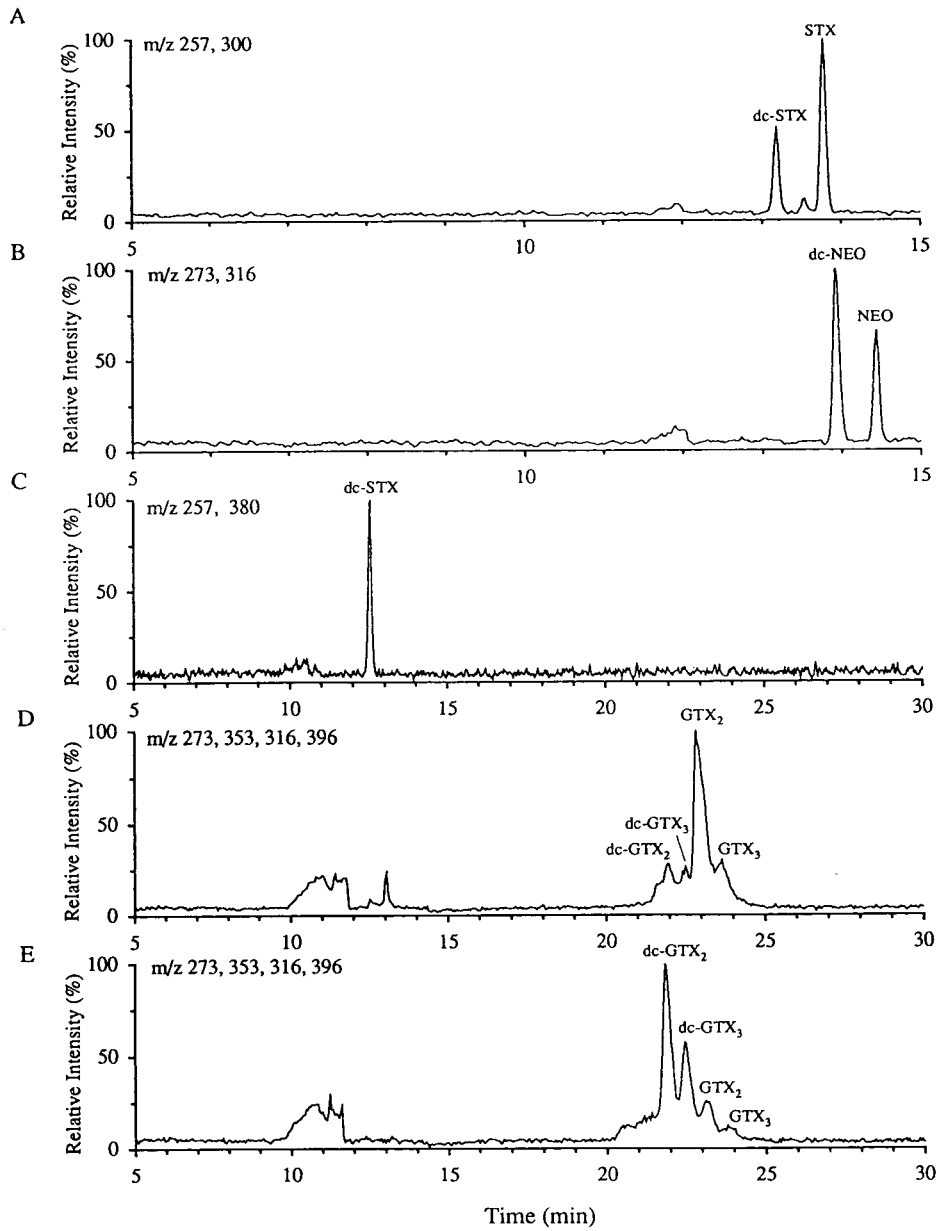

Fig. 6. CE–ES-MS analyses of different PSP standards following 15 h carbamoylase digestion. Reconstructed ion electropherograms for characteristic ions corresponding to substrates and decarbamoyl products of STX, 300 μM (A), NEO, 300 μM (B), B_1, 210 μM (C), GTX_2, 250 μM and GTX_3, 60 μM (D) and C_1, 180 μM and C_2, 110 μM (E). Conditions as in Fig. 3, concentrations given correspond to initial substrate concentrations.

toring mode (data not shown). However the exact structures of these dc-$GTX_{2,3}$ isomers are still not known at present. The occurrence of such dc-$GTX_{2,3}$ isomers was found only in digests of the C toxins, and could possibly arise from $C_{1,2}$ isomers present in the original substrate solution. Interestingly, a similar situation was encountered for STX where a small peak

was observed at 13.5 min in Fig. 6A. This component, which migrates just before STX, was also observed in CE–UV analyses of the STX standard solution, and accounted for approximately 3% of the STX peak area. The extracted mass spectrum of this minor component showed an abundant ion at m/z 300, suggesting that this compound could be an isomer of STX. Unfortunately, no previous report has documented such an observation, possibly reflecting the difficulties in obtaining sizable amounts of these two closely related PSP toxins using preparative chromatographic techniques.

The present CE stacking technique also facilitated the structural characterization of products released during the enzymatic hydrolysis using CE–ES-MS–MS. Examples of MS–MS spectra obtained are shown in Fig. 7A–D for MH^+ ions of dc-STX, dc-NEO, dc-GTX_2 and dc-GTX_3, respectively. In each case the extracted spectrum was obtained from the injection of 20 nl of the reaction mixture, and corresponded to the average of 3 to 4 scans across the CE peak. The MS–MS spectrum of the MH^+ ions of dc-STX (Fig. 7A) was characterized by sequential losses of H_2O and NH_3 giving rise to fragment ions at m/z 239 and 222. An abundant fragment ion at m/z 180, possibly arising from a rearrangement reaction favoring the elimination of a molecule of HN=C=NH from m/z 222, was also observed in Fig. 7A. Similar fragmentations were observed (Fig. 7B) in the MS–MS spectrum of MH^+ from dc-NEO with one additional fragment ion at m/z 225 possibly arising from the consecutive or concomitant losses of the C-17 side chain plus the hydroxyl group on N-1 (Fig. 1). Such a dissociation would lead to the formation of a conjugated double bond between N-1 and C-6, providing additional stability to the resulting fragment ion [19].

In comparison, the MS–MS spectra of MH^+ ions of dc-GTX_2 (Fig. 7C) and dc-GTX_3 (Fig. 7D), obtained from the enzymatic digestion of $C_{1,2}$ toxins, yielded much simpler fragmentation patterns than those of dc-STX or dc-NEO. The MS–MS spectra of these 11-sulfate derivatives were mostly dominated by losses of SO_3 and/or H_2O from the precursor ion. These two epimers, which only differ in the stereochemistry of the sulfate group on C-11 (Fig. 1), can be distinguished on the basis of the relative intensities of the fragment ions at m/z 255 and 273. For dc-GTX_3 the sulfate group is stabilized through interaction with the hydroxyl group on C-17, in a fashion similar to that described for $GTX_{2,3}$ [22], thus preventing the formation of the m/z 273 ion. Fragment ions observed in the MS–MS spectra of these decarbamoyl toxins formed as enzymatic hydrolysis products, were consistent with those of native PSP toxins [19,22], thus confirming the proposed assignments.

In order to determine the relative specificity and affinity of the crude preparation of the carbamoylase enzyme toward different substrates, the temporal profile of the digestion was monitored using CE–UV for a series of PSP toxins. Results obtained in these experiments are presented separately in Fig. 8 for the carbamate toxins (STX and NEO), the 11-sulfate carbamate toxins (GTX_{1-4}) and for the N-sulfocarbamate toxins (B_1 and $C_{1,2}$). The initial concentrations of PSP toxin substrates ranged from 70 to 440 μM while a constant aliquot of the concentrated enzyme extract was added to each of the toxin solutions. These initial substrate concentrations were not limiting, and comparisons of specificities for the different toxins are based on initial reaction rates only. Furthermore, it was not possible to use identical toxin concentrations to study these reactions because of the rapid formation of epimeric equilibria for solutions of the 11-sulfate analogues (as described later).

Amongst the three groups of toxins studied, the N-sulfocarbamate derivatives exhibited the fastest rate of hydrolysis. For example, incubation periods of approximately 0.5 and 3 h were required to convert 50% of the B_1 toxin and $C_{1,2}$ toxins into their corresponding decarbamoyl products, whereas more than 8 h was necessary to hydrolyse the same proportion of any of the other PSP toxins. This is evidenced in Fig. 8 from the slopes of the different digestion profiles. The formation of dc-STX from B_1 rapidly levelled off to its maximum value of approximately 200 μM after only 1.5 h. The production of dc-GTX_3 from the C_2 toxin followed a profile

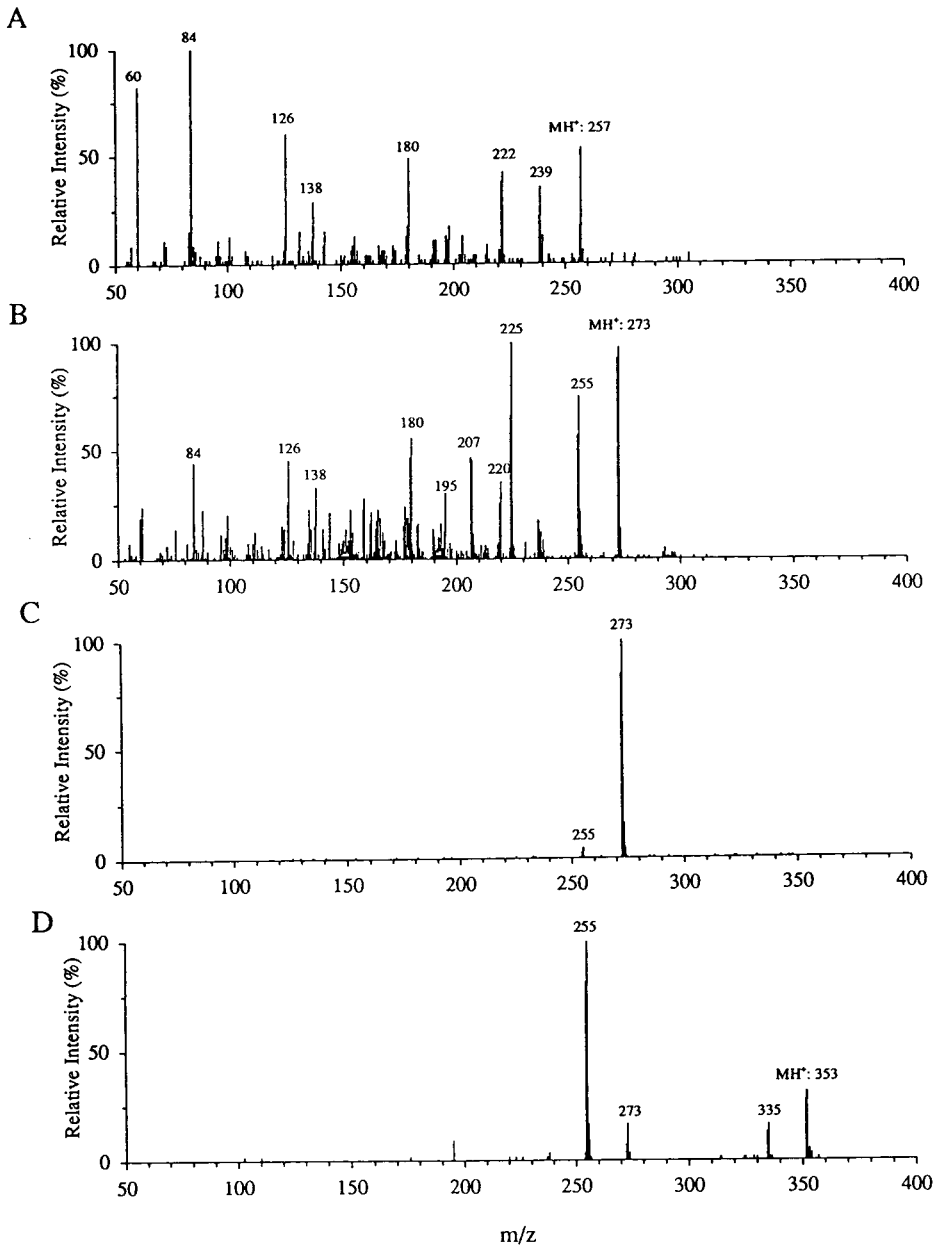

Fig. 7. CE–ES-MS–MS analyses of enzymatic products released during the carbamoylase digestion. Product ion mass spectra for dc-STX, *m/z* 257 (A), dc-NEO, *m/z* 273 (B), dc-GTX_2, *m/z* 353 (C) and dc-GTX_3, *m/z* 353 (D). Electrophoretic conditions as in Fig. 3, collision energies of 25 eV (laboratory-frame of reference) with Ar at collision gas thickness of $3.8 \cdot 10^{15}$ atoms cm^{-2}.

of hydrolysis similar to that of B_1 reaching a plateau after 1–2 h. The formation of dc-GTX_2 from C_1 appears to be more gradual reaching concentrations even higher than that of dc-GTX_3 after 6 h of incubation. The first-order rate constants were determined from the slopes of the

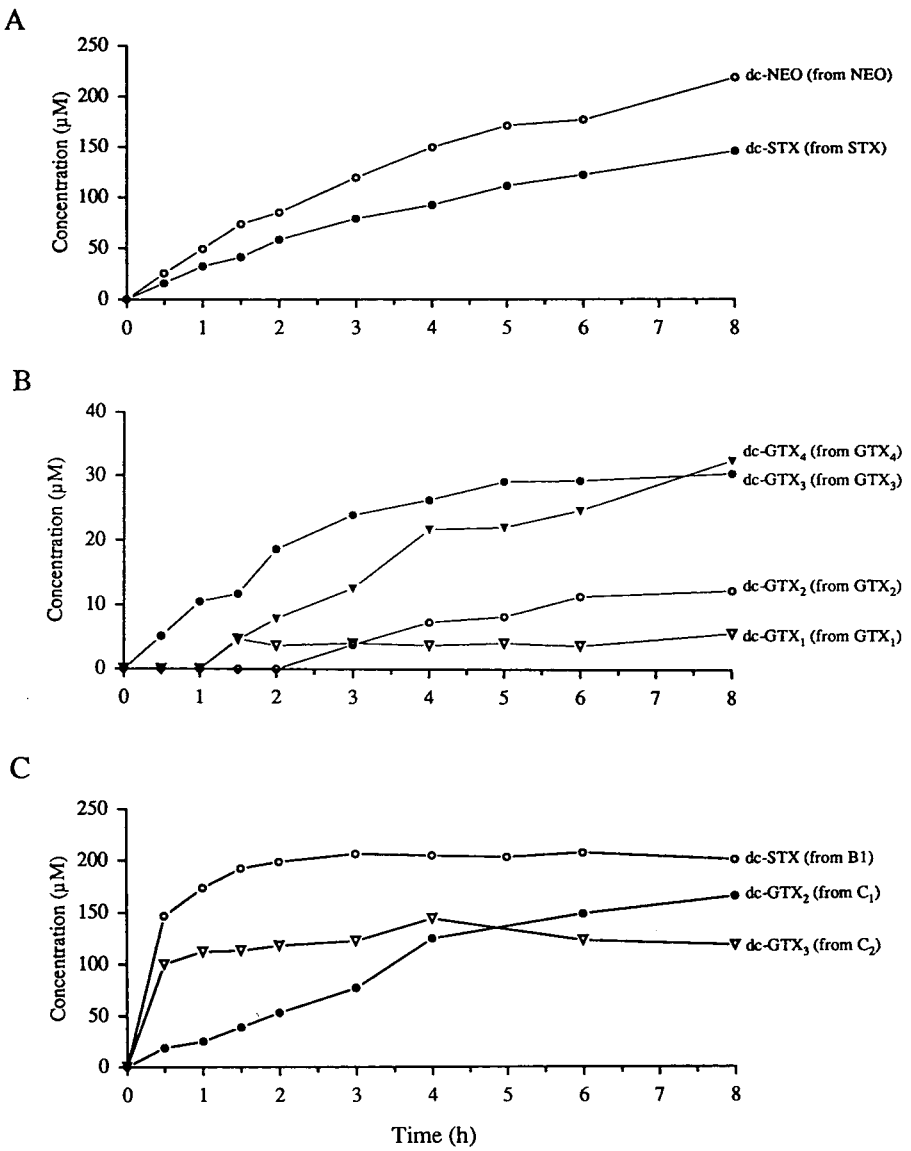

Fig. 8. Concentrations of decarbamoyl toxins released during the carbamoylase digestion of different PSP toxin substrates. Concentration profiles for carbamate toxins (A), 11-sulfocarbamoyl toxins (B) and N-sulfocarbamoyl toxins (C). Electrophoretic conditions as in Fig. 2, all concentrations were determined from CE–UV corrected peak areas. All toxin solutions were incubated with 140 μl of a crude clam homogenate extract. The initial substrate concentrations were as follows: STX (370 μM), NEO (440 μM), GTX_2 (120 μM), GTX_3 (90 μM), GTX_1 (310 μM), GTX_4 (70 μM), B_1 (210 μM), C_1 (180 μM), C_2 (110 μM).

natural logarithm of concentration vs. time for the first 2 h to be 1.1, 2.5 and 0.32 h^{-1} for B_1, C_2 and C_1, respectively.

The fact that the concentration of dc-GTX_2 overtakes that of dc-GTX_3 over a longer digestion period may reflect epimerization of the toxins in neutral buffers. The epimerization of substituents at the C-11 position follows a thermodynamic equilibrium with the α-epimer (C_1, C_3, GTX_1 and GTX_2) being more stable

than the β-epimer (C_2, C_4, GTX_3 and GTX_4) [4]. This trend was also noted in Fig. 8B, though to a much lesser extent, for dc-GTX_2 and dc-GTX_3 produced directly from the corresponding GTX_2 and GTX_3 toxins. In this latter case, the concentration of dc-GTX_3 declined after 5 h of incubation as a result of the epimerization of the C-11 sulfated derivatives. For the GTX toxins which are more resistant to decarbamoylation, the rate of individual toxin hydrolysis is complicated by epimerization reactions taking place at the same time.

The rate of hydrolysis of PSP toxins such as STX and NEO were found to be intermediate between the N-sulfocarbamoyl and the GTX toxins. For a given enzyme extract concentration, the natural logarithmic plots of STX and NEO concentrations vs. time gave good linearity with correlation coefficients $r^2 > 0.985$ over the 8-h incubation period. For these two toxins the plots of the natural logarithm of concentration vs. time showed an inverse linear relationship, consistent with a first-order reaction. The rate constants obtained from the slopes of these plots were $6.2 \cdot 10^{-2}$ and $8.3 \cdot 10^{-2}$ h^{-1} for STX and NEO, respectively, and indicated that 50% hydrolysis is reached at 11 and 8 h for the same two toxins. Unfortunately the rate constants for the GTX toxins could not be determined precisely from this preferred procedure using the integrated rate expression, since both the substrates and their enzymatic products are affected by epimerization reactions taking place under the present conditions. However, it is possible to evaluate approximately the relative reaction rates from the initial slopes of formation of dc-GTX toxins (Fig. 8B). Accordingly, the rate of GTX toxin hydrolysis increased progressively for GTX_2, GTX_1, GTX_3 and GTX_4. It is noteworthy that the concentration at which a plateau is observed appears to depends on the initial substrate concentration. Based on the above observations, the relative rate of hydrolytic conversion of PSP toxins into their corresponding decarbamoyl derivatives appears to observe the following progression: $C_2 > B_1 > C_1 > NEO > STX > GTX_4 > GTX_3 > GTX_1 > GTX_2$.

Although the relative susceptibilities of these toxins to hydrolysis is not a precise measure of their specific activities, the above progression is however indicative of the affinity of the enzyme for a given substrate. The fast hydrolysis rates noted for the N-sulfocarbamoyl toxins suggests the participation of the sulfo group in the enzymatic reaction. The presence of such a polar group near the hydrolysis site might facilitate the interaction of the substrate with basic residues of the catalytic site. Interestingly, hydrolysis rates were also found to be dependent on the orientation of the sulfate group on C-11, faster rates being observed for the β-epimers. While the configuration of the β-epimers would lead to more proximal interactions between the carbamoyl and 11-sulfate functional groups, it is possible that significant steric hindrance of the substrate as it approaches the catalytic site might be responsible for the lower hydrolytic activity of the carbamoylase for the 11α-sulfate toxins. Additional insights on the interactions of the substrate with the carbamoylase enzyme will possibly be obtained by comparison with similar hydrolytic enzymes, and through detailed structural analyses from X-ray diffraction studies. The development of isolation and purification procedures of the carbamoylase from *P. staminae* using the present screening method are presently in progress, and results from this latter study will be reported separately.

4. Conclusions

Improvements in sample focusing prior to zone electrophoresis separation were obtained for PSP toxins dissolved in high-ionic-strength buffers using on-column sample stacking. With proper choice of leading and terminating electrolytes, the method developed can be used with uncoated capillaries. The application of this stacking procedure is demonstrated for the analysis of products released during the digestion of PSP toxins by a carbamoylase isolated from viscera of little neck clams (*P. staminea*). This CE method was also used for detecting the desired enzymatic activity in fractions obtained from preparative chromatographic procedures. The ease of operation, flexibility, high resolution, and short analysis time of CE combined

with either UV or MS detection make this technique an attractive method for the monitoring of carbamoylase activity in shellfish extracts.

The identity of products formed during the enzymatic digestion of the PSP toxins was established directly by combined CE–ES-MS and CE–ES-MS–MS analyses. Results from this study provide direct evidence of the transformation of PSP toxins to decarbamoyl derivatives, and support a previous proposals made on the basis of indirect evidence from HPLC–FLD analyses of compounds obtained following re-carbamoylation of the enzymatic products [14]. The possibilities of conducting fast (less than 15 min) and reproducible analyses on crude clam extracts enabled determination of enzymatic profiles for different PSP toxin substrates. The rate of hydrolysis was also found to be highly dependent on the substrate structure. Amongst all PSP toxins investigated, the fastest rate of hydrolysis was found for the N-sulfocarbamoyl derivatives (B_1, C_1 and C_2) with rate constants ranging from 0.3 to 2.5 h^{-1}. In contrast, the formation of decarbamoyl products from any of the other PSP toxins proceeded more slowly with rate constants of less than $9 \cdot 10^{-2}$ h^{-1}. Furthermore, faster hydrolysis rates were observed for 11β-sulfate toxins such as C_2, GTX_3 and GTX_4 compared to their corresponding α-epimers (C_1, GTX_1 and GTX_2). This presumably reflects the steric hindrance of the substrate approaching the catalytic site.

Acknowledgements

The authors would like to thank R. Richards for technical assistance in preparing several of the PSP standards used in the present study, and Dr. A.D. Cembella and Dr. R.K. Boyd for valuable discussions.

Note added in proof

Additional experiments using CE–UV and CE–ES–MS enabled identification of neosaxitoxinol as the minor component observed at 13.5 min in Fig. 6A. Neosaxitoxinol is a C_{12} dehydroxy derivative of NEO, and can be obtained from reduction of NEO using sodium borohydride.

References

[1] S. Hall, P.B. Reichardt, in E.P. Ragelis (Editor), *Seafood Toxins (ACS Symposium Series*, No. 262), American Chemical Society, Washington, DC, 1984, p. 113.
[2] Y. Shimizu, in A.T. Tu (Editor), *Handbook of Natural Toxins, Vol. 3, Marine Toxins and Venoms*, Marcel Dekker, New York, 1988, p. 63.
[3] A.D. Cembella, J.J. Sullivan, G.L. Boyer, F.J.R. Taylor, R.J. Andersen, *Biochem. System. Ecol.*, 15 (1989), 171.
[4] A.D. Cembella, S.E. Shumway and N.I. Lewis, *J. Shellfish Res.*, 12, (1993) 389.
[5] P. Lassus, J.M. Frémy, M. Ledoux, M. Bardouil and M. Bohec, *Toxicon*, 27 (1989) 1313.
[6] P. Lassus, M. Bardouil, M. Ledoux, I. Murail, M. Bohec, P. Truquet, J.-M. Frémy and V. Rohmer, *Aquat. Liv. Res.*, 5 (1992) 319.
[7] V.M. Bricelj, J.H. Lee, A.D. Cembella and D.M. Anderson, *Mar. Ecol. Prog. Ser.*, 63 (1990) 177.
[8] V.M. Bricelj, J.H. Lee and A.D. Cembella, *Mar. Ecol. Prog. Ser.*, 74 (1991) 33.
[9] M.K. Beitler and J. Liston, in E. Granéli, B. Sundström, L. Edler and D.M. Anderson (Editors), *Toxic Marine Phytoplankton*, Elsevier, New York, 1990, pp. 257–262.
[10] Y. Shimizu, W.E. Fallon, J.C. Wekell, D. Gerber and E.J. Gauglitz, *J. Agric. Food Chem.*, 26 (1978) 878.
[11] Y. Shimizu and M. Yoshioka, *Science*, 212 (1981) 547.
[12] Y. Kotaki, Y. Oshima and T. Yasumoto, in D.M. Anderson, A.W. White and D.G. Baden (Editors), *Toxic Dinoflagellates —Proc. 3rd Int. Conf. on Toxic Dinoflagellates*, Elsevier, New York, 1985, pp. 287–292.
[13] Y. Oshima, in P. Lassus (Editor), *Proceedings of the 6th International Conference on Toxic Phytoplankton, Nantes, 18–22 October 1993*, Elsevier, p. 153.
[14] J. Sullivan, W.T. Iwaoka and J. Liston, *Biochem. Biophys Res. Commun.*, 114 (1983) 465.
[15] J. Sullivan, M.M. Wekell and L.L. Kentala, *J. Food Sci.*, 50 (1985) 26.
[16] Y. Oshima, M. Machida, K. Sasaki, Y. Tamaoki and T. Yasumoto, *Agric. Biol. Chem.*, 48 (1984) 1707.
[17] P. Thibault, M.V. Laycock and S. Pleasance, *J. Chromatogr.*, 542 (1991) 483.
[18] S. Pleasance, P. Thibault and J.F. Kelly, *J. Chromatogr.*, 591 (1992) 325.
[19] S.J. Locke and P. Thibault, *Anal. Chem.*, 66 (1994) 3436.
[20] M.V. Laycock, P. Thibault, S.W. Ayer and J.A. Walter, *Natural Toxins*, 2 (1994) 175.
[21] R.D. Smith, J.A. Olivares, N. Nguyen and H.R. Udseth, *Anal. Chem.*, 60 (1988) 436.
[22] S. Pleasance, S.W. Ayer, M.V. Laycock and P. Thibault, *Rapid Commun. Mass Spectrom.*, 6 (1992) 14.

ELSEVIER

Journal of Chromatography A, 688 (1994) 317–327

JOURNAL OF CHROMATOGRAPHY A

Separation of phenoxy acid herbicides and their enantiomers by high-performance capillary electrophoresis

A.W. Garrison*, P. Schmitt, A. Kettrup

Institut für Ökologische Chemie, GSF-Forschungszentrum für Umwelt und Gesundheit, Neuherberg, D-85758 Oberschleissheim, Germany

First received 6 January 1994; revised manuscript received 12 September 1994

Abstract

Capillary electrophoresis conditions in the free solution mode (capillary zone electrophoresis) were established for the separation and detection of 2,4-dichlorophenoxyacetic acid and three optically active phenoxy acid herbicides (dichlorprop, mecoprop and fenoprop).

A 50 m*M* acetate buffer at pH 4.5 gave the best separation, using a 50 cm (to detector) × 75 μm I.D. fused-silica column; the column temperature was 30°C, separation voltage 20 kV and optimum detector wavelength 230 nm. Separation of the four herbicides required less than 15 min under these conditions. Baseline separation of the two enantiomers of each of the three optically active herbicides, separately and in mixtures of the three, was accomplished by the addition of 25 m*M* tri-O-methyl-β-cyclodextrin to the acetate separation buffer. Di-O-methyl-β-cyclodextrin or α-cyclodextrin (CD) separated enantiomers of dichlorprop and mecoprop, but not those of fenoprop; β-CD provided very little separation and γ-CD gave no separation. Addition of methanol to the separation buffer increased separation, but doubled migration times. Over a variety of sample concentrations and injection times, reproducibilities of migration times of racemates and enantiomers ranged from 1.3 to 4.6% R.S.D.; peak area and peak height reproducibilities ranged from 1.6 to 17.9% R.S.D.

1. Introduction

The recent advent of high-performance capillary electrophoresis (HPCE or CE) adds a separation tool of unprecedented efficiency to the more conventional chromatographic instrumentation, and CE has been applied to numerous pharmaceutical and biochemical separation problems [1], but not often to pesticide analysis or to other environmental problems [2–7].

Currently available chiral solid phases for gas chromatography (GC) and high-performance liquid chromatography (HPLC) columns and chiral reagents allow the chromatographic separation of optical isomers, and a fertile field of investigation has ensued, especially for pharmaceutical products and amino acids. Techniques for chiral separations by CE, usually involving addition of chiral reagents such as cyclodextrins (CDs) to the separation buffer [8,9], are now also available, and have been widely applied in

* Corresponding author. Visiting Scientist at GSF, now returned to the Athens Environmental Research Laboratory, US Environmental Protection Agency, Athens, GA 30605-2720, USA.

0021-9673/94/$07.00
SSDI 0021-9673(94)00893-0

the pharmaceutical and biomedical fields during the past few years [10–13].

Biological activity in soil or water environments may result in the preferential reactivity of one enantiomer or other optical isomer of a pesticide in terms of microbial degradation, biological uptake, metabolism or toxicity [14,15]. Investigations of this preferred reactivity phenomenon could produce important results; manufacturers, for example, may be able to tailor pesticide formulations that are more selective for target organisms and vegetation, thereby reducing total chemical application significantly. Improved targeting of pests also should result in a direct reduction in adverse environmental impacts [14].

Investigations of preferential reactivity require advanced separations technology, as do the analyses required for research and monitoring during development, testing and production of optical isomers of insecticides and herbicides. Analysis usually involves GC or HPLC with chiral solid phases [16,17].

Phenoxy acid herbicides, including the well known 2,4-dichlorophenoxyacetic acid (2,4-D), are important as selective pre- and post-emergence herbicides; their toxicity and herbicidal effects have been studied in detail, and a variety of methods have been developed for their analysis, most being based on HPLC or GC [18–20]. Their environmental persistence also has been studied; for example, the degradation kinetics of 2,4-D and dichlorprop (Fig. 1) in soils were measured in the early 1980s [21]. Several of these herbicides are optically active —those with the phenoxy substituent on the 2-position of propionic acid, for example. Enantiomers of dichlorprop and mecoprop [17] have been separated by HPLC and their biological properties studied; in each case, only the (+)-isomer is herbicidally active [22].

These phenoxy acids are excellent candidates for separation by CE. Their pK_a values are such as to allow separation by the simplest form of CE, free solution CE (FSCE), otherwise known as capillary zone electrophoresis (CZE). For example, Nielen [31] recently described the CZE separation of several phenoxy acid herbicides

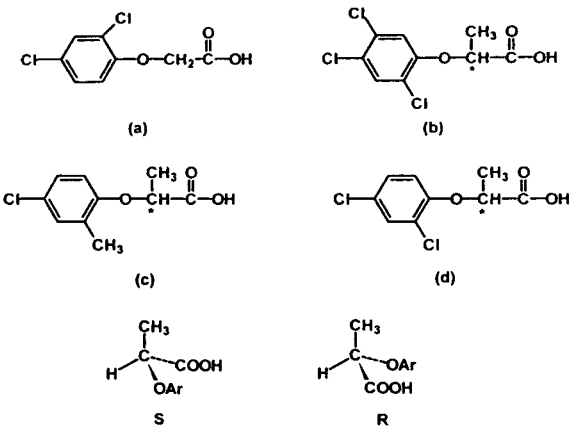

Fig. 1. Structures phenoxy acid herbicides. a = 2,4-Dichlorophenoxyacetic acid (2,4-D); $pK_a = 3.3$ (SPARC), 2.64 (literature). b = 2-(2,4,5-Trichlorophenoxy)-propionic acid (fenoprop); $pK_a = 3.2$ (SPARC), 2.84 (literature). c = 2-(4-Chloro-2-methylphenoxy)propionic acid (mecoprop); $pK_a = 3.4$ (SPARC); d = 2-(2,4-Dichlorophenoxy)propionic acid (dichlorprop); $pK_a = 3.3$ (SPARC). *S* and *R* = designation of absolute configuration of enantiomers of the optically active compounds; Ar is the substituted phenyl group. * = Optically active carbon.

and related impurities originating from production processes, as well as chiral separation of some phenoxypropionic acid herbicides using CD chiral selectors. Of special interest in our study was the optimization of separation of the enantiomers of the optically active herbicides by CZE with CD reagents. Our objective was to establish the optimum conditions necessary for CZE analysis of representative phenoxy acid herbicides and their enantiomers.

2. Experimental

Instrumentation consisted of a Beckman P/ACE 2100 series HPCE with Beckman System Gold chromatography software. The fused-silica CE column [65 cm (50 cm to the detector) × 300 μm O.D. × 75 μm I.D.] was obtained from Beckman and fitted into a 100 × 200 μm aperture cartridge. Usual CE conditions for separation of the phenoxy acid compounds were: temperature, 30°C; voltage, 20 kV; detector wavelength, 230 nm.

The three buffers were composed as follows: (a) acetate [50 m*M*, pH 4.45; 0.05 *M* glacial acetic acid–0.05 *M* sodium acetate (1:1, v:v)], (b) borate [100 m*M*, pH 7.0; 0.1 *M* boric acid–0.4 *M* sodium tetraborate (6.5:2.5, v:v)] and (c) phosphate [100 m*M*, pH 6.95; 0.1 *M* sodium dihydrogenphosphate–0.1 *M* disodium hydrogenphosphate (85:15, v:v)]. Buffer stock solutions were stored under refrigeration.

The phosphate buffers were apparently not stable for more than about 2 days, even when kept cold. Older solutions caused "spikes" on the electropherograms, perhaps because of bacterial growth. Filtration (through 0.45-μm syringe filters) followed by sonication for various times usually resulted in even more "spikes".

CD solutions were prepared in small volumes, as needed, in the acetate separation buffer. It was usually necessary to sonicate for 30 s or longer to achieve solution except for the methylated CDs, which were very soluble. β-CD was the least soluble; it was necessary to warm the solution to reach even 25 m*M* concentration. These CD solutions were not filtered. In the experiments where methanol was added in an attempt to enhance enantiomeric separation, solutions of α-CD and β-CD in buffer and methanol were filtered through 0.2-μm syringe filters.

Phenoxy acid analyte stock solutions were prepared as follows: 40 mg of each analyte were dissolved in 100 ml of pesticide-grade methanol; this was diluted 1:100 to give a final solution concentration of 4 μg/ml. This solution was used directly for CE analysis.

Typically, analyses were performed automatically by the Beckman P/ACE system and the System Gold software, using the software's sample table. One or two samples could be run to optimize conditions, or up to ten samples could be automatically analyzed. In any case, the run sequence always included the following steps: (1) 2-min rinse with the separation buffer, in a separate inlet vial; (2) hydrodynamic sample injection from the sample vial, for 5 to 15 s; (3) sample separation run for 15 to 20 min with separation buffer in inlet and outlet vials; and (4) 2-min rinse with 0.1 *M* sodium hydroxide. At the beginning of the day, the column was rinsed with 0.1 *M* sodium hydroxide for 20 min, followed by distilled water for 15 min, and finally by 0.1 *M* sodium hydroxide for 2 min just before beginning a run sequence. For step 3, separation, inlet and outlet buffers were usually renewed for each sample; however, there were many exceptions. If the buffer appeared to be stable (i.e., provided fairly reproducible migration times) the same solutions (in the same inlet and outlet vials) were often used for as many as four samples. This also held true for buffers containing CDs.

Chemical sources and purity: distilled/deionized water was obtained from a "Milli-Q plus" still (Millipore, Bedford, MA, USA). Dichlorprop, mecoprop, fenoprop and 2,4-D were obtained in greater than 99% purity from Dr. Ehrenstorfer GmbH, Augsburg, Germany. *R*-(+)-Mecoprop, *R*-(+)-dichlorprop, (designated "D" instead of "*R*" by the supplier) and methanol (Pestanal grade) were obtained from Riedel-de Haen, Munich, Germany. α-, β- and γ-CDs were from Serva, Heidelberg, Germany. Heptakis(2,6-di-O-methyl)-β-cyclodextrin and heptakis(2,3,6-tri-O-methyl)-β-cyclodextrin were from Sigma, Deisenhofen, Germany. Boric acid (electrophoresis grade) and sodium tetraborate (99% pure) were also from Sigma. Sodium dihydrogenphosphate, disodium hydrogenphosphate, sodium acetate and glacial acetic acid, all analytical-reagent grade, were from E. Merck, Darmstadt, Germany.

3. Results

3.1. Separation of the racemic herbicides

Fig. 1 shows the structures, and the caption the pK_a values, of the four phenoxy acid herbicides studied. The pK_a values of 2,4-D and fenoprop were available from the literature; values for all four compounds were also calculated using SPARC [23], a computer program developed for calculation of chemical and physical properties of chemicals strictly from their structures. Fig. 1 also shows the absolute con-

figuration of the three optically active herbicides. Only the *R*-isomers of dichlorprop and mecoprop are herbicidally active [22]; these are correctly named *R*-(+)-2-(2,4-dichlorophenoxy)-propionic acid and *R*-(+)-2-(4-chloro-2-methylphenoxy)propionic acid, respectively, since they each rotate the plane of polarized light in a clockwise direction (+).

Selection of the appropriate buffer (background electrolyte) was critical in separation of the closely related racemates. Buffer components, pH and ionic strength are all important variables [24,25]. Neither phosphate nor borate buffers provided adequate separation of dichlorprop, fenoprop and mecoprop (2,4-D was not included in these particular experiments) at pH levels within their optimum pH ranges (Fig. 2). A 50 m*M* acetate buffer of about pH 4.5 gave the best separation; higher pH acetate buffers were unsuccessful. Fig. 2 also shows the effect of changing ionic strength on resolution of these three compounds; increasing the buffer concentration from 20 to 50 m*M* at pH 4.47 increased resolution.

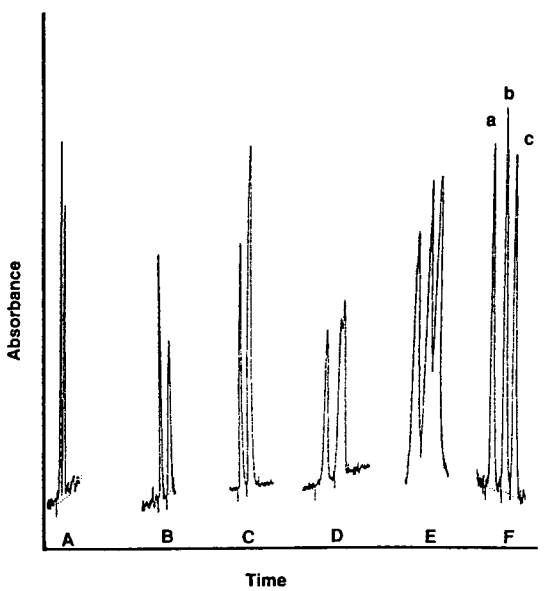

Fig. 2. Buffer trials for separation of fenoprop (a), mecoprop (b) and dichlorprop (c). (A) 100 m*M* borate, pH 8.35; (B) 100 m*M* phosphate, pH 6.40; (C) 50 m*M* acetate, pH 5.80; (D) 50 m*M* acetate, pH 5.20; (E) 20 m*M* acetate, pH 4.47; (F) 50 m*M* acetate, pH 4.47. Other separation conditions as in Fig. 3B. Concentration of each analyte in sample is 1.5 μg/ml.

Apparently the balance between the electroosmotic flow and the electrophoretic mobility of the analytes (corresponding to their pK_a values) is optimum at about pH 4.5 and 50 m*M* buffer concentration. At pH much below this value, a significant fraction of each analyte would exist in its neutral form, because their pK_a values range between 3.2 and 3.4, and the net charge on the analyte would decrease. In earlier trials with a different acetate buffer system, we found that resolution decreased when pH decreased from 4.8 to 4.0. On the other hand, the lack of complete separation with borate and phosphate buffers at relatively high pH values where the analytes are completely ionized suggests some sort of secondary buffer effect on mobilities.

Use of a 10 kV separation voltage instead of the usual 20 kV approximately doubled migration times, but did not significantly increase resolution. This was as expected, because efficiency is proportional to voltage [24]. Temperature of the column was maintained at 30°C for all analyses. This was a stable temperature for the Beckman CE system, which employs a liquid bath to control column temperature.

3.2. Detection and reproducibility of the racemates

Fig. 3 shows that 230 nm is the optimum wavelength for detection of the four herbicides with the Beckman standard UV detector. The herbicides do not absorb at 254 nm. Although the absorbance for fenoprop is about three times higher at 214 nm than at 230 nm, the latter wavelength gives only slightly poorer absorbances (about 25% less) for the other three compounds; in addition, the absorbances of all four compounds are more uniform at 230 nm. Finally, the acetate buffer gives a much smaller negative peak at 230 nm. Electropherogram peaks were identified by spiking with standards.

The detection limit for each herbicide is 0.05 μg/ml, or about $5 \cdot 10^{-7}$ *M*, at a signal-to-noise

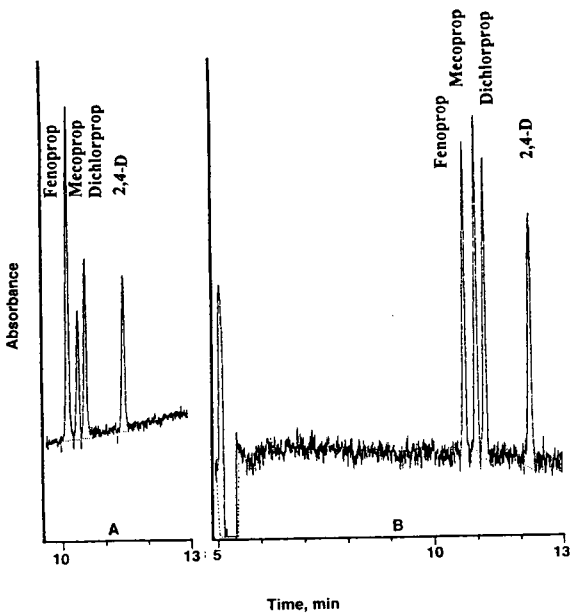

Fig. 3. Absorbances of phenoxy acid herbicides at (A) 214 and (B) 230 nm. Buffer: 50 m*M* acetate, pH 4.45. Capillary: 50 cm (to detector) × 0.075 mm I.D., fused silica. Separation voltage/current: 20 kV (400 V/cm)/41 μA. Hydrodynamic injection: 5 s. Temperature: 30°C. Concentration of each analyte in (A) and (B): 1 μg/ml. Signal at 5.07 min in (B) is the neutral peak.

ratio of 2. Table 1 gives reproducibility data for migration time, peak area and peak height for CE analysis of these herbicide racemates at 1 and 10 μg/ml and at two different injection times.

3.3. Separation of the herbicide enantiomers

Fig. 4 depicts the degree of enantiomeric separation of the three optically active herbicides (Fig. 1) achieved through addition of 10 m*M* α- or β-CD or di-O-methyl-β-cyclodextrin (DMBCD) to the acetate run buffer (50 m*M*, pH 4.45). γ-CD had no effect on the resulting electropherogram; no separation occurred. The addition of β-CD caused slight peak splitting of fenoprop and mecoprop, but no separation of dichlorprop enantiomers. DMBCD caused baseline separation of mecoprop and dichlorprop enantiomers, but had no effect on fenoprop. Finally, the addition of α-CD resulted in almost baseline separation of dichlorprop and mecoprop enantiomers, but, as with DMBCD, had no effect on fenoprop. Surprisingly, α-CD caused a major shift in migration times of the herbicides; fenoprop and dichlorprop changed relative migration times.

Higher concentrations of these CDs had little effect on separation results, although an increase of β-CD concentration from 10 to 25 m*M* decreased enantiomeric separation to almost zero. Higher concentrations sometimes caused very noisy baseline levels and spikes. The γ-CD background/baseline was very noisy, even at 10 m*M*. Table 2 summarizes the interactions among the five cyclodextrins and the three optically active herbicides. (2,4-D always existed as a single peak, of course, because it is not optically active).

The best enantiomeric separation was achieved by addition of tri-O-methyl-β-cyclodextrin (TMBCD) to the acetate run buffer. Fig. 5 shows two representative electropherograms of 2,4-D and the six enantiomers of fenoprop, mecoprop and dichlorprop. Resolution is better at 25 m*M* than at 12.5 m*M*, but the baseline is noisier, probably because of the lower concentration of analytes. Spiking the Fig. 5B sample solution with 1 μg/ml *R*-(+)-dichlorprop and *R*-(+)-mecoprop enantiomer standards showed the second peak of each pair of enantiomers to be the *R*-(+) isomer. No standards were commercially available for the enantiomers of fenoprop.

Experiments were conducted to determine the optimum level of TMBCD. Fig. 6 shows the relationship between the α value [26] for separation of each (+) and (−) pair of isomers and the concentration of TMBCD. $\alpha = t_{R2}/t_{R1}$, where t_{R2} is the migration time of the later-eluting peak (the + isomer) and t_{R1} is the migration time of the first peak. Based on these data, 25 m*M* was deemed to be the optimum concentration of TMBCD in the run buffer, even though 50 m*M* gives a slightly higher α value for dichlorprop.

Table 1
Reproducibility of CE data for herbicides and their enantiomers

Herbicide	Concentration (μg/ml)	Injection time (s)	Migration time (min)			Peak area		Peak height	
			n	Mean	R.S.D.	*n*	R.S.D.	*n*	R.S.D.
Fenoprop									
Racemate	1	15	6	13.13	3.91	6	6.84	6	13.08
	10	15	6	12.31	3.05	6	4.78	6	4.36
	10	5	7	14.77	1.30	7	13.05	7	11.55
(−)-Isomer	1	15	4	10.76	2.91	4	1.55	4	11.13
(+)-Isomer	1	15	4	11.20	3.05	4	4.97	4	6.80
Mecoprop									
Racemate	1	15	6	13.53	3.91	6	8.70	6	12.24
	10	15	6	12.63	3.12	6	5.31	6	5.31
	10	5	7	15.26	1.34	7	12.03	7	13.78
(−)-Isomer	1	15	4	12.69	3.42	4	5.57	4	6.37
(+)-Isomer	1	15	4	13.19	3.69	4	8.06	4	7.62
Dichlorprop									
Racemate	1	15	6	13.84	4.08	6	8.37	6	12.67
	10	15	6	12.97	3.11	6	5.75	6	5.51
	10	5	7	15.64	1.29	7	13.96	7	16.11
(−)-Isomer	1	15	4	13.87	4.14	4	2.46	4	9.78
(+)-Isomer	1	15	4	14.19	4.27	4	7.50	4	9.92
2,4-D	1	15	6	15.45	4.56	6	9.44	6	13.13
	10	15	6	14.32	3.25	6	6.32	6	8.25
	10	5	7	17.68	1.54	7	17.86	7	15.45

3.4. *Effects of methanol on enantiomeric separation*

Even though use of TMBCD under the above conditions gave good separations of all three enantiomer pairs, the effects of methanol addition were briefly investigated. Experiments were conducted with 0, 5, 10 or 20% methanol added to each run buffer, which also contained 12.5 m*M* of one of the five CD reagents. With one exception, qualitative results were the same with as without methanol: (1) α-CD with methanol separated the isomers of dichlorprop and mecoprop, and not those of fenoprop, while shifting the migration order of the herbicides in the same way as without methanol; (2) DMBCD separated the isomers of dichlorprop and mecoprop, and not those of fenoprop; (3) β-CD slightly separated the isomers of fenoprop but not those of the other two herbicides (without methanol, the mecoprop peak was also very slightly split); and (4) TMBCD still afforded the best separation, giving good baseline separation of all three pairs of isomers. A methanol content of 10% resulted in even better separation using the TMBCD reagent than that obtained with no methanol added. This was generally also true with the α-CD, DMBCD and β-CD reagents; i.e., whenever separation of isomers occurred upon the addition of a CD, the addition of 10% methanol increased the separation.

The one exception with methanol addition mentioned above was that γ-CD in the presence of methanol did cause some separation of the dichlorprop and mecoprop optical isomers, as opposed to the absence of methanol, where γ-CD caused no separation at all. Separation was maximum with 20% methanol, in which case the

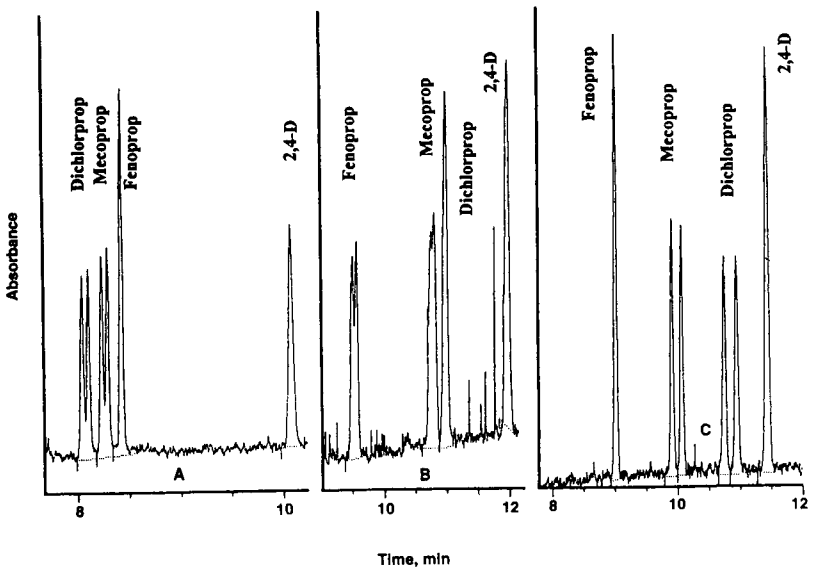

Fig. 4. Separation of (+) and (−) isomers of optically active herbicides by cyclodextrin reagents. (A) 10 m*M* α-CD; (B) 10 m*M* β-CD; (C) 10 m*M* DMBCD. Conditions as in Fig. 3B, except for addition of 10 m*M* CD to the acetate run buffer.

dichlorprop isomers had an α value of 1.01, showing peak splitting but not baseline separation.

One disadvantage of methanol addition was the increase in migration time for all optical isomers and for 2,4-D. This increase correlated with the amount of methanol added; for example, with TMBCD but without methanol, the latest migrating peak, 2,4-D, required 13.57 min for elution. With the addition of 10% methanol, migration time increased to 24.17 min, and with 20%, to 29.67 min. This degree of increase of migration time with addition of methanol was about the same when the other four CDs were used; i.e., addition of 20% methanol more than doubled the migration times for the optical isomers and for 2,4-D.

3.5. Reproducibility of enantiomer electropherograms

Table 1 presents data on the reproducibility of migration times, peak heights and peak areas of the (+) and (−) isomers of the three herbicides at a concentration of 1 μg/ml, separated by complexation with TMBCD at 25 m*M* as described above.

Table 2
Separation of herbicide enantiomers by cyclodextrins

	α-CD	β-CD	γ-CD	DMBCD	TMBCD
Fenoprop	−	+	−	−	+
Mecoprop	+	+	−	+	+
Dichlorprop	+	-	−	+	+

+ = Some degree of separation; − = no separation.

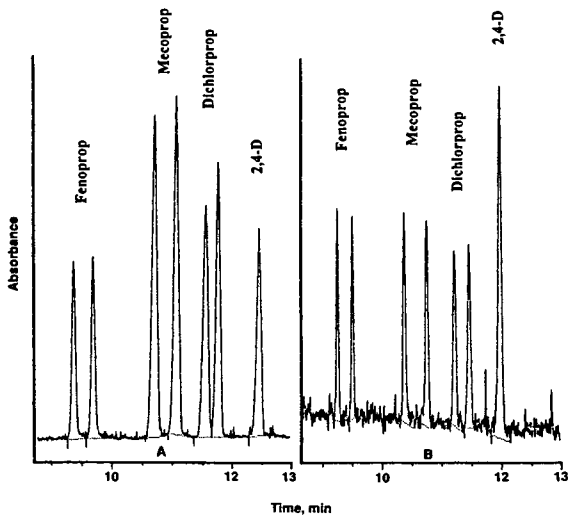

Fig. 5. Separation of (+) and (−) isomers of optically active herbicides by TMBCD. (A) 12.5 m*M* TMBCD, concentration of each herbicide is greater than 100 μg/ml; (B) 25 m*M* TMBCD, 1 μg/ml each herbicide. Other conditions as in Fig. 3B.

4. Discussion

TMBCD added to the acetate run buffer at 25 m*M* results in excellent separation of the optical isomers of the three herbicide racemates. None of the other four cyclodextrin derivatives used in this study separated all six optical isomers.

Both cavity size and hydrogen bonding and/or hydrophobic interactions at the larger lip of the truncated CD cone may play a role in its complexation with phenoxy acids [8,9,27]. Apparently, cavity size alone does not determine whether there is sufficient difference in the complexation constants of the (+) and (−) phenoxy acid isomers to cause separation. Racemic dichlorprop, the phenoxy acid with the smallest effective molecular diameter —corresponding to the molecular volume of the substituted phenoxy moiety (molecular volume of 2,4-dichlorophenol = 112 ml/mol)— is separated by the α-CD, which has the smallest cavity size, but not by the β-CD, which may simply be too large for differential complexation. This size restriction is logical, since the usual complexation mechanism involves insertion of the more hydrophobic (usually the aromatic) portion of the molecule into the hydrophobic CD cavity [8,9]. However, the fact that the dichlorprop racemate is separated by DMBCD and TMBCD, which have the same inner diameter as β-CD, implies an additional complexation mechanism.

Fenoprop, which has the largest effective molecular diameter (molecular volume of 2,4,5-trichlorophenol = 124 ml/mol) probably does not fit into the small α-CD cavity. Its isomers are separated by TMBCD and to a small extent by β-CD, but not at all by DMBCD. This apparent

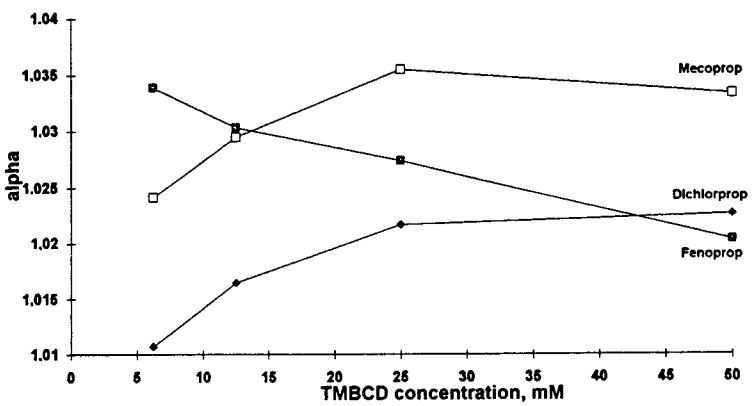

Fig. 6. Relative migration times (α) of (+) and (−) isomers of three herbicides at varying concentrations of TMBCD. Conditons as in Fig. 3B.

anomaly also implies an additional interaction mechanism. Mecoprop, the middle-sized (molecular volume of 2-methyl-4-chlorophenol = 118 ml/mol) of the racemic phenoxy acids, is separated to some extent into its optical isomers by all CDs used here except for γ-CD. γ-CD did not separate any of the racemates; its internal diameter is apparently too large.

The effects of methanol addition on these enantiomeric separations should provide clues to the CD–phenoxy acid complexation mechanisms [27]. For example, the partial separation of dichlorprop and mecoprop isomers with γ-CD in the presence of methanol may be caused by inclusion of a phenoxy acid–methanol adduct into the CD cavity, which may be too large to form effective complexes with the phenoxy acid alone. The general increase in optical isomer separation with addition of methanol, as well as the overall increase in migration times of all analytes, is likely caused by reduction of electroosmotic flow because of solvent interactions with the column wall [25]. Migration times in the presence of methanol could probably be reduced while retaining good separation by increasing the voltage from 20 to 30 kV.

Another puzzling phenomenon is the large shift in migration time observed with some of the optical isomers after CD complexation, relative to the migration time of the uncomplexed racemate. The complexes are new chemical species, of course, and would be expected to have different migration times from the uncomplexed racemates. An extreme case, however, is the large reduction in migration times of mecoprop and dichlorprop after the addition of α-CD; this large shift does not occur with other CDs. In this case, fenoprop's migration time changes very little; since its isomers are not resolved with α-CD, as mentioned above, and since fenoprop is the largest of the three herbicides, it is assumed that it does not form a complex. The greatly reduced migration time of mecoprop, which is even more reduced for dichlorprop, means that the α-CD complexes of these enantiomers have lower electrophoretic mobilities than do the uncomplexed racemates. Perhaps the pK_a values of the complexed analytes are increased relative to the uncomplexed forms, resulting in a net reduction of charge at the pH of the buffer.

Carbon-14 and proton nuclear magnetic resonance experiments are underway in an attempt to provide explanations for these complexation processes and mechanisms.

Changes in migration times upon CD complexation can cause confusion in identification of optical pairs, and it is necessary to spike samples with at least one of the optical isomers of each pair to assure positive identification. Sample spiking would be particularly important in the analysis of complex matrices, e.g., environmental samples. It should also be realized that migration time depends on the concentration of the CD used for separation, as well as on the CD structure.

Reproducibility of migration times of 2,4-D and the three optically active racemates and their (+) and (−) isomers is good; relative standard deviations (R.S.D.s) range from 1.3 to 4.6%. The R.S.D.s are considerably better for 5- than for 15-s injections. It is also noteworthy that the migration time R.S.D.s corresponding to 10 μg/ml sample concentrations are slightly better than those for 1 μg/ml levels at a 15-s injection time. On the other hand, reproducibility of quantitative parameters, i.e. peak areas and heights, varies from about 1.6 to 11.1% R.S.D. for the complexed optical isomers, and is even higher for most of the racemates, ranging from 4.4 to 17.9%. R.S.D.s for these parameters for the racemates are much better for 10 μg/ml than for 1 μg/ml concentrations at 15-s injection times. Area and peak-height R.S.D.s are much better for 15- than for 5-s injection times at the 10 μg/ml concentrations. For the optical isomers, peak area reproducibility was better than that for peak height.

In summary, the best quantitative precision occurs by using peak area measurements at the higher sample concentration and longer injection time. Under these conditions, migration time reproducibility is lower but still acceptable. For these optimal conditions, R.S.D.s for migration times range from 3.1 to 3.3%, and R.S.D.s for peak areas range from 4.8 to 6.3% for the

racemates. Similarly, migration time R.S.D.s range from 2.9 to 4.3% and peak area R.S.D.s range from 1.6 to 8.1% for the optical isomers, which were only run at the 1 μg/ml concentration.

5. Conclusions

A 50 m*M* acetate run buffer of pH 4.5 provides for baseline separation of 2,4-D, dichlorprop, mecoprop and fenoprop, using FSCE at 20 kV and 30°C. UV detection at 230 nm allows a lower detection limit of 0.05 μg/ml (about $5 \cdot 10^{-7}$ *M*).

TMBCD added to the acetate run buffer at 25 m*M* results in baseline separation of the (+) and (−) isomers of the three optically active herbicides; none of the other four CD derivatives used in this study separates all six isomers. NMR studies in progress should help explain the interactions between these phenoxy acids and the various CDs. The addition of methanol to the run buffer along with the CD reagent is not overall advantageous; separations are marginally improved, but migration times are generally doubled.

Reproducibility of migration times of 2,4-D and the three optically active racemates and their enantiomers is good. Reproducibility of peak areas and heights is acceptable; best results are obtained by using peak area instead of peak height measurements at higher concentrations and longer injection times.

5.1. Environmental applications

Possible applications of these results to environmental problems are obvious. HPCE has particular advantages over GC or HPLC: resolution is better; chiral separation is simpler; analysis is faster; and finally, less sample preparation is necessary, mostly because in the FSCE mode used here, only anions are detected. This latter advantage eliminates the need for derivatization, as well as screening out all cationic and neutral interferences.

CE also has disadvantages relative to GC or HPLC; for one, reproducibility is lower. In addition, CE does not have the apparent sensitivity of GC or HPLC separation/detection techniques; although the inherent sensitivity (mass sensitivity) is excellent in terms of the amount on column, the injection volume is very small. Detection levels are adequate, however, for many environmental analyses. Furthermore, laser-induced fluorescence detectors provide very high sensitivity for certain types of analytes. Another important current disadvantage of CE over the other techniques is that interfaces with mass spectrometers are still more or less in the experimental stage; positive identification of unknown peaks, therefore, is not the routine procedure possible with GC–MS or HPLC–MS. Current research is rapidly changing this situation, however [28,29].

The CE methods described here have recently been applied to determine the relative degradation of the two optical isomers of dichlorprop with time in soil samples from an agricultural site treated with a commercial herbicide formulation [30].

Acknowledgements

A.W.G. is grateful to the US Environmental Protection Agency (EPA) for an 11-month research assignment to the Institute for Ecological Chemistry (IOC) of the GSF, Neuherberg (Munich), Germany; special thanks are due Rosemarie Russo, George Bailey, Eric Weber and Linda Exum of EPA's Environmental Research Laboratory (ERL), Athens, GA, USA. Appreciation also is expressed to Gerd Pfister and his research group at the IOC for laboratory space and logistical assistance. We thank Mac Long and Sam Karickhoff of ERL-Athens for SPARC calculations of pK_a and molecular volume values. Finally, we wish to thank personnel of Beckman Instruments, Munich, Germany for their timely instrumentation and applications support.

References

[1] W.G. Kuhr and C.A. Monnig, *Anal. Chem.*, 64 (1992) 389R.

[2] G. Dinelli, A. Vicari and P. Catizone, *J. Agric. Food Chem.*, 41 (1993) 742.
[3] W.C. Brumley, *J. Chromatogr.*, 603 (1992) 267.
[4] W.C. Brumley and C.M. Brownrigg, *J. Chromatogr.*, 646 (1993) 377.
[5] M. Tomita, T. Okuyama, Y. Nigo, B. Uno and S. Kawai, *J. Chromatogr.*, 571 (1991) 324.
[6] S.K. Yeo, C.R. Ong and S.F.Y. Li, *Anal. Chem.*, 63 (1991) 2222.
[7] F. Foret, V. Sustacek and P. Boček, *Electrophoresis*, 11 (1990) 95.
[8] R. Kuhn and S. Hoffstetter-Kuhn, *Chromatographia*, 34 (1992) 505.
[9] J. Snopek, I. Jelinek and E. Smolková-Keulemansová, *J. Chromatogr.*, 609 (1992)1.
[10] S. Fanali, *J. Chromatogr.*, 545 (1991) 437.
[11] L. Cellai, C. Desiderio, R. Filippetti and S. Fanali, *Electrophoresis*, 14 (1993) 823.
[12] P. Gareil, J.P. Gramond and F. Guyon, *J. Chromatogr.*, 615 (1993) 317.
[13] R. Kuhn, F. Stoecklin and F. Erni, *Chromatographia*, 33 (1992) 32.
[14] D.W. Armstrong, G.L. Reid, III, M.L. Hilton and C.-D. Chang, *Environ. Pollut.*, 79 (1993) 51.
[15] M.D. Muller, M. Schlabach and M. Oehme, *Environ. Sci. Technol.*, 26 (1992) 566.
[16] W.A. Konig, D. Ichein, T. Runge, B. Pfaffenberger, P. Ludwig and H. Huhnerfuss, *J. High Resolut. Chromatogr.*, 14 (1991) 530.
[17] B. Blessington, N. Crabb and J. O'Sullivan, *J. Chromatogr.*, 396 (1987) 177.
[18] L. Chiang, R.J. Magee and B.D. Jones, *Anal. Chim. Acta*, 225 (1991) 187.
[19] W. Schussler, *Chromatographia*, 29 (1990) 24.
[20] R. Hamann and A. Kettrup, *Chemosphere*, 16 (1987) 527.
[21] D.G. Thompson, G.R. Stephenson, K.R. Solomon and A.V. Skepasts, *J. Agric. Food Chem.*, 32 (1984) 578.
[22] C.R. Worthing and S.B. Walker (Editors), *The Pesticide Manual*, British Crop Protection Council, Thornton Heath, 8th ed., 1987.
[23] S.L. Hilal, L.A. Carreira, G.L. Baughman, S.W. Karickhoff and C.M. Melton, *J. Phys. Org. Chem.*, 7 (1994) 122.
[24] S. Terabe, T. Yashima, N. Tanaka and M. Araki, *Anal. Chem.*, 60 (1998) 1673.
[25] R. Kuhn and S. Hoffstetter-Kuhn, *Capillary Electrophoresis: Principles and Practice*, Springer, Berlin, 1993, section 3.3.
[26] A. Guttman, A. Paulus, A.S. Cohen, N. Grinberg and B.L. Karger, *J. Chromatogr.*, 448 (1988) 41.
[27] G.N. Okafo and P. Camilleri, in P. Camilleri (Editor), *Capillary Electrophoresis: Theory and Practice*, CRC Press, Boca Raton, FL, 1993, Ch. 5.
[28] R.D. Smith, H.R. Udseth, C.J. Barinaga and C.G. Edmonds, *J. Chromatogr.*, 559 (1991) 197.
[29] F. Garcia and J. Henion, *J. Chromatogr.*, 606 (1992) 237.
[30] A.W. Garrison, P. Schmitt, D. Martens and A. Kettrup, *J. Agric. Food Chem.*, submitted for publication.
[31] M.W.F. Nielen, *J. Chromatogr.*, 637 (1993) 81.

ELSEVIER

Journal of Chromatography A, 688 (1994) 329–337

JOURNAL OF CHROMATOGRAPHY A

Enantiomeric differentiation of a wide range of pharmacologically active substances by cyclodextrin-modified micellar electrokinetic capillary chromatography using a bile salt

Anthony Aumatell*, Robert J. Wells

Australian Government Analytical Laboratory, 1 Suakin Street, Pymble, NSW 2073, Australia

First received 25 July 1994; revised manuscript received 9 September 1994

Abstract

This paper shows the versatility of modified charged and non-charged β-cyclodextrins in micellar systems for optically resolving β-agonists, β-antagonists, phenylethylamines stimulants and diclofensine an antidepressant. A total of 22 compounds were optically resolved using hydroxypropyl-β-cyclodextrin with sodium taurodeoxycholate and sodium sulfobutyl ether-β-cyclodextrin with sodium dodecyl sulfate.

1. Introduction

Bile salts are chiral naturally occurring anionic surfactants found in vertebrate species [1]. The primary physiological function of bile salts is to assist in the solubilization of dietary lipids, such as cholesterol, aiding in the excretion of insoluble endogenous lipids [2]. Bile salts have a flat-shaped steroid portion with the hydroxyl groups oriented in the same direction (hydrophilic face) nearly perpendicular to the steroidal frame (hydrophobic face). This induces the formation of small primary micelles [3] possessing a helical structure with the hydrophilic region facing the interior of the micelle [4,5]. Bile salt micelles are more polar, have a lower critical micelle concentration and aggregation number than the commonly used sodium dodecyl sulfate (SDS) [6]. They have been used in micellar electrokinetic capillary chromatography (MECC) for the separation of mainly hydrophobic solutes having rigid planer chemical structures [4,7–21], and optical resolution of racemates [11–17]. The separation principle of MECC using bile salts is based on the large anionically charged micelles electrophoretically migrating towards the anodic end of the capillary; however, since electroosmotic flow (EOF) is in the opposite direction, the net effect is that the micelles are slowly swept towards the detector. The slowly moving micelles create a pseudostationary phase. Analytes in the mobile EOF are separated by differential interactions with the micelles and by

* Corresponding author. Present address: Beckman Instruments, P.O. Box 218, Gladesville, NSW 2111, Australia.

SSDI 0021-9673(94)00885-X

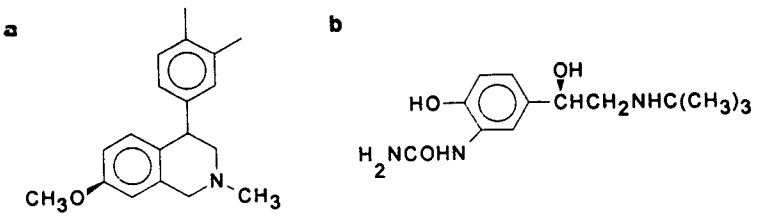

Fig. 1. Chemical structures of (a) diclofensine and (b) carbuterol.

their electrophoretic mobilities. The chiral recognition mechanism for bile micelles in MECC systems appears to be by solute structure compatibility with the helical cavity, enabling a specific interaction with one enantiomer and the micelle polar interior [15,20].

In a previous paper only positively charged drug compounds (β-agonists, β-antagonists, phenylethylamines and alcohols) were optically resolved by cyclodextrin (CD) capillary zone electrophoresis (CZE) [22], although drugs can exist as charged and/or neutral species. Both charged and neutral species can be resolved by incorporating a surfactant into the buffer system [23]. A CD MECC system that optically resolves both phenylethylamines and diclofensine enantiomers has not been reported.

Reported in this paper are CD MECC separation methods using sodium taurodeoxycholate (STDC) and SDS as surfactants and ether derivatives of β-CD to resolve a wide range of pharmacologically active drugs including diclofensine (Fig. 1a) and β-agonists, β-antagonists, phenylethyamines and alcohol stimulants (the chemical structure of carbuterol is illustrated in Fig. 1b, and others have been shown previously [22]). *R,S*-Diclofensine is a tricyclic antidepressant and widely used in the treatment of depression by inhibiting the re-uptake of dopamine, noradrenaline, and serotonin [24].

2. Experimental

2.1. Reagents

R,S-Diclofensine hydrochloride was kindly supplied by F. Hoffmann–La Roche, Basel, Switzerland. *R,S*-Clenbuterol, *R,S*-terbutaline, *R,S*-cimaterol, *R,S*-salbutamol, *R,S*-pirbuterol, *R,S*-atenolol, *R,S*-nadolol, *R,S*-propranolol, *R,S*-timolol, *R,S*-oxprenolol, *R,S*-pindolol, *R,S*-alprenolol, *R,S*-labetalol, *R,S*-acebutolol, *R,S*-metoprolol, *R,S*-amphetamine, *R*-amphetamine, *R,S*-carbuterol, *S*-amphetamine, *R*-methylamphetamine, *S*-methylamphetamine, *R,S*-methyldimethoxyamphetamine, *R,S*-methyldimethoxymethylamphetamine, *R,S*-methyldimethoxyethylamphetamine, *R,S*-2,5-dimethoxy-4-methylamphetamine, *R,S*-4-bromo-2,5-dimethoxyamphetamine, *R,S*-norephedrine, *S*-ephedrine, *R*-ephedrine, *S*-pseudoephedrine and *R*-pseudoephedrine were supplied by the Curator of Standards, Australian Government Analytical Laboratories (Pymble, Australia). Hydroxypropyl-β-cyclodextrin [HP-β-CD, average molar substitution (MS) 0.6 and 0.8], dimethyl-β-cyclodextrin, trimethyl-β-cyclodextrin, γ-cyclodextrin, sodium taurodeoxycholate, *R*-propranolol, *S*-propranolol, *R,S*-epinephrine and *S*-epinephrine were supplied by Sigma (St. Louis, MO, USA). *R*-Atenolol, *S*-atenolol, *S*-alprenolol-*S*-tartrate were supplied by Aldrich. Sodium sulfobutyl ether-β-cyclodextrin (SBE-β-CD) was supplied by Isco (Lincoln, NE, USA). SDS was obtained from E. Merck, Kilsyth, Australia. SDS was recrystallised three times from absolute ethanol. Analytical-reagent grade propan-1-ol was redistilled under vacuum from activated charcoal prior to use. All other chemicals and solvents were of analytical-reagent or HPLC grade and were used without further purification.

2.2. Preparation of buffers

A stock buffer solutions of 0.100 *M* sodium

tetraborate adjusted to pH 9.5 with 5.0 *M* sodium hydroxide, 0.100 *M* SDS and 0.100 *M* STDC were used to prepare running buffers. The running buffers were prepared by the appropriate volume of stock buffer and surfactant, propan-1-ol and mass of cyclodextrin. The resulting running buffer was degassed by sonication and filtered through a 0.2-μm PTFE filter (Micro Filtration Systems, Dublin, CA, USA) before use.

2.3. Apparatus

Qualitative work was performed with fused-silica capillary tubes (Isco) (100 cm × 50 μm I.D.) with an effective length of 50 cm to the detector window. An Isco Model 3140 electropherograph was used for all analyses. The instrument was operated at 30 kV and at a temperature of 23°C with the detector placed on the cathode side. The sample solution was loaded into the capillary under vacuum (vacuum level 4.0 kPa/s for Isco 3140 electropherogram). The compounds were detected at 200 nm and 0.01 AUFS. Electropherograms were recorded and processed with the ICE data management and control software supplied with the Model 3140 electropherograph.

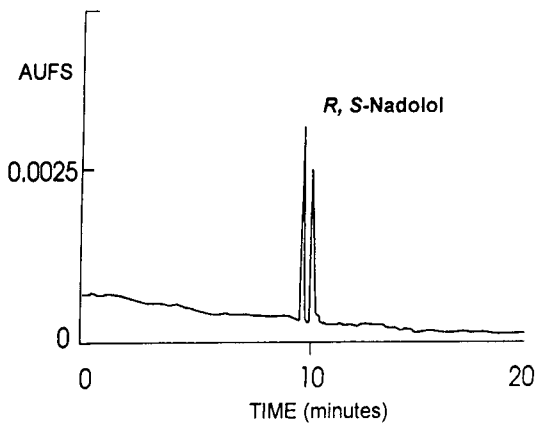

Fig. 2. Electropherogram of a 100 μg/ml *S,R*-nadolol standard. Conditions: 50 kPa/s injection, 30 kV, 220 nm [1.45 m*M* SBE-β-CD, 20 m*M* borate, 20 m*M* SDS, 5% (v/v) propan-1-ol at pH 9.05].

2.4. Procedure for capillary preparation and handling

Prior to extended use, the capillary was filled with 1 *M* sodium hydroxide and allowed to stand for 1 h. This solution was replaced with 0.1 *M* sodium hydroxide, allowed to stand for another hour and washed with deionised water before filling with the running buffer (between sample injections capillary was flushed with 20 μl of running buffer). The capillary was used for a maximum of 40 sample injections before rinsing with 1 *M* sodium hydroxide (200 μl), deionised water (200 μl) and running buffer (200 μl); it was then left filled with running buffer ready for sample injection.

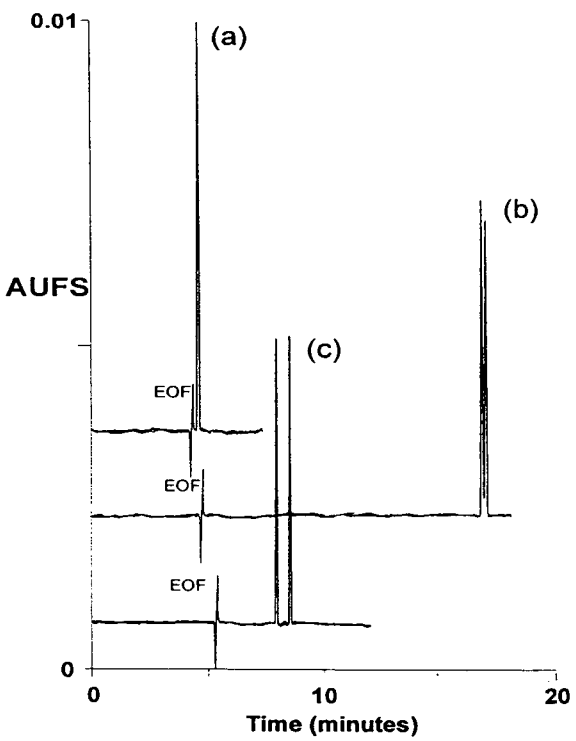

Fig. 3. Electropherogram of a 300 μg/ml *S,R*-diclofensine standard injected into (a) 30 m*M* HP-β-CD (average MS 0.6), 50 m*M* borate buffer at pH 9.5; (b) 2 m*M* HP-β-CD (average MS 0.6), 50 m*M* STDC, 50 m*M* borate buffer at pH 9.5; (c) 30 m*M* HP-β-CD (average MS 0.6), 50 m*M* STDC, 50 m*M* borate buffer at pH 9.5. Other conditions: 2 kPa/s injection, 30 kV, 200 nm.

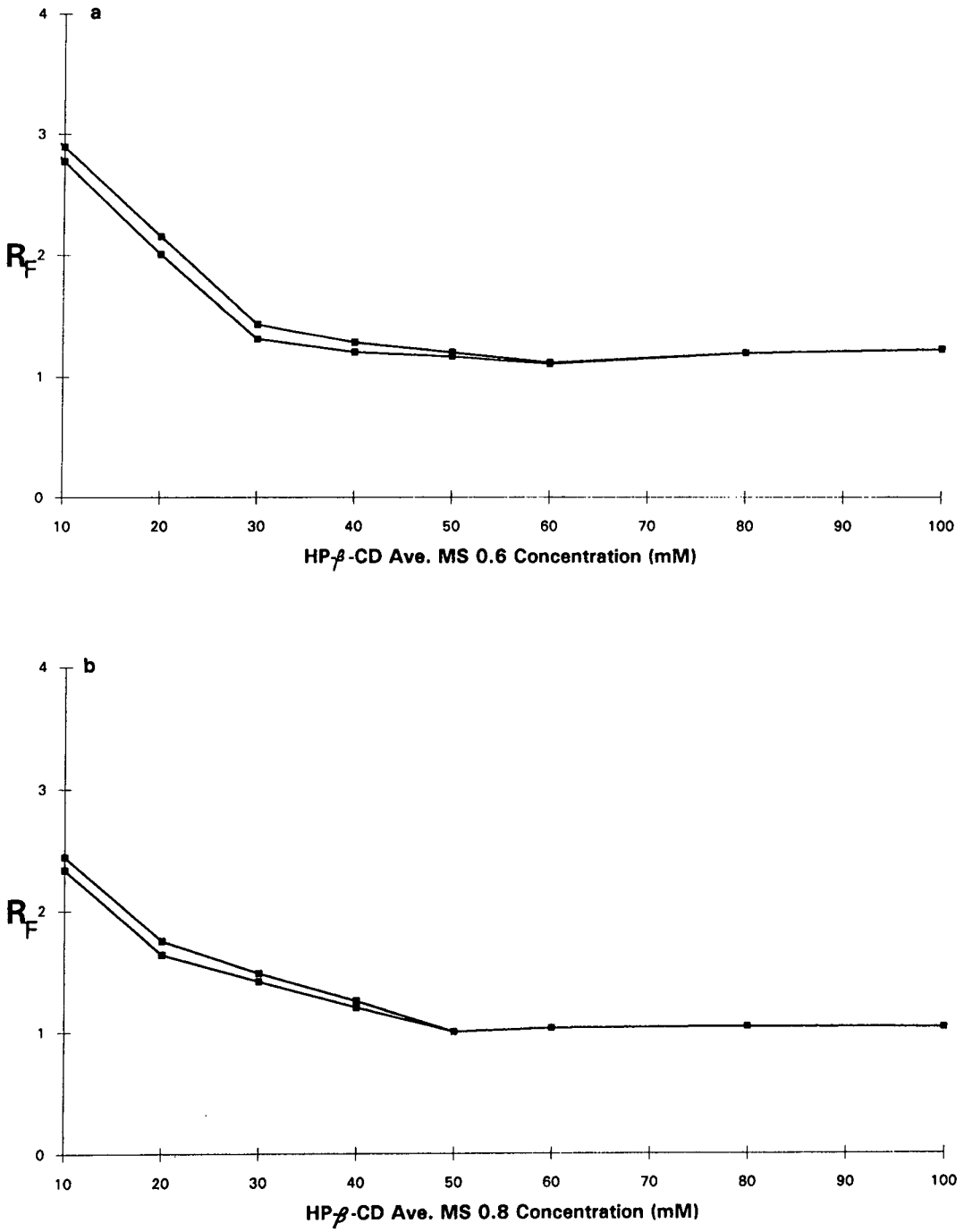

Fig. 4. Plots of *S,R*-diclofensine R_F versus (a) HP-β-CD (average MS 0.6), (b) HP-β-CD (average MS 0.8) and (c) STDC concentration (standard buffer composition 50 m*M* borate at pH 9.5, 50 m*M* STDC and 30 m*M* HP-β-CD).

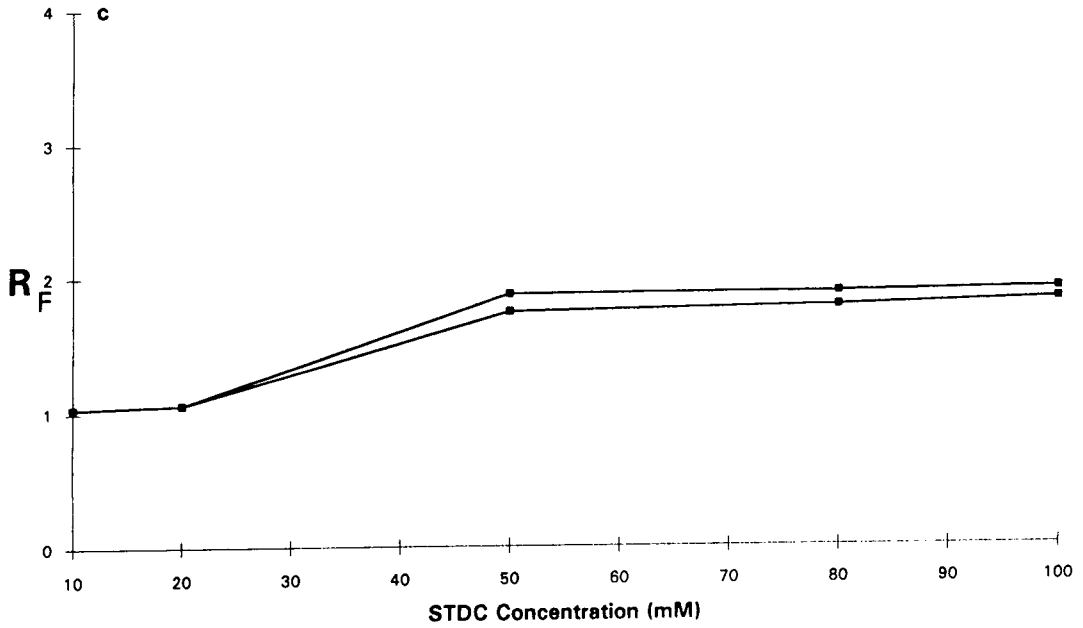

Fig. 4 (*continued*)

Table 1
R_F values of β-agonists and β-antagonists with 60 and 120 m*M* HP-β-CD (average MS 0.6 and 0.8) in 50 m*M* STDC, 5% (v/v) propan-1-ol and 50 m*M* borate buffer at pH 9.5

Compound	R_F [a]	R_F [b]	Compound	R_F [a]	R_F [b]
60 mM HP-β-CD			*120 mM HP-β-CD*		
R,S-Atenolol	0.98	0.98	*R,S*-Timolol	0.95, 1.0	0.98
R,S-Nadolol	0.98	0.98	*R,S*-Atenolol	0.98	0.98
R,S-Oxprenolol	0.98	0.98	*R,S*-Nadolol	0.98	0.96, 0.98
R,S-Cimaterol	0.98	0.98	*R,S*-Oxprenolol	0.98	0.97, 0.98
Methanol	1.0	1.0	*R,S*-Pindolol	0.98	0.98
R,S-Timolol	1.0	0.98, 0.99	*R,S*-Metoprolol	0.98	0.98
R,S-Pindolol	1.0	0.98, 0.99	*R,S*-Terbutaline	0.98	0.98
R,S-Pirbuterol	1.1	1.0	*R,S*-Propranolol	0.98	0.98
R,S-Acebuterol	1.1	1.0	*R,S*-Cimaterol	0.98, 0.99	0.97, 0.98
R,S-Alprenolol	1.1	1.0	Methanol	1.0	1.0
R,S-Clenbuterol	1.05, 1.06	1.0	*R,S*-Clenbuterol	1.01, 1.02	1.02, 1.03
R,S-Metoprolol	1.1	0.97, 0.99	*R,S*-Alprenolol	1.1	1.15
R,S-Terbutaline	1.1	1.1	*R,S*-Pirbuterol	1.1	1.1
R,S-Carbuterol	1.1	1.1	*R,S*-Carbuterol	1.1	1.1
R,S-Salbutamol	1.2	1.2	*R,S*-Diclofensine	1.10, 1.11	1.10, 1.11
R,S-Propranolol	1.2	1.25	*R,S*-Salbutamol	1.2	1.18
R,S-Diclofensine	1.2, 1.3	1.2, 1.3	*R,S*-Labetalol	1.3	1.3
R,S-Labetalol	1.3	1.3			

[a] HP-β-CD: average MS 0.6.
[b] HP-β-CD: average MS 0.8.

3. Results and discussion

Initial attempts to resolve enantiomers of β-agonists, β-antagonists, phenylethylamines and diclofensine were unsuccessful using β-CD, γ-CD, dimethyl- and trimethyl-β-CD, HP-β-CD (average MS 0.6 and 0.8 and SBE-β-CD in association with SDS, propan-1-ol at pH 9.0. Nadolol was only resolved optically using an SDS–propan-1-ol–SBE-β-CD system (Fig. 2).

Propranolol, atenolol, phenylethylamines and alcohols were not optically resolved with CD MECC systems employing SDS or STDC as surfactants at both pH 9 and 11 [25,26]. However, MECC systems employing bile salts and organic modifiers such as alcohols and CDs have optically resolved drugs structurally similar to phenylethylamines and diclofensine [11–17]. Diclofensine has a pK_a value of ca. 7 and is deprotonated at pH 9.5 migrating with the EOF in a CD CZE system (Fig. 3a). Addition of STDC to the CD CZE system optically resolved diclofensine and longer migrations times were observed, shown by Fig. 3a and b. This was attributed to diclofensine partitioning between the slower migrating micellar pseudostationary phase, and resulting in a specific optical interaction between the micelle polar interior and CD buffer phase. Increases in HP-β-CD (average MS 0.6 and 0.8) concentration decreased the relative migration time (R_F = solute migration time/methanol migration time) of diclofensine, and HP-β-CD (average MS 0.6 and 0.8) concentrations greater than 60 and 50 m*M*, respectively did not change diclofensine R_F (Figs. 3b and c and 4a and b). Similar results were observed with other CD MECC systems employing bile surfactants [16,17]. Also, β-agonists and β-antagonists R_F values decreased with increases in HP-β-CD concentration, reflected by $R_F < 1$ for atenolol, nadolol, oxprenolol, cimaterol, timolol and pindolol at 60 m*M* HP-β-CD concentration, and increasing HP-β-CD concentration to 120 m*M* resulted in atenolol, nadolol, oxprenolol, cimaterol, timolol, pindolol, timolol, pindolol, terbutaline and propranolol giving $R_F < 1$ (Table 1). β-Agonists, β-antagonists and phenylethylamines have pK_a values between 9.2 and 11 [25,27] and are protonated at pH 9.5 electromigrating in the same direction as EOF. A number of phenylethylamines, β-agonists and β-antagonists studied gave $R_F < 1$; suggesting weak interactions between the drug and the negatively charged STDC (Tables 1 and 2). Conversely, increases in STDC concentration up to 50 m*M* increased the R_F of diclofensine, and further increases in STDC concentration did not appear to change diclofensine R_F values (Fig. 4c). CD can associate weakly with the hydrophilic face of STDC within the micelle via hydrogen bonding

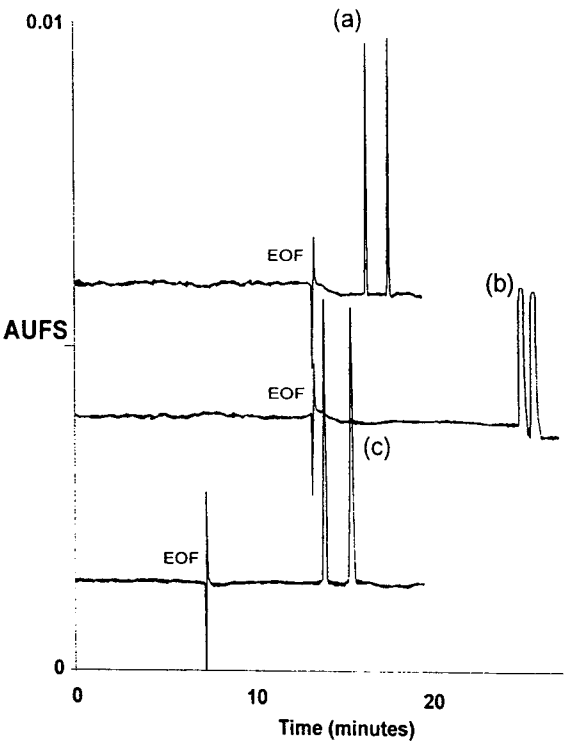

Fig. 5. (a, b) Electropherogram of a 300 μg/ml (a) *S,R*-nadolol and (b) *S,R*-diclofensine standard injected into 20% (v/v) propan-1-ol, 30 m*M* HP-β-CD (average MS 0.6), 50 m*M* STDC, 50 m*M* borate buffer at pH 9.5. (c) Electropherogram of a 300 μg/ml standard *S,R*-diclofensine injected into 5% (v/v) propan-1-ol, 30 m*M* HP-β-CD (average MS 0.6), 50 m*M* STDC, 50 m*M* borate buffer at pH 9.5. Other conditions: 2 kPa/s injection, 30 kV, 200 nm.

Table 2
R_F values of phenylethylamine and alcohols with 60 and 120 m*M* HP-β-CD (average MS 0.6 and 0.8) in 50 m*M* STDC, 5% (v/v) propan-1-ol and 50 m*M* borate buffer at pH 9.5

Compound	R_F [a]	R_F [b]	Compound	R_F [a]	R_F [b]
60 mM HP-β-CD			*120 mM HP-β-CD*		
R,S-Methyldimethoxymethyl-amphetamine	0.92, 0.93	0.96, 0.97	*R,S*-Methylamphetamine	0.92, 0.93	0.90, 0.91
R,S-2,5-Dimethoxy-4-methyl-amphetamine	0.93	0.92	*R,S*-Methyldimethoxymethyl-amphetamine	0.93	0.97, 0.98
R,S-Epinephrine	0.94	0.96	*R,S*-Epinephrine	0.94	0.98
R,S-Methyldimethoxyethyl-amphetamine	0.94, 0.95	0.92, 0.93	*R,S*-4-Bromo-2,5-dimethoxy-amphetamine	0.94	0.95
R,S-Methylamphetamine	0.95, 0.96	0.93, 0.94	*R,S*-2,5-Dimethoxy-4-methyl-amphetamine	0.96	0.97
R,S-Methyldimethoxy-amphetamine	0.95	0.93	*R,S*-Amphetamine	0.98	0.98
R,S-Amphetamine	0.98	0.93	*R,S*-Ephedrine	0.98	0.98
R,S-Ephedrine	0.98	0.98	*R,S*-Pseudoephedrine	0.98	0.98
R,S-Pseudoephedrine	0.98	0.98	*R,S*-Methyldimethoxy-amphetamine	0.98	0.95
R,S-Norephedrine	0.98	0.98	*R,S*-Norephedrine	0.98	0.97
R,S-4-Bromo-2,5-dimethoxy-amphetamine	0.98	0.98	*R,S*-Methyldimethoxyethyl-amphetamine	0.98	0.98

[a] HP-β-CD: average MS 0.6.
[b] HP-β-CD: average MS 0.8.

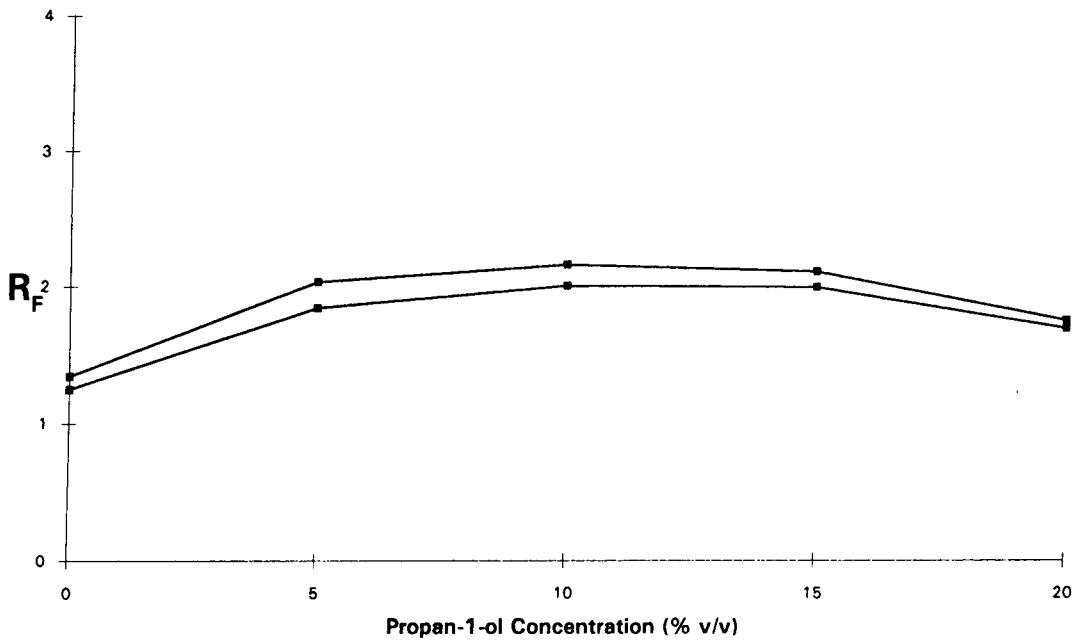

Fig. 6. A plot of *S,R*-diclofensine R_F versus propan-1-ol concentration [50 m*M* STDC, 30 m*M* HP-β-CD (average MS 0.8), 50 m*M* borate buffer at pH 9.5].

[16] decreasing the micelle hydrophobicity, reflected in this work by decreases in R_F values for β-agonists, β-antagonists and diclofensine with increases in CD concentration.

Resolution in MECC can be improved by modifying the buffer with short-chain alcohols, decreasing the EOF and affinity of the hydrophobic solute for the micellar phase [28,29]. The STDC–HP-β-CD system at pH 9.5 studied was modified with propan-1-ol at various concentrations and β-agonists, β-antagonists, phenylethylamines and diclofensine were injected separately to obtain the modifier concentration which optically resolved the greatest number of compounds. The optical resolution of diclofensine was observed to increase with propan-1-ol concentration up to 5%, and further increases in propan-1-ol concentration degraded the chiral resolution (Figs. 3c, 5b and c and 6). Timolol, pindolol, metoprolol, clenbuterol, diclofensine, oxprenolol, cimaterol, methylamphetamine, methyldimethoxymethylamphetamine and methyldimethoxyethylamphetamine were optically resolved with STDC–HP-β-CD modified with 5% (v/v) propan-1-ol (Tables 1 and 2 and Figs. 5c, 7–9. The STDC–HP-β-CD system modified with 20% (v/v) propanol could only resolve optically nadolol and diclofensine (Fig. 5a and b).

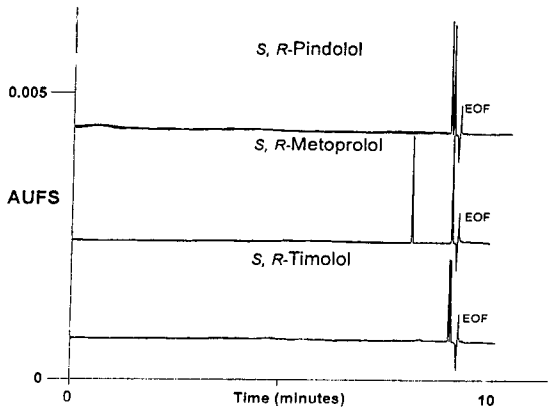

Fig. 8. Electropherogram of a 300 μg/ml *S,R*-pindolol, *S,R*-metoprolol and *S,R*-timolol standard injected into 5% (v/v) propan-1-ol, 60 m*M* HP-β-CD (average MS 0.8), 50 m*M* STDC, 50 m*M* borate buffer at pH 9.5 (2 kPa/s injection, 30 kV, 200 nm).

The optical isomers of β-agonists, β-antagonists, ephedrines and amphetamines resolved at pH 2.5 with HP-β-CD migrated with the "*S*" form first, followed by the "*R*" [22]. In this work methylamphetamine migrated with the "*S*" form

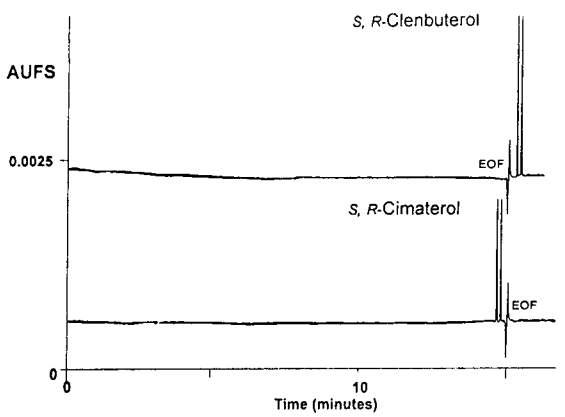

Fig. 7. Electropherogram of a 300 μg/ml *S,R*-clenbuterol and *S,R*-cimaterol standard injected into 5% (v/v) propan-1-ol, 30 m*M* HP-β-CD (average MS 0.8), 120 m*M* STDC, 50 m*M* borate buffer at pH 9.5 (2 kPa/s injection, 30 kV, 200 nm).

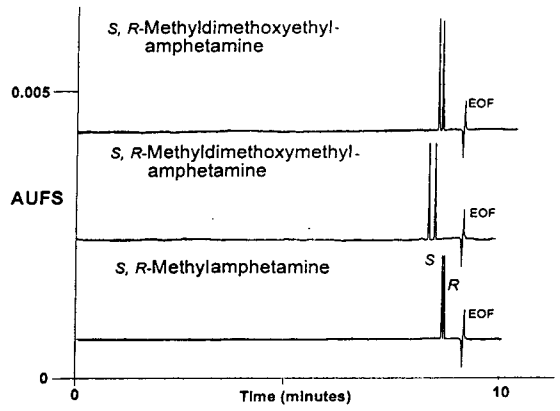

Fig. 9. Electropherogram of a 300 μg/ml *S,R*-methyldimethoxyethylamphetamine, *S,R*-methyldimethoxymethylamphetamine and *S,R*-methylamphetamine standard injected into 5% (v/v) propan-1-ol, 60 m*M* HP-β-CD (average MS 0.8), 50 m*M* STDC, 50 m*M* borate buffer at pH 9.5 (2 kPa/s injection, 30 kV, 200 nm).

first, followed by the "*R*" (Fig. 9), suggesting a common mechanism to the HP-β-CD CZE system [22]. Chiral resolution for metoprolol at pH 2.5 with HP-β-CD appeared to be impaired by the protruding aromatic substituent preventing the aromatic ring from sufficient penetration into CD for hydrogen bonding to occur with the stereogenic centre [22]. Conversely, optical resolution appeared impaired with timolol by the large distance between the stereogenic centre and hydrogen bonding groups on the CD [22]. In this work, the combination of HP-β-CD with STDC appeared to produce a synergetic effect optically resolving metoprolol and timolol. Similar effects have appeared using dansylamino acid derivatives with STDC–CD systems [17,18].

4. Conclusions

Mixtures of modified charged and non-charged β-CDs in association with SDS or STDC at pH 9.0 and 9.5 have shown to be useful in optically resolving a wide variety of pharmacologically active drugs by CD MECC. These systems are further being evaluated for resolving a number of other drugs.

Acknowledgement

Thanks are due to the Australian Government Analyst, Dr. C.J. Dahl, for the support of this work.

References

[1] A. Hofmann, *Gastroenterology*, 48 (1965) 484.
[2] D. Oakenfull, in E. Wyn-Jones and J. Gormally (Editors), *Aggregation Processes in Solution*, Elsevier, Amsterdam, 1983, pp. 118–137.
[3] D. Attwood and A.T. Florence, *Surfactant Systems*, Chapman & Hall, London, 1983, pp. 185–196.
[4] R.O. Cole, M.J. Sepaniak, W.L. Hinze, J. Gorse and K. Oldiges, *J. Chromatogr.*, 557 (1991) 113.
[5] A.R. Campanelli, S.C. De Sanctis, E. Chiessi, M. D'Alagni, E. Giglio and L. Scardmuzza, *J. Phys. Chem.*, 93 (1989) 1536.
[6] M. Vesikel, in U. Pfüller (Editor), *Mikroemulsionen*, Springer, Berlin, 1986, p. 26.
[7] L. Valtcheva, J. Mohammad, G. Pettersson and S. Hjertén, *J. Chromatogr.*, 638 (1993) 263.
[8] P. Lukkari, H. Vuorela and M. Riekkola, *J. Chromatogr. A*, 652 (1993) 451.
[9] A. Shafaati and B.J. Clark, *Anal. Proc.*, 30 (1993) 481.
[10] G.L. Chee and T.S.M. Wan, *J. Chromatogr.*, 612 (1993) 172.
[11] S. Terabe, M. Shibata and Y. Miyashita, *J. Chromatogr.*, 480 (1989) 403.
[12] S. Terabe, H. Nishi, T. Fukuyama and M. Matsuo, *J. Microcol. Sep.*, 1 (1989) 234.
[13] H. Nishi, T. Fukuyama, M. Matsuo and S. Terabe, *Anal. Chim. Acta*, 236 (1990) 281.
[14] H. Nishi, T. Fukuyama, M. Matsuo and S. Terabe, *J. Chromatogr.*, 515 (1990) 233.
[15] R.O. Cole, M.J. Sepaniak and W.L. Hinze, *J. High Resolut. Chromatogr.*, 13 (1990) 579.
[16] G.N. Okafo, C. Bintz, S.E. Clarke and P. Camilleri, *J. Chem. Soc., Chem. Commun.*, 17 (1992) 1189.
[17] M. Lin, N. Wu, G.E. Barker, P. Sun, C.W. Huie and R.A. Hartwick, *J. Liq. Chromatogr.*, 16 (1993) 3667.
[18] H. Nishi, T. Fukuyama, M. Matsuo and S. Terabe, *J. Chromatogr.*, 498 (1990) 313.
[19] H. Nishi, T. Fukuyama, M. Matsuo and S. Terabe, *J. Chromatogr.*, 513 (1990) 279.
[20] N.V. Pavel, E. Giglio, G. Eposito and A. Zanabi, *J. Phys. Chem.*, 91 (1987) 356.
[21] W.C. Brumley and C.M. Brownrigg, *J. Chromatogr. Sci.*, 32 (1994) 69.
[22] A. Aumatell, R.J. Wells and D.K.Y. Wong, *J. Chromatogr. A*, 686 (1994) 293.
[23] A. Aumatell and R.J. Wells, *J. Chromatogr. Sci.*, 31 (1993) 502.
[24] R. Capponi, *Neuropsychobiology*, 14 (1985) 173.
[25] I.S. Lurie, *J. Chromatogr.*, 605 (1992) 269.
[26] T.E. Peterson, *J. Chromatogr.*, 630 (1992) 353.
[27] J. Jumppanen, H. Sirén and M.-L. Riekkola, *J. Chromatogr. A*, 652 (1993) 451.
[28] A.T. Batchunas and M.J. Sepaniak, *Anal. Chem.*, 59 (1987) 1466.
[29] S. Terabe, K. Otsuka and T. Ando, *Anal. Chem.*, 57 (1985) 834.

ELSEVIER

Journal of Chromatography A, 688 (1994) 339–349

JOURNAL OF CHROMATOGRAPHY A

Simultaneous separation of ammonium and alkali, alkaline earth and transition metal ions in aqueous–organic media by capillary ion analysis

Qing Yang, Johanna Smeyers-Verbeke, Wen Wu, Mikhail S. Khots, Desire L. Massart*

Farmaceutisch Instituut, Vrije Universiteit Brussel, Laarbeeklaan 103, B-1090 Brussels, Belgium

First received 11 April 1994; revised manuscript received 19 August 1994

Abstract

The simultaneous separation of the mono-, di- and trivalent cations NH_4^+, K^+, Na^+, Li^+, Mg^{2+}, Ca^{2+}, Sr^{2+}, Ba^{2+}, Mn^{2+}, Ni^{2+}, Zn^{2+}, Cu^{2+} and Cr^{3+} by capillary ion analysis was studied in a background electrolyte system composed of imidazole, 2-hydroxyisobutyric acid, 18-crown-6 and methanol. The effects of this system on the electroosmotic and electrophoretic mobility were studied in detail. A competitive complexation between 2-hydroxyisobutyric acid and sulphuric acid was observed which determined the cation mobility. Applying a central composite design, a quantitative description of the electrophoretic behaviour of the inorganic cations as a function of the system parameters was made and the optimum separation could be predicted. It was found in most instances that a linear model is sufficient for mobility modelling. Using a full factorial design, the main effects on the electroosmotic flow were estimated and methanol was found to be the dominating factor. The applicability of the capillary electrophoresis method was examined by separating ions in Chinese tea infusions. Five metal cations (K^+, Na^+, Ca^{2+}, Mg^{2+} and Mn^{2+}) were detected. A limit of detection at the $\mu g/l$ level could be achieved using electromigration injection.

1. Introduction

Different types of capillary electrophoresis (CE), namely capillary zone electrophoresis (CZE) [1,2], micellar electrokinetic capillary chromatography (MEKC) [3,4] and isotachophoresis (ITP) [5], have been applied to the separation of inorganic cations. Among these, CZE is the simplest. By adding a complexing reagent to the electrolyte buffer, such as 2-hydroxyisobutyric acid (HIBA) [6,7], 8-hydroxyquinoline-5-sulfonic acid [2] or 1,2-cyclohexanediamine-N,N,N,N′-tetraacetic acid (CyDTA) [8], efficient separation of metal cations has been achieved. The separation is based on the difference in complex formation between individual cations and the ligand. The larger the formation constant, the lower is the apparent charge of a complexed cation and therefore the slower its movement.

Foret et al. [6] proposed a CZE method for the separation of lanthanides which employed a mixture of creatinine and HIBA as a background electrolyte (BGE). Later, Weston et al. [7]

* Corresponding author.

0021-9673/94/$07.00
SSDI 0021-9673(94)00800-0

developed the method for separating alkali, alkaline earth and transition metal cations. Beck and Engelthardt [9] proposed imidazole–H_2SO_4 as the BGE system for the separation of alkali and alkaline metal cations. The method was successfully adapted to the quantitative analysis of pharmaceutical electrolyte solutions and fruit juices, and compared with atomic spectrometry in our previous work [10]. Recently, Shi and Fritz [11] investigated the use of lactate, phthalate and tartrate as complexing reagents for CZE separation of metal cations.

A special complexation mechanism is the formation of inclusion complexes by using crown ethers, such as 18-crown-6 and 15-crown-5. They have been used in the CE separation of alkali and alkaline earth metal cations and some transition metal cations [5,12,13]. Use of 18-crown-6 has also been considered in the chiral separation of organic compounds [14]. The crown ether can strongly bind K^+ through its specific cyclic ring structure, lined inside with oxygen atoms carrying unshared pairs of electrons. Therefore, it is added to the BGE to moderate the mobility of K^+. As a result, K^+ and NH_4^+ are separated.

The addition of organic solvents for the CE analysis of organic compounds has been proposed by several groups [15,16]. The organic solvents are added to the running buffer to improve analyte solubility and detection sensitivity, to control electroosmotic flow (EOF) and to provide an additional selectivity. Motomizu et al. [8] have shown the effects of organic solvents such as acetone, ethanol, ethylene glycol and hexanesulfonic acid on the CZE separation of metal–CyDTA complexes. Recently, Janini et al. [15] confirmed that the addition of organic solvents to the electrolyte buffer causes a large change in buffer viscosity. This change is responsible for variations in electroosmotic mobility (μ_{eof}) and electrophoretic mobility (μ_{ep}). The influence on μ_{ep} depends on the extent of solute dissociation and therefore is pH dependent in an acid–base equilibrium system. So far, the CZE separation of metal cations has rarely been considered in mixed organic aqueous media. We decided to study this possibility in more detail.

In this work, we studied an aqueous–organic BGE system composed of imidazole, HIBA, 18-crown-6 and methanol, investigating the effects of the important system parameters on migration and EOF. In addition to a one-variable-at-a-time optimization approach, modelling the electrophoretic behaviour of the inorganic cations as a function of the concentrations of HIBA, 18-crown-6 and methanol was investigated. A central composite design was applied to determine the model coefficients accurately and to predict the optimum separation. The practical applicability of the CE method was evaluated by separating ions in Chinese tea infusions.

2. Experimental

2.1. Instrumentation

The CE instrument was a Waters Quanta 4000 capillary electrophoresis system with a twenty-sample carousel and a zinc lamp detector (214 nm). Accusep fused-silica capillaries (60 cm × 75 μm I.D.) were used in all analyses. A positive voltage of 20 kV was applied. The detector time constant was 0.3 s. Samples were introduced either by hydrostatic or electromigration injection. The electropherograms were recorded and treated with a Waters 810 data workstation equipped with a W51 watch-dog interface. Temperature control was carried out as described in Ref. [10]. The SPSS program [17] was used with an IBM PC2 computer for statistical calculations.

2.2. Capillary preparation and cleaning

Every morning, the capillary was washed for 1 min with 0.5 *M* KOH, for 2 min with water obtained from a Milli-Q system (Millipore) (Milli-Q water) and for 3 min with the electrolyte buffer. Subsequently it was conditioned for at least 15 min. Between each injection, the capillary was washed for 1 min each with 0.1 *M* KOH and Milli-Q water and for 3 min with the electrolyte buffer. At the end of the day, the capillary was rinsed with Milli-Q water for 5 min and left in the water.

2.3. Reagents and standards

Water used for the preparation of all solutions was obtained from a Milli-Q water purification system and contained no detectable analyte cations.

Titrisol concentrates of 1000 μg/ml of Na^+, K^+, Mg^{2+}, Ca^{2+}, Mn^{2+}, Ba^{2+}, Sr^{2+}, Cr^{3+}, Zn^{2+} and Cu^{2+} (Merck, Darmstadt, Germany) were used. Stock standard solutions containing 1000 μg/ml of Ni^{2+}, NH_4^+ and Li^+ were prepared from their chloride or nitrate salts (Merck). Working standard solutions containing different concentrations of the above elements were prepared by mixing the appropriate amounts of the stock standard solutions.

Imidazole was of analytical-reagent grade and methanol of chromatography grade. H_2SO_4 and HCl were of Suprapur grade (Merck), 2-Hydroxyisobutyric acid and 18-crown-6 were 99% pure reagents (Aldrich).

2.4. Preparation of background electrolyte

First, three stock standard solutions containing 130.6 m*M* HIBA, 50.0 m*M* 18-crown-6 and 500.0 m*M* imidazole were prepared. The background electrolytes used in CZE analysis were prepared by mixing appropriate amounts of these stock standard solutions and corresponding volumes of reagent methanol in a 100-ml plastic volumetric flask. The pH was then adjusted by titration first with 5 *M* and subsequently with 0.5 *M* H_2SO_4. For all the BGEs, the pH was kept at ca. 4.5. The electrolyte solutions were stored in a refrigerator. Just before use they were filtered through a 0.45-μm syringe filter (Millipore, Molsheim, France). In modelling mobility experiments, the dilute H_2SO_4 was replaced with 1 *M* HCl for the adjustment of the buffer pH.

2.5. Samples

Chinese green and black teas were bought in a local tea shop in China. The tea infusions were prepared in the following way: ca. 0.5 g of each of teas was weighed in quartz cups and infused in 15 ml of boiling Milli-Q water for 10 min. The infusions were then filtered through a 0.45-μm syringe filter. For the analysis, the solutions were diluted two-fold (1 + 1). The green tea infusion was spiked as follows: 1 ml of the tea infusion and 6 ml of 100 μg/ml ammonium nitrate were pipetted in a 100-ml flask and diluted to volume with Milli-Q water. The solution was again diluted sixfold with Milli-Q water.

3. Results and discussion

3.1. Competitive complexation effect between HIBA and sulfate

Fig. 1 is a plot of cation mobilities as a function of the concentration of HIBA. For

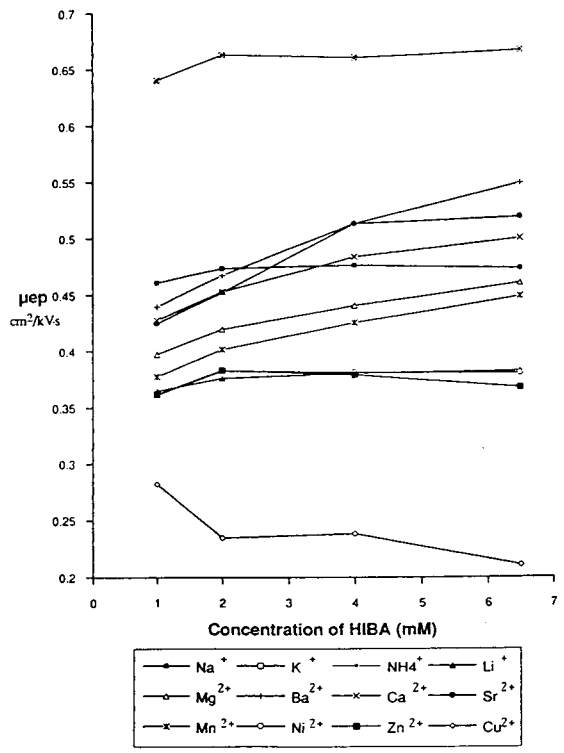

Fig. 1. Dependence of the ionic mobility μ_{ep} on the concentration of HIBA. 2 μg/ml each of NH_4^+, K^+, Na^+, Li^+, Mg^{2+}, Ca^{2+}, Sr^{2+}, Ba^{2+}, Mn^{2+}, Ni^{2+}, Zn^{2+} and Cu^{2+}. Experimental conditions: applied voltage, +20 kV; hydrostatic injection from 10 cm height for 30 s; BGE, 5 m*M* imidazole at pH 4.5.

NH_4^+, Li^+ and K^+, the mobilities are hardly affected by HIBA because they do not form any complexes with HIBA [7] and also have very small formation constants with sulfate [16]. For the alkaline earth metal cations Mg^{2+}, Ca^{2+}, Sr^{2+} and Ba^{2+} the mobilities increase as the HIBA concentration increases. This is also observed for the transition metal cation Mn^{2+}. This observation, however, is contradictory to that in the UVCat1-HIBA BGE, where the mobility decreased with increasing HIBA concentration [7]. This is a result of the competition between sulfate and HIBA for the cations. The effective electrophoretic mobility of each resulting CZE band is regulated by the relative contribution of the various possible chemical forms, such as free metal cation and metal–HIBA and metal–sulfate complexes. As the concentration of HIBA increases there is more $M(HIBA)^+$ complex and less uncharged sulfate complex, so the mobility increases. For Cu^{2+}, Zn^{2+} and Ni^{2+}, which have high formation constants (Table 1 [18]), probably $M(HIBA)_2^0$ is formed. Therefore, a decrease in the mobilities of Zn^{2+}, Ni^{2+} and Cu^{2+} is noticed in Fig. 1. As the HIBA complexation becomes more important with increasing concentration, the selectivity of the separation increases as the formation constants of HIBA complexes are more different for different ions than the sulfate complexes. As we shall see later, by replacing H_2SO_4 with HCl for BGE pH adjustment, a linear mobility dependence on the HIBA concentration is experimentally confirmed. Bächmann et al. [12] also observed the effect of SO_4^{2-} on the ionic mobility in a $Ce_2(SO4)_3$–18-crown-6 BGE system (indirect fluorimetric detection) and found differences of up to 20% between the measured mobilities and the values cited in the literature [19], attributing this to the formation of sulfate salts.

Table 1
Logarithm of overall complex formation constants (β) of HIBA and sulfate with cations [18]

Cation	Log β	
	HIBA	SO_4^{2-}
Mg^{2+}	MgL 0.81, MgL_2 1.47	2.25
Ca^{2+}	CaL 0.92, CaL_2 1.42	2.30
Sr^{2+}	SrL 0.55, SrL_2 0.73	2.31
Ba^{2+}	BaL 0.36, BaL_2 0.51	2.55
Mn^{2+}	MnL 0.96, MnL_2 1.54	2.26
Zn^{2+}	ZnL 1.71, ZnL_2 3.01	2.38
Ni^{2+}	NiL 1.67, NiL_2 2.85, NiL_3 2.84	2.32
Cu^{2+}	CuL 2.74, CuL_2 4.34, CuL_3 4.05	2.36

Fig. 2 shows a plot of μ_{eof} as a function of the concentration of HIBA. μ_{eof} decreases when the concentration of HIBA in the BGE increases (without the addition of 18-crown-6 and methanol). With 1 m*M* HIBA, $\mu_{eof} = 0.48$ cm^2/kV·s and the relative standard deviation (R.S.D.) of the μ_{eof} calculated from 15 independent measurements is 4%. The μ_{eof} and R.S.D. decline rapidly to 0.42 cm^2/kV·s and 2% ($n = 15$), respectively, when the concentration of HIBA is increased to 2 m*M*. A further increase in the HIBA concentration to 6.5 m*M* does not change μ_{eof} significantly but results in an R.S.D. of 1%. We conclude that sufficient amounts of HIBA can improve the stability of the capillary surface.

3.2. *Effect of methanol*

HIBA provides an efficient selectivity of the separation for most of the cations studied here, but as shown in Fig. 3a, the separation between Li^+, Ni^{2+} and Zn^{2+} is insufficient even at 6.5 m*M* HIBA. A further increase in HIBA concentration was found to produce an interference

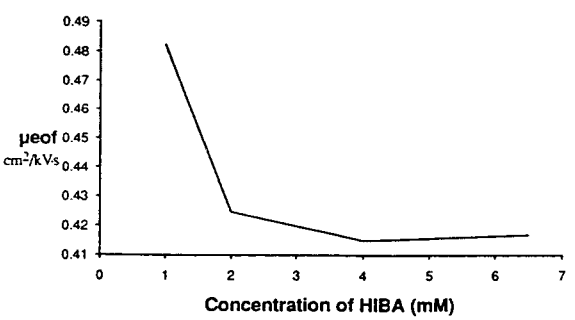

Fig. 2. Dependence of electroosmotic mobility μ_{eof} on the HIBA concentration. Experimental conditions as in Fig. 1.

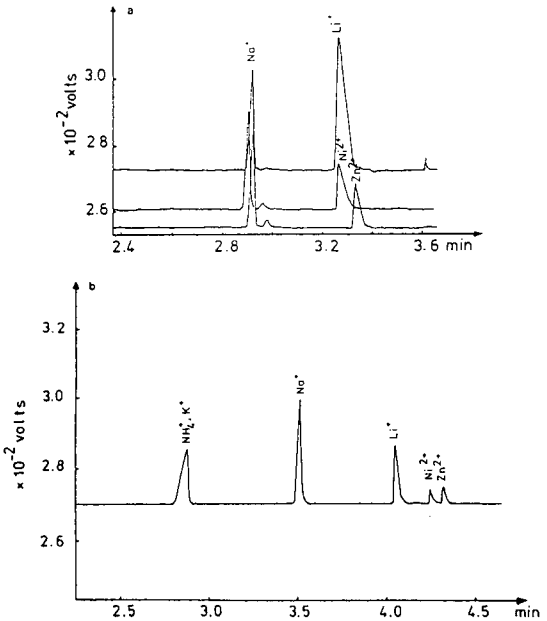

Fig. 3. Separation of Li^+, Ni^{2+} and Zn^{2+} (a) without methanol and (b) with 10% (v/v) methanol in the BGE. Experimental conditions: applied voltage, +20 kV; hydrostatic injection from 10 cm height for 30 s; BGE, 5 m*M* imidazole–6.5 m*M* HIBA at pH 4.5.

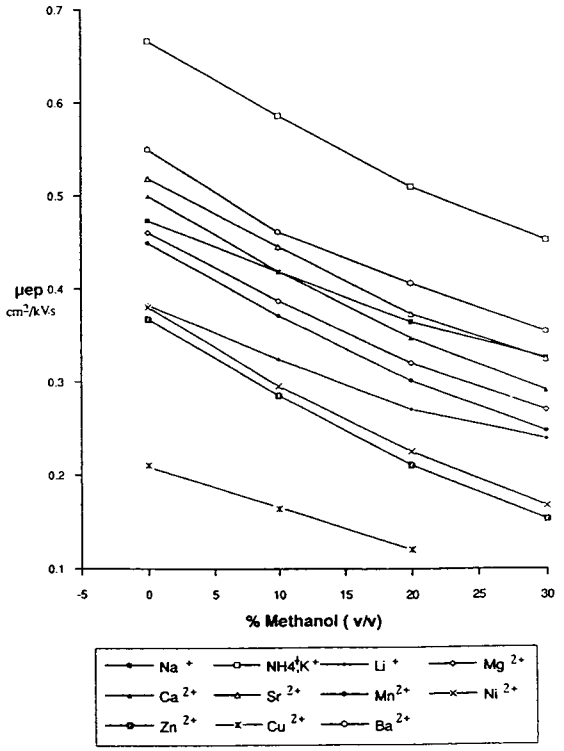

Fig. 4. Dependence of the ionic mobility μ_{ep} on the methanol concentration in the BGE. 2 μg/ml each of NH_4^+, K^+, Na^+, Li^+, Mg^{2+}, Ca^{2+}, Sr^{2+}, Ba^{2+}, Mn^{2+}, Ni^{2+}, Zn^{2+} and Cu^{2+}. Experimental conditions as in Fig. 3.

peak, which can interfere with the other cations. The cause is not clear. For this reason, the amount of HIBA in the BGE was not increased further. As shown in Fig. 3b, however, by adding 10% (v/v) methanol to the electrolyte buffer, the mobilities of Ni^{2+} and Zn^{2+} are greatly decreased, so that they are separated from Li^+.

The effect of methanol on the electrophoretic mobility of the cations was investigated systematically. This was carried out by changing the percentage of methanol in the BGE up to 30% (v/v) while keeping the concentration of HIBA constant. The resulting plot is given in Fig. 4. With increasing percentage of methanol, the mobilities of all the cations decrease almost linearly and elution of the cations is greatly delayed. Methanol affects Li^+ and Na^+ comparatively less, so that peak cross-over occurs when the amount of methanol in the BGE is continuously increased. It follows that methanol modifies the selectivity of CZE separation for inorganic cations.

However, overuse of methanol can produce a negative effect on the separation efficiency owing to broadening of the peak shape. Others [20] also argued that large amounts of organic solvents can cause electrical breakdown and have no advantages except for the improvement of the solubility of hydrophobic compounds. Therefore, 30% (v/v) methanol in the BGE is the maximum amount we studied.

As expected, a strong effect of methanol on μ_{eof} was also observed. Fig. 5 shows that an increase in the methanol content results in a decrease in μ_{eof} when the concentration of HIBA in the BGE is kept constant. The stability of μ_{eof} does not change significantly since the R.S.D. values are always below 1%. The excel-

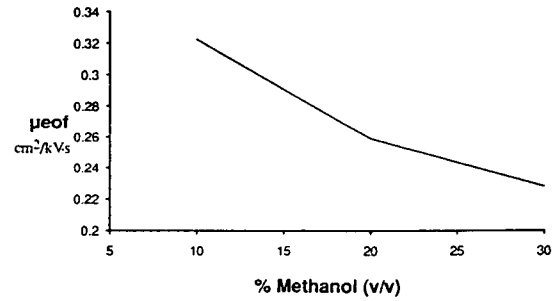

Fig. 5. Dependence of electroosmotic mobility μ_{eof} on the methanol concentration. Experimental conditions as in Fig. 3.

lent repeatability of μ_{eof} is indicative of the stability of the capillary surface. This is one of the important factors in ensuring a repeatable electrophoretic performance. At 30% methanol, $\mu_{eof} = 0.23\ cm^2/kV \cdot s$, which is about half of that in the absence of methanol. Comparing Figs. 4 and 5, the electroosmotic mobility (μ_{eof}) is smaller than the ionic mobility in most instances. The decline in the EOF is attributed mainly to the change in buffer viscosity caused by methanol [15].

Organic solvents may influence electrophoretic behaviour: (i) change the viscosity of the electrolyte buffer; (ii) solvate the solutes [15]; and (iii) affect the chemical equilibrium [21,22].

(i) A change in the viscosity of the electrolyte buffer causes a variation in μ_{ep}. The effects of organic solvents can be derived from the following equation [23]:

$$\mu_{ep} = q/6\pi\eta r \quad (1)$$

where q is the net charge of the solute, r the Stokes radius and η the viscosity of the medium. According to Janini et al. [15], an increase in the viscosity of the medium, η, resulting from the addition of organic solvents, leads to a decrease in μ_{ep}. The effect on μ_{ep} also depends on the charge and size of the solute.

(ii) The influence of organic solvents on the migration can also occur through the ion–dipole bonds that exist between a charged ion and a polar solvent molecule. The solvated cations are altered in geometry and therefore their movement in the electrical field is slowed. According to Freiser [21], depending on the specific properties of the ions and the solvent molecules, the size and type of solvation shell around the ions will differ and therefore the mobilities of the ions are altered differently. The ultimate result is a maximization of the separation due to the increased mobility difference.

(iii) There is an alternative view on the effect of the solvents. Methanol has a lower dielectric constant than water. The lower the dielectric constant of a medium, the easier it is for ions to be associated in the medium. This means that a complexation reaction, where charge neutralization occurs, will be favoured by a decrease in the dielectric constant, and the formation of high-degree complexes, e.g., $M(HIBA)_2^0$, can be promoted. This then decreases the cation mobility and provides an additional possibility for improving the separation.

3.3. Effect of 18-crown-6

K^+ and NH_4^+ have almost the same mobility, which is not significantly affected by HIBA and methanol. Two approaches have been used to facilitate their separation, increasing the pH of the BGE to decrease the mobility of NH_4^+ [24] or employing inclusion complexation by adding 18-crown-6 [12,13]. Fig. 6 shows the variation of the cation mobility as the concentration of 18-crown-6 changes from 0 to 2.7 m*M*, at 6.5 m*M* HIBA, pH 4.5 and 20% (v/v) methanol. A sharp decline in the mobility of K^+, Sr^{2+} and Ba^{2+} is observed. The effect of the crown ether is the most significant for Ba^{2+}, with the most rapid decrease in the Ba^{2+} mobility occurring when the concentration of the complexing reagent changes from 0 to 0.5 m*M*. Except for K^+, which shows a strong dependence on 18-crown-6 over the whole concentration range, the mobilities of Sr^{2+} and Ba^{2+} change less if more than 1 m*M* of 18-crown-6 is present in the BGE. The mobilities of the other cations are not significantly affected.

The effect of 18-crown-6 on the cations can be attributed to the fact that the oxygen of the reagent carries unshared pairs of electrons, through which cations are strongly solvated. This

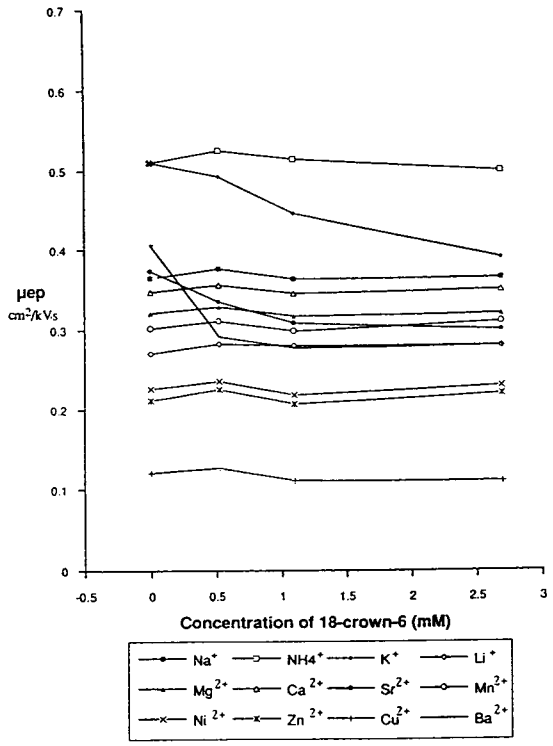

Fig. 6. Dependence of the ionic mobility μ_{ep} on the concentration of 18-crown-6. 2 μg/ml each of NH_4^+, K^+, Na^+, Li^+, Mg^{2+}, Ca^{2+}, Sr^{2+}, Ba^{2+}, Mn^{2+}, Ni^{2+}, Zn^{2+} and Cu^{2+}. Experimental conditions: applied voltage, +20 kV; hydrostatic injection from 10 cm height for 30 s; BGE, 5 m*M* imidazole–6.5 m*M* HIBA–20% (v/v) methanol at pH 4.5.

leads to a new cation with a much larger size, which therefore moves more slowly than the bare cation in an electrical field. The stability of the newly formed cation depends on the fit between the ionic diameter of the cation and the cavity diameter of the crown ether. As reported [25], 18-crown-6 has a cavity diameter of 2.7 Å, which closely matches the ionic diameter of Ba^{2+}, 2.68 Å. Therefore Ba^{2+} can be tightly held by 18-crown-6. With a low concentration of 18-crown-6 present in the BGE, most of the Ba^{2+} is complexed. Therefore, its mobility changes only slightly when the concentration of 18-crown-6 is further increased. K^+ and Sr^{2+} have ionic diameters of 2.66 and 2.24 Å, respectively [26], and log $\beta = 3.87$ for Ba^{2+}, 2.72 for Sr^{2+} and 2.03 for K^+ [27]. 18-Crown-6 was not found to produce a significant effect on the μ_{eof} because methanol is the predominant factor in determining μ_{eof}. This conclusion is based on a statistical estimation of main effects on the EOF. The concentrations of HIBA and 18-crown-6 and also methanol were changed simultaneously according to the 2^3 full factorial design [28]. The statistical results are given in Table 2. Only the methanol effect is significant at $\alpha = 0.05$. No interaction effects were found. This also agrees with the previous observation: as shown in Fig. 2, with more than 2 m*M* present in the BGE, the HIBA effect on μ_{eof} approaches a constant, whereas the effect of methanol on μ_{eof} is significant, as shown in Fig. 5.

3.4. Description of electrophoretic behaviour and prediction of the optimum separation

Using the preceding relationship, it is possible to find an optimum combination of the experimental parameters. As we have seen from

Table 2
Statistics for the evaluation of the main effects of μ_{eof}

Effect	Estimate	Mean square	Variance ratio
HIBA	−0.0018	0.0000	
Crown	0.0040	0.0000	
Methanol	−0.0287	0.0016	$27.28 > F_{0.05,1,4} = 7.7$[a]
HIBA/crown	−0.0046	0.0000	
HIBA/methanol	−0.0049	0.0000	
Crown/methanol	0.0024	0.0000	
HIBA/crown/methanol	−0.0084	0.0001	

[a] The value is larger than the critical *F* value, so that only the effect of methanol on μ_{eof} is statistically significant.

Fig. 6, the optimum separation conditions are located around 0.5 m*M* 18-crown-6 with 6.5 m*M* HIBA, 20% methanol and pH 4.5. An alternative approach is to apply experimental design and we wanted to investigate whether such an approach is feasible in this context and also if it would confirm our earlier findings.

In this set of experiments, dilute H_2SO_4 was replaced with dilute HCl for adjustment of the pH of the BGE because of the better solubility of chlorides than sulfates. Also, we intended to study the mobility dependence on HIBA without the presence of H_2SO_4 to confirm our previous explanation concerning the effect of HIBA and H_2SO_4.

A central composite design [28] was applied to select experimental points. The experimental set-up was composed of fifteen experimental runs, in each of which two to five injections were performed to calculate the mean of the cation mobility. The concentration of HIBA varied from 2 to 6.5 m*M*, methanol from 10 to 20% and 18-crown-6 from 0.5 to 2.0 m*M*. The structure of the design is given in Table 3. For each cation, the effective mobility was calculated using the following equation:

$$\mu_{ep} = \frac{L_t L_d}{V}\left(\frac{1}{t} - \frac{1}{t_0}\right) \quad (2)$$

Table 3
Central composite design for three factors at three levels

Run	Design matrix	HIBA (m*M*)	18-Crown-6 (m*M*)	Methanol (%, v/v)
1	0,0,0	4.25	1.25	15
2	1,1,1	5.85	1.78	18.5
3	−1,−1,−1	2.65	0.72	11.5
4	1,1,−1	5.85	1.78	11.5
5	−1,−1,1	2.65	0.72	18.5
6	1,−1,−1	5.85	0.72	11.5
7	−1,1,−1	2.65	1.78	11.5
8	1,−1,1	5.85	0.72	18.5
9	−1,1,1	2.65	1.78	18.5
10	1.414,0,0	6.5	1.25	15
11	−1.414,0,0	2	1.25	15
12	0,1.414,0	4.25	2	15
13	0,−1.414,0	4.25	0.5	15
14	0,0,1.414	4.25	1.25	20
15	0,0,−1.414	4.25	1.25	10

where L_t is the total length of the capillary, L_d the distance from the injector to the detector, V the applied voltage, t the migration time of the analyte cation and t_0 the migration time of water, which is used as the marker of EOF.

The modelling assumes a mathematical equation which relates the cation mobility (μ_{ep}) to the concentrations of HIBA (C_{HL}), 18-crown-6 (C_{crown}) and methanol ($C_{Me.}$):

$$\begin{aligned}\mu_{ep} = {} & k_0 + k_1 C_{HL} + k_2 C_{crown} + k_3 C_{Me.} \\ & + k_{12} C_{HL} C_{crown} + k_{13} C_{HL} C_{Me.} \\ & + k_{23} C_{crown} C_{Me.} + k_{11} C_{HL}^2 \\ & + k_{22} C_{crown}^2 + k_{33} C_{Me.}^2 \end{aligned} \quad (3)$$

where k represents the empirical parameter. The subsequent statistical evaluation by the SPSS program [17] gives the significant coefficients for individual cations,which are listed in Table 4. For all the cations, k_0 is significant. For NH_4^+, Li^+ and Na^+, only k_3 is significant. The fact that k_1 and k_2 are not significant is because there is no complexation between these cations and HIBA or 18-crown-6. For Mg^{2+}, Ca^{2+}, Mn^{2+}, Ni^{2+} and Zn^{2+}, k_1 and k_3 are significant. The coefficient k_{13} is never significant, indicating the absence of an interaction effect between HIBA and methanol. As we use HCl for electrolyte pH adjustment, a negative linear dependence of the mobilities of the alkaline earth and transition

Table 4
Significant coefficients for individual cations in Eq. 4

Cation	k_0	k_1	k_2	k_3	k_{22}
NH_4^+	0.6332			−0.0073	
Li^+	0.3786			−0.0052	
Na^+	0.4696			−0.0055	
K^+	0.6437		−0.0371	−0.0088	
Sr^{2+}	0.5047		−0.0619	−0.0070	−0.0163
Ba^{2+}	0.4302		−0.0449	−0.0055	0.0149
Mg^{2+}	0.4860	−0.0059		−0.0063	
Ca^{2+}	0.5341	−0.0083		−0.0067	
Mn^{2+}	0.4906	−0.0082		−0.0067	
Ni^{2+}	0.4935	−0.0185		−0.0067	
Zn^{2+}	0.5013	−0.0212		−0.0069	

$\mu_{ep} = k_0 + k_1 C_{HL} + k_2 C_{crown} + k_3 C_{Me.} + k_{22} C_{crown}^2$. C_{HL} and C_{crown} are in m*M* and $C_{Me.}$ in % (v/v).

metal cations on the HIBA concentration is obtained. This is different from the results in Fig. 1 with H_2SO_4 which has been explained by the competition between HIBA and sulfate for the cations. Therefore, our previous explanation that sulfate, introduced by titration, serves as a complexing reagent has been confirmed by the experiments.

For K^+, Sr^{2+} and Ba^{2+}, k_2 and k_3 are significant and for the later two k_{22} is also important for a more accurate mobility prediction. Again, the interaction effects k_{12}, k_{13} and k_{23} are not significant. Therefore, Eq. 3 can be simplified to

$$\mu_{ep} = k_0 + k_1 C_{HL} + k_2 C_{crown} + k_3 C_{Me.} + k_{22} C^2_{crown} \quad (4)$$

In most instances, a linear model is sufficient for the description of ionic mobility as a function of the system parameters. For Sr^{2+} and Ba^{2+}, an additional polynomial coefficient is included. The usefulness of the model for the optimization will be examined. The mobility of Cu^{2+} was not modelled because it moves much more slowly than the others and will not cause any problem in the separation.

The absolute value of $\Delta\mu_{min.}$ was used as the criterion to search for the optimum experimental conditions. This is a more suitable criterion in our case than the α value (ratio of the migration times for two adjacent peaks) because peak cross-over is expected. Two neighbouring cations can be well resolved when their mobility difference is at least 0.005. Using the mobility equations given in Table 4, the mobility of each cation in the whole experimental domain is predicted. At each set of experimental conditions, the minimum mobility difference between each pair of cations was obtained, and consequently the maximum of the minimum within the whole experimental area was found. The maximum separation (maximum $\Delta\mu_{min.}$) is always achieved at HIBA $\approx$ 6.5 m*M*. This means that the highest HIBA concentration should be used. However, as mentioned previously, the concentration is restricted. In the subsequent experiments, the HIBA concentration was set at 6.5 m*M*. Two optimum domains are obtained, which are shown in Fig. 7. Two sets of experimental

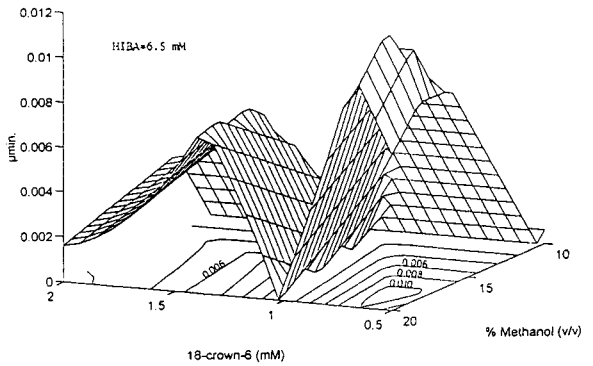

Fig. 7. Response surface for minimum differences in mobility ($\Delta\mu_{min.}$).

conditions were selected from the two domains, namely HIBA = 6.5 m*M*, methanol = 20% and 18-crown-6 (a) 0.53 m*M* (found also by the preliminary experiments) or (b) 1.33 m*M*.

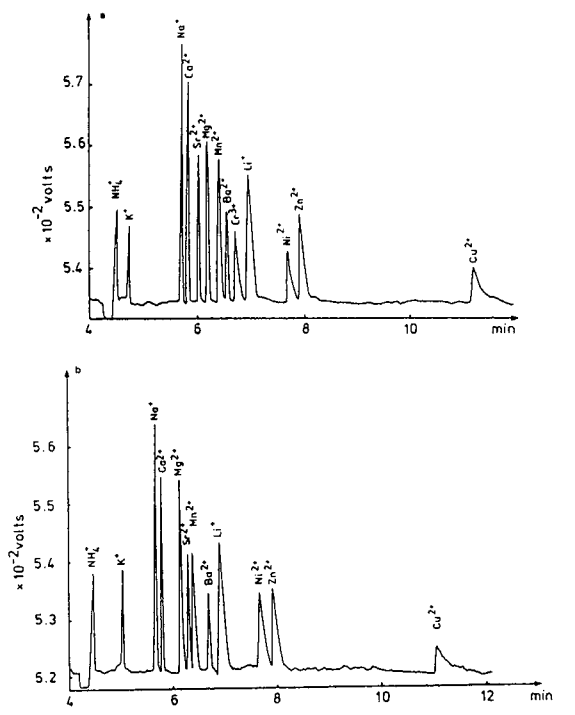

Fig. 8. Separation of a mixture containing NH_4^+, K^+, Na^+, Li^+, Mg^{2+}, Ca^{2+}, Cr^{3+} (2 μg/ml), Sr^{2+}, Ba^{2+}, Mn^{2+}, Ni^{2+}, Zn^{2+} (4 μg/ml) and Cu^{2+} (6 μg/ml). Experimental conditions: applied voltage, +20 kV; hydrostatic injection from 10 cm for 20 s; $I \approx 6.0$ μA; $T \approx 23$°C; BGE, 5 m*M* imidazole–6.5 m*M* HIBA–20% (v/v) methanol at pH 4.5 with (a) 0.53 and (b) 1.33 m*M* 18-crown-6.

Fig. 8a shows the separation of a mixture containing thirteen inorganic cations performed under the two sets of experimental conditions. Baseline separation for all the cations is achieved under conditions (a). One additional cation, Cr^{3+}, is also well resolved. Fig. 8b shows the separation performed under conditions (b). Simultaneous separation of the twelve cations is obtained. It is noted that sometimes the ammonium ion appears with the system peak, but this is not the case in the samples. A good linear relationship was obtained between the peak area and the concentration of ammonium ions. In this BGE system, ammonium ions do not interfere in the determination of potassium.

There is good agreement between the predicted and experimental mobilities as shown in Fig. 9.

3.5. Practical applicability of the selected BGE system

The practical applicability of the selected BGE was investigated by separating ions in different types of Chinese tea infusions under the optimum conditions. Good separation was achieved for all the samples. In Fig. 10a, an electropherogram of a green tea infusion is shown; five metal cations, K^+, Na^+, Ca^{2+}, Mg^{2+} and Mn^{2+}, are detected. Fig. 10b shows an electropherogram for the separation of ions in the tea sample spiked with ammonium nitrate, NH_4^+ and K^+ being well separated.

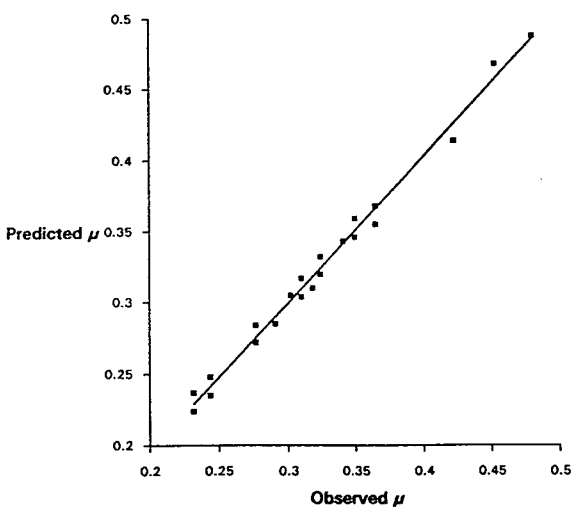

Fig. 9. Correlation plot of observed and predicted ionic mobilities of the cations under the two optimum experimental conditions (μ in $cm^2/kV \cdot s$). The correlation coefficients (R^2) is 0.992. The line represents the case of perfect correlation.

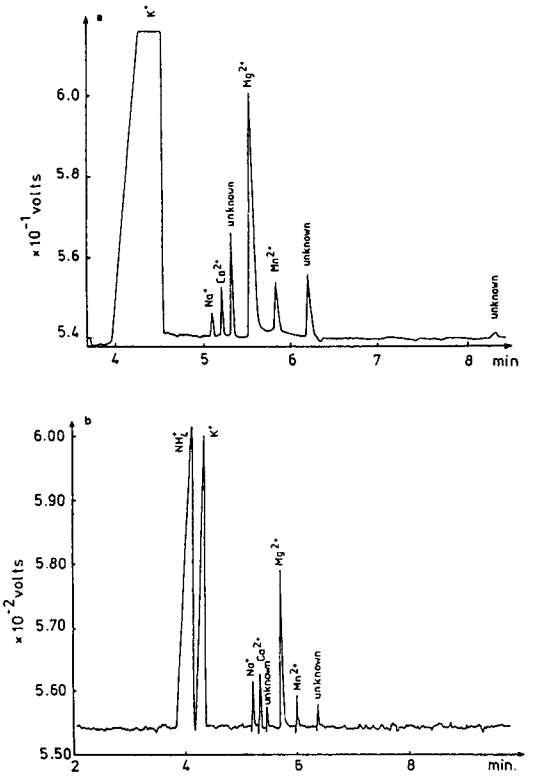

Fig. 10. Separation of Chinese green tea infusion. (a) Twofold dilution of green tea infusion; (b) 600-fold dilution of green tea infusion containing 1 μg/ml of NH_4^+. Experimental conditions: applied voltage, +20 kV; electromigration injection, 30 kV for 10 s; $I \approx 6.0$ μA; $T \approx 23$°C; BGE, 5 m*M* imidazole–6.5 m*M* HIBA–20% (v/v) methanol–0.53 m*M* 18-crown-6 at pH 4.5.

3.6. Limit of detection

CZE separation is very efficient for a variety of substance types. The limit of detection attainable with the generally used UV detector is restricted, however. Sample injection by electromigration allows better results than hydrostatic injection. Therefore, we checked the limits of detection (LODs) with electromigration injec-

tion at 20 kV for 30 s. The LODs based on three times the baseline noise are as follows: 0.4 μg/l for Li^+ and Mg^{2+}, 1 μg/l for NH_4^+ and Ca^{2+}, 2.5 μg/l for Na^+, 10 μg/l for K^+, 120 μg/l for Sr^{2+}, Mn^{2+}, Cr^{3+} and Zn^{2+}, 500 μg/l for Ba^{2+} and Ni^{2+} and 1000 μg/l for Cu^{2+}.

As observed in our experiments, the improvement in detectability with electromigration injection has a greater impact on those cations which move faster. For a slowly moving cation such as Cu^{2+}, no significant effect was found.

Acknowledgements

The authors thank P. Fernandes de Aguiar for assistance with the calculation of parameters. A. Vander Straeten is gratefully acknowledged for technical assistance. The Diensten voor Programmatie van het Wetenschapsbeleid are thanked for financial support.

References

[1] P. Jandik, W.R. Jones, A. Weston and R.P. Brown, *LC·GC*, 5 (1991) 20.
[2] D.F. Swalle and M.J. Sepaniak, *Anal. Chem.*, 63 (1991) 179.
[3] K. Saltoh, C. Klyohara and N. Suzuki, *Anal. Sci.*, 7 (1991) 269.
[4] K. Saltoh, C. Klyohara and N. Suzuki, *J. High Resolut. Chromatogr.*, 14 (1991) 245.
[5] K. Fukushi and K. Hiiro, *J. Chromatogr.*, 523 (1990) 28.
[6] F. Foret, S. Fanali, A. Nardi and P. Bocek, *Electrophoresis*, 11 (1990) 780.
[7] A. Weston, P.R. Brown, A.L. Heckenberg, P. Jandik and R. Jones, *J. Chromatogr.*, 602 (1992) 249.
[8] S. Motomizu, S. Nishimura, Y. Obata and H. Tanaka, *Anal. Sci.*, 7 (1991) 253.
[9] W. Beck and H. Engelhardt, *Chromatographia*, 33 (1992) 313.
[10] Q. Yang, M. Jimidar, T. Hamoir, J. Smeyers-Verbeke and D.L. Massart, *J. Chromatogr.*, 673 (1994) 275.
[11] Y.C. Shi and J. Fritz, *J. Chromatogr.*, 640 (1993) 473.
[12] K. Bächmann, J. Boden and I. Haumann, *J. Chromatogr.*, 626 (1992) 259.
[13] W. Beck and H. Engelhardt, *Fresenius' Anal. Chem.*, 346 (1993) 618.
[14] R. Kuhn, F. Stoecklin and F. Erni, *Chromatographia*, 33 (1992) 32.
[15] G.M. Janini, K.C. Chan, J.A. Barnes, G.M. Muschik and H.J. Issak, *Chromatographia*, 35 (1993) 497.
[16] C. Schwer and E. Kenndler, *Anal. Chem.*, 63 (1991) 180.
[17] *SPSS/PC+ Statistics 4.0*, SPSS, IL, 1990.
[18] J. Inczédy, in J. Tyson (Editor), *Analytical Application of Complex Equilibria*, Ellis Horwood, Chichester, 1976, p. 347.
[19] R.C. Weast (Editor), *CRC Handbook of Chemistry and Physics*, CRC Press, Boca Raton, FL, 67th ed., 1986, p. F87.
[20] I.M. Johnasson, E.C. Huang, J.D. Henion and Z. Weigenbaum, *J. Chromatogr.*, 554 (1991) 331.
[21] H. Frieser, *Concepts and Calculations in Analytical Chemistry —A Spreadsheet Approach*, CRC Press, Boca Raton, FL, 1992, Ch. 2, p. 34.
[22] O.A. Shpigun and Yu.A. Zolotov, *Ion Chromatography in Water Analysis*, Ellis Horwood, Chichester, 1988, Ch. 10, p. 148.
[23] Y. Xu, *Anal. Chem.*, 65 (1993) 425R.
[24] A. Weston, P.R. Brown, P. Jandik, W.R. Jones and H. Heckenberg, *J. Chromatogr.*, 593 (1992) 289.
[25] R.T. Morrison and R.N. Boyd, *Organic Chemistry*, Allyn & Bacon, Boston, MA, 5th ed., 1987, Ch. 6, p. 223.
[26] K.D. Altria and C.F. Simpson, *Anal. Proc.*, 23 (1986) 453.
[27] R.M. Smith and A.E. Martell, *Critical Stability Constants*, Plenum Press, New York, 1975.
[28] E. Morgan, *Chemometrics: Experimental Design*, J. Wiley, Chichester, 1991.

ELSEVIER

Journal of Chromatography A, 688 (1994) 350–356

JOURNAL OF CHROMATOGRAPHY A

Short communication

Neutral carrier-based ion-selective electrode with similar sensitivity to different monovalent cations as a detector in ion chromatography

Kyung-Hee Kwon[a], Ki-Jung Paeng[a], Dong Kwon Lee[b], Ihn Chong Lee[b], Uk Sun Hong[c], Geun Sig Cha[c,*]

[a]*Department of Chemistry, Yonsei University, Wonju 222-701, South Korea*
[b]*Department of Chemistry, Hallym University, Chunchon 200-702, South Korea*
[c]*Department of Chemistry, Kwangwoon University, 447-1 Wolgye-Dong, Nowon-Ku, Seoul 139-701, South Korea*

First received 10 May 1994; revised manuscript received 5 October 1994

Abstract

A variety of neutral carrier-type ionophores were employed to prepare cation-selective electrodes for use as a detector in single-column ion chromatography. A polymer membrane electrode doped with a new siloxane-based bis-crown ether exhibited similar selectivity to ammonium and all alkali metal ions except lithium. The lithium ion selectivity was induced by further incorporating an appropriate amount of lithium ionophore ETH 1810 into the bis-crown ether-doped membrane. A single-ionophore membrane electrode doped with monensin methyl ester, known as a sodium ionophore, was shown to exhibit the most comparable sensitivity towards all alkali metal ions and ammonium ion.

1. Introduction

There is a growing interest in polymer membrane ion-selective electrodes (ISEs) to be used in flow-through detectors in ion chromatography (IC) [1–7]. These devices may offer the advantages of rapid and reproducible response, low detection capabilities, and ease of fabrication and miniaturization. Unlike conductometric detectors, the response of the potentiometric ISE detectors does not depend on the area of the electrode [4]. This will be a useful property in situations where a small detector is necessary, such as in capillary IC.

However, direct application of common potentiometric membrane electrodes to IC systems does not allow the detection of different ions with comparable detectabilities. Most of these ISEs are highly selective for specific ions, and exhibit negligible response toward other ionic species. Therefore, the design of ISEs with similar selectivity to many different ions is one essential aspect in the use of such potentiometric detectors for chromatographic applications. Recently, several research groups have examined various approaches to employ neutral carrier-based ISEs in chromatographic detectors [1–7]. For instance, four different cation ionophores (i.e., valinomycin, benzo-15-crown-5, nonactin and tetranactin) were examined to prepare chro-

* Corresponding author.

0021-9673/94/$07.00
SSDI 0021-9673(94)00963-5

matographic ISE detectors [1]. In this study, single-ionophore membrane electrodes were prepared by incorporating each of these ionophores into poly(vinyl chloride) (PVC)-matrix membranes and employed as monovalent cation detectors in IC. Of these neutral carriers, tetranactin provided a membrane with the most similar sensitivity to alkali metal and ammonium ions. Another effort to balance the detectability of different ions includes the use of multiion-selective membranes incorporating several different ionophores [5,6]. The detection characteristics of the multiionophore membranes are controlled by the amounts and ratios of the ionophores incorporated in the membranes.

The aim of this work is to examine a wider range of neutral carrier-doped ISEs as monovalent cation detectors in IC. These neutral carriers include compounds known as sodium ionophores (i.e., ETH 157, ETH 2120, Fluka sodium ionophore VI and monensin methyl ester), lithium (ETH 1810), ammonium (nonactin) and potassium (valinomycin) ionophores, crown ethers (dibenzo-18-crown-6, benzo-18-crown-6 and benzo-15-crown-5), and a siloxane-based bis-crown ether recently synthesized by Chang and Kim [8].

2. Experimental

2.1. Reagents

PVC, bis(2-ethylhexyl) adipate (DOA), 2-nitrophenyl octyl ether (NPOE), potassium tetrakis(*p*-chlorophenyl) borate (KTpClPB), nonactin, N,N′-dibenzyl-N,N′-diphenyl-1,2-phenylenedioxydiacetamide (ETH 157), N,N,N′,N′-tetracyclohexyl-3-phenylenedioxydiacetamide (ETH 2120), bis[(12-crown-4)methyl] dodecylmethyl malonate (sodium ionophore VI), N,N-dicyclohexyl-N′,N′-diisobutyl-*cis*-cyclohexane-1,2-dicarboxamide (ETH 1810), and benzo-15-crown-5 were obtained from Fluka (Switzerland). Monensin methyl ester was purchased from Calbiochem-Novabiochem (La Jolla, CA, USA) and valinomycin from Sigma (St. Louis, MO, USA). A new bis-crown ether compound connected through a siloxane chain, 1,1,3,3,5,5-hexamethyl-1,5-dipentaoxacyclohexadecamethyl trisiloxane (BCE 11), was a gift from Professor Seung Hyun Chang, Taegu University, South Korea. It was prepared according to the procedure published previously elsewhere [8].

All other chemicals used were analytical-reagent grade. Standard solutions and buffers were prepared with the use of deionized water.

2.2. Ion-selective membrane electrodes

The polymeric membrane composition was 1% (w/w) neutral carrier, 33% (w/w) PVC and 66% (w/w) plasticizer (DOA or NPOE) except the membrane for sodium ionophore VI [6.5% (w/w) ionophore, 26.8% (w/w) PVC and 66.7% (w/w) plasticizer]. DOA was used for membranes doped with valinomycin, nonactin, ETH 159 and ETH 2120, and NPOE for membranes with ETH 1810, sodium ionophore VI, monensin methyl ester, benzo-15-crown-5 and BCE 11. Membranes with monensin methyl ester and ETH 1810 further incorporated 0.35 and 0.4% (w/w) of KTpClPB, respectively.

All membranes were cast as described elsewhere [9]. Smaller disks were punched from the cast films and mounted in Philips electrode bodies (IS-561; Glasbläserei Möller, Zürich, Switzerland). For all types of electrodes, 0.1 *M* KCl was employed as the internal filling solution. The external reference electrode was an Orion sleeve-type double junction Ag/AgCl electrode (Model 90-02).

Initial potentiometric evaluation of various membranes was conducted by employing a static arrangement. Electrodes were connected through a high impedance amplifier to an IBM AT-type computer equipped with an analog-to-digital converter. The cell potentials were measured at ambient temperature (22°C) by immersing ISEs and the reference electrode in a beaker containing 200 ml of the working buffer (0.05 *M* Tris–HCl, pH 7.2), and the calibration data were obtained from additions of standard solutions. The solutions were magnetically stirred through-

out and equilibrium potentials were recorded. Selectivity coefficients were determined by using the separate solution-matched potential method [10–12] at an interfering cation concentration of 0.1 *M*. The detection limits of the membrane electrodes were obtained from the calibration curves as described elsewhere [10].

2.3. Ion chromatography

Chromatographic measurements were carried out using a HPLC pump (Model CCPD; Tosoh, Japan), a sample injector (Model 7125; Rheodyne, Cotati, CA, USA) equipped with a 20-μl sample loop, a cation separation column (Shodex IC Y-521; Showa Denko, Tokyo, Japan), a column heater (CH-30; Eppendorf North America, Madison, WI, USA), and an ISE detector. The design used for incorporating ISEs into a flow-through detection unit was a large volume wall-jet cell electrode design described elsewhere [6,13]. In addition to the HPLC pump, a peristaltic pump (Ismatech Model 7331-00, Zürich, Switzerland) was placed behind the outlet of the column to help maintain a constant level of effluent in the wall-jet detector cell. Electrodes were connected to an Accumet pH-mV meter (Model 925; Fisher Scientific, Romulus, MI, USA), and analog outputs were recorded on an integrator (HP 3394A; Hewlett-Packard, Avondale, PA, USA).

The eluent used was 2 m*M* nitric acid, and the column temperature was maintained at 40°C. For an optimal performance of the wall-jet electrode detector, the eluent stream (1.5 ml/min) from the outlet of the column was merged with a buffer stream (2.0 ml/min) of 0.05 *M* Tris–HCl, pH 9.0 and through a coiled length (35 cm × 0.81 mm I.D.) of PTFE tubing to the detector.

3. Results and discussion

Preliminary potentiometric evaluation of membranes doped with various types of neutral carriers was conducted by employing the static arrangement. Table 1 summarizes the results. For comparison purposes, the data values are presented with respect to potassium (i.e., as the primary ion) for all types of membranes. The more positive the value of log $k^{pot}_{K^+,j}$ [10], the greater the electrode's response for the interfering ion. When the value of log $k^{pot}_{K^+,j}$ is zero, the membrane electrode exhibits equal sensitivity

Table 1
Electrochemical characteristics of cation-selective membranes doped with various types of neutral carrier

Neutral carrier	Slope (*mV/dec*)	Selectivity coefficient (log $k^{pot}_{K^+,j}$					*Detection limit* (*M*)
		Li^+	Na^+	NH_4^+	Rb^+	Cs^+	
Valinomycin	55.4	−4.96	−4.48	−2.01	0.42	−0.49	$7.4 \cdot 10^{-7}$
Nonactin	53.2	−4.13	−2.15	0.87	−0.60	−1.77	$3.0 \cdot 10^{-6}$
Dibenzo-18-crown-6	53.9	−4.86	−2.20	−1.79	−0.79	−0.22	$1.5 \cdot 10^{-6}$
Benzo-18-crown-6	49.1	−4.85	−2.21	−1.57	−1.01	−1.41	$2.5 \cdot 10^{-6}$
Benzo-15-crown-5	51.1	−3.54	−2.15	−1.62	−0.67	−1.15	$3.8 \cdot 10^{-6}$
ETH 157	43.1	−1.46	0.40	−0.63	−0.53	−0.94	$2.0 \cdot 10^{-5}$
ETH 2120	31.3	0.33	1.48	−0.25	−0.61	−0.41	$3.7 \cdot 10^{-5}$
Sodium ionophore VI	33.3	−1.28	1.87	−1.39	−0.38	−0.11	$2.6 \cdot 10^{-5}$
Monensin methyl ester	52.8	−0.28	0.79	−1.14	−0.88	−1.16	$4.9 \cdot 10^{-6}$
ETH 1810	24.0	2.71	0.35	−0.09	−0.09	0.09	$4.6 \cdot 10^{-5}$
BCE 11	52.1	−3.52	−1.07	−0.90	0.27	−0.82	$1.7 \cdot 10^{-6}$
BCE 11/ETH 1810[a]	50.9	−1.13	−0.96	−0.87	0.26	−0.85	$2.3 \cdot 10^{-6}$

Selectivity coefficients and detection limits calculated with respect to K^+ by employing a static arrangement (see the Experimental section and Refs. [10–12] for details).

[a] Prepared with 1% (w/w) of BCE 11 plus 1% (w/w) of ETH 1810.

toward the primary (potassium) and interfering ions. When the value of log $k^{pot}_{K^+,j}$ is positive, the electrode exhibits even greater response toward the interfering ion than toward potassium. Therefore, more universal non-selective chromatographic detectors can be devised with ISEs having their log $k^{pot}_{K^+,j}$ values closer to zero. In Table 1, the detectability of the electrode for different ions may be estimated roughly by comparing its selectivity coefficients, knowing the detection limit [10] of the electrode for potassium.

Valinomycin and nonactin are now commonly used for preparing potassium and ammonium-selective membrane electrodes, respectively. In addition to sodium ionophore VI, ETH 157, ETH 2120 and monensin methyl ester are used for sodium-selective electrodes, and ETH 1810 for lithium. The crown ether-type compounds have been examined for their cation selectivities, previously [7,14,15]. The selectivity values listed for the ionophores in Table 1 are in accordance with those previously reported elsewhere [11,16]. It can be seen that all neutral carriers resulted in membranes with a negligible response toward lithium, except monensin methyl ester which provided the membrane with similar sensitivity toward all monovalent cations including lithium.

The electrochemical properties of the PVC membranes doped with the siloxane-based bis-crown ethers such as 1,3-bis(trimethylsiloxyl)-1,3-dimethyl-1,3-dipentaoxacyclohexadecamethyl disiloxane (BCE 9) and BCE 11 have been reported previously [7]. Interestingly, the membranes doped with such bis-crown ether compounds as the ionophore exhibited quite a similar selectivity toward ammonium and all alkali metals except lithium. In this work, the BCE 11 membrane was employed for comparison purposes. When the BCE 11 membrane was further incorporated with ETH 1810 to induce selectivity toward lithium, the resulting BCE 11/ETH 1810 membrane achieved a comparable response toward all alkali metals and ammonium ion (see Table 1).

The use of multiple ionophores for a single membrane matrix is thought to be beneficial in that the selectivity of the membrane can be controlled by varying the types and amounts of ionophores incorporated [5,6]. The previous K^+/NH_4^+/Na^+/Ca^{2+} ion-selective membrane electrode employs four different ionophores (i.e., valinomycin, nonactin, ETH 2120 and ETH 129) [6]. Because of their different lipophilicity values, the ionophores in this membrane will leach at different rates, with the membrane lifetime being determined by the one which leaches most rapidly. Furthermore, different leach rates of the ionophores can alter the initial selectivity of such membrane electrodes since the selectivity of the multiple-ionophore membrane electrodes depends upon the amount and ratio of the ionophores present in the membrane phase. The BCE 11/ETH 1810 membrane employed in this study incorporates only two different ionophores for multiion selectivity. This membrane maintained its initial response slope and selectivity at least for 40 days when stored in buffer. The reproducibility of the characteristics in these multiion membranes seems to be a function of our ability to control the exact quantities of ionophores incorporated into the membrane phase, just as is the case in conventional single-ionophore membranes.

Fig. 1 compares typical ion chromatograms obtained by using ISE detectors with some of the membrane electrodes listed in Table 1. Potentiometric detection was carried out with the wall-jet flow-injection system described in the Experimental section. The chromatograms were obtained by injecting 20 μl of standard mixture containing monovalent cations (Li^+, Na^+, NH_4^+, K^+, Rb^+ and Cs^+) in an equal concentration of 1.0 m*M*. In this study, an additional buffer stream was merged with the eluent stream to help maintain a constant level of effluent in the wall-jet detector cell, and to increase the pH of the eluent stream for an optimal performance of the ISE detectors. It should be noted, however, that a post-column addition of buffer and a mixing coil employed in the experimental set-up will have an adverse effect on chromatographic efficiency (i.e., band dispersion, a reduced signal magnitude due to dilution, etc.).

In static measurements, the electrode response was reasonably rapid, with equilibrium reached

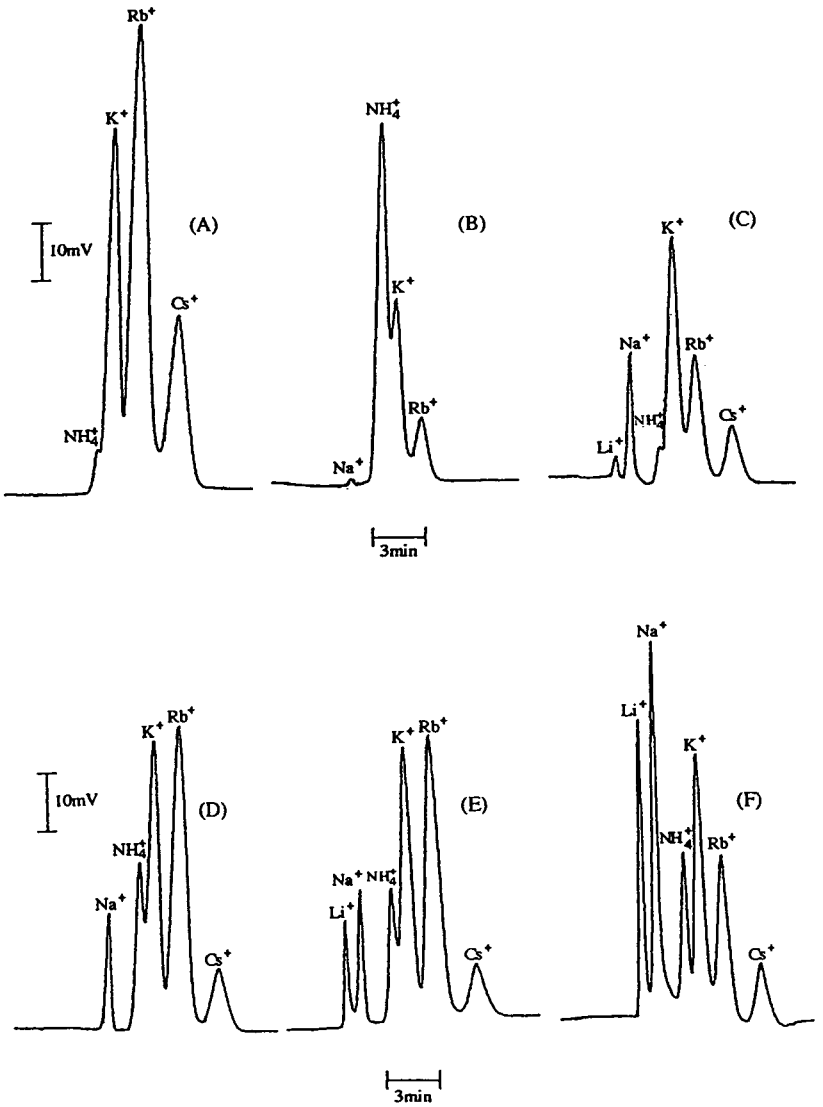

Fig. 1. Ion chromatograms obtained by using ISE detectors doped with (A) valinomycin, (B) nonactin, (C) benzo-15-crown-5, (D) BCE 11, (E) BCE 11 plus ETH 1810 and (F) monensin methyl ester: eluent, 2 m*M* HNO_3, pH 2.5, 1.5 ml/min; sample, 1.0 m*M* each cation (Li^+, Na^+, NH_4^+, K^+, Rb^+ and Cs^+); injection volume, 20 μl.

in less than 10 s; but a large tailing peak was observed in the chromatogram when a sample was injected at a very high concentration, but in most cases the response returned reasonably fast to the baseline level previously observed.

As can be seen in Fig. 1, the response magnitude of the detector was related basically to the selectivity sequences of the ISE employed. A significant response to Li^+ was observed only with the ISE detectors based on ETH 1810, BCE 11/ETH 1810 and monensin methyl ester. Compared to other single-ionophore detectors (e.g., valinomycin, nonactin, lithium and sodium ionophores except monensin methyl ester), all crown ether-based detectors showed better sensitivities toward most of the injected cations. Among the

detectors examined, the BCE 11/ETH 1810 and monensin methyl ester electrodes exhibited most balanced detectability for the cations. However, it should be mentioned that even a highly selective ISE system with less universal detection capability may prove useful for a particular application in IC. For instance, the chromatographic determination of Na^+ and K^+ in the human serum matrix (i.e., a high-sodium and low-potassium medium) was reported by Watanabe et al. [4], employing an ISE detector of which the selectivity is higher for K^+ and lower for Na^+.

It is a very common opinion that the logarithmic nature of the response limits the precision of the ISE measurements; a 4% error results from an uncertainty of ± 1 mV with a monovalent ion and 8% for a divalent ion. However, calibration curves of the ISE detector employed in this study were still quite useful because of their good reproducibility. The response of the electrodes doped with BCE 11/ETH 1820 or monensin methyl ester is linear when plotted against logarithmic concentrations of the monovalent cations.

Since the BCE 11/ETH 1810- and monensin methyl ester-based ISE detectors were found to provide universal detection capabilities for monovalent cations, the detection limits were estimated from the calibration plots obtained for the chromatographic system employed. The amplitude of the baseline noise (0.42 mV) was compared with the signal magnitude obtained for the injection of the examined ions. The evaluation was made by assuming that, in the range of small potential changes, the peak height is linearly related to the concentration of injected cations [1–4]. For a signal-to-noise ratio of 2 and a sample volume of 20 μl, the detection limits were as follows: BCE 11/ETH 1810-based, 28 μM (3.9 ng) for Li^+, 4.2 μM (1.9 ng) for Na^+, 21 μM (7.6 ng) for NH_4^+, 2.8 μM (2.2 ng) for K^+, 2.8 μM (4.8 ng) for Rb^+ and 42 μM (110 ng) for Cs^+; monensin methyl ester-based, 1.2 μM (0.17 ng) for Li^+, 0.42 μM (0.19 ng) for Na^+, 4.2 μM (1.5 ng) for NH_4^+, 2.8 μM (2.2 ng) for K^+, 4.2 μM (7.2 ng) for Rb^+ and 84 μM (220 ng) for Cs^+. In this study, no direct comparison was made between ISE and conductometric detection methods. However, it has been reported that, in certain instances, the detectabilities obtainable with potentiometric ISE detection are comparable to those with conductivity detection in single column (non-suppressed) chromatography [1,3,6]. The detectability obtained in this work, without any preconcentration step, is considered to be also satisfactory.

In summary, cation-selective electrodes doped with a variety of neutral carrier-type ionophores were examined for application in flow-through detectors in ion chromatography. The ISE detectors prepared with both monensin methyl ester and a new siloxane-based bis-crown ether compound achieved a comparable response for different alkali metal and ammonium ions. Such ISE detectors could be used as alternative detectors for eluting monovalent cations in IC.

Acknowledgement

We wish to thank Professor Seung Hyun Chang, Taegu University, South Korea for providing the bis-crown ether compounds used in this study. We gratefully acknowledge the Korea Science and Engineering Foundation for supporting this work.

References

[1] K. Suzuki, H. Aruga and T. Shirai, *Anal. Chem.*, 55 (1983) 2011.
[2] M. Trojanowicz, E. Pobozy and M.E. Meyerhoff, *Anal. Chim. Acta*, 222 (1989) 109.
[3] M. Trojanowicz and A. Ivaska (Editors), *Contemporary Electroanalytical Chemistry*, Plenum Press, New York, 1990, pp. 255–266.
[4] K. Watanabe, K. Tohda, H. Sugimoto, F. Eitoku, H. Inoue, K. Suzuki and S. Nakamura, *J. Chromatogr.*, 566 (1991) 109.
[5] Y.S. Park, M.J. Cha, S.H. Han, D.S. Shin, H.D. Kim and G.S. Cha, *J. Korean Chem. Soc.*, 37 (1993) 259.
[6] S.H. Han, K.S. Lee, G.S. Cha, D. Liu and M. Trojanowicz, *J. Chromatogr.*, 648 (1993) 283.
[7] D.K. Lee, I.C. Lee, J.Y. Kim, S.H. Chang, S.H. Han and G.S. Cha, *J. Korean Chem. Soc.*, 38 (1994) 529.

[8] S.H. Chang and J.Y. Kim, *J. Korean Chem. Soc.*, 38 (1994) 377.
[9] U. Wuthier, H.V. Pham, R. Zund, D. Welti, R.J.J. Funk, A. Bezegh, D. Ammann, E. Pretsch and W. Simon, *Anal. Chem.*, 56 (1984) 535.
[10] G.G. Guilbault, R.A. Durst, M.S. Frant, H. Freiser, E.H. Hansen, T.S. Light, E. Pungor, G. Rechnitz, N.M. Rice, T.J. Rohm, W. Simon and J.D.R. Thomas, *Pure Appl. Chem.*, 48 (1976) 129.
[11] Y. Umezawa, *Handbook of Ion-Selective Electrodes: Selectivity Coefficients*, CRC Press, Ann Arbor, MI, 1990.
[12] V.P.Y. Gadzekpo and G.D. Christian, *Anal. Chim. Acta*, 164 (1984) 279.
[13] W. Frenzel, *Analyst*, 113 (1988) 1039.
[14] G.A. Rechnitz and E. Eyal, *Anal. Chem.*, 44 (1972) 370.
[15] M. Mascini and F. Pallozzi, *Anal. Chim. Acta*, 73 (1974) 375.
[16] D. Ammann, P. Anker, P.C. Meier, W.E. Morf, E. Pretsch and W. Simon, *Ion-Sel. Electrode Rev.*, 5 (1983) 3.

ELSEVIER

Journal of Chromatography A, 688 (1994) 357–362

JOURNAL OF CHROMATOGRAPHY A

Short communication

Preparative isolation of the lectin jacalin by anion-exchange high-performance liquid chromatography

S. Giovanni De Simone[a,b,*], R. Santos[a], M.F. Araujo[a], R.T. Pinho[c]

[a]*Protein Microsequence Laboratory, Department of Biochemistry and Molecular Biology, Oswaldo Cruz Institute, Fiocruz, Avenue Brasil 4365, 21040-900 Rio de Janeiro, RJ, Brazil*

[b]*Department of Celular and Molecular Biology, Federal Fluminense University, Ni, Brazil*

[c]*Department of Immunology, Oswaldo Cruz Institute, Fiocruz, Rio de Janeiro, RJ, Brazil*

First received 27 July 1993; revised manuscript received 20 September 1994

Abstract

The lectin jacalin from *Artocarpus integrifolia* was purified to homogeneity in a single step by preparative anion-exchange high-performance liquid chromatography (HPLC). Selection of the optimum chromatographic parameters in gradient elution allowed a rapid procedure to be obtained for the qualitative and quantitative isolation of the most important α- and α'-jacalin components. A recovery of 27–33% was obtained from a total soluble extract using a polyacrylate–DEAE HPLC column. The identities of the two isolated polypeptides were established by N-terminal amino acid sequence analysis and from the IgA_1 binding lectin activity.

1. Introduction

The biological and selective stimulation of T- and B-cell functions of the α-D-galactose-specific lectin jacalin isolated from jack fruit seeds were first described by Bunn-Moreno and Campos-Neto [1] and Roque-Barreira and Campos-Neto [2]. This interesting lectin displays a 200-fold preference for the α-anomer over the β-anomer, a property not observed in the other α-galactoside binding lectins [3]. It binds very strongly to the CD4-bearing T-lymphocytes Galβ1–3GalNAc [4], the Thomsen–Friedenreich tumour-associated antigen Galβ1–3GalNAc·Ser [5] and specifically to human IgA_1 subclass [6] and IgA from several mammalian species [7] except mice and rat [8].

Several previous studies [3,9,10] have indicated that the lectin is tetrameric and bivalent, with no interaction between the two binding sites [5] and contains 3% of neutral sugars [3]. However, recent structural and electron microscopic analysis suggest that in addition to the α- and α'-chains, the lectin contains three distinct types of non-covalently associated polypeptides (β-subunits) with 20 amino acids forming an M_r 65 000 tetrameric protein [11]. Although its quaternary structure is still controversial, jacalin is present to the extent of 30–56% in jack fruit seeds [2,8]. Its isolation in a pure state is tedious and time-consuming, involving affinity chromatography on an IgA-Sepharose column [1,2], Minileak–melibiose [12] or cross-linked guar

* Corresponding author. Address for correspondence: Protein Microsequence Laboratory, Department of Biochemistry and Molecular Biology, Oswaldo Cruz Institute, Fiocruz, Avenue Brasil 4365, 21040-900 Rio de Janeiro, RJ, Brazil.

0021-9673/94/$07.00
SSDI 0021-9673(94)00907-4

gum [5] followed by one or more chromatographic steps by ion-exchange chromatography [11,13] and partition chromatography or analytical C_4 reversed-phase high-performance liquid chromatography (HPLC) [14].

As the lectins may serve as useful probes in cell biology and isolation and in the characterization of carbohydrate-containing macromolecules, we decided to develop a simple procedure for the isolation of the active jacalin compounds by direct preparative HPLC. We employed a DEAE column and a gradient of NaCl (0–0.3 *M*) in 10 m*M* phosphate buffer (pH 7.4).

The N-terminal amino acid sequence data are in excellent agreement with recently published work [11,15]. The described HPLC method has certain advantages over some other reported chromatographic methods and it is suitable for the qualitative and quantitative recovery of jacalin in total *Artocarpus integrifolia* extract preparations.

2. Experimental

Preparative and analytical HPLC studies were carried out on Shimadzu (Kyoto, Japan) Model LC-7A and LC-6A systems, respectively, linked to a C-R6A data processor. A polyacrylate (PA)–DEAE (Shimpack PA–DEAE, 10 μm) anion-exchange column (10 cm × 20 mm I.D.) was used for preparative work and a Shimpack Diol 150 column (50 cm × 7.9 mm I.D.) for gel filtration analysis. The HPLC systems and the columns were obtained from Shimadzu. The peaks were detected with a Shimadzu SPD-7AV or SPD-6A detector at 280 nm.

2.1. Obtaining the lectin extract

Dried seeds of *A. integrifolia* were ground and suspended in 10 m*M* phosphate buffer (pH 7.2) containing 150 m*M* NaCl (PBS) for 16 h at 4°C (10%, w/v) [1]. The decanted supernatant was centrifuged at 2000 *g* for 20 min at 4°C and the supernatant solution was stored at −20°C.

2.2. Isolation of pure jacalin by preparative HPLC

A 250–600-mg amount of the phosphate extract residue was dialysed against 10 m*M* phosphate buffer (pH 7.4), centrifuged at 15 000 *g* to remove insoluble matter, concentrated through Amicon Centripep-10 microconcentrators, filtered and then injected into the preparative column and eluted with a gradient of 0–0.3 *M* NaCl. The flow-rate was adjusted to 5 ml min^{-1}. Under these conditions, seven peaks were obtained. A broad peak centred at 19.5–19.7 min was collected in two fractions (A and B) for further analysis.

2.3. Preparation of standard sample

Human IgA_1 (Behring Institut, Marburg, Germany) was covalently linked to Sepharose CL-4B (Pharmacia, Uppsala, Sweden) (5 mg of IgA_1 per ml of Sepharose) and a volume of 5 ml of PBS–jacalin extract was applied to a 4.0-ml column. The unbound material was collected by washing the column with PBS. The bound material was eluted with 0.8 *M* galactose in PBS, following which it was dialysed against PBS. The bound fraction was concentrated to 1 ml and compared with a sample isolated by DEAE HPLC.

2.4. Polyacrylamide gel electrophoresis and protein determination

Sodium dodecyl sulphate polyacrylamide gel electrophoresis (SDS-PAGE) was performed using 15% polyacrylamide gels in Laemmli buffers [16] under reducing conditions. The gels were stained with Coomassie Brilliant Blue. Bovine serum albumin (M_r 66 000), ovalbumin (M_r 45 000), carbonic anhydrase (M_r 29 000), soybean trypsin inhibitor (M_r 21 000) and lysozyme (M_r 14 500) were used as standards for the characterization of molecular mass. Protein concentration was determined according to the method of Lowry et al. [17] using serum albumin as a standard.

2.5. Isoelectricfocusing (IEF)

Analytical IEF was carried out in precast gels containing 5% polyacrylamide gel and 2% Biolyte 3–10 (Bio-Rad, Richmond, CA, USA). A 2-μl portion of a 5–8 mg ml^{-1} total jacalin extract, DEAE-purified protein and standard p*I* marker proteins (cytochrome *c*, lentil lectin, human haemoglobins a and c, equine myoglobin, human carbonic anhydrase, β-lactoglobulin B and phycocyanin) were applied to the gel. Focusing was performed in a Bio-Rad mini IEF cell (Model 111) at room temperature in a stepped fashion (100 V for 15 min, 200 V for 15 min and 450 V for 1 h). Gels were stained with Crocein Scarlet and Coomassie Brilliant Blue R-250.

2.6. Electroblotting and sequencing

For sequencing experiments, the DEAE–jacalin fractions A and B from peaks 2 and 3 were subjected to SDS-PAGE (15%) and the proteins were blotted on to a PVDF membrane (Bio-Rad) using a semi-dry blotting apparatus (Bio-Rad). After electroblotting, the blots were stained for 5–10 min with 0.1% (w/v) Coomassie Brilliant Blue R-250 in 50% (v/v) methanol and destained with 60% (v/v) methanol.

Amino-terminal amino acid sequence analysis were carried out on a Model PSQ-1 gas-phase protein sequence system, consisting of an Edman reaction unit, an on-line phenylthiohydantoin (PTH)-amino acid analyzer and a C-R4A chromatogram integrator (Shimadzu). Edman degradation was performed according to the standard programme supplied by Shimadzu. The released PTH-amino acid derivatives were identified using an on-line HPLC system (Model 6A) with a Wako-Pak WS-PTH column (250 × 4.6 mm I.D.) (Wako, Osaka, Japan). All separations of PTH-amino acids were performed in the isocratic mode, with 40% acetonitrile, 0.014% SDS and 20 m*M* sodium acetate buffer (pH 4.7) at a flow-rate of 1.0 ml min^{-1} and with detection at 269 nm.

The alignment of the α- and α'-chain sequences determined in this study was carried out on a VAX 800 computer using the FASTA program [18]. This program searchs regions of sequence similarities using the PAM250 matrix [19].

2.7. Double diffusion in agarose gel

The agarose plates for lectin precipitation analysis were prepared as described by radial immunodiffusion [20]. Briefly, the plates were incubated overnight at room temperature with 10 μl (2 μg) of human IgA and approximately 2 μg of each DEAE HPLC peak, concanavalin A (Sigma, St. Louis, MO, USA) and a rabbit serum anti-human IgA (Behring Institut), then washed for two days in PBS containing 0.2% NaN_3 at room temperature and stained with 0.25% Coomassie Brilliant Blue R in ethanol–acetic acid–water (5:1:5) for 5 min. The plates were destained in 35% (v/v) ethanol–10% (v/v) acetic acid and photographed.

2.8. Gel-filtration HPLC

An amount of 100–300 μg (20 μl) of the pooled DEAE chromatographic peak 2 (fractions A and B) was injected on to a Shinpack Diol 150 HPLC column, previously equilibrated in 50 m*M* phosphate buffer (pH 7.2), and the proteins were fractioned at a flow-rate of 1 ml min^{-1} for 28 min at 25°C. For molecular mass characterization the column was calibrated in the same buffer with β-galactosidase (*M*r 105 000), bovine serum albumin (M_r 66 000), carbonic anhydrase (M_r 29 000) and cytochrome *c* (M_r 12 400) (MW-GF-70 kit; Sigma).

3. Results and discussion

An HPLC column was used to purify to apparent homogeneity the lectin jacalin from seeds of *A. integrifolia* with high recovery, and the N-terminal sequences of the α- and α'-chains were determined. The purification procedure described here differs from those reported previously. The soluble protein extract obtained from 500 mg yielded 135–165 mg of purified jacalin with a recovery of 27–33% (relative to the

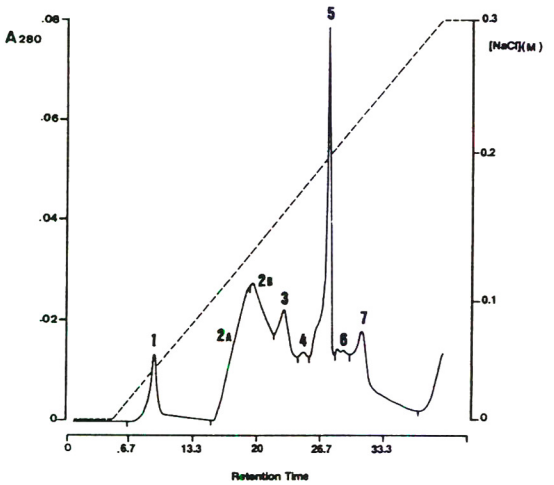

Fig. 1. High-performance anion-exchange chromatography on a DEAE preparative column (100 × 20 mm I.D.) of the crude PBS seed extract. Elutions were performed with a linear NaCl gradient from 0 to 0.3 *M* in 10 m*M* phosphate buffer (pH 7.4) at a flow-rate of 5 ml min^{-1}. Retention time in min.

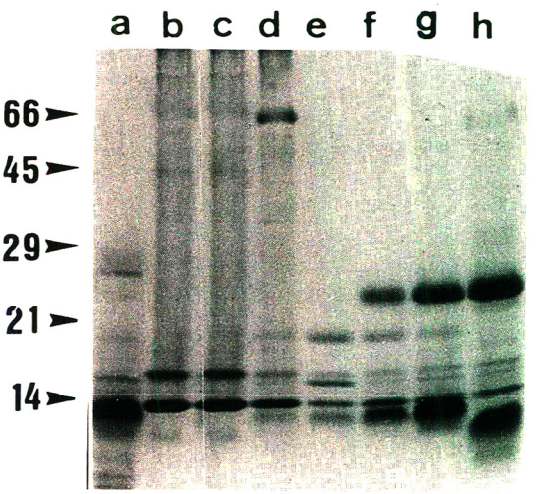

Fig. 2. SDS-PAGE (15%) analysis of pooled peaks from PA–DEAE (Fig. 1) columns followed by staining with Coomassie Brilliant blue. Lanes: a = crude PBS extract; b and c = fractions A and B, respectively, from peak 2; d–h = proteins from peaks 3–7, respectively. Approximately 50–70 μg of protein were applied in each slot. The values of the M_r standard [bovine serum albumin (66 000), ovalbumin (45 000), carbonic anhydrase (29 000), soybean trypsin inhibitor (21 500) and lysozyme (14 400)] are indicated on the left.

DEAE column). By passing the PBS-soluble material through the PA–DEAE column, several peaks were obtained (Fig. 1). Peak 2 (fractions A and B) contained proteins of M_r 12 000 and 15 000 (Fig. 2) and IgA_1 lectin binding activity (Fig. 3). SDS-PAGE analysis of the eluted proteins suggested that contaminating proteins with similar molecular mass that bind to the anion exchanger were eluted in subsequent peaks (Figs. 1 and 2). The apparent molecular masses of the α- and α'-chains were 12 000 and 15 000, respectively, by SDS-PAGE (Fig. 2) and gel filtration (Fig. 4). This difference in molecular mass has been attributed to different degrees of glycosylation [11].

Although previous workers [21] observed a considerable p*I* range for the lectin jacalin, our analysis of peak 2 (fractions A and B) containing protein showed only a band with p*I* 7.0–7.2 (Fig. 5). Whether this difference reflects a genetic variation or different degree of purification remains to be determined.

The partial amino N-terminal sequence (GKAFDDGAFTGIREINLSYNKETAIGDFQ-VVYDLNGSPYVGQNHISFI) of the first 48 amino acids of both chains revealed a very high degree of homology (initial amount loaded 100 pmol; repetitive yield 95–96%) with the jacalin α- and α'-chains confirming recently published data sequences results [9,10], except that in position 45 the lysine (K) was replaced by isoleucine (I).

The band with a similar molecular mass (12 000) that appears at peak 3 (Fig. 2, lane d) presented a distinct N-terminal amino acid sequence (TTLPPAVVDISGNLGEYTLLAWPY-AATLIHTVEPLVAYTT), showing it to be a different molecule. Moreover, no reactivity with IgA was observed by double diffusion (Fig. 3).

The use of affinity chromatography culminated in a highly active preparation of purified jacalin (Fig. 6). However, this procedure is time-consuming and could be used only for small-scale preparation. The results presented in Figs. 3 and 6 show that the jacalin obtained by the preparative HPLC method is identical in all respects

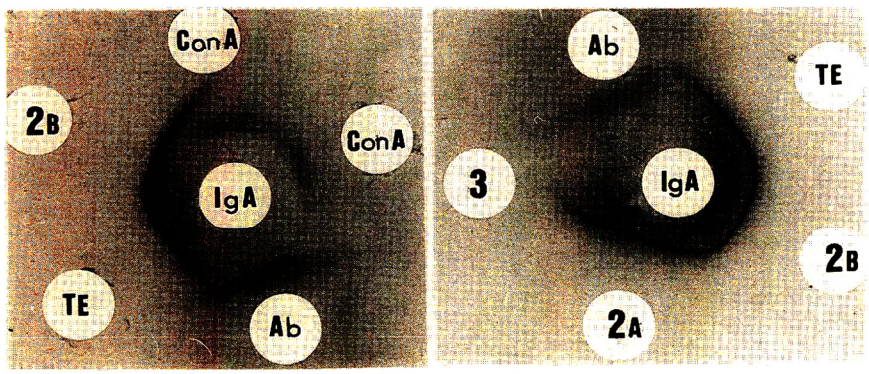

Fig. 3. Gel precipitation analysis of HPLC-purified jacalin. Portions (about 2 μg) of DEAE HPLC peaks 2 (2), 3 (3), 4 (4), total lectin extract (TE), concanavalin A (ConA), antibodies anti-IgA (Ab) and human IgA_1 (IgA) were incubated on agarose plates overnight at room temperature, washed for two days in PBS containing 0.02% NaN_3, stained with Coomassie Brilliant Blue for 5 min and destained as described in the text.

with a sample prepared by affinity chromatography on an IgA-Sepharose column. These include molecular mass, human IgA_1 reactivity and N-terminal amino acid sequence.

In conclusion, using a PA–DEAE column of 20 mm I.D., the optimum batch size was 500 mg of the protein from the total phosphate extract. Using the described procedure, each run could be completed in about 40 min, yielding 135–165 mg of jacalin α- and α'-chains, and several runs can be effected in succession. Using larger preparative columns (I.D. $\geqslant$50 mm), which are

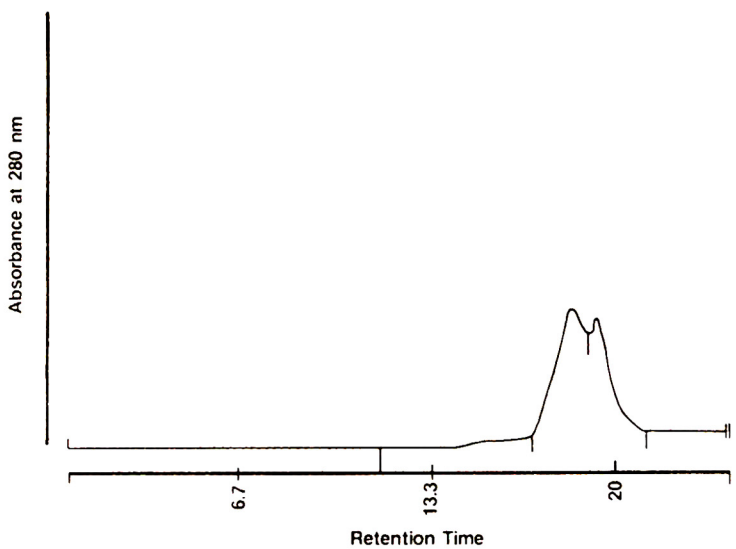

Fig. 4. Gel filtration chromatographic analysis of the DEAE HPLC jacalin-containing peak 2B using a Shinpack Diol-150 HPLC column (50 cm × 7.9 mm I.D.). About 100 μg of protein were analysed and elution was performed using 50 m*M* phosphate buffer (pH 7.2) at a flow-rate of 1 ml min^{-1}. Retention time in min.

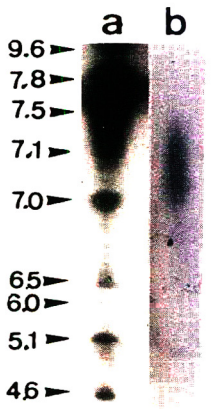

Fig. 5. IEF analysis of the purified jacalin. Lanes: a = total lectin extract; b = purified jacalin (peak 2B). On the left side are shown the values of the p*I* standard marker proteins.

commercially available, the batch size can be increased to 5 g.

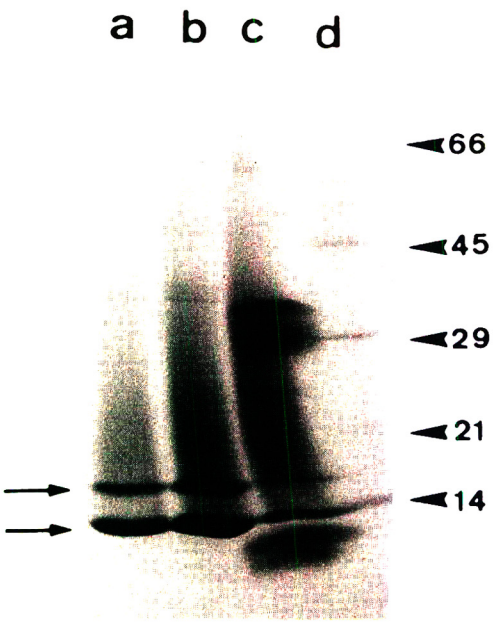

Fig. 6. SDS-PAGE comparison of IgA-Sepharose column-isolated jacalin (a) and DEAE (fraction 2B)-purified lectin (b). Lane c represents the analysis of the total lectin extract. Each lane contained 40–60 μg of protein. The M_r standards are shown in lane d ($M_r \times 10^{-3}$).

Acknowledgements

We are grateful to the CNPq and Fiocruz for financial support. R.S. and M.F.A. are fellows of CNPq and Fiocruz, respectively.

References

[1] M.M. Bunn-Moreno and A. Campos-Neto, *J. Immunol.*, 127 (1981) 429.
[2] M.C. Roque-Barreira and A. Campos-Neto, *J. Immunol.*, 134 (1985) 1740.
[3] P.S. Appukuttan and D. Basu, *FEBS Lett.*, 180 (1985) 331.
[4] G.F. Springer and P.R. Dessai, *Carbohydr. Res.*, 40 (1975) 83.
[5] M.V. Krishna Sastry, P. Banerjee, S.R. Patanjali, M.J. Swamy, G.V. Swarnalatha and A. Surolia, *J. Biol. Chem.*, 261 (1986) 11726.
[6] H. Kondoh, K. Kobayashi, K. Hagiwara and T. Kajii, *J. Immunol. Methods*, 88 (1986) 171.
[7] R. Wilkinson and S. Neville, *Vet. Immunol. Immunopathol.*, 18 (1988) 195.
[8] D.L. Skea, P. Christopoulous, A.G. Plaut and B.J. Underdown, *Mol. Immunol.*, 25 (1988) 1.
[9] H. Ahmed and B.P. Chatlerjee, *J. Biol. Chem.*, 264 (1989) 9365.
[10] P. Aucouturier, N. Pineau, J.C. Brugier, E. Mihaesco, F. Duarte, F. Skuaril and J.L. Preud'homme, *J. Clin. Lab Anal.*, 3 (1989) 244.
[11] E. Ruffet, N. Paquet, S. Frutiger, G. Hughes and J.C. Jaton, *Biochem. J.*, 286 (1992) 131.
[12] K. Hagiwara, D. Collet-Cassart, K. Kobayashi and J.P. Vaerman, *Mol. Immunol.*, 25 (1988) 69.
[13] C. Capron, F. Pillar, J.M. Wieruszeski, Y. Leroy and L. Fournet, *Carbohydr. Res.*, 199 (1990) 121.
[14] N.M. Young, R.A. Johnston, A.G. Szabo and D.C. Watson, *Arch. Biochem. Biophys.*, 270 (1989) 596.
[15] S.K. Mahanta, S. Sanker, N.V.S.A.V. Prasad Rao, M.J. Swamy and A. Surolia, *Biochem. J.*, 284 (1992) 95.
[16] U.K. Laemmli, *Nature*, 227 (1970) 680.
[17] O.H. Lowry, N.J. Rosebrough, A.L. Farr and R.J. Randall, *J. Biol. Chem.*, 193 (1951) 265.
[18] W.R. Pearson, *Methods Enzymol.*, 183 (1990) 88.
[19] M.O. Dayhoff, in M.O. Dayhoff (Editor), *Atlas of Protein Sequence and Structure*, Vol. 5, Suppl. 3, National Biomedical Research Foundation, Washington, DC, 1979, pp. 345–358.
[20] O. Ouchterlony, *Acta Pathol. Microbiol. Scand.*, 26 (1949) 507.
[21] T. Vijayakumar and J.A. Forrester, *Biol. Plant.*, 28 (1986) 370.

ELSEVIER

Journal of Chromatography A, 688 (1994) 363–367

JOURNAL OF CHROMATOGRAPHY A

Short communication

Selectivity effects in semi-polar columns. II

Pilar Fernandez, Rosa Vilanova, Lourdes Berdie, Joan O. Grimalt*

Department of Environmental Chemistry (CID–CSIC), Jordi Girona 18, 08034-Barcelona, Catalonia, Spain

First received 26 May 1994; revised manuscript received 13 September 1994

Abstract

Significant selectivity differences between semi-polar capillary gas chromatographic columns involving the elution order of acyclic and polycyclic lipid molecules have been observed. These differences occur despite these columns being reported to be "equivalent" in catalogue specifications. In Part I, the changes in retention indices between columns manufactured by different companies were described. In this paper, it is shown that these variations in selectivity may even be observed among semi-polar columns originating from the same manufacturer.

1. Introduction

In Part I [1], we showed that the use of different capillary columns in the trace organic analysis of environmental samples may give rise to significant changes in the relative retentions of several major compounds. These selectivity changes essentially concerned the elution order of linear vs. polycyclic molecules such as squalene and benzopyrenes and alkan-1-ols and sterols, and were observed among semi-polar stationary phase columns (5% phenyl–95% methyl type) which are reported to be equivalent in commercial catalogues. The study involved a comparison of semi-polar columns from J & W Scientific (DB-5), Carlo Erba (SE-52 and SE-54), Chrompack (CP-Sil 8 CB) and Hewlett-Packard (HP-5).

In the context of the chromatographic work on environmental problems regularly performed in our Department, we have found that these previously described differences [1] may even involve columns manufactured by the same company. In this paper we present one of these cases, which extends the previous description of selectivity differences between semi-polar columns.

2. Experimental

2.1. Materials

Chromatography quality *n*-hexane, methanol, dichloromethane, isooctane and neutral silica gel (Kieselgel 40, 70–230 mesh) were obtained from Merck (Darmstadt, Germany). The silica gel was extracted with dichloromethane–methanol (2:1, v/v) in a Soxhlet apparatus for 24 h. After solvent evaporation, the silica was heated for 12 h at 120°C. A total of 5% (w/w) of water obtained with a Milli-Q system (Millipore) was then added to the chromatographic adsorbents for deactivation. The purity of the solvents was checked by concentrating under vacuum 100 ml of solvent to 10 μl for GC analysis. Blank

* Corresponding author.

0021-9673/94/$07.00
SSDI 0021-9673(94)00898-1

requirements were as follows: splitless injection of 2 μl should result in chromatograms with no unresolved GC envelope and only a few peaks, representing up to 1 ng in terms of their flame ionization detector response.

2.2. Sampling, extraction and fractionation

Samples were obtained by sediment coring in high-altitude lakes. The cores were divided into sections at the sampling site and frozen at −20°C until analysis in the laboratory. Lipids were extracted by sonication after freeze-drying. About 1 g of sediment was extracted with dichloromethane–methanol (2:1, v/v) (3 × 20 ml; 20 min), the extract was vacuum and nitrogen evaporated almost to dryness and diluted to 0.5 ml with *n*-hexane, then fractionated by column chromatography according to previously established methods [2]. A column filled with 2 g of 5% water-deactivated silica was used. The hydrocarbon and alcohol fractions were obtained by successive elution with 8 ml *n*-hexane–dichloromethane (1:1) and 12 ml of dichloromethane–methanol (18:2), respectively. These fractions were vacuum and nitrogen concentrated almost to dryness and silylated with isooctane–bis(trimethylsilyl)trifluoroacetamide (1:1) (60 min, 70°C).

2.3. Instrumental analysis

The samples were analysed by GC and GC–MS. These analyses were performed with a Carlo Erba HRGC Mega 2 Series gas chromatograph

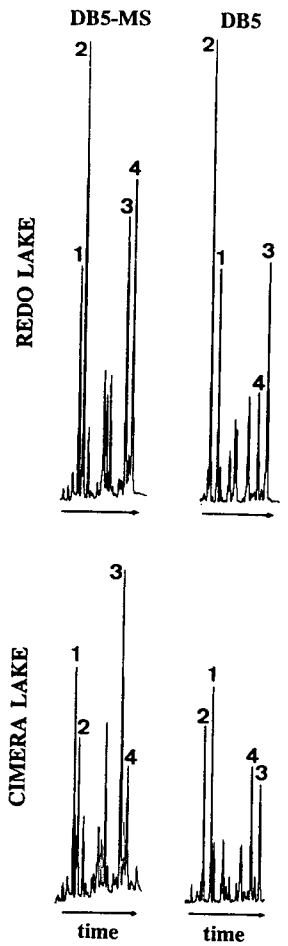

Fig. 1. GC profiles showing the elution order of the TMS ether derivatives of alkan-1-ols and Δ^5-sterols with the DB-5 and DB5-MS semi-polar columns. Peaks: 1 = cholest-5-en-3β-ol; 2 = octacosan-1-ol; 3 = β-sitosterol; 4 = triacontan-1-ol.

Table 1
Semi-polar capillary columns compared in this study

Column	Stationary phase[a]	Dimensions	Film thickness (μm)	Manufacturer
DB-5	5% phenyl–95% methyl	30 m × 0.25 mm I.D.	0.2	J & W Scientific (Folsom, CA, USA)
DB5-MS	5% phenyl–95% methyl	30 m × 0.25 mm I.D.	0.2	J & W Scientific

[a] As defined by the manufacturer.

equipped with a flame ionization detector and with a Carlo Erba GC8000 Series gas chromatograph coupled to a Fisons MD 800 mass spectrometer, respectively. The GC analyses were performed with the capillary columns described in Table 1. The oven temperature was programmed from 90 to 300°C at 6°C/min, and the injector and detector temperatures were set at 280 and 330°C, respectively. Hydrogen was used as the carrier gas at a flow-rate of 50 cm/s. The oven temperature programme for the GC–MS analyses was from 90 to 300°C at 4°C/min, the injector and transfer line temperatures were 280 and 300°C, respectively, and helium was used as the carrier gas at a flow-rate of 50 cm/s. Data were acquired in the electron impact mode (70 eV), scanning from 50 to 550 mass units at 1 s per decade. In both instances the injector was in the splitless mode (1 μl; hot needle technique), the split valve being closed for 35 s.

3. Results and discussion

C_{20}–C_{30} alkan-1-ols constitute the dominant compounds in the polar fractions of the sediments considered in this study. In addition to these, sterols are also major compounds, encompassing a mixture of C_{27}–C_{29} homologues dominated by cholest-5-en-3β-ol and β-sitosterol. The gas chromatograms corresponding to the analysis of the alcohol–sterol mixtures with the two columns indicated in Table 1 are shown in Fig. 1. These chromatograms illustrate that important changes in relative retention are observed when using the different columns. Thus, with the DB-5 column, the trimethylsilyl (TMS) ethers of octacosan-1-ol and triacontan-1-ol elute before than the TMS ethers of cholest-5-en-3β-ol and β-sitosterol, respectively, whereas with the DB-5 column the elution order is the reverse.

Repeated analyses with several columns and comparison of the resulting relative retention indices (I) of the sterols (Table 2) showed that the discrepancy is maintained despite using columns from different manufacturing batches. The I dispersion is low (relative standard deviation 0.17–0.26%) in comparison with the DB-5–DB5-MS I discrepancies (1.4–1.8%), which results in very significant mean I differences between the two column types (confidence level in Student's t-test $\gg 0.9995$).

These selectivity effects parallel the elution order changes observed in our previous work [1] and show that this new J & W Scientific column, DB5-MS, behaves similarly to CP-Sil 8 CB, SE-54 and HP-5, with which the elution of the linear compounds follows that of the polycyclic molecules occurring at close retention times (Table 3). In particular, the retention index of β-sitosterol with this column is coincident with that with CP-Sil 8 CB.

The difference in selectivity is independent of the specific functionality of the analyte mole-

Table 2
Relative retention indices (I) of alkan-1-ols and sterols with the DB-5 and DB5-MS columns

Column	I			
	Octacosan-1-ol	Cholest-5-en-3β-ol	Triacontan-1-ol	β-Sitosterol
DB-5	2800.0	2831.1	3000.0	3037.7
	2800.0	2825.6	3000.0	3035.2
	2800.0	2827.9	3000.0	3035.8
	2800.0	2819.7	3000.0	3020.3
DB5-MS	2800.0	2781.6	3000.0	2973.2
	2800.0	2791.7	3000.0	2983.5
	2800.0	2787.5	3000.0	2979.2
	2800.0	2781.4	3000.0	2974.0

I values relative to alkan-1-ols.

Table 3
Average relative retention indices (I) of alkan-1-ols and sterols with the semi-polar columns listed in Table 1 and those considered in a previous study [1]

Column	I			
	Octacosan-1-ol	Cholest-5-en-3β-ol	Triacontan-1-ol	β-Sitosterol
DB-5	2800.0	2826.1	3000.0	3032.2
SE-52	2800.0	2803.6	3000.0	2998.2
CP-Sil 8 CB	2800.0	2776.9	3000.0	2974.1
SE-54	2800.0	2782.5	3000.0	2985.3
HP-5	2800.0	2774.4	3000.0	2969.1
DB5-MS	2800.0	2785.6	3000.0	2977.5

I values relative to alkan-1-ols.

cules. Thus, the comparison of the elution order of C_{29}–C_{32} n-alkanes and several triterpenes and triterpanes [taraxer-14-ene, olean-12-ene, hop-17(21)-ene, glutinane, heterolupene, diploptene and (22R)-17α(H),21β(H)-homophopane] in the two columns shows the same displacement towards higher I for the polycyclic molecules eluting in the DB-5 column (Fig. 2 and Table 4). With these hydrocarbons, the general displacement effect gives rise to elution order inversions between hop-17(21)-ene and n-hentriacontane and between heterolupene and n-dotriacontane.

The same type of I differences between the DB-5 and the CP-Sil 8 CB, SE-54 and HP-5 columns was observed in our previous study [1] when comparing the elution time of squalene and benzopyrenes. Hence the selectivity effect

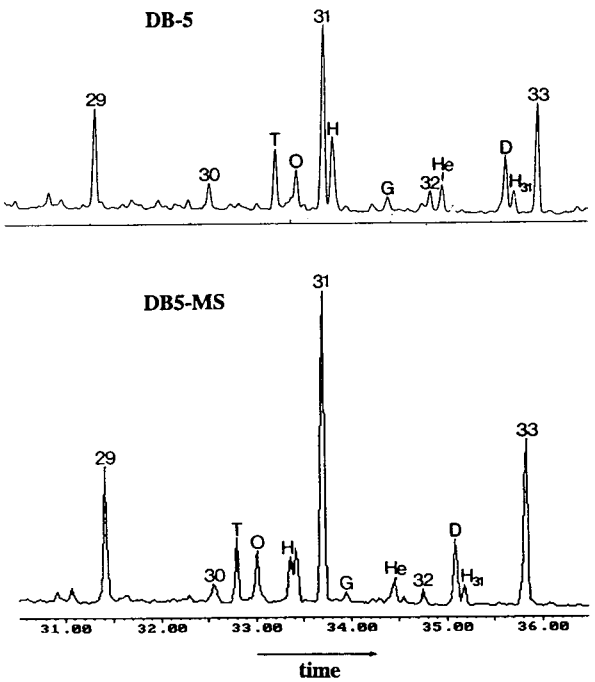

Fig. 2. GC profiles showing the elution order of n-alkanes and triterpanes with the DB-5 and DB5-MS semipolar columns. Numbers on peaks refer to n-alkane chain length. T = taraxer-14-ene; O = olean-12-ene; H = hop-17(21)-ene; G = glutinane; He = heterolupene; D = diploptene; H_{31} = (22R)-17α(H),21β(H)-homohopane. Time scale in min.

Table 4
Relative retention indices (I) of linear and polycyclic hydrocarbons with the DB-5 and DB5-MS columns

Compound	I	
	DB-5	DB5-MS
n-Triacontane	3000.0	3000.0
Taraxer-14-ene	3059.0	3020.7
Olean-12-ene	3077.0	3040.7
n-Hentriacontane	3100.0	3100.0
Hop-17(21)-ene	3109.8	3070.0[a]
Glutinane	3161.0	3124.1
n-Dotriacontane	3200.0	3200.0
Heterolupene	3210.8	3170.4[a]
Diploptene	3271.4	3231.2
(22R)-17α(H),21β(H)-Homohopane	3278.4	3240.4
n-Tritriacontane	3300.0	3300.0

I values relative to n-alkanes.
[a] Compounds showing reversal of elution order with respect to the n-alkane with the nearest retention.

which differentiates the DB-5 column essentially concerns the elution time of cyclic vs. polycyclic molecules.

4. Conclusions

The important changes in relative retention on analysis of organic compounds with different semi-polar columns described in Part I [1] are also observed even with columns produced by the same manufacturer. Catalogue specifications do not allow differentiation between semi-polar columns corresponding to one or another group. Hence, the use of a standard mixture containing linear and polycyclic molecules with similar retention times is recommended as a guideline for environmental applications where both types of molecules are easily encountered. This is particularly relevant when comparing GC traces obtained with different detectors, such as flame ionization and mass spectrometric types. Important peak assignment errors may be produced from the straightforward comparison of "equivalent" semi-polar capillary columns such as those described here.

Acknowledgements

Financial support from ALPE-II Project (EEC Project EV5V-CT92-0205) is acknowledged. P.F. thanks CIRIT (Generalitat de Catalunya) for a research contract. L.B. thanks the Spanish Ministry of Education for a Ph.D. fellowship.

References

[1] M. Aceves and J.O. Grimalt, *J. Chromatogr.*, 607 (1992) 261.
[2] M. Aceves, J.O. Grimalt, J. Albaiges, F. Broto, L. Comellas and M. Gassiot, *J. Chromatogr.*, 436 (1988) 503.

ELSEVIER

Journal of Chromatography A, 688 (1994) 368–374

JOURNAL OF CHROMATOGRAPHY A

Short communication

Build-up of artifacts on adsorbents during storage and its effect on passive sampling and gas chromatography–flame ionization detection of low concentrations of volatile organic compounds in air

Xu-Liang Cao*, C. Nicholas Hewitt

Institute of Environmental and Biological Sciences, Lancaster University, Lancaster LA1 4YQ, UK

First received 13 June 1994; revised manuscript received 20 September 1994

Abstract

The levels of blank artifacts on four adsorbents commonly used for air sampling (Tenax-TA, Tenax-GR, Carbotrap and Chromosorb 106) were observed to increase during storage. This may determine the detection limits and hence their suitability for the passive sampling of volatile organic compounds in ambient air. Blank build-up on Chromosorb 106 was very high, and this material cannot be used for passive sampling in ambient air. The blank build-up on Carbotrap was also high, especially in the chromatographic range corresponding to hydrocarbons of $\leq C_5$, but that on Tenax-TA and Tenax-GR was very low. Simultaneous sampling was carried out using different adsorbents, and for compounds that are the main artifacts on adsorbents (e.g., benzene on Tenax, benzene and toluene on Carbotrap) the results from Carbotrap are much higher than those from Tenax-TA and Tenax-GR, and the results from Tenax-TA and Tenax-GR also vary.

1. Introduction

One of the main limitations in the application of passive samplers (e.g., Perkin-Elmer diffusion tubes) to the determination of low concentrations of organic compounds in air [typically sub-ppb (v/v) (ppbv) in rural air] is the blank build-up on adsorbents due to artifact formation during storage and exposure. Although blank levels can be made extremely low by meticulous conditioning of the adsorbing material, artifacts may build up on the unexposed matrix during storage. They may also build up during exposure of the sampler by reaction of ozone with the adsorbent [1,2], and this may raise the detection limits to unacceptable levels. The responses of the reduction gas detector to the blank build-up signals resulting from different adsorbents have been investigated recently [3], and it was found that some adsorbents (e.g., Chromosorb 106) are not suitable for the passive sampling of low concentrations of volatile organic compounds (VOCs) in air. As gas chromatography–flame ionization detection (GC–FID) is widely employed in analyses for hydrocarbons (e.g., Refs. [4] and [5]), it is necessary to study the FID responses to the artifact build-up signals on different adsorbents, and to assess their suitabili-

* Corresponding author.

0021-9673/94/$07.00
SSDI 0021-9673(94)00908-2

ty for the passive sampling and determination of VOCs at low concentrations in ambient air.

In this work, four different adsorbents were used for the passive sampling of VOCs in rural air, and their artifact build-up problem was investigated. The problems with water vapour during passive sampling and analysis are also discussed.

2. Experimental

GC–FID measurements were made using a Hewlett-Packard 5890 Series II instrument. The carrier gas was helium and the make-up gas was nitrogen. The capillary column used was an Ultra 2 (cross-linked 5% phenyl–methyl silicone) (25 m × 0.2 mm I.D., 0.33 μm film thickness) from Hewlett-Packard. The exposed passive sampling tubes were thermally desorbed by a Chrompack thermal desorption cold trap (TCT) injector, interfaced with the gas chromatograph. The flow-rate of the desorption carrier gas (helium) through the tube was 35 ml/min. The desorbed analytes were retrapped by a deactivated fused-silica capillary trap (40 cm × 0.53 mm I.D.) [6] cooled by liquid nitrogen. After sample concentration, the trap was flash-heated to 220°C at 15°C/s for 1 min, and the trapped vapours were injected on to the capillary column in the splitless mode.

Four commonly used adsorbents were studied: Tenax-TA (60–80 mesh, specific surface area 20 m^2/g; Chrompack), Carbotrap (20–40 mesh, specific surface area 100 m^2/g; Supelco), Tenax-GR (60–80 mesh, specific surface area 25 m^2/g; Chrompack) [7–9] and Chromosorb 106 (60–80 mesh, specific surface area 800 m^2/g; Supelco). These adsorbents were conditioned for at least 16 h with a helium flow of 35 ml/min at the maximum temperature possible for each adsorbent. Details of the conditioning and desorption conditions for each adsorbent have been given previously [3]. Perkin-Elmer stainless-steel diffusion tubes packed with adsorbents were used for the sampling of VOCs in a rural area in the vicinity of Lancaster, North-west England, during May–July 1992. The relative humidity varied from 40 to 80% and the temperature from 8 to 25°C. Membrane diffusion caps were used in all instances to reduce the amount of water vapour adsorbed on the adsorbents. The concentrations of organic compounds in air were calculated using the following expression [10]:

$$\text{analyte concentration (ppm)} = \frac{\text{mass uptake (ng)}}{\text{uptake rate (ng/ppm} \cdot \text{min)} \times \text{exposure time (min)}} \quad (1)$$

The uptake rate in Eq. 1 was calculated using the following equation [10];

$$\text{uptake rate (ng/ppm} \cdot \text{min)} = \frac{DA}{L} \quad (2)$$

where D is the diffusion coefficient in air (cm^2/s), A is the cross-sectional area of the diffusion tube and L is the diffusion length of the tube. The uptake rates of the Perkin-Elmer diffusion tube were calculated for some compounds and are given in Table 1.

Table 1
Ideal uptake rate for Perkin-Elmer diffusion tube with diffusion cap

Compound	Uptake rate [ng/ppm (v/v) · min]
Benzene	1.75
Toluene	1.84
Ethylbenzene	1.92
p-Xylene	1.86
o-Xylene	2.02
1,2,4-Trimethylbenzene	1.88

3. Results and discussion

In order to investigate the problem of increasing contamination or artifact formation on adsorbents during storage, sampling tubes were packed with different adsorbents, rigorously conditioned and sealed with Swagelok caps. After storage for one week they were thermally desorbed and analysed by GC–FID as mentioned above. Typical blank chromatograms before and after storage are shown in Figs. 1 and 2, respectively.

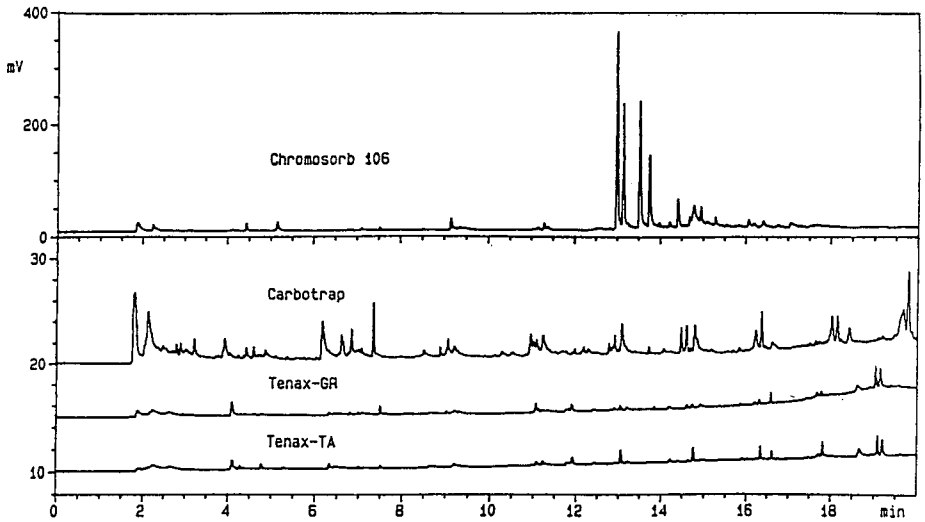

Fig. 1. Chromatograms of blank build-up for different adsorbents before storage. Temperature programme: increased from 35°C (held for 3 min) to 200°C at 10°C/min.

It can be seen from Fig. 1 that after conditioning both Tenax-TA and Tenax-GR are very clean, Carbotrap less so and Chromosorb 106 much less so. Some peaks, e.g., the benzene peaks from Tenax-TA, Tenax-GR and Carbotrap and the unidentified peaks from Chromosorb 106, in Fig. 1 are very small. This is in contrast to the response of the reduction gas detector [3], which has much higher sensitivity and selectivity towards the reactive hydrocarbons than does the flame ionization detector. Fig. 2 shows the chromatograms of the different adsorbents after storage for one week. All four adsorbents showed increased levels of contamination. It is unlikely these peaks represent contaminants from ambient air, adsorbed during storage, as the tubes were sealed with Swagelok caps. Rather it seems likely that they represent residual compounds not completely removed and/or compounds generated within the adsorbents themselves during storage, possibly by degradation of the polymers, or oxidation of the residual compounds by the oxidizing groups on the surface of the Carbotrap. The decomposition and oxidation could take place during conditioning and the compounds then released later during storage. Moreover, the significant increase of the characteristic peaks from Chromosorb 106 (retention times >12.5 min) indicates that the artifact peaks on the adsorbents after storage are produced by the adsorbents themselves and are not contaminants. Such artifact formation processes may be unavoidable, and shortening the sampling and storage period to the minimum practicable or decreasing the amount of adsorbent used may be the only steps that can be taken to obviate the problem.

Fig. 3 shows representative chromatograms of samples collected with different adsorbents after exposure for about one week to ambient air at the same site. It can be seen that for the very clean adsorbents (e.g., Tenax-TA and Tenax-GR), the amount of analytes adsorbed on the adsorbents is significant compared with their corresponding blank build-up levels (shown in Fig. 2). Even for the Carbotrap, which is less clean than the Tenax materials, the signal-to-noise ratio is also large enough for the successful determination of some hydrocarbons ($\geq C_6$) in ambient air. However, this is not so with Chromosorb 106, where artifact formation is too severe a problem for this matrix to be used successfully for this application. The differences in retention times between the separations on

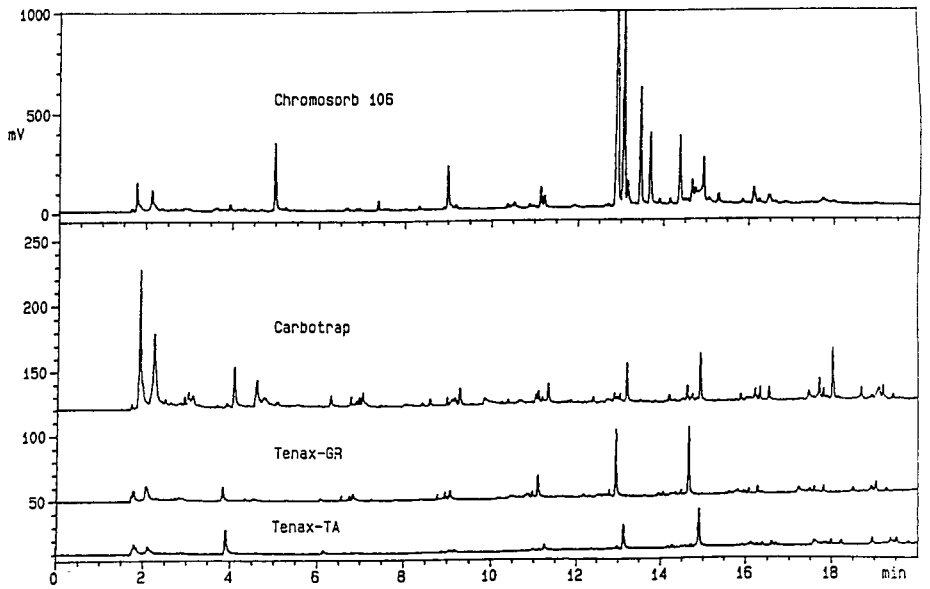

Fig. 2. Chromatograms of blank build-up for different adsorbents after storage for one week. Temperature programme as in Fig. 1.

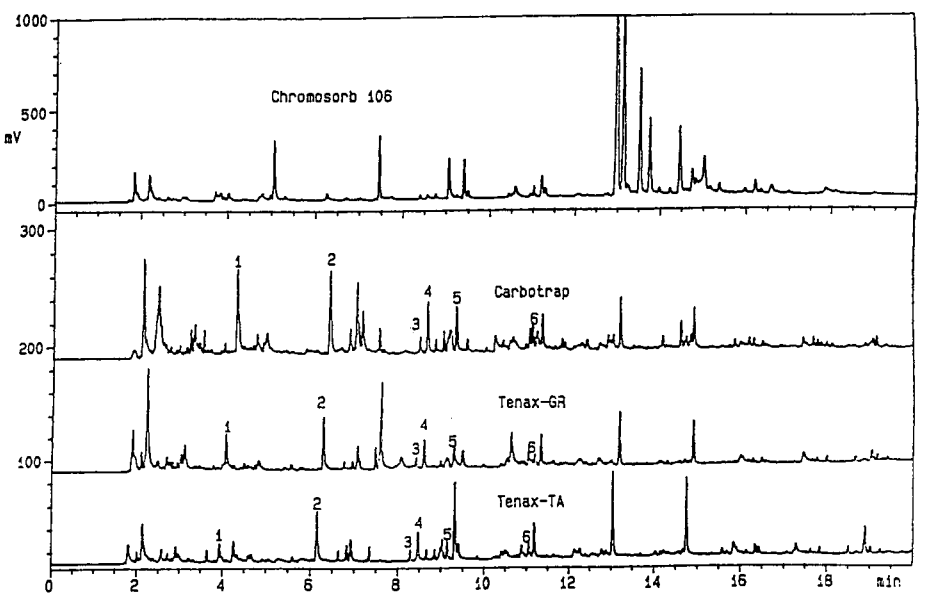

Fig. 3. Chromatograms of passive sampling in ambient air for about one week for different adsorbents. Temperature programme as in Fig. 1. Peaks: 1 = benzene; 2 = toluene; 3 = ethylbenzene; 4 = *p*-xylene; 5 = *o*-xylene; 6 = 1,2,4-trimethylbenzene.

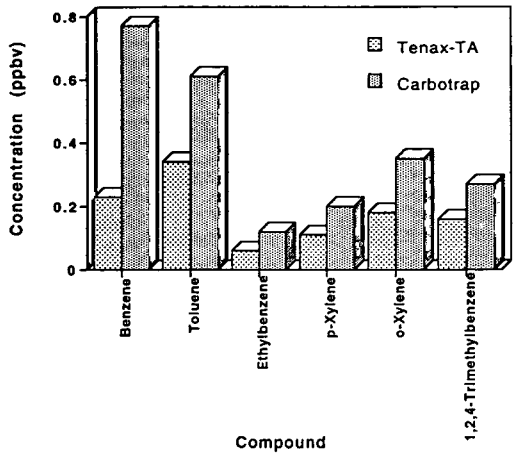

Fig. 4. Concentrations of hydrocarbons in air obtained from simultaneous sampling using Tenax-TA, Tenax-GR and Carbotrap during the period 14–19 June 1992.

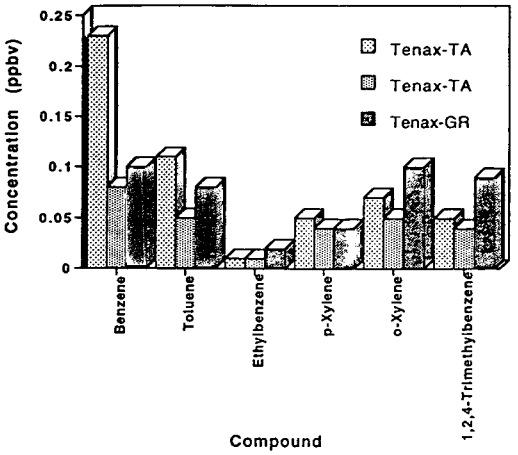

Fig. 6. Concentrations of hydrocarbons in air obtained from simultaneous sampling using Tenax-TA and Tenax-GR during the period 28 July–2 August 1992.

the various adsorbents are due to the variation in the head pressure of the GC capillary column. As Chromosorb 106 cannot be used for passive sampling in rural air, the peaks from it were not identified.

The concentrations of selected organic hydrocarbons in rural air were calculated from the results of Tenax-GR, Tenax-TA and Carbotrap desorption according to Eq. 1. Figs. 4–6 show representative results obtained from simultaneous sampling using different adsorbents. It can be seen that for ethylbenzene, *p*-xylene, *o*-xylene and 1,2,4-trimethylbenzene, which are not present or are present at very low levels as artifacts, the results obtained from Carbotrap generally agree well with those from Tenax-TA and Tenax-GR. The results from Tenax-GR also agree well with those from Tenax-TA for toluene. However, the results for benzene and toluene from Carbotrap are much higher than those from Tenax-TA and Tenax-GR, and the results for benzene from Tenax-TA and Tenax-GR also vary. This is due to the fact that toluene and, especially, benzene, are the main artifacts on the adsorbents, and they exist at higher levels on Carbotrap than on Tenax adsorbents. The uptake rate of benzene on Tenax adsorbent is relatively lower than that on Carbotrap and this may also contribute to this difference. The results from replicate sampling using Tenax-TA (shown in Fig. 6) also show good agreement, except for benzene, which may be due to the difference between the benzene blank levels on these two Tenax-TA sampling tubes before sampling. The average concentrations of the different compounds derived from different adsorbents and the total average values are summarized in Table 2. It can be seen that the results

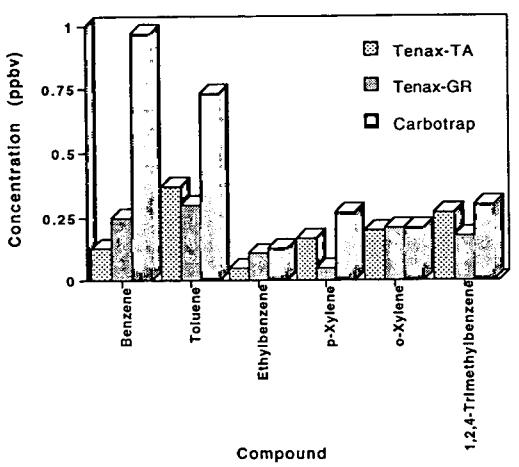

Fig. 5. Concentrations of hydrocarbons in air obtained from simultaneous sampling using Tenax-TA and Carbotrap during the period 18–23 June 1992.

Table 2
Mean concentrations of selected pollutants in ambient rural air in North-west England obtained from different adsorbents during May-July 1992.

Compound	Concentration (mean ± S.D.) (ppbv)			
	Tenax-TA	Tenax-GR	Carbotrap	Total
Benzene	0.21 ± 0.08 (11)[a]	0.19 ± 0.11 (8)	0.51 ± 0.30 (10)	0.33 ± 0.25 (29)
Toluene	0.36 ± 0.19 (11)	0.25 ± 0.18 (8)	0.66 ± 0.54 (10)	0.43 ± 0.38 (29)
Ethylbenzene	0.08 ± 0.08 (10)	0.06 ± 0.04 (6)	0.12 ± 0.05 (8)	0.09 ± 0.07 (24)
p-Xylene	0.20 ± 0.16 (10)	0.09 ± 0.07 (6)	0.24 ± 0.10 (8)	0.21 ± 0.19 (24)
o-Xylene	0.23 ± 0.18 (10)	0.15 ± 0.08 (6)	0.31 ± 0.13 (8)	0.26 ± 0.16 (24)
1,2,4-Trimethylbenzene	0.18 ± 0.09 (10)	0.12 ± 0.07 (6)	0.25 ± 0.04 (7)	0.20 ± 0.10 (23)

[a] Number of samples.

obtained from Tenax-TA and Tenax-GR generally agree well, whereas the results for benzene and toluene from Carbotrap are higher than those from the Tenax adsorbents. Therefore, although it is possible to measure the compounds in air after subtraction of their blank signal following artifact formation, the precision and accuracy of the results may be poor, depending on the level of the artifacts on the adsorbents.

The other problem encountered in the passive sampling of VOCs in ambient air is the humidity. The relative humidity of ambient air is highly variable, and may range from 30 to 40% on a fine day, from 60 to 70% during the night and be more than 85% during fog or rain. Water vapour adsorbed on sampling adsorbents may cause two problems: on desorption it may extinguish the flame of the flame ionization detector, and it may block the cold trap, especially the capillary cold trap, which has only a single path, used for sample preconcentration, by the formation of ice. Although the latter problem can be eased by using a multi-path packed cold trap, the large difference between the carrier gas flow-rate through a packed cold trap and that through a capillary GC column necessitate the use of split injection, causing most of the sample to be lost by venting. This causes a severe loss of sensitivity. However, by using a flow-rate restrictor in the packed cold trap, the splitting ratio may be decreased significantly. Although the membrane diffusion cap available for Perkin-Elmer diffusion tubes may be used during sampling to lower the amount of water vapour adsorbed, it does not eliminate it completely under conditions of high relative humidity. Therefore, further development of membrane diffusion caps to exclude water, while allowing the analytes to pass, is required.

4. Conclusions

The main problem in the passive sampling of low concentrations of volatile hydrocarbons in rural air concerns the sensitivity of the method, which is highly dependent on the signal-to-noise ratio in the resultant chromatogram. It is possible to clean the adsorbents used to acceptable levels by the use of rigorous conditioning procedures. However, with time, artifacts form in or on the adsorbent, resulting in an increasingly noisy blank signal. This occurs during storage prior to sampling, during exposure to ambient air and during storage after sampling prior to analysis. Artifact formation on four adsorbents during storage was studied. The problem is at a minimum with Tenax-TA and Tenax GR, is more acute with Carbotrap, especially in the $\leq C_5$ range, and is so severe with Chromosorb 106 that it prevents the use of this material for this application.

The results of simultaneous sampling using different adsorbents show that for compounds that are not present or are present at very low levels in the blank build-up on each adsorbent,

the results obtained from Carbotrap generally agree well with those from Tenax-TA and Tenax-GR. The results from Tenax-GR also agree well with those from Tenax-TA for toluene. However, for compounds which are the main artifacts on adsorbents (e.g., benzene and toluene), the results obtained from Carbotrap are much higher than those from Tenax-TA and Tenax-GR, and the results from Tenax-TA and Tenax-GR also vary. Hence, although it is possible to measure the compounds in air by subtraction of their corresponding blank signals on adsorbents, the precision and accuracy of the results may be poor, depending on the amount of the artifact on the adsorbent.

Storage and exposure times should be as short as possible in order to keep the blank build-up level on adsorbents as low as possible. This would be facilitated by the design of a new thermally desorbable passive sampler with much higher uptake rates (by increasing the ratio of A/L of the sampler) and by development of more sensitive detection methods.

The adsorption of water vapour by even the most hydrophobic adsorbents remains a problem and further development of membrane diffusion caps to exclude water, while allowing the analytes to pass, is required.

Acknowledgements

We thank the Government of the People's Republic of China, the British Council and the Natural Environment Research Council for funding and Dr. R.H. Brown for useful discussions.

References

[1] J.M. Roberts, G.C. Feshenfeld, D.L. Albritton and R.E. Sievers, in L.H. Keith (Editor), *Identification and Analysis of Organic Pollutants in Air*, Butterworth, London, 1984, pp. 371–387.
[2] X.-L. Cao and C.N. Hewitt, *Environ. Sci. Technol.*, 28 (1994) 757–762.
[3] X.-L. Cao and C.N. Hewitt, *J. Chromatogr.*, 648 (1993) 191–197.
[4] M.A. Cohen, P.B. Ryan, Y. Yanagisawa, J.D. Spengler, H. Ozkaynak and P.S. Epstein, *JAPCA*, 39 (1989) 1086–1093.
[5] H.C. Shields and C.J. Weschler, *JAPCA*, 37 (1987) 1039–1045.
[6] X.-L. Cao and C.N. Hewitt, *J. Chromatogr.*, 627 (1992) 219–226.
[7] W.T. Sturges and J.W. Elkins, *J. Chromatogr.*, 642 (1993) 123–124.
[8] K. Ventura, M. Dostal and J. Churacek, *J. Chromatogr.*, 642 (1993) 379–382.
[9] X.-L. Cao and C.N. Hewitt, *Atmos. Environ.* 27A (1993) 1865–1872.
[10] R.H. Brown, J. Charlton and K.J. Saunders, *Am. Ind. Hyg. Assoc. J.*, 42 (1981) 865–869.

ELSEVIER

Journal of Chromatography A, 688 (1994) 375–382

JOURNAL OF CHROMATOGRAPHY A

Short communication

Determination of salicylate- and benzophenone-type sunscreen agents in cosmetic products by gas chromatography–mass spectrometry

K.W. Ro*, J.B. Choi, M.H. Lee, J.W. Kim

Pacific Co. R and D Center, 314-1, Bora-ri, Kiheung-Eup, Yong in-Kun, Kyung gi-Do, 449-900, South Korea

Received 4 August 1994

Abstract

A novel simple method to detect salicylate- and benzophenone-type sunscreen agents in cosmetic products by gas chromatography–mass spectrometry (GC–MS) has been developed. Seven sunscreen agents (two salicylate-type and five benzophenone-type) were used for this study. Sunscreen agents and cosmetic product solutions were prepared by dissolving in dimethylformamide, and silylated with bis-trimethylsilyltrifluoroacetamide–trichloromethylsilane (BSTFA). Silylated sunscreen agents were separated on a cross-linked methyl silicone gum column. The identification of each sunscreen agent was accomplished by retention time and mass spectrum library search with a computer, and the quantitation was made in the selected-ion monitoring (SIM) mode of GC–MS. Silylation increased the detection limits of all sunscreen agents about 20–170-fold. Linearity was maintained over the range 1–300 μg/ml for each sunscreen agent. Each cosmetic product (i.e. sun lotion, sun cream and sun cream foundation) was found to contain amounts of the sunscreen agents. This method was sensitive and gave 95.2–104.1% recovery of each sunscreen agent from these cosmetic products. From these results, we concluded that silylation with BSTFA followed by GC–MS analysis allows the simple, convenient and exact determination of sunscreen agents from cosmetic products.

1. Introduction

Sunscreen agents in cosmetics are used to protect the skin from aging and sunburn and to prevent discoloration or fading of cosmetic products due to sunlight. A variety of sunscreen agents have been developed and used in cosmetic products, especially skin care (e.g., lotion, cream) and make-up products (e.g., foundation, twin cake).

To detect the sunscreen agents in cosmetic products, thin-layer chromatography (TLC) [1], high-performance liquid chromatography (HPLC) [1–5], and gas–liquid chromatography (GC) [1,6,7] have been used. Confirmation of sunscreen agents by these methods has been done on the basis of retention time, and spectral characteristics of sunscreen agents on UV spectrophotometers.

Recently, a gas chromatography–mass spectrometry (GC–MS) method for the identification of sunscreen agents was reported [7]. The GC–MS method in selected-ion monitoring (SIM) mode allowed the accurate determination and

* Corresponding author.

0021-9673/94/$07.00
SSDI 0021-9673(94)00949-X

confirmation of sunscreen agents among many ingredients of the cosmetic products.

We propose a new simple method based on GC–MS for the detection of two salicylate- and five benzophenone-type sunscreen agents [2-ethylhexylsalicylate (octylsalicylate), 3,3,5-trimethylcyclohexylsalicylate (homosalate), 2,4-dihydroxybenzophenone (benzophenone-1), 2,2′,4,4′-tetrahydroxybenzophenone (benzophenone-2), 2-hydroxy-4-methoxybenzophenone (benzophenone-3), 2,2′-dihydroxy-4,4′-dimethoxybenzophenone (benzophenone-6), and 2,2′-dihydroxy-4-methoxybenzophenone (benzophenone-8)] in cosmetic products.

Since most of the benzophenone-type sunscreen agents have low sensitivity and volatility for gas chromatography, derivatization such as silylation has been used to overcome these drawbacks. According to Cumpelik [6], a silylation method using HMDS (hexamethyldisilazane) and TMS-Cl (trichloromethylsilane) requires the complete removal of water from all solvents and samples. We adapted a simple silylation method using BSTFA which was used by Valdez [8] and Molever [9].

2. Experimental

2.1. Reagents and materials

Benzylbenzoate, 2,4-dihydroxybenzophenone (benzophenone-1), dimethylformamide (DMF) and bis-trimethylsilyltrifluoroacetamide–1% trichloromethylsilane (BSTFA) were purchased from Sigma (USA). All reagents were analytical grade and used without further purification. Commercially available sunscreen agents used in this study are listed in Table 1.

2.2. Instruments and conditions

Analysis of sunscreen agents was performed on a Model HP 5890 Series II gas chromatograph (Hewlett-Packard, USA) interfaced with a Model HP 5971A mass selective detector, and a Model HP 7673A automatic sampler. Electron impact (EI) mass spectra were recorded at an ionization potential of 70 eV. The mass spectrometer was scanned from m/z 35 to 550 rate of 1.1 scan per second. Fused-silica capillary column (HP-1, Hewlett-Packard), 25 m × 0.20 mm I.D. was used which had been coated with methyl silicone gum (cross-linked) of 0.33 μm film thickness.

Both the injection and the transfer line temperature were 280°C. The oven temperature was held at 170°C for 3 min, then increased at a rate of 5°C/min to a final temperature of 280°C, and kept there for 5 min. The carrier gas was helium at a column head pressure of 8 p.s.i. (1 p.s.i. = 6894.76 Pa), and the split ratio was 20:1. Using an automatic sampler, 1 μl-aliquots of the prepared standard and sample solutions were analysed under the operation conditions described above.

Quantitation was made based on peak area

Table 1
List of sunscreen agents studied

Chemical name	Synonym	Supplier
2-Ethylhexylsalicylate	Octylsalicylate	Vandyk
3,3,5-Trimethylcyclohexylsalicylate	Homosalate	Merck
2-Hydroxy-4-methoxybenzophenone	Benzophenone-3	BASF
2,4-Dihydroxybenzophenone	Benzophenone-1	Sigma
2,2′-Dihydroxy-4-methoxybenzophenone	Benzophenone-8	Sigma
2,2′-Dihydroxy-4,4′-dimethoxybenzophenone	Benzophenone-6	Vandyk
2,2′,4,4′-Tetrahydroxybenzophenone	Benzophenone-2	Vandyk

Table 2
Retention times and detection limits of sunscreen agents before and after silylation

Peak no.	Sunscreen agent	Before silylation		After silylation	
		t_R (min)	Detection limit (μg/ml) [b]	t_R (min)	Detection limit limit (μg/ml) [b]
1	Benzylbenzoate (I.S.) [a]	5.60	0.3	5.59	0.30
2	Octylsalicylate	6.18	2.0	7.69	0.03
3	Homosalate	6.81, 7.08	2.0	8.09, 8.53	0.03
4	Benzophenone-3	8.40	2.0	9.05	0.03
5	Benzophenone-1	9.21	5.0	9.83	0.03
6	Benzophenone-8	9.74	7.0	10.75	0.03
7	Benzophenone-6	12.52	7.0	12.57	0.10
8	Benzophenone-2	N.D. [c]	N.D.	13.69	0.30

[a] I.S. = Internal standard.
[b] Detection limits were measured in GC–MSD-SIM mode.
[c] N.D. = Not detected.

with GC–MS in SIM mode using benzylbenzoate as an internal standard.

2.3. Standard solutions

Standard stock solutions were prepared by dissolving the appropriate amount of sunscreen agent in DMF. A set of working standard solutions were made by diluting aliquots of the stock solutions with DMF to 100 ml in volumetric flasks containing 5 ml internal standard solution. Then, each 200-μl aliquot of the mixed solutions was transferred to an automatic sampler vial and 400 μl of BSTFA were added. The concentration of each compound for the calibration curves is in the range of 1–300 μg/ml.

2.4. Sample solutions

About 5 g of cosmetic product was weighed into a 100-ml beaker, dissolved in about 40 ml of DMF by sonication and transferred into a 100-ml volumetric flask. The beaker was rinsed three times with 10-ml portions of DMF. The solution was diluted with DMF to 100 ml in volumetric flasks containing 5 ml internal standard solution. An aliquot of the solution was filtered through a 0.45-μm membrane filter. Then, each 200 μl

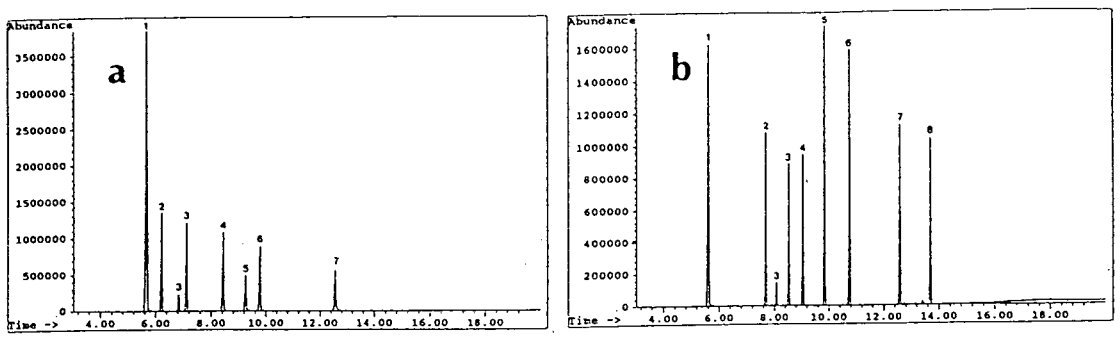

Fig. 1. Total-ion chromatogram of sunscreen agents (a) before and (b) after silylation.

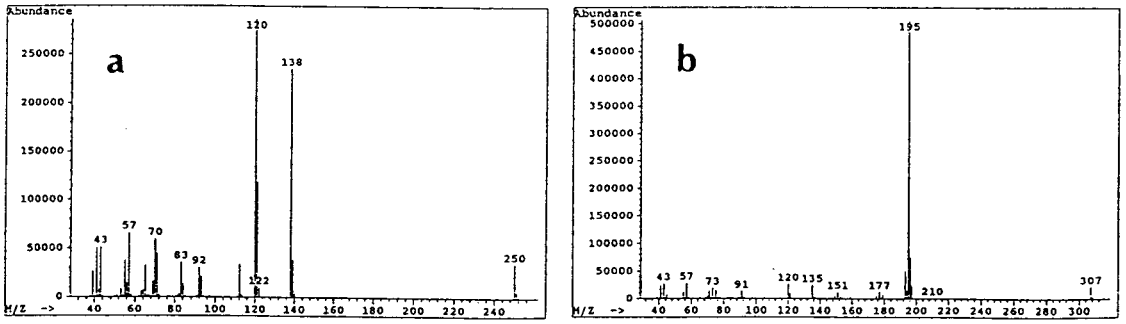

Fig. 2. EI mass spectra of (a) octylsalicylate and (b) silylated octylsalicylate.

aliquot was transferred to an automatic sampler vial and 400 μl of BSTFA were added.

2.5. Internal standard solutions

About 2.0 g of benzylbenzoate was weighed into a 50-ml volumetric flask and diluted to the volume with DMF.

3. Results and discussion

The retention times and the detection limits for the investigated sunscreen agents before and after silylation are shown in Table 2. The total-ion chromatograms (TIC) obtained with the proposed GC–MS method are shown in Fig. 1a (before silylation) and Fig. 1b (after silylation). After silylation, all studied sunscreen agents showed remarkable increases (20–170 times) in the sensitivities and the detection limits. Benzophenone-2 was detected with a high sensitivity and a good detection limit in Fig. 1b (peak 8), but not in Fig. 1a. The seven sunscreen agents were found to be well separated after silylation.

The electron impact (EI) mass spectra of the sunscreen agents are shown in Fig. 2–8. Octylsalicylate and homosalate showed intense peaks at m/z 195 due to the 2-dimethylsilyloxybenzoic acid moiety. All the benzophenone-type sunscreen agents showed strong $[M-CH3]^+$ ion peaks as base ions. The base and characteristic mass ion peaks of the sunscreen agents after silylation are listed in Table 3.

Sometimes, the peaks of the sunscreen agents in practical GC analysis overlap with those of other ingredients in cosmetic products. In this case, the GC–MS information obtained from monitoring the characteristic molecular and major ions helped to detect the presence of particular sunscreen agents, and to determine the exact amounts of sunscreen agents in cosmetic products. In this study, the selected-ion

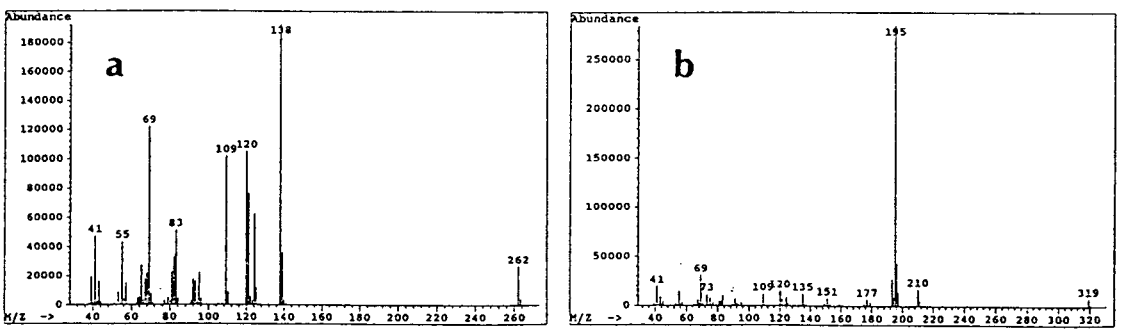

Fig. 3. EI mass spectra of (a) homosalate and (b) silylated homosalate.

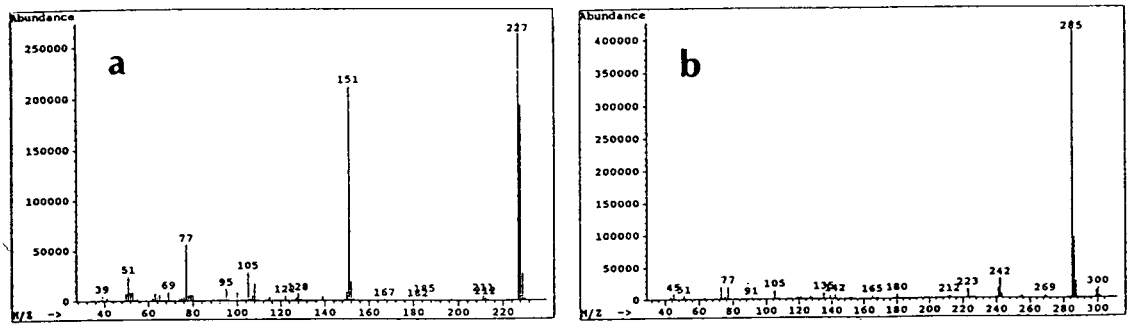

Fig. 4. EI mass spectra of (a) benzophenone-3 and (b) silylated benzophenone-3.

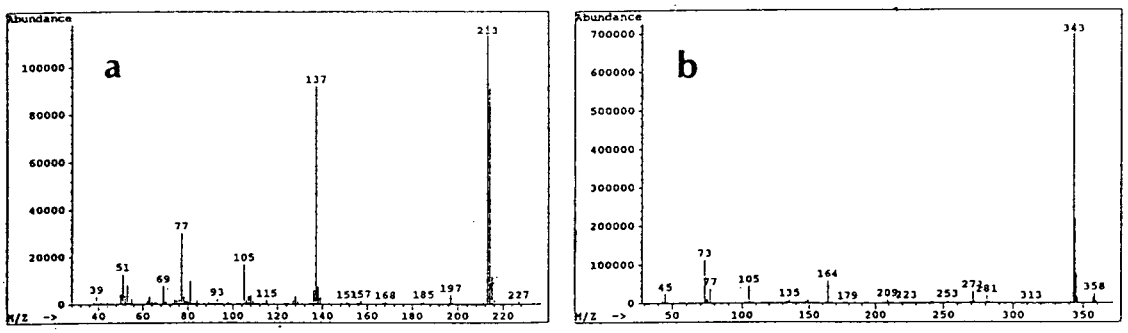

Fig. 5. EI mass spectra of (a) benzophenone-1 and (b) silylated benzophenone-1.

monitoring (SIM) mode of GC–MS was used as a selective detector for sunscreen agents

A calibration curve was constructed by plotting the peak areas against the concentration of the silylated standards injected in GC–MS-SIM mode. Correlation coefficients were in the range of 0.991–1.000, and linear relationship was maintained over the range of 1–300 μg/ml for each silylated sunscreen agent.

Recovery tests were carried out to evaluate the reproducibility and accuracy of the proposed method. A proprietary sun lotion, a sun cream, and a sun cream foundation were spiked with the amounts of agents reported in Table 4 and subjected to the described analytical procedure. Quantitation was made in GC–MS-SIM mode with internal standard, and selected mass ions for the SIM mode were the same as those listed

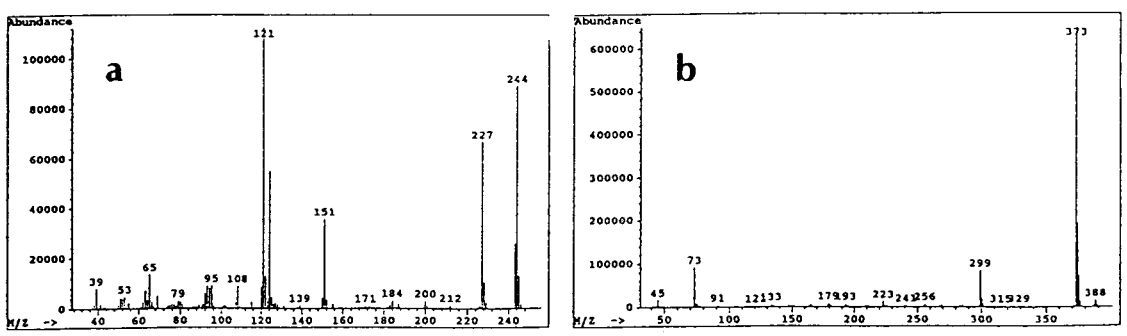

Fig. 6. EI mass spectra of (a) benzophenone-8 and (b) silylated benzophenone-8.

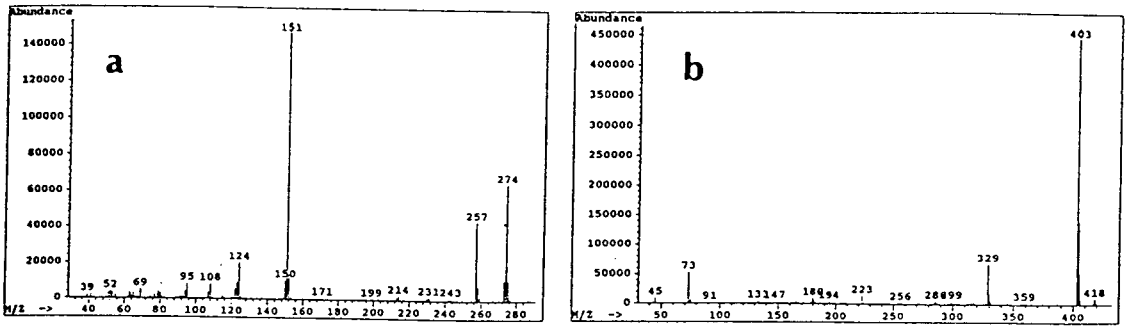

Fig. 7. EI mass spectra of (a) benzophenone-6 and (b) silylated benzophenone-6.

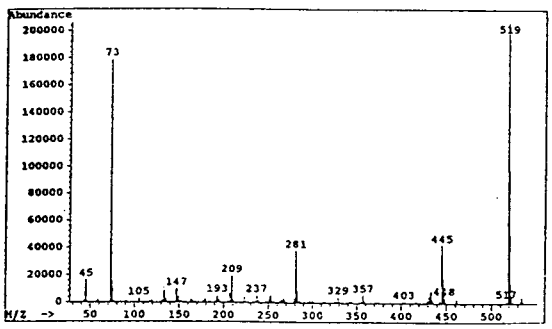

Fig. 8. EI mass spectrum of benzophenone-2.

in Table 3. Excellent recovery with precision was observed, as shown in Table 4. From the total-ion chromatogram (Fig. 9a, 10a and 11a) and selected-ion chromatogram (Fig. 9b, 10b and 11b) of sun lotion, sun cream and sun cream foundation, it was seen that GC–MS-SIM could be used as a selective detector for sunscreen agents. Therefore, in GC–MS-SIM mode, it was possible to exclude the unwanted peaks of ingredients in cosmetic products and determine the amounts of sunscreen agents with accuracy.

4. Conclusion

A novel method was developed for the determination of sunscreen agents in cosmetic products by GC–MS. Simple silylation with BSTFA followed by GC–MS analysis allowed a remarkable increase in the sensitivity and the detection limit as well as the accurate determi-

Table 3
The characteristic mass ions of sunscreen agents after silylation

Peak no.	Sunscreen agent	*m/z*	*m/z*
1	Benzylbenzoate (I.S.)	105 $[M - C_7H_7O]^+$	212 $[M]^+$
2	Octylsalicylate	195 $[M - C_9H_{19}]^+$	307 $[M - CH_3]^+$
3	Homosalate	195 $[M - C_{10}H_{19}]^+$	319 $[M - CH_3]^+$
4	Benzophenone-3	285 $[M - CH_3]^+$	300 $[M]^+$
5	Benzophenone-1	343 $[M - CH_3]^+$	358 $[M]^+$
6	Benzophenone-8	373 $[M - CH_3]^+$	388 $[M]^+$
7	Benzophenone-6	403 $[M - CH_3]^+$	418 $[M]^+$
8	Benzophenone-2	445 $[M - C_4H_{13}Si]^+$	519 $[M - CH_3]^+$

Table 4
Recoveries of sunscreen agents from cosmetic samples

Peak no.	Sunscreen agent	Amount added (%, w/w)	Recovery ± S.D.(%) [a]		
			Lotion	Cream	Cream foundation
2	Octylsalicylate	3.0	97.0 ± 0.9	98.8 ± 0.7	99.7 ± 0.6
3	Homosalate	3.0	96.5 ± 1.3	97.2 ± 1.1	97.6 ± 0.8
4	Benzophenone-3	3.0	98.3 ± 0.8	98.1 ± 1.6	98.8 ± 1.1
5	Benzophenone-1	3.0	98.0 ± 0.9	97.7 ± 1.2	100.6 ± 1.8
6	Benzophenone-8	3.0	97.6 ± 1.9	98.7 ± 1.3	99.9 ± 0.5
7	Benzophenone-6	3.0	98.8 ± 1.1	98.0 ± 0.8	99.5 ± 0.8
8	Benzophenone-2	3.0	101.6 ± 3.1	100.8 ± 1.4	101.3 ± 2.8

[a] Each value is the average of five determinations.

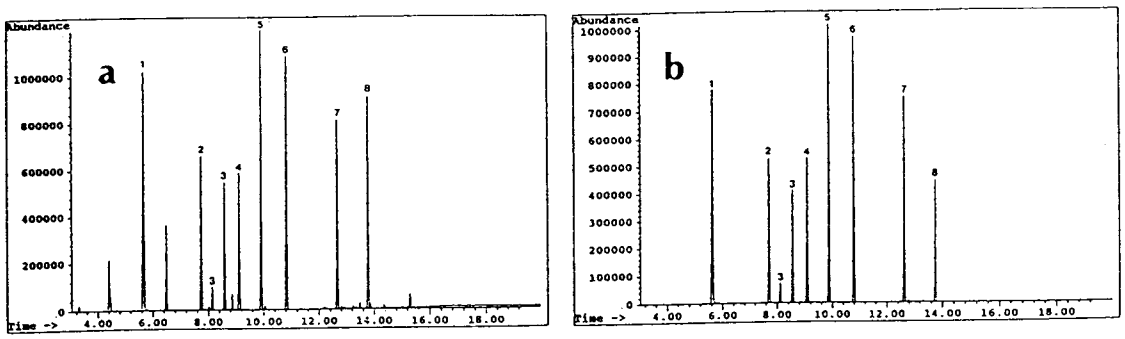

Fig. 9. (a) Total- and (b) selected-ion chromatogram of silylated sun lotion.

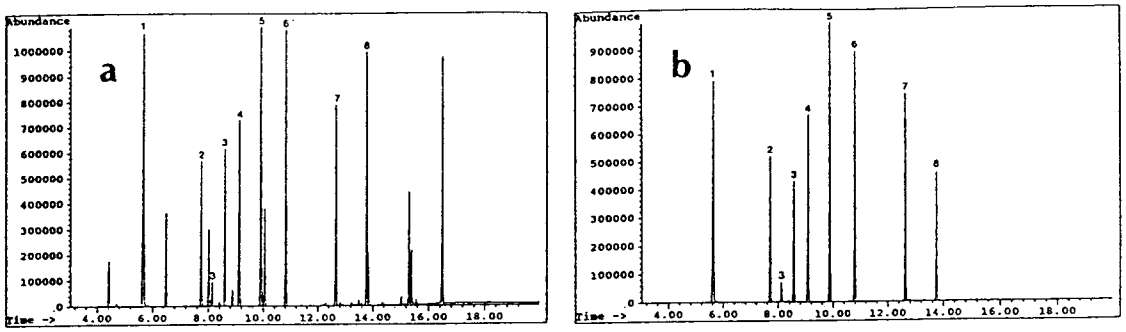

Fig. 10. (a) Total- and (b) selected-ion chromatogram of silylated sun cream.

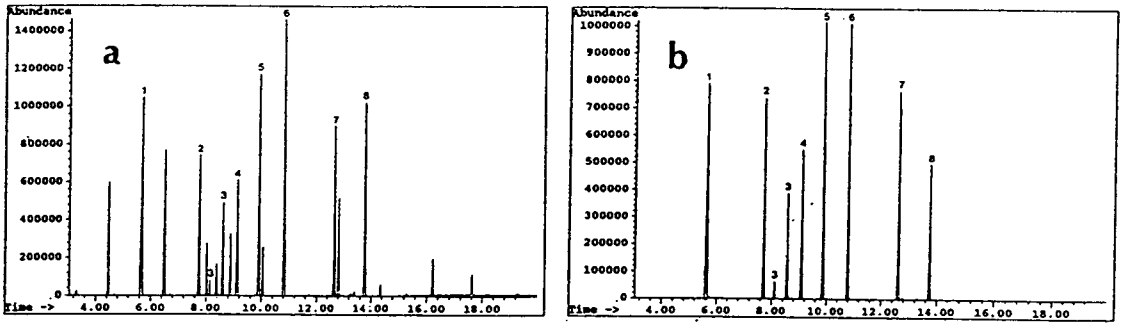

Fig. 11. (a) Total- and (b) selected-ion chromatogram of silylated sun cream foundation.

nation and confirmation of sunscreen agents in cosmetic products containing many ingredients.

References

[1] N.A. Shaath, *Cosmet. Toiletries*, 104 (1989) 75–84.
[2] H.S.I. Tan, R. Sih, S.E. Moseley and J.L. Lichtin, *J. Chromatogr.*, 291 (1984) 275–282.
[3] L. Gagliard, A. Amato, A. Basili, G. Cavazzutti, E. Gattavecchia and D. Tonelli, *J. Chromatogr.*, 362 (1986) 450–454.
[4] L. Gagliard, A. Amato, A. Basili, G. Cavazzutti and D. Tonelli, *J. Chromatogr.*, 408 (1987) 409–415.
[5] L. Gagliardi, G. Cavazzutti, L. Montanarella and D. Tonelli, *J. Chromatogr.*, 464 (1989) 428–433.
[6] B.M. Cumpelik, *Cosmet. Toiletries*, 97 (1982) 67–75.
[7] K. Ikeda, S. Suzuki and Y. Watanabe, *J. Chromatogr.*, 513 (1990) 321–326.
[8] D. Valdez, *J. Chromatogr. Sci.*, 23 (1985) 128–131.
[9] K. Molever, *J. Am. Oil Chem. Soc.*, 170 (1993) 101–103.

ELSEVIER

Journal of Chromatography A, 688 (1994) 383–389

JOURNAL OF CHROMATOGRAPHY A

Short communication

Determination of atrazine and simazine in drinking and surface waters by solid-phase extraction and high performance thin layer chromatography

Helena Zahradníčková[a,*], Petr Šimek[a], Pavla Hořicová[b], Jan Tříska[b]

[a]*Institute of Entomology, Laboratory of Analytical Chemistry, Academy of Sciences of the Czech Republic, Branišovská 31, 370 05 České Budějovice, Czech Republic*

[b]*Institute of Landscape Ecology, Department of Analytical Chemistry and Biochemistry, Academy of Sciences of the Czech Republic, Branišovská 31, 370 05 České Budějovice, Czech Republic*

First received 13 July 1993; revised manuscript received 13 October 1994

Abstract

A simple high-performance thin layer chromatographic (HPTLC) method has been developed for the determination of atrazine and simazine herbicides in drinking and surface waters. The method involves solid-phase extraction on C_{18} Bakerbond cartridges followed by development of the concentrated extracts on HPTLC silica plates with a nitromethane–tetrachloromethane (1:1, v/v) mobile phase and quantitation by UV scanning densitometry. Using the proposed mobile phase composition, pronounced background suppression on the chromatograms of the real water samples was accomplished. The detection limits of the method were 30 and 60 ng/l for atrazine and simazine, respectively, at the 80–400 ng/l fortification level in the surface waters. The method was successfully applied to the analyses of tap and surface waters with overall recoveries between 58 and 93% and a relative standard deviation below 12%. The results show, that the HPTLC method is sufficiently selective and sensitive to be employed in screening of contaminated waters containing the triazines below the maximum residues limits of the European Community.

1. Introduction

Triazine herbicides such as atrazine and simazine have been extensively applied in agriculture over the last three decades. Triazines are usually used for pre- and post-emergent control of broadleaf and grassy weeds in corn, soybeans and other field crops. As a result of the extensive application, the herbicides may contaminate crops and also drinking, surface and ground waters. In European countries, the maximum residue limit (MRL) of individual pesticide in drinking water is 100 ng/l. Routine analysis of large series of samples is therefore needed to monitor environmental pollution and satisfy the regulatory requirements.

A number of sample processing and quantitation schedules has been used for the determination of triazines including thin-layer chromatography (TLC) [1–5]. Up to now, application of TLC in the field of pesticide residue analysis has been limited, particularly because of its lack of its selectivity [6]. Since the 1960s, various approaches have been proposed in order to over-

* Corresponding author.

0021-9673/94/$07.00
SSDI 0021-9673(94)00982-1

come this problem, including post-chromatographic labeling of the pesticide spots [2–4], the use of HPTLC layers precoated with modified hydrophilic surfaces [5] or automated multiple wavelength detection [6,7]. In this paper, a simple HPTLC method is described for the determination of atrazine and simazine residues in tap and surface waters. The method is based on solid-phase extraction (SPE) with C_{18} cartridges followed by elution of the extracts on the fluorescently labeled silica HPTLC plates with a mobile phase allowing sensitive and sufficiently selective detection of the pesticide spots by UV scanning densitometry.

2. Material and methods

2.1. Chemicals

Methanol, tetrachloromethane, chloroform, acetone, ethyl acetate and anhydrous sodium sulfate were purchased from Lachema (Brno, Czech Republic); dichloromethane, toluene, hexane and isooctane from Fluka (Buchs, Switzerland); nitromethane from P.P.H. Polskie Odczynniki Chemiczne (Gliwice, Poland); and [$^2H_{10}$]anthracene from Aldrich (Milwaukee, WI, USA). Atrazine and simazine were obtained from Supelco (Gland, Switzerland). All the chemicals and solvents used were of analytical grade. Methanol, toluene and water were redistilled in glass prior to use.

2.2. Standard solutions

Working calibration standards of each triazine were prepared by serial dilution from the individual stock solutions (1 mg/ml) in methanol and used for spiking of water samples and formation of calibration plots.

2.3. Samples

Surface water samples were obtained from Římov and Orlík water reservoirs located in south and central Bohemia (Czech Republic), respectively. Drinking water samples originating from Římov water reservoir were collected from the municipal water supply in the authors' laboratories. The samples were taken in February–June 1992 and stored in 2-l glass bottles rinsed with Nanopure, deionized water prior to sampling.

2.4. SPE and HPTLC equipments

Bakerbond spe octadecyl 6-ml cartridges (1000 mg) and a vacuum manifold Baker SPE 10 column processor system from J.T. Baker (Gross-Gerau, Germany) were used for extraction of the pesticides from water samples. HPTLC precoated silica gel 60 F_{254} plates, 10 × 10 cm, article No. 5628, series 19760707 (Merck, Darmstadt, Germany) and HPTLC Nano-Plates SIL-20 UV 254, 10 × 10 cm, article No. 811 022, charge 11.88 from Macherey–Nagel (Düren, Germany) were used for chromatography. The samples were applied on the plates with a Linomat IV applicator from Camag (Muttenz, Switzerland). A Camag horizontal developing chamber and a Camag TLC Scanner II densitometer were used for the elution and detection of the pesticides. The plates were scanned in the reflectance mode at 220 nm. Data were processed with a SP 4270 integrator (Spectra-Physics, Darmstadt, Germany).

2.5. SPE

Atrazine and simazine were removed from water samples by using Bakerbond C_{18} SPE cartridges according to a procedure similar to that described elsewhere [8]. Shortly, each sample was split in six 250-ml aliquots; four of these were fortified with two known concentrations of each triazine in the range of 80–400 ng/l. The cartridges were conditioned with 2 × 6 ml of methanol followed by 2 × 6 ml of redistilled water. Each sample aliquot was then aspirated through the preconditioned cartridge at a flow-rate of 8.3 ml/min. The cartridges were further washed with 3 × 6 ml of redistilled water, 3 × 6 ml of 5% aqueous methanol and dried under vacuum for 15 min. Triazines were desorbed from the cartridges with 4 × 500 μl of methanol into 4-ml screw vials. The eluate was evaporated to dryness under a stream of nitrogen on a water

bath at 45°C, redissolved in 200 μl of methanol and used for HPTLC and/or GC–MS analysis.

2.6. HPTLC analysis

A 40-μl volume of each SPE methanolic extract was applied by means of the Linomat IV applicator in 3-mm strips at a rate of 8 s per μl on the HPTLC plates. The samples and the triazine standards were applied alternatively at 2-mm intervals to both halves of the plates, 18 strips on each side, 8 mm from the edge. The calibration was based on the peak heights obtained from densitometric responses of the standards applied on each plate. The plates were developed using an appropriate eluent on the 45-mm developing path at ambient temperature (25°C). The spots were dried under a stream of air and scanned immediately. The conditions for the quantitative evaluation were: deuterium lamp wavelength, 220 nm; monochromator bandwidth, 30 nm; slit width, 0.4 mm; slit length, 2 mm; scanning speed 1 cm/min.

2.7. GC–MS analysis

Two aliquots of each water sample processed by the SPE procedure, a spiked and an untreated one, were subjected to the GC–MS analysis. A 80-μl volume of each methanolic SPE extract was evaporated to dryness under a mild stream of nitrogen and redissolved in 100 μl of toluene, containing [$^2H_{10}$]anthracene as an internal standard (2 ng/μl). Analyte identity in the water samples was verified by GC–MS on a 30 m DB-5 column using a Finnigan MAT ion trap detector as described by Pereira et al. [9]. The detection limit of the GC–MS method ($S/N = 5$) was in our hands about 10 ng/l for both triazines.

3. Results and discussion

In order to meet criteria of the pesticide MRLs, conventional SPE in combination with chromatographic techniques, such as HPLC [10–14], was utilized prior to the HPTLC analysis. Optimization of the HPTLC step was primarily focused on two factors which showed to be critical in preliminary experiments; the mobile phase composition and performance of the HPTLC plates. A series of solvent mixture eluents was evaluated in terms of selectivity. R_F values of atrazine and simazine calculated for the examined mobile phase compositions are summarized in Table 1. The triazines can easily be separated on the HPTLC silica gel plates with most tested eluents, which is consistent with the results reported by other authors [2]. Moreover, using UV scanning densitometry triazine spots were easily detected at the low nanogram level, corresponding to 100 ng/l of each herbicide in a water sample. The results were less satisfactory when spiked real water samples were subjected to the analysis; this was evidently due to the background effects. Fortunately, as only small amounts of mobile phase were needed (typically 4.8 ml for up to 18 analysis runs available on a HPTLC plate), rather uncommon solvents could be used as eluents for the selectivity adjustment. We found nitromethane–tetrachloromethane (50:50, v/v) the best elution system leaving impurities mostly on the start and front positions of the eluent, which resulted S/N values approximately 5 times higher than those achieved with other tested eluents. For calculations of sensitivity (S = peak height/ng of each standard on the HPTLC plate) and detectability [16] ($D = 2 \times$ noise/S), six spiked surface water samples, obtained from the Římov water reservoir and preliminary checked to be free of triazines by GC–MS, was analysed by the developed method. The results, summarized in Table 2, show detection limits of the method ($S/N = 2$) to be 30 and 60 ng/l for atrazine and simazine, respectively.

Performance of the HPTLC plates was found to be another critical factor considerably influencing the HPTLC analysis at the MRL concentration level. With a batch of Merck HPTLC silica gel plates sensitivity and selectivity obtained from densitometric detection was acceptable for trace analysis of both triazines in water samples. However, when a similar batch of the Macherey–Nagel HPTLC silica gel plates was examined, the results were less satisfactory. This

Table 1
R_F values of atrazine and simazine obtained with the 12 tested mobile phases on the Merck silica gel 60 F_{254} plate by UV scanning densitometry

Mobile phase	R_F		Ref.[a]
	Atrazine	Simazine	
$CHCl_3$–MeOH (80:20, v/v)	0	0	[15]
$CHCl_3$–acetone (90:10, v/v)	0	0	[2]
Hexane–MeOH (90:10, v/v)	0.09	0.06	[3]
Toluene–acetone (85:15, v/v)	0	0	[4]
$CHCl_3$–MeOH–water (97:2:1, v/v)	0.53	0.43	
$CHCl_3$–MeOH–water (97:2.5:0.5, v/v)	0.80	0.69	
$CHCl_3$–MeOH–water (96.5:2.5:1, v/v)	0.57	0.51	
$CHCl_3$–MeOH–EtAc[b]–water (97:2:0.5:0.5, v/v)	0.73	0.63	
CH_2Cl_2–MeOH–water (97:2.5:0.5, v/v)	0.51	0.44	
CH_2Cl_2–MeOH–water (97:2:1, v/v)	0.43	0.36	
Nitromethane–$CHCl_3$ (50:50, v/v)	0.58	0.45	[2]
Nitromethane–CCl_4 (50:50, v/v)	0.61	0.47	[2]

[a] References, where the same solvents were employed for the elution of the triazines on TLC silica gel plates.
[b] EtAc = Ethyl acetate.

is illustrated in Fig. 1, where densitograms of 15 ng of atrazine and simazine applied on these two HPTLC silica gel plates are depicted. As the silica gel layer on the Merck HPTLC plates proved also to be more compact and mechanically resistant to manipulation, only these plates were further evaluated for quantitative analysis.

3.1. HPTLC calibration curves

Calibration curves exhibited good linearity on the Merck HPTLC precoated silica gel plates in the range of 2–45 ng for both triazines. Typical linear regression equations calculated from the densitometric peak height measurements were $y = 3.504 \times + 3.604$ ($r^2 = 0.999$) for atrazine and $y = 1.803 \times + 0.576$ ($r^2 = 0.999$) for simazine.

The calibration curves were found to be non-linear in the range 50–250 ng.

3.2. Quantitation of atrazine and simazine in real water samples

The proposed HPTLC method was further evaluated by determining atrazine and simazine levels in tap and surface waters collected from various water reservoirs in central and south Bohemia. The overall recoveries of atrazine and simazine from real water samples and their relative standard deviations (R.S.D.) are sum-

Table 2
Sensitivity, detectability, detection limits (DLs) and precision of the HPTLC method calculated from the determination of atrazine and simazine in six surface water samples fortified at the 100 ng/l level

Analyte	Sensitivity (mm/ng)	Detectability (ng/spot)	DL (ng/l)	R.S.D.[a] (%)
Atrazine	3.8	2	30	3
Simazine	1.9	3	60	4

Each sample obtained from the Římov water reservoir in March 1992 was analysed in triplicate.
[a] Relative standard deviation of the densitometric peak height measurement.

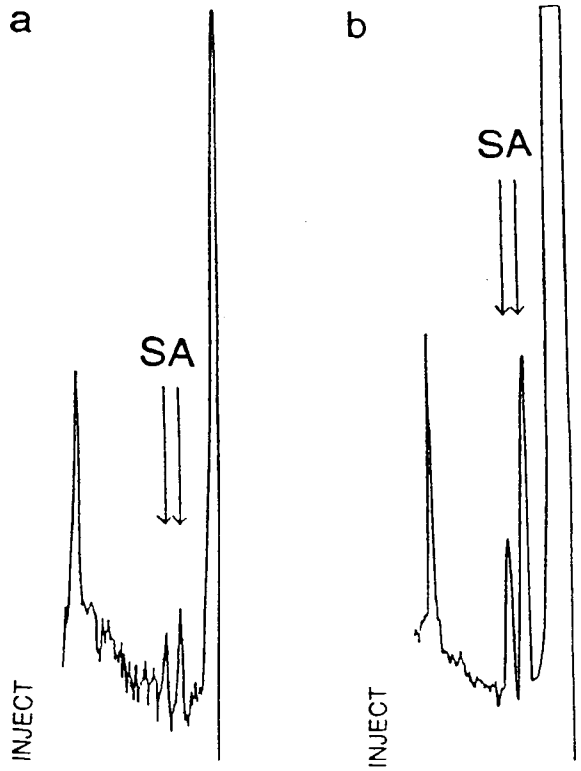

Fig. 1. Densitograms of 15 ng of atrazine (peak A) and simazine (peak S) obtained by UV scanning densitometry on the Macherey–Nagel (a) and Merck (b) HPTLC silica gel plates. Mobile phase: nitromethane–tetrachloromethane (1:1, v/v); 220 nm.

marized in Table 3. The results are satisfactory showing recoveries in the range of 58–93% and R.S.D. values not exceeding 12%. Rather varying recoveries in some cases may be explained by occurrence of the herbicides below the detection limit of the method that could influence recovery calculations on the 100 ng/l concentration level.

Typical densitograms obtained from a HPTLC analysis of a surface water sample from the Římov water reservoir and the same sample spiked with each triazine at 400 ng/l level (sample 8 in Table 3) are shown in Fig. 2a and b, respectively. Although the water samples were collected in Spring and early Summer period, when pollution of water reservoirs in central Europe from run-off waters is most serious, the amounts of atrazine and simazine in all tap and natural waters were found below the detection limit of the HPTLC method as well as below the legal tolerance levels. This knowledge was further checked by the GC–MS method, used as a confirmatory technique. The use of another independent method such as GC–MS is essential in cases when spots corresponding to atrazine and simazine are present on the densitograms in order to avoid false positive results. Using GC–MS only traces of atrazine (at 15 ng/l) were found in samples collected from the Orlík water reservoir in April 1992.

Sample throughput of the HPTLC method is high because 36 analysis runs can be performed simultaneously on each HPTLC plate. The time of analysis is limited by the SPE procedure; particularly by the capacity of the vacuum manifold column processor and sample evaporation

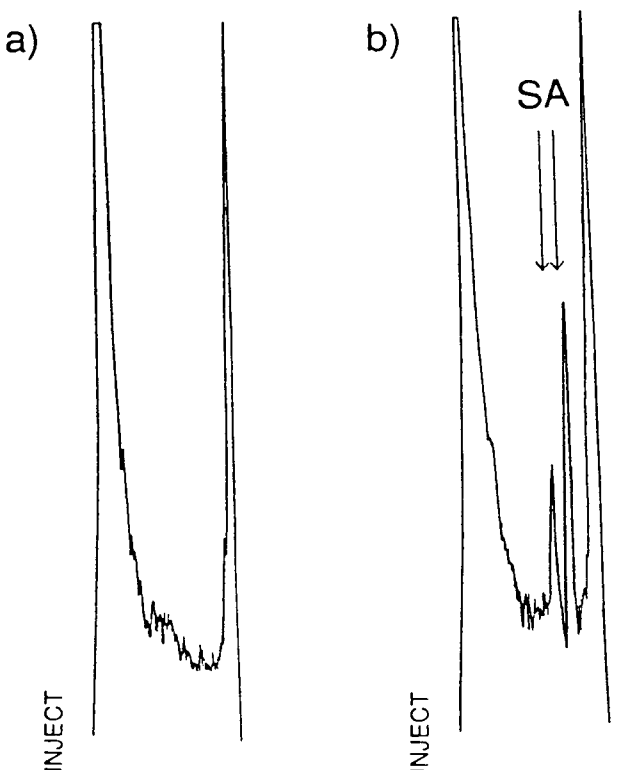

Fig. 2. Densitograms of (a) the SPE extract obtained from the Římov water reservoir collected 13 April 1992 and (b) the SPE extract of the same sample aliquot spiked with each triazine at the 400 ng/l level.

Table 3
Mean recovery and R.S.D. of atrazine and simazine in real tap and surface water samples

Water sample	No.	Date[a]	Atrazine			Simazine		
			Spike[b] (ng/l)	Recovery (%)	R.S.D. (%)	Spike[b] (ng/l)	Recovery (%)	R.S.D. (%)
Tap water	1	19 February 1992	80	93	4	80	79	4
	2	19 February 1992	200	85	3	200	70	3
Římov reservoir	3	19 February 1992	120	77	8	120	67	10
	4	19 February 1992	240	81	4	240	58	4
	5	20 March 1992	120	79	8	120	84	9
	6	20 March 1992	240	64	6	240	62	7
	7	13 April 1992	200	72	8	200	70	8
	8	13 April 1992	400	62	5	400	65	6
	9	15 June 1992	200	93	5	200	74	5
	10	15 June 1992	400	88	6	400	79	7
Orlík reservoir	11	23 April 1992	200	62	8	200	65	12
	12	23 April 1992	400	73	7	400	72	7
	13	9 June 1992	200	84	9	200	88	9
	14	9 June 1992	400	62	10	400	66	10

The triazines were detected only in the spiked samples. Each value is the average from the analysis of four replicates ($n = 4$).
[a] Date of the water sample collection.
[b] Spiking sample level.

after desorption of analytes from the SPE column. Considering the HPTLC step only, which involves application of six standards for calibration, application of a sample and the corresponding spike, development of the spots, densitometric scanning, and integrator data processing, 15 water sample extracts can be analysed on each HPTLC plate in 2 h; i.e. complete quantitation of 60 water samples can be achieved by the proposed HPTLC method within 8 working hours.

4. Conclusions

The proposed HPTLC method is sufficiently selective and sensitive for determination of atrazine and simazine in drinking and surface waters below the MRLs established in the European Community. Due to its performance, particularly high sample throughput, the method seems to be suitable for routine screening of contaminated waters, reducing the use of more powerful and expensive methods such as GC–MS for confirmatory purposes.

Acknowledgements

The authors thank Dr. Josef Hejzlar, Institute of Hydrobiology, Czech Academy of Sciences, České Budějovice, for sample collection from the Czech water reservoirs.

References

[1] V.N. Kaveckii, L.I. Bublik and G.V. Fuzik, *Zh. Anal. Khim.*, 42 (1987) 1302–1304.
[2] D.C. Abbott, J.A. Bunting and J. Thomson, *Analyst*, 90 (1965) 356–361.
[3] J. Sherma, *J. Liq. Chromatogr.*, 11 (1986) 2121–2130.
[4] G. Szökely, P. Weick and B. Abt, in P. Henschel and P.G. Lauberean (Editors), *Proceedings of a Workshop organized within the framework of Working Party 1 of the Concerted Action "Organic Micropollutants in the Aquatic Environment" COST 641, Berlin (West), 16–17 March 1989*, Guyot, Bruxelles, 1989, pp. 102–110.

[5] H.-E. Hauck, M. Mack, S. Reuke and H. Herbert, *J. Planar Chromatogr.*, 2 (1989) 268–275.
[6] K. Burger, *Fresenius' Z. Anal. Chem.*, 318 (1984) 228.
[7] U. de la Vigne and D.E. Jänchen, *J. Chromatogr.*, 553 (1991) 489–496.
[8] *Bakerbond Application Note EN-022*, J.T. Baker, Gross-Gerau, 1991.
[9] W.E. Pereira, C.E. Rostad and T.J. Leiker, *Anal. Chim. Acta*, 228 (1990) 69–75.
[10] M. Battista, A. Di Corcia and M. Marchetti, *Anal. Chem.*, 61 (1989) 935–939.
[11] A. Di Corcia, M. Marchetti and R. Samperi, *J. Chromatogr.*, 405 (1987) 345.
[12] R.J. Bushway, L.B. Perkins, L. Fukal, R.O. Harrison and B.S. Fergusson, *Arch. Environ. Contam. Toxicol.*, 21 (1990) 365–370.
[13] M. Stahl, M. Lührmann, H.-G. Kicinski and A. Kettrup, *Z. Wasser-Abwasser-Forsch.*, 22 (1989) 124–127.
[14] C. Schlett, *Fresenius' J. Anal. Chem.*, 339 (1991) 344–347.
[15] R.W. Frei, N.S. Nomura and M.M. Frodyma, *Microchim. Acta*, 6 (1967) 1099–1104.
[16] C.F. Poole, M.E. Coddens, H.T. Butler, S.A. Schuette, S.S.J. Ho, S. Khatib, L. Piet and K.K. Brown, *J. Liq. Chromatogr.*, 8 (1985) 2875–2926.

ELSEVIER

Journal of Chromatography A, 688 (1994) 390

JOURNAL OF CHROMATOGRAPHY A

Book Review

Basic Relationships of Gas Chromatography, by L.S. Ettre and J.V. Hinshaw, Advanstar Communications, Cleveland, OH, 1993, XII + 177 pp., price US$ 34.95 (hardbound), US$ 24.95 (paperback), ISBN 0-929870-19-0 (hardbound).

This small book contains in eleven parts the whole spectrum of relationships connected with chromatograms, column performance, analyte retention, detector characteristics and fundamental equations. In four supplements, calculations of the hold-up time, film thickness and three versions of basic relationships between efficiency, resolution, selectivity and retention, as well as a critically compiled review of books on gas chromatography, are presented in detail.

The subject matter is presented in a perfectly clear form using the latest internationally accepted nomenclature, and where more versions of data presentation are known, comparative values give an evaluated picture. Although the book is stated to be a gas chromatographic aid, in fact the majority of the relationships discussed are valid also for liquid and supercritical fluid chromatography.

Both authors are well known scientists at Perkin-Elmer who have been working and teaching for many years in the field of (gas) chromatography. The first author is one of the main organizers of the IUPAC chromatography nomenclature and the second is the Editor of the "GC connections" column in the *LC · GC Magazine*. They have produced a valuable book which will be welcomed both by GC beginners and by advanced chromatographers, and also by students and teachers in undergraduate and graduate chemistry courses.

Summarizing, this is not just another publication on gas chromatography, but a book that should be present in personal, school and industrial libraries for day-to-day use covering a broad spectrum of interests. The "1993 Edition" on the cover page is a signal that more editions are to be expected. Congratulations.

Brno, Czech Republic Jaroslav Janák

SSDI 0021-9673(94)00915-5

Author Index

Chromatography in the Petroleum Industry

Edited by **E.R. Adlard**

Journal of Chromatography Library, Volume 56

Petroleum mixtures consist primarily of relatively unreactive complex hydrocarbons covering a wide boiling range. Such mixtures are difficult to separate by most analytical techniques. Therefore, the petroleum industry has for many years played a leading role in the development of chromatographic methods of analysis. Since the last book specifically concerned with chromatographic analysis of petroleum appeared 15 years ago, numerous advances have been made including developments in liquid and supercritical fluid chromatography, the advent of silica capillary columns with bonded stationary phases and the commercial availability of new selective detectors.

The current book contains chapters written by experts concerning the analysis of mixtures ranging from low boiling gases to waxes and crude oils.

Although the volume is specifically aimed at the petroleum analyst, there is much information of general interest which should be of benefit to a very wide readership.

Contents:

©1995 452 pages Hardbound
Price: Dfl. 435.00 (US$ 255.75)
ISBN 0-444-89776-3

ELSEVIER
An imprint of Elsevier Science

ORDER INFORMATION

ELSEVIER SCIENCE B.V.
P.O. Box 330
1000 AH Amsterdam
The Netherlands
Fax: +31 (20) 485 2845

For USA and Canada:
P.O. Box 945, New York
NY 10159-0945
Fax: +1 (212) 633 3680

US$ prices are valid only for the USA & Canada and are subject to exchange rate fluctuations; in all other countries the Dutch guilder price (Dfl.) is definitive. Customers in the European Union should add the appropriate VAT rate applicable in their country to the price(s). Books are sent postfree if prepaid.

Hyphenated Techniques in Supercritical Fluid Chromatography and Extraction

Edited by **K. Jinno**

Journal of Chromatography Library Volume 53

This is the first book to focus on the latest developments in hyphenated techniques using supercritical fluids. The advantages of SFC in hyphenation with various detection modes, such as FTIR, MS, MPD and ICP and others are clearly featured throughout the book. Special attention is paid to coupling of SFE with GC or SFC.
In this edited volume, chapters are written by leading experts in the field. The book will be of interest to professionals in academia, as well as to those researchers working in an industrial environment, such as analytical instrumentation, pharmaceuticals, agriculture, food, petrochemicals and environmental.

Contents:

ELSEVIER SCIENCE B.V.

© 1992 x + 334 pages Hardbound
Price: Dfl. 275.00 (US$ 157.25)
ISBNN0-444-88794-6

"...will be a good guide to the scope of successful applications of supercritical fluids and clearly demonstrates the ability of SFC to provide a wealth of information about analytes."
Chromatographia

"...a valuable new source of information describing the latest developments in SFC and SFE hyphenated techniques. The book is highly recommended for advanced undergraduate students and chromatographers."
LC-GC International

ORDER INFORMATION

For USA and Canada
ELSEVIER SCIENCE INC.
P.O. Box 945
Madison Square Station
New York, NY 10160-0757
Fax: (212) 633 3880

In all other countries
ELSEVIER SCIENCE B.V.
P.O. Box 330
1000 AH Amsterdam
The Netherlands
Fax: (+31-20) 5862 845

US$ prices are valid only for the USA & Canada and are subject to exchange rate fluctuations; in all other countries the Dutch guilder price (Dfl.) is definitive. Customers in the European Union should add the appropriate VAT rate applicable in their country to the price(s). Books are sent postfree if prepaid.

PUBLICATION SCHEDULE FOR THE 1995 SUBSCRIPTION

Journal of Chromatography A and *Journal of Chromatography B: Biomedical Applications*

MONTH	O 1994	N 1994	D 1994	
Journal of Chromatography A	683/1 683/2 684/1	684/2 685/1 685/2 686/1	686/2 687/1 687/2 688/1 + 2	The publication schedule for further issues will be published later.
Bibliography Section				
Journal of Chromatography B: Biomedical Applications				

INFORMATION FOR AUTHORS

(Detailed *Instructions to Authors* were published in *J. Chromatogr. A*, Vol. 657, pp. 463–469. A free reprint can be obtained by application to the publisher, Elsevier Science B.V., P.O. Box 330, 1000 AH Amsterdam, Netherlands.)

Types of Contributions. The following types of papers are published: Regular research papers (full-length papers), Review articles, Short Communications and Discussions. Short Communications are usually descriptions of short investigations, or they can report minor technical improvements of previously published procedures; they reflect the same quality of research as full-length papers, but should preferably not exceed five printed pages. Discussions (one or two pages) should explain, amplify, correct or otherwise comment substantively upon an article recently published in the journal. For Review articles, see inside front cover under Submission of Papers.

Submission. Every paper must be accompanied by a letter from the senior author, stating that he/she is submitting the paper for publication in the *Journal of Chromatography A* or *B*.

Manuscripts. Manuscripts should be typed in **double spacing** on consecutively numbered pages of uniform size. The manuscript should be preceded by a sheet of manuscript paper carrying the title of the paper and the name and full postal address of the person to whom the proofs are to be sent. As a rule, papers should be divided into sections, headed by a caption (*e.g.*, Abstract, Introduction, Experimental, Results, Discussion, etc.). All illustrations, photographs, tables, etc., should be on separate sheets.

Abstract. All articles should have an abstract of 50–100 words which clearly and briefly indicates what is new, different and significant. No references should be given.

Introduction. Every paper must have a concise introduction mentioning what has been done before on the topic described, and stating clearly what is new in the paper now submitted.

Experimental conditions should preferably be given on a *separate* sheet, headed "Conditions". These conditions will, if appropriate, be printed in a block, directly following the heading "Experimental".

Illustrations. The figures should be submitted in a form suitable for reproduction, drawn in Indian ink on drawing or tracing paper. Each illustration should have a caption, all the *captions* being typed (with double spacing) together on a *separate sheet*. If structures are given in the text, the original drawings should be provided. Coloured illustrations are reproduced at the author's expense, the cost being determined by the number of pages and by the number of colours needed. The written permission of the author and publisher must be obtained for the use of any figure already published. Its source must be indicated in the legend.

References. References should be numbered in the order in which they are cited in the text, and listed in numerical sequence on a separate sheet at the end of the article. Please check a recent issue for the layout of the reference list. Abbreviations for the titles of journals should follow the system used by *Chemical Abstracts*. Articles not yet published should be given as "in press" (journal should be specified), "submitted for publication" (journal should be specified), "in preparation" or "personal communication".

Vols. 1–651 of the *Journal of Chromatography*; *Journal of Chromatography, Biomedical Applications* and *Journal of Chromatography, Symposium Volumes* should be cited as *J. Chromatogr.* From Vol. 652 on, *Journal of Chromatography A* (incl. Symposium Volumes) should be cited as *J. Chromatogr. A* and *Journal of Chromatography B: Biomedical Applications* as *J. Chromatogr. B.*

Dispatch. Before sending the manuscript to the Editor please check that the envelope contains four copies of the paper complete with references, captions and figures. One of the sets of figures must be the originals suitable for direct reproduction. Please also ensure that permission to publish has been obtained from your institute.

Proofs. One set of proofs will be sent to the author to be carefully checked for printer's errors. Corrections must be restricted to instances in which the proof is at variance with the manuscript.

Reprints. Fifty reprints will be supplied free of charge. Additional reprints can be ordered by the authors. An order form containing price quotations will be sent to the authors together with the proofs of their article.

Carbohydrate Analysis

High Performance Liquid Chromatography and Capillary Electrophoresis

Edited by **Z. El Rassi**

Journal of Chromatography Library, Volume 58

The objective of the present book is to provide a comprehensive review of carbohydrate analysis by HPLC and HPCE by covering analytical and preparative separation techniques for all classes of carbohydrates including mono- and disaccharides; linear and cyclic oligosaccharides; branched heterooligosaccharides (e.g., glycans, plant-derived oligosaccharides); glycoconjugates (e.g., glycolipids, glycoproteins); carbohydrates in food and beverage; compositional carbohydrates of polysaccharides; carbohydrates in biomass degradation; etc.

The book will be of interest to a wide audience, including analytical chemists and biochemists, carbohydrate, glycoprotein and glycolipid chemists, molecular biologists, biotechnologists, etc. It will also be a useful reference work for both the experienced analyst and the newcomer as well as for users of HPLC and HPCE, graduates and postdoctoral students.

Contents: Part I. The Solute.
1. Preparation of carbohydrates for analysis by HPLC and HPCE (A.J. Mort, M.L. Pierce).
Part II. Analytical and Preparative Separations.
2. Reversed-phase and hydrophobic interaction chromatography of carbohydrates and glycoconjugates (Z. El Rassi).
3. High performance hydrophilic interaction chromatography of carbohydrates with polar solvents (S.C. Churms).
4. HPLC of carbohydrates with cation- and anion-exchange silica and resin-based stationary phases (C.G. Huber, G.K. Bonn). 5. Analysis of glycoconjugates using high-pH anion-exchange chromatography (R.R. Townsend). 6. Basic studies on carbohydrate - protein interaction by high performance affinity chromatography and high performance capillary affinity electrophoresis using lectins as protein models (S. Honda). 7. Modern size exclusion chromatography of carbohydrates and glycoconjugates (S.C. Churms). 8. High performance capillary electrophoresis of carbohydrates and glycoconjugates (Z. El Rassi, W. Nashabeh). 9. Preparative HPLC of carbohydrates (K.B. Hicks).
Part III. The Detection.
10. Pulsed electrochemical detection of carbohydrates at gold electrodes following liquid chromatographic separation (D.C. Johnson, W.R. LaCourse). 11. On-column refractive index detection of carbohydrates separated by HPLC and CE (A.E. Bruno, B. Krattiger). 12. Mass spectrometry of carbohydrates and glycoconjugates (C.A. Settineri, A.L. Burlingame). 13. Evaporative light scattering detection of carbohydrates in HPLC (M. Dreux, M. Lafosse). 14. Chiroptical detectors for HPLC of carbohydrates (N. Purdie). 15. Pre- and post-column detection-oriented derivatization techniques in HPLC of carbohydrates (S. Hase). 16. Post-column enzyme reactors for the HPLC determination of carbohydrates (L.J. Nagels, P.C. Maes). 17. Other direct and indirect detection methods of carbohydrates in HPLC and HPCE (Z. El Rassi, J.T. Smith). Subject index.

©1995 692 pages Hardbound
Price: Dfl. 425.00 (US$250.00)
ISBN 0-444-89981-2

ELSEVIER
An imprint of Elsevier Science

ORDER INFORMATION

ELSEVIER SCIENCE B.V.
P.O. Box 330
1000 AH Amsterdam
The Netherlands
Fax: +31 (20) 485 2845

For USA and Canada:
P.O. Box 945, New York
NY 10159-0945
Fax: +1 (212) 633 3680

US$ prices are valid only for the USA & Canada and are subject to exchange rate fluctuations; in all other countries the Dutch guilder price (Dfl.) is definitive. Customers in the European Union should add the appropriate VAT rate applicable in their country to the price(s). Books are sent postfree if prepaid.

151

15